PB80-196124

Proceedings of the Tenth International Technical Meeting on Air Pollution Modeling and Its Application, Held at Rome, Italy on October 22-26, 1979

NATO Committee on the Challenges of Modern
Society, Brussels (Belgium)

Oct 79

U.S. Department of Commerce
National Technical Information Service
NTIS

PB80-196124

COMMITTEE ON

THE CHALLENGES OF

MODERN SOCIETY

PROCEEDINGS OF THE TENTH INTERNATIONAL TECHNICAL MEETING ON AIR POLLUTION MODELING AND ITS APPLICATION

Number [redacted] 108

REPRODUCED BY
NATIONAL TECHNICAL
INFORMATION SERVICE
U.S. DEPARTMENT OF COMMERCE
SPRINGFIELD, VA 22161

NORTH ATLANTIC TREATY ORGANIZATION

TECHNICAL REPORT DATA

(Please read Instructions on the reverse before completing)

1. REPORT NO. NATO/CCMS No. 108	2.	3. RECIPIENT'S ACCESSION NO. PB 80 196124
4. TITLE AND SUBTITLE Proceedings of the Tenth International Technical Meeting on Air Pollution Modeling and Its Application		5. REPORT DATE October 1979
		6. PERFORMING ORGANIZATION CODE
7. AUTHOR(S)		8. PERFORMING ORGANIZATION REPORT NO.
9. PERFORMING ORGANIZATION NAME AND ADDRESS A report of the Air Pollution Pilot Study, NATO Committee on the Challenges of Modern Society		10. PROGRAM ELEMENT NO.
		11. CONTRACT/GRANT NO.
12. SPONSORING AGENCY NAME AND ADDRESS NATO Committee on the Challenges of Modern Society (CCMS) Environmental Proteciton Agency Room 819 W 401 M Street, S.W., Washington D.C. 20460		13. TYPE OF REPORT AND PERIOD COVERED
		14. SPONSORING AGENCY CODE

15. SUPPLEMENTARY NOTES

16. ABSTRACT

The growing energy demand in industrialized countries requires the construction of an increasing number of power plants fired with sulfur containing fossil fuels in already polluted areas. The construction of high stacks seemed to be the best solution. Standardized Gaussian models if at all suitable, are not yet tested for an application to this problem. This document includes discussions and research findings of this problem.

17. KEY WORDS AND DOCUMENT ANALYSIS

a. DESCRIPTORS	b. IDENTIFIERS/OPEN ENDED TERMS	c. COSATI Field/Group

18. DISTRIBUTION STATEMENT	19. SECURITY CLASS *(This Report)*	21. NO. OF PAGES 743
	20. SECURITY CLASS *(This page)*	22. PRICE

EPA Form 2220-1 (9-73)

PROCEEDINGS OF THE TENTH INTERNATIONAL TECHNICAL MEETING ON AIR POLLUTION MODELING AND ITS APPLICATION

October 22-26, 1979

ROME, ITALY

A Report of the Air Pollution Pilot Study
NATO Committee on the Challenges to Modern Society
1979

Preface

In 1969 the North Atlantic Treaty Organization established a Committee on the Challenges of Modern Society which under the impression of the increasing public concern about the human environment focussed its work program mainly on environmental issues. For carrying out its program the Committee created a new system of initiating so-called pilot studies which should be run by one country, the pilot country, and which should complete its work in not more than two to three years. This system was chosen in order to collect information and make them widely available as long as they are yet current. Participation in these pilot studies is not restricted to members of the Alliance only but open to every country concerned or interested.

Air pollution was immediately identified as one of the priority problems of environmental protection and already in the year of its establishment the Committee initated a pilot study on Air Pollution chaired by the United States of America. One of the subjects to be dealt with was air quality modeling which found increasing interest and soon the air quality modeling working group decided to annually invite air quality modelers from all over the world to discuss recent findings and developments. The tradition of these International Technical Meeting of Air Pollution Modeling and its Application was not abandoned when the first Air Pollution Pilot Study was completed: In 1975 the Federal Republic of Germany proposed and initiated another pilot study about Air Pollution Assessment Methodology and Modeling and, in the same time, decided to continue to annually organize the international modeler symposia. The success of these conferences and their response in the scientific work more than justified this decision. We can now look back with satisfaction at ten successful international conferences.

During our pilotship in the last five years air quality modeling made a remarkable development and progress. This is increasingly proven by the wide use of this new technique in policy making, administration and management.

Last year the second pilot study on air pollution was completed; this year the Committee on the Challenges of Modern Society adopted another proposal of the Federal Republic of Germany to continue work in this area with a new pilot study, again under the chairmanship of the Federal Republic of Germany. The International Technical Meetings on Air Quality Modeling, however, will no longer be organized by us. With the publication of the present proceedings of the 10th International Technical Meeting which was held in Rome in October 1979 we are glad to hand the stick over to Belgium, our co-pilot during the years 1975 - 1978, for maintaining the tradition of an annual international exchange of research findings and innovations in air quality modeling.

We herewith would like to express our gratitude to all authors of papers and discussion reports as well as to the session chairmen for their cooperation together with our sincere thanks to our Italian hosts for their outstanding hospitality in Rome!

Dieter Jost

Dieter Jost
Chairman

Christa Morawa

Christa Morawa
Secretary

NATO /CCMS Air Pollution Pilot Study,
Assessment Methodology and Modeling
1975 - 1978

Berlin, November 30, 1979

CONTENTS

Page:

Introductory Papers:

LUIGI SANTOMAURO:
TALL STACKS - MANAGEMENT 3

WERNER KLUG:
TALL STACKS - IMPACTS ON THE ATMOSPHERE 9

Discussion: 24

CHAPTER I
TALL STACKS

1. FORECAST OF FUMIGATION EPISODES AROUND A TALL STACK

(P. Bolzern, G. Fronza, Istituto di Elettrotecnica ed Elettronica; Centro Teoria dei Sistemi; Politecnico di Milano; MILANO, Italy) 29

Discussion: 44

2. HOW DO TALL STACKS INFLUENCE ON LONG RANGE TRANSPORT?

(M. Benarie, Institut national de recherche chimique appliquée - IRCHA - Boite postale No. 1;
91710 Vert Le Petit, France) 45

Discussion: 52

3. MODELING OF DISPERSION FROM TALL STACKS

(A. Venkatram, Ontario Ministry of the Environment, Air Quality and Met. Section, 135 St. Clair Avenue West, TORONTO, Ont. MAV 1P5;
R. Vet, Vet Consultants Ltd., TORONTO, Ont. Canada) 53

Discussion: 69

4. ON THE EFFECTIVENESS OF EXTREMELY TALL STACKS

(H. Fortak, Freie Universität Berlin, Theoretische Meteorologie, Thielallee 49, 1 BERLIN 33) 71

Discussion: 83

5. DISPERSION OF POLLUTANTS FROM TALL STACKS STUDIED BY REMOTE SENSING TECHNIQUES DURING EEC JOINT CAMPAIGNS

(P. Guillot, Commission of the European Communities; Environment and Raw Materials Research Programme, 200 Rue de la Loi, 1049 BRUSSELS, Belgium) 85

Discussion: 94

Page:

6. THE NANTICOKE STUDY: EXPERIMENTAL INVESTIGATION OF DIFFUSION FROM TALL STACKS IN A SHORELINE ENVIRONMENT

(R. V. Portelli, Atmospheric Environment Service;
Fisheries and Environment Canada; 4905 Dufferin Street,
DOWNSVIEW, Ont. M3H 5T4, Canada) .... *

Discussion: .... *

7. EXPERIMENTAL INVESTIGATION OF ATMOSPHERIC SULFUR TRANSPORT AND TRANSFORMATION IN THE STATE PROGRAM

(Wm. E. Wilson, F. Schiermeier, US Environmental
Protection Agency, Environmental Sciences Research
Laboratory, MD-84, RESEARCH TRIANGLE PARK, North
Carolina 27711, USA) 95

Discussion: 105

8. DEVELOPMENT OF PRACTICAL CALCULATIONS FOR ESTIMATING DISPERSION FROM ELEVATED SOURCES

(A. E. Saab, J. P. Granier, Electricité de France,
Direction des études et recherches, 6, Quai Watier,
78400 CHATOU, France) 107

Discussion: 117

9. EXPERIMENTAL OBSERVATIONS OF THE PLUME FROM A TALL STACK OUT TO 400 km

(M. M. Millàn, Atmospheric Environment Service;
Fisheries and Environment Canada; 4905 Dufferin Street,
DOWNSVIEW, Ont. M3H 5T4, Canada) .... *
Discussion: .... *

10. ELEVATED SOURCE SF$_6$-TRACER DISPERSION EXPERIMENTS IN THE COPENHAGEN AREA

(S. E. Gryning, E. L. Petersen, Risø National Laboratory,
Met. Section, 4000 Roskilde;
E. Lyck, National Agency of Environmental Protection,
Air Pollution Lab., Risø National Laboratory,
4000 Roskilde, Denmark) 119

Discussion: 132

11. A REVIEW OF HORIZONTAL AND VERTICAL DISPERSION COEFFICIENTS APPLIED IN THE CALCULATION OF GROUND LEVEL POLLUTANT CONCENTRATION RESULTING FROM EMISSIONS FROM TALL STACKS UNDER VERY UNSTABLE ATMOSPHERIC CONDITIONS

(D. A. Trout, US Environmental Protection Agency, Region V,
CHICAGO, Illinois, USA) 133

Discussion: 143

SUMMARY OF PANEL DISCUSSION ON TALL STACKS
(R. V. Portelli and M. M. Millan)............................ 145

*Manuscripts not available.

CHAPTER II
COMPLEX TERRAIN AND WEAK WIND CONDITIONS

12. A GROSS PARAMETER PLUME MODEL: THEORY AND APPLICATION FOR NON-PLANAR TOPOGRAPHY AND FOR NEGATIVELY BUOYANT EFFLUENTS

(B. Henderson-Sellers, University of Salford, Dept. Civil Eng. SALFORD M5 4WT, England) 153

13. BUOYANT PLUME RISE OVER A TWO-DIMENSIONAL HILL

(J. C. Weil, Martin Marietta Corp., Environmental Center, 1450 South Rolling Road, BALTIMORE, Maryland 21117, USA) .. 163

Discussion: 174

14. ANALYSIS BY MEANS OF METEOROLOGICAL AND PHYSICAL CONSIDERATIONS ABOUT THE TRANSPORT AND GROUND DEPOSITION OF THE TCDD EMITTED THE 10/7/76 FROM THE ICMESA FACTORY

(A. Cavallaro; G. Tebaldi; R. Gualdi; Laboratorio Provinciale Igiene e profilassi - Reparto Chimico, Via Juvara 22, MILANO, Italy) 175

Discussion: 185

15. STATIONARITY OF THE CONCENTRATION INTERMITTENCY IN SHORT-RANGE ATMOSPHERIC DISPERSION

(C. D. Jones, Porton Down, SALISBURY, WILTS SP4 oJQ, England) 187

Discussion: 197

16. THE INFLUENCE OF LOW LEVEL INVERSIONS ON THE DISPERSION OF ATMOSPHERIC POLLUTANTS

(H. Kolb, H. Reuter, Universität Wien, Institut für Meteorologie und Geophysik, Hohe Warte 38, 1190 WIEN, Austria) 199

17. NUMERICAL SIMULATIONS OF AIR FLOW POLLUTANT DISPERSION OVER COMPLEX TERRAIN

(Gisela Tangermann, Meteorologisches Institut der Universität Karlsruhe, 7500 KARLSRUHE, Federal Republic of Germany) 209

18. TEMPERATURE INVERSION DESTRUCTION IN MOUNTAIN VALLEYS - IMPLICATIONS FOR AIR POLLUTION DISPERSION

(C. D. Whiteman, T. B. McKee, Colorado State University, Dept. of Atmospheric Science, FORT COLLINS, Colorado 80523, USA) 217

Page:

19. TRAJECTORIES UNDER A STRONG TEMPERATURE INVERSION IN A MOUNTAINOUS AREA

(F. Wippermann, H. J. Koppert, Technische Hochschule Darmstadt, Institut für Meteorologie, Hochschulstr. 1, 6100 DARMSTADT, Federal Republic of Germany) 225

Discussion: 237

20. DEVELOPMENT AND VALIDATION ON AN AIR POLLUTION MODEL FOR COMPLEX TERRAIN APPLICATIONS

(M. W. Chan, Sara J. Head, S. Machiraju, Aero Vironment, Inc., 145 Vista Avenue, PASADENA, California 91107, USA).. 239

Discussion: 249

21. PHYSICAL MODELING OF PLUME DISPERSION IN COMPLEX TERRAIN WITH AN ELEVATED INVERSION

(H. T. Liu, Flow Research Com., 21414 68th Avenue South Kent, Washington 98031, USA;
J. T. Lin, United Industries Corp. Bellevue, WASHINGTON, USA) 253

22. A STUDY OF DISPERSION OVER COMPLEX TERRAIN IN THE SOUTHEASTERN UNITED STATES

(George C. Holzworth, Meteorology and Assessment Division, Envir. Sciences Research Lab., EPA, RESEARCH TRIANGLE PARK, North Carolina 27711, USA;
K. E. Pickering & R. C. Koch, Geomet. Inc., 15 Firstfield Road, GAITHERSBURG, Maryland 20760, USA) 269

Discussion: 293

23. EXPERIMENTAL DETERMINATION OF DIFFUSION COEFFICIENTS ABOVE AN URBAN AREA

(L. Santomauro, V. Maestro, C. Barberis, Osservatorio Meteorologico di Brera, Via Brera 28, MILANO, Italy) 295

Discussion: 306

24. A COMPARISON OF SOME INTEGRAL PLUME RISE MODELS WITH FIELD OBSERVATIONS

(G. A. Davidson, P. R. Slawson, University of Waterloo, Dept. of Mechanical Engineering, WATERLOO, Ont. N2L 3G1;
S. G. Djurfors, Syncrude Canada Ltd. 10030-107 Street, EDMONTON, Alberta T5J 3E5, Canada) 309

Discussion: 324

25. ANALYSIS OF SEVERAL LOW WIND SPEED TRACER EXPERIMENTS

(R. J. Yamartino, Argonne National Laboratory, 9700 South Cass Avenue, ARGONNE, Illinois 60439, USA;

Page:

P. G. Lühring, R. Stern, Freie Universität Berlin,
Institut für Geophysikalische Wissenschaften,
Thielallee 50, 1000 BERLIN 33) 325

Discussion: 338

26. DIFFUSION OF ATMOSPHERIC POLLUTANTS BEING EMITTED FROM TALL STACKS

(W. G. Hübschmann, K. Nester, P. Thomas, Kernforschungszentrum Karlsruhe GmbH, Postfach 3540, 7500 KARLSRUHE,
Federal Republic of Germany) 339

Discussion: 345

27. TESTS ON ATMOSPHERIC DIFFUSION WITH TRACERS IN URBAN AREA

(D. Camuffo, CNR Laboratorio Chimica e Tecnologia Radioelementi, Corso Stati Uniti, 35100 PADOVA;
M. De Bortoli, P. Gaglione, JRC EURATOM, Chemical Div.
ISPRA, Varese, Italy) 347

Discussion: 360

28. AN EXTENSION OF THE GAUSSIAN PLUME MODEL FOR THE CASE OF CHANGING WEATHER CONDITIONS

(K. J. Vogt, J. Straka, H. Geiß, Kernforschungsanlage
Jülich GmbH, Postfach 365, 5170 JÜLICH, Federal
Republic of Germany) 361

CHAPTER III

MULTIPLE SOURCES

29. REGIONAL SOURCE QUANTIFICATION

(L. P. Prahm, National Agency for Environmental Protection
Danish Air Pollution Laboratory, Risø National Lab.
4000 ROSKILDE;
K. Conradsen, L. B. Nielsen, Institute of Mathematical
Statistics and Operations Research, Denmark's Technical
University, 2800 LYNGBY; Denmark;
A. Eliassen, Norwegian Meteorological Institute,
Postbox 320, BLINDERN, OSLO 3, Norway) 373

Discussion: 376

Page:

30. AN EXPERIMENTAL AND THEORETICAL INVESTIGATION OF PHOTOCHEMICAL POLLUTION IN TURIN

(J. H. Weaving, S. F. Benjamin, Browns Lane Allesley, Coventry CV5 9DR, England;
P. P. Gaddo, F. Repetto, Committee of Common Market Automobile Constructors (CCMC), 18 Square de Meeûs, 1040 BRUSSELS, Belgium) 377

Discussion: 396

31. MULTIVARIATE REAL-TIME PREDICTORS OF SULPHUR DIOXIDE CONCENTRATIONS IN MILAN CITY

(D. Barbieri, M. Baroni, G. Finzi, Centro Teoria dei Sistemi CNR c/o Istituto di Elettrotecnica ed Elettronica; Politecnico di Milano, Piazza Leonardo da Vinci, 32, 20133 MILANO, Italy) 397

Discussion: 410

32. SOME COMMENTS ON THE VALIDATION OR VERIFICATION OF MULTIPLE SOURCE MODELS FOR IMPACT ASSESSMENT

(J. G. Kretzschmar, Studiecentrum voor Kernenergie, S.C.K. /C.E.N., Boeretang 200, 2400 MOL, Belgium).......... 411

Discussion: 418

33. COMPARISON OF FINITE DIFFERENCE AND GALERKIN TECHNIQUES APPLIED TO THE NUMERICAL TREATMENT OF ADVECTION AND DIFFUSION OF AIR POLLUTANTS

(E. Runca, P. Melli, Centro Scientifico IBM Italia, ROMA, Italy) 421

Discussion: 431

CHAPTER IV

MESOSCALE DIFFUSION

34. THE DEVELOPMENT AND APPLICATION OF A MATHEMATICAL MODEL OF MESOSCALE DIFFUSION OF ATMOSPHERIC POLLUTANTS

(D. Henderson, United States Dept. of the Interior, National Park Service WASO Air Quality Office, P.O. Box 25287 DENVER, Colorado 80225;
Mei-Kao Liu and Michael Wojcik, Systems Applications, Inc. 950 Northgate Drive, SAN RAFAEL, California 94903, USA) ... 435

Discussion: 442

Page:

35. APPLICATION OF THE MESO-SCALE DIFFUSION MODELS MESOS AND TALD TO ACCIDENTAL RELEASES OF RADIO ACTIVITY

(H. ApSimon, J. Wrigley, Imperial College,
London, England;
J. Le Grand, A. Després, Commissariat à l'Energie
Atomique, Fontenay-Aux Roses, France) 443

Discussion: 457

36. VARIATION OF ACID RAIN CONCENTRATIONS WITH SUMMER PRECIPITATION EVENTS IN THE SCHEFFERVILLE, QUEBEC AREA

(J. E. Lewis, B. Hrebenyk, McGill University,
Department of Geography, Burnside Hall, 805 Sherbrooke
Street West, MONTREAL, PQ, H3A 2K6, Quebec, Canada) 459

Discussion: 468

37. THE USE OF TIME AVERAGED PRECIPITATION FOR WET REMOVAL IN A REGIONAL AIR POLLUTION ASSESSMENT MODEL

(W. E. Davis, W. J. Eadie, Battelle Pacific Northwest
Lab., Battelle Boulevard, RICHLAND, Washington 99352, USA). 469

38. SPECTRAL TURBULENT DIFFUSIVITY THEORY APPLIED FOR POINT SOURCE DISPERSION

(R. Berkowicz, Danish Meteorological Institute,
100 Lyngbyvey, 2100 COPENHAGEN, Denmark;
L. P. Prahm, National Agency for Environmental Protection,
Air Pollution Lab., Risø National Laboratory, 4000 ROSKILDE,
Denmark) 479

Discussion: 486

39. MODELING DRIFT OF FOREST PESTICIDE SPRAY USING THE MONTE CARLO METHOD

(J. D. Reid, Atmospheric Environment Service, Boundary
Layer Research Division, 4905 Dufferin Street,
DOWNSVIEW, Ont. M3H 5T4, Canada) 487

Discussion: 496

40. A STATISTICAL STUDY OF AIR TRAJECTORIES IN CONNEXION WITH THE OBSERVED LEVEL OF MESO-SCALE POLLUTION

(A. Berger, G. Deman, Cl. Demuth, P. Hecq, Université
Catholique de Louvain, Institut d'Astronomie et de
Géophysique Georges Lemaitre, Chemin du Cyclotron 2,
1348 LOUVAIN-LA-NEUVE, Belgium) 497

Discussion: 508

Page:

41. THE MATHEMATICAL MODELLING OF THE MESO-SCALE AND LONG-RANGE TRANSPORT OF SULPHUR COMPOUNDS

(P. R. Maul, Central Electricity Generating Board, Scientific Sciences Department, RATCLIFFE-ON-SOAR, Nottingham, NG II OEE, England) 509

Discussion: 519

42. MODELLING INTERREGIONAL TRANSPORT OF SO_2

(K. Herrmann, BASF Aktiengesellschaft, Abt. TUU/L1 - K 210, 6700 LUDWIGSHAFEN, Federal Republic of Germany) ... 521

Discussion: 530

43. EVALUATION OF A MESO-SCALE MODEL OF THE DISPERSION OF SULPHUR DIOXIDE

(N. D. van Egmond, Rijksinstituut voor de Volksgezondheid, BILTHOVEN;
C. Huygen, IMG/TNO Div. of Technology for Society, P. O. Box 342, 7300 AH APELDOORN, The Netherlands) 533

Discussion: 543

44. AIR POLLUTION MODEL FOR CALCULATING SHORT-TERM (DAILY) REGIONAL PATTERNS AND TRANSFRONTIER EXCHANGES OF AIRBORNE SULFUR IN EUROPE

(C. M. Bhumralkar, W. B. Johnson, R. L. Mancuso, D. E. Wolf, Stanford Research International, 333 Ravenswood Ave, MENLO PARK, California 94025/USA;
J. Pankrath, Umweltbundesamt, Bismarckplatz 1, 1000 BERLIN 33) 545

CHAPTER V

REGULATORY APPLICATIONS

45. THE CHANGING REGULATORY ENVIRONMENT: AN APPRAISAL OF MODEL NEEDS IN THE ANALYSIS AND EXAMINATION OF POTENTIAL AIR QUALITY IMPACTS OF NO_x EMISSIONS FROM LARGE POINT SOURCES

(S. R. Hayes, P. M. Roth, D. R. Souten, R. W. Bergstrom, Systems Applications, Inc., 950 Northgate Drive, SAN RAFFAEL, California 94903, USA)........................ 563

Discussion: 575

Page:

46. THE CURRENT ROLE OF TALL STACKS IN THE UNITED STATES - TECHNOLOGY VERSUS POLITICS

(M. E. Smith, Meteorological Evaluation Services Inc., Broadway, AMITYVILLE, N. Y. 11701, USA) 577

Discussion: 584

47. SENSITIVITY OF MODEL CALCULATIONS ON THE METEOROLOGICAL DATA AND ITS RELEVANCE TO REGULATORY ASPECTS

(L. Kropp, W. Bahmann, Technischer Überwachungsverein Rheinland e.V., Postfach 101750, 5000 KÖLN 1, Federal Republic of Germany) 587

Discussion: 600

48. TOTAL ENVIRONMENTAL PREDICTION - AIR QUALITY COMPONENT

(J. W. S. Young, Atmospheric Environment Service Canada, Dispersion Div., 4905 Dufferin Street, DOWNSVIEW, Ontario M3H 5T4, Canada) 603

Discussion: 611

49. THE USE OF GOOD ENGINEERING PRACTICE STACK HEIGHTS IN AIR POLLUTION CONTROL

(J. A. Tikvart, Alan H. Huber, United States Environmental Protection Agency, Office of Air Quality Planning and Standards MD - 14, RESEARCH TRIANGLE PARK, North Carolina 27711, USA) 613

Discussion: 623

CHAPTER VI

HEAVY GASES

50. FAILURE PROBLEMS AND DISPERSION PROCESSES OF HEAVY GASES

(B. Gutsche, Freie Universität Berlin, FB 24/WE 4 - Fachrichtung Meteorologie, Thielallee 49, 1000 BERLIN 33; Christina Ludwig, Fritz Vahrenholt, Umweltbundesamt, Bismarckplatz 1, 1000 BERLIN 33) 627

51. THE UNSTEADY GRAVITY SPREAD OF A DENSE CLOUD IN A CALM ENVIRONMENT

(A. P. van Ulden, Koninklijk Nederlands Meteorologisch Instituut, Postbus 201, 3730 AE DE BILT, The Netherlands).. 645

Discussion: 654

Page:

52. THE INVESTIGATION INTO THE SPREADING AND DISPERSION OF A HEAVY GAS CLOUD BY MEANS OF PLANT DAMAGES IN THE AFFECTED AREA

(C. G. Booij, van Hueveenstraat 46, 6824 ARNHEM, The Netherlands) 655

53. FIELD TRIALS ON THE RELEASE OF HEAVY GASES

(J. McQuaid, Research and Laboratory Services Division, Health and Safety Executive, RED HILL Sheffield S3 7HQ, England) 663
Discussion 673

54. HEAVY GAS IN THE ATMOSPHERE

(K. J. Eidsvik, Norwegian Institute for Air Research, P. B. 130, 2001 LILLESTROM, Norway) 675
Discussion 688

55. PHYSICAL MODELING OF ATMOSPHERIC DISPERSION OF HEAVY GASES RELEASED AT THE GROUND OR FROM SHORT STACKS

(R. N. Meroney, Colorado State University, Department of Civil Engineering, FORT COLLINS, Colorado 80523, USA) 689

Discussion: 699

56. COMPARISON OF A WIND TUNNEL MODEL OF A DENSER-THAN-AIR GAS SPILL WITH FIELD EXPERIMENTS

(D. J. Hall, Warren Spring Laboratory, Stevenage, Herts, United Kingdom) 701

AGENDA 711

LIST OF PARTICIPANTS 728

TOPIC 1

Tall Stacks

TALL STACKS - Management

L. Santomauro

1. Foreword

Some aeriform substances contained in industrial effluents are known to alter the quality of the atmosphere if protective measures are not taken at their release.

The air quality can be kept within acceptable limits from the standpoint of health by proper operational procedures or by engineering techniques:

The operational procedures include:

(a) the containment and/or reduction of pollutant emission;

(b) the variation of the physical conditions of the effluents (increased temperature and speed, load reduction, use of low-sulphur fuel).

The engineering techniques include:

(a) abatement or purification of the gaseous effluents before their release to atmosphere;

(b) discharge of polluting effluents at an appropriate elevation above ground so as to favour dispersion, dilution and self-purification of the pollutants in the air.

The operational procedures mentioned above can also be applied together. As concerns engineering methods, abatement or purification will become a valid alternative when the technique will be available for prompt aplication to large combustion processes. A general method utilized today to reduce the ground concentration of pollutants at parity of emission is to release the effluents at an elevation that, within reasonable limits, will make the most of the diluting capability of the air.

Therefore, the dynamic climatology and the orography at the plant site, condition the height of the stack.

In addition, it should be recalled that the dynamics of the transport and dispersion of pollutants are governed by "internal" parameters that depend on the design and operational characteristics of the plant as a whole and by "external", environmental and meteorological parameters which, of course, cannot be affected in any way.

On the other hand, the vicissitudes that the primary and secondary pollutants will go through from the emission to their ground deposition involve extremely complex processes that affect the ground concentration

Preceding page blank

and thus the quality of the air, which is an important requisite for the survival of mankind.

2. Definition of tall stack

To be an effective means of dispersion, a tall stack must evidently be capable of utilizing the natural dispersion and self-purification characteristics of the atmosphere and of suitably reducing the ratio between the pollutant concentration at ground level (immission) and at the release point (emission).

Such a structure must therefore be sufficiently high above ground and the surrounding obstacles to utilize the potential self-diluting characteristics of the atmosphere.

This leads to the need for the tall stacks usually employed in some industries (thermal power stations, foundries, etc.) where large amounts of sulphur and nitrogen oxides are produced.

Though such tall stacks have been and are rather extensively used all over the world, as yet there is not a general agreement on the definition of a tall stack.

At present, a tall stack is defined according to one of the following three main criteria: geometrical, diffusive and micrometeorological.

The first criterion of geometrical nature, followed by many experts, consists in taking an arbitrary heigh of 200 m over which a stack is called "tall".

The second criterion, which takes into account the effect of downwash, is the rule of 2 1/2; this level marks the geometrical limit between "low" and "tall" stacks.

The third criterion - micrometeorological - is that of defining "tall" a stack when the effluents are released above the average boundary layer in the involved area.

It is evident that the last criterion is the most complex to apply since it requires the development and utilization of models with an acceptable degree of confidence and reliability in the definition of the boundary layer and in the determination of the effluent plume rise over the stack outlet.

The practical development of this criterion obviously implies the performance of ad hoc experimental surveys to acquire the data necessary for a correct utilization of the meteorological and plume rise models.

From the logistical and economical points of view this type of operation should not represent a major problem, because tall stacks are built in large plants that call for detailed siting studies under various aspects including the ecological.

3. Tall stacks as alternative means for the reduction of ground level concentration

It should be recalled, that in November 1975, the U. N. Commission for Europe (ECE) sponsored the "Second Seminar on Desulphurization of Fuels and Combustion Gases" in Washington, D. C. and I was invited to deliver an introductory statement on "Alternatives and Supplements to Technical Methods-Large Industrial Sources", that is, for industries with SO_2 emissions over 1.5 ton/hour.

Regarding the utilization of tall stacks as alternative and supplemental methods to fuel and combustion gas desulphurization, it was concluded at the Seminar that the principle stated in the introductory Italian paper should be accepted, that is, that a stack is a system to disperse pollutants in the atmosphere and to reduce their ground concentration; also, that their geometrical size is determined by the type and by the operating parameters of the plant together with the physical conditions of the environment.

Finally, among the recommendations to the ECE countries' Governments for alternative methods, it was established that "not only must the emission rate be considered but also the emission height, the distribution of emitters and the distance of transport as well as the effects of meteorological conditions and naturally occurring chemicals".

From the above it must be clear that a designer, to be reasonably sure that the emissions from a plant remain within the limits established by law, must:

(a) firstly, assess which are the worst meteorological conditions for the site, that is, the conditions that will give, for the source, the highest ground concentration;

(b) secondly, by utilizing said conditions as restraint, determine the height of the stack and the operational parameters (temperature and speed of effluents, etc.) in accordance with the limits imposed by law.

Special attention is to be given to the concept of worst meteorological conditions to be assumed; such conditions shall have a significant probability of occurrence (the importance of statistical data is evident here); in the case of exceptionally unfavourable conditions it is always possible to resort the exceptional measures already described, such as the utilization of clean fuels, increasing gas temperature, load reduction, etc.

4. Impact of tall stack management

In recent years all the major industrial countries have enforced legislations on atmospheric pollution with various legal measures either original or taken from other countries' legislations.

These various laws differ a good deal both in their basic principles and in the restraint measures enforced, so that an analytical and detailed comparison is difficult.

In any case it is easy to understand that, by having to establish restraints in the absence of precise indications from epidemiological studies the legislator has taken precautions, in the definition of the air quality, by establishing the limits with ample safety margins.

Nonetheless it must be recalled that not only the numerical immission limits vary widely in the various national legislations but also the philosophy of the various laws controlling the atmospheric pollution has been in many cases conditioned both by the available technologies and by technical solutions adopted.

The basic elements that characterize this type of legislation and on which the legislator is required to make precise choices, can be listed as follows:

1. Monitoring and limitation of the emissions to the atmosphere and /or monitoring and limitation of the ground concentrations;
2. Restraints and limitations in the use of fuels with regard to their polluting characteristics and sulphur content;
3. Requirement to adopt flue-gas purification plants;
4. Utilization of surveillance networks to monitor air quality.
5. Appointment of qualified bodies for examination and judgement in the controversial cases of atmospheric pollution;
6. Classification of territory in controlled areas.

When examining the legislation of ten European Countries (Austria, Denmark, France, Germany, Holland, Italy, Poland, Sweden, Switzerland and U. K.) the following observations, as regards the various types of pollution, can be made:

(a) for sulphur dioxide: no limitation to the emissions are provided for with the exception of those deriving from the limits to sulphur content of the fuels; provision is generally made for limitation of the immissions;

(b) for particulates: some limitations to the emissions are provided for;

(c) limitations to CO emissions are provided for in some countries.

To our knowledge, in no country flue-gas cleaning plants are required while some legislations contain generic recommendations for the adoption of the best available technology for purification.

Only one national legislation mentions flue-gas desulphurization plants since such practice is considered substitutive or equivalent to the use of low-sulphur fuels.

Finally, in two European countries, the installation of surveillance networks for the monitoring of SO_2 and sulphur oxides around the new plants is required.

In other countries, surveys are requested for a limited time since, once the thermal plant contribution has been determined, it is considered unnecessary to maintain permanent monitoring.

In such a scenario of different laws, the technique of tall stacks, as utilized in modern thermal plants, gives assurance of amply maintaining the immissions within the limits imposed by the most stringent legislations.

By integrating such a technique with the selected use of low-sulphur fuels and, in some cases, with the use of monitoring networks, it is possible to cope with particularly adverse conditions both from the meteorological and the existing background pollution points of view.

This procedure is successfully applied in all those cases in which compliance with immission limits must be assured; in particular, such technique is mainly used to reduce the ground concentration of sulphur and nitrogen oxides.

On a world-wide scale an exception is represented by the USA where the control is imposed on the emissions; moreover there is a tendency to question the required height of the stacks.

This subject will be discussed by our colleague Mr. Tikvart of EPA in one of the next sessions.

The policy presently applied to power plants in our country is that of utilizing tall stacks as a means of reducing ground pollution.

Such policy is mainly justified by the particular meteorological conditions in our country with regard to the diffusion of air pollution.

These conditions range from the atmospheric instability at the sea coasts to the stability of the Po valley.

Therefore the Italian approach on the use of tall stacks, which is shared by other European Community Countries (U. K., France, etc.), is based other than on the plant size, also on the early surveys of the meteorological conditions prevailing in the zone expected to be influenced by the emission.

To conclude my paper, I wish to repeat, in agreement with Prof. Scorer, that the recommendations in favour of increasing tall stack height are made as an obvious precaution but they become useless without quantitative evaluations of their effect.

This subject will now be discussed further by our friend and colleague Professor Klug.

IMPACTS ON THE ATMOSPHERE

W. KLUG:

When I was asked about 9 months ago by Dieter Jost whether I would give a review paper on tall stacks, the time distance to this conference was large and I was in an optimistic mood; so I agreed.But when I began to write up this paper I realized that nearly all I can present here is a statement on the problems but not the solution and in a few cases I can review the knowledge we have.

Before we start off I want to explain what I understand under tall stacks, that is

stacks with building heights >200 m,

which gives in many cases effectiveheights in the order of 300 - 500 m. There are two main aspects under which I shall deal with the topic of tall stacks:

1. How much or better how little do we know when we want to evaluate the diffusion of material released from tall stacks?
2. What are the advantages or disadvantages of tall stacks regarding air pollution problems?

1. The problems we encounter when we deal with diffusion of material released from tall stacks are manifold and shall try to describe why this is so:

   a) The heights of tall stack and especially their effective heights are a substantial fraction of the height of the boundary layer most of the time.

   At night they are very often at the top or even above the nocturnal boundary layer. In order to evaluate the diffusion of material released by the tall stack we must have realistic descriptions of the whole boundary layer, such as turbulence characteristics, wind profiles, etc. as function of the external parameters. Unfortunately, such descriptions are very meager or cumbersome to obtain.

b) In air pollution problems we are very often concerned with surface concentrations of the material released. Since the maximum surface concentration moves under indifferent and stable stratifications to large distances from the source when the effective source heights are large, it takes some time until the material reaches the point of maximum grand level concentration. That is to say that the problem of instationarity caused by diurnal or advective changes of the meteorological situation comes into the picture. Quite apart from this fact, the inhomogeneity of the ground is more likely to occur over large distances. And finally, for longer travel times removal and transformation processes are becoming important.

c) When we deal with diffusion from low level sources we can - with reasonable success - estimate the diffusion characteristics of the lower layers of the atmosphere by means of rather simple, i. e. synoptic, observations alone. This is in many circumstances not possible any more with elevated sources, where the characteristics of a much deeper layer are involved. For example, it is very difficult, if not impossible to determine the height of the nocturnal boundary layer by means of synoptic surface observations alone. Even if we would utilise sophisticated models of the boundary layer - such as second-order-closure-models - to predict the relevant diffusion parameters, we would not have on a routine basis the input parameters to such models, such as surface heat flux, baroclinicity, initial profiles, etc. which influence the results in a complex way.

After having mentioned many difficulties which we encounter with diffusion from tall stacks, we have one meteorological situation where some reliable results are available from water tank experiments (Willis & Deardorff 1978), which can give us some guidance on our problems. This is the meteorological situation of a convective boundary layer, which gives - we can say, fortunately enough, the highest concentrations from an elevated release. Deardorff stated earlier, that for an elevated source in a mixed layer the scaling approach used in convective boundary modelling is "most applicable". Since we have this detailed knowledge from the water tank experiments we can compare those results with the conventional Gaussian plume approach and see what the differences are.

Deardorff shows that the important scale parameters of a convective boundary layer are

h = the height of the mixed layer and

$w_* = \left(\frac{g}{T} H_o h\right)^{1/3}$, where g is the gravity parameter,

T = mean temperature and

H_o = the kinemetic surface heat flux.

We can therefore define dimensionless coordinates and concentration

$$X = \frac{w_x}{U}\frac{x}{h}, \quad Y = \frac{y}{h}, \quad Z = \frac{z}{h}, \quad C = \frac{c \cdot h^2 \cdot U}{Q},$$

Where C is concentration

U mean wind velocity and

Q source strength.

The source height in the experiment was at $Z_h = 0.24$.

The first result from the model experiment is that the center of gravity of the released material remains for some distance near the height of the source or even subsides before starting to rise. Secondly the σ_z-curve levels off at distances $X \cong 1$, which is obviously caused by the capping inversion and which distance is also agreement with the Turner Workbook advice how to treat a capping inversion. Thirdly, the maximum in the vertical concentration distribution does not stay at the surface beyond the point of maximum ground level concentration, but rises again.

If we use plausible values of the scaling parameters then we can compare the experimental data with conventional forecasts, e. g. the Gaussian model with Pasquill-Giffort σ-values. Although it is quite clear that these values were given for low level sources. We choose

$$h = 1500 \text{ m}$$

$$w_x = 2.2 \text{ m se}^{-1} \text{ (surface heat flux 25 mw cm}^{-2}$$

The dimensionless source height of 0.24 is then at 390 m, which is in the order of effective source heights of power plants.

Obviously, the Gaussian model cannot describe the features of the vertical concentration distribution as obtained by the water tank experiments and as described above. But it is interesting to compare the results for the surface concentration and the equivalent σ-values.

Experiment Equivalent σ-Values		Gauss-Model
Dimensionless	With parameter Values above	Turner-Values For Class A
$\sigma_z(X=.2) = 0.11$	$\sigma_z(x= 300 \text{ m}) = 160 \text{ m}$	$\sigma_z(x= 300 \text{ m}) = 48 \text{ m}$
$\sigma_z(X=.4) = 0.22$	$\sigma_z(x= 600 \text{ m}) = 320 \text{ m}$	$\sigma_z(x= 600 \text{ m}) = 160 \text{ m}$
$\sigma_z(X=1.0) = 0.35$	$\sigma_z(x=1500 \text{ m}) = 525 \text{ m}$	$\sigma_z(x=1500 \text{ m}) = 1100 \text{ m}$
$\sigma_y(X=.2) = 0.09$	$\sigma_y(x= 300 \text{ m}) = 135 \text{ m}$	$\sigma_y(x= 300 \text{ m}) = 72 \text{ m}$
$\sigma_y(X=.4) = 0.16$	$\sigma_y(x= 600 \text{ m}) = 240 \text{ m}$	$\sigma_y(x= 600 \text{ m}) = 136 \text{ m}$
$\sigma_y(X=1.0) = 0.30$	$\sigma_y(x=1500 \text{ m}) = 450 \text{ m}$	$\sigma_y(x=1500 \text{ m}) = 300 \text{ m}$

$X_{max} = 0.38$ $\quad$ $_{max} = 570$ m $\quad$ $x_{max} = 780$ m

$C_{max} = 5.9$ $\quad$ $\frac{C_{max} \cdot \overline{u}}{Q} = 2.6.10^{-6}\ m^{-2}$ $\quad$ $\frac{C_{max} \cdot \overline{u}}{Q} = 3.0.10^{-6}\ m^{-2}$

The comparison shows that the maximum surface concentration is reached in the experiment at a shorter distance from the stack than the results from the Turner Workbook-values. The concentrations near to the stack are therefore much higher than the conventional ones. The maximum concentration, however, is not very different, the difference is about 20 %. The conclusion we can draw is following: When taking average values for the scaling parameters under convective conditions the water tank experimental values of σ do not agree with the Pasquill-Gifford values, however, the maximum surface concentration is only 20 % different. One important point should be noted here:

We have used Pasquill diffusion category A and assumed certain average parameter values for h and w_*. However, the Workbook estimates can be off to a layer degree from the model values if other parameter values are taken.

In other words: The Pasquill classification does not use the pertinent sealing parameters under convective conditions.

2. We are coming now to the next problem: How effective are tall stacks for air quality management?

   It is well known that the maximum ground level concentration from an elevated point source is approximately inversely proportional to h^2, the square of the effective source height and directly proportional to Q, the source strength. If we want to control the m.g.l.C. we can do this by increasing $h \propto \sqrt{Q}$. But if we go to distances from the source where the concentration is well mixed in the boundary layer, i. e. practically constant with height, then the surface concentration is independent of source height, inversely proportional to the height of the mixed layer and directly proportional to Q. For very unstable convective conditions this is already for source distances > 4 km (for mixing height 1500 m), for indifferent stability (mixing height 1000 m) for distances > 50 km. These simple facts are very often camouflaged by the diurnal and other variability of the meteorological conditions. But there are conditions where this variability is rather small and then we can observe that high surface concentrations are maintained over large distances, in the order of several hundred kilometers. These conditions are not too seldom in Middle-Europe and can determine the monthly mean values of the surface concentration at a certain place far away from large sources to a high degree. I shall show you an example of such a situation:

In the north-east of the Ruhr-area a network of SO_2-ground-level sampling stations has been established which records hourly mean values of SO_2. The geographical positions are shown in the following graph (Scale 1 : 550 000). When we constructed SO_2-windroses at the different locations we assumed that we could get highest concentrations when the air is coming with SWesterly winds from the Ruhr-area, roughly 30 - 100 km away. To our surprise, however, the windroses showed high average concentrations for easterly and northwesterly winds. So we picked one episode with high concentrations connected with easterly winds for a more detailed case study. The episode was from the 5. - 9. December 1978. Line averages are shown for the whole month of December. When we look at the concentration field we can see that there is typically a gradient in the concentration field from East to West. We picked one time with high concentrations and computed backward trajectories, one with surface winds, the other with winds measured at roughly 900 m and at a few mountain stations. It is earily recognised that both trajectories point after a travel time of about 20 hours into heavily industrialized area south of Leipzig, about 300 km away. There is no other area with large sources in the neighborhood of the trajectories. The radiosonde ascents during this period look typically like the ones shown here.

A rough estimate shows the magnitude of the concentrations to be expected. From a published Emission-inventory for the year 1973 (Semb (1978)) we take that the area source strength of a square 127 km x 127 km to be 10^6 to SO_2/a. Since we have rather low surface temperatures around -5^0 C, allowing for an increase still 1973 and for background from upwind area sources, we double this amount to $2 \cdot 10^6$ to SO_2/a.

This amount is divided up according to the following graph. We take now the simple Gaussian model with a mixing height of 800 m, wind-velocity 5 m sec^{-1} and obtain the order of magnitude which is shown on the graph and what is roughly, what is observed.

From this I conclude: We can expect high surface concentrations even at distances of the order of 500 km away from highly industrialized areas when we have a strong subsidence inversion in 500 - 1000 m height with relatively strong winds which cause mechanical turbulent mixing below the inversion. Since these situations are mostly connected with quasi-persistent high pressure areas there is no wet deposition and therefore this situation is typical for "not-home-made" or "imported" air pollution episodes, which can last for some days and therefore determine the monthly average to a large degree.

The point I wish to make at the end of this introductory paper is that we should try to get away from looking at maximum ground level concentrations only and consider also the frequency of occurrence of such meteorological situations where high level concentrations are advected over large distances and where local air pollution management measures are more or less useless. Since the advection can take place over distances of 500 - 1000 km. I pledge that an international cooperation at least in Europe is absolutely necessary.

Abb.1 Geographische Lage der SO_2-Meßstationen

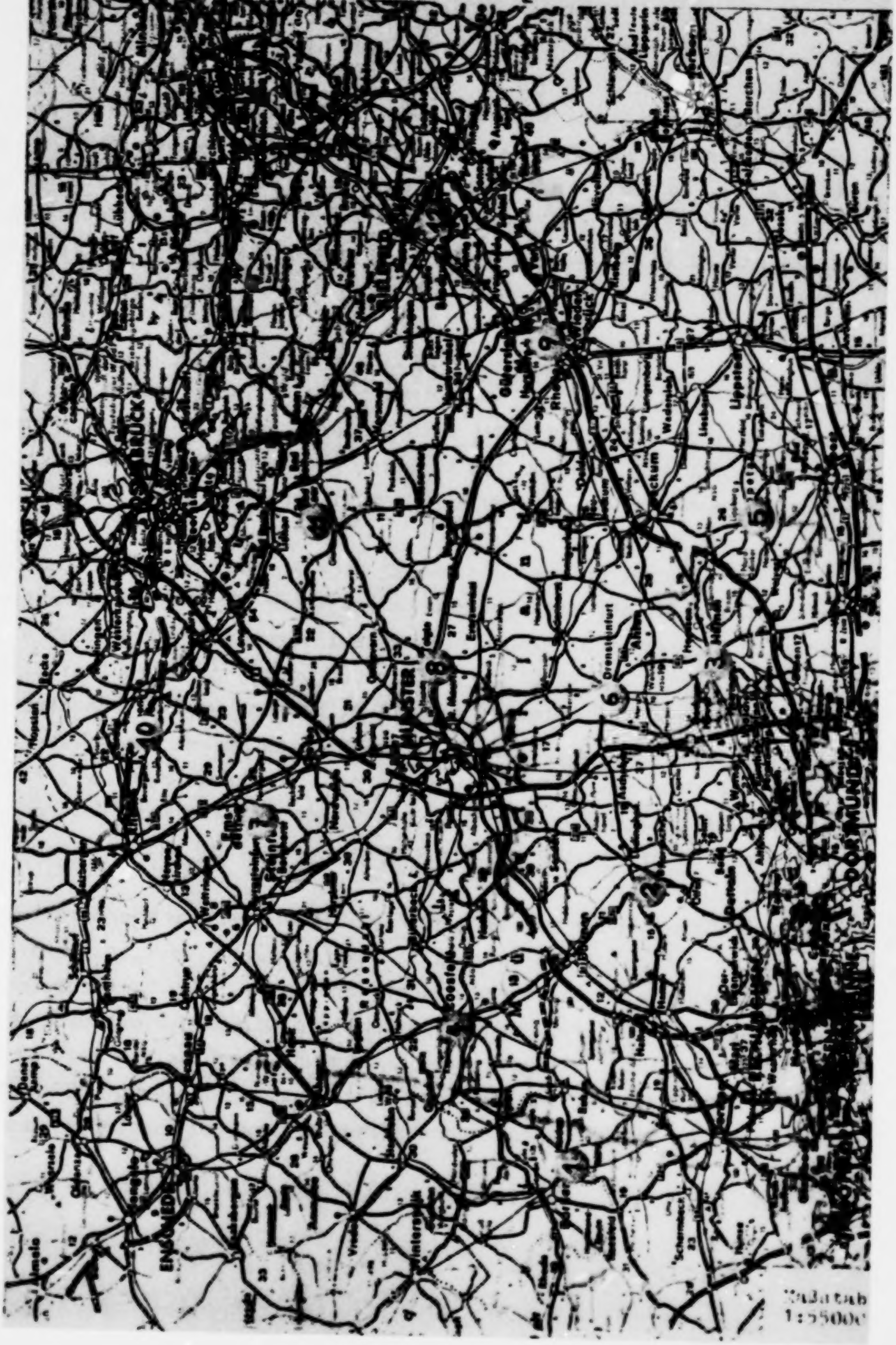
Gütersloh
Beckum
Lippstadt
Drensteinfurt
Ahlen
9
5
8
6
10
3
12
Maßstab
1:55000

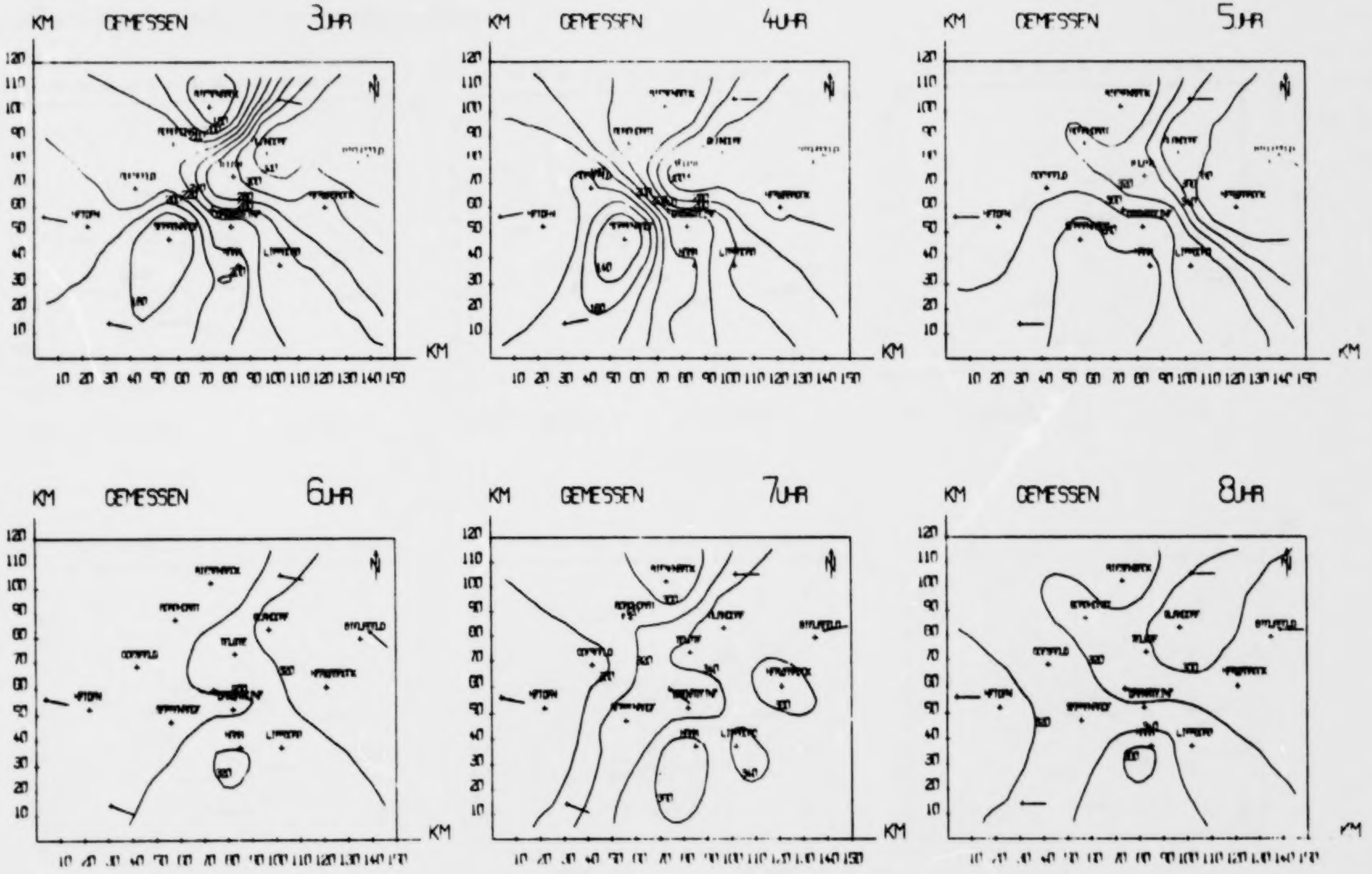
KM
GEMESSEN
3UHR
4UHR
5UHR
6UHR
7UHR
8UHR
10 20 30 40 50 60 70 80 90 100 110 120
10 20 30 40 50 60 70 80 90 100 110 120 130 140 150
KM

SO$_2$-Konzentrationsfeld am 06.12.1978

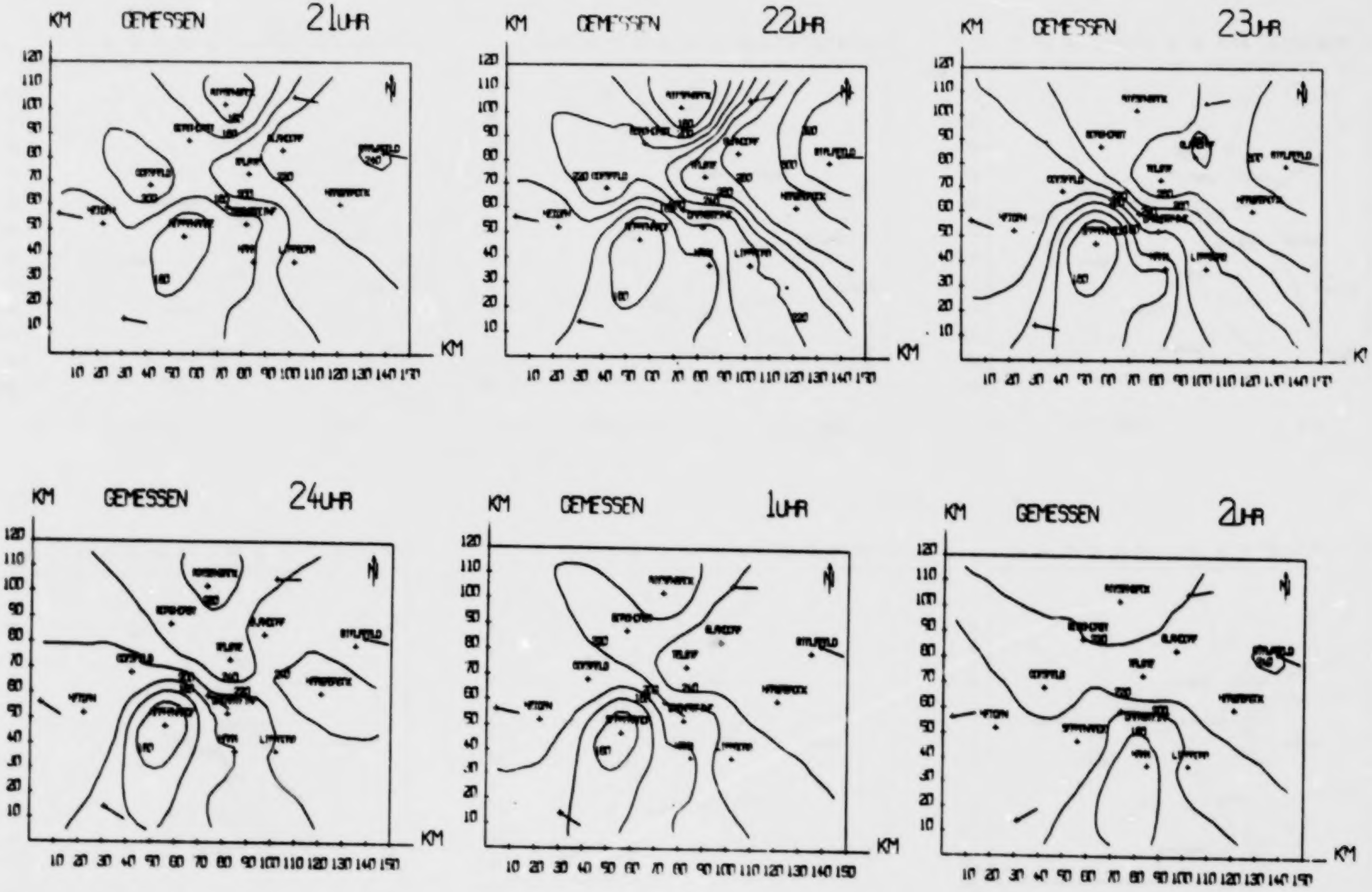
KM
GEMESSEN
21UHR
KM
GEMESSEN
22UHR
KM
GEMESSEN
23UHR
KM
GEMESSEN
24UHR
KM
GEMESSEN
1UHR
KM
GEMESSEN
2UHR
120
110
100
90
80
70
60
50
40
30
20
10
10 20 30 40 50 60 70 80 90 100 110 120 130 140 150
KM

SO$_2$-Konzentrationsfeld am 06./07.12.1978

TOTAL SOURCE STRENGTH: $2 \cdot 10^6$ to SO_2/a

- DOMESTIC HEATING
  $2 \cdot 10^5$ to SO_2/a
  SOURCE HEIGHT 15m
- INDUSTRY
  $1{,}8 \cdot 10^6$ to SO_2/a
  - 2 CONCENTRATED AREAS
    $1{,}44 \cdot 10^6$ to SO_2/a
    SOURCE HEIGHT 200m
  - ALL OVER
    $0{,}36 \cdot 10^6$ to SO_2/a
    SOURCE HEIGHT 100m

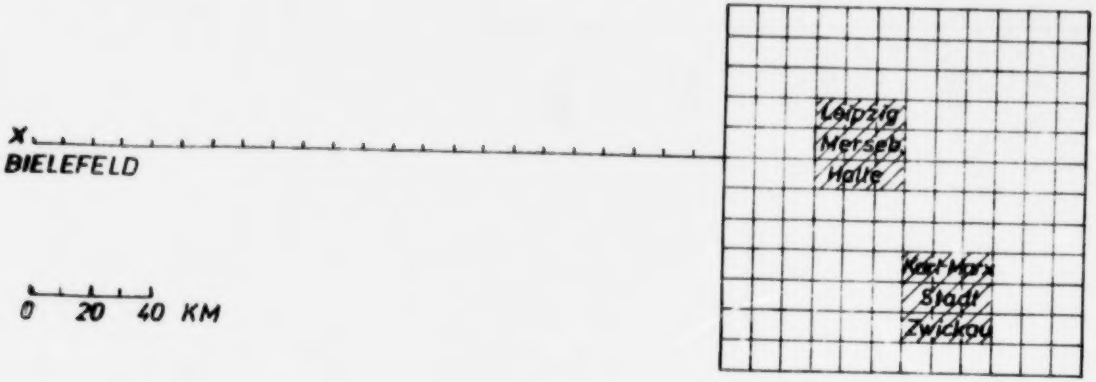
x
BIELEFELD
Leipzig
Merseb.
Halle
Karl-Marx-
Stadt
Zwickau
0 20 40 KM

MIXING HEIGHT: 800m
WIND VELOCITY: 5m sec^{-1}
NO DEPOSITION

RESULTS:
$C_{BIELEFELD}$ [$\mu g/m^3$]
STABLE : ~300
INDIFF. : ~150

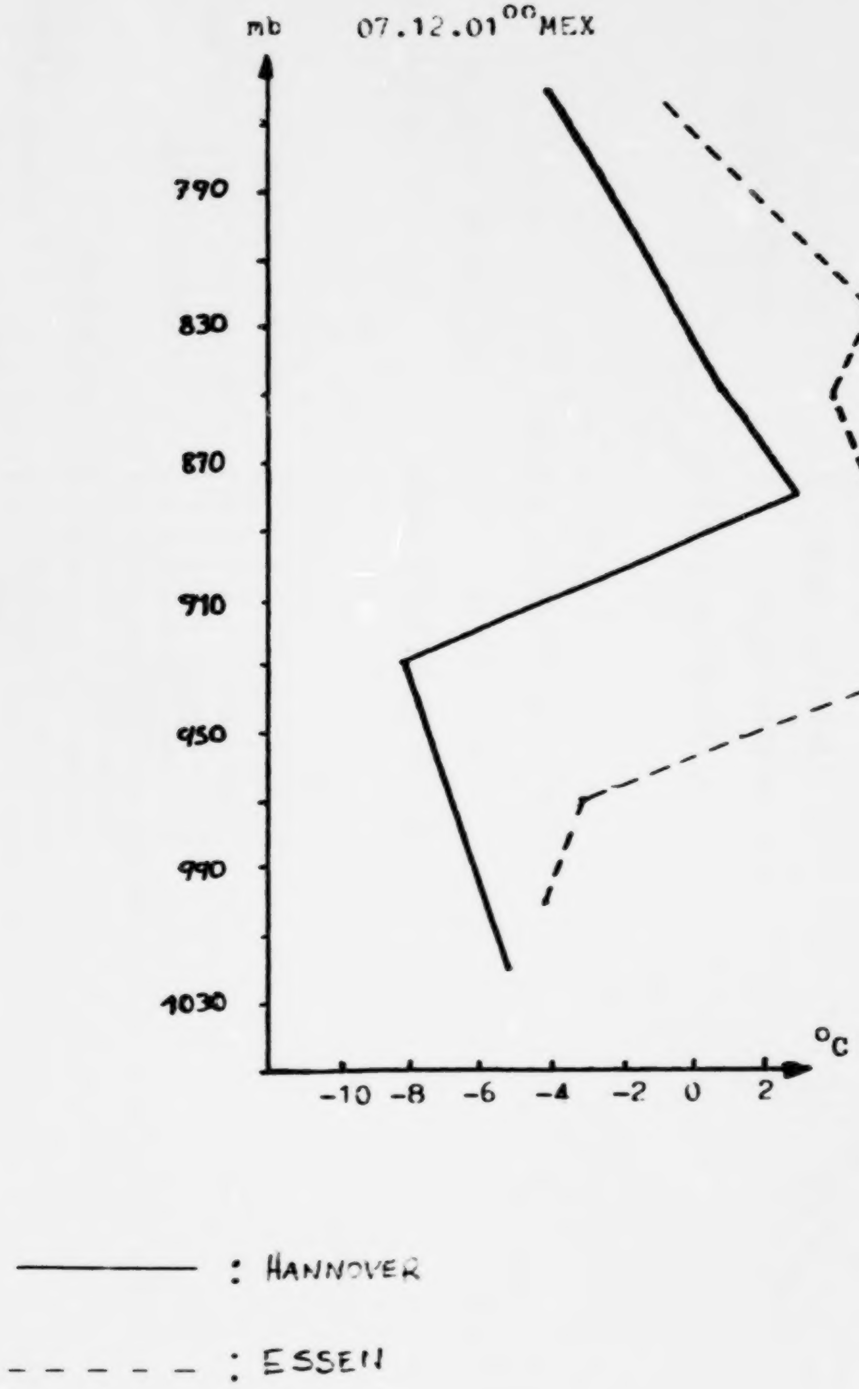
mb
07.12.01 00 MEX
790
830
870
910
950
990
1030
°C
-10
-8
-6
-4
-2
0
2
: HANNOVER
: ESSEN

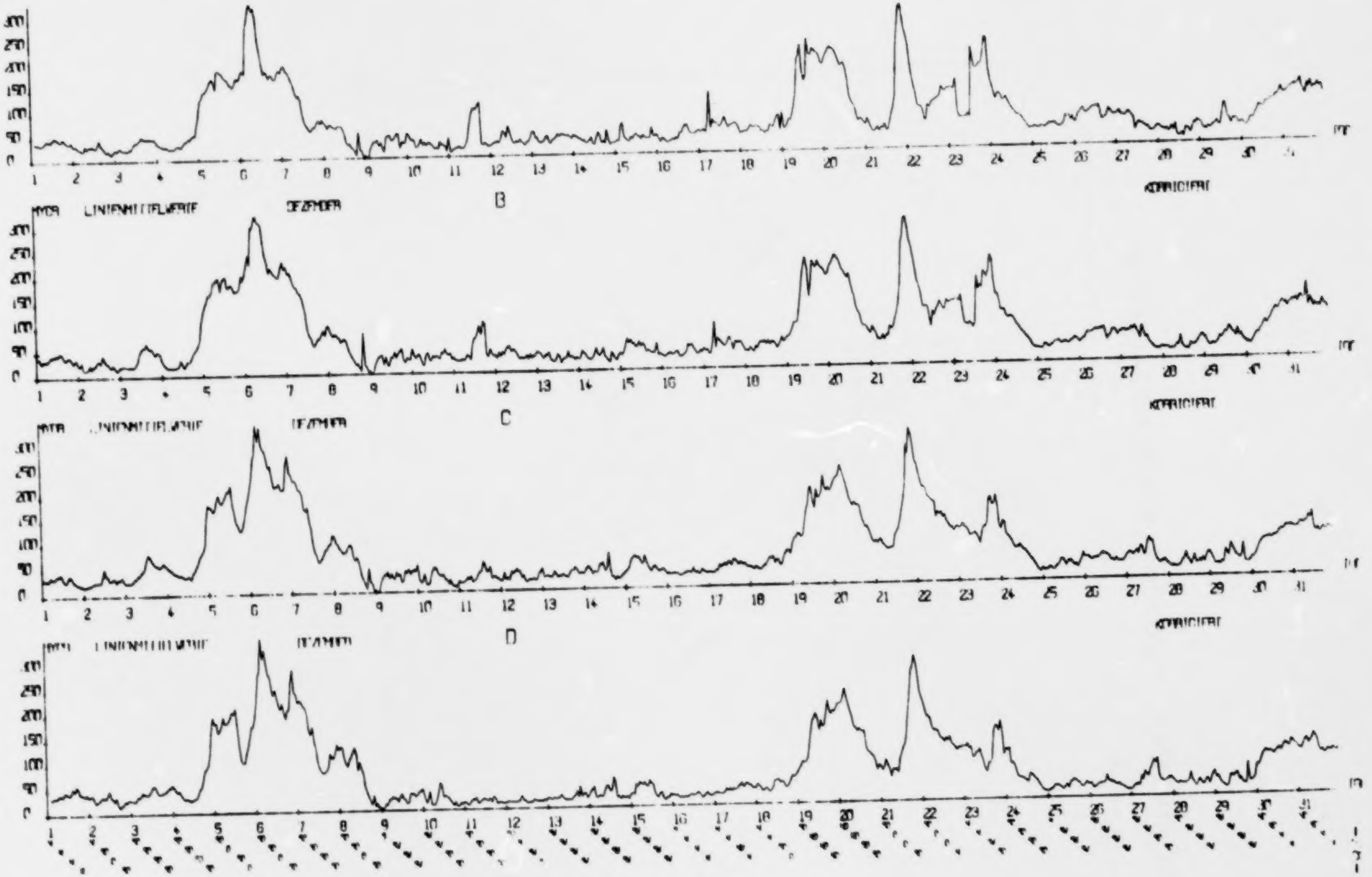
300
250
200
150
100
50
0
1 2 3 4 5 6 7 8 9 10 11 12 13 14 15 16 17 18 19 20 21 22 23 24 25 26 27 28 29 30 31
TT
KORRIGIERT
B
MYGR LINIENMITTELWERTE DEZEMBER
KORRIGIERT
C
MYGR LINIENMITTELWERTE DEZEMBER
KORRIGIERT
D
MYGR LINIENMITTELWERTE DEZEMBER
TT

KM SO2 WINDROSEN GESCHWINDIGKEITSUNABHANGIG

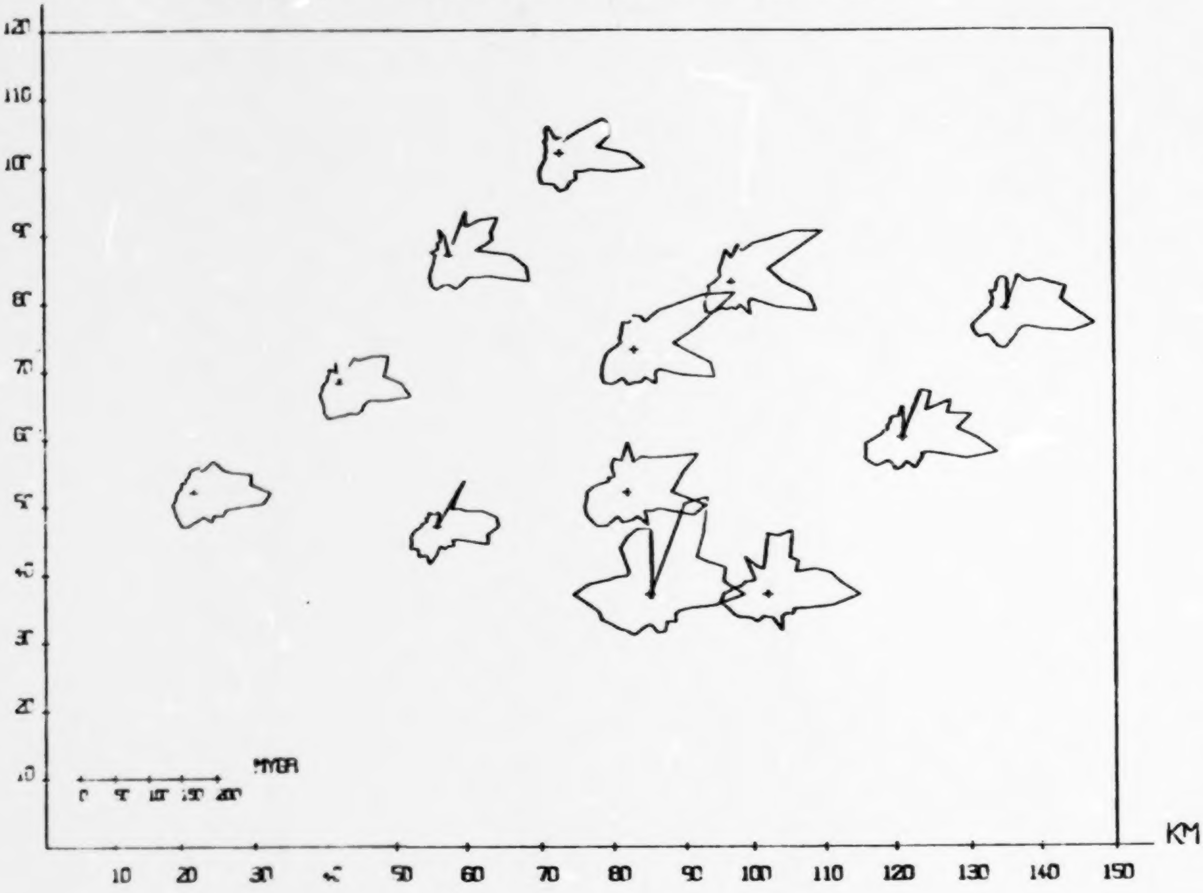

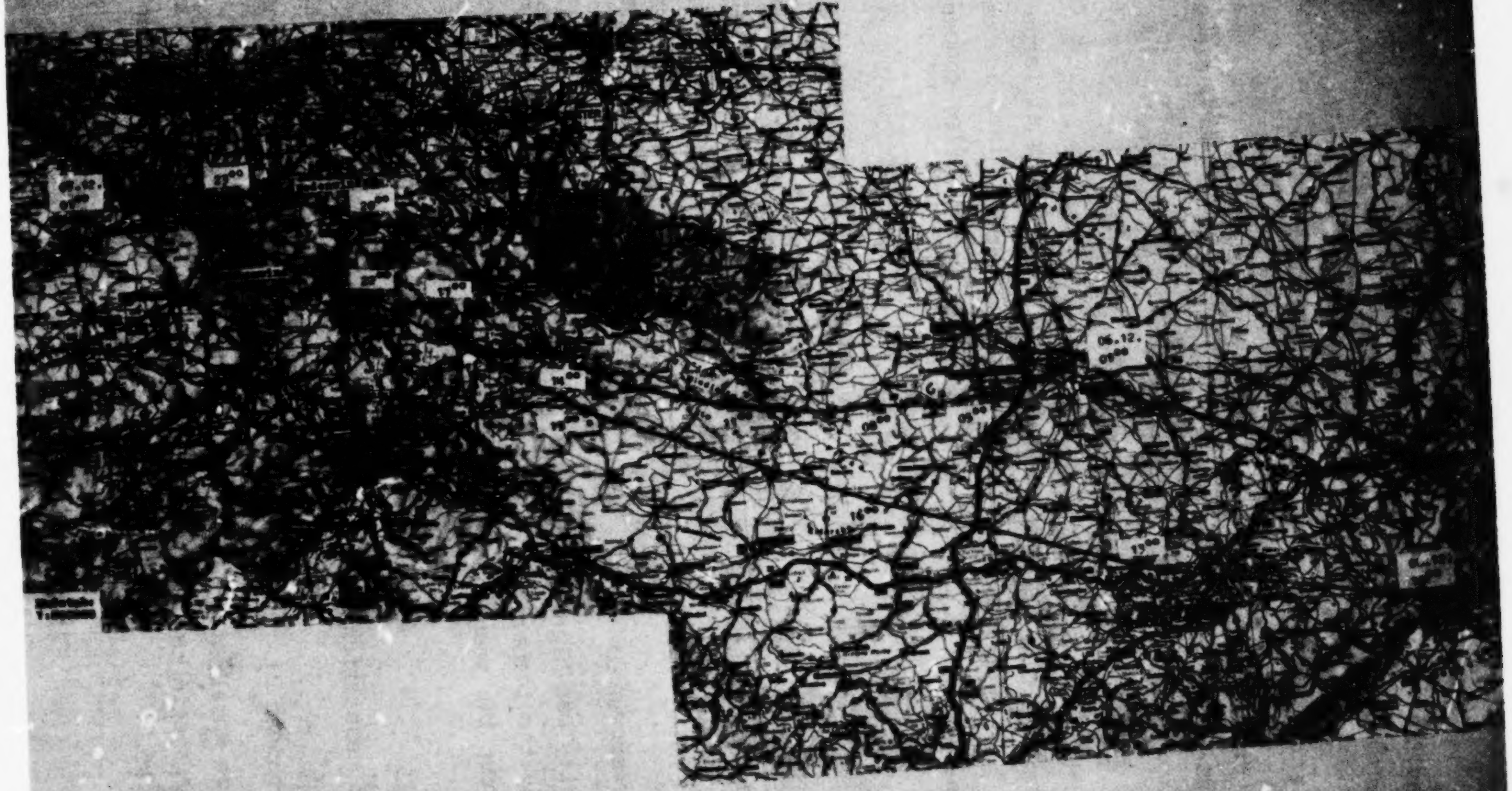
06.12.
16^{00}

Discussion:
(Rapporteur: R. V. Portelli)

Bénarie:

How do high stacks contribute to concentrations at long distances when compared to low stacks?

Klug (response):

The point of my presentation was that concentrations at large distances are independent of source height due to the well mixed boundary layer at such distances. No attention was paid to identifying concentrations by source height.

Gutsche:

The estimates you gave of SO_2 ground-level concentration did not take into account transformation processes (i. e. SO_2 to sulphate). What was the humidity in this case and what would have been the effect on transformations ?

Klug (response):

The humidity was high but the transformation processes are strongly steered by the temperature, which in this case was low and therefore I would expect the transformations to have been negligible.

Bhumralkar:

What about deposition considerations?

Klug (response):

The Gaussian model was run with and without a deposition term. There was a 10 % decrease in the estimates of concentration when deposition was accounted for.

Berger:

When considering the impact of tall stacks, one must take account of the increased pollutant residence times.

Klug (response):

True, however, the main interest to the present has been in the maximum ground level concentrations near the source and I have tried to emphasis in my presentation that the frequence of occurrence of various concentration levels must also be taken into consideration. The data I showed indicate that in December, the monthly average was dominated by 2 episodes.

Venkatram:

You have compared the P-G method to connective scaling techniques. In doing this, there exists a certain amount of subjectivity, would'nt you agree?

Klug (response):

Yes, but the values used in the cases described are plausible for middle Europe.

Kretzschmar:

Based on your trajectory analysis, you concluded that the sources responsible for the easterly peaks in the SO_2 roses in the region around Münster had to be somewhere in the neighbourhood of Leipzig. Did you have any data on the SO_2 levels east of Leipzig and between Leipzig and Münster to show that these peaks were actually caused by tall stacks near Leipzig?

Klug (response):

No concentration measurements were available from the GDR but an SO_2 concentration of 600 ug/m^3 was observed near the border between the GDR and the Federal Republic of Germany.

Berger:

In the pollution wind roses shown were the winds at these sites used or, were the wind observations at the source employed?

Klug (response):

Surface winds were used and a map analysis was done.

Gutsche:

Can you exclude local pollutant accumulations in the case described?

Klug (response):

I do not believe there would be accumulations in this case due to the high wind speeds.

M. E. Smith:

You noted that Deardorff's technique predicts a maximum concentration of about the same order as the Gaussian Pasquill A prediction, but that the predicted distance to the maximum is much closer. In the United States, we have seen little data supporting a predicted maximum occurring very close to the source. Have you found any data in Europe to verify Deardorff's prediction?

Klug (response):

No, I do not know of any ambient data supporting the prediction.

Trout:

I would like to respond to the Smith's comment which suggested that Prof. Klug's results are contrary to observations (i. e., based on observations, maximum concentrations do not appear to occur as close to the stack as these predictions indicate). Very limited data exist to assess such cases since there are not very many monitors located within short distances (< 2 km) of tall stacks were either the Deardorff or Gaussian Pasquill A model predict the maximum to occur. However, these limited monitoring data have been reviewed and concentrations as high or higher than the Gaussian Pasquill A model predictions have been found. My paper this afternoon will cover some of these data sets.

Fortak:

Would you say that tall stacks are better or worse than short stacks, considering other situations such as a boundary layer which is not well mixed?

Klug (response):

At night, for example, when the boundary layer is not well mixed concentrations at ground level would be much lower than from short stacks. In general, I do feel that tall stacks are better for reducing the impacts of emitted pollutants.

FORECAST OF FUMIGATION EPISODES AROUND A TALL STACK

by

P. Bolzern, G. Fronza

Istituto di Elettrotecnica ed Elettronica
Centro Teoria dei Sistemi
Politecnico di Milano
IIASA - Schloss Laxemburg - Austria

Abstract. An ARMAX-type stochastic model of SO_2 pollution around a tall stack is illustrated. Specifically, the model describes the dynamics of short-term Dosage Area Product (DAP) in a sector of the region around the stack. Model exogeneous inputs are a variable accounting for emission, wind direction and a properly defined "atmospheric stability class". A real-time predictor is derived from the stochastic model in order to supply with forecasts of future DAP at the beginning of each time step. The performance of such predictor is checked on a historical DAP time series and in particular, the quality of the forecast in correspondence with fumigation intervals is illustrated.

1. Introduction

As it is well-known, fumigation phenomena around tall stacks (see for instance Slade[1]), namely sharp enhancements and subsequent decreases of pollutant concentration, occur during a few central hours of some sunny days and are related to plume breakdown by the enhancing mixing layer. While Gaussian-type mathematical representations offer an inadequate description of such a phenomenon, advection-diffusion models require extremely detailed information about meteorology, knowledge of concentration dynamics at the boundary of the integration region and complex numerical solution schemes [2-5].

Hence, an alternative approach [6-8] is being followed in the present paper. It bases on the use of a stochastic model of the ARMAX-type (Auto Regressive Moving Average with eXogenous inputs, see for instance Box and Jenkins[9]), which describes the diurnal dynamics of a variable, chosen as representative of SO_2 pollution around the tall stack of a power plant in the summer period (two-hour Dosage Area Product or DAP, see Section 2). Precisely, in the model the DAP in a certain interval is expressed as a linear combination of previous DAP and power generated by the plant. Moreover, the coefficients of the linear combination depend upon wind direction and a suitably defined atmospheric stability class (see Section 3).

Preceding page blank

From the model (Section 4), a real-time predictor is derived, namely a recursive relationship which, at the begining of each time step, supplies with forecasts of future DAP on the basis of current information about DAP, meteorology and generated power. The two and four-hour forecast performances of such predictor are measured by suitable quality indexes, in particular, to test the effectiveness in presence of fumigation episodes.

A crucial point is represented by the circumstance that the meteorological inputs of the pollution predictor are measures not available at the instant when the forecast is made. Specifically, as shown in Section 4, future (and not present or past) wind direction and stability class must be introduced into the pollution forecast recursive algorithm. Hence, it is necessary to :

a) set up two separate "meteorological predictors", for forecasting wind direction and the stability class respectively;
b) use such meteorological forecasts as inputs of the pollution predictor.

Naturally, the quality of pollution forecasts turns out to be lower with respect to the ideal (but obviously unrealistic) situation, where the future true values of the meteorological inputs are perfectly guessed at each time step. However, as shown in Section 4, such loss of performance, though singificant, is not intolerable (approximately 10-15%) in the case analysed in the paper, namely themeteorological predictors give acceptable forecasts.

2. Definition and Evaluation of the two-hour Dosage Area Product

The region under consideration is shown in Fig. 1, together with the polluting source PS and the monitoring network, supplying with SO_2 thirty-minute concentration averages. The pollutant is released through a stack of 120m.

Hourly wind speed and direction have been recorded by two anemometers located at opposite positions on the top of the stack. Hourly solar radiation (in Kcal cm^{-2} hr^{-1}) has been recorded through a pyranometer. Finally, Pasquill's category at the end of the night, a datum required for the evaluation of a model input (see next section) has been determined by wind and cloudiness data[10].

The variable taken as pollution representative has been the two-hour DAP (Dosage Area Product, see Duckworth and Kupchanko[11]) over the sector Ω of prevailing fallout, namely the average of the two-hour dosage over Ω . Specifically, if a coordinate system is superimposed to the region under consideration, like in Fig. 1, the k-th two-hour dosage in point (x,y) of the region is defined as (Δt = 2 hours)

$$D(x,y,k) = \int_{(k-1)\Delta t}^{k\Delta t} c(x,y,t)dt$$

where c(x,y,t) is the pollutant concentration in (x,y) at the instant t.

Moreover, the k-th two-hour DAP over the sector Ω is defined as

$$DAP(k) = \frac{1}{A\Delta t} \iint_{\Omega} D(x,y,k)\ dxdy \qquad (1)$$

where A is the area of the sector Ω .

For each k, the integral in eq. (1) can be approximately evaluated from sensor measurements by the "polygons method", i.e. by assuming that the dosage in each point of the sector is equal to the dosage recorded in the nearest monitoring station :

$$DAP(k) = \frac{1}{A\Delta t} \sum_{i=1}^{20} A_i D_i(k) \qquad (2)$$

where

$D_i(k)$ = two-hour dosage in the i-th monitoring station of the sector (i=1,2,...,20); its derivation from the four thirty-minute averages recorded by the i-th sensor during the interval $[(k-1)\Delta t,\ k\Delta t]$ is straightforward;

A_i = "area of influence of the i-th station" = area of the region of points for which the i-th station is the nearest one.

Naturally, since the network is very thick inside the sector Ω, approximation (2) gives an acceptable estimation of the true DAP defined by eq. (1). Through eq. (2), the time series of two-hour DAP in the period June 1st, 1973 - September 30th, 1973 has been evaluated.Such series will from now onwards be referred to as the "historical DAP series".

3. Description of the Stochastic Model

The following stochastic model for describing the dynamics of the two-hour DAP, defined in the previous section, has been considered:

$$DAP(k+1)=\alpha(s(k+1),d(k+1))DAP(k)+\beta(s(k+1),d(k+1))p(k+1)+w(k) \quad (3)$$

where:

$p(k)$ = average power (in Megawatt) generated during the k-th interval, i.e. during $[(k-1)\Delta t, k\Delta t]$ (it is an indirect measure of overall source emission in such interval);

$s(k)$, $d(k)$ = respectively, atmospheric stability and wind direction class in the k-th interval (see below for their precise definition);

$\alpha(s(k+1), d(k+1))$, $\beta(s(k+1), d(k+1))$ = model parameters, depending upon atmospheric stability and wind direction classes (see below for their estimation by a fitting procedure of DAP, meteorological and generated power data);

$\{w(k)\}_k$ = stochastic process (noise), whose statistical characteristics are also specified below.

Model (3) is explained and completed by the following comments and definitions :

(i) The model describes only the diurnal dynamics of the DAP during the "summer season" (June 1st-September 30th). Thus, for each day, the time indexing is as follows: the value k=2, namely the time interval $[\Delta t, 2\Delta t]$ corresponds to the two-hour interval during which sunrise occurs (precisely, to 4 a.m. - 6 a.m. in the period June 1st - September 14th and to 6 a.m. - 8 a.m. in the period September 15th - September 30th). Therefore, k=1, namely the interval $[0, \Delta t]$ corresponds to the last two-hour interval of the previous night. Moreover, the time index k takes increasing values during the day, until sunset occurs. The index is reset to 1 at the end of the following night and so on.

(ii) Model (3) can be given the following rough "physical" interpretation. Delete for a while the noise term $w(k)$ at the right-hand side of eq. (3), namely consider DAP (k+1) as equal only to the "deterministic part of the model", i.e. to the linear combination of DAP(k) and $p(k+1)$. The value DAP (k) is grossly correlated to the pollutant existing at the beginning of the (k+1)-th interval, while $p(k+1)$ is representative of the pollutant released in such interval. Thus, the model structure means that DAP (k+1) is assumed to be a linear combination (the simplest type of function) of "already existing" and "new" pollutant. Moreover, the coefficients of the combination depend upon the meteorological situation. Naturally, such arbitrary model structure does not exactly reproduce the true DAP dynamics, namely the deterministic part alone cannot entirely explain the true value of DAP(k+1). That "portion" of such value, which is not accounted for by the deterministic part, is ascribed to random fluctuations, i.e. is represented by the random variable $w(k)$ added to the right-hand side of eq. (3).

(iii) The atmospheric stability class $s(k)$ is defined as follows : first let

$C_p(1)$ = Pasquill's stability category at the end of the previous night, namely in the interval $[0, \Delta t]$;

$r(j)$ = solar radiation (in Kcal cm^{-2}) in the j-th time interval;

$S(k)$ = total solar radiation since sunrise =

$$\sum_{j=2}^{k} r(j); \qquad (4)$$

$v(k)$ = average wind speed in the interval $[(k-3)\Delta t, k\Delta t]$, namely in the six hours before the instant $k\Delta t$.

Then the category $s(k)$ is defined as :

$$s(k) = \begin{cases} \text{I} & \text{if } S(k) < T_1(C_p(1), v(k)) & (5a) \\ \text{II} & \text{if } T_1(C_p(1), v(k)) \leq S(k) \leq T_2(C_p(1), v(k)) & (5b) \\ \text{III} & \text{if } T_2(C_p(1), v(k)) < S(k) & (5c) \end{cases}$$

where $T_1(C_p(1), v(k))$ and $T_2(C_p(1), v(k))$ are class thresholds, depending upon the atmospheric status at the end of the previous night and upon the average wind speed in the three previous intervals.

Definition (5) aims at characterising the status of the air in the k-th interval from the viewpoint of the pollution fumigation phenomenon. Precisely, formula (5) points out three distinct atmospheric conditions. Such three conditions (obviously together with wind direction, previous DAP and generated power) allow model (3) to reproduce respectively the situations of absent (or not yet started), increasing and decreasing fumigation.

Class I.	The total radiation is below the lower threshold. Either no mixing layer has developed or its height is not enough to reach the plume.
Class II.	The total radiation passes the lower threshold. The mixing layer reaches the plume and the pollutant begins to be carried to the ground.
Class III.	The total radiation passes the upper threshold. The mixing layer overtakes the plume and the dilution effect begins.

The phenomenon is also influenced by the strength of the inversion at the end of the previous night and by wind speed, which affects both plume rise and heat propagation through the lower layers of the atmosphere (namely the "speed of enhancement" of the mixing layer). Such factors have been taken into account by making the thresholds depend upon both $C_p(1)$ and $v(k)$. In particular, the choiche of $v(k)$ as wind speed variable has been simply made through empirical analysis of the data.

Also from empirical data analysis, the most suitable thres-

Table 1. Values of $T_1(C_p(1), v(k))$

$C_p(1)$ \ $v(k)$ (m sec^{-1})	≤ 1	>1, ≤ 2	>2, ≤ 2.7	>2.7
D	∞	∞	∞	∞
E	91	89	89	89
F	95	97	95	92

hold-versus-v(k) functions have turned out to be the ones shown in Tables 1 and 2, respectively.

Finally, the basic difference between the classes defined by (5) and the usual atmospheric stability class definitions (such as the one due to Pasquill) must be underlined. Here, the atmospheric situation in the k-th time interval is not only characterised by the meteorological data recorded in that interval, but also the whole past "history" of the atmosphere since sunrise, as well as the starting condition at sunrise. This different approach is vital in order to account for the fumigation mechanism, strictly related to a variable (present height of the mixing layer) which cannot be explained only by the current meteorological measurements. For instance, if the class in the k-th interval were defined just on the basis of solar radiation in the k-th interval itself, the same class would often be ascribed to the atmosphere in correspondence with both concentration increase and decrease, namely model (3) would not be able to fit the fumigation peak at all.

Table 2. Values of $T_2(C_p(1), v(k))$

$C_p(1)$ \ $v(k)$ (m sec^{-1})	≤ 1	>1, ≤ 2	>2, ≤ 2.7	>2.7
D	-	-	-	-
E	355	255	255	255
F	355	419	364	255

(iv) Wind direction class $d(k)$ is simply defined as a binary variable :

$$d(k) = \begin{cases} 1 & \text{if the wind blows towards sector } \Omega \\ 0 & \text{otherwise} \end{cases} \qquad (6)$$

Though drastic, definition (6) does not create ambiguous situation, since wind blowing towards nearly outside of the sector is rather infrequent (see Fig. 2).

(v) The noise $\{w(k)\}_k$ has been assumed to be zero-mean purely random stochastic process (white noise), namely process having covariance ($E[\cdot]$= expectation operator) :

$$E[w(k)w(k+\zeta)] \begin{cases} = 0 & \zeta \neq 0 \\ \neq 0 & \zeta = 0 \end{cases}$$

Naturally the zero-mean-whiteness assumption on $\{w(k)\}_k$ must be validated a posteriori, after model parameter estimation ("diagnostic checking", see again Box and Jenkins[9]).

Since it has been assumed $\beta(s(k+1),0)=0$ for all $s(k+1)$, there were nine parameters of model (3) to be estimated by historical data, precisely :

6 parameters of the AR-part, i.e. one α-type parameter for each of the three atmospheric classes and for each of the two wind direction classes;
3 parameters of the X-part, i.e. one β-type parameter for each of the three atmospheric classes, for $d(k+1)=1$.

The estimation of such parameters has been made by fitting DAP, meteorological and generated power data of the period June 1st, 1973 - August 31st, 1973, in accordance with the standard Recursive Least Squares technique (see for instance Goodwin and Payne [12]). The process $\{w(k)\}_k$ has turned out to be acceptably zero-mean and white (whiteness has been checked by means of the cumulative periodogram of the residual).

4. The Real-time DAP Predictor

From the stochastic model described in the previous section, a real-time predictor can be derived, namely a recursive relationship, which, at the end of each time interval, supplies with forecasts of future DAP (see for instance Box and Jenkins [9]). Specifically in the case of model (3), the recursive forecast algorithm takes the simple form :

$$\hat{DAP}(k+1/k)=\alpha(s(k+1),d(k+1))DAP(k)+\beta(s(k+1),d(k+1))p(k+1) \qquad (7a)$$

$$\hat{DAP}(k+2/k)=\alpha(s(k+2),d(k+2))\hat{DAP}(k+1/k)+\beta(s(k+2),d(k+2))p(k+2) \quad (7b)$$

where, for $q = 1,2$

$\hat{DAP}(k+q/k)$ = forecast of DAP(k+q) made at the end of the k-th interval, i.e. at the instant $k\Delta t$.

Eq. (7a) points out the basic difficulty inherent to the use of the DAP predictor. Specifically, the forecast $\hat{DAP}(k+1/k)$ is also based upon s(k+1) and d(k+1), which are not available information at $k\Delta t$, the instant when the forecast is made. In particular, the unavailability of s(k+1) is due to its dependence both upon S(k+1), (which in view of eq. (4), depends upon r(k+1), the radiation in the (k+1)-th interval) and v(k+1). The very same argument holds for $\hat{DAP}(k+2/k)$, which (see eq. (7b)) is based upon s(k+2) and d(k+2).

Hence, at each time step, it is necessary to generate separate forecasts of radiation, wind speed and wind direction, in order to supply the pollution predictor (7) with all the required inputs.

a) Radiation predictor

A real-time radiation predictor has been heuristically derived through the following considerations. The starting point has been the radiation model developed by Bacci et al.[13], on the basis of experimental evidence. Precisely, they suggest the continuous-time formula for the intensity of solar radiation

$$\rho(t) = \frac{\pi\bar{S}}{2N} \sin\left[\pi(t-t_o)/N\right] \qquad t_o \leq t \leq t_s \quad (8)$$

where

$\rho(t)$ = intensity of solar radiation at instant t (in Kcal cm^{-2} hr^{-1});
t_o = sunrise instant;
t_s = sunset instant;
N = average number of sunlight hours in the current month;
$\bar{S}$ = average total daily radiation (in Kcal cm^{-2}) in the current month.

By definition

$$r(k)=\begin{cases} \int_{t_o}^{2\Delta t} \rho(t)dt & k = 2 \quad (9a) \\ \int_{(k-1)\Delta t}^{k\Delta t} \rho(t)dt & k=3,4,.., k_s-1 \quad (9b) \\ \int_{(k_s-1)\Delta t}^{t_s} \rho(t)dt & k = k_s \quad (9c) \end{cases}$$

where k_s denotes the two-hour interval containing the sunset instant t_s.

In view of eq. (8), eq. (9) turns out to be via some cumbersome computations :

$$r(k)=\begin{cases} \frac{\bar{S}}{2}\{1-\cos\{\pi[2\Delta t-t_o]/N\}\} & k=2 \quad (10a) \\ \frac{\bar{S}}{2}\{\cos\{\pi[(k-1)\Delta t-t_o]/N\}-\cos\{\pi[k\Delta t-t_o]/N\}\} & k=3,4,...,k_s-1 \quad (10b) \\ \frac{\bar{S}}{2}\{\cos\{\pi[(k_s-1)\Delta t-t_o]/N\}+1\} & k=k_s \quad (10c) \end{cases}$$

Eq.(10) already represents a "predictor", in the sense that at the sunrise of each sunny day, one can forecast all future radiation values for that day (in fact, both N and $\bar{S}$ are monthly parameters, estimated by pyranometer records in a certain number of summers). However, eq. (10) is not a real-time predictor, since at each $k\Delta t$ the forecast is not updated on the basis of radiation measurements recorded up to $k\Delta t$. In order to derive a proper real-time predictor, first note that by straightforward computations eq. (10) can be given the equivalent recursive form :

$$r(k+1) = r(k) + \delta(k) \qquad (11)$$

where

$$\delta(k) = \begin{cases} \frac{\bar{S}}{2}\{2\cos\{\pi[2\Delta t-t_o]/N\}-1-\cos\{\pi[3\Delta t-t_o]/N\}\} & k=2 \\ \frac{\bar{S}}{2}\{2\cos\{\pi[k\Delta t-t_o]/N\}-\cos\{\pi[(k-1)\Delta t-t_o]/N\}- \\ \quad -\cos\{\pi[(k+1)\Delta t-t_o]/N\}\} & k=3,4,\dots,k_s-2 \\ \frac{\bar{S}}{2}\{2\cos\{\pi[(k_s-1)\Delta t-t_o]/N\}+1-\cos\{\pi[(k_s-2)\Delta t-t_o]/N\}\} & \\ & k=k_s-1 \end{cases}$$

Eq.(11) suggests to write the radiation real-time predictor in the form :

$$\hat{r}(k+1/k) = r(k) + \delta(k) \tag{12a}$$

$$\hat{r}(k+2/k) = \hat{r}(k+1/k) + \delta(k+1) \tag{12b}$$

where $\hat{r}(k+q/k)$ is the forecast of $r(k+q)$ made at the instant $k\Delta t$ $(q=1,2)$.

The basic difference between eq. (11) and eq. (12a) must be underlined. In the right-hand side of the "batch predictor" (11), $r(k)$ is a computed quantity, namely it is the radiation value computed by the previous iteration of eq. (11) itself or by the equivalent eq. (10) (and for all k, such radiation "forecast"can be made once for all at sunrise). On the contrary, in the right-hand side of the real-time predictor (12a), $r(k)$ is the measure of the pyranometer during $[(k-1)\Delta t, k\Delta t]$ (just available at the instant $k\Delta t$ when the forecast is made).

Of course, the updated predictor (12a) has a better performance. The sequential introduction of pyranometric measurements, as far as they become available, allows, for instance, to account for the occurrence of cloudy intervals during the day.

b) Predictor for $v(k+q)$

A simple persistence predictor has been used :

$$\hat{v}(k+q/k) = v(k) \tag{13}$$

where

$\hat{v}(k+q/k)$ = forecast of $v(k+q)$, made at $k\Delta t$.

The choice of eq. (13) is motivated by two considerations; first $v(k)$ is wind speed average over three consecutive intervals, hence it is a rather smooth variable, namely there are no strong variations between $v(k)$ and $v(k+1)$. Moreover, $v(k)$ is a discretized variable (see Tables 1 and 2). Thus, the persistence predictor (13) is a good one, in this case.

c) Wind direction predictor

A probabilistic predictor has been used :

$\hat{d}(k+q/k)$ = solution of the maximization problem

$$\max_{d(k+q)} \left[\mathrm{Prob}\ (d(k+q)/d(k),\ v(k),\ k)\right] \tag{14}$$

where
$\hat{d}(k+q/k)$ = forecast of $d(k+q)$, made at $k\Delta t$;
$\mathrm{Prob}(d(k+q)/d(k),\ v(k),\ k)$ = probability of $d(k+q)$, conditioned to the fact that $d(k)$ is the direction class recorded in the k-th interval, $v(k)$ is the average wind speed recorded during $[(k-3)\Delta t,\ k\Delta t]$ and that the interval under consideration is the k-th. Such conditioned distribution has been estimated by wind data June 1st, 1973 - August 31st, 1973.

Thus, predictor (14) corresponds to forecast the wind direction class having maximum probability to occur, conditioned to current and recent wind records and to the forecast instant.

Let $\hat{s}(k+q/k)$ be the forecast of atmospheric stability class, made via eqs. (4), (5), on the basis of $\hat{r}(k+q/k)$ and $\hat{v}(k+q/k)$, supplied by predictors (12) and (13) respectively. By introducing $\hat{s}(k+q/k)$, as well as $\hat{d}(k+q/k)$ given by eq. (14), into eqs. (7), the DAP predicotr takes the form :

$$\hat{DAP}(k+1/k)=\alpha(\hat{s}(k+1/k),\hat{d}(k+1/k))DAP(k)+\beta(\hat{s}(k+1/k),\hat{d}(k+1/k))p(k+1) \tag{15a}$$

$$\hat{DAP}(k+2/k)=\alpha(\hat{s}(k+2/k),\hat{d}(k+2/k))\hat{DAP}(k+1/k)+\beta(\hat{s}(k+2/k),\hat{d}(k+2/k))p(k+2) \tag{15b}$$

Note that in eqs. (15), both $p(k+1)$ and $p(k+2)$ are regarded as available data at the end of the k-th period. This is quite reasonable, since $p(k)$ is a manipulated variable, namely since the generated power is scheduled in advance.

Predictor (15) has been tested (on a computer) in correspondence with the period September 1st, 1973 - September 30th, 1973, different from the one used for estimating the parameters of both model (3) and predictor (14). The result is summarized in the first two columns of Table 3. The quality indexes of Table 3 are :

θ = correlation between predicted and observed DAP;
θ_F = correlation between predicted and observed DAP during fumigation episodes.

Table 3. Performance of the DAP predictor under forecast (columns 1 and 2) and true (columns 3 and 4) future meteorology.

DAP Predictor Forecast Quality Index	2h Ahead with Forecast Meteorology	4h Ahead with Forecast Meteorology	2h Ahead with True Meteorology	4h Ahead with True Meteorology
θ	.87	.76	.91	.84
θ_F	.72	.60	.80	.68

A similar performance (only slightly better) has been obtained in correspondence with the period June 1st, 1973 - August 31st, 1973, namely with the same period used for estimating the parameters of model (3).

To measure the effectiveness of the meteorological predictors (12) - (14), the pollution predictor (7) has also been run again in correspondence with September 1973 data but introducing the future true values of s(k+q) and d(k+q) at each forecast step. The result is summarized in Table 3 (third and fourth column) and shows the loss due to the imperfect meteorological forecasts (12)-(14).

The loss is significant (around 10% of performance, approximately), but not so high as one might have feared by the gross nature of meteorological predictors. A step-by-step analysis shows that the most conspicuous losses occur during fumigation episodes, and are due to wrong direction forecast or wrong class prediction. Hence, sometimes either the start of the episodes is forecast with delay or the episode is forecast longer than its actual duration.

References

1. D.H. Slade, (editor), Meteorology and atomic energy, U.S. Atomic Energy Commission, TID 24190, 1968.

2. D. Randerson, "A numerical experiment in simulating the transport of sulphur dioxide through the atmosphere", Atmosph. Envir; 4:615-632, 1970.

3. C.C. Shir, and L.J. Shieh, "A generalized urban air pollution model and its application to the study of SO_2 distributions in the St.Louis Metropolitan Area", J. of Appl. Meteor., 13:185-204, 1974.

4. S.G. Bankoff, and E.L. Hanzevack, "The adaptive filtering transport model for prediction and control of pollutant concentration in an urban airshed", Atmosph. Envir., 9:793-808, 1975.

5. E. Runca, P. Melli, and A. Spirito, "Real-time forecast of air pollution episodes in the Venetian region. Part I: the advection-diffusion model", Appl. Math. Mod. (in press), 1979.

6. G. Finzi, G. Fronza, and A. Spirito, "Univariate stochastic models and real-time predictors of daily SO_2 pollution in Milan", Proc. of the 8th NATO international Technical Meeting on Air Pollution Modelling and its Application, Louvain-La Neuve (in press), 1977.

7. G. Finzi, G. Fronza, and S. Rinaldi, "Stochastic modelling and forecast of the Dosage Area Product", Atmosph. Envir., 12:831-838, 1978.

8. G. Finzi, P.Zannetti, G. Fronza, and S. Rinaldi, "Real-time prediction of SO_2 pollution in the Venetian Lagoon area", Atmosph. Envir. (in press), 1979.

9. G.E.P. Box, and G.M. Jenkins, Time Series Analysis, Forecasting and Control, Holden Day, San Francisco 1970.

10. F. Pasquill, Atmospheric diffusion, Van Nostrand, 1971.

11. S. Duckworth, and E. Kupchanko, "Air analysis: the standard Dosage Area Product", J. Air Poll. Contr. Ass., 17: 379-387, 1967.

12. G.C. Goodwin, and R.L. Payne, Dynamic System Identification: Experiment Design and Data Analysis, Academic Press, New York, 1977.

13. P. Bacci, et al., "Meteorological and radioecological researches, in the years 1972, 1973, 1974 around Caorso power plant", Proc. of AEI Annual Meeting, paper A. 29: 1-24 (in Italian), 1975.

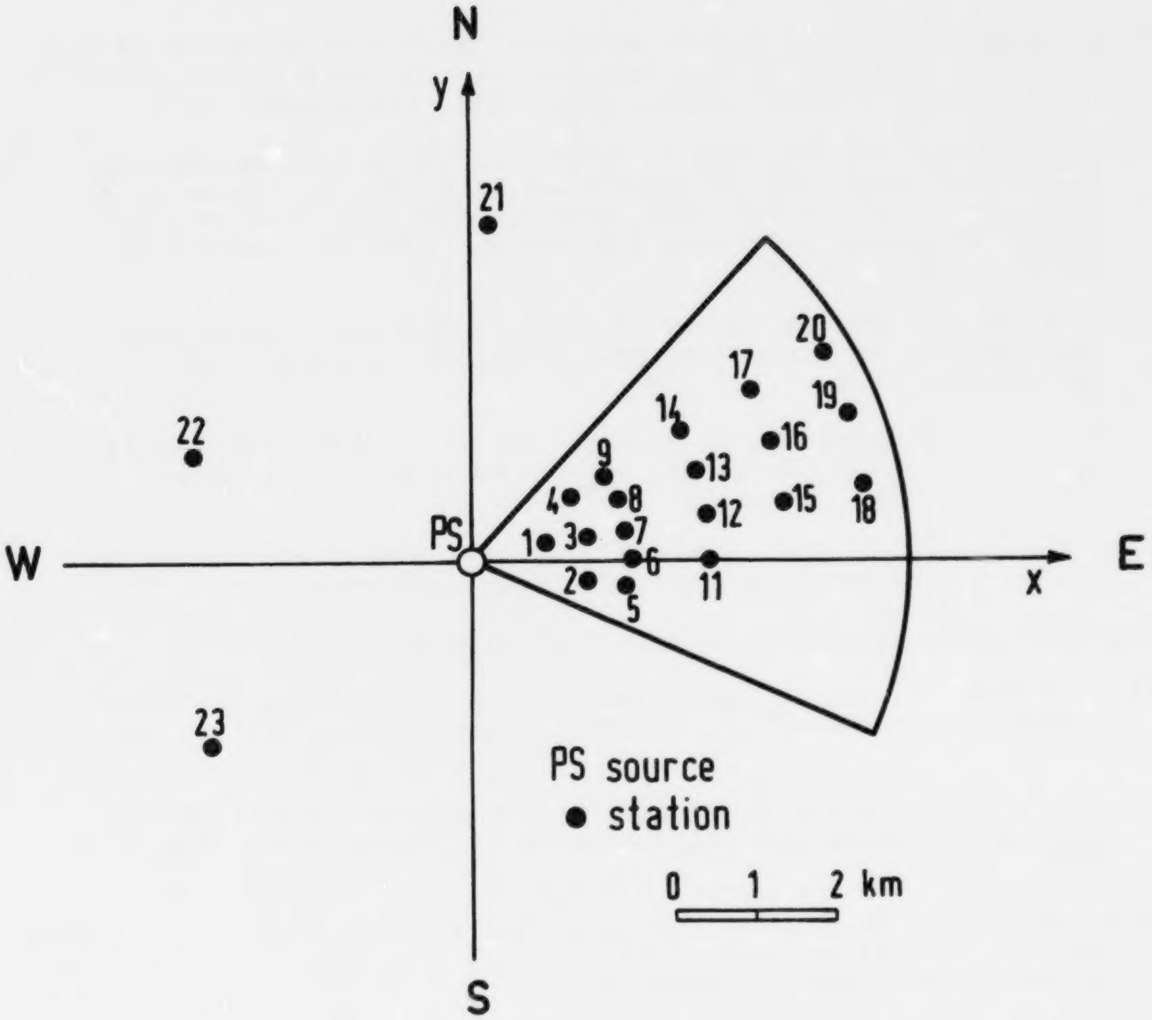
N
y
21
20
17
19
14
16
22
9
13
4
8
15
18
12
PS
7
1
3
W
6
E
11
2
x
5
23
PS source
● station
0 1 2 km
S

Fig. 1. Pollutant source and monitoring network

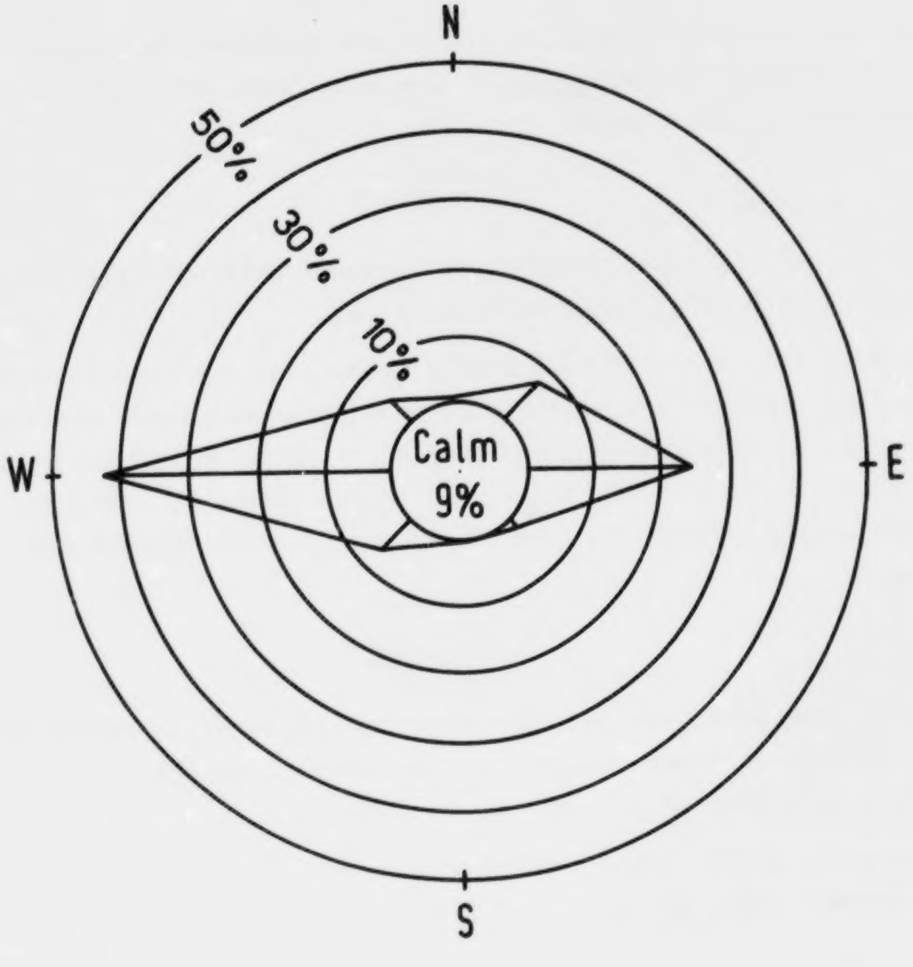

Fig. 2. Daily wind-rose

Discussion:

(Rapporteur: C. Whiteman)

A. Berger:

1. Is your model a purely linear one or a logarithmic-linear one?
2. What are the significance levels of the different correlation coefficients? Does the amplitude of the calculated pollution curve fit the observed curve well?

Fronza (response) :

1. Yes, we did, but the resulting differences were not relevant when compared with model input uncertainties.
2. The results fit rather well in the sense that the forecast peak coincides generally with the true peak. However, there are cases of error in forecasting the beginning of episodes and the ending of episodes. As for the first part of the question, different forecast quality indices have been used, but the conclusions are the same.

Dr. Hübschmann :

Mr. Fronza, you based the decision referring to emission reductions on the average of concentrations in the sampling sector.
Is the objective of this method to limit

- maximum ground level concentration, or
- average concentrations in a given area?

Fronza (response):

The variable taken as representative of pollution is an option in our approach. Simulations which use other variables (the maximum ground level concentrations in the area, for instance) and other unit time intervals are presently being carried out. In particular we are considering the variables on which the ambient standards are defined.

HOW DO TALL STACKS INFLUENCE ON LONG RANGE TRANSPORT ?

by

Michel M. Benarie
IRCHA - Centre de Recherche
91710 - VERT-le-PETIT - France.

Abstract. Empiral evidence from published dispersion experiments concerning long travel times, ranging over release heights from 0m to 9 km demonstrates that beyond 10^4s travel time, the dilution factor is independent from the source height. Therefore, it is concluded that the dimensions of a cloud which travelled more than 10^4s, do not contain any information about the release height.

Introduction

The well-know fact, that the ground-level concentration maximum *is* a function of the effective height of the source, suggests the popular fallacy, that the higher the source, the longer the travel distance of the pollutant.

First of all "travel distance" as such is devoid of sense. It is known that volcanic dust and nuclear debris circle the globe several times. Thus "distance" depends on analytical acuity. The essential parameters are :

1.- The total mass transported and

2.- The volume in which the mass is to be found, i.e. the concentration. With inert, passive material, the mass of which is being conserved, concentration depends only on the dilution volume. This is the product of $\sigma_x \sigma_y h$, where σ_x is the longitudinal and σ_y the lateral measure of the cloud and h its height. In fact this reasoning follows narrowly that outlined by PASQUILL (1974, p.366-373 see especially Fig.6.11 there), where he arrives at the conclusion that beyond 10 km distance, the same concentration is recorded, wether the source is at ground level or at 100 m height. PASQUILL (p. 368, l.c.) states that "... for 100 km... very speculative estimates based on limited observations of dispersion (were used)..." Here, on the contrary, the experimental evidence presented by the dispersion parameters will be examined in some detail.

It is outside the scope of this discussion to look into short and medium range (say, less than 100 km) material balance, a topic widely discussed in other papers. As it is common knowledge, that emission height *and* deposition velocity are essential parameters of the short- and medium range transport, the conclusions to be drawn from this inquiry will be strictly applicable only the inert, non settling pollutant. In other instances, they represent an approximating inference .

Empirical evidence.

Our purpose is to examine the dilution volume $\sigma_x \sigma_y h$ at long distance.

At distances which are of concern here, the pollutant is well mixed within a boundary layer, the thickness of which may be assumed as being constant and of the order of 2 km. The reason of this assumption is the well known diurnal evolution of the mixed layer (HOLZWORTH 1972; GILLIANI and HUSAR 1977) which progresses over the continents from the shallow nocturnal inversion through the afternoon maximum back again to the nocturnal stability. With travel times larger than 1d, the pollutant participates at least once in the afternoon convective growth of the layer and becomes well-mixed up to the afternoon mixed height. Consequent thermal re-structuration cannot change the molecular mixing ratio, therefore, a component once diluted in the volume between 0 and 2 km stays that way, unless deposition, chemical transformation or admixture with other molecules occurs.

By the same argument, it is of little concern, if the chimney plume does or does not penetrate an atmospheric inversion layer. After having undergone at least one full afternoon mixing, the pollutant is distributed at least up to the height to which the thermal convection reached.

Due to influence of meandering, we cannot simply ignore σ_x as usual for short range, continuous releases, but there is almost no information available about the longitudinal spread. Many tracer experiments, e.g. tetroons, hardly distinguish between σ_x and σ_y therefore, as it is generally done, we assume that $\sigma_x = \sigma_y$ and the dilution volume is proportional to σ_y^2.

A major critical compilation of σ_y (also of σ_z) as function of travel time has been published by HAGE et al. (1966). BAUER (1974) added to this survey further data pertaining mainly to the strastosphere and to the mesosphere, which are not of immediate concern here. HAGE'S diagram is the backbone of Fig. 1. To these, hitherto unpublished results of Belgian and French dispersion experiments have been joined. Other, recently published investigations, with special consideration to long travel times (distances) are : ANGELL et al. (1971), tetroons 4 km altitude, followed up to approx. one day ; BIGG et al. (1978), smelter plume from a 154 m tall stack, distances from 56 to 560 km; DOURY et al. (1975), SF_6 tracer emitted at 8 m and followed 160 km; MILLAN (1978) smelter plume from a 387 m - stack, followed by correlation spectroscopy at 315 km; RANDERSON (1968), forest fire plume of about 100 km length surveyed by satellite photography; RANDERSON (1972) nuclear cratering debris cloud, for travel times up to 2 days; ZETTWOOG and HAULET (1978); volcanic plume of the Etna (3200m) up to 100 km from the crater, also by correlation spectroscopy. To avoid overburdening the diagram, only the data from the here expressly quoted references are displayed in Fig.1; for the others shown only by contours, HAGE (l.c.) should consulted.

Fig. 1 does not show the points of the Jülich (Germany) diffusion experiments (VOGT 1977) because they pertain to shorter distances (< 10 km). Nevertheless, they are highly significant as our argument goes. Radioactive tracers were released from 50 and 100 m height, with simultaneous emission of different tracer nuclides to assure identical weather conditions. Beyond the distance of 2 km, no measurable height dependence of the diffusion parameters subsisted.

Discussion.

The original feature of Fig. 1 is to display the emission height as parameter. The whole set of data displayed, from a few seconds to about three or four day's travel time are clustered along a straight line represented by the exponential.

$$\sigma_y = 0.26\ t^{1.08} \qquad (1)$$

It appears obviously that there is no segregation of the data as a function of emission height. This is especially true for travel times longer than approx. 10^3s, as shown in Fig. 2. Here, each series of experiment has been represented by one point situated at the center of gravity of the respective contour or line of Fig. 1. It can be seen even more clearly, that emission height is not a discriminating criterion. Source altitudes from 0m to 9 km are intermingled.

We may therefore conclude, that beyond 10^4 - 10^5s travel time, the dilution factor $\sigma_y{}^2$ is independent from source height. Conversly, this is equivalent to the statement that the lateral dimensions of a cloud that travelled more than 10^4s, do not contain any information about the release height.

This finding contradicts the popular model of a puff or a release lifted rapidly at some great hight, transported almost undiluted at long distance and then descending somewhere two or three days later. Would this image be true, the σ_y of two or three day's travel time should be more or less similar to those belonging to shorter travel times, that is, the point in Fig. 1 should show some tendency to level off. No such leveling off is evidenced by the data.

The main mechanism explaining the independence of the dilution factor from the emission height at travel times longer than one day, seems to be the abovementioned diurnal cycle of the mixing process. While this factor is positively at work over dry land, much less is known about what happens over extended oceanic surfaces. This point concerns some of the nuclear plumes plotted in Figs. 1 and 2, which were released from small islands surrounded by thousands of kilometers of water. In fact, I am not aware if analogous studies to that of HOLZWORTH (1972), but for large water surfaces, have ever been made. They would be of considerable interest for a betterunderstanding of dispersion and long range transport in general and over seas in special.

The data points are spread in both figures well beyond the limit which may reasonably be expected due to the inhomogeneity of the methods (tetroons, volcanic and stack plumes, etc..) and to individual error within each experimental set. The explanation of this range is found in the fact, that the experiments referred to in the Figs. 1 and 2 relate to releases made under widely different stability conditions. Even if the conditions of the release pertain to the same stability class, for observations lasting one or more days, stability changes, if not for an other reason, then because of the alternance of day and night. In Fig. 2, the dispersion parameters derived from A.S.M.E. (1968) are shown for the two extreme stability classes (stable and very unstable) and for two wind velocites (5 and 15 m^{-1}). It is not expected that this approximation derived from short range observations should quantitatively represent the long range results, but the order of magnitude of the spread between the stable and the very unstable situations makes the advanced explanation quite likely.

It has been attempted but without success, to plot Fig. 2 as data pertaining to the main stability conditions of the release. Most pertinent information lacks in the available references; many of the releases were oceanic and the observations were not made; finally the remaining few well-documentaed points thin out to random insigficance.

By recognizing that at long distance there is no measurable difference between an emission at ground level and another at 9 km height, we must also admit that from the point of view of the diffusive and advective properties of the long range transport, a source at 0m height and another at 200 m height must also be indistinguisable. This affirmation does not take into consideration, that at transport times where full mixing did not yet occur, that is below 10^3 - 10^4s, differences due to several other reasons may subsist (see e.g. GILLIANI and HUSAR, 1977).

The physical precesses involved in the spread of the cloud do not enter in our purely empirical considerations. Indeed, from a meteorological standpoint the distinction between advection and turbulent diffusion is arbitrary and depends on the choice of the averaging scale.

Model results.

Schooled in precepts of the Gaussian plume model, which predicts that a distinct maximum concentration occurs at the source height Z_s at all distances from the source, one is somewhat taken aback by the empirical evidence of Sect. 2, *vis*, that the plume width at ground level is independent of the relase height. The full theoretical explanation has been given by LAMB (1978 and undated draft) and therefore, only his conclusions should be inserted here. Using the numerical turbulence model of DEARDORFF (1974) in conjunction with Lagrangian diffusion theory , he has demonstrated the following properties of the ground-level concentrations of non-buoyant material released by continuous point sources at various height Z_s in the convective planetary boundary layer with the mixed depth h :

1.- The lateral spread of material is completely independent of source height for sources above $Z_s > 0.1$ h. This is true to a lesser extent also for the vertical spread.

2.- The maximum concentration occurs along a descending path from elevated sources and an ascending path from surface releases.

LAMB (e.c.) proposed suitable modifications of the standard Gaussian expressions to resolve the discrepancy between them and the results produced by his numerical simulations, for which his papers should be consulted.

References.

ANGELL J.K., ALLEN P.W. and JESSUP E.A. 1971 : Mesoscale relative diffusion estimates from tetroon flights J. Appl . Meteor 10 p. 43-46

A.S.M.E. (The American Soc. of Mechanical Engineers) 1968 : Recommended Guide of the prediction of the dispersion of airborne effluents. 85 pp.

BAUER E. 1974 : Dispersion of tracers in the atmosphere and ocean : survey and comparison of experimental data. J. Geophys. Res. 79 p. 789-795.

BIGG E.K., AYERS G.P. and TURVEY D.E. 1978 : Measurement of dispersion of a smoke plume at large distances from the source. Atm. Env. 12 p. 1815-1818.

DEARDORFF J.W. 1974 : Three-dimensional study of the height and mean structure of a heated planetary boundary layer. Boundary Layer Met. 7 p. 81-106.

DOURY A., DEVILLE-CAVELIN G., MAIGNE J.P., RZEKIECKI R., BRUN J. and GEISSE C. 1975 : Simulation de transferts atmosphériques à grande distance. Rapport (CEA) SESR-R-33, 15 pp.

GILLIANI N.V. and HUSAR R.B. 1977 : Project MISST : Plume modeling of the dispersion, transformation and ground removal of SO_2 over the β-mesoscale range (25-250 km). Eigth Internat. Techn. Meeting NATO/CCMS Louvain-la-Neuve, Belgique, Sept. 20-23, p. 428-480.

HAGE K.D., ARNASON G., BOWNE N.E., BROWN P.S., ENTREKIN H.D., LEVITZ M. and SEKORSKI J.A. 1966 : Particle fallout and dispersion in the atmosphere. Final Report Sandia Corp. SC-CR-66-2031, available from NTIS, 102 pp.

HOLZWORTH G.C. 1972 : Mixing heights, wind speeds, and potential for urban air pollution throughout the contiguous United States. U.S. Env. Prot. Agency AP-101, 118 pp.

LAMB R.G. 1978 : A numerical simulation of dispersion from an elevated point source in the convective planetary boundary layer. Atm. Env. 12 p. 1297-1304.

LAMB R.G., undated draft : The effects of release height on material dispersion. Communicated by letter, Jan. 1979, 16 pp.

MILLAN M.M. 1978 : Recent advances in correlation spectroscopy for the remote sensing of SO_2. Proceedings of the 4th Joint Conf. on Sensing Environmental Pollutants, Am. Chem. Soc., p.40-43.

PASQUILL F. 1974 : Atmospheric diffusion. Wiley & Sons, New-York, 429 pp.

RANDERSON D. 1968 : A study of air pollution sources as viewed by Earth satellites. J. Air Poll. Contr. Assoc. 18 p. 249-253.

RANDERSON D. 1972 : Temporal changes in horizontal diffusion parameters of a single nuclear debris cloud. J. Appl. Meteor. 11 p. 670-673.

VOGT K.J. 1977 : A new system of release height dependent diffusion parameters for the Gaussian plume model. Fourth Internat. Clean Air Congr. 16-20 May; Tokyo, p. 171-175.

ZETTWOOG P. and HAULET R. 1978 : Experimental results on the SO_2 transfer in the Mediterranean obtained with remote sensing devices. Atm. Env. 12 p. 795-796.

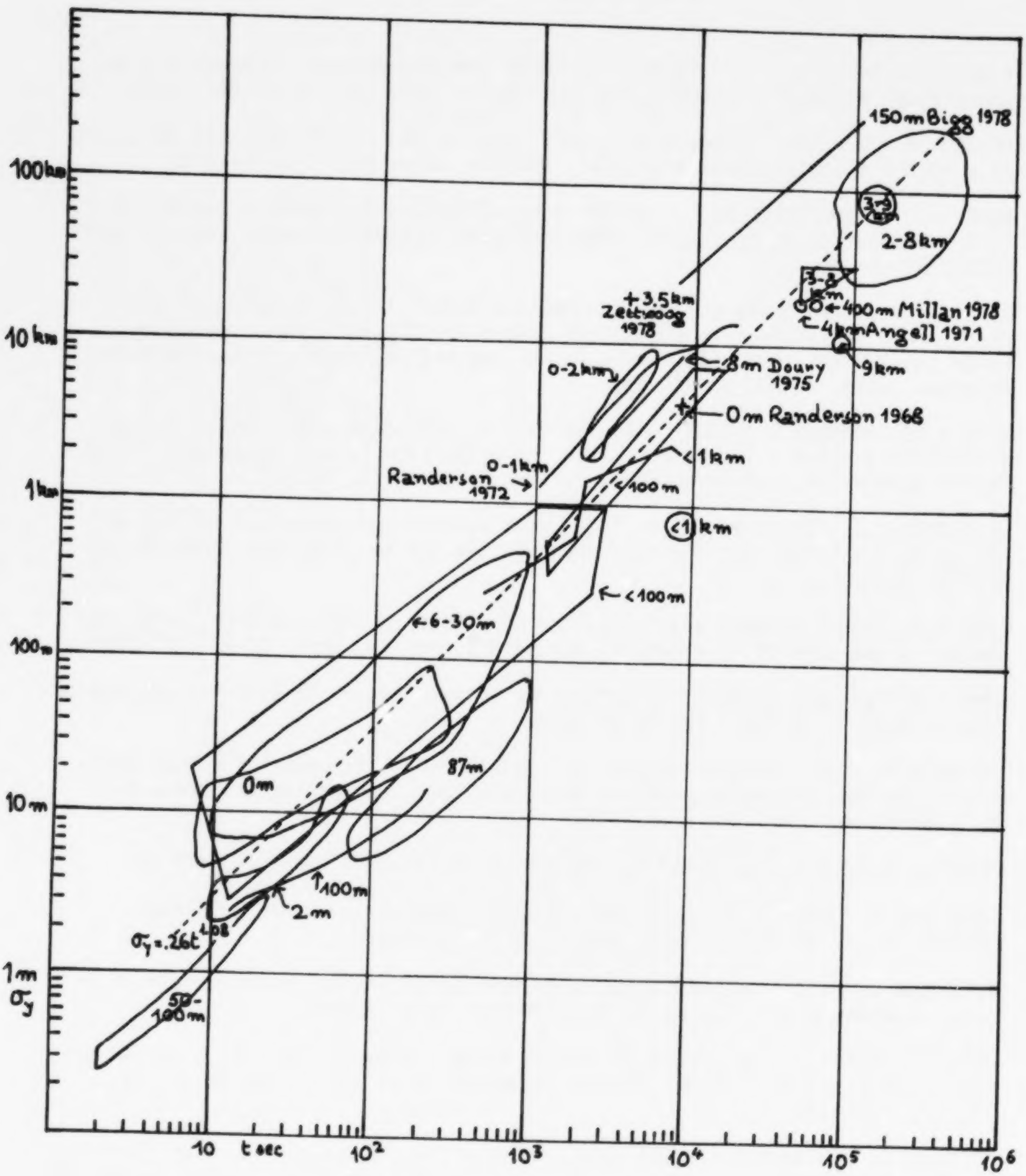

Fig. 1 - Lateral spread as function of the travel time, mainly after HAGE et al. (1966), with some more recent data added. The numbers refer to the emission heights in m or km.

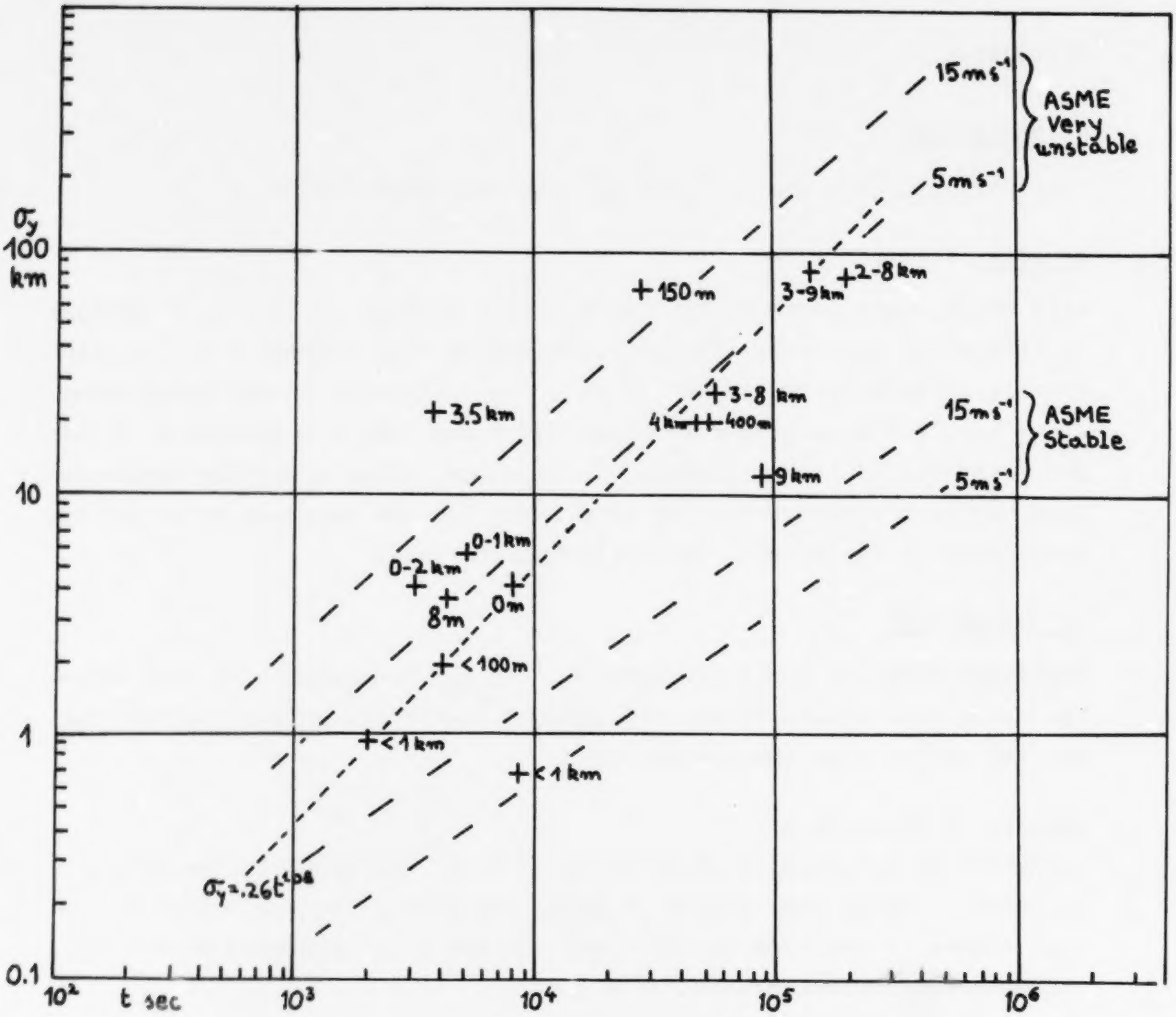

Fig. 2 - Enlarged section of Figure 1, representing the emission height dependence of the lateral spread for travel times larger than 10^3s.

Discussion:

A. Venkatram:

Does vertical wind shear affect the concentration field?

Bénarie (response):

Wind shear has a profound influence on the process of mixing. Therefore it influences the concentration field before full mixing (i. e., vertically uniform concentration field) has occurred. On the other hand, after perfect mixing no mechanical force can induce a de-mixing (Second Principle of Thermodynamics). Therefore, after a uniform concentration has been attained neither wind shear nor the build-up of a temperature gradient can affect the concentration field.

T. Schneider:

Professor Bénarie, could you estimate the percentage of time that plumes from very tall stacks do not mix through the boundary layer within the one day period that you mentioned?

Bénarie (response):

Experimental evidence accumulated up to now (as shown in the body of my paper) shows that beyond 24 hours transport time the emission from tall stacks (and from ground-level sources) is thorughly mixed throughout the planetary boundary layer.
Therefore the percentage is exactly 100 percent.
On the other hand, observations show that full mixing may occur after 10^3 or 10^4 seconds. I do not have statistical data in hand, just the percentage of time full mixing occurs after 10^3 seconds, 10^4 seconds and so on. It would perhaps be worthwhile to investigate.

MODELING OF DISPERSION FROM TALL STACKS

by

A. Venkatram
Ontario Ministry of the Environment
Toronto, Canada

and

R. Vet
R. Vet Environmental Consulting
Unionville, Canada

Abstract. This paper proposes a model for dispersion of pollutants emitted from an elevated source into a convective boundary layer. The model incorporates some of the most recent understanding of dispersion in the mixed layer. For example, we relate the horizontal plume spread σ_y to the convective velocity scale w_*. Our formulation for the vertical spread σ emphasizes the role of the mixed layer height z_i and the associated time scale z_i/w_* in controlling dispersion in the vertical direction.

An important ingredient of our model is the concept of plume impingement distributed around a mean distance x_i at ground level. The computation of x_i has been guided by the recent work of Lamb and that of Briggs.[1,2]

The model has been tested by comparing predictions with concentrations measured around the Dickerson and Morgantown power plants in Maryland and the INCO nickel smelter in Sudbury, Ontario. The results of the verification are very encouraging.

Introduction

The main advantage of a tall stack lies in the fact that pollutants emitted from the stack are unaffected by the turbulent boundary layer most of the time. For example, pollutants emitted from a 200 m stack will be seldom dispersed by the shear generated turbulence of the nocturnal boundary layer which usually does not exceed 100 m. Therefore, during stable conditions elevated emissions do not cause ground-level concentrations. On the other hand, convective turbulence, which can extend to heights of the order of kilometers, will bring the plume down to the ground very effectively. Thus, emissions from a tall stack are a problem primarily during sunny (summer) days with considerable convective activity. The term "looping" graphically illustrates the behaviour of the tall stack plume under such conditions. Apart from this qualitative understanding of dispersion from tall stacks, there is little guidance in the literature on the estimation of ground-level concentrations during plume "looping".

It is only recently that attempts have been made to understand dispersion in the convective boundary layer. Deardorff and Willis studied dispersion in the laboratory using a water tank while Lamb has investigated particle diffusion using numerical techniques.[3,4,5] These experiments show that conventional modeling techniques are not applicable to dispersion in the convective boundary layer. In response to a need for concentration estimates, these investigators have suggested various parameterizations to describe the concentration field associated with a source emitting pollutants in the unstable boundary layer. Unfortunately, these results have not been applied, to any extent, to operational prediction of concentrations. Furthermore, validation with field data has not been attempted. One of the reasons for this is that the parameterizations refer to passive releases while most "real" releases are associated with considerable buoyancy. Also, some of the variables of these concentration formulations cannot be directly related to the type of meteorological measurements which are conventionally made.

In this paper we propose a model to estimate concentrations associated with elevated releases in the daytime unstable boundary layer. The model incorporates the principal results of the investigations of Deardorff, Willis and Lamb. In addition, its formulation relies heavily on actual ground-level concentration measurements. Thus, it represents a significant step towards an operational model.

The Model

Before going into the details of the model it is instructive to review the principal results of recent studies (Deardorff, Willis and Lamb) of dispersion in the convective boundary layer. As we are primarily interested in ground-level concentrations we will pay little attention to the results pertaining to the detailed vertical structure of the concentration field.

The turbulent velocities σ_v and σ_w in the upper part of the PBL ($z > 0.1z_i$) are proportional to the convective velocity scale w_* given by

$$w_* = \left[\frac{g}{T_o} H_o z_i\right]^{1/3} \qquad (1)$$

where H_o is the heat flux, T_o is the average temperature of the mixed layer and z_i is the mixed layer height. Thus, w_* is one of the controlling parameters for dispersion of pollutants emitted at heights much greater than the thickness of the shear dominated surface layer. We recall that this surface layer does not extend much higher than $z = |L|$ where L, the Monin-Obukhov length is

$$L = -\frac{T_o u_*^3}{gk\, H_o} \qquad (2)$$

In (2), u_* is the surface friction velocity and k is the von-Karman constant.

As the most energetic eddies in the mixed layer scale with z_i, the integral time scale τ_m relevant to dispersion is z_i/w_*. We also see that τ_m is roughly the time taken after release for pollutants to become well mixed through the depth of the mixed layer. This interpretation of τ_m allows us to appreciate the definition of the non-dimensional travel distance X,

$$X \equiv \frac{w_* x}{u \; z_i} \tag{3}$$

In (3), x is the distance from the pollutant source and u is the mean mixed layer wind.

With the preliminaries of the preceding paragraphs we are now in a position to describe our dispersion model. We will find it convenient in our development to deal initially with the crosswind integrated concentration

$$\bar{C}^y = \int_{-\infty}^{\infty} C(x, y, 0)\, dy \tag{4}$$

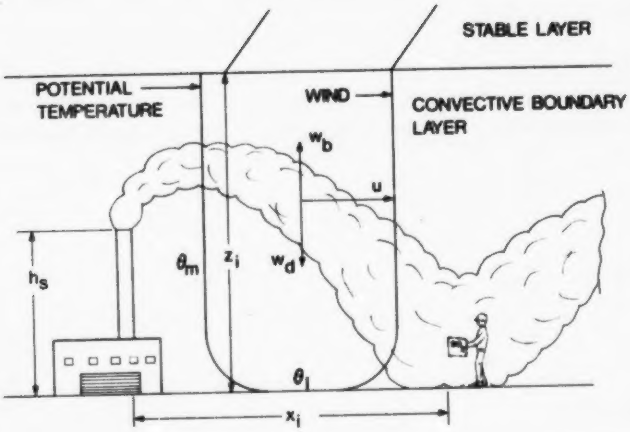
STABLE LAYER
POTENTIAL TEMPERATURE
WIND
CONVECTIVE BOUNDARY LAYER
w_b
u
h_s
θ_m
z_i
w_d
θ_l
x_i

Figure 1

Schematic of physical system under study

Figure 1 shows a schematic of the physical system being considered. Based on visual evidence of the behaviour of the looping plume we will assume that we can separate the small scale spreading of the plume about its centerline and the larger scale up and down motion. The vertical meandering of the plume is associated with the convective updrafts and downdrafts extending through the depth of the PBL. As these downdrafts (or updrafts) have relatively long lifetimes it is reasonable to assume that a plume segment emitted into a downdraft will remain in it until it impinges on the ground. The figure illustrates such a situation. Note that the vertical velocity of the plume can be resolved into an upward acting buoyant velocity and an opposing downdraft velocity which eventually brings the plume down to the ground. As the emission point is taken to be well above the shear dominated surface layer most of the downward travel of the plume occurs in a region in which the velocity (and potential temperature) is virtually uniform.

It is reasonable to assume that a nonzero concentration (crosswind integrated) is detected at a receptor x_r whenever the plume impinges on the ground at a distance $x \leq x_r$. Then if $P_d(x)$ is the probability density of plume impingement, the fraction of the time δ the plume is seen at x_r is given by

$$\delta = \int_0^{x_r} P_d(x, \nu)\, dx \tag{5}$$

In (5), ν refers to variables such as stack height, buoyancy and atmospheric turbulence which determine P_d.

It is always possible to associate an average vertical dimension σ to the collection of plume segments detected at x_r. Then, for a given wind speed u in the mixed layer we can express the average plume segment concentration at x_r as

$$C_p \sim \frac{Q}{u\,\sigma} \tag{6}$$

where Q is the emission rate. Note that Q/u is the mass per unit length of the plume segment.

We assume that the ensemble averaged concentration $\bar{C}^y(x_r, 0)$ can be approximated by

$$\bar{C}^y(x_r, 0) \sim \frac{Qf}{u\,\sigma} \tag{7}$$

Note that (7) implies that we are modeling the concentration time series at x_r by top-hat profiles whose constant magnitude is given by (6). In other words, the concentration at x_r is either zero or C_p. We point out that Davidson and Halitsky based a successful dispersion model on this idea.[6]

In order to be able to use (7) we need formulations for f and σ. As plume impingement can occur at any downwind distance ranging from 0 to ∞ a convenient choice for $P_d(x)$ is the lognormal distribution. The precise form of $P_d(x)$ is not expected to be critical in computing $\bar{C}^y(x_r, 0)$ as f depends on the integral of the distribution. Then, we can express f as

$$f = \frac{1}{\sqrt{2\pi}\;\ell n s_g} \int_0^{x_r} exp\left[\frac{-(\ell n x - \ell n m_g)^2}{2\ell n^2 s_g}\right] d(\ell n x) \tag{8}$$

In (8), m_g and s_g are the geometric mean and standard deviation of the lognormal distribution. These parameters can be estimated by examining the results of the numerical experiments of Lamb.[5] His study shows that the plume centerline descends when particles are released from an elevated source. The rate of descent of the centerline (locus of the maximum crosswind integrated concentration) is approximately $0.5\ w_*$. Then, for particles released at a height h_s, the plume centerline impinges at a distance $2uh_s/w_*$ from the source. Briggs had a similar picture in mind when he proposed the "touchdown" model for plume rise.[2] According to him the buoyant plume rises relative to a region of convective downdrafts. As the buoyant plume rise rate decreases with time the downdrafts eventually bring the plume down to the ground at at distance x_i given by the solution of the following equation

$$\frac{\alpha F^{1/3}\, x_i^{2/3}}{u} - \frac{w_d x_i}{u} = -h_s \tag{9}$$

where F is the buoyancy parameter and w_d is the downdraft velocity which is about $0.5w_*$. The first term on the left is the buoyant rise and the second term represents the effect of convective downdrafts. Some preliminary studies indicate that the constant α in (9) is $\approx$ 1.0.[7]

In view of the preceding discussion we feel that is reasonable to assume that the mean impingement distance m_g is proportional to x_i . The model testing, described in a later section, indicated that the simplest relationship $m_g = x_i$ was adequate. We can estimate s_g by using Lamb's (personal communication) results on the statistics of convective velocities in the PBL. He found that the magnitude of the downdraft velocity one standard deviation away from the mean ($= 0.5w_*$) was approximately $0.75\, w_*$ ($=1.5w_d$). The impingement distance corresponding to $0.75\ w_*$ would be a lower limit on possible plume impingement distances. We can then approximate s_g by

$$s_g = \frac{x_i(w_d = 0.5w_*)}{x_i(w_d = 0.75w_*)} \tag{10}$$

It is interesting to note that for the cases considered s_g computed from (10) was around 2, the value used in an earlier version of this model.[8]

For the behaviour of σ we propose

$$\frac{\sigma}{z_i} \sim X \quad ; \text{ small x} \tag{11a}$$

$$\frac{\sigma}{z_i} \sim \text{constant}; \text{ large x} \tag{11b}$$

Note that σ is the vertical extent of a plume segment and thus corresponds to an averaging time roughly equal to the time the plume segment is detected at a receptor. Assuming that z_i is the relevant length scale controlling dispersion in the convective boundary layer, we can estimate the averaging time for σ with the Eulerian time scale z_i/u. Taking typical values of z_i =1500 m and $u = 5$ ms^{-1} we find that the averaging time is approximately 5 minutes. For this time interval we are partially justified in using the small time limit for dispersion (statistical theory) in Eq. (11a). Equation (11b) reflects the observation that at large X the vertical spread is limited by the capping inversion at z_i .

A plausible interpolation for σ between the limits for small and large X can be written as

$$\frac{\sigma}{z_i} = A\left[1 - exp(-1.5X)\right] \tag{12}$$

where A is a constant to be determined from the subsequent analysis. The constant 1.5 in (12) was chosen on the basis of model tesing described in a later section. Also, it is seen that for $X > 3$, σ is within 1% of its maximum value. This result agrees with the observations of Willis and Deardorff.[4]

We can now write the expression for the centerline ground-level concentration as

$$C(X,\ 0,\ 0) = \frac{BQf(x)}{u\,\sigma_y\,\sigma} \qquad (13)$$

We can determine the constant B/A in (13) by noting that the expression for C(X,0,0) should reduce to that corresponding to the well-mixed PBL for large X

$$C(X,\ 0,0) = \frac{Q}{\sqrt{2\pi}\ u\,\sigma_y\,z_i} \qquad (14)$$

From (14) we see that B/A = $1/\sqrt{2\pi}$. Note that (14) implies that the concentration distribution in the crosswind direction is Gaussian, a description which is adequate according to the tank experiments of Willis and Deardorff.[4]

Based on the results of Islitzer and Willis and Deardorff we selected the simplest formulation of σ_y.[8,9]

$$\frac{\sigma_y}{z_i} = 0.45\ X \qquad (15)$$

It is noted that Islitzer's measurements did not extend beyond X = 0.5 . As partial support for applying his results to much larger X we cite Moore's results on the determination of ground-level σ_y values due to elevated sources.[10] The results corresponding to sampling times of approximately one hour indicated that σ_y varied linearly up to 14 km which translates roughly to X = 4. This behaviour was followed under a wide variety of meteorological conditions. One possible explanation for this enhanced plume spreading is the conversion of vertical kinetic energy of downdrafts into horizontal kinetic energy as the sinking fluid strikes the ground.

We point out that our formulations for σ_y and σ are empirical in the sense that they were derived by fitting concentration measurements to the expression for the ground-level concentration. However, Lamb suggests that this is the most practical method to derive sigmas.[11] According to him "theoretical" expressions for σ's are not compatible with simple Gaussian type models which cannot account for the complex dispersion processes occurring near the ground.

It is useful to note that the expressions for the σ's do not include the effects of self-induced spread due to plume buoyancy. The model testing described in a later section indicated that these effects were minor.

It should be apparent from the preceding discussion that each stage of model development relied heavily on comparison with concentration observations. Thus, this model is essentially a concise description of the observations made under a variety of meteorological and stack conditions. We point out that a model is of little value if it has to be "tuned" everytime the dispersion conditions change. As will be seen in the next section our model has been applied to three independent sets of data with no site specific "tuning".

Model Testing

The model was tested with three sets of data. Two of them, reported by Weil, refer to measurements made in the vicinity of the Dickerson and Morgantown power plants situated in Maryland.[12] The third set consists of measurements made around a nickel smelter in Sudbury, Ontario. Simultaneous meteorological data were also obtained during these field studies.

For the sake of completeness, we will describe some of the relevant information given in Weil's report. The coal-fired Dickerson plant consists of three 185 MW generated units with two 122-m stacks, 60 m apart. It is situated in the rolling terrain of Montgomery county. Measurements at the Dickerson plant extended from October 1972 through April 1973.

The Morgantown power plant is also situated in relatively flat terrain next to the Potomac River in southern Charles County. It has two 575 MW units exhausting through two 213 m stacks, 76 m apart. Measurements at the plant were made during February 1975 through June 1975.

The International Nickel Company (INCO) smelter is situated on rolling ground in Sudbury, Ontario. There are a number of small lakes in the vicinity of the plant. Waste gases from the smelter are exhausted through a 381 m stack. The high sulphur content of the local nickel ore results in the emission of approximately 3000 tons of SO_2 per day. The field experiment to study the concentrations associated with this emission was conducted during a two week period in June 1978.

The method of measurement of SO_2 was similar in all three fields studies. An instrumented mobile van was used to measure ground-level SO_2 concentrations. Using available roads, repeated passes were made across the direction of plume travel. The traverses lasted from ½ to 1 hour and resulted in about 6 to 10 instantaneous concentrations profiles. Some of the traverses in the Sudbury field study were done with an instrumented twin engined Aztec aircraft flying at tree top level (~ 30m).

Concentration profiles obtained from the traverses were combined to form an Eulerian average profile corresponding to an averaging time of approximately 1 hour. The maximum of this composite profile was taken to represent the ground-level centerline concentration. These centerline concentrations were compared with predicitions from our model. Following Deardorff and Willis we used data corresponding[3] to the range $1.5\ w_* \leqslant u \leqslant 6w_*$ to ensure the applicability of convective scaling.

As the surface heat flux was not measured we assumed that it was 0.3 times the incoming solar radiation. We believe that this is not critical as the heat flux is used in the computation of the convective velocity w_* which depends on the one third power of the heat flux.

Concentration observations were compared with model predictions using the following three steps:

1) Compute percentage of predictions within a factor-of-two of the observations. The factor-of-two criterion is based on experience with dispersion modeling and is the time-honored method of testing model performance (A Position Paper of the AMS 1977 Committee on Atmospheric Turbulence and Diffusion). Model predictions meeting this accuracy criterion are further tested using curve fitting procedures.

2) Regress observations on predictions using the following equation:

$$C(\text{observed}) = a + b\,C(\text{predicted}) \quad , \qquad (16)$$

The value of the coefficient of determination r^2 is an indication of the performance of the model. Furthermore, the regression coefficients 'a' and 'b' should not be significantly different from their expected values of 0.0 and 1.0 respectively.

3) Regress observations on predictions using the equation

$$C(\text{observed}) = a\left[C(\text{predicted})\right]^{b} \qquad (17)$$

Equation (17) would be relevant for model testing if observations are lognormally distributed about the predicted ensemble mean. As observations show that this indeed the case (13) we feel that the r^2 associated with (17) is a good test of model accuracy. Note that the expected value of 'a' and 'b' is unity.

Table 1 summarizes the results of model testing on three sets of data. It is seen that model predictions compare well with observed concentrations. More than 80% of the predictions are within a factor-of-two of the measurements. The value of r^2 for the Dickerson data set is above 0.70. This indicates a high degree of association between model predictions and observations. For the Morgantown data there is a tendency for the model to slightly underpredict although the r^2 is as high as 0.80 for the logarithmic correlation analysis.

For the Sudbury data, the model does not perform as well as it does for Dickerson and Morgantown. This could be related to the fact that our assumption of constant downdraft velocity might be questionable when the emission point is in the upper part of the convective PBL. Recall that the Sudbury stack is 381 m tall.

Figures 2, 3 and 4 illustrate the details of the comparision between model predictions and observations. In Fig. (2a) we have plotted the ratio of C (observed) to C (predicted) against X/X_i. It is seen that the model performs as well for $X/X_i > 1$ as it does for $X/X_i < 1$. This gives us some confidence in our choice of the lognormal distribution to "smear" the concentration distribution around the mean impingement distance x_i. The scattergram of Fig. (2b) shows in more detail the excellent agreement between predicted and observed concentrations.

It is seen from the table that the averaging times for most of the observations are less than one hour. Furthermore, the concentrations represent averages derived from about six instantaneous values corresponding to ground level traverses. In view of this, substantial deviations of observed concentrations from predicted ensemble

TABLE 1*

Data Set Name	No. of Data Points	Percentage Meeting Factor-of-two criterion	Mean Value of C(obs)/C(pred) (filtered data set)	Linear			Logarithmic		
				r^2	a	b	r^2	a	b
Dickerson	26	85	0.98(0.34)	0.70	-0.15	0.98	0.74	0.91	1.00
Morgantown	22	86	1.20(0.37)	0.65	18.86	0.87	0.80	2.21	0.84
Sudbury	25	80	1.02(0.27)	0.53	9.95	1.00	0.60	0.89	1.02

*Summary of model testing for the Dickerson, Morgantown and Sudbury data sets. Numbers in parenthesis are the standard deviations.

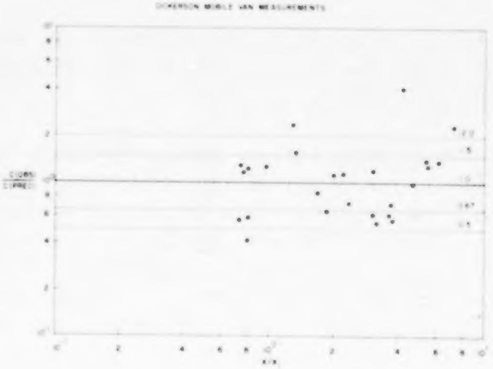

Figure 2a

Variation of the ratio C(observed)/C (predicted) as a function of X/X_i Horizontal lines correspond to selected values of the ratio. Data set refers to the Dickenson Power Plant.

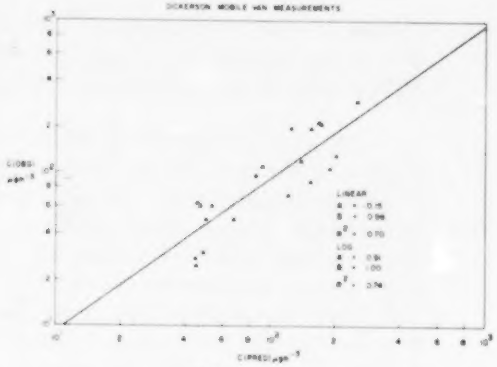

Figure 2b

Scattergram of predicted concentrations against observed concentrations. Data set refers to measurements around the Dickenson Power Plant. Only data meeting the factor-of-two criterion have been used. The best fit line corresponds to regression of log-transformed concentrations.

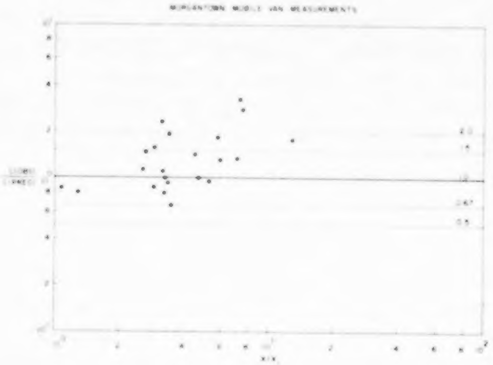

Figure 3a

Same as 2a except for Morgantown Power Plant.

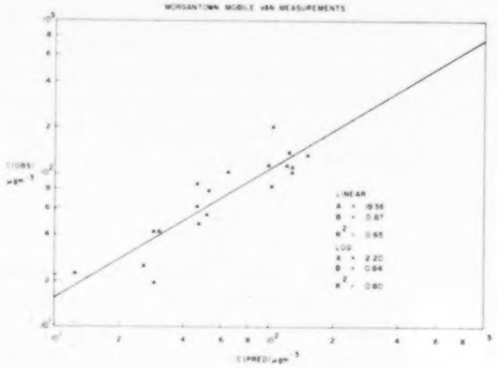

Figure 3b

Same as 2b except for Morgantown Power Plant.

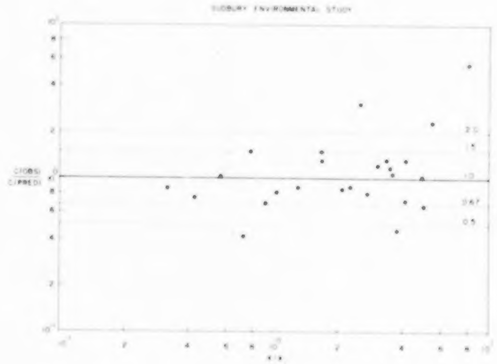

Figure 4a

Same as 2a except for Sudbury.

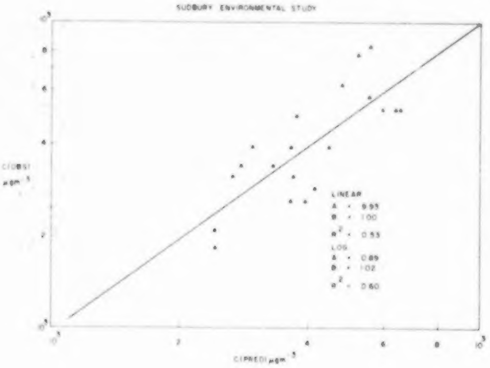

Figure 4b

Same as 2b except for Sudbury.

means is not unexpected.[14] However, as seen in Fig. (4a), this scatter is well within the accepted norms (See AMS position paper on this subject, BAM). In fact, 80% of the data is within a factor of 1.5 of the predictions.

In performing a regression analysis between observations and predictions we have chosen only those data points which meet the factor-of two criterion. This filtering is justifiable, in our opinion , only if the rejected data points are a small percentage of the observations. Furthermore, this process ensures (approximately), that the expected variances of the observed concentrations are comparable. Note that linear regression is valid only if this condition is satisfied.[15] Figure (3a) indicates as seen before, that the model slightly underpredicts concentrations for the Morgantown data set. However, better than 65% of the predictions are within a factor of 1.5 of the measured concentrations. The high degree of association between model results and observations is also evident in Fig. (3b).

The details of the meteorological and source conditions for the Dickerson and Morgantown concentration observations are given elsewhere.[8] In this paper we only present the relevant information for the observations made in Sudbury, Ontario during June 1978. Note that (Table 2) $u \leqslant 6w_*$ for all the data indicating that the PBL is dominated by buoyant production of turbulence. This also justifies the use of convective scaling in the analysis of dispersion.[3] Figure 4b illustrates the comparison between observed and predicted concentrations. Considering the expected variances in measurements the comparison is gratifying. In addition to the r^2 being as high as 0.6 the best fit values of 'a' and 'b' are very close to their expected values.

Summary

This paper proposes a model to describe the dispersion of pollutants emitted from a point source into a convective boundary layer. The model is primarily applicable to elevated sources as the micrometeorological variables used in its formulation pertain to the upper part of the planetary boundary layer. However, this does not limit its usefulness as present day stacks tend to be tall and are associated with high concentrations usually during convective conditions. Thus the model is useful during the time that elevated releases are of most concern.

At this point it is useful to summarize the equations on which our model is based.

$$\overline{C}\,(X,\ 0,\ 0) = \frac{f(X)}{\sqrt{2\pi}\ \overline{\sigma}\ \overline{\sigma}_y} \qquad (18a)$$

$$\overline{C} \equiv C z_i^2 u/Q\ ; \quad X \equiv w_*\, x/z_i u \qquad (18b)$$

$$\overline{\sigma}_y = \sigma_y/z_i = 0.45\ X \qquad (18c)$$

$$\overline{\sigma} \equiv \sigma/z_i = 1 - exp\ (-\ 1.5\ X) \qquad (18d)$$

TABLE 2*

SUDBURY ENVIRONMENTAL STUDY

DA	MO	YR	START TIME	END TIME	F (m^4s^{-3})	Q (gs^{-1})	x (m)	z_i (m)	w_* (ms^{-1})	u (ms^{-1})	x_i (m)	C(PRED) (ugm^{-3})	C(OBS) (ugm^{-3})	C(OBS)/C(PRED)
10	06	78	13:45	14:32	2082	28213	3100	1040	2.13	11.3	9372	241	208	0.86
10	06	78	14:02	15:00	2149	32224	39000	940	2.16	11.7	9479	361	260	0.72
10	06	78	15:56	17:12	2072	22958	32000	740	2.31	10.2	7650	373	494	1.32
11	06	78	16:10	17:11	1897	22958	3000	1540	2.80	13.8	6987	241	182	0.75
13	06	78	13:34	15:00	2590	33330	9200	1640	2.58	10.5	6994	593	520	0.88
13	06	78	13:01	13:35	2703	33884	15500	1640	2.48	8.9	6744	444	390	0.88
13	06	78	16:30	17:04	2481	27383	15100	1840	2.66	10.3	6493	519	780	1.50
13	06	78	16:44	17:20	2481	27383	18000	1840	2.66	11.5	7029	272	832	3.05
13	06	78	17:23	17:54	2489	3426	13800	1940	2.64	10.3	6576	367	312	0.85
13	06	78	10:28	12:43	2761	32086	6000	1140	1.93	9.0	10543	552	572	1.04
14	06	78	13:03	13:26	2768	35681	12000	1740	2.28	7.6	7082	553	832	1.50
14	06	78	13:31	14:05	2753	35681	21000	1740	2.35	6.0	5792	363	390	1.07
14	06	78	16:00	16:30	2477	25171	18000	1440	2.54	5.8	4750	336	156	0.46
14	06	78	16:03	16:49	2425	23649	38000	1340	2.54	5.7	4662	164	910	5.54
14	06	78	16:34	17:10	2534	37894	23500	1440	2.55	5.6	4654	391	260	0.66
20	06	78	12:02	12:43	2375	24479	18000	790	2.22	6.8	6535	651	520	0.80
20	06	78	12:27	13:24	2445	18671	6500	940	2.32	7.0	6232	636	520	0.82
20	06	78	12:53	13:38	2416	21575	29000	840	2.40	7.0	5854	329	338	1.03
20	06	78	16:18	17:26	2454	26830	23500	1590	2.38	8.3	6676	265	312	1.18
23	06	78	12:56	13:23	1965	14660	15500	1240	2.37	5.0	5033	277	338	1.22
23	06	78	13:05	14:32	1854	11064	4100	1240	2.44	5.5	4436	412	286	0.69
23	06	78	17:02	17:55	2327	22820	10500	1340	2.55	9.0	6195	476	624	1.31
27	06	78	15:37	16:38	2495	28075	4700	1690	2.51	9.0	6494	558	234	0.42
27	06	78	16:21	16:57	2495	28075	2000	1640	2.55	8.1	5889	295	390	1.32
27	06	78	17:08	17:39	2474	28628	3200	1740	2.58	8.1	5762	178	416	2.33

*Listing of meteorological and stack conditions for the Sudbury concentration measurements during June 1978. Model predicts the impingement distance x_i and C (predicted).

$$f(X) = \frac{1}{\sqrt{2\pi}} \int_{-\infty}^{p} \exp(-t^2/2)\, dt \tag{18e}$$

$$p = \ln(X/X_i)/\ln s_g \tag{18f}$$

$$X_i = w_* x_i / z_i u \tag{18g}$$

In (18f), the mean impingement distance x_i is the solution of

$$F^{1/3} x_i^{2/3} - w_d x_i + h_s u = 0 \tag{19a}$$

$$w_d = 0.5 w_* \tag{19b}$$

$$s_g = \frac{x_i(w_d = 0.5 w_*)}{x_i(w_d = 0.75 w_*)} \tag{19c}$$

The results form an earlier paper[14] indicate that using a constant value $s_g = 2.0$ yields acceptable model predictions.

In summary, the model uses some of the most recent understanding of dispersion in the convective planetary boundary layer. Furthermore, model predictions have seen compared with field data and the results of the comparison are very encouraging. The model is simple to use and can be used with routinely available meteorological measurements. The mixed layer height can be estimated from temperature soundings. It can also be predicted with simple models such as the one described by Carson and Smith.[16] Similarly, the convective velocity can be related to the solar heat flux or the mixed layer height using formulations described by Venkatram.[17]

References

1. R.G. Lamb, "The effects of release height on material dispersion in the convective planetary boundary layer," Preprint volume, Fourth Symposium on Turbulence, Diffusion and Air pollution, Reno, Nevada, 27 -33., Jan. 15 -18, 1979.

2. G. Briggs, "Plume rise predictions," Lectures on Air Pollution and Environmental Impact Analyses, D.A. Haugen, Editor, AMS, Boston, Mass., 59-105, 1975.

3. J.W. Deardorff, and G.E. Willis, "A parameterization of diffusion into the mixed layer." J. Appl. Met., 14, 1451 - 1458, 1975.

4. G.E. Willis, and J.W. Deardorff," A laboratory model of diffusion into the convective planetary boundary layer," Quart. J.R. Met. Soc., 102, 427 -445, 1976.

5. R.G. Lamb," A numerical simulation of dispersion from an elevated point source in the convective boundary layer, " Atmospheric Enviornment, 12, 1297 - 1304, 1978.

6. B. Davidson, and J. Halitsky," A method of estimating the field of instantaneous ground concentrations from tower bivane data," JAPCA, 7, 316 - 319, 1958.

7. A. Venkatram, and J. Kurtz, "Models to study the impact of large point sources," Preprint volume of the Fourth Symposium on Turbulence, Diffusion and Air Pollution, Reno, Nevada, 79-84, 1979.

8. A. Venkatram,"Dispersion from an elevated source in a convective boundary layer," To appear in Atmospheric Environment, 1979.

9. G.E., Willis, and J.W. Dearorff,"A laboratory study of dispersion from a elevated source within a modeled convective planetary boundary layer," Atmospheric Environment, 12, 1305-1312, 1978.

10. D.J. Moore, "A simple boundary-layer model for predicting time mean ground-level concentrations of material emitted from tall chimneys," Paper presented for ordinary meeting of the institution (Thermodynamics and Fluid Mechanics Group) in London, November 1974.

11. R.G. Lamb,"Mathematical principles of turbulent diffusion modeling," Lectures presented at the International School of Atmospheric Physics, Erice, Sicily, Feb. 1978.

12. J.C. Weil,"Evaluation of the Gaussian plume model at Maryland power plants," Report No. PPSP-MP-16, Martin Marietta Corporation, Baltimore, Maryland, 1977.

13. G.T. Csanady,"Turbulent Diffusion in the Environment," Geophysics and Astrophysics Monographs, D. Reidel Publishing Company, Dordrecht -Holland, 248 pg, 1973.

14. A. Venkatram,"A note on the measurement and modeling of pollutant concentrations associated with point sources," To appear in Boundary-layer Meteorology, 1979.

15. A.M. Neville, and J.B. Kennedy,"*Basic Statistical Methods for Engineers and Scientists*," International Textbook Company, Scranton, Penn., 325 pg, 1964.

16. D.J. Carson, and F.B. Smith,"Thermodynamic model for the development of a convectively unstable boundary layer," Adv. Geophys. 18 A, Academic Press, 111-124, 1974.

17. A. Venkatram,"Estimating the convective velocity scale for diffusion applications," Boundary-layer Meteorology,15, 447-452, 1978.

Discussion:

Nieuwstadt :

How do you take into account in your model when the plume is caught in an updraft and does not reach the ground until very far from the source?

A. Venkatram (response):

The plume impingement probability function does not distinguish between plume segment caught in downdrafts and those caught in updrafts. The only major assumption is that the mean impingement distance is determined by the mean downdraft velocity.

ON THE EFFECTIVENESS OF EXTREMELY TALL STACKS

by

H. G. Fortak
Freie Universität Berlin, Germany

Abstract. The effectiveness of extremely tall stacks is investigated on the basis of absolute maximum ground-level concentrations and, in addition, on the basis of a sensitivity analysis taking into account all relevant parameters for transport and dispersion. It follows, that the effectiveness decreases with increasing stack height. Furthermore, conditions of strong thermal convection are considered. It is shown, that convection must be responsible for the very high concentrations found in inversion layers. For high stacks, this leads to possibly very high concentrations far away from the source.

1. Introduction

There is no doubt about the fact that tall stacks are favourable with regard to effective air pollution protection of its surroundings. However, the investments for building tall stacks increase tremendously with increasing height, whereas the effectiveness of reduction of ground-level concentration decreases faster than linearily. From this point of view, there should exist a certain limiting stack height that represents a reasonable compromise between both effects. On the other hand, most time of the year inversion layers limit vertical dispersion. Therefore air pollution emitted by very high stacks may be trapped in such layers. As a result, receptors far away from the source are affected. Trapping by inversions is enhanced under convective conditions in the atmosphere. In many of such conditions vertical convective transport of air pollution takes place against the concentration gradient. Very high concentrations in the inversion layer develop if convective elements loaded with high concentrations are embeded in that layer. This effect is more pronounced if the sources already emit into layers close to inversion layers. As inversion layers are found around 1.000 meters above the ground, we get an additional reason to limit the height of tall stacks.

Investigations of the effectiveness in the sense mentioned at the beginning can be done by utilizing the well known Gaussian theory. It is believed, that at least the genreal conclusions are correct. The effect of trapping caused by strong convection can be investigated only by solving numerically the extended equation for transport and turbulent diffusion together with proper boundary conditions.

2. Absolute maximum ground-level concentration

As one possible criterion for the effectiveness of tall stacks maximum ground-level concentration is chosen. However, since maximum ground-level concentration varies as a function of meteorological transport and dispersion conditions, the highest of all possible values of maximum concentration is used as a criterion. Such an "absolute" maximum concentration does exist if Gaussian type of simulations are used [1].

Let be

$$S_0(x,y) = \frac{Q}{\pi \bar{U}_1 \sigma_y \sigma_z} \exp\left[-\frac{1}{2}\left(\frac{y^2}{\sigma_y^2} + \frac{H^2}{\sigma_z^2}\right)\right] \tag{1}$$

the well known representation of Gaussian ground-level concentration with dispersion parameters F, G, f, g in

$$\sigma_y = F x^f ; \quad \sigma_z = G x^g \tag{2}$$

effective stack height H, where E is a function of source distance

$$H = h + \Delta h = h + \frac{E}{\bar{U}_2} ; \qquad E = E^* x^{\epsilon} \tag{3}$$

and where vertical mean transport velocity $\bar{U}_1$ and velocity $\bar{U}_2$ for plume rise calculation are obtained from a power law representation of the wind profile according to

$$U(z) = U_A\left(\frac{z}{z_A}\right)^m ; \quad \bar{U}_1 = \frac{1}{MH}\int_0^{MH} dz\, U(z) ; \quad \bar{U}_2 = \frac{1}{N\Delta h}\int_h^{h+N\Delta h} dz\, U(z) \tag{4}$$

then the effective stack height is obtained as

$$H = \frac{1}{N}\left[(N-1)h + \left(h^{m+1} + \frac{N(m+1)\, z_A^m E}{U_A}\right)^{\frac{1}{m+1}}\right] \tag{5}$$

and ground level concentration becomes a function of a large number of parameters:

$$x, y \;\; ; h, Q, E(E^*, \epsilon) ; \; U_A, m, M, N \; ; F, G, f, g$$

in particular it is

$$\bar{U}_1(U_A, m; M, N; h, E) \quad \bar{U}_2(U_A, m; N; h, E) \quad H(U_A, m; N; h, E).$$

Two free parameters M and N are introduced for testing the sensitivity of (1) aganist various processes of averaging the wind profile.

The absolute maximum ground-level concentration is sought in terms of source distance and of wind velocity U_A in anemometer level, i. e.

$$\left.\frac{\partial S_o}{\partial x}\right|_{U_A} = 0 \qquad\qquad \left.\frac{\partial S_o}{\partial U_A}\right|_{x} = 0 .$$

Performing partial differentiation of this type one gets source distance x_{max}

$$x_{max} = \left[\frac{H_{max}}{G\sqrt{2R}}\right]^{\frac{1}{g}} \qquad \text{with} \qquad R = \frac{f+g+\epsilon}{2g} \tag{6}$$

and absolute maximum ground level concentration $S_{o,max}$

$$S_{o,max} = \frac{Q}{\pi(\bar{U}_1)_{max}} \; \frac{\exp[-R]}{FG\; x_{max}^{f+g}} \tag{7}$$

where the following functions have to be introduced

$$(\bar{U}_1)_{max} = \frac{(U_A)_{max}}{m+1}\left(\frac{2\,H_{max}}{z_A}\right)^m \qquad (U_A)_{max} = (2R-1)\,\frac{z_A^m}{h^{m+1}}\,E^* x_{max}^{\epsilon}$$

$$H_{max} = \left[\frac{2R+m}{2R-1}\right]^{\frac{1}{m+1}} h \tag{8}$$

As an example we take one of Briggs plume rise formulae, i. e. [2]

$$E^* = 1.6\,F^{*\,1/3}, \qquad \epsilon = 2/3 \quad : x \leqq 3.5\,x^*$$

$$E^* = 1.6\,F^{*\,1/3}(3.5\,x^*)^{2/3}, \quad \epsilon = 0 \quad : x > 3.5\,x^* \tag{9}$$

$$x^* = 14\,F^{*\,5/8} \;:\; F^* \leqq 55\,; \qquad x^* = 34\,F^{*\,2/5} \;:\; F^* > 55$$

$$F^* = 3.18 \cdot 10^{-6}\,\mathcal{R}\,\Delta T$$

The x-axis represents the physical stack height h[m] ranging from 10^0 = 1 m to 10^3 = 1000 m. The left-hand y-axis represents the absolute maximum ground-level concentration divided by source strength Q. Values range from 10^{-8} to 10^{-3} s/m^3 if Q is measured in mg/s and S_o in mg/m^3. The right-hand y-axis represents source distance x_{max} ranging from 10^1 = 10 m to 10^6 = 1000 km. It is obvious which system of lines belongs to the two vertical axises. As a parameter besides h the heat flux parameter of the effluent gases F* is used. Shown are the results for three stability categories only: class 3 (slightly unstable: f = g = 0,81, F = 0,34, G = 0,27, m = 0,250), class 4 (neutral: f = g = 0,78, F = 0,32, G = 0,22, m = 0,288) and class 5 (slightly stable: f = g = 0,76, F = =,315, G = 0,18, m = 0,325). The curvature of the falling lines (concentration) indicate clearly the decreasing effectiveness of the class of tall stacks. This fact is seen qualitatively. Quantitativ arguments are obtained from sensitivity investigations.

3. Sensitivity analysis

Logarithmic differentiation of (1) and algebraic manipulation leads to a representation of relative changes of ground-level concentration as function of relative changes of all (except ϵ) relevant parameters:

$$
\begin{aligned}
\frac{\delta S_o}{S_o} = {} & \frac{\delta Q}{Q} - \left[1 - \frac{y^2}{\sigma_y^2}\right]\left(\frac{\delta F}{F} + \ln x^f \frac{\delta f}{f}\right) - \left[1 - \frac{H^2}{\sigma_z^2}\right]\left(\frac{\delta G}{G} + \ln x^g \frac{\delta g}{g}\right) - \\
& - A\left[1 - (m+1)B\right]\frac{\delta h}{h} - AB\frac{\delta E}{E} - \left[1 - AB\right]\frac{\delta U_A}{U_A} + \\
& + \left[1 + \ln\left(\frac{z_A}{MH}\right)^{m+1} - AB\left(1 + \ln\left(\frac{z_A}{h}\right)^{m+1}\right) - A\,\frac{NH-(N-1)h}{NH}\ln\left(\frac{h}{NH-(N-1)h}\right)\right]\frac{\delta(m+1)}{m+1} - \\
& - m\frac{\delta M}{M} + \left[1 - B + \frac{h}{H}\right]\frac{\delta N}{N}
\end{aligned}
\qquad (10)
$$

where

$$
A = \frac{H^2}{\sigma_z^2} + m > 0 \quad : x \neq x_{max} \qquad A = 2r + m > 1 \quad : x = x_{max} \qquad (11)
$$

$$
B = \frac{\dfrac{z_A^m E}{U_A}}{H\left[NH-(N-1)h\right]^m} \qquad \frac{H^2}{\sigma_z^2} = 2r = \frac{f+g}{g}
$$

With regard to tall stacks the relative changes of h and E are connected with each other. Given h and E* as well as an "initial situation" determining the factors A and B, equation (10) allows to study the influences on relative changes of ground-level concentration. According to (11) A does not vary significantly with stack height h in the vicinity of maximum ground-level concentration. Further, B is a function increasing with increasing h. Therefore, the factor of the relative change of h is a decreasing function of h itself. This result is in agreement with the qualitative arguments following the discussion of figure 1. A relative increase of E* produces a compensating effect since B increases with h. Numerical calculations however, show that the δh -term is dominating.

4. The effects of strong thermal convection

Oberservations show increasing concentrations of air pollution components with increasing height under conditions which are predominantly convective. This is the case even if the sources are located close to the ground. Due to normal vertical turbulent transport, concentration should decrease with height even in the presence of an inversion in higher layers. Figure 2 reflects the observations. In all parts of this figure, the vertical axis is height above ground. The horizontal axis represents either temperature or relative humidity. Therefore, the vertical temperature profile as well as the vertical profile of relative humidity is illustrated. Among all convective conditions (normal (Normaltyp)), type A (Konvektionstyp A), type B (Konvektionstyp B), and the most instense type (Böentyp) the inversion layer is a layer of highest concentration.

The physical mechanism which produces this effect even if the sources are all in the lowest layers is the following. Organized convection is created fairly close to the ground. Low level convergence (entrainment) collects air pollution which is transported upwards in each individual thermal. A scale-handover mechanism leads to the creation of larger thermals in the middle of the convective layer. Here entrainment is still predominant. Detrainment becomes dominant in the vicinity of the inversion layer where the turbulent downward transport becomes weak. As a result, the statistical properties of rising thermals in connection with its physical behaviour may result in an organized convective vertical transport of air pollution from the ground to an inversion layer. This is a counter-grandient transport which does not violate the second law of thermodynamics.

In order to model this mechanism, the transport equation for concentration S in averaged form, i. e.

$$\frac{\partial \bar{\varrho} \hat{S}}{\partial t} + \nabla \cdot \left[\bar{\varrho} \hat{\mathbf{v}} \hat{S} + \overline{\varrho \mathbf{v}'' S''} \right] = \bar{\varrho} \hat{Q} \tag{12}$$

is averaged over a scale which contains many convective elements. Assuming a flat earth's surface, the averaged vertical velocity vanishes according to the kinematic boundary condition and we get

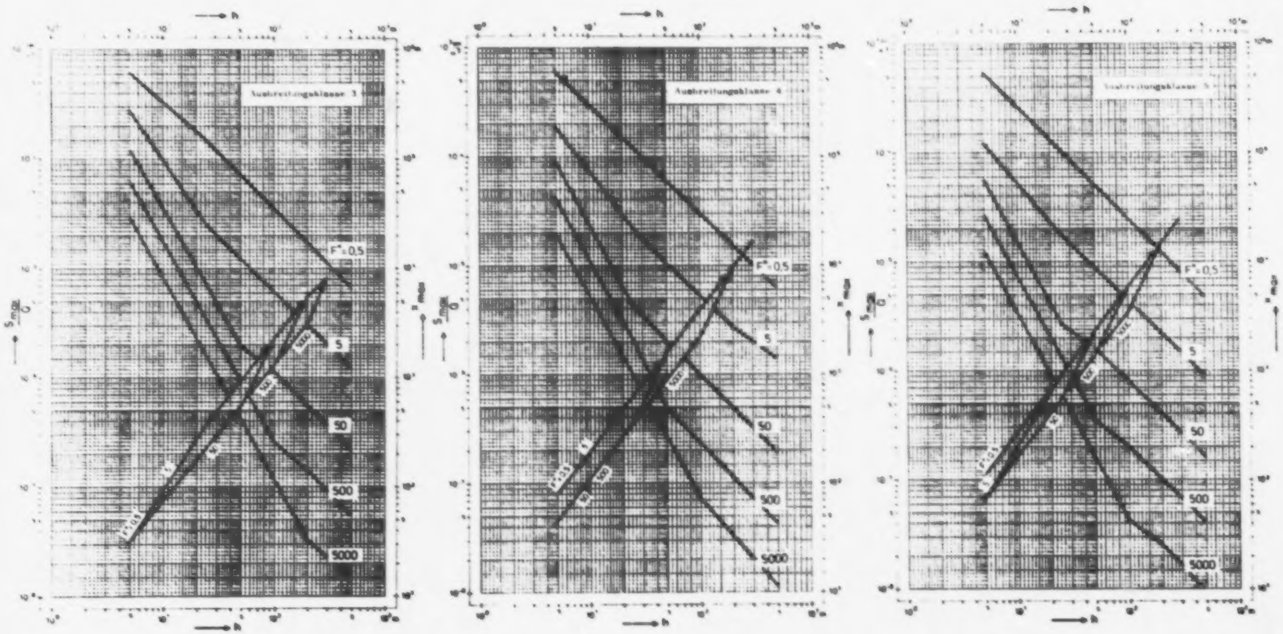

Figure 1. Absolute ground-level concentration and corresponding source distance for three dispersion categories (Turner 3, 4, 5).

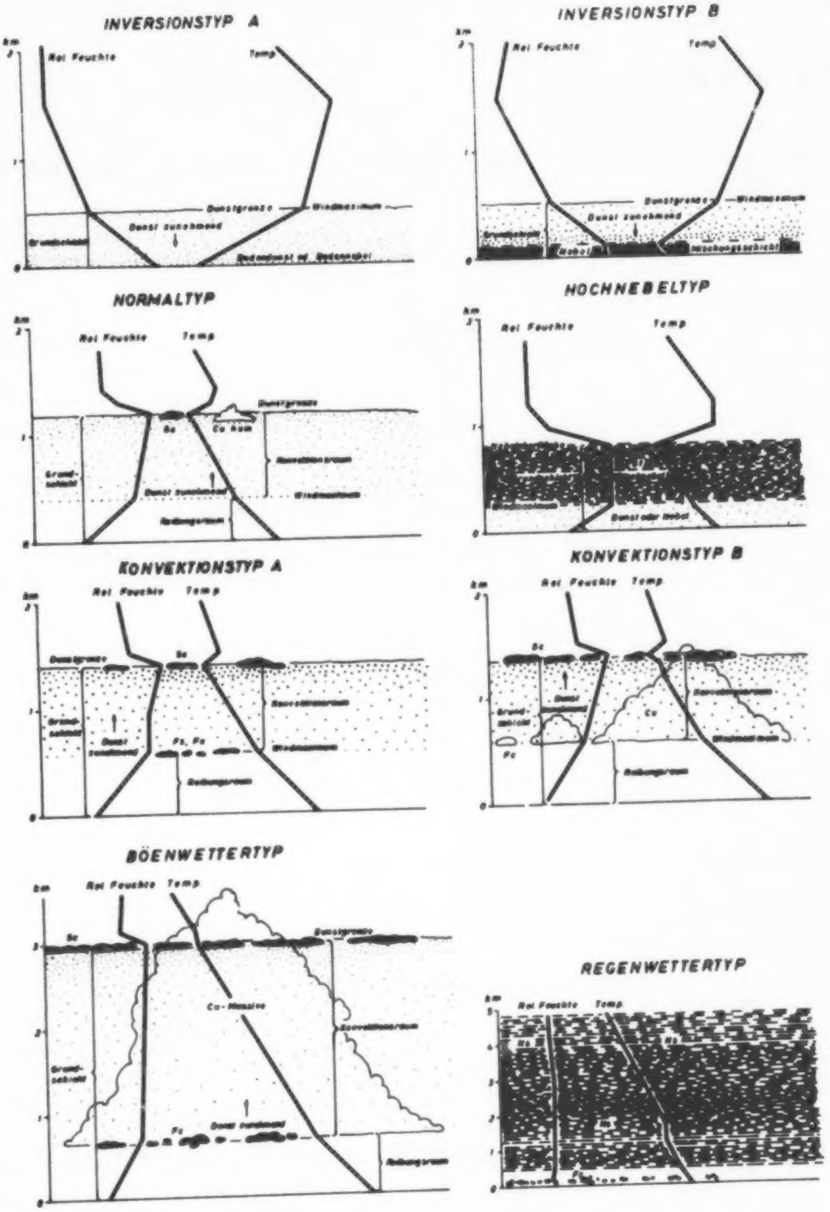
INVERSIONSTYP A
INVERSIONSTYP B
km
Rel Feuchte
Temp
Dunstgrenze
Windmaximum
Dunst zunehmend
Grundschicht
Nebel
NORMALTYP
HOCHNEBELTYP
Sc
Cu hum
Grund-schicht
Dunst oder Nebel
KONVEKTIONSTYP A
KONVEKTIONSTYP B
Fs, Fc
Fc
Cu
BÖENWETTERTYP
Cu-Massive
Fc
REGENWETTERTYP
Ns

Figure 2. Types of frequent atmospheric stratification and corresponding dust layers in the vicinity of temperature inversions.

$$\frac{\partial \bar{\bar{\rho}} \hat{\hat{S}}}{\partial t} + \nabla_h \cdot \left[\bar{\bar{\rho}} \hat{\hat{\mathbf{v}}}_h \hat{\hat{S}} + \bar{\bar{\rho}} \overline{\mathbf{X}}_h \right] + \frac{\partial}{\partial z} \left[\overline{\bar{\rho} \hat{v}_z'' \hat{S}''} + \bar{\bar{\rho}} \overline{X}_z \right] = \bar{\bar{\rho}} \hat{\hat{Q}} \tag{13}$$

where horizontal and vertical turbulent transports are given by

$$\bar{\rho} \overline{\mathbf{X}}_h = \overline{\bar{\rho} \hat{\mathbf{v}}_h'' \hat{S}''} + \overline{\overline{\rho \mathbf{v}_h'' S''}} \qquad \bar{\rho} \overline{X}_z = \overline{\overline{\rho v_z'' S''}} \tag{14}$$

It should be mentioned, that weighted averaging has been applied to both scales.

The vertical advective turbulent transport in (13) is modelled according to

$$\overline{\bar{\rho} \hat{V}_z'' \hat{S}''} \approx \bar{\bar{\rho}} w_c \hat{\hat{S}} > 0 \tag{15}$$

where w_c is a convective vertical velocity due to organized thermal convection. The reasoning leading to assumption (15) is found by modelling thermals and by averaging over sufficiently large areas. Clearly, w_c is a function of height above the ground.

A simple model may demonstrate the effects in question. Under steady-state and two-dimensional conditions equation (14) reads as

$$\frac{\partial}{\partial x} \left[\bar{\bar{\rho}} \hat{\hat{U}} \hat{\hat{S}} + \bar{\bar{\rho}} \overline{X}_x \right] + \frac{\partial}{\partial z} \left[\bar{\bar{\rho}} w_c \hat{\hat{S}} + \bar{\bar{\rho}} \overline{X}_z \right] = 0 \tag{16}$$

with area sources at x = 0 only.

Let be

$$\overline{T}_x = \bar{\bar{\rho}} \hat{\hat{U}} \hat{\hat{S}} + \bar{\bar{\rho}} \overline{X}_x \qquad \overline{T}_z = \bar{\bar{\rho}} w_c \hat{\hat{S}} + \bar{\bar{\rho}} \overline{X}_z \tag{17}$$

the components of the total transport vector

$$\overline{\mathbf{T}} = \mathbf{i} \overline{T}_x + \mathbf{k} \overline{T}_z \qquad \nabla_2 \cdot \overline{\mathbf{T}} = 0 \tag{18}$$

it is obvious, that a "stream-function" ψ according to

$$\overline{\mathbf{T}} = -\mathbf{j} \times \nabla_2 \psi \quad ; \quad \overline{T}_x = -\frac{\partial \psi}{\partial z} \quad , \quad \overline{T}_z = \frac{\partial \psi}{\partial x} \tag{19}$$

fullfills equation (16).

The proper boundary conditions are the following:

$$\begin{aligned}
x = 0: &\quad \overline{T}_x = \bar{\bar{\varrho}}\,\hat{\hat{U}}\,\hat{\hat{S}} + \bar{\varrho}\,\overline{X}_x = -\frac{\partial\psi}{\partial z} = F(z) \\
x \to \infty: &\quad \overline{T}_z = \bar{\bar{\varrho}}\,w_c\,\hat{\hat{S}} + \bar{\varrho}\,\overline{X}_z = \frac{\partial\psi}{\partial x} = 0 \\
z = 0: &\quad \overline{T}_z = \cdots\cdots\cdots\cdots = \frac{\partial\psi}{\partial x} = 0 \\
z = H_I: &\quad \overline{T}_z = \cdots\cdots\cdots\cdots = \frac{\partial\psi}{\partial x} = 0\,.
\end{aligned} \tag{20}$$

Integrating the boundary condition at x = 0 and defining the upper boundary (inversion) by $\psi(0,H_I) = 0$ we get, instead of (20),

$$\begin{aligned}
x = 0: &\quad \psi(0,z) = \int_z^{H_I} dz\, F(z) \\
x \to \infty: &\quad \frac{\partial\psi(x,z)}{\partial x} = 0 \\
z = 0: &\quad \psi(x,0) = \int_0^{H_I} dz\, F(z) = C \\
z = H_I: &\quad \psi(x,H_I) = 0\,.
\end{aligned} \tag{21}$$

Now it can be shown that the "stream-function" ψ fullfills the same equation (16) as S does if one assumes

$$\overline{X}_x = -K_H \frac{\partial\hat{\hat{S}}}{\partial x} \qquad \overline{X}_z = -K_z \frac{\partial\hat{\hat{S}}}{\partial z} \tag{22}$$

Here $K_H = K_H(z)$, $K_z = K_z(z)$, $\hat{\hat{U}} = U(z)$ and $w_c = w_c(z)$. After having solved (16) for ψ together with boundary conditions (21) numerically, concentration $\hat{\hat{S}}$ is obtained from

$$\bar{\bar{\varrho}}\,\hat{\hat{U}}\,\hat{\hat{S}} - \bar{\bar{\varrho}}\,K_H \frac{\partial\hat{\hat{S}}}{\partial x} = -\frac{\partial\psi}{\partial z} \qquad \bar{\bar{\varrho}}\,w_c\,\hat{\hat{S}} - \bar{\bar{\varrho}}\,K_z \frac{\partial\hat{\hat{S}}}{\partial z} = \frac{\partial\psi}{\partial x} \tag{23}$$

The "initial condition" at x = 0 is of a line source type according to

$$F(z) = \frac{q}{\sqrt{2\pi}\,\sigma} \exp\left[-\frac{(z-H)^2}{2\sigma^2}\right] \quad ; \quad \int_0^{H_I} dz\, F(z) = C = Q \tag{24}$$

with small values of σ and centered at the effective height H of a source. The factor q is chosen such that $C = Q$.

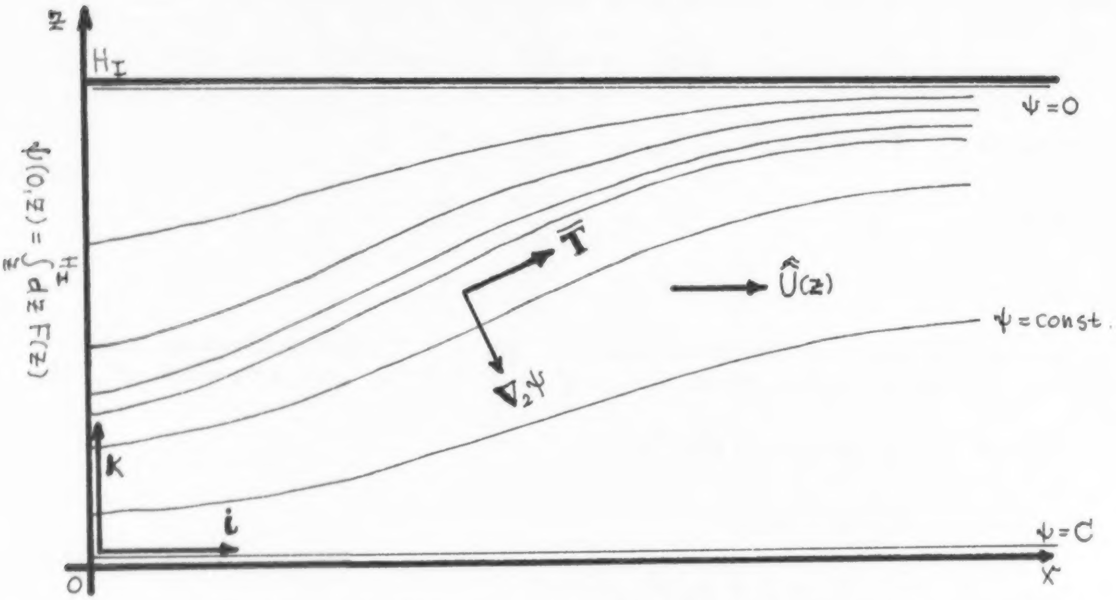

Figure 3. The domain of integration, boundary conditions and total transport vector

Numerical values used in one typical numerical experiment are: $Q = 1$ kg/ms, $\sigma = 50$ m, $H_I = 1000$ m. In addition mean values of $\hat{U}$, K_H and K_z were $\hat{U} = 3$m/s, $\tilde{K}_H = 50$ m^2/s, $\tilde{K}_z = 50$ m^2/s. Mean values for w_c ranged between $\tilde{w}_c = 0$ to $\tilde{w}_c = 23$ cm/s, effective stack heights between $H = 200$ m to $H = 900$ m.

In the following figures 4 and 5 the uppermost "stream line" $\psi = 0$ is located at ($H_I = 1000$ m). The one at the earth's surface is given by $\psi = 1,0$, not shown in the figures itself since heights below 100 m were not included in the figures. Spacing between the lines is 0,1. In both cases, $w_c = 0$ represents the pure influence of reflecting barriers at both boundaries. Equal spacing of the ψ-lines for large x means that concentration is independent of height above the ground. Cases with $w_c > 0$ show increasing gradients of the ψ-fields with height. This means increasing total transport of air pollution components. It should be mentioned, that all vertical distributions for equal w_c-values are identical at $x \to \infty$ whatever the emission height H was.

References

1. H. G. Fortak, "Absolute Imissionsmaxima im Lee einer Punktquelle". Fortschrittberichte der VDI-Zeitschriften, Reihe 15, Nr. 14, Düsseldorf, 1979.
2. G. A. Briggs, "Discussion of chimney plumes in neutral and stable surroundings". Atmos. Environ., 6, 1972.

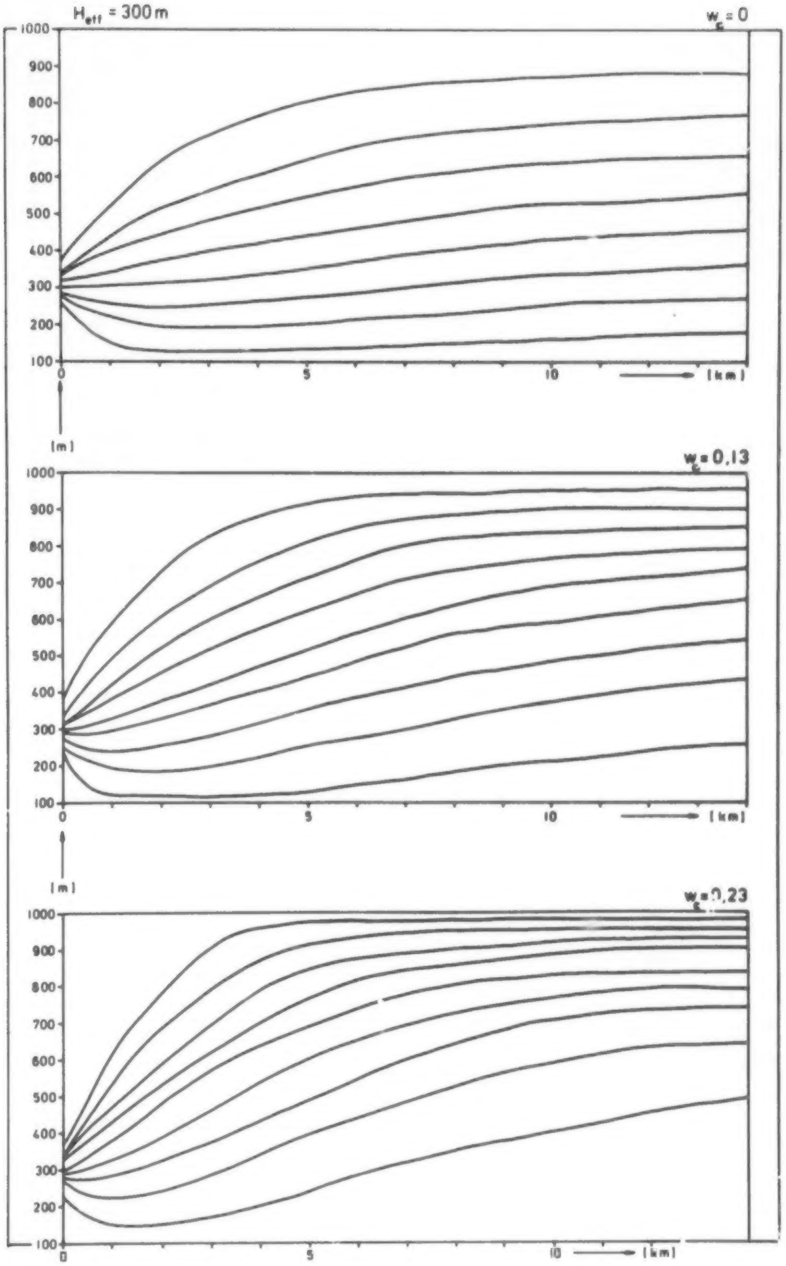

Figure 4. Result of numerical integration of equ. (16) for different convective vertical transport velocities w_c. Represented are "stream lines" ψ. Emission height is H = 300 m.

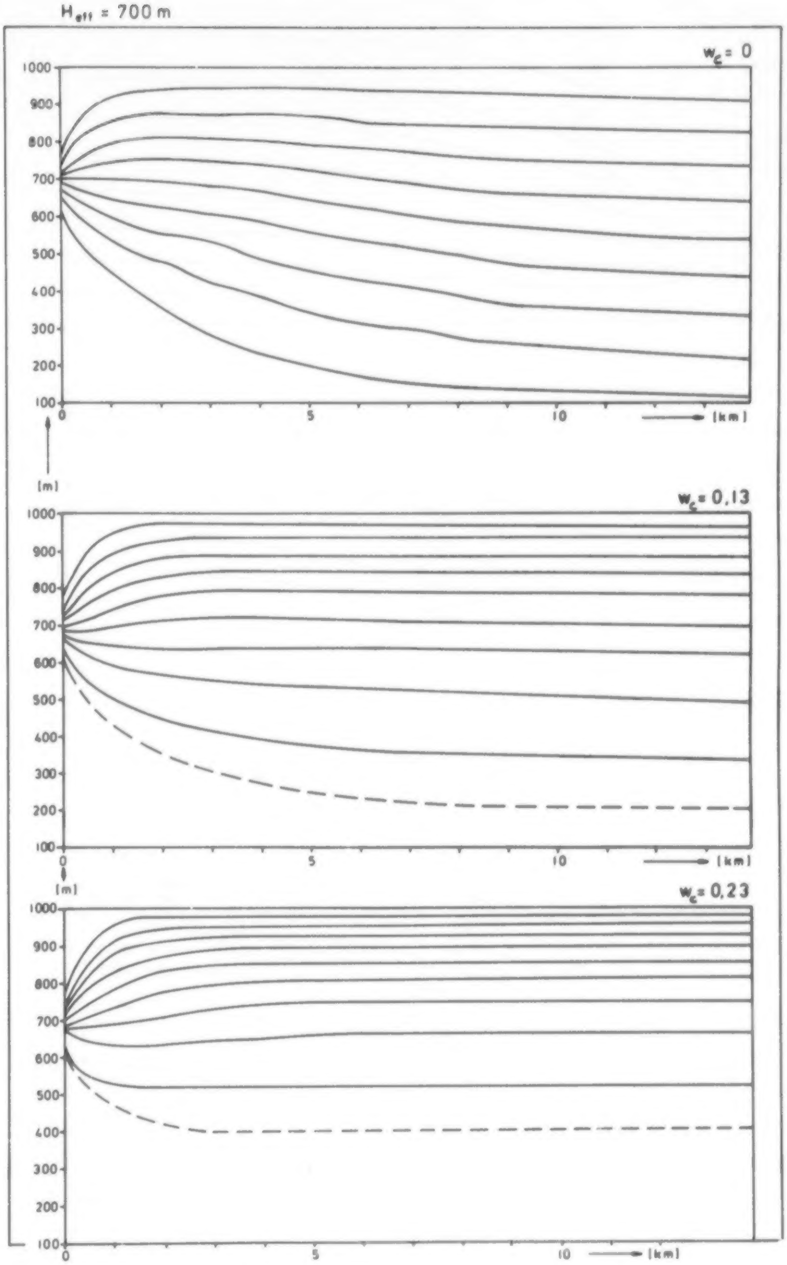

Figure 5. Same as figure 4. Emission height is H = 700 m.

Discussion:

Fronza:

You detected a "saturation effect" for the usefulness of tall stacks. That is proportional to the square root of the maximum concentration reduction. You showed the effect by sensitivity and analysis on dispersion models by showing the percentage of concentration reduction corresponding to the percent enhancement of stack height. Do you plan to collect experimental evidence of this effect by analyzing concentrations from tall stacks of different heights?

Fortak (response):

Yes! However, not on the basis of ground-level concentrations alone but utilizing an instrumented aircraft. This was done in connection with sulfur reduction measures at Wilhelmshaven power station (stack height 275 m). There plume rise was investigated as a function of varving gas exit temperatures. Low level flights are planned for the near future.

DISPERSION OF POLLUTANTS FROM TALL STACKS STUDIED BY REMOTE SENSING TECHNIQUES DURING EEC JOINT CAMPAIGNS

by

P. Guillot
Environment and Raw Materials Research Programmes
Commission of the European Communities
200 rue de la Loi
1049 Brussels Belgium

Abstract. The Commission of the European Communities with the help of national energy producers in EEC States organized joint campaigns to study the pollution dispersion around large sources of SO_2 and NO_x by a variety of remote sensors, measuring simultaneously meteorological parameters and pollutants concentrations in the boundary layer. Three campaigns have been achieved, one is planned for September 1979, gathering fifteen to twenty teams for about ten days to measure the pollutants distribution at distances up to 30 km from the stacks with ground based equipment, fixed or mobile. These sets of measurements have been proved useful for following the temporal and spatial variations of the pollution dispersion and estimating the chemical transformations of NO_x. Some examples from these campaigns are given and prospects for future campaigns are discussed.

Introduction

Since nearly a decade, new techniques and equipment for measuring air pollutants amounts and concentrations at a distance from ground level have been existing and demonstrated in many occasions and countries. At the European level the Commission of the European Communities encourage these remote sensing techniques since 1973 through :

- either a "direct action" research performed at the Joint Research Centre of the CEC at Ispra (I)
- or an "indirect action" research achieved by national laboratories under contracts partially funded by the CEC.

This research and development of new equipment and techniques was complemented by field campaigns of measurements of pollution dispersion aiming at :

1) checking in real conditions the performances and reliability of equipment already tested in laboratory conditions
2) assessing the limits and drawbacks of these techniques which cannot be deduced from laboratory tests
3) studying practical situations of pollution around large sources to understand the mechanisms of the dispersion of pollutants in relation to a variety of meteorological parameters
4) supplying data in the three dimensions to check the predictions of models of pollution dispersion

Preceding page blank

Last but not least these campaigns were also felt as a good opportunity to encourage cooperation to exchange information and technical knowledge between laboratories teams from European Countries who were already experienced in these techniques or were interested in using them.

For these campaigns it was necessary to dispose of a large source of air pollutants like SO_2, NO_x, particulates of which the emission flow-rate would be as constant as possible and known or monitored by another way. Ideally this source should be isolated from any other source in a rather flat terrain with stationary meteorological consitions in order to have time enough for repeated measurements. Although these conditions were not all met in any campaign, three campaigns were achieved : the first (1975) in France around a gas plant at Lacq, the second in England at Drax around an electricity power plant (1976) and the third one at Cordemais (France, 1977) around an electricity power plant. All these plants are emitting regularly amounts of SO_2 of some hundreds of metric tons per day through tall stacks to disperse it in the atmosphere. With the help of the managers of the plants who maintained the emission conditions rather steady during the measurements and supplied all the necessary informations on the emission, in a rather short period of ten days during which about 80 to 100 people were measuring a huge variety of parameters, it was possible to accumulate data and information in order to meet the different objectives.

The general results of these campaigns have been or will be published and only some interesting examples are given[1,2,3,4,5] to illustrate the advantages of such campaigns.

Simultaneous measurements of the total vertical burdens

The benefits of making simultaneous measurements at different distances from the source with three apparatus mounted in vans running along parallel roads are illustrated in figures 1 and 2, (results of the Lacq campaign[2]). These drawings show the variations of the total burden of SO_2 measured in a vertical cylinder of 1 m^2 section above the apparatus moving to and fro along one of the three roads, during the morning and then the afternoon of one day. Clearly in the afternoon there was an accumulation of SO_2 above one valley above the middle road, route G, due to particular meteorological phenomena occurring in a restricted atmospheric volume, a local fumigation process due to the orographic situation and the solar heating. This evidence would not have been possible with one apparatus only because of the time necessary to run along long distances.

Measurements of the plume width and height

By comparing results from meteorological soundings and from Lidars scanning the height of the aerosols plume, one can follow the plume trajectory at different distances from the stack at different times in relation with the height of the temperature inversion layers ; figure 3 compares the measurements and the theoretical plume trajectories (results of the Drax campaign[3]) in two different conditions of the same day early in the morning when the plume is above the inversion layer and later when the inversion layer has lifted up and mixed with the plume. Figure 4 indicates how the lifting of the inversion layer during the day influences the height of the plume (results of the Cordemais campaign[5]). These simultaneous measurements with different Lidars are very fruitful to follow the plume changes. In future it will be possible to compare the aerosols plume and the SO_2 plume using an UV Lidar for SO_2 ; these two plumes might be quite separate.

Figure 5 shows the increase of the σ_y of the plume with the distance from the stack measured in different stability conditions compared to theoretical curves from Pasquill-Turner.

Chemical conversion of NO into NO_2 in the plume

Because of the high temperature of the burner practically only NO is emitted from the chimneys.When the emission conditions of the plant and the meteorological conditions are stationary, the simultaneous measurements of the total NO_2 vertical burden in the plume at increasing distances from the source allow to calculate the velocity of transformation of NO into NO_2 in the plume. Figure 6 shows the increase of NO_2 burden in the plume which doubles within about 7 km downwind from the stack that is in about 50 minutes at noon, on a warm and sunny day (results from the Cordemais campaign[5]).

Conclusions and prospects for future campaigns

These joint campaigns which assemble for a rather short time a large variety of instruments and teams for a detailed study of a real field situation of pollution dispersion are very fruitful for all participants provided that :

1) the teams and equipment are selected to complement each other and cross check their results
2) the campaign plans are prepared and discussed with the active collaboration of the manager of the pollution source to be studied
3) the meteorological parameters are carefully monitored as often as possible up to 1500 m above the area where the remote sensors are surveying the pollution. This is often the most difficult condition to meet, specially when the meteorological situation is changing very rapidly during the surveys.

Up to now only the pollution dispersion from power plants stacks have been studied for practical organisation reasons. For future campaigns more complicated emission conditions and/or dispersion conditions (orographic, meteorological) as well as physicochemical transformations between air pollutants can be studied by this combination of remote sensing techniques and other point sensors which increases the usefulness of both results. It is also hoped that future campaigns can extend the geographical origin of the teams to countries other than EEC States.

References

1. P. Guillot, "Joint European Community campaign on remote sensing of SO_2 pollution from a gas plant at Lacq. Proceedings of the 4th Joint Conference on sensing of Environmental Pollutants, New Orleans, 1977".
Published by the American Chemical Society 1978

2. P. Guillot, G. Bonometti, H. Hasenjaeger, A. van der Meulen, P.M. Hamilton, R. Haulet, J. Laurent, S. Sandroni, C. Cerutti, G. Giovanelli, T. Tirabassi, O. Vittori, P. Piccinini "Atmospheric Environment 1979, 13, 895-917
First European Community campaign for remote sensing of atmospheric pollution, Lacq (France) 7-11 July 1975"

3. P.M. Foster, S. Sutton, R.H. Varey,
"Lidar measurements on the plume at Drax. Report RD/L/N53/78, August 1978. Central Electricity Research Laboratories, Leatherhead, Surrey (UK)"

4. R.A. Scriven, "Measurement of air pollution at Drax during the 1976 CEC remote sensing campaign. Report RD/L/R 1984. Central Electricity Research Laboratories, Leatherhead, Surrey, (UK)"

5. M.C. Robé-Naudy, "Etude de la pollution en oxydes d'azote et dioxyde de soufre d'un site industriel" Thèse Doctorat 3ème cycle présentée le 26 janvier 1979 à l'Université Paris VII - Paris (F).

FIG. 1

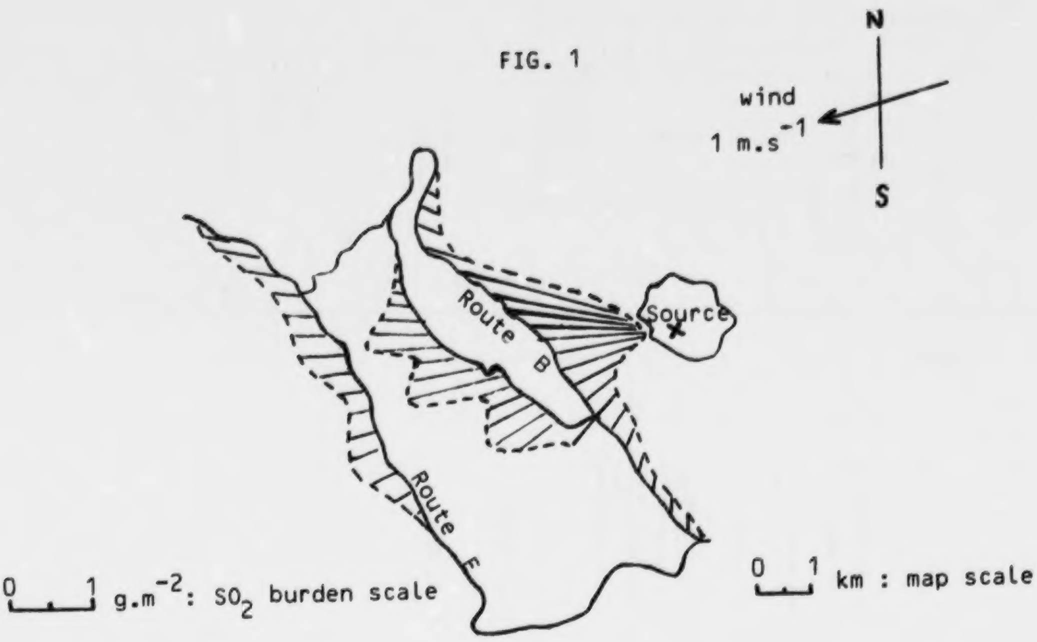
N
wind
1 m.s^{-1}
S
Source
Route B
Route E
0 1 g.m^{-2}: SO_2 burden scale
0 1 km : map scale

Simultaneous measurements of SO_2 burdens on morning of 9th July 1975 at Lacq, on three routes. The hatched areas are proportional to the total SO_2 over the route.

FIG. 2

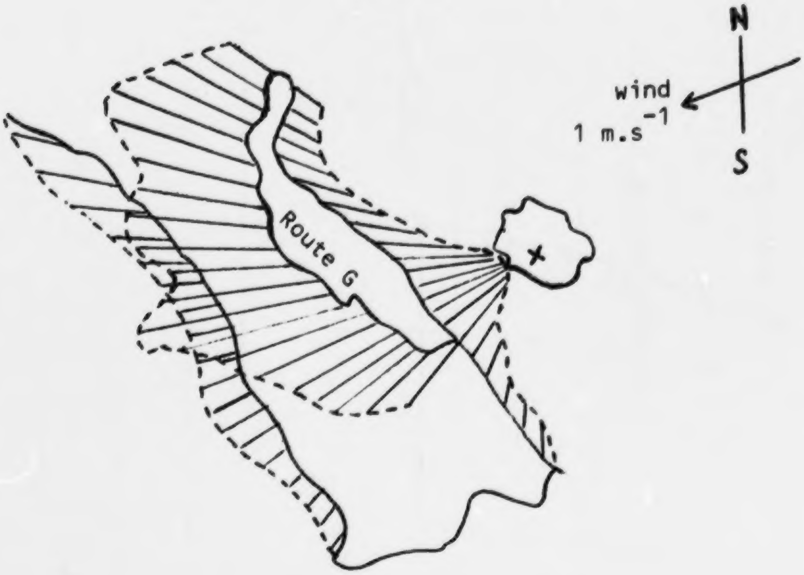
N
wind
1 m.s^{-1}
S
Route G

Same as figure 1, but measurements on afternoon of 9th July at Lacq. Over the route G, there is an accumulation of SO_2 three times bigger than over B and E.

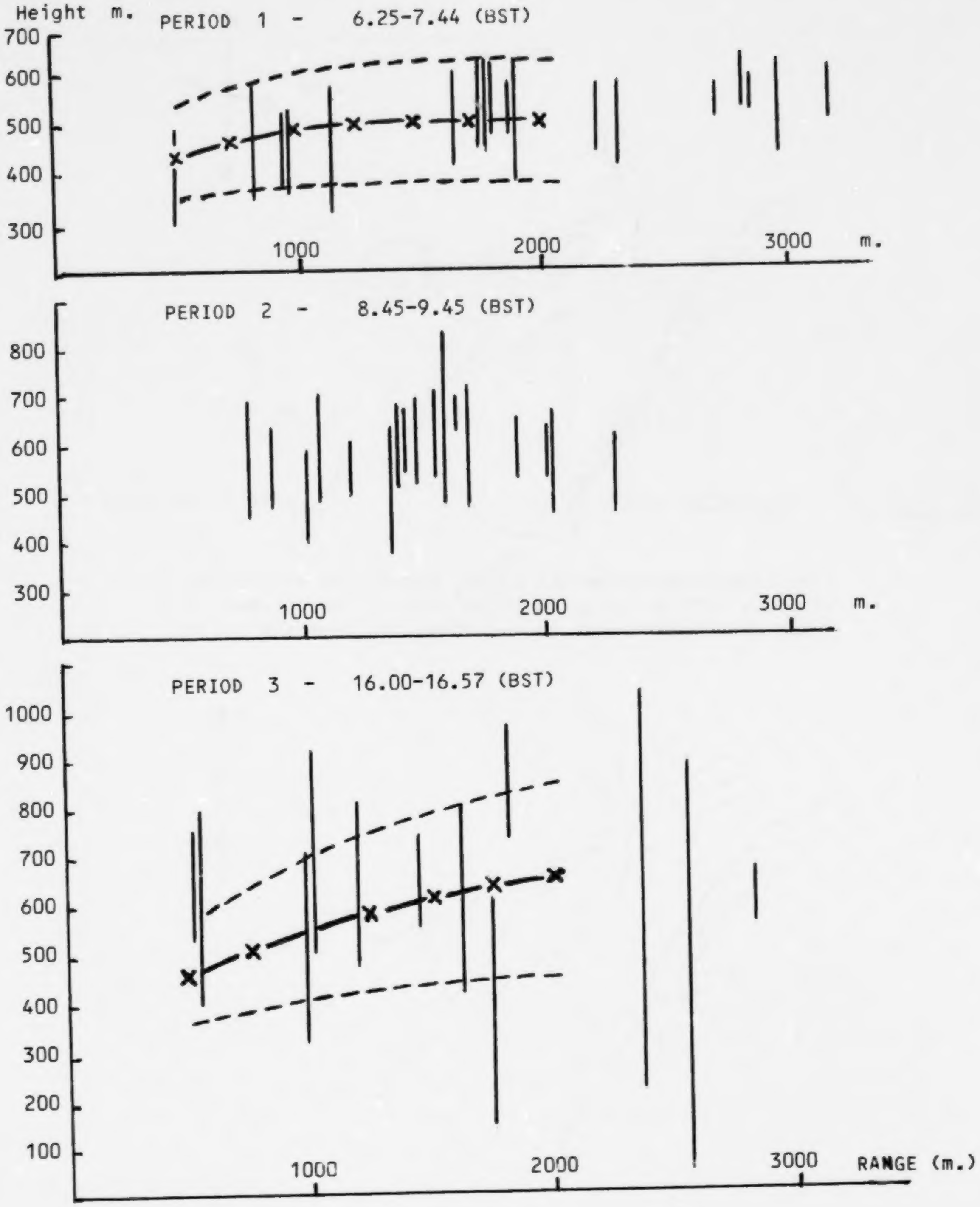

FIG. 3

Vertical plume dimensions measured at Draxon 13th September 1976

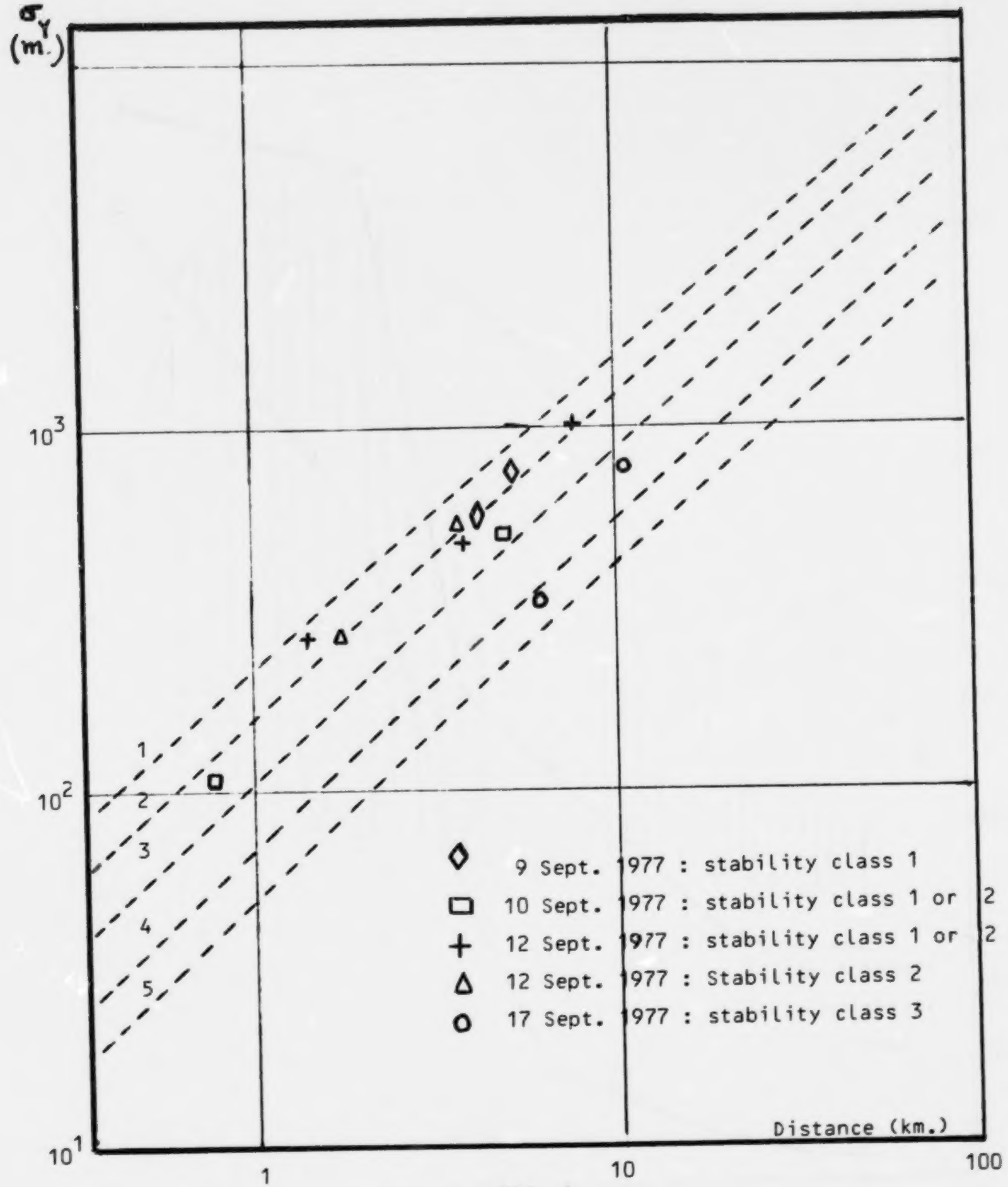

FIG. 4

Standard deviation σ_y of the plume measured at Cordemais as a function of the distance to the stack.

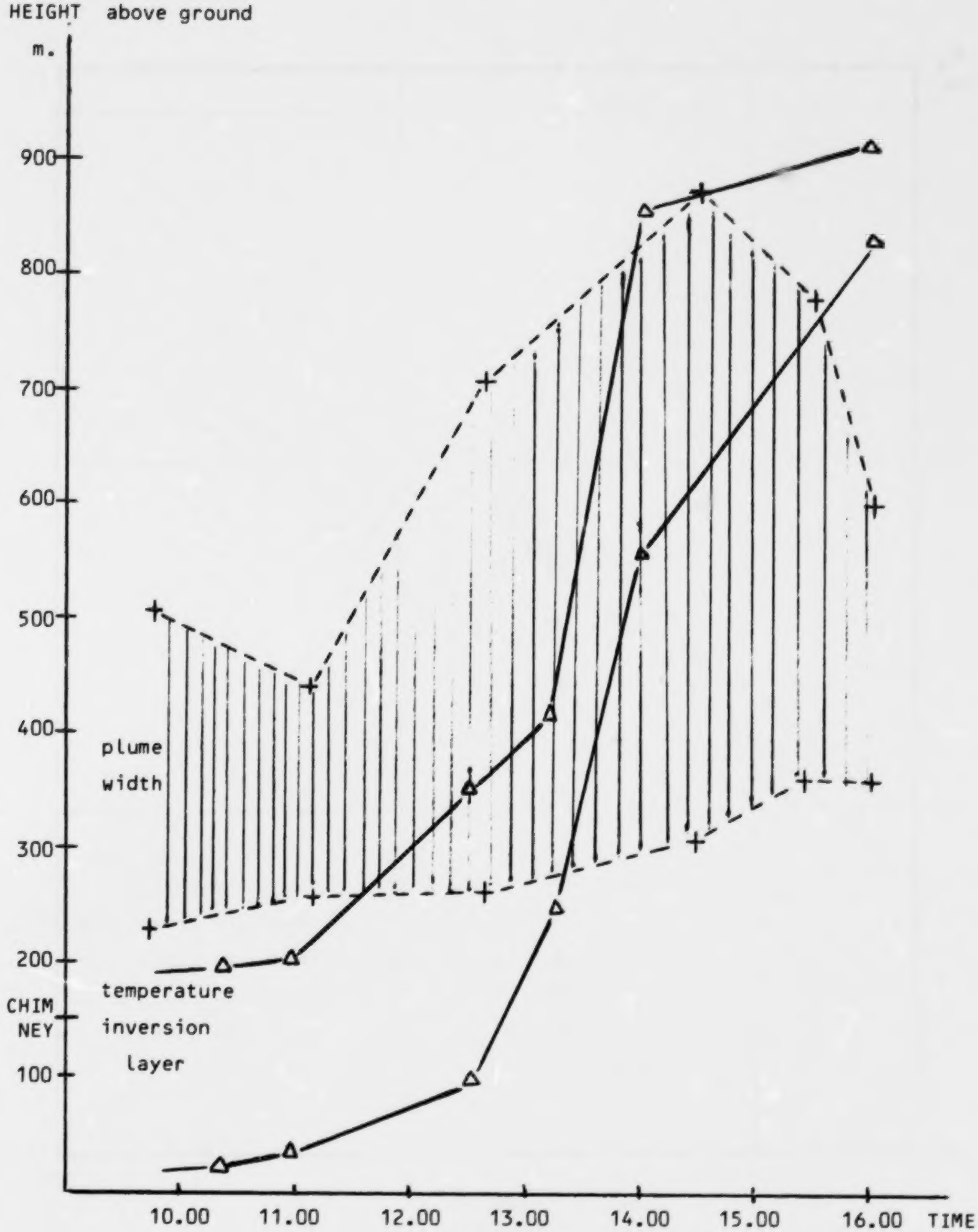

FIG. 5

Vertical plume width measured by Lidars at Cordemais on 12 September 1977

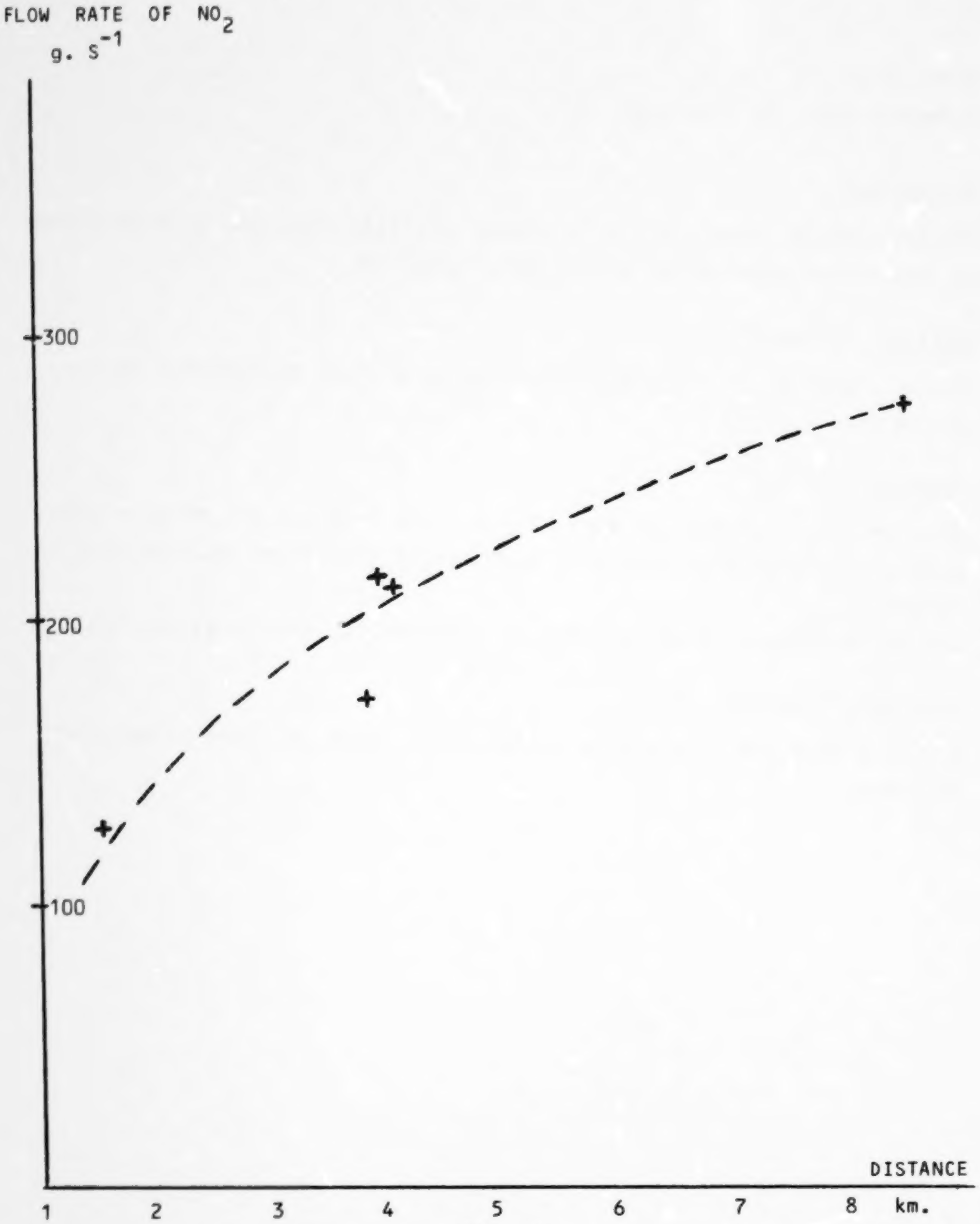

FIG. 6

Measured flow rate of NO_2 at Cordemais on 12th Sept. 1977 from NO.

Discussion
(Rapporteur: A. Venkatram)

Nieuwstadt:

Remote sensing gives you instantaneous profiles. How do you relate them to hourly averages which are normally required?

Guillot (response):

You can combine instantaneous profiles to produce approximate hourly averages.

Bénarie:

Your results indicate the mass flux derived from one of profiles measured in the same time period is much larger than those derived from the others.
Can you explain this discrepancy in relation to mass conservation.

Guillot (response):

I cannot give you an explanation but this seemed to happen from time to time.

EXPERIMENTAL INVESTIGATION OF ATMOSPHERIC SULFUR TRANSPORT AND TRANSFORMATION IN THE STATE PROGRAM

Francis A. Schiermeier*, Francis Pooler*, Noor V. Gillani[1],
John F. Clarke*, Jason K.S. Ching*, and William E. Wilson

Environmental Sciences Research Laboratory
Environmental Protection Agency
Research Triangle Park, North Carolina 27711

[1]Department of Mechanical Engineering
Washington University
St. Louis, Missouri 63130

*On assignment from the National Oceanic and Atmospheric Administration.

Abstract

Spurred by the rising sulfate concentrations in the northeastern United States, the EPA has established the Sulfur Transport and Transformation in the Environment (STATE) program to quantitatively determine the impact on local air quality of distant source pollutants and their transformation products. The first major STATE field study was the August 1978 Tennessee Plume Study conducted near the Cumberland Steam Plant in northwestern Tennessee. Representatives from 25 governmental agencies, universities, research institutes, and private contractors participated in this joint meteorological/chemical study in an attempt to define plume transport, dispersion, transformation, and removal rates under various meteorological conditions. Included herein are some examples of the types of meteorological and plume chemistry measurements collected during the field study.

Introduction

During recent years, air pollution scientists have become increasingly concerned with the high ambient sulfate concentrations observed in the northeastern quadrant of the United States. The recent formulations of national energy goals, which advocate a shift from oil and natural gas to more abundant coal as a fuel source for electrical generating stations and industrial plants, are likely to result in even higher ambient levels of sulfur oxides, nitrogen oxides, and other pollutants. There is growing awareness in the scientific community that these pollutants, particularly fine particle sulfates and nitrates, may be transported over long distances without appreciable loss by removal processes.

In an attempt to quantitatively determine the impact of emitted pollutants and transformation products from distant sources on local air quality, the Environmental Sciences Research Laboratory (ESRL), a division of the EPA's Office of Research and Development (ORD), initiated the Sulfur Transport and Transformation in the Environment (STATE) program. Combining the disciplines of meteorology and chemistry, the STATE program will examine the relationships between source emissions of sulfur oxides and the high sulfate levels of the northeastern United States.

The STATE program includes two kinds of studies, delineated by consideration of the scale at which pollutant plumes from discrete sources or source complexes can be distinguished from one another.

- Plume studies, encompassing travel distances up to several hundred kilometers, have the objective of quantifying spatial distributions and physico-chemical forms of pollutants from identifiable single sources by means of studies of dispersion, transformation, and removal processes acting on emitted pollutants.
- Regional studies, encompassing areas up to sub-continental scale, have the objective of quantifying the cumulative impact on local air quality of the many discrete sources contributing to the pollutant loading of an air mass as it moves over source regions.

Tennessee Plume Study

The first major field experiment performed under STATE auspices was the August 1978 Tennessee Plume Study (TPS)[1]. In cooperation with the Tennessee Valley Authority (TVA), this study was conducted in the area surrounding the Cumberland Steam Plant in northwestern Tennessee (Fig. 1). The field effort was designed to characterize the plume from a coal-fired power plant during summertime conditions of strong daytime mixing, strong sunlight intensi high frequency of nocturnal inversions, and significant background levels of r active pollutants. This study, by concentrating on a single plume several hundred kilometers nominally upwind of the northeastern United States during the summer season, pursued the first STATE objective.

The Cumberland Steam Plant possesses a generating capacity of 2600 MW fro two 1300 MW boilers, each connected to its own 305 m stack by three ducts. The coal supply nominally contains 3% sulfur and is fairly homogeneous, being mined from a single seam. As part of its existing air quality programs, TVA conducts an extensive pollutant monitoring and meteorological forecasting program in the Tennessee Valley, encompassing the Cumberland Plant.

To more particularly meet the objective of quantifying plume characteristics and compositional changes, a basic study design made up of four principal scenarios was developed. Taken together, these scenarios cover the complete diurnal range of ambient conditions to which plumes are subject. For each scenario, chemical sampling of plume constituents was planned in a Lagrangian frame in order that changes within an identifiable plume segment could be measured. An extensive turbulence and boundary layer structure measurement program was developed so that plume dispersion and associated constituent changes could be related to meteorological causes.

The objective of Scenario 1 was to describe the vertical mixing process and dispersion rate during conditions of rapid convective mixing by sampling t distances of approximately 50 km downwind as the plume became vertically well mixed. Scenario 2 was designed to quantify horizontal plume spreading by nocturnal wind shear as well as to measure "second-day" chemical changes within the previously well mixed plume. By following the same plume segment emitted during convective conditions through the night to distances of 300-500 km, this scenario also provided data for long range trajectory model verification.

The objective of Scenario 3 was to document and parameterize plume dispersion from an elevated source under stable conditions out to approximately 400 km. The experimental period began during early evening and continued past inversion breakup the following morning until about noon. Scenario 4 was intended to describe the vertical and lateral rates of dispersion of a plume segment initially released above a developing mixed layer, subsequently becoming well mixed in the convective boundary layer, and finally restabilizing during the development of a nocturnal stable layer with attendant directional shears.

For the daytime portions of the scenarios, two component programs were included to better define the boundary layer turbulent structure and energy inputs. The first of these was an aircraft turbulence program to determine the mean/turbulent wind, temperature and moisture structures and the variations of the surface and planetary boundary layers in the plume transport area, which was characterized by non-uniform, non-homogeneous terrain. In addition, these experiments observed the values of and relationships between Eulerian and Lagrangian turbulence scales. The second component program utilized an aircraft with upward and downward sensing radiation instruments. Solar and longwave radiation measurements obtained over various land use areas, when combined with the turbulent flux measurements, will provide estimates of the boundary layer energy balance. In-plume measurements were also obtained to determine the amount of radiation depletion by plume pollutants.

During the last few days of the study, the Lagrangian orientation of the scenarios was changed to Eulerian. Sets of plume chemistry measurements were made at constant distances downwind of the plant to sample the diurnally ranging effects of ambient meteorological and background pollutant conditions at approximately the same plume travel times.

Measurement Plan

The TPS was a coordinated study, with the primary emphasis that measurements from each of the sampling platforms be designed to supplement and reinforce those of other platforms. In this manner, sufficient meteorological data were collected to define plume transport and dispersion, and appropriate chemical measurements were made to determine pollutant transformation and removal rates.

Three chemical-sampling aircraft, fully equipped to measure a variety of plume chemical and meteorological parameters, participated in the performance of all four scenarios and the plume chemistry missions. Surface chemical and meteorological measurements were simultaneously obtained by instrumented vans which operated in both mobile and stationary modes. Specially instrumented aircraft were deployed to measure the mean and turbulent structure and energy budgets in the time dependent planetary boundary layer, and the intensity of radiation in and around the plume.

Remote sensing played an important role in the TPS. A correlation spectrometer mounted in a mobile van monitored overhead SO_2 and NO_2 burdens. A mobile ground-based lidar and an airborne lidar were instrumental in providing real-time plume geometry and mixing depth determination. Acoustic echo sounders obtained remote measurements of the diurnal variation of the mixed layer.

In order to mark discrete plume segments for downwind Lagrangian sampling by airborne and surface measurement vehicles, three methods were utilized. The first involved the insertion of transponder-equipped tetroons (tetrahedral balloons) into the plume near the Cumberland stacks, either individually or in vertical "stacks" of two to four, depending on the scenario being performed. A second tracking technique consisted of inserting a manned balloon into the plume to serve not only as a location reference, but also to monitor pollutants in the same plume segment as it moved downwind. The third plume marker consisted of one to three hour releases of SF_6 into the Cumberland stack(s). This comprised the most reliable plume identification technique since the tracer gas exited along with the plume. SF_6 was measured in both real-time and by subsequent analysis of grab samples.

Upper-air meteorological support for both real-time planning purposes and for subsequent data analyses was provided by TVA personnel and by the National Weather Service. During operation of TPS scenarios and missions, radiosondes were released and tracked at 3-hr intervals at the TVA New Johnsonville Steam Plant, located 50 km southwest of Cumberland. Simultaneously, a double theodolite pibal team operated at the Cumberland Plant and three mobile single theodolite pibal teams were available for dispatch contingent on plume position. Extra rawinsondes were released from nearby National Weather Service stations to provide soundings at 6-hr intervals during the month of the study.

In fulfillment of a quality assurance program, an independent contractor performed on-site configuration, procedures, and performance audits of several of the TPS measurement platforms and related ground monitoring stations. In an effort to determine emission rates from the Cumberland stacks, TVA recorded operational parameters and performed frequent coal analyses while stack gas measurements were independently performed by EPA contractors.

Data Reduction and Analysis

The TPS data base is maintained at Washington University in St. Louis. After preliminary on-site field review of the data to ensure the proper working order of sampling instrumentation, off-site detailed data validation and compilation were performed upon completion of the field study. Compilation of the data base included creating backup tapes, automatic error checks, appropriate data conversions and reductions, and entering manually collected data. Several data volumes containing meteorological and chemical measurements have already been prepared. A data exchange and cooperative reporting protocol has been adopted which provides for data collected by each TPS principal investigator to be furnished to the remaining investigators through the TPS data bank. Data will be available to the entire scientific community in about a year.

Planning and coordination meetings have been held to focus on analyzing, interpreting, and reporting the results of the TPS. Priorities have been established and various investigators are performing the analyses; principal results are to be presented at a symposium planned for May 1980, with subsequent journal publication. Included herein are some examples of the types of meteorological and plume chemistry measurements collected during the field study.

Airborne Plume Traverse

On August 10, during the course of a Scenario 1 experiment, the air flow carried the plume from the Johnsonville Plant south of the Cumberland Plant, then in a northerly course east of Cumberland during the early afternoon hours. An aircraft traverse starting at about 1410 CDT shows plumes from both plants (Fig. 2) with the Johnsonville plume located east of the Cumberland plume. The travel time for the Cumberland plume was about 1.5 hours, with transport during this time occurring in an unstable boundary layer. The portion of the Johnsonville plume sampled had travelled for about eight hours, the first half of which was as a fairly compact plume in the dissipating nocturnal inversion layer, and the last half in the unstable boundary layer.

It may be noted that the Cumberland plume was fresh enough to show an O_3 deficit due to NO emissions, whereas for the Johnsonville plume, a slight O_3 excess is suggested. The width of the Johnsonville plume indicated by the SO_2 registrations is considerably greater than that of the Cumberland plume, both because of the greater travel time involved, and because the traverse route cuts obliquely across that segment of the plume sampled, due to the turning of the wind transporting the plume. The differences in the continuous sulfate traces is the most notable feature: whereas the sulfate excess in the Cumberbland plume is similar to the SO_2 profile, suggesting the excess is primary sulfate emission, the sulfate excess in the Johnsonville plume suggests maxima at the edges of the SO_2 plume, indicating the importance of plume dilution and mixing with background air in sulfate formation rates.

Calculations of sulfur conversion rates based on the excess of SO_2 and sulfate above background yield an upper limit of about 2% per hour for both plumes. For the Johnsonville plume, surface removal would lower this average rate, but accounting for the diurnal increase of conversion rates would suggest a value of about 3% per hour at the time of sampling.

Ground-Level Plume Traverse

A Scenario 4 experiment was conducted on August 23. Winds were southerly all during the experiment, with speeds decreasing during the forenoon as the mixing layer developed, settling down to 2-to-4 m sec^{-1} during the afternoon hours. The ground van instrumented with the correlation spectrometer was deployed to make repeated traverses along a road essentially normal to the plume, at a distance of about 17 km from the Cumberland Plant. Data were analyzed to obtain the mean position (center of mass) and standard deviation of the horizontal distribution about the mean of both the ground-level concentration and the vertically integrated plume.

After about 1100 CDT, the plume was stirred to ground-level, producing surface SO_2 concentrations of 200-300 ppb until the boundary layer began to restabilize late in the day (Fig. 3b). For most of the day, the integrated plume was slightly clockwise from the surface plume (Fig. 3a), which would be the shear expected if the classical Ekman spiral existed in the boundary layer. The indicated shear on this particular day was slightly greater and more persistent than found on other sampling days, however. The computed plume standard deviations (Fig 3c) indicate that the surface plume and the integrated plume are of comparable widths, with the surface plume tending generally to be slightly narrower, which is consistent with the fact that it represents only one level within the total plume. It may also be noted that plume width increased to a sustained maximum during the afternoon hours, with a decrease in width late in the day as the boundary layer began to restabilize.

Dispersion Statistics

Turbulence velocity statistics, σ_v and σ_w, which are related to the lateral and vertical spread of a plume, were observed by means of a NOAA aircraft platform. On-board fast response sensors included gust probes and a pitot tube for measurement of wind components, and thermistors and a microwave refractometer for obtaining temperature and humidity fluctuation statistics. Aircraft motions measured with an inertial navigation system were subsequently removed from the gust probe data to obtain the wind field relative to the ground. Products of the data processing include the mean and first, second and third moments of the velocity, temperature and humidity statistics as well as the turbulent fluxes of momentum, heat and moisture.

Table 1 summarizes preliminary results of three flights designed to study the spatial variability of the planetary boundary layer based on land use patterns. Measurements obtained during sequential low level flights over an agricultural site and a forest indicate significant differences in both the vertical and lateral velocity statistics, σ_w and σ_v, and in the sensible heat flux, H, for the different land uses. Both surface and mixed layer similarity theory predict the ratio of the sigmas to be governed by the corresponding ratio of the heat flux to the 1/3 power. In these missions, it appears that the results are consistent with theory. The obvious conclusion is that large spatial variations in the turbulent structure of the planetary boundary layer do exist and therefore must be considered in evaluating plume dispersion statistics.

Table 1. Preliminary Results of Land Use Variation of Velocity and Heat Flux in the TPS Study Area.

Julian Day 1978	Time CDT		σ_{ag} $m \cdot sec^{-1}$	σ_f $m \cdot sec^{-1}$	σ_{ag}/σ_f	H_{ag} watts·m^{-2}	H_f watts·m^{-2}	$(H_{ag}/H_f)^{1/3}$
221	1320-1437	(w)	37.5	84.8	0.44	52	213	0.62
		(v)	54.0	142.5	0.38			
226	1048-1154	(w)	40.0	57.0	0.70	44	96	0.77
		(v)	35.0	51.0	0.69			
239	1045-1200	(w)	38.5	51.8	0.74	37	83	0.76
		(v)	77.0	74.0	1.04			

Lidar Plume Depiction

In the pre-dawn hours on August 18, the boundary layer winds reflected the combined influences of the inertial oscillation associated with the nocturnal stabilizing of the boundary layer, and the effects of frictional drag on the air flow near the surface. These influences yielded a wind profile with the direction veering (turning clockwise) with height in the lower layers and backing (turning counterclockwise) at higher levels. A traverse with the lidar van made at a distance of about 40 km from the Cumberland Plant on a road normal to the direction of plume travel (Fig. 4) shows a good correspondence between the wind profile and the horizontal position of the plume with height. It may be noted that the plume shows as a sideways "V", with the vertex of the "V" pointing east, and the plume top and bottom stretching off to the west.

The crosswind spread of the plume due to wind directional shear shown in this example was not particularly large. There are numerous other cases in which the horizontal spread of the stable plume as detected by the lidar is considerably greater than that found with daytime unstable plumes, and consequently, the nocturnal shear should be considered a significant factor in plume dispersion.

Ground-Level Tracer Pattern

A Scenario 2 experiment was planned for August 15. During the day, the winds were moderately strong (approximately 8 m sec^{-1}) from the south-southwest, and quite steady in direction. During the evening, the wind speed in the boundary layer increased significantly in response to the onset of nocturnal stability, coupled with an increase of the synoptic scale pressure gradient force. Wind speeds aloft after midnight were in excess of 20 m sec^{-1}. Wind directional shear slowly developed during the evening, such that directions aloft were somewhat to the right (more toward the east) of winds near the surface.

Tracer (SF_6) was released through the stacks at the Cumberland Plant for three hours during the afternoon, and sampled by the aircraft as well as by mobile ground crews. Sampling traverses were made along four roads, ranging from about 17 to 110 km from the plant. The pattern of ground level concentration of tracer was well defined by the sampling traverses (Fig. 5) being very similar to that which might be calculated from standard Gaussian plume formulae. A total of ten tetroons was released during the experiment, and both the mean tetroon trajectory as well as the crosswind dispersion of individual flights conformed quite closely to the pattern of tracer at the surface, out to beyond the 60-km sampling route. (For clarity, only two of the trajectories are shown in Fig. 5). At the 110 km distance, the tracer cloud arrived about sunset, and the subsequent development of the stable nocturnal layer with associated shear caused the tracer plume to slow down considerably and thus increase the duration of tracer dosage at that distance. The principal effect of the shear, with winds near the surface decreasing while winds aloft increased, was to stretch the tracer cloud longitudinally, such that it was about 60 percent longer than it had been at the termination of tracer release.

Summary

The authors believe that the quantity and quality of chemical and meteorological information collected during the 1978 Tennessee Plume Study will provide a useful data base for evaluating the effects of a single large pollutant source on air quality a few hundred kilometers downwind. Design of the next STATE field study to characterize regional scale episodes of elevated pollution is now being formulated. This second phase is designated as PEPE, for Persistent Elevated Pollution Episodes. Use of advanced measurement techniques such as satellite imagery and remote sensing are anticipated. Also, further experiments are planned to characterize dispersion and transformation processes in plumes from power plants and urban complexes within the larger regional scale. The eventual end product of the STATE program is expected to be air quality simulation models that describe distribution of sulfates and nitrates over the northeastern United States.

Reference

1. Schiermeier, F.A., W.E. Wilson, F. Pooler, J.K.S. Ching, and J.F. Clarke, 1979. Sulfur Transport and Transformation in the Environment (STATE): A Major EPA Research Program. Bull. Am. Meteorol. Soc., 60:11.

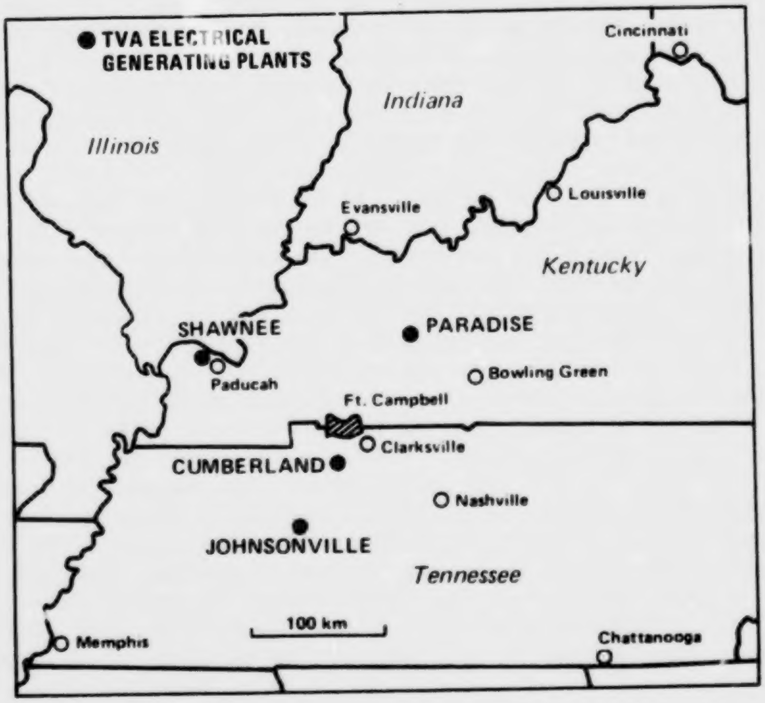
● TVA ELECTRICAL GENERATING PLANTS
Cincinnati
Indiana
Illinois
Louisville
Evansville
Kentucky
SHAWNEE
PARADISE
Paducah
Bowling Green
Ft. Campbell
Clarksville
CUMBERLAND
Nashville
JOHNSONVILLE
Tennessee
100 km
Memphis
Chattanooga

Figure 1. Area of Tennessee Plume Study

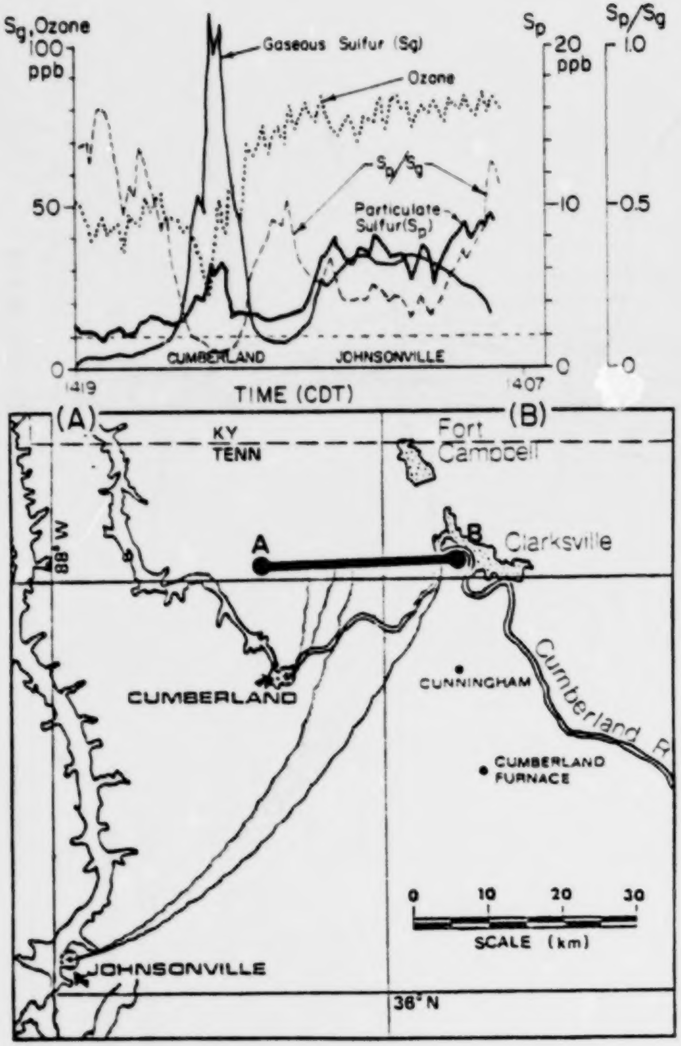
Sg, Ozone
100 ppb
50
0
Sp
20 ppb
10
0
Sp/Sg
1.0
0.5
0
Gaseous Sulfur (Sg)
Ozone
Sp/Sg
Particulate Sulfur (Sp)
CUMBERLAND
JOHNSONVILLE
1419
1407
TIME (CDT)
(A)
(B)
KY
TENN
Fort Campbell
88° W
A
B
Clarksville
CUMBERLAND
CUNNINGHAM
Cumberland R
CUMBERLAND FURNACE
0
10
20
30
SCALE (km)
JOHNSONVILLE
36° N

Figure 2. Aircraft traverses of Cumberland and Johnsonville plumes.

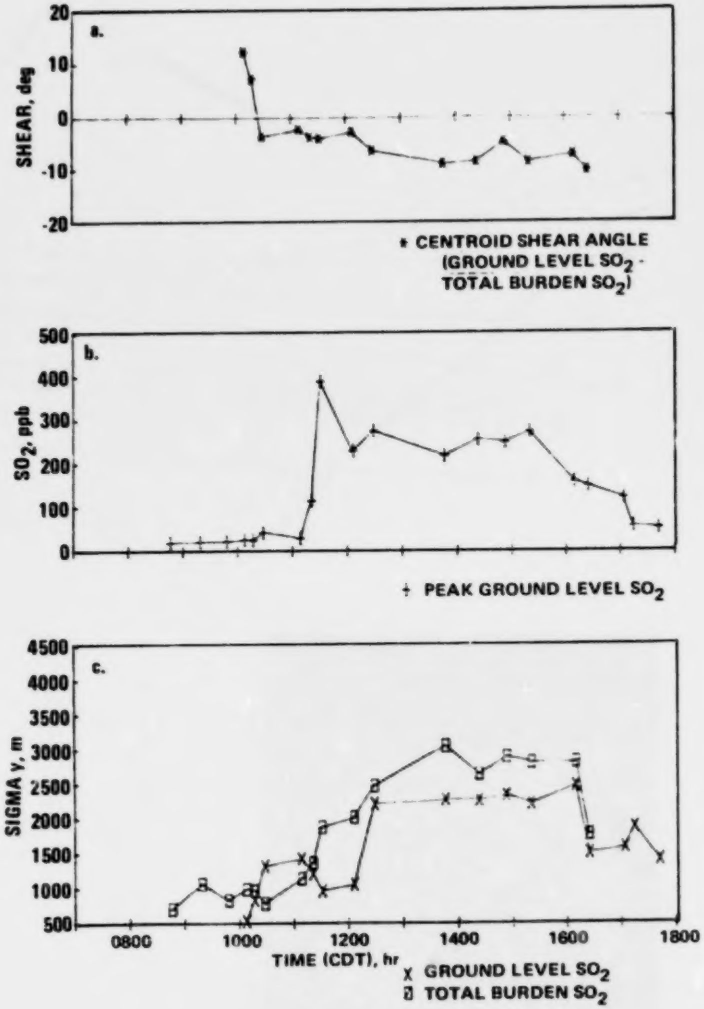

Figure 3. Comparison of ground-level and integrated plume measurements.

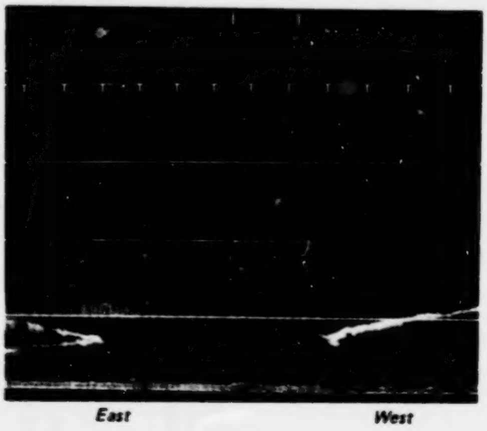

Figure 4. Lidar depictions of Cumberland plume.

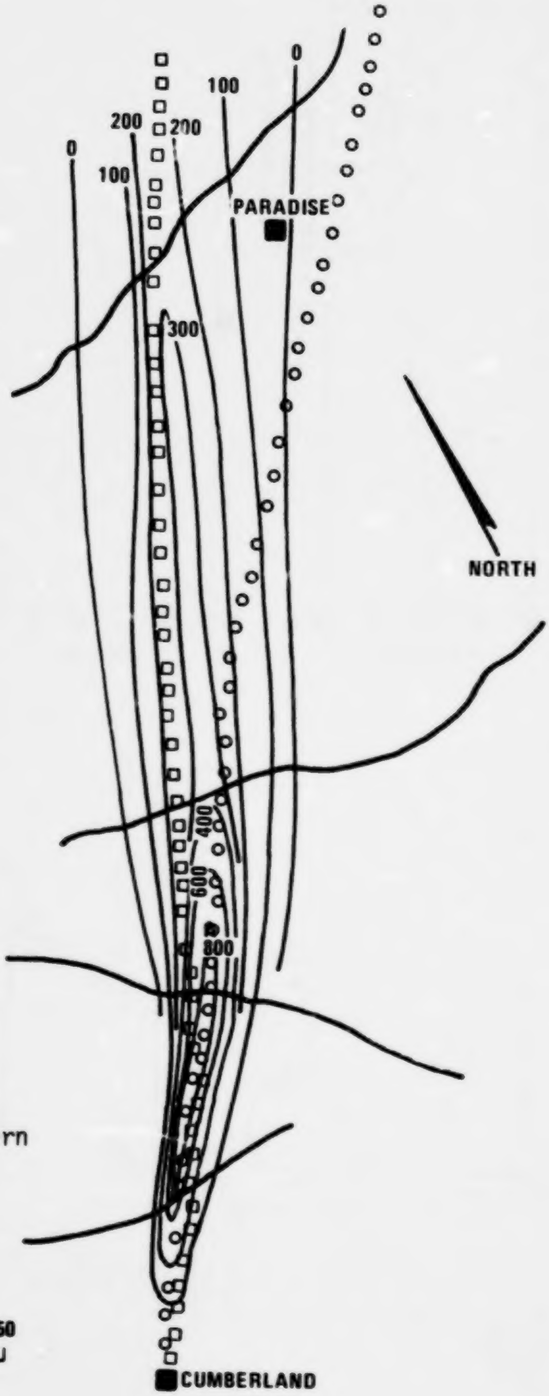
0
100
200
200
100
0
300
400
600
800
PARADISE
CUMBERLAND
NORTH
○ TETROON RELEASED 1330
□ TETROON RELEASED 1600
0
10
20
30
40
50
SCALE, km

Figure 5. Ground-level SF_6 tracer pattern of Cumberland plume.

Discussion:

Hübschmann:

When and where will your data set be published?

Gillani (response):

They will be published in journals in the near future. Furthermore, we in co-operation with EPA are organizing a conference on plumes sometime next year. At that time the data set and the field experiments will be discussed and published in the proceedings.

DEVELOPMENT OF PRACTICAL CALCULATIONS FOR ESTIMATING DISPERSION FROM ELEVATED SOURCES

by

A.E. Saab - J.P. Granier
Direction des Etudes et Recherches
Electricité de France

Abstract. Neither the statistical approach nor the gradient transfert theory are capable of representing all the effects induced by elevated sources, when the vertical wind shear, plume meandering and buoyancy are frequently predominant. Nevertheless, a judicious application of these theories in combination with second order closure modeling allows to define the turbulent diffusion parameters suitable for simple models using corrected velocity, length and time scales (Lumley's and Launder's [6] formalisms).

The computed values are compared with different sets of measurements obtained on the sites of Cordemais (EEC campaign) and Jumeauville (EDF experimental site).

Introduction

As many contributors pointed out in the recent NATO Meetings, the difficulties to describe satisfactorily, on one hand, the atmospheric boundary layer and, on the other hand, the process of turbulent diffusion are such that, untill now, no general theory works -specially in the case of estimating dispersion from elevated sources where the whole description of the atmospheric boundary layer is necessary-.

The suggestions are that a "judicious application of the conventional theories in combination with second order closure modeling could provide some better approach" (Pasquill [1]).

Starting from that basis, we can analyze the difficulties to develop a working theory of the turbulent diffusion in the atmosphere :

- Concerning the atmospheric boundary layer, a multiparametric similarity theory is needed :
  - a one scale theory like Monin theory allows only the description of the atmospheric surface layer,
  - to take into account the vertical inhomogeneity of the atmosphere due to the buoyant effect, gravitational effect or wind shear, at least two or three similarity parameters are necessary : 2 parameters to describe thermal stability and 1 Coriolis effect,
  - to take into account some properties related to the unsteadiness or the non-homogeneous characteristics of boundary limit conditions, some other similarity parameters are necessary to represent the geostrophic wind acceleration, baroclinicy and horizontal homogeneity.

Preceding page blank

- Modeling the turbulent diffusion process, there are some restrictive limits related to the conventional theories :

  - the statistical theory needs some more information on relations between lagrangian and eulerian scales in non-homogeneous turbulence with gravitational and buoyant effects,
  - the gradient transfer approach is not satisfactory to reproduce some effects related to spatial inhomogeneity and buoyancy.

So there is a challenge with second order closure theories to seek a representation of turbulent transport of mass taking into account the influence of the main similarity parameters for the representation of atmospheric boundary layer and the turbulent diffusion process.

In the following, we will try to develop shortly two parts :

1 - How to proceed with second order closure modeling respecting a compromise between available input data and model accuracy.

2 - How to improve simple models.

Basic analysis

At NATO last meeting in Louvain-la-Neuve, the authors [2] presented a three-dimensional model using turbulent diffusivities profiles deduced from a simplified second order closure model reducing the turbulent fluxes equations to algebraic ones. The idea was to incorporate, in the description of turbulent diffusivities, the influence of gravitational, buoyant and wind shear effects which are very important in the case of estimating dispersion from tall stacks.

A validation is obtained from a sensitivity test on the order of magnitude of the different terms introduced in the second order fluxes equations : advection, production, diffusion and pressure terms. Generally it prevails that as the plume develops the significance of the advection and diffusion terms decreases rapidly (specially with unstability), and a balance is reached between production and pressure redistribution terms except for special conditions such as strong spatial variations in the turbulence field or fast thermal evolution when a quasi-equilibrium state is not respected.

Using the tensorial forms for diffusivity $\overline{u_i c} = - K_{ij}\ \partial C/\partial x_j$, which is more reliable than a scalar form, we can express the components of tensor diffusivity :

$$K_{zz} = \frac{-\dfrac{1}{\gamma_1}\left[\overline{w^2} + \dfrac{1+\gamma_2}{\gamma_3}\,\dfrac{g}{\Theta_o}\,\overline{w\theta}\right]}{\left[1 + \dfrac{g}{\Theta_o}\,\dfrac{1-\gamma_2}{\gamma_1\ \gamma_3}\,\dfrac{\partial\theta}{\partial z}\right]}$$

$$K_{x_i x_i} = \frac{-\dfrac{1}{\gamma_1}\left[\overline{u_i^2} - K_{zz}\,\dfrac{\partial U_i}{\partial z}\right]}{\left[1 + \dfrac{g}{\Theta_o}\,\dfrac{1-\gamma_2}{\gamma_1\ \gamma_3}\,\dfrac{\partial\theta}{\partial z}\right]} \qquad i = 1,2$$

$$K_{zx_i} = \frac{-\frac{1}{\gamma_1}\left[\overline{u_i w} + \frac{1+\gamma_2}{\gamma_3}\frac{g}{\Theta_o}\overline{u_i\theta}\right]}{\left[1 + \frac{g}{\Theta_o}\frac{1-\gamma_2}{\gamma_1\ \gamma_3}\frac{\partial\Theta}{\partial z}\right]} \qquad i = 1,2$$

All tensor diffusivity components are expressed in terms of explicit variables of the flow (mean values, momentum and heat turbulent fluxes) and characteristic kinetic energy and length scales (q, Λ).

We used different field dispersion experiments carrying out fine measurements of atmospheric turbulent structure and spatial pollutant concentrations to investigate the choice of characteristic turbulent scales and all constant appearing in the modeling of unknown terms in the exact transport equations (Saab [3] - 1978).

The parameters γ_1, γ_2 and γ_3 introduced in the closure modeling provide the correct dimensional homogeneity by means of characteristic length and kinetic energy scales. Their dependance on stability is highly correlated to turbulent Schmidt number $S_{c_t} = \overline{uw}\ \partial C/\partial z / \overline{wc}\ \partial U/\partial z$, as it is shown in this table :

L Monin length	- 15 m	- 30 m	- 150 m	∞
S_{c_t} Schmidt number	0.55	0.63	0.82	0.84
$\gamma_1, \gamma_3 / -\left(\frac{q}{\Lambda}\right)$	0.60	0.6 - 0.7	0.7 - 0.8	0.8 - 1
γ_2	0.25	0.25	0.40	0.45

A correction on the dependance of length scale with downwind distance is now obtained, taking into account the height of the mixing layer. This allows to cope with the major objections to the gradient transfer approach which is not adequate when used to model the lateral plume spread : $K_{x_i x_i} = K_{x_i x_i}(x,z)$, as it is shown in the statistical theory

$$\Lambda^* = \Lambda^*_o + k_1 z^*[1 - \exp(-k_2 x^*)]$$

where Λ, z and x are non-dimensionalised by the height of mixing layer z_i ; k_1 and k_2 are constants depending on stability ; Λ_o is related the initial plume width.

A sensitivity test on the variation of diffusivity profiles with downwind distances is presented on Figure 1.

The profiles of mean wind components, temperatures and turbulent covariances, are settled from a one-dimensional turbulent model using the local-equilibrium approximation. The differential equations for the evolution of second order turbulent moments (momentum $\overline{u_i u_j}$, and heat flux $\overline{u_i\theta}$) are thus reduced to algebraic relations, and expressed in terms of kinetic energy and length scales.

Applications

An experimental validation of this approach using the available data of CEC Campaign at Cordemais (1977) is carried out. Cordemais is a large power station, with a total capacity of 2000 MW built by EDF in the West of France (in a flat region between Nantes and Saint-Nazaire). In its present configuration the effluents are released by means of two 150 stacks, on serving a 600 MW unit, another serves 2 × 700 MW units. The measurements facilities available during the campaign consisted of two survey vehicles for measuring ground level concentrations (TECO and BENDIX) and overhead burdens (COSPEC) of SO_2 and NO_x together with meteorological variables and plume characteristics (Robé [8])

Keeping in mind the limitations of both the numerical and the experimental approaches, the agreement between computed and experimental results is satisfactory, as it is shown on Figure 2. As a critical test the model results on September 12 are compared to the instantaneous values measured by a survey vehicle for ground level concentration and overhead burden in the crosswind direction at a distance of 8400 m.

For the practical use of this model, we can run it for different heights of release and different meteorological situations, solving the convective-diffusion equation with the simplified closure turbulent schemes for the tensor of eddy diffusivity. Using the moment concentration method, we can generate from the three-dimensional concentration fields various sets of sigma-curves which could be used in gaussian models.

In Figure 3, we present the variations of crosswind dispersion coefficients with distance for different atmospheric stabilities and for three release heights (100, 300 and 500 m). The main effect of increasing release height from 150 to 500 m squares with an increasing value of the crosswind dispersion coefficients with stability specially at large distances (at 10 km downwind, the variation of σ_y is around 50 per cent in stable conditions).

The results depicted in Figure 4 point out the effects of some factors on crosswind dispersion coefficients for a 300 m release height : atmospheric stability, wind shear and surface roughness. It is interesting to note that these results agree qualitatively with the general conclusions drawn by some researchers (Briggs [4], Gifford [5]) based on their theoretical and experimental studies.

A parametrization study is now developped in order to provide the characteristic turbulent scales (turbulent intensity and time-scale) which can be used in gaussian formulation. In neutral and stable conditions with wind shear effect, a correction on lagrangian time-scale using Lumley's [6] formalism provides a correct prediction on sigmas σ_y and σ_z. The semi-empirical expressions used to estimate turbulent intensities are based on similarity theory :

$$\tau_L^* = \tau_L\left(1 - \frac{\partial U}{\partial x_i}\,\tau_L\,\frac{\overline{u_i\,u_j}}{\overline{u_i^2}}\right)$$

τ_L^* is a corrected lagrangian time-scale.

In unstable conditions, untill additional sensitivity tests are performed, we use the scheme proposed for the convectively mixing layer introducing a convective velocity scale and the depth of the mixed layer (Panofsky [7]).

References

[1] F. Pasquill, "The dispersion of materials in the atmospheric boundary layer. The basis for generalization", Lectures on Air Pollution and Environmental Impact Analysis, 296 p., A.M.S., Boston, 1975.

[2] A.E. Saab, J.P. Granier, "New techniques of estimating dispersion coefficients. Generalization of the diffusivity concept", 8th I.T.M. on Air Pollution Modeling (Louvain-la-Neuve), 1977.

[3] A.E. Saab, "Contribution à l'étude du transport turbulent de masse dans l'atmosphère. Etude théorique et expérimentale", Doctorate thesis, Paris, 1978.

[4] G. Briggs, "Plume rise predictions", Lecture on Air Pollution and Environmental Impact Analysis, A.M.S., Boston, 1975.

[5] F. Gifford, "Turbulent diffusion typing schemes : a review", Nuclear Safety, 17, pp. 68-86, 1976.

[6] J. Lumley, "Computational modeling of turbulent flows", V.K.I.-L.S. 1978, n° 7, (Rhode-St-Genese), 1978.

[7] H. Panofsky, D.H. Lenschow, H. Tennekes, J.C. Wyngaard, "The characteristics of turbulent velocity components in the surface layer under convective situations", Boundary Layer Meteor., 11, pp. 355-361, 1977.

[8] M.C. Robé-Naudy, "Etude de la pollution en oxydes d'azote et dioxyde de soufre d'un site industriel", Bulletin D.E.R.-E.D.F. 2/3/1979

[9] A.G. ROBINS, J.E. FACKRELL, "Continuous Plumes - Their Structure and prediction" CEGB memorandum TF 212, 1979

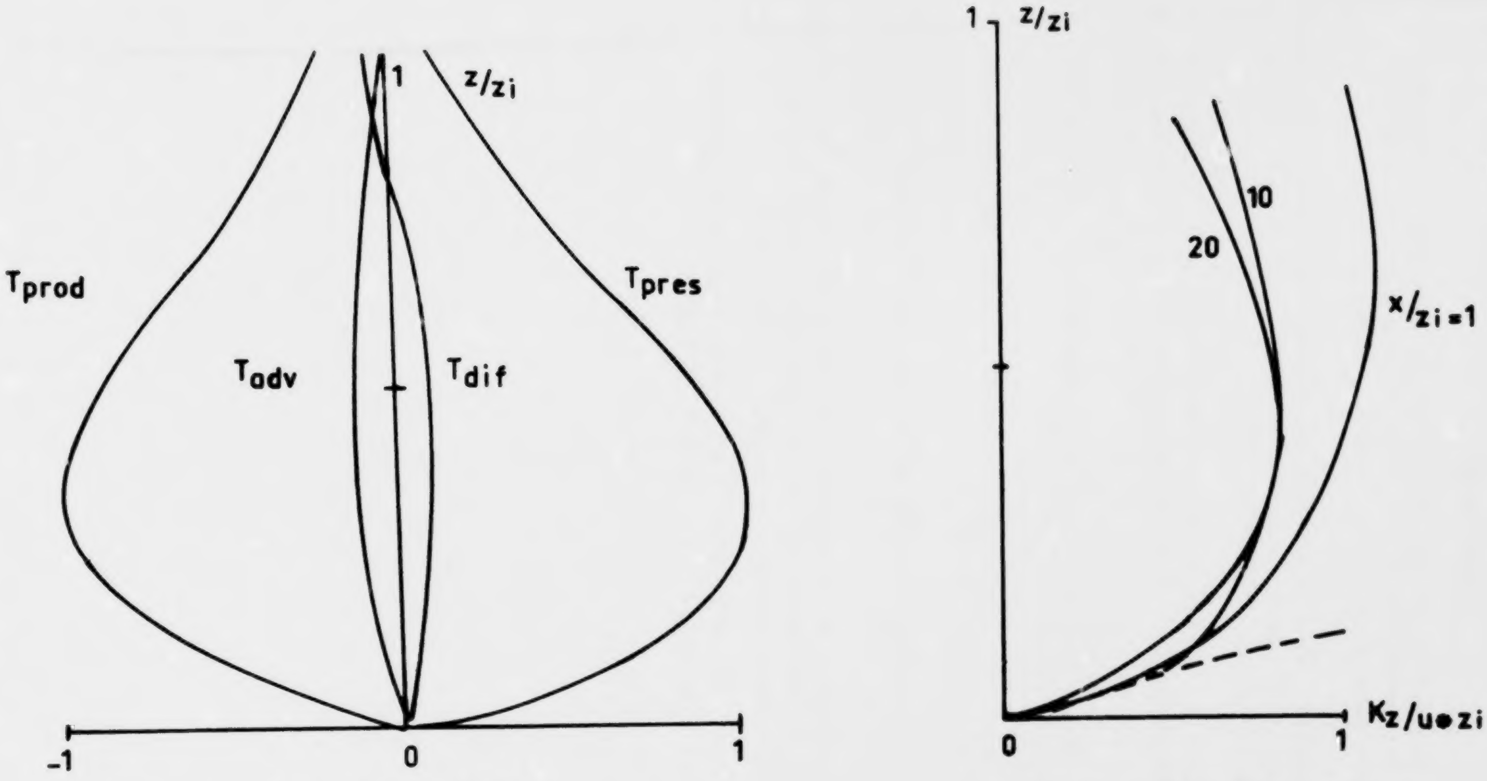

Bilan de l'équation de $(\overline{wc})$
flux vertical de masse. (Robins [9])

Profil de diffusivité verticale

Fig. 1

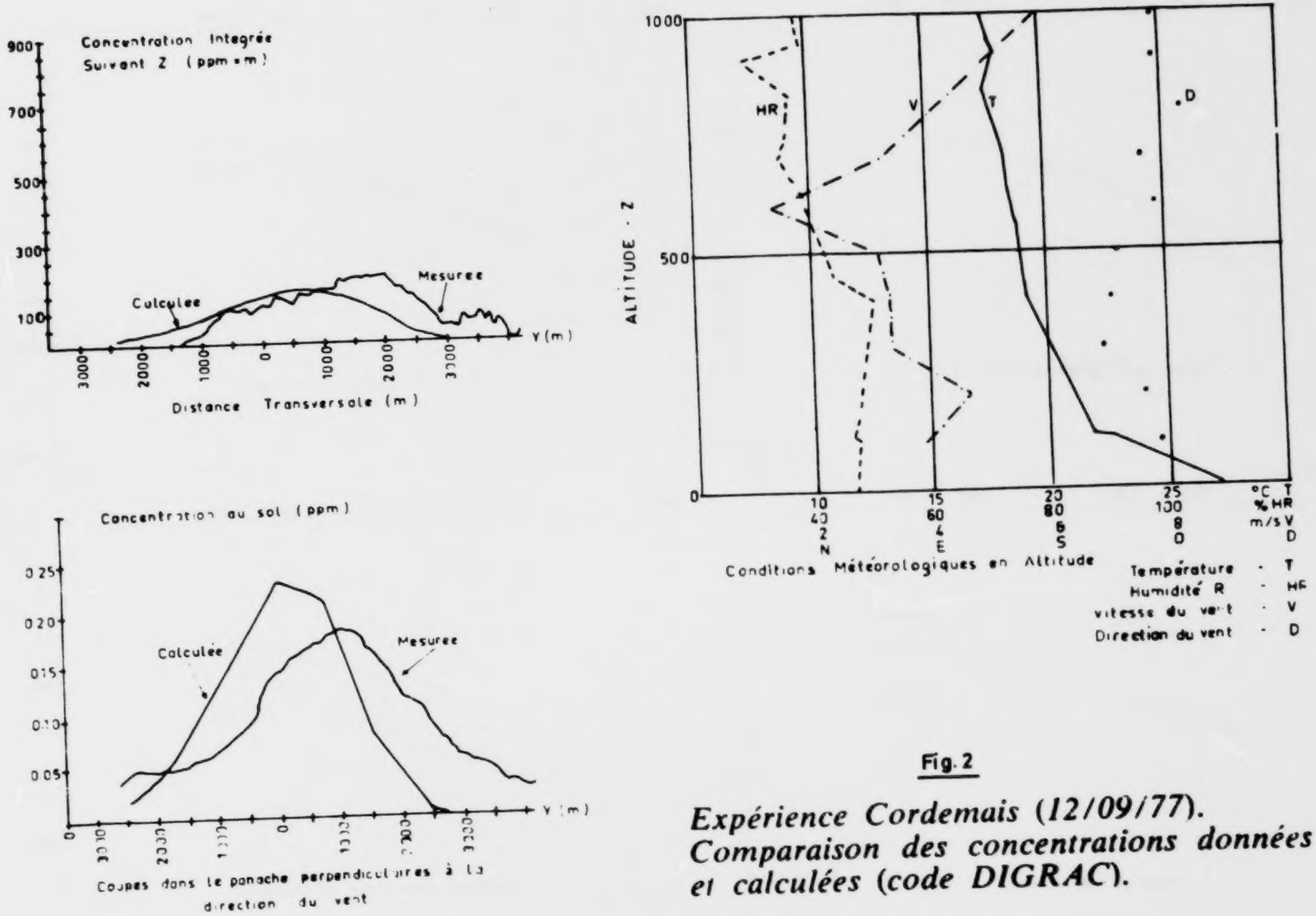

Fig.2

Expérience Cordemais (12/09/77).
Comparaison des concentrations données et calculées (code DIGRAC).

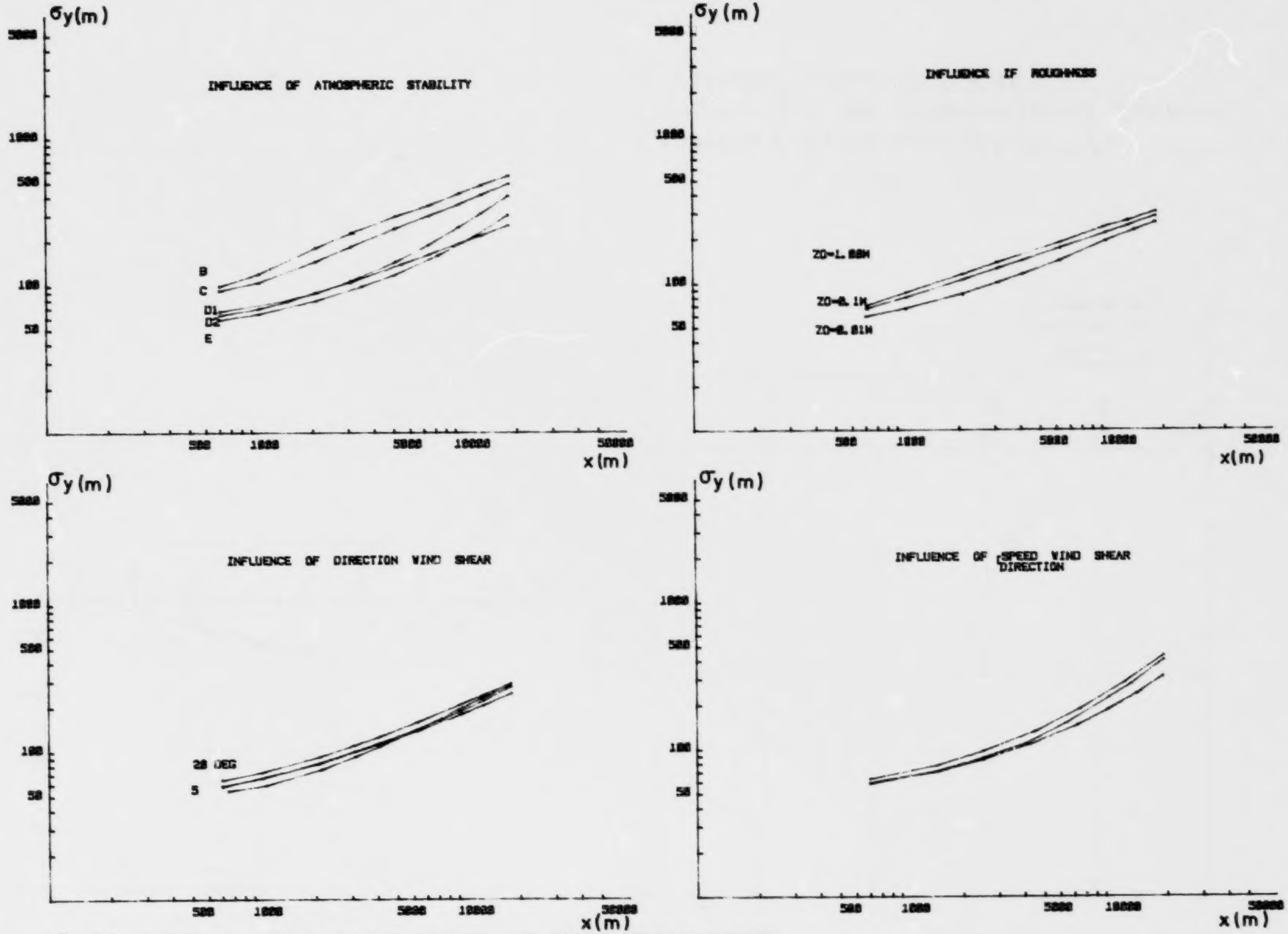

Fig.3A INFLUENCE OF ATMOSPHERIC STABILITY, ROUGHNESS, WIND SHEAR ON CROSSWIND DISPERSION

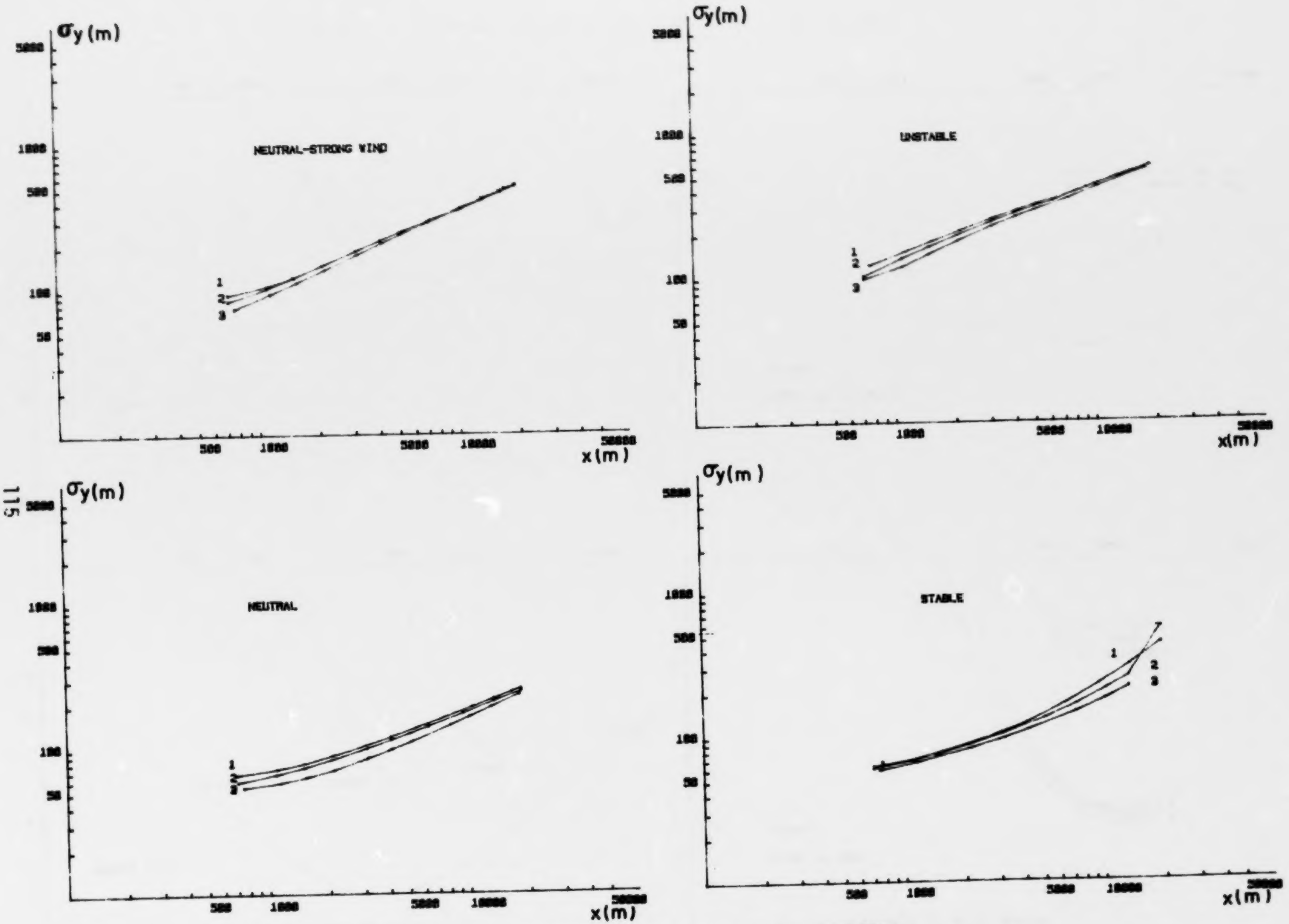

Fig. 3B INFLUENCE OF RELEASE HEIGHT ON CROSSWIND DISPERSION FOR DIFFERENT ATMOSPHERIC STABILITIES
1-H=300 M 2-H=200 M 3-H=150M

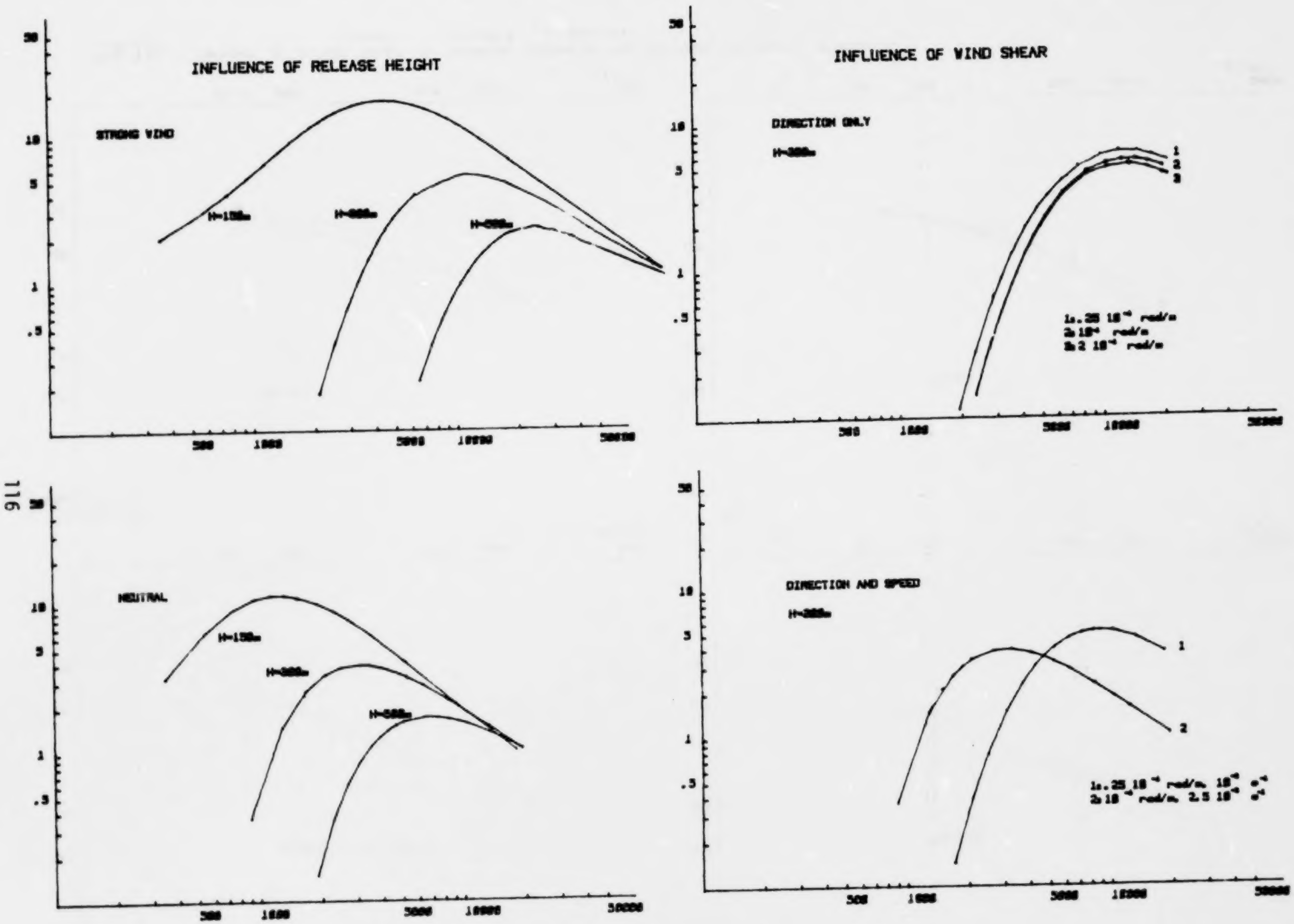

Fig. 4 Cmax*U/Q(10^{-6} m^{-2}) VS X(m)

Discussion:

Venkatram:

How do you account for plume induced turbulence in your second order model?

Saab (response):

This can be accounted for approximately in the turbulent kinetic energy equation.

ELEVATED SOURCE SF_6-TRACER DISPERSION EXPERIMENTS IN THE COPENHAGEN AREA

Preliminary results I

by

Sven-Erik Gryning and Erik L. Petersen
Meteorology Section
Risø National Laboratory, Roskilde, Denmark

Erik Lyck
Danish National Agency of Environmental Protection
Air Pollution Laboratory
Risø National Laboratory, Roskilde, Denmark

Abstract. For an ongoing, full scale tracer experiment in the Copenhagen area, results from 6 experiments are reported. The tracer sulphurhexafluoride was released at the height 115 m and was sampled at ground-level at up to 6 km downwind. σ_y was estimated from the tracer concentrations and from the lateral standard deviation of the wind fluctuations by using Pasquill's computational scheme. The experiments seem to indicate a significant wind velocity dependence for the f_y-function that is not included in the computational scheme. An assumed Gaussian distribution of the vertical concentration distribution was found to be inconsistent with the measured crosswind integrated tracer concentrations in some of the experiments.

Introduction

A project has been started to investigate experimentally the ability of the atmosphere to disperse nonbuoyant effluents released from elevated point sources in an urban environment.

The investigation is performed by carrying out dispersion experiments by use of the tracer sulphurhexafluoride, SF_6. The tracer is horizontally released from the TV-tower at Gladsaxe, a suburb of Copenhagen, at a height of 115 m. The dispersed tracer is then sampled at ground-level positions in up to three crosswind series about 2, 4 and 6 km downwind from the point of release. The experimental range is limited by the coast of Øresund (Fig. 1).

The ongoing experiments in the Copenhagen area were started in September 1978; in this paper preliminary results from 6 out of 7 experiments are presented, one experiment was excluded from this analysis due to malfunctions of the meteorological instruments.

Site

The experimental site is a suburban area in the northern part of Copenhagen. The experimental area consists of 2 opposing 110 degree winddirection sec-

Preceding page blank

tors where the roughness characteristics of the residential area are pretty much alike. About 0.5 km south of the TV-tower, a complex of up to 15-storey buildings makes the use of the remaining sectors too complicated. Positions suitable for mounting tracer-sampling-units were marked out in advance along carefully selected roads. These were chosen as a compromise between the wish to have the potential sampling-unit positions along arcs with center at the TV-tower and the practical requirements for an easy and quick set-up, which is of fundamental importance for the success of this kind of experiments. At the present, experiments are only performed in the sector that includes the prevailing westerly winds, because this sector turned out to contain the best pattern of roads for the experiments.

Experimental

The experimental procedure, the tracer analysis technique and the tracer sampling units were rather similar to those used in previous experiments.[1] In summary the set-up is as follows. In addition to the routine measurements of wind speed (10,60,120,200 m;10 minutes average), direction (10,120,200 m; 10 minutes average), and temperature (2,40,80,120,160,200; 10 seconds every 10th minute), at the tower at Gladsaxe, the turbulent wind velocity components were measured during the experiments. These measurements at the height of release were performed with a combination of a leightweight cupanemometer, vane sensor and vertical propeller.[2] The signals from the instruments were recorded on an analog Ampex FM-recorder and were later digitized with a frequency of 1 or 2 Hz depending on wind-velocity.

The tracer was discharged from a cylinder at the base of the tower at a constant rate and piped to the point of release. Immediately prior to an experiment the automatic, completely selfcontained tracer sampling units were transported to positions marked out in advance (Fig. 1) and distributed according to the actual wind direction. In the experiments about 20 tracer-sampling-units were used in each series, 40 of the sampling-units are radiocontrolled, the rest have a preselected starting time. The distance between the sampling-units in the three series corresponds to an angular separation of about 2 degrees. Three consecutive air samples were taken, each collected over 20 min., so that the total averaging time of the 3 bags was 60 min. The intake tube of the units was located 2-3 m above the ground. Tracer samples were brought back to the laboratory immediately after each experiment and later analyzed for content of SF_6 by use of electron capture detector gas chromatography.The uncertainty of the absolute tracer concentrations is about 20% and the short-term reproducibility is about 2%. The calibration results show that SF_6-concentrations could be detected down to about $2 \cdot 10^{-12}$ ppp (parts SF_6 per parts of air) with a signal-to-noise ratio of 4.

Analysis

Analysis of Tracer Concentrations

As the sampling units during the experiments were placed near ground-level at preselected positions along roads, the measured tracer concentrations primarily allowed for an estimation of the lateral standard deviation of the tracer concentration distribution, $(\sigma_y)_{mea}$. In this paper calculations of $(\sigma_y)_{mea}$ are based on 60 minute averaged tracer concentration distributions derived from the three 20 minute samples. It was derived as the square root of the second order moment of the tracer concentration distribution projected on the crosswind line through the position of the measured maximum concentration.

As the vertical distribution of tracer concentration was not measured, the vertical standard deviation, σ_z, could only be indirectly estimated from continuity considerations, for example by assuming that the tracer concentration distribution is Gaussian. Then

$$\frac{\chi}{Q} = \frac{1}{\pi u \sigma_y \sigma_z} \cdot \exp(-\frac{1}{2}(\frac{y}{\sigma_y})^2) \cdot \exp(-\frac{1}{2}(\frac{h_r}{\sigma_z})^2) \qquad (1)$$

where h_r is the height of the tracer release, χ is the tracer concentration, Q is the tracer release rate, and u is the mean wind speed at the height release. This expression implies conservation of mass and specular reflection of the tracer at the ground. By crosswind integration of (1), we obtain

$$u \cdot \int_{-\infty}^{\infty} \chi dy/Q = \sqrt{2/\pi} \cdot \exp(-\frac{1}{2}(\frac{h_r}{\sigma_z})^2)/\sigma_z \qquad (2)$$

$\chi_{CWI} = \int_{-\infty}^{\infty} \chi dy$ has been approximated by $\frac{1}{2}\Sigma(\chi_i + \chi_{i-1})\Delta y_i$, where χ_i is the 60-minute tracer concentration at position i and Δy_i is the cross-wind distance between position i-1 and i. The relation, (2), between the vertical dispersion parameter and crosswind integrated tracer concentration distribution is shown in Fig. 2. It is characteristic that there is an upper limit for χ_{CWI}. Observed values of χ_{CWI} larger than this limit indicate that (2) cannot any more describe the vertical tracer concentration distribution.

Analysis Based on Wind Variances

From the measurements of the turbulent wind velocity fluctuations performed with the instrument package at the release height, we determined the standard deviations of the turbulent wind fluctuations in the crosswind and vertical direction, σ_θ and σ_ϕ.

Pasquill has developed a relation between the crosswind spread from a continuous point source and the lateral component of the wind-velocity fluctuations, σ_θ, in terms of Taylor's statistical dispersion theory.[3,4] The relation for the lateral dispersion parameter has been put into the form

$$\sigma_y = \sigma_\theta \cdot x \cdot f_y(T/t_L) \qquad (3)$$

where T is the travel time, t_L the Lagrangian integral time scale, and x the downwind distance from the point of release. The travel time assuming Taylor's hypothesis, is T = x/u. Pasquill argues that (3) approximately implies that[5]

$$\sigma_y = \sigma_\theta \cdot x \cdot f_y(x) \qquad (4)$$

so that t_L is inversely proportional to u.

For x less than 10 km a number of discrete values of $f_y(x)$ and for greater x a formula, has been suggested.[5] For the determination of σ_z, it is recommended to use the curves by Turner, which are based on the Pasquill stability classification of the atmospheric spread conditions.[5,6,3] We determined the stability class from measurements of insolation and observation of cloudiness, further the heat island effect was taken into account by changing this stability class one half class towards more unstable conditions. The roughness is taken into account directly by enchanging the σ_z-values.[5]

Meteorological Conditions

Table 1 shows some important parameters for a description of the meteorological conditions during the experiments. Of 6 experiments 5 were performed in conditions that can be characterised by Pasquill stability class C without taking the heat island effect into account. In the various experiments the mean wind velocity (one hour average) at the source height varied from 3.4 to 10.6 m/s, and the temperature gradient, determined from the temperature measurements at 2 and 40 m, varied from -3.34 to -0.97°C/100m. Table 1 also shows the height of the lowest inversion estimated from the routine radiosonde launches, which are performed only 5 km from the TV-tower. The synoptic times are quite close to the time of the experiments. Except from the experiment on November 3 where z_i = 390 m, the height of the lowest inversion is seen to be far larger than the height of tracer release.

Table 1. Meteorological Conditions.

Experiment 1978	Mean wind speed 115 m u (m/s)	Lateral standard deviation 115 m σ_θ degree	Temperat. gradient 2-40 m $\Delta T/\Delta z$ (°C/100 m)	Inversion height z_i (m)	Monin-Obukhov length L (m)	Pasquill stability class. Heat island effect not incl.	incl.
Sept. 14.	8.9	7.5	-0.97	-	-1100	D	C-D
Sept. 20.	3.4	16.0	-3.34	1980	-24	C	B-C
Sept. 26.	10.6	7.7	-3.08	1920	-244	C	B-C
Oct. 19.	5.0	10.1	-2.53	1120	-51	C	B-C
Nov. 3.	4.5	6.1	-2.05	390	-67	C	B-C
Nov. 9.	6.7	6.9	-1.53	820	-169	C	B-C

Results

In all experiments the 60 minute averaged tracer concentration distributions were well covered by the sampling-unit network. The tracer concentrations from the experiment November 9, is illustrated in Fig. 3.

Lateral Dispersion Parameter

Table 2 lists values of σ_y derived from the measured tracer concentrations, $(\sigma_y)_{mea}$, and values computed on basis of the wind fluctuation measurements during the experiment by means of (4), $(\sigma_y)_{EPA}$.

The values of $(\sigma_y)_{mea}$ for the Pasquill class C experiments is seen to vary widely: at a distance of 2 km downwind, the range is 184 m to 254 m, and at 4 km the range is 279 m to 444 m. $(\sigma_y)_{EPA}$ is in all cases except for one, smaller than $(\sigma_y)_{mea}$. The mean percentage deviation is -25%.

Pasquill argues that to a reasonable degree of accuracy the f_y-function is dependent on x only.[5] Functional relationship between the f_y-function and sampling time, downwind distance and wind velocity can, for a given instrument system and atmospheric stability, be established by Taylor's formula. Accordingly, Doran finds that the f_y-function depends heavily on the sampling time and shows that atmospheric stability and the mean wind speed affects the f_y-function.[8] For relatively higher wind speeds, the value of the f_y-function is reported to increase.[8]

Table 2. Results of the analysis on the lateral dispersion.

Experiment	Distance (km)	$(\sigma_y)_{mea}$ (m)	$(\sigma_y)_{EPA}$ (m)
Sept. 14.	3.9	375	207
Sept. 20.	1.9	254	269
	3.7	444	425
Sept. 26.	2.1	239	140
	4.2	438	224
Oct. 19.	1.9	184	170
	3.7	283	268
	5.4	404	358
Nov. 3.	4.0	301	170
Nov. 9.	2.1	185	125
	4.2	279	201
	6.1	376	274

In Fig. 4 $(\sigma_y)_{mea}/\sigma_\theta \cdot x$ is shown as a function of x. The points are seen to vary systematically with the wind speed as expected. It must be stressed, however that only a very limited number of experiments were available for use in Fig. 4. The experiment on November 3, is seen not to follow the general behaviour.

Doran reports that this dependence upon wind speed can be observed in the data from the Prairie Grass ground level dispersion experiment.[8] Results from a series of high source dispersion experiments at Cabauw in the Netherlands did not show the dependence on f_y on the wind speed.[9]

Vertical Dispersion Parameter

Values of σ_z derived from (2), $(\sigma_z)_{est}$, and $(\sigma_z)_{EPA}$ from the Pasquill method are shown in table 3.[5]

To investigate the effect on $(\sigma_z)_{est}$ that originates from the uncertainty in the absolute calibration of the gaschromatograph table 3 includes values of $(\sigma_z)_{est}$, derived by increasing/decreasing the measured concentration by 20%. $(\sigma_z)_{est}$ is seen to be very sensitive to variations in the absolute tracer concentrations, especially for the series closest to the source. Due to the larger roughness in the urban area as compared to a rural area, larger values of σ_z are expected over cities in comparison with σ_z for rural areas. At the present, this effect is not possible to isolate due to the sensitivity in (2) on the absolute calibration.

Table 3. Results of the analysis on the vertical dispersion and of the maximum concentration comparisons.

Experiment	Distance (km)	$(\sigma_z)_{est}$ (m)	measured concentration decreased 20% (m)	measured concentration increased 20% (m)	$(\sigma_z)_{EPA}$	$(\frac{\chi}{Q})_{EPA} / (\frac{\chi}{Q})_{mea}$
Sept. 14.	3.9	x)	185	x)	197	1.1
Sept. 20.	1.9	340	435	275	221	1.3
	3.7	1010	1265	840	426	2.3
Sept. 26.	2.1	x)	x)	x)	244	0.8
	4.2	225	295	170	480	1.0
Oct. 19.	1.9	135	210	x)	221	1.0
	3.7	225	295	170	426	0.7
	5.4	350	450	285	614	0.8
Nov. 3.	4.0	x)	125	x)	464	0.6
Nov. 9.	2.1	x)	180	x)	241	1.2
	4.2	155	225	x)	480	0.7
	6.1	205	275	145	708	0.5

x) no solution

For some experiments, the value of χ_{CWI} u/Q is too large to allowe an estimate of $(\sigma_z)_{est}$ (table 3). Since the experiments are performed under slightly unstable to unstable conditions, the flow field is believed to resemble convective mixing. From tank experiments, as well as numerical work, it has been reported that the height of the maximum crosswind integrated concentration for an elevated plume released into a fully convective flow follows a descending path immediately after release. The plume descends close to the ground and remain there for a considerable distance.[10, 11] Further downwind, the plume is swept up by the convective cells. It is characteristic for the Gaussian distribution that the maximum crosswind integrated concentration behaves in a somewhat similar way. It follows a descending path out to the distance, where $\sigma_z = h_r$. From here the maximum remains at ground-level.Although there is this similarity, it is not possible for all experiments to solve (2) for $(\sigma_z)_{est}$ by use of χ_{CWI} u/Q.

This might be due to the Gaussian distribution being a poor approximation to the actual tracer concentration distribution. To obtain a value of $(\sigma_z)_{est}$ for all experiments, either the shape of the vertical concentration distribution must be altered and/or the plume centerline, h_r, must be lowered as a function of downwind distance. In order to obtain solutions of $(\sigma_z)_{est}$ from (2), values of h_r down to 85 m are required and down to 71 m when the tracer concentrations are increased by 20% (uncertainty in absolute calibration of the gaschromatograph). It is characteristic that for the series farthest away, it is always possible to estimate $(\sigma_z)_{est}$.

Maximum Tracer Concentrations

In order to investigate the ability to predict ground-level concentrations at the experimental distances, using σ_y and σ_z derived from the semiempirical method by Pasquill, the ratio, $(\frac{\chi}{Q})_{EPA}/(\frac{\chi}{Q})_{mea}$, has been calculated (table 3).[5] χ represents the centerline ground-level concentration at the actual distance. The numerator is based purely on the computational method and meteorological data, whereas the denominator is based solely on measured tracer concentrations. If perfect agreement is obtained, the ratio should be 1. Actually, $(\frac{\chi}{Q})_{mea}$ does not represent the real ground-level maximum concentration, because the measurements are made at discrete positions. The difference is, however, believed to be small.

In table 3, $(\frac{\chi}{Q})_{EPA}/(\frac{\chi}{Q})_{mea}$ is seen to scatter around unity, the ideal value. No systematic deviation with downwind distance is seen. Looking at the experiments as a whole, $(\chi/Q)_{EPA}$ is seen in 2 cases to be more than 20% bigger than $(\chi/Q)_{mea}$, and in 4 cases to more than 20% smaller; 20% is the calibration uncertainty of the absolute tracer concentrations. The mean value of the deviation between $(\chi/Q)_{EPA}$ and $(\chi/Q)_{mea}$, calculated from 6 experiments and a total of 12 estimates, is less than the uncertainty in the absolute tracer concentrations.

Acknowledgements

A group that consists of H. Flyger, N.O. Jensen, U. Torp, E. Lyck, and S.E. Gryning has been established to follow the project. E. Lund Thomsen carried out the calibration of the gaschromatograph and performed the tracer analyses. U. Torp collected meteorological information and took part in the experiments. The technical staff at the Air Pollution Laboratory and Meteorological Section provided practical support. H.S. Buch, the Danish Meteorological Institute, took care of forecasts for the experiments. The routine meteorological measurements at the TV-tower are performed by the Danish Meteorological Institute. The Danish Department of Post and Telecommunication made it possible to carry out the experiments from the TV-tower. The study was sponsored by the Danish National Agency of Environmental Protection and Risø National Laboratory.

References

1. S.E. Gryning, E. Lyck and K. Hedegaard, "Short-range diffusion experiments in unstable conditions over inhomogeneous terrain," Tellus 30, 1978.

2. S.E. Gryning and D.W. Thomson, "A "tall tower" instrument system for mean and fluctuating velocity, fluctuating temperature and sensible heat flux measurements," J. appl. Met.(in press, to appear 1979).

3. F. Pasquill, "Atmospheric Diffusion," John Wiley and Sons, New York, 1974.

4. G.I. Taylor, "Diffusion by continuous movement," Proc. London Math. Soc. 2, 1921.

5. F. Pasquill, "Atmospheric dispersion parameters in Gaussian plume modelling. Part II. Possible Requirements for Change in the Turner Workshop Values," EPA-600/4-76-030b. US Environmental Protection Agency, 1976.

6. D.B. Turner, "Workbook of atmospheric dispersion estimates," Public Health Service Pub. No. 999-AP-26. US Department of Health, Education, and Welfare, 1970.

7. D. Golder, "Relations among stability parameters in the surface layer," Boundary-Layer Meteorology 3, 1972.

8. J.C. Doran, T.W. Horst and P.W. Nickola, "Variations in Measured Values of Lateral Diffusion Parameters," J. appl. Met. 17, 1978.

9. F.T.M. Nieuwstadt and H.v. Duuren, "Dispersion experiments with SF_6 from the 213 m high meteorological mast at Cabauw in the Netherlands," Fourth Symposium on Turbulence, Diffusion and Air Pollution. American Meteorological Society, Reno, Nevada, 1979.

10. G.E. Willis and J.W. Deardorff, "A laboratory study of dispersion from an elevated source within a modelled convective planetary boundary layer," Atmospheric Environment 12, 1978.

11. R.G. Lamb, "Numerical simulation of dispersion from an elevated point source in the convective planetary boundary layer," Atmospheric Environment 12, 1978.

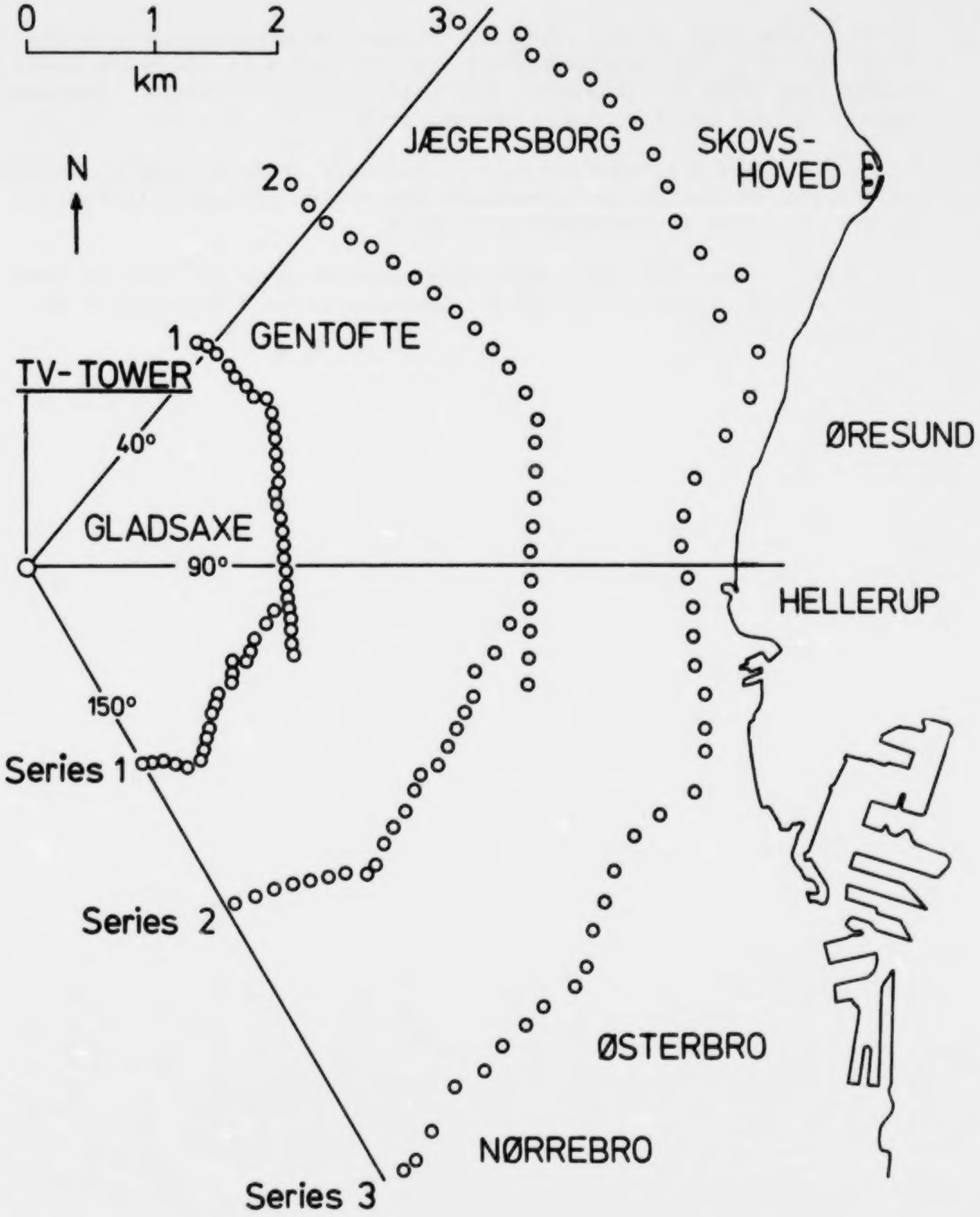
0
1
2
km
N
JÆGERSBORG
SKOVS-
HOVED
GENTOFTE
TV-TOWER
40°
GLADSAXE
90°
150°
ØRESUND
HELLERUP
ØSTERBRO
NØRREBRO
1
2
3
Series 1
Series 2
Series 3

Figure 1. The experimental site. Sampling unit positions used at the experiments are indicated by (o). In the experiments normally 20 sampling units were used per series.

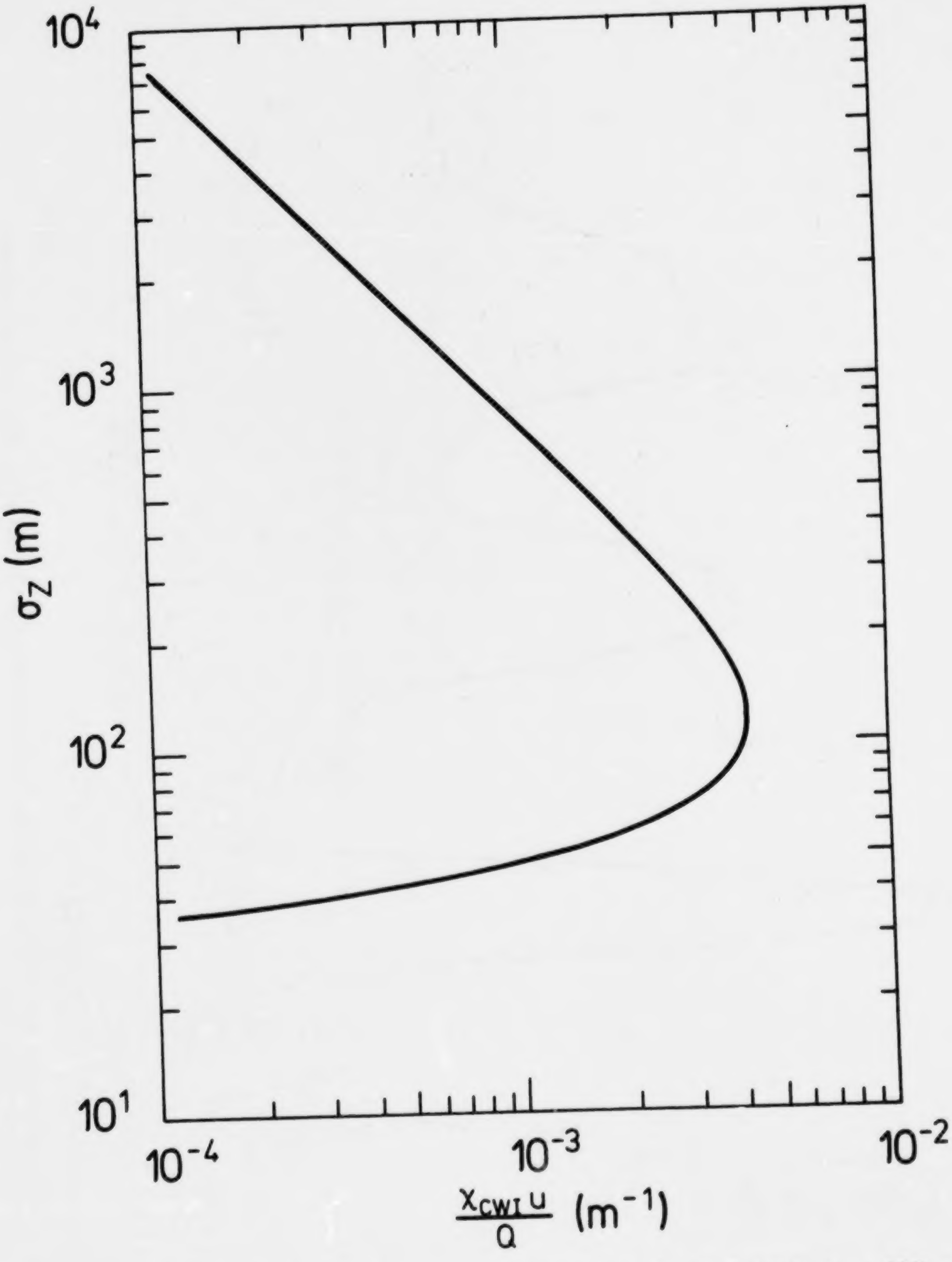

Figure 2. σ_z as a function of $\chi_{CWI} \cdot u/Q$ for the release height, h_r = 115 m.

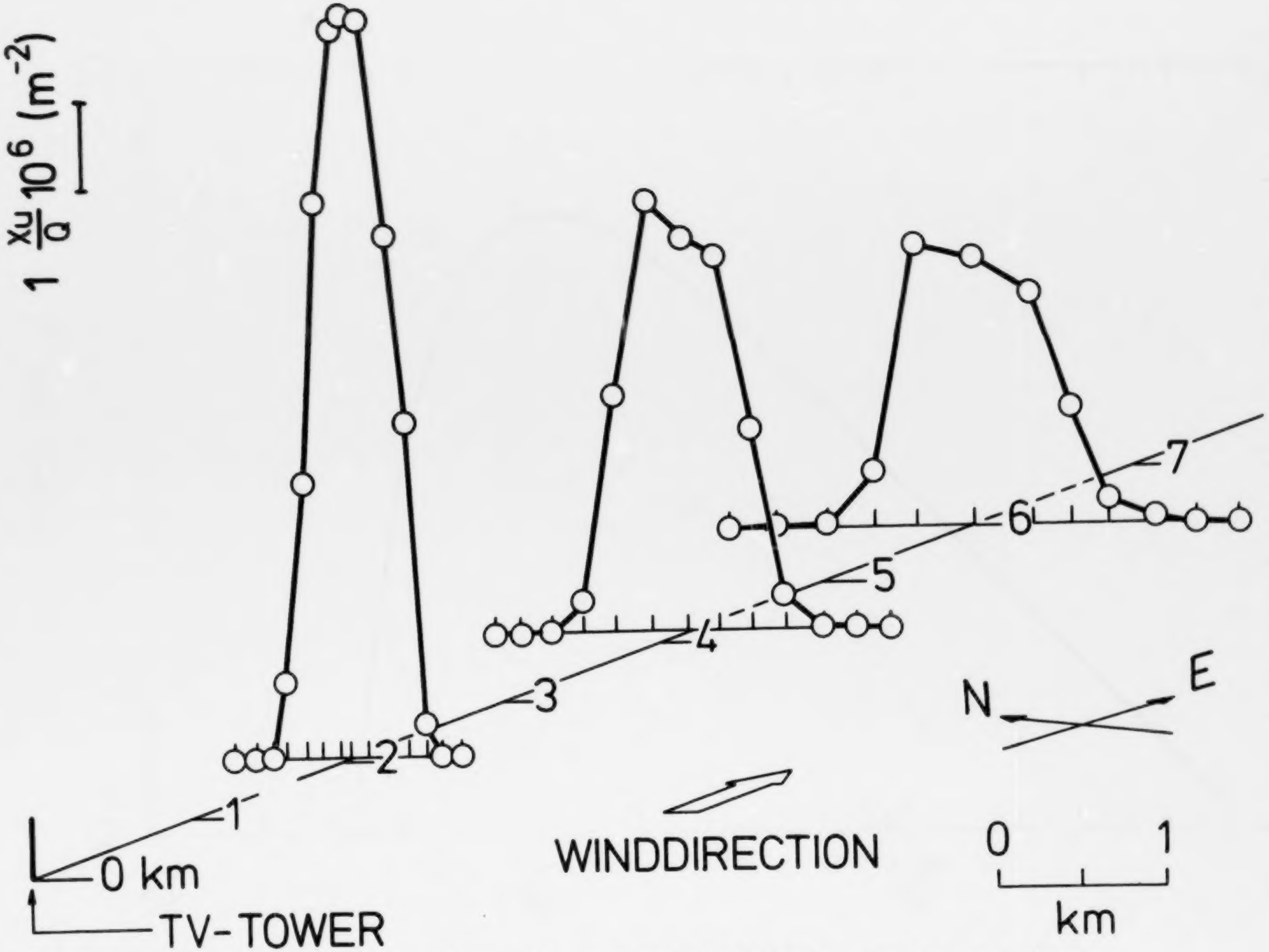

Figure 3. Normalized tracer concentrations (o), averaged over 60 min. for the experiment November 9, 1978.

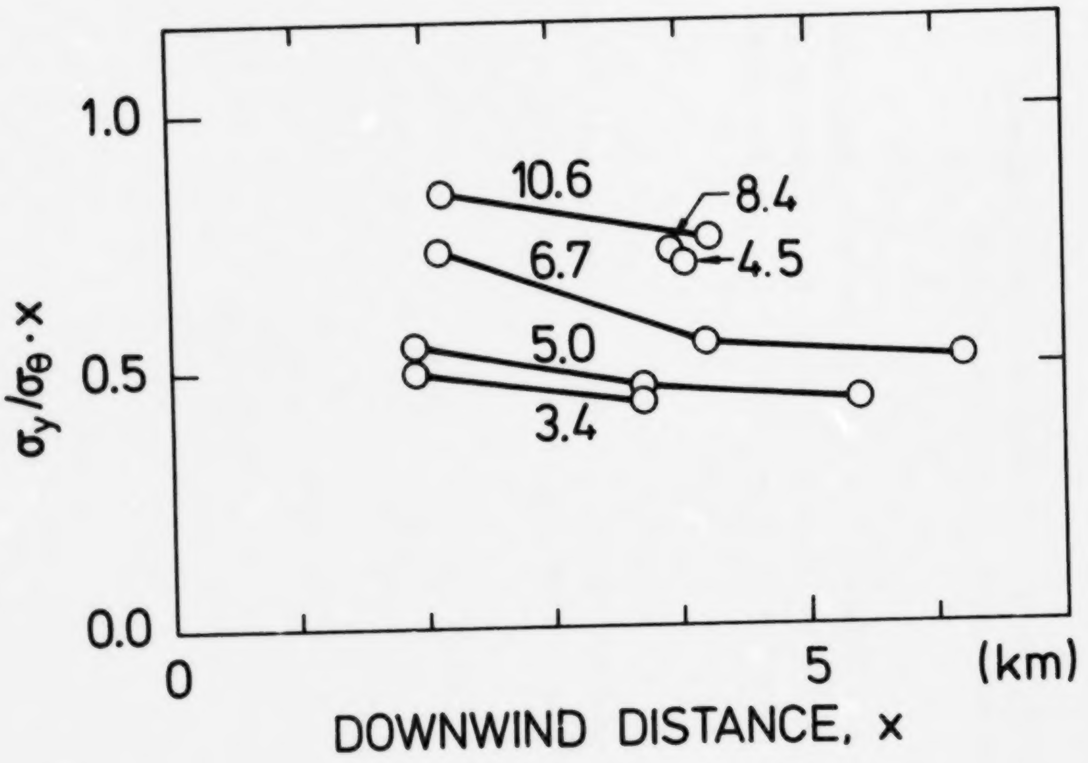

Figure 4. $\sigma_y/\sigma_\theta x$ as a function of downwind distance x. The mean wind velocity (m/s), is shown.

Discussion:

Venkatram:

Why did you assume the Lagrangian time scale (t_L) to be inversely proportional to the mean wind speed $(\bar{u})$?

Petersen (response):

It was an assumption made by Pasquill also.

Schulze:

In an urban area, σ_y and σ_z may be influenced by terrain roughness upwind. What upwind influence on the σ's did you observe?

Petersen (response):

There was no significant difference of terrain in the measurement area and the upwind stretch. Owing to the uncertainty in the estimate of σ_z it was not possible to determine any enhancement in σ_z over the urban area.

Benarie:

Your results appear to bear out McElroy and Pooler's results that there is an increase of one pasquill stability class in dispersion over an urban area.

A REVIEW OF HORIZONTAL AND VERTICAL DISPERSION COEFFICIENTS APPLIED IN THE CALCULATION OF GROUND LEVEL POLLUTANT CONCENTRATIONS RESULTING FROM EMISSIONS FROM TALL STACKS UNDER VERY UNSTABLE ATMOSPHERIC CONDITIONS

by

Dennis A. Trout
Regional Meteorologist
U.S. Environmental Protection Agency, Region V
Chicago, Illinois USA

Abstract. Reviewed herein are curves of horizontal and vertical dispersion coefficients, σ_y and σ_z, that have been developed by field experiments of various investigators as functions of downwind distance from elevated releases under very unstable atmospheric conditions. Comparisons of calculated concentrations using the different sets of σ_y and σ_z curves under the same conditions indicate that maximum calculated ground level concentrations and the distance of such impact from the source differ significantly. Measured maximum concentrations at monitoring sites within 2 km of sources with tall stacks (stack heights of 100 m or more) exceed the concentrations calculated using the different sets of dispersion coefficients. Caution is warranted in applying various dispersion coefficients to estimate impacts of tall stack effluents due to such effects as: increased initial plume growth during plume rise, enhanced plume rise due to multiple plumes, transitional plume rise, changes in height of the plume centerline downwind of final plume rise, and non-Gaussian conditions influencing transport and dispersion.

Introduction

Numerous investigators have traditionally used the Pasquill-Gifford (P-G) curves of dispersion coefficients (σ_y and σ_z) in calculating air quality impacts based on Gaussian modeling approximations. The P-G curves were developed based primarily on field studies of near ground level tracer releases over smooth terrain.[1] A controversy, however, has existed regarding the use of the P-G curves for class A (very unstable) atmospheric conditions in estimating ground level pollutant impacts due to effluents from tall stacks.[2] As a result of this controversy, a review of the curves of horizontal and vertical dispersion coefficients based on existing field studies has been conducted. Because the transport and dispersion of effluents from tall stacks (stack heights greater than 100 m) is the primary concern, only field studies for which tracers were released at heights of 100 m or higher are compared herein with the P-G class A and B curves.

Note, the P-G class B curves are also compared herein because several investigators have suggested that the use of the σ_z values of the P-G class A curves result in overestimates of ground level impacts for sources having tall stacks. Some of these investigators have suggested that the P-G class A curves be replaced by the P-G class B curves which yield smaller σ_z values and thus would result in smaller impacts being calculated for the most unstable atmospheric conditions.

In the following sections, the characteristics of the curves derived from the different tracer experiments are compared. Concentrations predicted by the alternative sets of curves are also compared with concentrations measured near sources with tall stacks.

Tracer Experiments

Three independent sets of field experiments have been found in the literature which investigate the dispersion of tracers released at heights of 100 m and higher under very unstable atmospheric conditions. Singer and Smith, Vogt et al., and Thomas et al. (see Kiefer and Koelzer) have derived σ_y and σ_z curves based on such field investigations.[3-6] Table 1 identifies curves of dispersion coefficients reviewed herein. Table 1 indicates the site, investigator, tracer release height, and surface roughness length (z_0) for each set of curves reviewed herein.

Table 1. Curves of Dispersion Coefficients (σ_y and σ_z) from Field Experiments.

Curve	Investigator	Experiment Site	Tracer Release Height (m)	Surface Roughness Length, z_0 (m)
P-G A	Pasquill-Gifford	O'Neill, Nebraska	< 1	≤ 0.03
P-G B	Pasquill-Gifford	O'Neill, Nebraska	< 1	≤ 0.03
BNL B_2*	Singer-Smith	Long Island, NY	≥ 100	≈ 1
Jülich A	Vogt et al.	Jülich, W. Germany	≥ 100	≈ 1
Karlsruhe A	Thomas et al.	Karlsruhe, W. Germany	≥ 195	≈ 1

* No σ_y or σ_z curves have been derived by Singer and Smith for the most unstable category of atmospheric conditions observed at the Brookhaven National Laboratory (BNL) experiment site on Long Island, NY. Singer and Smith indicate stability categories A, B_2, B_1, C, and D based on wind direction traces (A represents most unstable and D represents most stable; i.e., A is more unstable than B_2).[3] Curves were derived only for categories B_2, B_1, C, and D.[4]

Figures 1 and 2 graphically present curves of σ_y and σ_z respectively for the tracer studies identified in Table 1. It can be seen from these figures that the greatest differences are found between the different σ_z curves as compared to differences among the various σ_y curves.

From Figure 1 it can be seen that for distances of 1 to 3 km from the source, the P-G A, BNL B_2, and Karlsruhe A σ_y curves are in close agreement. However, the Jülich A σ_y values are as much as a factor of 2 larger than the others. The P-G B curve obviously indicates smaller σ_y values than the others.

Figure 2 indicates, for distances of 0.7 to 3 km from the source, that the Karlsruhe A, P-G A, Jülich A, BNL B_2, and P-G B curves yield the highest through lowest σ_z values respectively. This fact suggests that the calculated maximum

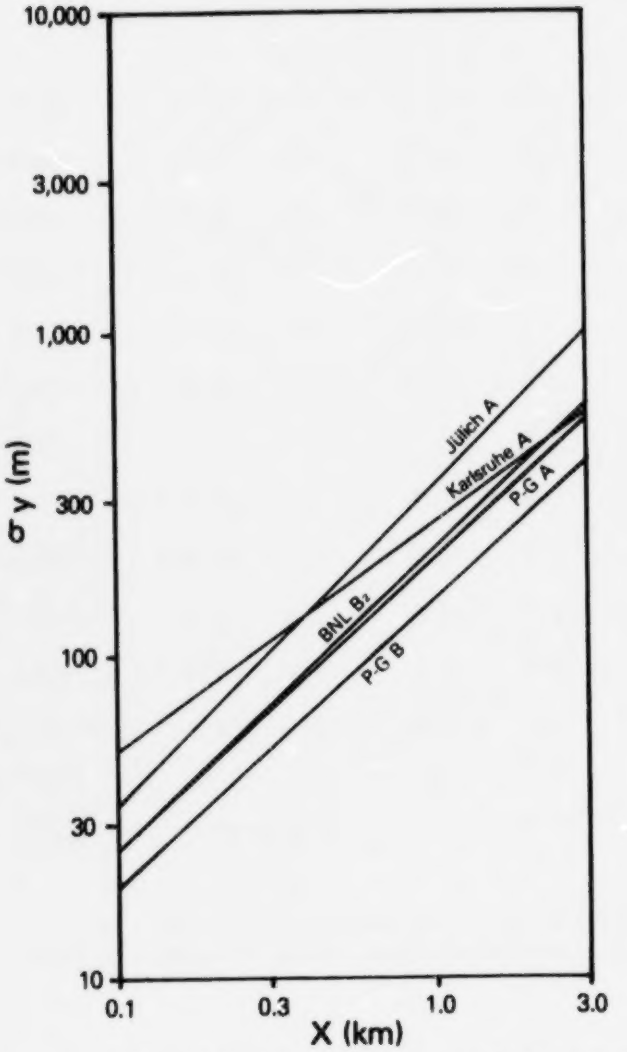

Figure 1. Horizontal dispersion coefficient (σ y) curves as a function of downwind distance (X) from the source.

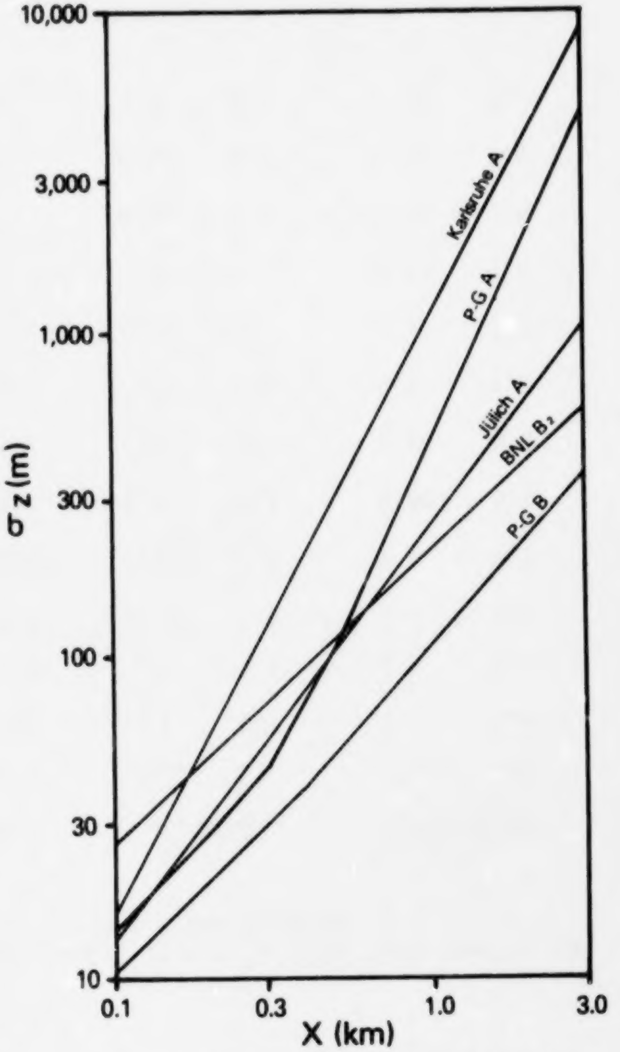

Figure 2. Vertical dispersion coefficient (σ z) curves as a function of downwind distance (X) from the source.

Table 2. Maximum Normalized Concentration, C ($10^{-6}/m^2$), and Distance, X (km), from the Source to the Calculated Point of Maximum Impact for Various Plume Heights.

Plume Height (m)	P-G A		P-G B		BNL B_2		Jülich A		Karlsruhe A	
	C	X	C	X	C	X	C	X	C	X
200	6.8	0.6	4.4	1.3	5.9	0.6	3.9	0.7	7.5	0.4
400	2.5	0.9	1.3	2.5	1.5	1.4	1.1	1.1	2.9	0.5
600	1.4	1.1	0.61	3.6	0.65	2.1	0.55	1.6	1.7	0.6
800	0.95	1.2	0.36	4.7	0.37	2.9	0.33	1.9	1.1	0.7
1000	0.69	1.3	0.24	5.8	0.23	3.7	0.22	2.3	0.82	0.8
1200	0.54	1.5	0.18	6.8	0.16	4.5	0.16	2.7	0.64	0.9
1500	0.39	1.6	0.12	8.3	0.10	5.8	0.11	3.2	0.47	1.1
2000	0.26	1.9	0.07	11.	0.06	7.9	0.06	4.0	0.32	1.2
2500	0.19	2.1	0.05	13.	0.04	10.	0.04	4.7	0.23	1.4
3000	0.15	2.2	0.03	16.	0.03	12.	0.03	5.5	0.18	1.5
4000	0.10	2.6	0.02	20.	0.02	17.	0.02	6.8	0.12	1.8
5000	0.07	2.9	0.01	25.	0.01	22.	0.01	8.1	0.09	2.0

ground level impacts for unstable conditions would occur closest to the source using the Karlsruhe A curves and farthest from the source using the P-G B curves.

Table 2 presents the maximum normalized concentrations ("diffusion factor"), C, and downwind distance to the maximum calculated impacts for various plume heights ranging from 200 to 5000 m above the surface. Table 2 demonstrates that the Karlsruhe A curves result in calculated impacts that are both larger and occur closer to the source. It can be seen from Table 2 that the P-G A and Karlsruhe A curves fortuitously agree well in resultant calculated impacts (both in magnitude and distance) even though they are based on entirely different field experiments. The other curves yield calculated maximum impacts that are smaller and occur at much greater distances from the source.

Comparison of Observations With Predictions

In order to further assess the alternative curves, maximum observed 3-hour average concentrations at monitoring sites nearest several sources having tall stacks were reviewed. Table 3 lists power plants having monitors within 2 km of their stacks and indicates the location of the plant as well as the nearest monitor and its location relative to the plant. It should be noted that reviews of monitoring data from monitors located at greater distances from these sources reveal that maximum 3-hour average concentrations at more distant monitors occur with more stable, higher wind speed conditions than those associated with the P-G class A stability category.

Table 3. Power Plants with SO_2 Monitors within 2 km of their Tall Stacks.

Power Plant	Location (County,State)	Monitor Number	Monitor Distance from Stacks (km)	Monitor Direction from Stacks (°)	Monitor Height above Stack Base (m)
John Sevier	Hawkins, TN	4	1.6	229	9
Widows Creek	Jackson, AL	24	1.6	139	4
Cumberland	Stewart, TN	6	1.8	97	26
Muskingum River	Washington, OH	5	1.3	37	78

Table 4 identifies the stack design and operating parameters and emission rates for each stack of each source. The stack parameters shown on Table 4 are used in conjunction with prevailing meteorological parameters to calculate plume height and position relative to the monitor site.

The wind speed and direction and plume height for each stack are shown on Table 5 for days of high monitored concentrations during unstable atmospheric conditions. The plume heights and transport wind velocities shown on Table 5 are used to calculate impacts at the monitoring sites using the alternative sets of dispersion coefficients with the standard Gaussian steady state dispersion equation for continuous point sources assuming an unlimited mixing layer.[7]

Table 4. Stack Design and Operating Parameters and Emission Rates.

Power Plant	Unit Number	Stack Number	Stack Height (m)	Stack Diameter (m)	Stack Exit Velocity (m/s)	Stack Exit Temperature (°K)	Emission Rate (g/s)
John Sevier*	1-2	1	107	7.2	12.3	412	1,925
	3-4	2	107	7.2	12.3	412	1,925
Widows Creek*	1-6	1	305	8.2	28.1	422	1,705
	7	2	152	6.3	28.1	399	4,917
	8	3	152	7.4	22.7	367	708
Cumberland*	1	1	305	9.5	32.9	422	10,544
	2	2	305	9.5	32.9	422	10,544
Muskingum River**	1-4	1	252	7.6	23.5	430	5,712
	5	2	252	6.7	11.7	450	4,465

* Operating parameters shown represent full load conditions. Emission rate is based on reported monthly average sulfur content of the fuel for the plant assuming full load conditions.

** Operating parameters shown represent lowest stack velocity and temperatures and highest emission rates reported for the period of interest.

Table 5. Plume Transport Parameters Used in Calculating Power Plant Impacts.

Power Plant	Date	Hour	Wind Speed* (m/s)	Wind Direction (°)	Calculated Plume Height above Monitor Site**		
					Stack 1 (m)	Stack 2 (m)	Stack 3 (m)
John Sevier	3/25/77	15	3	36	690	690	
		16	2	347	1080	1080	
		17	2	49	840	840	
Widows Creek	9/20/78	12	3	319	1190	770	Unit #8 Not in Service
		13	3	261	1270	830	
		14	2	339	1570	1030	
Cumberland	10/22/77	15	3	307	1850	Unit #2 Not in Service	
		16	3	261	1680		
		17	2	30	2590		
Muskingum River	9/5/78	14	1	360	2400	1500	
		15	1	(217)***	4630	2830	
		16	1	340	2400	1500	

* Wind speed scaled from highest anemometer height to stack top by the approximation: $u_1/u_2 = (z_1/z_2)^{0.1}$; where z_i is the height above the surface and u_i is the wind speed at that height.

** An unlimited mixing layer is assumed in all calculations.

*** Not reported, assumed value represents flow directly from source to monitor.

Table 6 compares the observed 3-hour average concentrations with concentrations calculated using the alternative sets of dispersion coefficients. It can be seen from Table 6 that all the predicted concentrations resulting from the use of each of the alternative sets of dispersion coefficients underpredict the observed 3-hour average values at each monitoring site. It should be noted, although not directly shown, that even if the mixing layer was assumed to be equal to plume height, the 3-hour average concentrations would still be underpredicted by use of the P-G B, BNL B_2 and Jülich A curves. Calculations based on the use of the P-G A and Karlsruhe A curves, however, appear to best approximate observations.

In order to determine if wind direction measurement and reporting errors could be the cause of the large degree of underpredictions, predicted concentrations are also calculated assuming the mean wind blew continually in the direction of the monitor. Table 7 presents the results of such calculations and compares them to measurements. It is noted that the concentrations monitored are still always underpredicted in each case by the P-G B, BNL B_2 and the Jülich A dispersion coefficients for this very conservative assumption. Again, calculations based on use of the P-G A and Karlsruhe A curves still appear to best approximate monitored values even for this conservative assumption. Note, due to lack of sufficient monitoring coverage at distances closer to the stacks, it is impossible to determine if the P-G A and Karlsruhe A curves locate the maximum impacts too close to the stacks and/or underpredict the magnitude of such impacts.

Table 6. Comparison of Observed and Calculated SO_2 Concentrations for the Fixed Monitoring Sites.*

			SO_2 Concentration (ppm)					
				Calculated to Occur at Monitor Site				
Power Plant	Date	Hour	Observed	P-G A	P-G B	BNL B_2	Jülich A	Karlsruhe A
John Sevier	3/25/77	15	.56	.21	---**	.09	.19	.11
		16	.44	---	---	---	---	---
		17	.28	.45	---	.08	.18	.21
		15-17	.43	.22	---	.06	.12	.11
Widows Creek	9/20/78	12	.33	.49	---	.12	.20	.23
		13	.37	---	---	---	---	---
		14	.15	.12	---	---	.04	.10
		12-14	.28	.20	---	.04	.08	.11
Cumberland	10/22/77	15	.27	.01	---	---	---	.02
		16	.15	.15	---	---	.01	.13
		17	.20	---	---	---	---	---
		15-17	.21	.05	---	---	---	.05
Muskingum River	9/5/78	14	.39	---	---	---	---	---
		15	.53	≤.01	---	---	---	≤.64
		16	.26	---	---	---	---	---
		14-16	.39	---	---	---	---	≤.21

* Observed concentrations include background SO_2 concentrations. Background concentrations for each period analyzed are estimated not to exceed 0.02 ppm. Calculated values shown do not include any background contributions.

** --- indicates that the calculated value is less than 0.005 ppm.

Table 7. Comparison of Observed and Calculated SO_2 Concentrations Assuming that the Mean Wind is Always Directly from the Source to the Monitoring Site for Calculation Purposes.*

			SO_2 Concentration (ppm)					
				Calculated for Plume Centerline				
Power Plant	Date	Hour	Observed	P-G A	P-G B	BNL B_2	Jülich A	Karlsruhe A
John Sevier	3/25/77	15	.56	.39	---**	.19	.24	.17
		16	.44	.52	---	.01	.08	.27
		17	.28	.45	---	.08	.18	.21
		15-17	.43	.45	---	.09	.17	.22
Widows Creek	9/20/78	12	.33	.49	---	.12	.20	.23
		13	.37	.52	---	.08	.18	.25
		14	.15	.59	---	.02	.10	.31
		12-14	.28	.53	---	.07	.16	.26
Cumberland	10/22/77	15	.27	.46	---	---	.01	.32
		16	.15	.46	---	---	.01	.29
		17	.20	.36	---	---	---	.41
		15-17	.21	.43	---	---	.01	.34
Muskingum River	9/5/78	14	.39	.41	---	---	---	1.05
		15	.53	.01	---	---	---	.64
		16	.26	.41	---	---	---	1.05
		14-16	.39	.28	---	---	---	.91

* Observed concentrations include background SO_2 concentrations. Background concentrations for each period analyzed are estimated not to exceed 0.02 ppm. Calculated values shown do not include any background contributions.

** --- indicates that the calculated value is less than 0.005 ppm.

Summary and Recommendations

The available alternative sets of dispersion coefficients for use in Gaussian modeling of effluents from tall stacks under very unstable atmospheric conditions vary significantly with respect to both the magnitude and location of their resultant predicted impacts. If the other modeling approximations as standardly employed in steady state Gaussian models are assumed to be appropriate (e.g., assumptions and modeling methodology as employed in the U.S. EPA CRSTER model), the results of the limited comparisons presented herein suggest that the P-G A and Karlsruhe A curves are better predictors of maximum impacts of tall stack effluents under unstable atmospheric conditions at monitors within 2 km of the stacks, than the P-G B, BNL B_2, or Jülich A curves. Comparisons also suggest that σ_z values larger than those of the P-G B, BNL B_2, or Jülich A curves are required to approximate the location of maximum impacts under unstable atmospheric conditions.

Due to the lack of measurements of plume height, trajectories of the elevated plumes, and mixing heights, caution is warranted. Furthermore, such factors as increased initial plume growth during plume rise, enhanced plume rise due to multiple stacks, transitional plume rise effects, changes in height of the plume centerline downwind of final plume rise, and non-Gaussian conditions influencing transport and dispersion have not been applied in the calculations made herein.

In order to better assess the impacts of tall stack effluent under unstable atmospheric conditions, more monitors are recommended to be placed in areas nearer such sources than has been standardly practiced to date. Downwind and crosswind arrays of monitors close to the source in the directions of expected impacts under unstable atmospheric transport conditions are warranted. Measurement of plume height and distribution of the effluent mass as a function of downwind distance is also recommended in order to better ascertain the transport and dispersion of tall stack effluents during unstable atmospheric conditions.

References

1. Gifford, F.A., Jr., 1961: Use of Routine Meteorological Observations for Estimating Atmospheric Dispersion, Nuclear Safety, 2(4), 47-51.

2. ANL, 1977: Report to the U.S. EPA of the Specialists' Conference on the EPA Modeling Guideline, Argonne National Laboratory, Chicago, IL, 322 p.

3. Singer, I.A., and M.E. Smith, 1966: Atmospheric Dispersion at Brookhaven National Laboratory, Int. J. of Air Water Pollution, 10, 125-135.

4. Smith, M.E. (ed), 1973: Recommended Guide for the Prediction of the Dispersion of Airborne Effluents, 2d ed., Am. Soc. of Mech. Engineers, 85 p.

5. Vogt, K.J. et al., 1978: New sets of diffusion parameters resulting from tracer experiments in 50 and 100 meters release height, Proceedings of the NATO/CCMS 9th International Technical Meeting on Air Pollution Modeling and its Application, August 28-31, 1978, Toronto, 221-239.

6. Kiefer, H. and W. Koelzer, 1979: Jahresbericht 1978 der Abteilung Sicherheit, Kernforschungszentrum Karlsruhe, 191-195.

7. Turner, D.B., 1970: Workbook of Atmospheric Dispersions Estimates, USDHEW, PHS Pub. No. 995-AP-26, 84 p.

Discussion:

Dr. Trout:

This paper serves to demonstrate that if a single model component is selected for potential revision, that great care must be exercised regarding any generalizations or conclusions that are to be derived. For example, some critics of a standard steady state Gaussian model (the US EPA CRSTER model) which uses the Pasquill Gifford (P-G) curves have suggested only that the P-G class A curves be replaced with the P-G class B curves or some other set of curves.

These critics have not chosen (at least to this point in time) to review or refine the other model algorithms and assumptions (as briefly summarized in the conclusion of this paper) which may be equally or more important to refining the understanding and modeling of tall stack effluents under very unstable atmospheric conditions.

We have shown that some alternative curves (e. g. the P-G class B and BNL B_2 curves) if substituted for the P-G class A curve without any other changes to the model would result in even greater under estimates of the higher concentration observed at monitoring sites within 2 km of tall stacks (based obviously on the very limited data set available). We should note that such critics previously have contended that the P-G A curves caused over estimates of ground level impacts as opposed to under estimates using the US EPA CRSTER model.

Note, we are not proposing or concluding from this very limited study that the P-G class A curves best represent the distribution of the mass of elevated plumes in reality, but only that when we must constrain ourselves to a given set of associated modeling assumptions (e. g. plume rise calculations, orographic and inversion effects, etc.) the P-G class A curves in comparison to the P-G B_2 or the BNL B_2 curves may perform fortuitously well in calculating short term (3-hr) maximum impacts at monitors with 2 km of tall stack sources during P-G class A conditions.

Therefore if revisions to a given or reference model are proposed, all associated model algorithms and assumptions must be evaluated. Otherwise we may improve only that component and perhaps lessen the overall performance of the given model because other components having compensating errors (with respect to the original single component now revised) still remain.

SUMMARY OF PANEL DISCUSSION ON TALL STACKS

Rapporteurs: R. V. Portelli & M. M. Millan

Panelists: W. Klug (Chairman), P. Maul, M. Smith, T. Schneider,
H. Fortak, A. Berger

Professor Klug opened the round table discussion by requesting each panelist to make some introductory comments on tall stacks suggesting that as a starting point, his presentation on the impacts of tall stacks on the atmosphere, could be referred to. An open discussion followed.

Smith:

He agreed with Klug's statements that not enough is known about tall stack plumes and their behavior in the boundary layer. However, he felt that the current studies are showing promise and indicated that the morning's presentations on experimental studies dealing with tall stacks were very encouraging.

Schneider:

He supportet Smith's view regarding the presentations of the morning session and then posed the question 'Can you really model dispersion from tall stacks?' He stated that if you want to determine impact the best approach with tall stacks is to utilize trajectory analysis.

Fortak:

He indicated that he was not as pessimistic about modelling tall stack plumes. His aircraft observations have supported his modelling efforts and indicate that Briggs' plume rise equations work well. The looping condition, however, cannot be described well by Gaussian models except perhaps for long averaging times when a statistical treatment can provide useful information.

Berger:

He considered it important to divide the horizontal scale into two parts:

1) short-range
2) long-range

Also, the vertical scale should be divided into:

1) diffusion into the PBL
2) diffusion into the free atmosphere

It is necessary that different scaling in the atmosphere and discontinuities be accounted for.

Maul:

The effectiveness of tall stacks depends on the diffusion climatology to large extent. In Britain, there are less frequent convective boundary layers. Therefore, tall stacks are more effective.

Q Yamartino:

He questioned the case for tall stacks in short, medium or long-range situations in convective conditions.

A Smith:

The tall stack is effective in convective conditions when long time periods are considered.

Q Klug:

Ground concentrations are one concern, however, to the nuclear industry, deposition, particularly wet deposition is an important consideration when identifying ingestion pathways.

R Klug:

Agreed.

C Trout:

He pointed to the scarcity of monitoring data near tall stacks which makes it difficult to assess the capabilities of models for tall stack applications.

C Hübschmann:

The highest concentrations occur at heights of 100 - 200 m above ground, as indicated by observations. In view of this, legislation based on ground level concentrations is not adequate.

C Schneider:

When using the word 'effective', it must be asked 'effective' for whom or for what?. For example, if 80 % of emissions from a tall stack travel a long distance, then the tall stack is effective in ensuring that the local ground level standard is met but what about the long-range transport and resulting transformations? The newly formed pollutants may be more dangerous than the original pollutants.

C Benarie:

We have only spoken of SO_2. It is necessary that we also address particulates.

C Gillani:

He pointed out that the U. S. STATE program has collected data over long travel distances (to 400 km) for other pollutants as well as SO_2 and that night observations were also made.

C Klug:

He indicated that the WMO is looking for complete experimental data sets and any information on such should be provided to him.

Q Jost:

Since dispersion from tall stacks is not well understood, particularly in looping conditions, what data sets do exist which can be used to assess the benefits of tall stacks?

R Millan:

He referred to Canadian tall stack data for Sudbury's INCO stack, but also indicated that with such tall stacks a much larger area needs to be covered when trying to 'catch the plume', and this obviously leads to greater experimental difficulties.

C Smith:

Agreed with Millan, then referred to the balance of costs: tall stacks versus emission control.

C Kretzschmar:

We have been discussing primarily tall stack data from Canada and the U. S. However, the results from these studies cannot necessarily be extrapolated to Europe, in view of differing problems such as a larger number of urban heat islands within a given region.

C Portelli:

Referred to Maul's earlier remarks about dispersion climatology. He pointed out that climatological studies, such as of regional mixing heights and mixing layer wind speeds, should be carried out to aid in impact assessments as well as in the design of experimental programs.

C Venkatram:

Referred to earlier statements about a lack of predictive capability for (looping) unstable conditions. He felt that people had missed the point of his presentation which showed that his model can predict 1-hour looping concentrations.

C Berger:

Stated that we must consider the total impact on the environment of pollutants from tall stacks, and therefore the energy /climate system must be studies as a whole.

Klug:

In his closing remarks he thanked the panelists and the audience and hoped that the discussions will stimulate further work on tall stacks.

Q = Question
R = Response
C = Comment

10TH NATO /CCMS INTERNATIONAL TECHNICAL MEETING
ON AIR POLLUTION MODELING AND ITS APPLICATION

TOPIC 2

Complex Terrain and Weak Wind Conditions

Preceding page blank

A GROSS PARAMETER PLUME MODEL: THEORY AND APPLICATION FOR NON-PLANAR TOPOGRAPHY AND FOR NEGATIVELY BUOYANT EFFLUENTS

by

Brian Henderson-Sellers
Department of Civil Engineering
University of Salford, U.K.

Abstract. A "three phase" plume model, based on initial work by Slawson and Csanady is described. The formulation extends the regions of applicability of this forced plume model to cases of non-planar natural and artificial topography. The case of a negatively buoyant plume (e.g. one containing a percentage of sulphur dioxide) is also shown to be well simulated. The results are expressed in terms of plume centreline trajectory, rates of spread of plume material (which depends upon the dominant mixing mechanisms) and ground level concentrations. Finally, it is demonstrated that the third phase of this model, designed primarily for calculations of plume rise, is in fact identical to the well-developed diffusion theories (K theory, statistical theory) derived for and applied to a passive, neutrally buoyant effluent.

Introduction

When an effluent is emitted into the atmosphere (e.g. from a tall stack) it is important to be able to calculate the trajectory this material takes and the rate at which it spreads (and thus becomes diluted). Many models already exist which adequately describe both plume rise and diffusive spreading in the idealised case of a neutrally stratified atmosphere and a flat terrain. Here one of these approaches (that of a gross parameter "three phase" model originally developed by Slawson and Csanady[1,2])is developed further to extend the range of applicability to non-vertical emissions, non-planar topography (e.g. hills, buildings) and to negatively buoyant effluents; and where the atmospheric stratification is specified in detail. Such a comprehensive simulation requires a finite difference formulation - the model described here uses a set of curvilinear coordinates first used by Hoult et.al.[3] with a grid length defined either by an incremental distance, Δs, or an incremental time, Δt. The results given here use a variable length step, which has a value of 0.0001 m for the first, relatively short, but critical section of the trajectory (usually about 100 m); and thereafter a default value of 0.05 m. (These parametric values have been optimised after several computer runs using various values for Δs).

Theory

Plume model

The forced plume simulation uses a gross parameter numerical model which takes parametric values integrated across the plume, although the assumed profile permits concentrations etc. to be determined at any point in the plume. The model is described in detail by Henderson-Sellers[4] and is a 2 or 3 dimensional model based on ideas of Fox[5] and on entrainment concepts first used by

Preceding page blank

Morton et.al.[6]. As a reasonable first approximation, it neglects both the zone of flow establishment and downwash and wake effects.

The four conservation equations are expressed in terms of the flux variables for mass, momentum and buoyancy V, M, B defined by

$$V = b^{a+1}\,W, \quad M = b^{(a+1)/2}\,W, \quad B = b^{a+1}\,W\Delta \tag{1}$$

where b is the length scale associated with the radius (see later discussion). W and Δ are the centreline (axial) values of velocity u and buoyancy parameter $\delta = g(\rho_e - \rho)/\rho_1 = g(\theta - \theta_e)/\theta_1$; where $\rho_1 = \rho_e(0)$. These equations are:

$$\frac{dV}{ds} = 2^{1-a}\,\frac{V_e}{I_1}\left(\frac{V}{M}\right)^{\frac{2a}{a+1}} \tag{2}$$

$$\frac{dM^4}{ds} = 2\,\frac{I_3}{I_2}\,B\,V\sin\phi \tag{3}$$

$$\frac{dB}{ds} = -\,\frac{I_1}{I_4}\,N^2\,V\sin\phi \tag{4}$$

$$\cos\phi = \left(\frac{B_o\,V_o}{M_o^2}\,\cos\phi_o\right)\frac{M^2}{BV} \tag{5}$$

Here V_e is the entrainment velocity, I_i constants related to the assumed cross-sectional profiles of density and velocity, ϕ the angle of the plume to the horizontal and N^2 is the Brunt-Väisälä frequency. The parameter a has the value unity for a three-dimensional (point source) and zero for a two-dimensional (line source) plume.

For most forced plumes it is found that in the initial stages of the plume rise, the turbulence responsible for diluting the plume is generated by the plume's motion itself. In this case the entrainment velocity V_e is simply related to the axial velocity W by

$$V_e = V_{e_1} = \alpha|W| \tag{6}$$

(Morton et.al.[6]) where α is the "entrainment coefficient". This is a function of the densimetric Froude number, F_D^2 [7,8]. In a neutrally stratified environment this relationship is strictly linear, but must be modified if the environment is non-neutrally stratified[5].

As the plume tends to its equilibrium height, the momentum effects decrease and the rise is controlled by the buoyancy effects. Turbulent mixing is no longer a result of a velocity shear but originates as eddies in the plume. (second phase) and then large scale energy containing eddies of the atmosphere (third phase). Although it has been suggested by several authors that the plume progresses naturally through these phases, there now appears to be some doubt whether the plume will remain in the third phase, or whether the internal eddy diffusivity which seems to grow with distance downwind[9] will once again become dominant. Assuming, for the present, that the third phase remains dominant at large distances downstream, it becomes possible to use this model to analyse the effects on plume rise and dispersion rates of non-linear lapse rates, topography etc.

Entrainment Velocity

It is possible to associate with the three phases an entrainment velocity V_{e_i} (i = 1 to 3). Slawson and Csanady[1] give expressions for V_{e_2} and V_{e_3}:

$$V_{e_2} = a_1 \; \epsilon^{1/3} \; b^{1/3} \tag{7}$$

$$V_{e_3} = a_2 \; v \; L/b \tag{8}$$

where a_1, a_2 are constants, ϵ is the turbulent energy dissipation, v the rms turbulent velocity and L the turbulent length scale. These expressions must be developed so that the length scales can be related to observable parameters and to the length scales of the obstacles creating the turbulence (the latter in the third phase only). This is discussed fully elsewhere[10]. Using mixing length theory, ϵ and v can be expressed in terms of the eddy diffusivity K; and using a formula[11] for the friction velocity, u gives

$$V_{e_2} = a_1 \frac{P}{P_o} \; f(S) \; \overset{*}{u} \left(\frac{b}{L_2}\right)^{1/3} \tag{9}$$

$$V_{e_3} = a_2 \frac{P}{P_o} \; f(S) \; \overset{*}{u} \; L_3/b \qquad (b > H^*) \tag{10}$$

where P is the turbulent Prandtl number and P_o its neutral value; L_2 and L_3 are length scales and $f(S)$ is given by

$$f(S) = (1 + 0.1\,S)^{-1} \tag{11}$$

(Sundaram and Rehm[12]) in which S is the Richardson number. Equation 10 is only applicable when the atmospheric eddies (length scale H^*) are of comparable size to the plume radius, (Perkins[13]).

The length scales are given as

$$L_2 = 2\,b \tag{12}$$

$$\text{and} \quad L_3 = k\,(z + h) \tag{13}$$

where $k \simeq 0.4$ is von Karman's constant, z is the height of the plume above ground and h is the height of the topography.

Rates of Spread

The model described above predicts the plume path given by the locus of the centreline of the effluent material. To calculate ambient concentrations, it is necessary to know the value of the plume radius at each point downstream of the stack. It is possible to calculate the rate of increase of radius db/ds using two approaches; the cross-sectional profiles of velocity, buoyancy, pollutant concentration can be described by either a "top hat" or a Gaussian profile. In the former approach, the plume material is assumed to be mixed homogeneously across the plume of radius R such that e.g. for velocity u(r,s)

$$u(r,s) = \text{constant} = W \quad \text{for } |r|<R \qquad (14)$$
$$= 0 \quad \text{elsewhere}$$

This may be a useful representation for the profile of some plumes instantaneously although it is unlikely to be consistent with a smooth trajectory for the centreline when evaluated as a function of s - notwithstanding this, the top hat profile has been used by several authors as a useful model[14]. The alternative approach is to use the Gaussian profile to describe the time averaged cross-sectional shape of the plume. This agrees more closely with observations, whilst introducing the problem of defining the radius. A standard definition would be the distance at which the concentration is 1/e th of its centreline value[6], $R_e = b$; although this definition is not very useful, for example, in determining where and when the plume first touches ground. A more useful definition would appear to be where the profile value is C of its centreline value (where C is say 10 or 1 or less) giving a radius R_C - the definition is thus arbitrary to a large extent.

Comparison of the top hat and Gaussian profiles shows that the respective values of the constants (I_i) are different[5] as are the values for the entrainment constant α. Morton[14] shows that

$$\frac{\alpha\ (\text{Gaussian})}{\alpha\ (\text{Top hat})} = \frac{1}{\sqrt{2}} \qquad (15)$$

- this can easily be shown to be consistent with a ratio of the centreline velocities for the two profiles given by

$$\frac{W(\text{Gaussian})}{W(\text{Top hat})} = \frac{2}{1} \qquad (16)$$

- a comparison worthy of further consideration.

(Note. This discussion assumes the plume to have a symmetrical, circular cross-sectional profile. This is observed not to be the case when the plume encounters an inversion - this has been discussed in detail[15] where models for the elliptical shape of e.g. fanning plumes are presented.

The spread rate, db/ds, can then be calculated. From the definition of M and V given previously, it is easily shown that

$$b = \left(\frac{V}{M}\right)^{2/(a+1)} \qquad (17)$$

and hence

$$\frac{db}{ds} = \frac{2}{a+1}\left(\frac{V}{M}\right)^{\frac{1-a}{1+a}} \frac{M\frac{dV}{ds} - V\frac{dM}{ds}}{M^2} \tag{18}$$

Substituting for dV/ds and dM/ds from equations 2 and 3 gives

$$(a+1)\,W\frac{db}{ds} = 2^{1-a}\,\frac{V_e}{I_1} - b\,\frac{dW}{ds} \tag{19}$$

In the first phase this gives

$$\frac{db}{ds} = \frac{2^{1-a}}{a+1}\,\frac{\alpha}{I_1} - \frac{b}{(a+1)W}\,\frac{dW}{ds} \tag{20}$$

and in the second and third phases

$$\frac{db}{ds} = \frac{2^{1-a}}{\overset{*}{W}\,(a+1)}\,\frac{V_e}{I_1} - \frac{b}{\overset{*}{W}(a+1)}\,\frac{d\overset{*}{W}}{ds} \tag{21}$$

where $\overset{*}{W}$ is the resultant centreline velocity (of plume rise velocity W and wind speed U).

For a plume in its first phase of rise, the equation is reduced to

$$\frac{db}{ds} = \frac{1}{2}\,\frac{\alpha}{I_1} = \alpha \tag{22}$$

This agrees with previous theories[14] and gives a value for db/ds $\simeq 0.1$. In the third phase, the lateral spread rate is considerably less. From equation 21 for a typical entrainment velocity of the order of 0.10 and a 6 m s^{-1} wind, db/ds $\simeq 0.02$. It is thus important to calculate the spread rate - assumptions that equation 22 can be applied to all three phases will predict erroneous values of ground level concentrations.

Final Phase

It is worth noting that in the third phase

$$\frac{db}{ds} = \frac{2^{1-a}\,V_{e_3}}{\overset{*}{W}\,(a+1)I_1} \simeq \frac{V_{e_3}}{\overset{*}{W}} \tag{23}$$

It has been shown[1] that equation 8 can be rewritten as

$$V_{e_3} = a_2\,K/b \tag{24}$$

Hence in the third phase (where $\dot{W} = U$),

$$\frac{db}{ds} = \frac{a_2 K}{bU} \tag{25}$$

On the other hand, the radius R_e of the standard Gaussian plume model can be shown to be given by

$$R_e = b = 2\sqrt{\frac{Kx}{U}} \tag{26}$$

and hence an entrainment velocity of

$$V_G = 2 K / b \tag{27}$$

The value of the constant here depends upon the choice of C in the definition of radius. The forms of equations 25 and 27 are identical, implying that using these definitions (above) of radius $a_2 = 2$. (Other authors e.g. Batchelor[16,17] suggest slightly larger values for a_2).

It would certainly appear from this analysis that the final phase of the Slawson and Csanady three phase model and the so-called Gaussian plume model are identical - a conclusion implied previously[1].

Simulations

Applications of this model to test cases have been presented in detail elsewhere[5,10]. The case of both a marginally buoyant and a strongly buoyant source is compared favourably with other models in Table 1. The third phase effects of underlying topography are most easily seen in a marginally buoyant plume. Assuming a constant friction velocity (a restriction which will be removed in a later paper), the model predicts a variation in centreline height of about 2-3% (see Table 2). Although this results in a difference of less than 1 metre in the cases chosen, this may well be sufficient to alter ground level concentrations either directly, or for instance, by changing the probability that a effluent becomes trapped in a building wake or cavity, where the resulting "downdraught"[18] may lead to changes in pollutant concentrations of several orders of magnitude.

Table 1. Plume Rise in Metres at 500 m Downstream of Source

$W_o = 0.01 \text{ m s}^{-1}$

Formula	T_o = 290K	T_o = 350K
i) CONCAWE	0.42	1.43
ii) Carson and Moses	0.16	0.50
iii) This model	0.28	1.96

Table 2. Final Rise Values at 5000 m Downstream of the Source ($W_o = 0.01 \text{ m s}^{-1}$)

	Planar topography	Non-planar natural topography	Non-planar artificial topography	
			Plume emitted upwind of city	Plume emitted in city centre
290K	0.511	0.500	0.509	0.510
350K	3.656	3.574	3.644	3.651

It must be remembered (see above discussion) that in addition to affecting the centreline trajectory, different levels of turbulence also alter the rate at which the plume spreads laterally - a further important factor in determining ground level concentrations.

The model can also be applied to negatively buoyant effluents. One important case is that of emissions of sulphur dioxide, where the comparatively high molecular weight of SO_2 may result in an overall buoyancy which is low or even negative upon emission. The momentum effect will often be sufficient to raise the effluent above the stack top, although it may later sink back, possibly to ground level. The model formulation allows for negative values of buoyancy and initial runs using a 10% and a 1.5% SO_2 plume show a decrease in height of rise compared to plume of molecular weight equal to ambient. For the marginally buoyant plume of Table 2, the rise is nullified and the plume reaches equilibrium just below the height of emission. Of course this should realistically result in downwash effects - a phenomenon not yet included in this model - and increase ground level concentrations even more.

The initial buoyancy Δ_o, calculated by

$$\Delta_o = g\left(\frac{\theta-\theta_e}{\theta_1}\right) \tag{28}$$

where θ is the potential temperature of the effluent, θ_e that of the environment and θ_1 a reference temperature, is now written as

$$\Delta_o = g\left(\frac{\theta-\theta_e}{\theta_1} + \frac{\rho_e-\rho}{\rho_1}\right) \tag{29}$$

where ρ represents the corresponding values of potential density due to change in molecular weight Hence in terms of molecular weight,

$$\Delta_o = g\left(\frac{\theta-\theta_e}{\theta_1} + \frac{m_e-m}{m_1}\right) \tag{30}$$

Noting that at the stack top, $\theta_e = \theta_1$ and $m_e = m_1$ we find that

$$\Delta_0 = g\left(\frac{\theta}{\theta_1} - \frac{m}{m_1}\right) \tag{31}$$

For a 10% SO_2 plume, the original buoyancy is negative if $\theta/\theta_1 \lesssim 1.1$.

For a typical reference temperature of 288K, the plume will rise if its temperature is greater than about 325K. Further investigative modelling is necessary to relate quantitatively SO_2 content, ambient temperature, effluent temperature.

Conclusions

The modelling of a stack emission within an urban environment must take into account many factors. It has been shown that a three phase plume is more applicable since atmospheric eddies created by urban topography are an important factor in determining plume characteristics during the latter stages of its rise. The model has been developed to illustrate the individual effects of non-planar natural topography and artificial urban topography. The spread rate also depends upon parameterisation of turbulent mixing at all stages. It also appears that the third phase of the model may be identical to Gaussian plume models implying that plume rise and plume dispersion models and techniques can be combined into a single theory.

References

1. P.R.Slawson and G.T.Csanady, "On the Mean Path of Buoyant Bent Over Chimney Plumes", J.Fluid Mech.,28,311,1967.
2. P.R.Slawson and G.T.Csanady, "The Effect of Atmospheric Conditions on Plume Rise", J.Fluid Mech.,37,33-48,1971.
3. D.P.Hoult, J.A.Fay and L.J.Forney, "A Theory of Plume Rise Compared to Field Observations", J.Air Poll. Control Assocn.,19,585-590,1969.
4. B.Henderson-Sellers, "Forced Plumes in a Stratified Reservoir", Procs. ASCE., J.Hyd.Div.,104,HY4,487-501,1978.
5. D.G.Fox., "Forced Plume in a Stratified Fluid", J.Geophys.Res.75,6918-6835,1970.
6. B.R.Morton,G.I. Taylor and J.S.Turner, "Turbulent Gravitational Convection from Maintained and Instantaneous Sources",Procs.Roy.Soc.,A234,1-23,1956.
7. E.J.List and J.Imberger, "Turbulent Entrainment in Buoyant Jets and Plumes",Procs.ASCE.,J.Hyd.Div.,99,HY9,1461-1474,1973.
8. E.Hirst, "Buoyant Jets Discharged to Quiescent Stratified Ambients", J.Geophys.Res.,76,7375-7384.
9. D.B.Turner, "Workbook of Atmospheric Dispersion Estimates", U.S.Public Health Service Publication,999-AP-26,1970.
10. B.Henderson-Sellers, "The Behaviour of Marginally Buoyant Plumes in an Urban Environment", Ecological Modelling, in press.
11. B.Henderson-Sellers, "Role of Eddy Diffusivity in Thermocline Formation", Procs.ASCE.,J.Env.Eng.Div.,102,EE3,517,1976.
12. T.R.Sundaram and R.G.Rehm, "Formation and Maintenance of Thermoclines in Temperate Lakes", AIAA J.,9,1322-1330,1971.
13. H.C.Perkins, "Air Pollution", McGraw-Hill, London,1974,p151.

14. B.R.Morton, "The Ascent of Turbulent Forced Plumes in a Calm Atmosphere". Int.J.Air Poll.,1,184-197,1959.

15. B.Henderson-Sellers, "The Cross-Sectional Asymmetry of Plumes in Inversion Conditions". Appl.Math.Modelling,3,327-331,1979.

16. G.K.Batchelor, "The Application of the Similarity Theory of Turbulence to Atmospheric Diffusion", Q.J.Roy.Met.Soc.,76,133-146.

17. G.K.Batchelor, "Diffusion in a Field of Homogeneous Turbulence", Proc.Camb. Phil.Soc.,48,345-362,1952.

18. J.Halitsky, "Gas Diffusion near Buildings", Trans.ASHRACE.,69,464-485,1964.

BUOYANT PLUME RISE OVER A TWO-DIMENSIONAL HILL

by

Jeffrey C. Weil
Environmental Center, Martin Marietta Corporation
Baltimore, Maryland 21227 USA

Abstract. A mathematical model has been formulated for the rise and spread of a buoyant plume in neutral and stably stratified flows over a two-dimensional hill. The plume characteristics were computed from an integral equation method developed for a plume in a two-dimensional flow, which is an extension of an earlier method for plumes in horizontal flows. The plume equations were combined with an ambient flow model for solution. The ambient flow was computed from the idealized model of Long, but the plume equations are general and can be coupled to a more general ambient flow calculation. A comparison of predicted plume height and vertical spread by the plume model with experimental wind tunnel data showed good agreement.

Introduction

Prediction of plume rise is a critical factor for estimating ground-level concentrations of stack pollutants in complex terrain. However, conventional plume rise formulas[1] for flat terrain do not apply when a stack is near enough to elevated terrain (within a few kilometers) that the plume rises in a nonhorizontal wind field. For this situation, a new approach for computing plume rise is needed to take into account the effects of the deformed wind field on the plume.

This paper presents a mathematical model for calculating buoyant plume rise and spread in neutral and stably stratified flows over a two-dimensional hill. A two-dimensional barrier was chosen as a first step because of the great complexity in modeling ambient flow fields with stratification and three-dimensional complex terrain. The mathematical model was tested by comparing predicted wind fields and plume characteristics to wind tunnel simulations under idealized flow conditions (uniform upstream velocity and density stratification) over a two-dimensional barrier. The model was also compared to two existing methods for computing plume heights in elevated terrain.

Mathematical Model

The mathematical model for a buoyant plume in a two-dimensional flow consists of 1) a description of the ambient wind and temperature fields, and 2) a model for the behavior of the plume in those fields. For the plume characteristics, we use an integral equation approach in which we write differential equations for the total fluxes of mass, momentum, and energy over a plume cross section. This approach is traditional for plumes and was used successfully in the past to predict the behavior of both dry plumes[1,2] and moist plumes[3] in horizontal winds (i.e., in flat terrain). The equations presented here for a dry plume in a two-dimensional flow are an extension of those for the horizontal wind case (see Weil[4] for the derivation of the equations). The system of

Preceding page blank

equations is closed with an entrainment assumption relating plume growth to plume kinematics.

In the analysis, the wind components, as well as other atmospheric variables -- density, temperature, and pressure -- are assumed to vary both with altitude and downwind distance. The flow is steady and incompressible, and density differences between the plume and ambient air are assumed to be small enough that the Boussinesq approximation can be used. Furthermore, changes in ambient flow variables with location are assumed to be sufficiently small that the gradients in the variables can be considered constant over a plume cross section.

The horizontal and vertical velocity perturbations due to the plume, Δu and Δw, respectively, and the temperature perturbation ΔT are average differences between plume and ambient characteristics taken over a cross section normal to the local plume centerline.

Conservation of mass is expressed by

$$\frac{d}{ds}(u_{sc}\, b^2) = 2b\, v_e \tag{1}$$

where u_{sc} and s are the velocity and distance, respectively, along the plume centerline; b is the effective plume radius; and v_e is the entrainment velocity. We use the entrainment assumption of Hoult et al.,[2] which states that the entrainment velocity is proportional to the velocity differences parallel and normal to the plume centerline:

$$v_e = \alpha|u_{sc} - u_a \cos\phi - w_a \sin\phi| + \beta|w_a \cos\phi - u_a \sin\phi| \tag{2}$$

where α and β are the proportionality constants for parallel and normal velocity differences, respectively; u_a and w_a are the horizontal and vertical components of the ambient wind, respectively; and ϕ is the angle of the plume centerline with respect to the horizontal. Equation (2) differs from the entrainment expression of Hoult et al. in that it allows for the vertical component of the ambient wind.

Equations for conservation of horizontal and vertical momentum along the plume are given respectively by

$$\frac{d}{ds}(b^2\, u_{sc}\, \Delta u) = -\frac{\partial u_a}{\partial x}(b^2\, \Delta u) - \frac{\partial u_a}{\partial z}(b^2\, \Delta w) - \frac{1}{\rho_a}\frac{\partial p_a}{\partial x}\left(b^2\, \frac{\Delta T}{T_a}\right) \tag{3}$$

and

$$\frac{d}{ds}(b^2\, u_{sc}\, \Delta w) = -\frac{\partial w_a}{\partial x}(b^2\, \Delta u) - \frac{\partial w_a}{\partial z}(b^2\, \Delta w) - \frac{1}{\rho_a}\frac{\partial p_a}{\partial z}\left(b^2\, \frac{\Delta T}{T_a}\right) \tag{4}$$

where p_a and ρ_a are the ambient pressure and density, x the distance downwind of the hill crest, and z the height above level ground far from the hill. The gradients in ambient wind, pressure, and temperature (below) are evaluated at the local plume centerline height. In contrast to the equation for a plume in a horizontal wind,[3] the horizontal momentum equation includes a horizontal pressure gradient term arising from flow over the hill and a horizontal transport term ($\partial u_a/\partial x$). The vertical momentum equation likewise differs from its analog in the horizontal wind case by the inclusion of the first two transport terms on the right hand side. It also differs in that the pressure distribution is not assumed a priori to be hydrostatic.

The energy equation for the plume is

$$\frac{d}{ds}\left(b^2 u_{sc} \frac{\Delta T}{T_a}\right) = -\frac{1}{T_a}\frac{\partial\theta_a}{\partial x}(b^2 \Delta u) - \frac{1}{T_a}\frac{\partial\theta_a}{\partial z}(b^2 \Delta w) + \frac{1}{\rho_a c_p T_a}\left(u_a \frac{\partial p_a}{\partial x} + w_a \frac{\partial p_a}{\partial z}\right)\left(b^2 \frac{\Delta T}{T_a}\right) \tag{5}$$

where c_p is the specific heat of air at constant pressure, and θ_a the potential temperature of ambient air at height z. The difference between this equation and its counterpart in the horizontal wind case is the $\partial\theta_a/\partial x$ term and the third term on the right hand side, representing work done by the ambient wind and pressure field on the density (or temperature) perturbation.

For the ambient wind model used here, the departure from hydrostatic conditions is quite small, and $\partial p_a/\partial z$ could be set equal to $-\rho_a g$ with little loss of accuracy. Similarly, $\partial p_a/\partial x$ could be assumed as zero. We have chosen to retain the equations in their present form so that they could be used with a more general ambient flow model where nonhydrostatic conditions might be more pronounced.

To solve for the plume trajectory (rise z' versus distance downwind of the stack x'), we must add the kinematic conditions,

$$\frac{dx'}{ds} = \cos\phi, \quad \frac{dz'}{ds} = \sin\phi \tag{6}$$

$$\phi = \tan^{-1}\left(\frac{w_a + \Delta w}{u_a + \Delta u}\right) \tag{7}$$

the initial conditions on the mass, momentum, and energy fluxes, and the ambient flow description.

The ambient wind, pressure, and temperature fields necessary for solving the equations are obtained here from Long's model.[5] This model predicts gross fluid behavior such as streamline divergence and convergence and the associated fluid deceleration and acceleration. It considers inviscid, stably stratified flow over a two-dimensional barrier in a channel, and was originally formulated and used to study lee wave phenomena. By considering a flow which has a uniform (with height) kinetic energy and stratification far upstream of an obstacle, Long was able to transform the full equations governing the flow to a single linear equation. However, the boundary condition on the obstacle was nonlinear. Miles[6] found a Green's function for the problem whereby the flow field could be obtained for any arbitrarily shaped obstacle. A numerical scheme to apply the Green's function found by Miles was established by Davis[7] and successfully used to predict the flow about bluff two-dimensional obstacles in a channel. Davis' method is used here to predict flow over a two-dimensional Gaussian hill. The equations governing the flow and details of the calculations can be found in Weil.[4] It should be noted that the plume equations (1)-(7) are general and can be coupled to a more general ambient flow model (e.g., Sykes[8]) if desired.

The plume equations were solved by a computer program using a Runge Kutta standard library routine. The program was checked against analytical results for the flat terrain case.

Wind Tunnel Tests

Similarity Parameters

To conduct physical model experiments, it is convenient to characterize the stack exit conditions in terms of two important dimensionless parameters, the speed ratio R and the stack densimetric Froude number Fr. These parameters are given by

$$R = \frac{w_i}{u_a}, \qquad Fr = \frac{w_i}{\sqrt{b_i g \Delta_i}} \tag{8}$$

where g is the gravitational acceleration; w_i, b_i, and Δ_i are the stack exit values of velocity, plume radius, and fractional temperature difference, and

$$\Delta_i = \frac{T_i - T_1}{T_i} \tag{9}$$

where T_1 and T_i are the temperature of ambient air and plume at stack exit. Hoult and Weil[9] have shown that R and Fr are the only two dimensionless parameters that need to be modeled to attain geometrically similar plumes in scaled-down physical models, provided that the plume is fully turbulent at stack exit.

In stably stratified flows over an obstacle, the critical parameter determining the character of the flow field is the Froude number F_h based on obstacle height h:

$$F_h = \frac{u_\infty}{\left(\frac{g}{T_\infty}\frac{d\theta_\infty}{dz}\right)^{1/2} h} \tag{10}$$

where subscript ∞ denotes ambient conditions far upstream of the obstacle. The Froude number indicates the presence and amplitude of waves in the lee of the obstacle. For flows in a channel, as is the case here, the ratio of the obstacle height to channel height is an additional important parameter.

Experiments

Experiments with buoyant plumes in neutral and stably stratified flows over a two-dimensional hill were conducted in the stratified wind tunnel[10] at the Colorado State University. This low-speed, open-circuit tunnel has a test section 0.5 x 0.6 m in cross section and 4.6 m long. A nearly constant stable density gradient was created at the tunnel inlet by passing the flow through a vertical array of horizontal, parallel, electrically heated plates, which established a positive temperature gradient. The temperature profile was maintained along the tunnel by electrically heated plates on the ceiling and by cooled water panels on the floor. The maximum temperature gradient attained during these tests was 0.6°C/cm.

Experiments were conducted for three different stability conditions: $F_h = 1.31$, 3.47, and ∞, where the lowest F_h was the smallest value attainable in the tunnel. Uniform velocity profiles (except for thin boundary layers) were established in neutral ($F_h = \infty$) and slightly stable ($F_h = 3.47$) flows by placing a honeycomb mesh in the tunnel cross section about 10 cm upwind of the model stack. For the most stable case ($F_h = 1.31$), the honeycomb was removed because it created wavelike disturbances that strongly affected the plume[4].

The hill had a Gaussian profile $z_g(x) = h \exp(-x^2/2W^2)$ with its axis aligned perpendicular to the mean wind. The maximum hill height h and hill width W were both 6 cm (= 1/10 the tunnel height). A model stack emitting a helium/air mixture was located upstream of the ridge; in addition to creating a density defect, the helium acted as a plume tracer. A total of eight tests were conducted with the following stack conditions: $b_i = 0.16$ cm, $\Delta_i = 0.218$, and $Fr = 12.6$ for all tests; stack height equal to 1 cm or 3 cm; R ranging from 3.5 to 6.8; and distance between stack and ridge crest either 19 cm or 50 cm. The plumes were made turbulent at the stack exit by inserting a V-notched disc in the model stacks.

Vertical velocity profiles were measured at seven locations along the axis of the tunnel, and helium concentration profiles were measured at six of the same locations to determine plume height and width.

Results

The mathematical model was tested first by comparing predicted wind fields about the hill with those measured in the wind tunnel. Figure 1 shows nondimensional velocity profiles above the hill surface for the neutral and slightly stable cases. Since the difference between the predicted profiles for the two conditions was negligible, only the neutral case was plotted. The observed profiles for both cases correlated quite well with the predicted profiles up to the crest of the hill ($x/h \leq 0$). The positive wind shear at low elevations, $(z - z_g)/h < 1$, and at distances $x/h \leq -1.5$ was caused by deceleration of the flow by the hill and not by viscous effects, although a thin viscous boundary layer was observed at very low elevations, $(z - z_g)/h < 0.2$. A typical root-mean-square (rms) deviation in the wind speed about the mean speed was 3%.

On the downstream side of the hill ($x/h > 0$), mean velocities were lower than predicted due to a turbulent wake below the hill crest. Above the crest, measured velocities were higher than predicted, probably due to vertical displacement of the mean flow by the wake. The rms velocities in the wake (typically 30% of the mean) were considerably higher than those above the wake. The presence and effects of the wake had little effect on the study results because our interest was primarily in the upstream side of the hill where there was good agreement between measurements and predictions.

For the most stable case ($F_h = 1.31$), a uniform upstream velocity profile could not be obtained (with or without the hill in place), and, therefore, the experiment did not satisfy one of the conditions of Long's model. As expected, the computed velocity profiles showed poor agreement with the measured values except in the region $(z - z_g)/h < 1$ and for distances upstream of and above the hill crest; there, the measured velocities were typically within 25% of the predictions.[4] Thus, it was possible to predict plume trajectories from tunnel tests for plumes close to the hill (see below).

The plume centerline chosen from the vertical concentration profile was the height midway between points on the profile where the helium concentration dropped to 30 percent of the peak value. This height was found to be a good approximation of the profile centroid. The height of the peak concentration was typically 10 percent above the centroid. The vertical standard deviation σ_z was estimated as 0.32 times the distance between the points where concentration was 30 percent of peak. The result, identically true for a Gaussian profile, was a good approximation of the σ_z computed from second moments of the concentration distribution, even though the measured profiles were not Gaussian.

Figure 2 shows the good agreement found between measured and computed plume trajectories for hill Froude numbers of ∞ and 3.47 and for a mean speed ratio of 3.55. The calculated trajectories in these and all other cases were computed using the entrainment parameters determined in the extensive analysis of plume data by Hoult and Weil[9]: $\alpha = 0.11$ and $\beta = 0.6$. The computed plume rise for $F_h = 3.47$ is slightly lower than in the neutral case because the stable stratification depletes plume buoyancy. The experimental data exhibited similar differences in height up to the crest of the hill. The higher-than-predicted plume heights measured at the most distant cross section may have been due to displacement of the plume by the hill's wake. For reference, we note that the ambient streamline passing through the stack top would be at a height $z/h \simeq 1.09$ at the crest of the hill. The plume heights shown at the hill crest clearly demonstrate the effects of stack momentum and buoyancy fluxes.

Figure 3 shows calculated and measured trajectories for $F_h = \infty$ and 1.31 and for a speed ratio averaging about 6.4. Again, the computed trajectories agree quite well with the measured, but there is a significant difference between the two cases in this comparison: in the lee of the hill, the plume in neutral flow is considerably higher than the one in stable flow. The difference is caused both by the greatly diminished plume rise rate, resulting from buoyancy depletion by the stable stratification, and by the strong downslope winds on the lee side of the hill. Although the model slightly overestimates the measured centerline for $F_h = 1.31$, agreement is remarkably good considering the differences in the observed and predicted velocity profiles.[4]

For the eight test cases (48 vertical profiles), the mean of the ratio of predicted-to-measured rise above the stack was 1.1, with a standard deviation of 0.14. If the height of maximum concentration had been chosen for the measured plume height, the mean ratio would have been 1.0, with a standard deviation of 0.12.

The σ_z's calculated from the mathematical model also correlate well with the experimental data, as demonstrated in Fig. 4 for the neutral and most stable tests. In the stable case, the nearly constant σ_z between $x/h = -1$ and 1.6 was due to the strong convergence of streamlines near the top and lee side of the hill. For the eight experiments, the mean of the ratio of predicted-to-measured σ_z was 1.0, with a standard deviation of 0.21.

Finally, we compared plume height predictions from our mathematical model to those from two "terrain correction" models currently used to estimate ground-level concentrations for pollution sources in complex terrain. The Environmental Research and Technology (ERT) model[11] assumes the plume height (above terrain) for neutral conditions to be the difference of the value for flat terrain and one-half the terrain rise above stack base; however, the resulting height may not be less than one-half the plume height in the terrain's absence. The Cramer et al. model[12] subtracts the full terrain rise from the plume height but does not permit the resultant height to be less than zero.

Figure 5 compares the three models and experimental data for neutral ambient conditions and for the initial rise region (where the plume rise in flat terrain would vary as $x'^{2/3}$). The ERT and Cramer plume height predictions fall significantly below those predicted by the present model and observed experimentally in the wind tunnel. The Cramer model predicts an intersection of the plume centerline with the terrain; the ERT model is in better agreement with the present results. We should note that both of these models were intended for use in arbitrary terrain and would probably agree better with experiment for a three-dimensional hill, although the plume centerline should not intersect the hill under neutral flow for the same stack conditions, hill height, and stack/hill separation used here.

With the success of the present model for two-dimensional flow, we plan to extend it to more realistic three-dimensional geometries, where the plume centerline is expected to pass closer to the terrain surface.[13]

Concluding Remarks

A mathematical model based on integral plume equations was formulated for the rise and spread of a buoyant plume in neutral and stably stratified flows over a two-dimensional hill. The plume equations were solved using the idealized ambient flow model of Long,[5] but the equations are general and could be solved using a more realistic ambient flow model if desired.

Comparison of the plume model with wind tunnel-simulated data showed that predicted plume heights and vertical spread agreed well with measurements over stability conditions ranging from neutral ($F_h = \infty$) to moderately stable ($F_h = 1.31$). The plume centerline came closer to the hill in stable flow than in neutral flow because of plume buoyancy depletion by the stable stratification. In the moderately stable case, the plume remained nearly parallel to the terrain in the lee of the hill due to plume buoyancy depletion and to the strong downslope winds there.

For neutral flow, plume height predictions with the present model agreed much better with the experimental wind tunnel data than did predictions with two commonly used "terrain correction" techniques. We believe that this result is due to the more general and realistic treatment of the physical situation by the present model than by the terrain correction techniques.

We plan to extend the model to more realistic three-dimensional terrain.

Acknowledgements

I wish to thank J.E. Cermak and R.E. Petersen for help in the design of the wind tunnel experiments and for supervising them; R.L. Showers for writing the computer programs used to calculate the ambient flow field; S.H. Maslen and W. Furth for analytical support in the ambient flow calculations and helpful discussions; S.C. Traugott and J. Jensen for helpful discussions; and T. Talbot for reducing the wind tunnel data. This work was sponsored by the Maryland Power Plant Siting Program, Department of Natural Resources under contract number P45-78-04.

References

1. G.A. Briggs, "Plume Rise Predictions," In Lectures on Air Pollution and Environmental Impact Analyses, American Meteorological Society, Boston, MA, pp. 59-111, 1975.

2. D.P. Hoult, J.A. Fay, and L.J. Forney, "A Theory of Plume Rise Compared with Field Observations," J. Air Pollut. Control Assoc. 19:585-590, 1969.

3. J.C. Weil, "The Rise of Moist, Buoyant Plumes," J. Applied Meteorology 13:435-443, 1974.

4. J.C. Weil, "Modeling of Buoyant Plume Dispersion in Complex Terrain," Draft Report prepared by Martin Marietta Corporation, Baltimore, MD for Maryland Power Plant Siting Program, 1979.

5. R.R. Long, "Some Aspects of the Flow of Stratified Fluids, I, A Theoretical Investigation," Tellus 5:42-58, 1953.

6. J.W. Miles, "Lee Waves in a Stratified Flow, Part I, Thin Barrier," J. Fluid Mech. 32:549-569, 1968.

7. R.E. Davis, "The Two-Dimensional Flow of a Stratified Fluid over an Obstacle," J. Fluid Mech. 36:127-143, 1969.

8. R.I. Sykes, "Stratification Effects in Boundary Layer Flow over Hills," Proc. Roy. Soc. Lond. A. 361:225-243, 1978.

9. D.P. Hoult and J.C. Weil, "Turbulent Plume in a Laminar Cross Flow," Atmos. Environ. 6:513-531, 1972.

10. T. Yamada and R.N. Meroney, "A Wind-Tunnel Facility for Simulating Mountain and Heated-Island Gravity Waves," Boundary-Layer Meteorology 7:65-80, 1974.

11. B.A. Egan, "Turbulent Diffusion in Complex Terrain," In Lectures on Air Pollution and Environmental Impact Analyses, American Meteorological Society, Boston, MA, pp. 112-135, 1975.

12. H.E. Cramer, H.V. Geary, and J.F. Bowers, "Diffusion-Model Calculations of Long-Term and Short-Term Ground-Level SO_2 Concentrations in Allegheny County, Pennsylvania," Report prepared for Environmental Protection Agency, Region III, by H.E. Cramer Company, Salt Lake City, Utah, Report No. EPA 903/9-75-018, 1975.

13. J.C.R. Hunt, J.S. Puttock, and W.H. Snyder, "Turbulent Diffusion from a Point Source in Stratified and Neutral Flows Around a Three-Dimensional Hill, Part I, Diffusion Equation Analysis," Atmos. Environ. 13:1227-1239, 1979.

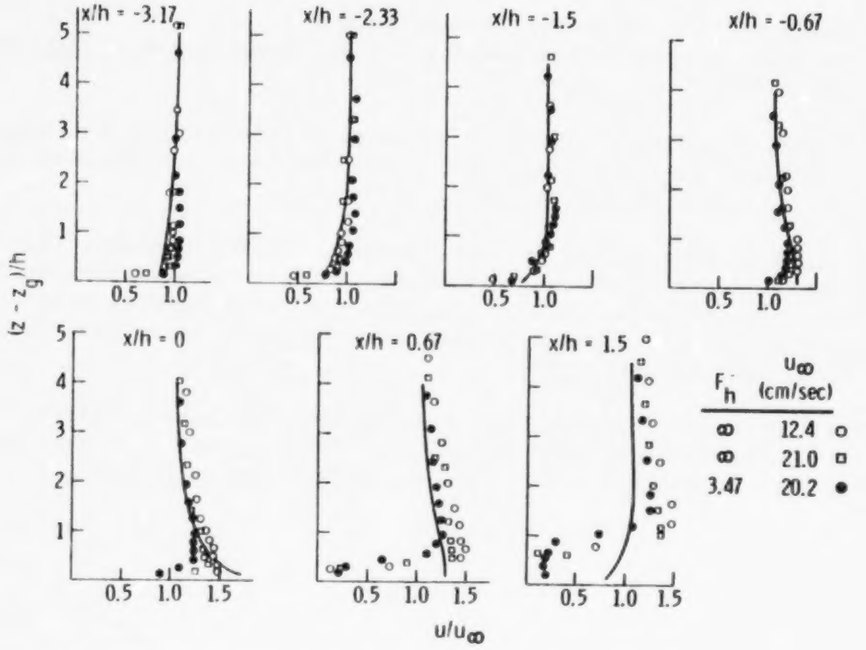

Figure 1. Theoretical predictions (solid line) and wind tunnel measurements of vertical velocity profiles over a two-dimensional Gaussian hill during neutral ($F_h = \infty$) and weakly stable ($F_h = 3.47$) conditions.

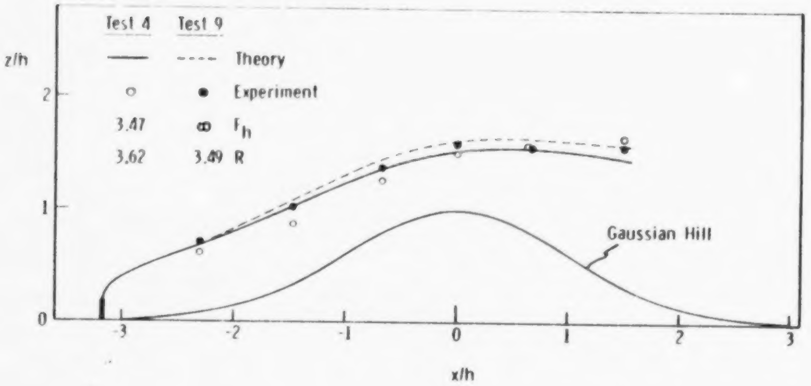

Figure 2. Theoretical and wind tunnel-measured trajectories of a buoyant plume in flow over a two-dimensional Gaussian hill during neutral and weakly stable conditions.

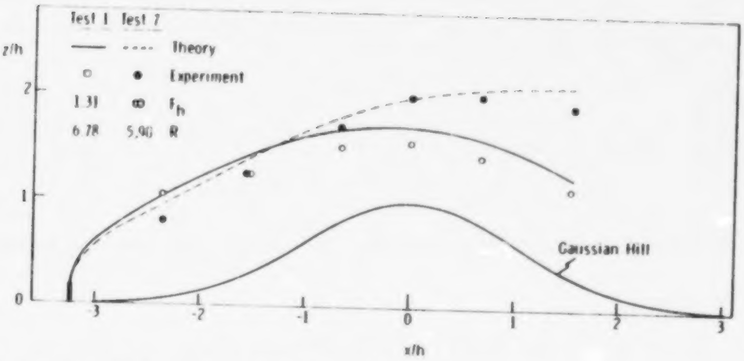

Figure 3. Theoretical and wind tunnel-measured trajectories of a buoyant plume in flow over a two-dimensional Gaussian hill during neutral and moderately stable conditions.

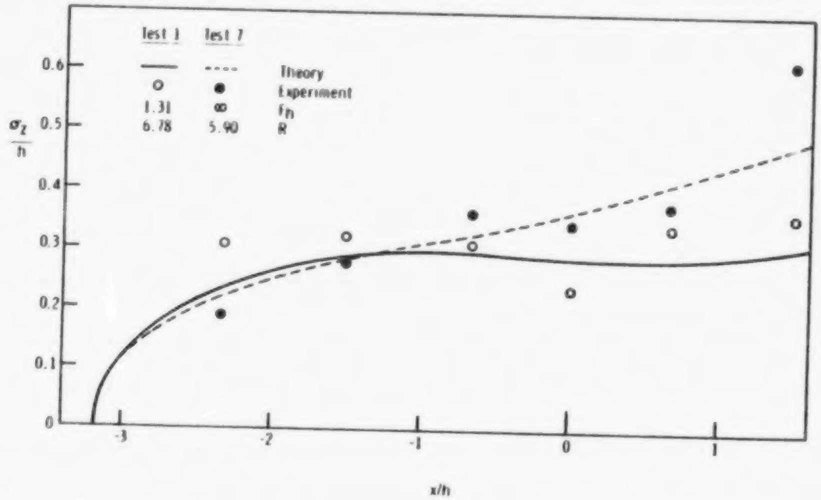

Figure 4. Theoretical and wind tunnel-measured vertical plume standard deviation for a buoyant plume in flow over a two-dimensional Gaussian hill during neutral and moderately stable conditions.

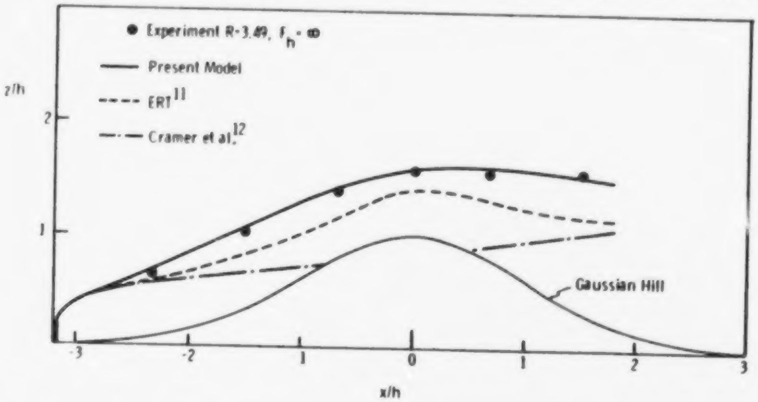

Figure 5. Comparison between predicted plume trajectories of three models and wind-tunnel measured trajectories during neutral flow over a Gaussian hill.

Discussion:

(Rapporteur: G. Fronza)

Djurfors:

Which entrainment parameter values did you use in your model?

Weil (response):

The same values used by Hoult, Fay and Forney.

Venkatram:

Has ambient turbulence an actual relevant effect on your simulation results?

Weil (response):

Yes, of course.

Hübschmann:

I understand your model on fits wind tunnel data better than other models. But what about fitting in reals cases?

Weil (response):

We are going to carry out model simulation aigainst field data in the next future.

ANALYSIS BY MEANS OF METEOROLOGICAL AND PHYSICAL CONSIDERATIONS ABOUT THE TRANSPORT AND GROUND DEPOSITION OF THE TCDD EMITTED THE 10/7/1976 FROM THE ICMESA FACTORY

by

A.Cavallaro G.Tebaldi R.Gualdi
Laboratorio Provinciale Igiene e Profilassi - Reparto Chimico -
Milano, Via Juvara 22 - Italy

Abstract. The areas interested by the contamination of TCDD emitted by the Icmesa factory have been determined, at first, through samples collected according to a cartesian grid. This map has been guided by human and animal epidemiology and by mathematical model. Afterwards it was necessary to determine the course of the toxic cloud with full particulars. By this aim we have determined the anemological field considering the data obtained by the six meteorological stations placed in the land around the factory. After determined the theoric path of the aeriform, we have studied the values of the ground concentration of TCDD drawn by previous map and we have looked for a deposition law.

The weather situation at the time of the ICMESA incident

On the 10th July 1976 during the period 10.40 GMT to 11.10 GMT, corresponding to the astronomical midday, the reaction in a batch reactor for the production of trichlorophenol went out of control, the bursting disc failed, allowing the reactor contents to be vented to the atmosphere. The cloud of material then dispersed downwind has contaminated a region on the south and east of the plant with the associated TCDD.

At the approximate time of the incident, in the areas of Meda and Seveso, it was a warm cloudless sunny day with north westerly winds, though highly variable. Data from the radiosonde station (Milano-Linate) indicated at about 11.00 GMT, slight instability in the lower layer (up to 1500 m above ground level). The wind vector (210°/09 kt above the surface) turned to the rights (280°/06 kt at 430 m a.g.l. and 320°/09 kt at 917 m a.g.l.) clockwise with respect to height and, after a decreasing in the first layer, its velocity was increasing with heigth (320°/13 kt at 1405 m a.g.l.).

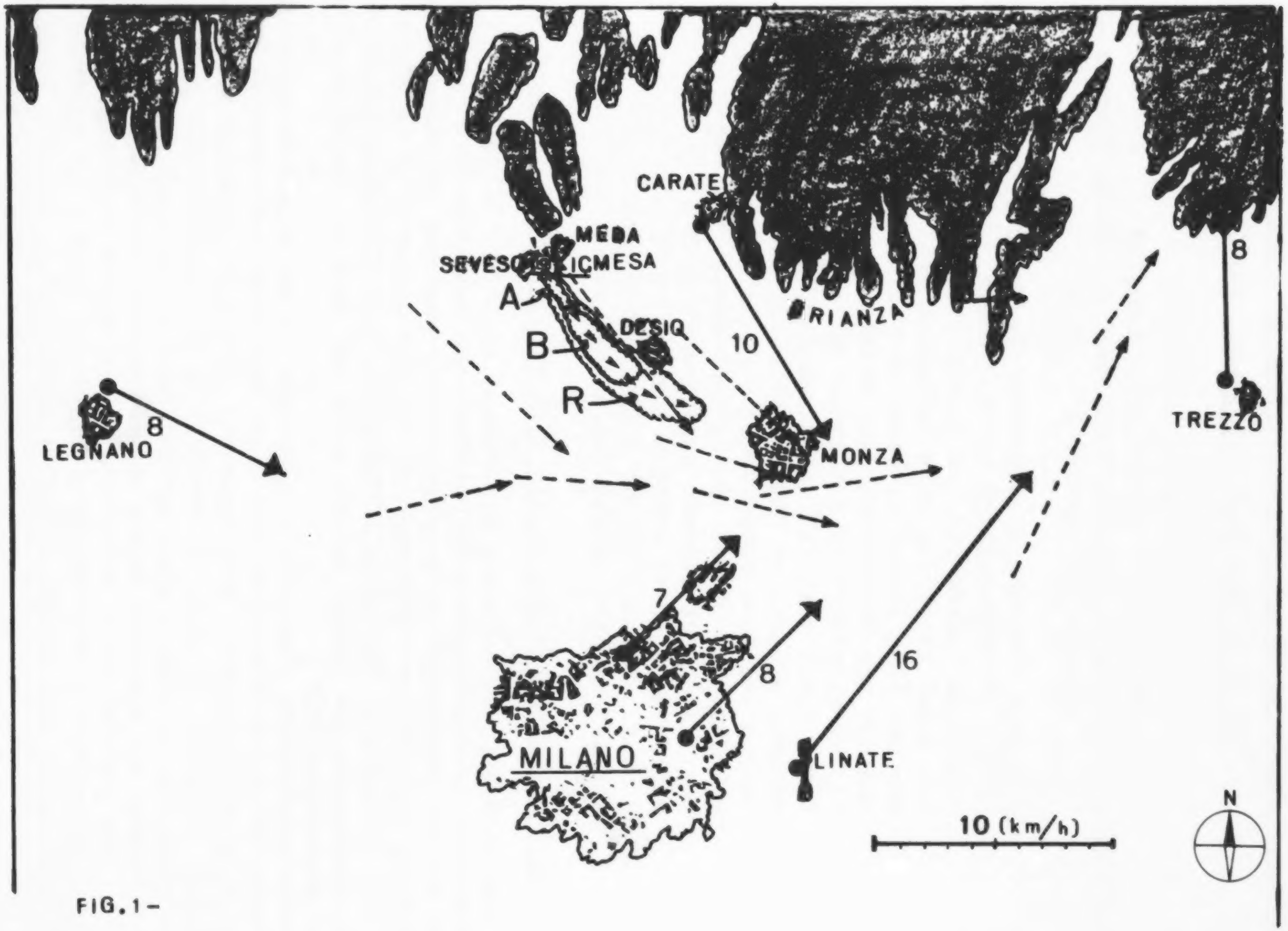
CARATE
MEDA
SEVESO
ICMESA
A
B
R
DESIO
10
BRIANZA
8
LEGNANO
MONZA
TREZZO
8
7
8
16
MILANO
LINATE
10 (km/h)
N

FIG.1-

Fig. 1 - Wind field analysis at 11.00 GMT.

Actually, on the area between the outskirts of Milan and Brianza hills, the streamlines, over the period of the incident, showed a confluence along a line across the Brianza plain with the main component in the east direction (Fig. 1). Exactly, in the northerly hilly area the mean wind direction was north westerly (Legnano, Carate Brianza), meanwhile in the North eastern side of the country (Trezzo d'Adda) the mean wind was coming from south, and in the Southern area the mean wind was coming from south west and therefore, at the approximate time of the accident at Seveso, the path of the toxic cloud couldn't be a straight line.
Really, the mean wind vectors, starting from ICMESA chemical plant, in the SSE direction, 2 km away turned in the SE direction and finally, in the E direction. Since the wind direction over the period of the discharge from the vent pipe was highly variable, the effects of wind direction fluctuations and that of atmospheric turbulence, added to the aerodynamic effect caused by the presence of buildings and the filtering effect from trees and tall crops (e.g. maize), the deposition process was not everywhere homogenous.
By wind field analysis, the locus of the toxic cloud corresponded remarkably with the boundaries of Zone A, for the first 2 km, and with the one of Zone B for the remaining path. This confirms the general shape of the contaminated area and gives reassurance that higher levels of contamination would not be expected further afield.

Statistical analysis of TCDD fall-out distribution

The isopleth lines over Zone A, fitted in $\mu g\ m^{-2}$ to the chemical map of 27 November 1976, inside a grid pattern with grid size of 50 m, and the trend of the measured values over Zone B, included in a grid pattern with grid size of 150 m, showed a steep reduction of TCDD ground concentration with down wind distance from the point of release. The spread of the maximum concentration nuclei starting by ICMESA, was all bounded in a narrow band, into Zone A, and widely dispersed into Zone B. Moreover, inside Zone B the reduction rate of TCDD ground concentration is less steeper than into Zone A, and since measured values were not uniformly decreasing and very little dense, we were not able to drawn any isoline over the Chemical map of Zone B.
Plotting on a semilogarithmic paper the outline of a vertical section along a broken line crossing the maximum concentration values of TCDD inside Zone A and B, i.e. along the path of the toxic cloud, we can see (Fig. 2) that it is possible to estimate the de

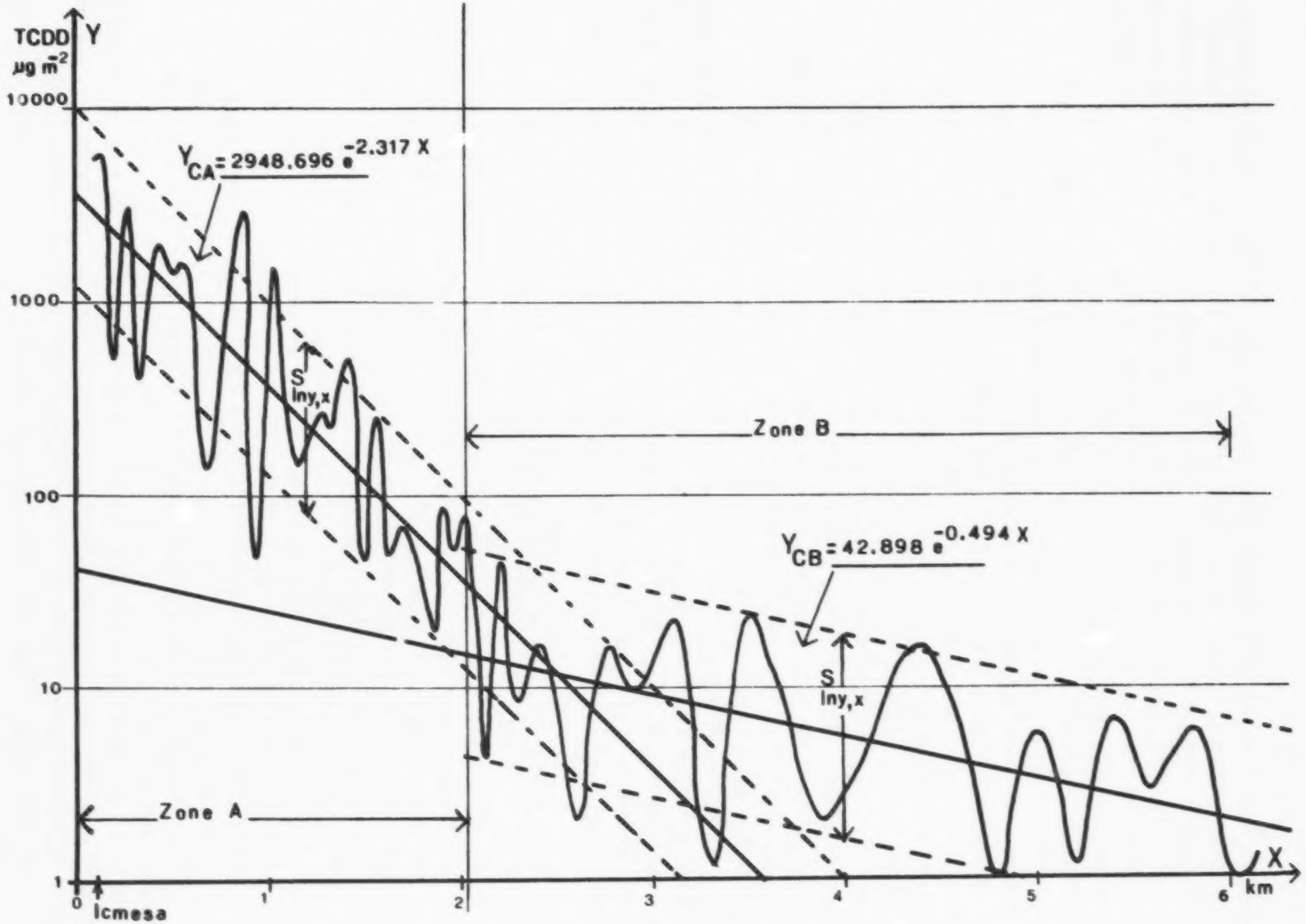

FIG.2-

Fig. 2 - TCDD ground concentrations with downwind distance.

creasing rate of TCDD ground concentration over Zone A and B by means of two different fitting lines of equation:

$$\text{Log } Y_c = \text{Log } a + b \,.\, X$$

where Y_c is the computed value of TCDD ground concentration in $\mu g\ m^{-2}$ and X is the downwind distance from ICMESA in km. The regression line corresponding to the deposition over Zone A, estimated through the nearest maximum or minimum points, is:

$$Y_{CA} = 2{,}948.696 \exp(-2.317\ X) \qquad (1)$$

with $0.1\ \text{km} < X < 2\ \text{km}$.
The TCDD ground concentration decreases exponentially with downwind distance and the overall correlation coefficient of - 0.814 confirms a reasonable agreement with the measured values. As expected, the exponential decay factor with downwind distance or travel time for the TCDD ground concentration is in good agreement with the hypothesis of a dry deposition process by means of a gravitational settling flux from a deplected Gaussian shaped plume. It is interesting to show that the zone of $\pm 1\ S_{\text{Log } y,x}$ around the estimating equation is too exponentially decreasing with downwind distance at a rate proportional to the local TCDD ground concentration:

$$\text{Sup } Y_{CA} - \text{Inf } Y_{CA} = (8{,}807.041 - 987.257)\exp(-2.317X) =$$

$$= 7{,}819.784 \exp(-2.317\ X). \qquad (2)$$

The estimating equation for the deposition over Zone B is:

$$Y_{CB} = 42.898 \exp(-0.494\ X) \qquad (3)$$

with $2\ \text{km} < X < 6\ \text{km}$.
The amplitude of the scatter is:

$$\text{Sup } Y_{CB} - \text{Inf } Y_{CB} = (130.535 - 14.097) \exp(-0.494\ X) =$$

$$= 116.438 \exp(-0.494\ X) \qquad (4)$$

and is relatively larger than the standard error of estimate of equation (1) for nearly whole Zone B, i.e. for $X > 2.3$ km. The smaller correlation coefficient $r = -0.534$ indicates a larger dispersion in the sample of TCDD measured values caused by wind turbulence. The slope of the two exponential equations (1) and (3), plotted on a semi-logarithmic paper (Fig.2) are significantly different at level of significance less than 0.001.

The TCDD decay law:

$$Y_C = Y_o \exp(-bX) \qquad (5)$$

means that the parameter Y_o is a function of the total mass of material emitted and that the coefficient b is a function of the deposition rate, larger for heavier particles. The different decay rate between Zone A and Zone B can be explained by a greater deposition velocity into Zone A than into Zone B. The very high measured concentrations closed to the source, up to 10,000 µg m^{-2}, tend to confirm the hypothesis that larger droplets or particles were emitted in the latter stages of the emission as the exit velocity subsided to less than sonic. This would give rise to localized high deposition while in the first stages, during the sonic discharge, any entrained liquid would be atomised to very small sizes droplets and should not have any appreciable settling velocity. Using the assumption that the profile of the actual TCDD ground-level concentration is espressed by a vertical distribution function similar to that one of the Gauss-formula:

$$C(X) = (A/X^a) \exp(-B/X^a) \qquad (6)$$

we have connected the negative exponential equations (5) with two functions of the tipe:

$$Y_{oC} = Y_o \exp(-1/2bX) \qquad (7)$$

with the same parameter Y_o and coefficient b of the equations (1) and (3). The maximum depositions are at about 0.30 km and 1.43 km from the source with the value of the maximum of 1,400 µg m^{-2} and 20 µg m^{-2} respectively, in according to the fact that, as the deposition velocity is increased, the peak values increase with the amount of pollutants emission and occurs closer to the source. Plotting on logarithmic paper the average profile of the TCDD ground concentrations into Zone A and B, we obtain the graphs of figure 3 which are in reasonable agreement with the literature on the models of atmospheric transport and deposition for pollutants emitted from an elevated point source over flat terrain. [1]
Making the assumption that the particles emitted are larger than 50 µm, their gravitational settling velocity (W) and their deposition velocity (V) are equal ($W = V > 0$), and thus the dry deposition is due entirely to gravitation settling. The graphs of figure 3 are proportional to the deposition flux along the plume centerline whose peak value increases without limit as the deposition velocity is increased and occurs closer to the source.

Figure 4 shows the deposition rate, namely the ratio of the amount of pollutant deposited on the ground between the source and the downwind distance X and the total amount of pollutant estimated on the ground surface. We can see that, according to the theory, as the deposition velocity is increased, deposition onto the ground occurs closer to the source. Consequently, a smaller ground surface area is contaminated but only at a higher concentration.

The graph of figure 5 shows the ratio of the cumulative amount of TCDD deposited on the ground along the cloud path across Zone A and B and the total amount of TCDD Fall-out, estimated by suitable integration of equations (1), (3) and (7). We can see that 50 per cent of total amount of TCDD deposited occurs within the first 400 m from ICMESA, 97 per cent occurs within the boundary of Zone A and 99.5 occurs within the limits of Zone B.

Extrapolation of the decay rate and in-field testing

The results of the statistical analysis of TCDD ground concentration distribution values are in a good agreement with the hypothesis of a dry deposition process involving at least two different classes of particles, both with size larger than 50 µm: the larger droplets, with a higher deposition velocity, give rise to localised high depositions over Zone A, while the smaller particles have been dispersed downwind over and beyond Zone B.

Solving equation (3) with respect to X we obtain the distance from ICMESA where we can find a selected value of TCDD average ground concentration: 1.00 µg m^{-2} at 7.6 km, 0.75 µg m^{-2} at 8.2 km and 0.20 µg m^{-2} at 10.9 km.

Since these distances have been extrapolated on the basis of values measured over the chemical network of Zone A and B, we wished to test the reliability of the computed results. For this purpose we set out a suitable grid to probing with a small number of samples the more and more distant areas that have been polluted by TCDD Fall-out. The inquiry has been carried out along the estimate mean path of the toxic cloud.

The soil samples have been drawn out by means of a square probe with 15 cm side and 5 cm depth. Chemical analysis was able to determine a value of 0.02 µg m^{-2}, by means of sophisticated cleaning methods.

Following the path of the toxic cloud and starting by a point near Desio, at a distance of 5,5 km from ICMESA and inside Zone B, we drew some diverging lines containing a wide angular sector crossed

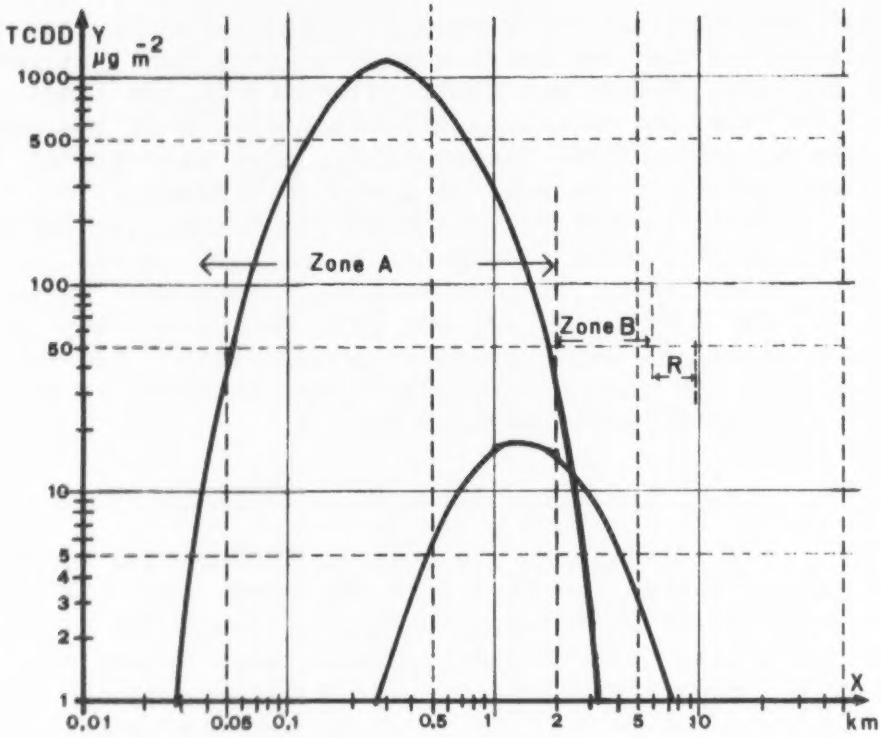

FIG, 3 —

Fig. 3 - Profile of the actual TCDD deposition.

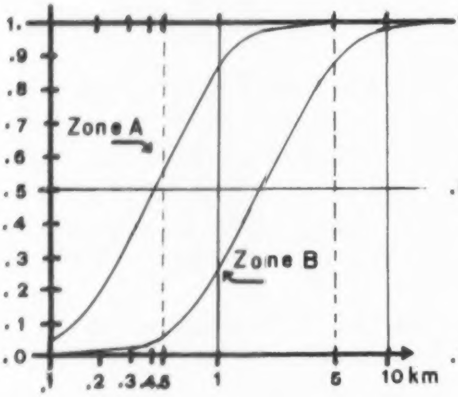

FIG. 4 -

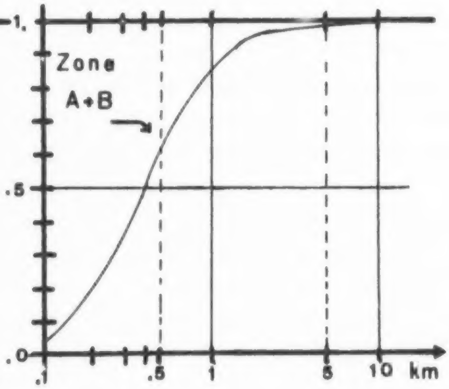

FIG. 5 -

-Fig. 4 - Single deposition rates

Fig. 5 - Cumulative deposition rate

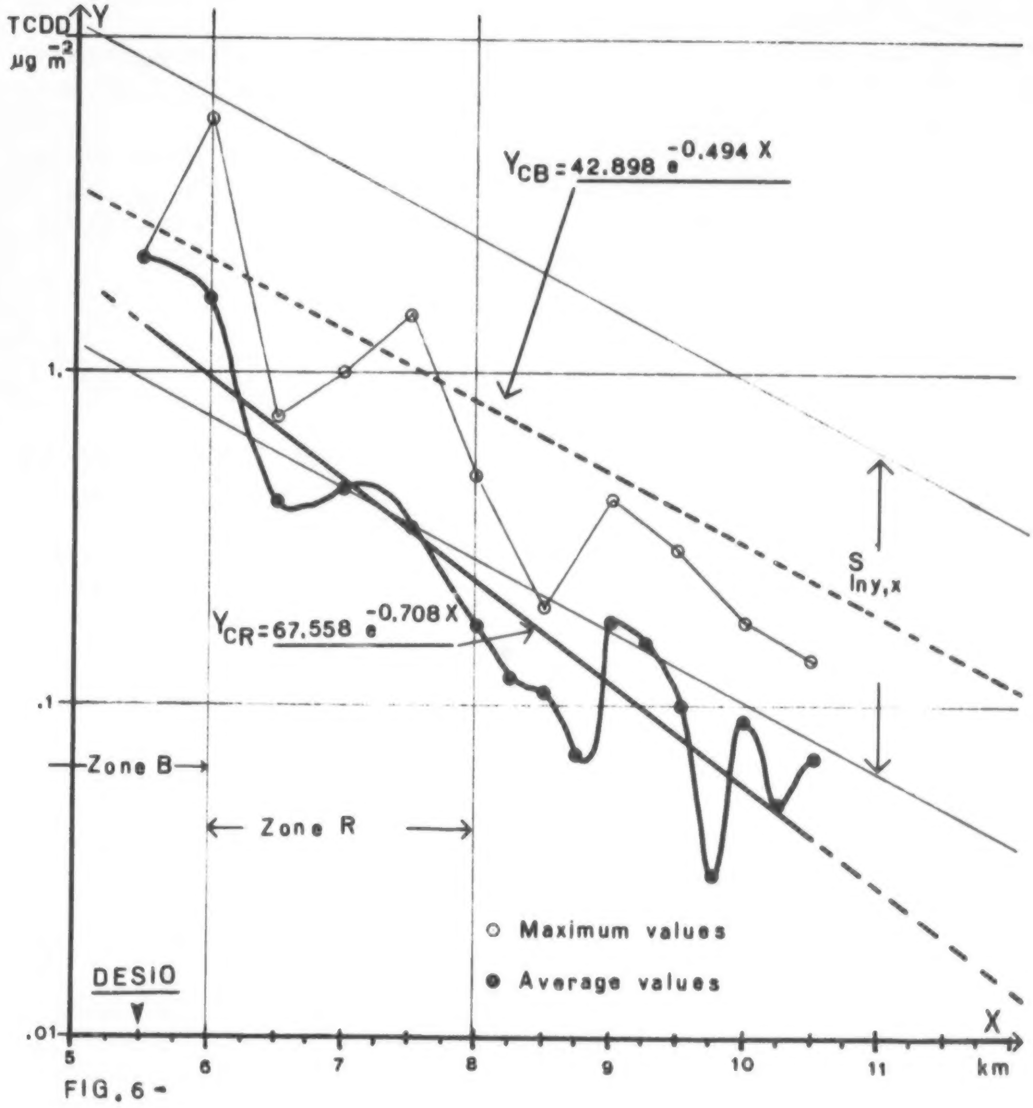

Fig. 6 - Comparison between actual and extrapolated TCDD concentrations.

by arches of circumference with radius multiple of 500 m (sometimes of 250 m) forming a polar grid.
We withdrew the samples, if possible near the grid intersection points, picking the areas far from autovehicular traffic out and avoiding cultivated fields.
Results are plotted on graph of figure 6 and are in a good agreement with the expected values: all maxima lie below Sup Y_{CB} and all TCDD average values are below Y_{CB}. Moreover, the estimating equation for the deposition beyond Zone B (Zone R) is:

$$Y_{CR} = 67.558 \exp(-0.708\ X)$$

with $5.5\ \text{km} < X < 10.5\ \text{km}$
and shows a faster decay rate than expected by eq (3).
Concluding:

a) - at a distance of about 10 km from ICMESA the distribution of measured values has a maximum value of 0.18 $\mu g\ m^{-2}$, in a good agreement with extrapolated values;
b) - the cross section along cloud path is gaussian-like shaped;
c) - TCDD ground concentration decreases at a costant rate with downwind distance and gets lower than 0.02 $\mu g\ m^{-2}$ at 11.5 km far from ICMESA.

Concluding remarks

As we pointed out, data analysis gave a more complete sight of the TCDD ground concentration patterns: first of all, the profile of the measured decay rate shows a good agreement with as expected by the estimating equation for the deposition over Zone B (3), in spite of the well known poor performance of each sample.
These results let us confirm the goodness of the chemical map data from which we drew the isopleth lines over Zone A, the maximum concentration values over Zone B and the boundaries of the most polluted areas.
Moreover, the exponential decay rate with downwind distance and the gaussian-like shaped cross sections indicates that the most polluted areas should lie all within the boundaries of Zone A and B.

References

1. Donald L. Ermak, "An analytical model for air pollutant transport and deposition from a point source", Atmospheric Environment Vol. 11, pp. 231-237.

Discussion:

Vogt:

Have you any information about deposition velocity?

Tebaldi (response):

I just have data from ground level chemical analysis. Actually, what happened in the reactor has not yet been well established.

Hübschmann:

What about the decrease of ground level contamination in the area?

Tebaldi (response):

Initially, there was rapid decrease (~ 65 %) due to relevant washout (the accident occurred on a dry period). The TCDD was partially washed into the Seveso River. But after there was practically no reduction, but strong stability in ground level concentrations.

STATIONARITY OF THE CONCENTRATION INTERMITTENCY IN SHORT - RANGE ATMOSPHERIC DISPERSIONS

C. D. Jones

CHEMICAL DEFENCE ESTABLISHMENT,
PORTON DOWN, SALISBURY, WILTS, U.K.

J. Murlis
CENTRE FOR OVERSEAS PEST RESEARCH
COLLEGE HOUSE,
WRIGHTS LANE,
LONDON W8 5SJ, U.K.

Preceding page blank

1. Introduction

Interest in the detailed structure of diffusing plumes (and puffs) is increasing because of its significance for, inter alia, the assessment of flammability and explosion hazards*), odour nuisance and in the formulation of pollution control standards generally. Three important factors in the assembly of a comprehensive description of plume structure are (i) the intermittency of the concentration fluctuations, (ii) the probability distribution of the amplitude of the concentration variations and (iii) the temporal distribution and statistics of concentration 'events'. These three elements are of course interrelated and a specification of one inevitably involves a partial specification of those remaining. However, it is conceptually convenient to employ this nomenclature for reasons which will become evident later. In this paper only the first two factors will be considered because special analytical techniques are required to determine the temporal distribution etc. of concentration events and these are still being developed.

The temporal non-stationarity and spatial inhomogeneity of atmospheric turbulence incurs major difficulties when attempts are made to obtain representative (i. e. widely applicable) data on dependent phenomena. At present very little high resolution data on the concentration fluctuations experienced downwind of a tracer source exist but in a recent series[1] of 45 min duration experiments it was evident that the intermittency (defined as the percentage of the 45 min for which the concentration was zero - or below some arbitrary threshold close to zero) of the concentration at locations up to 15 m downwind of a point source was ~ 90 %. Note that this was still the case even if the concentration sensor and tracer source were aligned accurately with the mean wind. Because of the small number of experiments conducted and the restricted range of meteorological and topographical conditions which have been explored to date it must be stressed that these conclusions must not be applied to other conditions /situations without very careful consideration. In view of this restriction additional experimental work has been carried out to examine the nature of the intermittency and the mechanisms responsible for it in more detail. It is hoped that this increased knowledge will facilitate more confident applications to other diffusion problems.

---

*) Strictly Lagrangian rather than Eulerian measurements are more appropriate here.

2. Experimental method and data handling

The results presented and examined in sec. 3 were obtained in two experiments (at 10 and 100 m downwind of a tracer source) performed on a flat coastal plain in NW Crete. The experimental technique, which is reported in the literature [1,2,3,4] employs unipolarly ionized air, produced by a controlled corona discharge, as the tracer. High resolution concentration (time constant typically 10 ms) measurements were made using specially developed ion collectors and high-speed current amplifiers. Ion concentration data were recorded on an FM reel-reel tape recorder for subsequent analysis in the laboratory. Intermittency measurements were made by playing back the data tape into a gated counter which incremented (in 0.1 s units) when the ion concentration level was above a given threshold. Ideally the threshold setting should be zero but in practice this is not possible because the counter would continually increment due to baseline drift and noise. 50 mV was found to be a satisfactory threshold and provided adequate immunity from noise together with good sensitivity.

Atmospheric stability, wind speed and direction were determined using aspirated thermocouples in conjunction with sensitive anemometers (and wind vanes) placed on a mast at heights of 1 and 11 m. This data was logged automatically every 2 min for subsequent analysis.

3. Results and Discussion

Both experiments were conducted in quite strong winds under clear skies during the daytime in summer - hence the conditions were unstable. Strong wind situations were found much more amenable to obtaining quasi-stationary data because systematic shifts, i. e. trends in direction appeared to be largely absent. In addition, since stationary (or as nearly stationary as possible) conditions were required if meaningful long period analyses of concentration intermittency etc. were to result it was essential to avoid working close to sunrise and sunset because of the marked changes in stability that occur at those times. Consequently one is restricted either to nocturnal experiments, which though feasible are difficult to carry out, or the period of the day when the sun is reasonably near its zenith. (The possibility of working under heavily clouded skies, i. e. in near-neutral conditions, was not considered practical in Crete in August!).

Table I

Details of the experimental conditions for the two trials

Distance down-wind from source (m)	Duration of trial (mins)	Mean wind speed at 1 m (ms^{-1})	Mean wind speed at 11 m (ms^{-1})	Mean air temperature at 1 m ^oC	Mean lapse rate $^oC\ m^{-1}$	Mean Richardson Number
10	120	4.1	6.2	26.5	-0.21	-0.15
100	180	5.3	7.3	26.3	-0.19	-0.16

Table II

Frequency distribution of total signal duration for 5 min. samples

Total signal Duration (s)	10 m Trial	100 m Trial
0 - 9.9	4	7
10.0 - 19.9	5	8
20.0 - 29.9	12	7
30.0 - 39.9	3	7
40.0 - 49.9	0	2
50.0 - 59.9	0	4
60.0 - 69.9	0	0
70.0 - 79.9	0	1
80.0 - 89.9	0	0

The total duration of signal (i. e. the total time that the concentration was above zero (in practice 50 m V)) in each 5 min. sampling period varied greatly in both the 10 and 100 m experiments, ranging from 3 to 32 s and 0 to 72 s respectively.

Table II gives the frequency distribution of signal duration in 10 s groups from which it can be seen that the 10 m data have a tighter distribution than the 100 m which are, comparatively, quite widely scattered. It was found that grouping the 5 min. values to give 20 min. averages, Tables IIIa and b, considerably diminished the variability in the results. Standard deviations, Table IV, were reduced from 6.01 to 3.28 in the 100 m case and, more modestly, from 3.02 to 2.18 in the 10 m. Note, however, that Table III shows that there is still considerable differences in the values even amongst the 60 min. means.

Table IIIa

Averaged intermittency ($\bar{\gamma}$), signal duration and wind speed for the 10 m trial

Elapsed time (mins)	$\bar{\gamma}$ 20 min. %	$\bar{\gamma}$ 60 min.	Signal Duration (s)	Wind Speed (ms^{-1})
20	93.95			
40	90.59			
60	94.40	92.98	252.7	4.1
80	96.57			
100	93.42			
120	91.28	93.76	224.6	6.2

Table IIIb

Averaged intermittency, signal duration, windspeed and direction for the 100 m trial

Elapsed time (mins)	$\bar{\gamma}$ 20 min. %	$\bar{\gamma}$ 60 min. %	Signal Duration (s)	Wind Speed ($m\ s^{-1}$)	Wind Direction (degrees)	Standard Deviation of Wind direction (degrees)
20	95.72					
40	92.76					
60	93.20	93.89	220.0	5.4	7.9	14
80	94.83					
100	91.40					
120	91.99	92.74	261.4	5.3	9.1	16
140	88.90					
160	88.36					
180	85.53	87.60	446.5	5.3	5.6	14

Table IV

Standard deviations of the averaged intermittencies as a function of sample length

Experiment	$\overline{\gamma}$ experiment (i. e. for entire experiment)	Standard Deviation of 5 min averaged intermittencies (σ5)	Standard Deviation of 20 min averaged intermittencies (σ 20)
10 m	93.37	3.02	2.18
100 m	91.41	6.01	3.28

During the 100 m trial there was little variation in the mean wind speed but slight changes in mean wind direction. The signal duration, however, increases both with a 1° increase and a 2° decrease in mean wind direction and, since the standard deviation of the direction fluctuations is of the order of 15°, the instantaneous wind direction would be outside these narrow limits for a very high percentage of the time in any case. It is therefore difficult to ascribe differences in signal duration to either wind speed or direction changes. There may, however, have been changes in large scale turbulence structure because, by the third hour of the trial, it was fairly late in the afternoon and the degree of instability would be beginning to reduce.

Higher resolution instrumentation and the use of a more sensitive stability parameter might help resolve this point in future.

Table V gives 20 and 60 min values for intermittency measured at a range of thresholds. By plotting these data on appropriate graph paper it emerges that both the 10 and 100 m data adhere quite closely to a logarithmic-normal distribution over the threshold range examined. However, the 100 m results do tend to deviate from log-normal for both sample durations at the higher threshold levels (a feature which has been shown by Jones[1] to be apparently characteristic of such data) and this suggests that they possess a smaller amplitude range than their 10 m counterparts.

Table V

Intermittency measurements at various threshold levels

Threshold level (mV)	Equivalent ion concentration (pCm^{-3})	20 min duration sample from trial		60 min duration sample from trial	
		$\overline{\gamma}$10 m trial	$\overline{\gamma}$100 m trial	$\overline{\gamma}$10 m trial	$\overline{\gamma}$100 m trial
50	225	93.95	95.72	92.98	93.82
75	338	97.33	97.77	96.99	97.03
100	450	98.48	98.41	98.24	98.02
150	675	99.38	99.40	99.28	99.60
200	900	99.68	99.88	99.66	99.93

It was also found, particularly at 100 m, that at threshold levels of 100 mV and less the adherence to the log-normal function was closer in the longer (i. e. 60 min.) sample. This is perhaps the clearest indication so far of the effect of sample duration and strongly suggests that at large source-detector separations considerable sample lengths are desirable in order to obtain fully representative data. However, for the purposes of initial estimation of the distribution of concentration amplitudes a sample as short as 10 min. may suffice at small separations.

5. Conclusions

(i) Even hourly averages of non-zero concentration duration are quite well scattered despite being derived from observations made in nominally stationary conditions.

(ii) Scatter in the data would appear not to be entirely due to errors in estimating mean wind directions for detector placement or indeed to subsequent slight shifts in that quantity. It may, however, be related to subtle changes in the structure of the turbulence.

(iii) For the estimation of the concentration amplitude distribution the duration of sampling should be increased with source-detector separation.

6. References

(i) JONES, C. D., 1978

Statistics of the concentration fluctuations in short range atmospheric diffusion.

Presented at a Conference on 'Numerical Modeling of turbulent diffusion' at Liverpool, U.K., September 1978.
(Proceedings to be published by the Academic Press).

(ii) JONES, C. D., 1977

Ion concentration variations at short distances downwind of continuous and quasi-instantaneous point sources.

Pesticide Science 1977, 8, 84 - 95.

(iii) JONES, C. D., 1977

Ionized air as a wind tunnel tracer.

J. Phys. E 1977, 10, 1287 - 91.

(iv) JONES, C. D. and GULLIFORD, N. T., 1978

Developments in the use of ionized air as a wind tunnel tracer.

J. Phys. E 1978, 12, 321 - 27.

Discussion:
(Rapporteur: J. Tikvart):

Discussants: Portelli, Venkatram, Millàn, Nieuwstadt

Differences in stationarity between stable and unstable conditions were not considered due to the difficulty of working at night. However, differences are not expected to be significant. The purpose of data collected was to study the behaviour of insects: information on stationarity is a secondary result.

The sensitivity of the instrument that was used is satisfactory for monitoring over several hundred meters. Due to the nature of the experiment, it was necessary to point the monitor in the general direction of the source; it was not possible to obtain a precise orientation.

THE INFLUENCE OF LOW LEVEL INVERSIONS ON THE DISPERSION OF ATMOSPHERIC POLLUTANTS

by

H. Reuter and H. Kolb
Vienna, Austria

Abstract. A theory is developed, which describes the direct influence of the height of the mixing layer on diffusion parameters. It takes into account that a shallow mixing layer influences dispersion not only through the boundary conditions, but also by a modification of the time dependancy of dispersion parameters.

Introduction

The mathematical treatment of turbulent diffusion processes corresponds to that of molecular diffusion processes, if the mean free path used in molecular theory is replaced by a different characteristic length. Generally, this length increases with the time of diffusion and it can attain the magnitude of the mixing depth (e.g. height of an inversion). A limiting vertical boundary can therefore influence dispersion processes in two ways: On the one hand reflexion takes place, similar to that at the ground, on the other the characteristic length itself is reduced. The first of these effects is accounted for by the analytical solution of the equation of diffusion using Jacobian Thetafunctions.[1],[3] The second, the reduction of the characteristic length, can be described by simple mathematical and geometrical considerations, as is to be shown in the following.

Deduction of a formula for the reduction of the characteristic length l by a limiting boundary in the height D

Two cases are considered:

a) the characteristic length l is smaller or equal to the mixing depth D,
b) l is equal or greater than D:

a) $l \leq D$
As fig. 1 shows, the following relations hold for the characteristic length l and the reduced length l*:

$$l = s \sec \delta_0 \qquad 0 \leq s \leq D$$
$$l^* = s \sec \delta$$

Averaging over the angle $d\Omega = \sin \delta d \delta d\phi$ and over s gives a mean characteristic length:

Preceding page blank

$$\overline{l^*}(s) = \frac{1}{4\pi}\left[\int_0^{2\pi}\int_0^{\delta_0} l^* d\Omega + \int_0^{2\pi}\int_{\delta_0}^{\pi} l d\Omega\right] = \frac{1}{4\pi}\left[2\pi s \int_0^{\delta_0} \mathrm{tg}\delta d\delta + 2\pi l \int_{\delta_0}^{\pi} \sin\delta d\delta\right] =$$

$$= \frac{1}{4\pi}\left[- 2\pi s \ln \cos\delta_0 + 2\pi l(\cos\delta_0 + 1)\right] = \frac{1}{2}\left[s \ln \frac{l}{s} + s + l\right]$$

Taking the symmetry of the upper and lower boundary into account for the integration over s:

$$\overline{l^*} = \frac{2}{D}\left[\int_0^{l} \frac{1}{2}\left(s \ln \frac{l}{s} + s + l\right) ds + \int_l^{\frac{D}{2}} l\, ds\right] =$$

$$= \frac{1}{D}\left[\frac{1}{2}\left(s^2 \ln \frac{l}{s} + \frac{s^2}{2}\right) + \frac{s^2}{2} + ls\right]_0^l + \frac{2l}{D} s \Big|_l^{D/2}$$

The mean characteristic length can therefore be expressed as:

$$\overline{l^*} = l\left(1 - \frac{l}{4D}\right) \qquad (1)$$

b) $l \geq D$

In addition to $l = s \sec \delta_0$, $l^* = s \sec \delta$, the following relations now hold (fig. 2)

$l = (D-s) \sec (\pi - \delta_1)$

$l^* = (D-s) \sec (\pi - \delta)$

Averaging first over dΩ

$$\overline{l^*}(s) = \frac{1}{4\pi}\left[\int_0^{2\pi}\int_0^{\delta_0} l^* d\Omega + \int_0^{2\pi}\int_0^{\delta_1} l d\Omega + \int_0^{2\pi}\int_{\delta_1}^{\pi} l^* d\Omega\right] =$$

$$= \frac{1}{2}\left[s \int_0^{\delta_0} \mathrm{tg}\delta d\delta + l \int_{\delta_0}^{\delta_1} \sin\delta d\delta + (D-s) \int_{\delta_1}^{\pi} \mathrm{tg}(\pi-\delta) d\delta\right] =$$

$$= \frac{1}{2}\left[s \ln \frac{D-s}{s} + D + D \ln \frac{l}{D-s}\right]$$

and then over s from 0 to D, the mean characteristic length is

$$\overline{l^*} = \frac{1}{2D}\left[\int_0^D s \ln \frac{D-s}{s} ds + \int_0^D D\, ds + \int_0^D \ln \frac{l}{D-s} ds\right].$$

These integrals are evaluated by partial integration:

$$\overline{1^*} = \frac{1}{2D}\{\frac{s^2}{2}\ln\frac{D-s}{s} - \frac{D^2}{2}[\frac{s}{D} + \ln(D-s)] + Ds + Ds\ln\frac{1}{D-s} +$$

$$+ D^2[\frac{s}{D} + \ln(D-s)]\}_0^D$$

$$= \frac{1}{4D}\{(D-s)^2\ln(D-s) - s^2\ln s + 3Ds + 2Ds\ln 1\}_0^D ,$$

which gives the final equation for the mean characteristic length:

$$\overline{1^*} = D(\frac{3}{4} + \frac{1}{2}\ln\frac{1}{D}) \qquad (2)$$

Dispersion of air pollutants below a limiting boundary, taking into account the reduction of characteristic length.

The diffusion equation under steady-state conditions for a continous point source and constant windspeed U in direction x is

$$U\frac{\partial s}{\partial x} = K_x(\tau)\frac{\partial^2 s}{\partial x^2} + K_y(\tau)\frac{\partial^2 s}{\partial y^2} + K_z(\tau)\frac{\partial^2 s}{\partial z^2} \qquad (3)$$

with K_x, K_y, K_z	diffusion coefficients
$\tau = x/U$	diffusion time
s	concentration of pollutant

and the initial- and boundary conditions are

$$\begin{array}{llll} z = 0 & \frac{\partial s}{\partial z} = 0 & s \to \frac{QS}{U}\delta(y)\delta(He-z) & (3a) \\ z = D & \frac{\partial s}{\partial z} = 0 & \tau \to 0 & \end{array}$$

QS	Source strength
He	effective source height

The solution of (3) with (3a) is [1,3]

$$s = \frac{QS}{2DU\sigma_y\sqrt{2\pi}}\exp(-\frac{y^2}{2\sigma_y^2})[\Theta_3(\frac{He-z}{2D}, \frac{\sigma_z^2}{2D^2}) + \Theta_3(\frac{He+z}{2D}, \frac{\sigma_z^2}{2D^2})] \qquad (4)$$

with

$$\Theta_3(v,w) = \frac{1}{\sqrt{\pi w}}\sum_{i=-\infty}^{+\infty}\exp[-\frac{(v+i)^2}{w}] \qquad \text{(Jacobian Thetafunction)}$$

$$K_y = \frac{d}{d\tau}\frac{\sigma_y^2}{2} \qquad K_z = \frac{d}{d\tau}\frac{\sigma_z^2}{2}$$

For all further considerations, $\sigma \equiv \sqrt{\sigma_y^2 + \sigma_z^2}$ is defined as a dispersion measure, which corresponds to the characteristic length. A reduction of this length in accordance with equation (1) or (2) implies similar reduction in σ.

An additional assumption to take the existing anisotropic conditions into account has to be made. It is assumed, that the relation of horizontal to vertical diffusion parameter is independant of mixing depth and constant. Now equation (1) and (2) can be applied to σ_y and σ_z, resulting in

$$\sigma \leq D \quad \sigma_z^* = \sigma_z \left(1 - \frac{\sqrt{\sigma_y^2+\sigma_z^2}}{4D}\right) \tag{5a}$$

$$\sigma \geq D \quad \sigma_z^* = \frac{\sigma_z \, D \left(\frac{3}{4} + \frac{1}{2} \ln \frac{\sqrt{\sigma_y^2+\sigma_z^2}}{D}\right)}{\sqrt{\sigma_y^2+\sigma_z^2}} \tag{5b}$$

and

$$\sigma_y : \sigma_z = \sigma_y^* : \sigma_z^* \tag{6}$$

Using the constants A, α, B and β given in table 1, the reduced diffusion parameters were calculated for different mixing depths according to (5) and (6)[2]. For a mixing depth of 200 m the result is shown for slightly unstable to stable dispersion classes in fig. 3. Very unstable and very stable conditions are not considered in this connection.

As was to be expected, there is little change in the diffusion parameters for small values of τ as compared with cases of unlimited dispersion. With the increase of σ_y and σ_z, σ and D are of the same order of magnitude, and the values of σ_y and σ_z are greately reduced. This effect could be interpreted as the change-over to higher stability classes, as the limited mixing depth becomes effective.

The influence of the reduction of σ_y and σ_z on the immission field at z = 0 for a continuous point source with an effective stack height of 100 m is shown in fig. 4 and 5. Mixing depth was taken to be 200 m, with neutral conditions within, a situation which frequently arises within cities or at the breakup of night time inversions. The mean windspeed for this case is 2 m/s. In fig. 4 the ground concentration along the x-axis (y = 0) is shown for a) unlimited vertical dispersion, b) limited vertical dispersion taking only reflexion into account and c) taking reflexion and reduction of σ_y and σ_z into account. Whereas the effect of reflexion is noticable only in distances above 1 km, the reduction of dispersion parameters shifts the whole immissionfield farther from the source and leads to much higher concentrations in greater distances.

The two-dimensional field is shown for the same three cases in fig. 5. Reflexion causes an increase in ground level pollution, and in the horizontal spread of the immission field. The effects accounted for by equations (5) and (6) however, lead to a narrowing of the field as a result of the reduction of σ_y.

References

1. H. Fortak, "Numerical Simulation of temporal and spatial distributions of urban air pollution concentration", Proceedings of Symposium on Multiple-Source Urban Diffusion Models, 1970.
2. H. Reuter, "Verwendung synoptischer Beobachtungen zur Klassifikation der Ausbreitungsbedingungen bei nächtlichen Temperatur-Inversionen", Lehrk.f.Theoret.Meteor.d.Univ.Wien, 1972.
3. A. Sommerfeld, "Vorlesungen über Theoretische Physik VI", Leipzig, 1948.

Table 1: Constants used to calculate diffusion parameters[2]:

$\sigma_z = A\tau^{\alpha}$ [m] , $\sigma_y = B\tau^{\beta}$ [m] for τ [s]

Stability class	A	α	B	β	
3	0.8684	1.105	0.8891	0.8335	slightly unstable
4	0.8353	1.067	0.7615	0.9000	neutral
5	0.7959	0.943	0.6989	0.6404	slightly stable
6	0.7993	0.504	0.5663	0.7365	stable

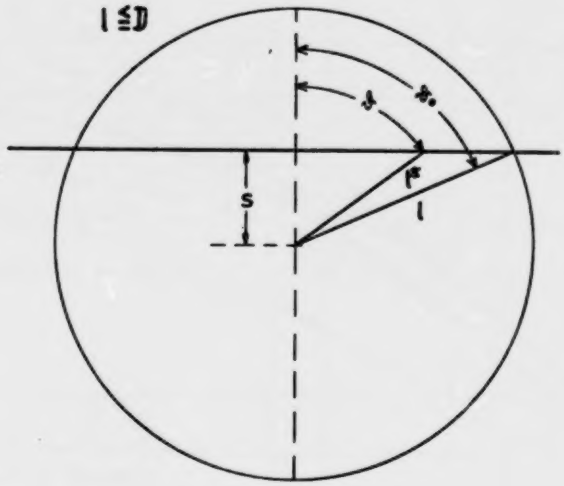

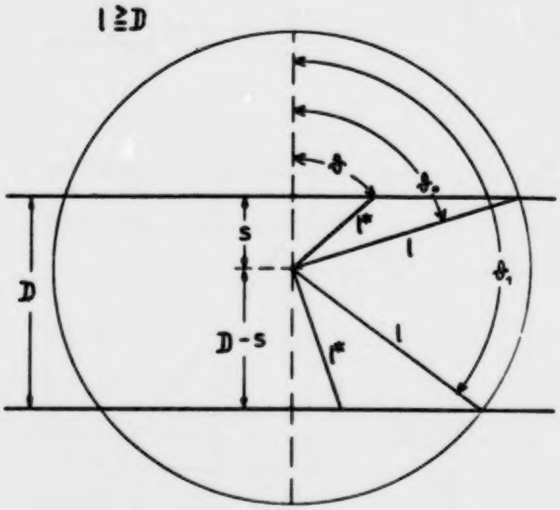
l ≧ D
ϑ
ϑ₀
s
l*
l
ϑ₁
D
D-s
l*
l

Figure 1. Reduction of the characteristic length l by a limiting boundary in the height D if $l \leq D$.

Figure 2. Reduction of the characteristic length l by a limiting boundary in the height D if $l \geq D$.

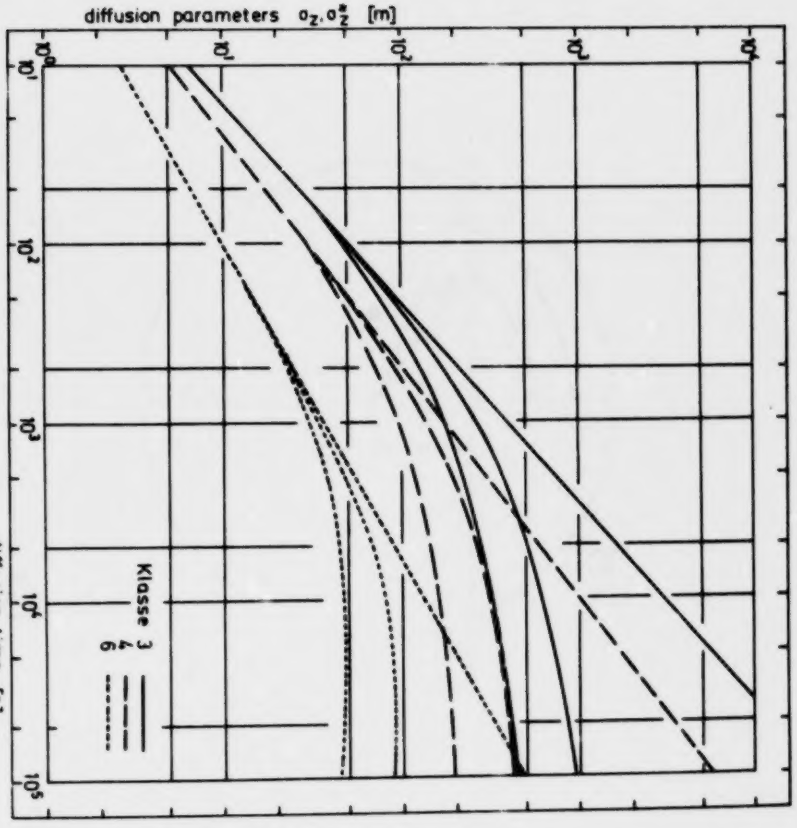

Figure 3. Vertical diffusion parameters σ_z* for different stability classes and mixing depths (∞, 500 m, 200 m).

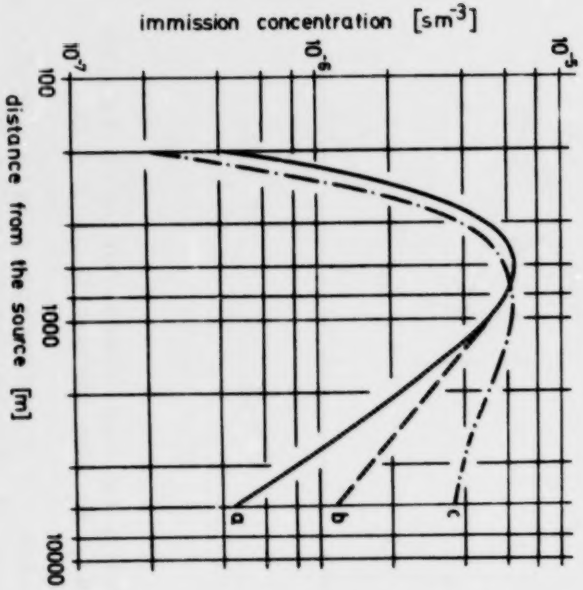

Figure 4. Ground concentration along the x-axis for a) unlimited vertical dispersion, b) limited vertical dispersion (200 m) taking only reflexion into account, and c) taking reflexion and reduction of σ_y and σ_z into account.

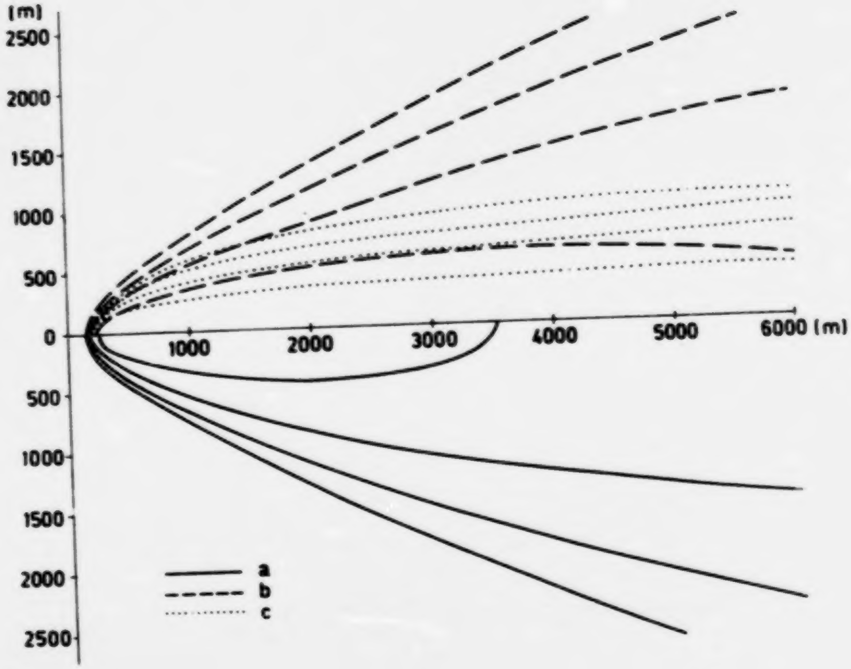

Figure 5. Two dimensional immission field a), b), c) as in fig. 4.

NUMERICAL SIMULATIONS OF AIR FLOW AND POLLUTANT DISPERSION OVER COMPLEX TERRAIN

Gisela Tangermann - Dlugi
Meteorologisches Institut, Universität Karlsruhe
D-7500 Karlsruhe 1, Germany

Abstract: A time-dependent, finite-difference model of air flow and pollutant dispersion over an irregular lower surface is described. The model, designed for mesoscale studies, is based on the hydrostatic equations of motion and a dispersion equation for inert contaminants. Complex terrain is included using a terrain-following coordinate transformation. Numerical results of flow and concentration patterns are presented which take into account different synoptic situations and source configurations.

Introduction

Considerable progress has been made in the last decade toward a better numerical simulation of dispersion processes without topography. The simulation of pollutant transports above terrain (irregular lower boundary) is made more difficult by the fact that using the usual Cartesian coordinate system, one has to deal with complicated boundaries. Correct boundary conditions are easy to apply if the model equations are formulated in a generalized nonorthogonal coordinate system. Particular coordinate transformation methods which transform a domain with an irregular lower boundary into a cube have been presented by several authors, e.g. (1). In this paper a similar method is used and the dispersion process of pollutants in a neutrally stratified boundary layer flow is computed.

The Model

The governing equations are reformulated in a nonorthogonal, noncartesian coordinate system suggested by (2). The Cartesian system (x,y,z) is transformed into a terrain-following system (x,y,η) by

$$x = x, y = y, \quad \eta = \frac{z - H}{h(x,y) - H}$$

The Jacobian of this transformation is

$$\sqrt{g} = h\,(x,y) - H$$

there $h\,(x,y)$ is the topographic height and H is the domain height of the model.

In this study a time-dependent, two-dimensional version of an air flow model and a time-dependent, three-dimensional version of a dispersion model have been adopted. The results decribe the flow field over a valley or ridge which is infinitely wide in the y-direction and the concentration field downwind from a point-source which is placed in the flow.

Preceding page blank

In the model diabatic motions are neglected and the potential temperature is assumed to be constant ($\theta=\theta_o$). The pressure field is hydrostatic in the vertical and geostrophic in the horizontal directions. The vertical velocity component $\dot{\eta}=d\eta/dt$ is calculated by solving the Richardson equation. With these assumptions the model equations can be written as

$$\frac{\partial u}{\partial t} + u\frac{\partial u}{\partial x} + \dot{\eta}\frac{\partial u}{\partial \eta} - f\,v = -c_p\theta_o\frac{\partial \pi}{\partial x} - g\eta\frac{\partial h}{\partial x} + \frac{1}{\sqrt{g}}\frac{\partial}{\partial x}\left[\sqrt{g}\,K_H\frac{\partial u}{\partial x}\right] + \frac{1}{\sqrt{g}}\frac{\partial}{\partial \eta}\left[\frac{K_V}{\sqrt{g}}\frac{\partial u}{\partial \eta}\right] \tag{1}$$

$$\frac{\partial v}{\partial t} + u\frac{\partial v}{\partial x} + \dot{\eta}\frac{\partial v}{\partial \eta} + f\,u = -c_p\theta_o\frac{\partial \pi}{\partial y} + \frac{1}{\sqrt{g}}\frac{\partial}{\partial x}\left[\sqrt{g}\,K_H\frac{\partial v}{\partial x}\right] + \frac{1}{\sqrt{g}}\frac{\partial}{\partial \eta}\left[\frac{K_V}{\sqrt{g}}\frac{\partial v}{\partial \eta}\right] \tag{2}$$

$$\frac{\partial \pi}{\partial \eta} = -\frac{g\sqrt{g}}{c_p\theta_o} \tag{3}$$

$$\frac{\partial^2 \dot{\eta}}{\partial \eta^2} - \frac{g\gamma\sqrt{g}}{c^2}\frac{\partial \dot{\eta}}{\partial \eta} = -\frac{1}{\pi(\gamma-1)}\left[\frac{\partial u}{\partial \eta}\frac{\partial \pi}{\partial x} + \frac{\partial v}{\partial \eta}\frac{\partial \pi}{\partial y}\right] + \frac{(\gamma-1)g\sqrt{g}}{c^2}\frac{\partial u}{\partial x} - \frac{\partial^2 u}{\partial x\partial \eta} + \frac{\gamma g}{c^2}u\frac{\partial h}{\partial x} - \frac{1}{\sqrt{g}}\frac{\partial u}{\partial \eta}\frac{\partial h}{\partial x} \tag{4}$$

$$\frac{\partial c}{\partial t} + \frac{1}{\sqrt{g}}\frac{\partial}{\partial x}\left[\sqrt{g}\,u\,c\right] + \frac{1}{\sqrt{g}}\frac{\partial}{\partial y}\left[\sqrt{g}\,v\,c\right] + \frac{1}{\sqrt{g}}\frac{\partial}{\partial \eta}\left[\sqrt{g}\,\dot{\eta}c\right] = \frac{1}{\sqrt{g}}\frac{\partial}{\partial x}\left[\sqrt{g}\,K_H\frac{\partial c}{\partial x}\right] + \frac{1}{\sqrt{g}}\frac{\partial}{\partial y}\left[\sqrt{g}\,K_H\frac{\partial c}{\partial y}\right] + \frac{1}{\sqrt{g}}\frac{\partial}{\partial \eta}\left[\frac{K_V}{\sqrt{g}}\frac{\partial c}{\partial \eta}\right] + Q \tag{5}$$

The terms u, v and $\dot{\eta}$ are the flow velocity components in the x, y and η directions, c is the pollutant concentraion, Q is the pollutant source term, the constants f, g, R, c_p and c_v are the Coriolis parameter, the gravity acceleration, the gas constant and the specific heats of the air at constant pressure and constant volume, respectively. γ is the ratio of c_p and c_v, $c^2 = \gamma R\pi\theta_o$ is the square of the adiabatic sound speed and $\pi = (p/p_o)^{R/c_p}$ is the Exner function used instead of the pressure variable p. The horizontal pressure gradients are given by the geostrophic wind velocity components u_g and v_g

$$c_p\,\theta_o\frac{\partial \pi}{\partial x} = f\,v_g - g\,\eta\frac{\partial h}{\partial x}$$

$$c_p\,\theta_o\frac{\partial \pi}{\partial y} = -fu_g$$

The turbulent viscosity coefficients K_V and K_H are related to the shear of the mean horizontal flow w

$$K_V\,(x.y,\eta,t) = \frac{l^2}{|\sqrt{g}|}\left|\frac{\partial w}{\partial \eta}\right| \qquad \text{for } \eta_i < \eta < 1$$

$$K_H\,(x,y,\eta,t) = \frac{1}{3}\,\Delta x\Delta y\left\{\left[\frac{\partial v}{\partial x}\right]^2 + \frac{1}{2}\left[\frac{\partial u}{\partial x}\right]^2\right\}^{1/2} \qquad \text{for } \eta_i < \eta < 1$$

with

$$l\,(x,y,\eta,t) = \frac{bu_*}{f}\ \tanh\left[\frac{k((H-h)\,(1-\eta)+z_0)}{bu_*/f}\right]$$

and

$$u_* = k\,|v|\ /\ \left\{\ln\left[((H-h)\,(1-\eta)+z_0)\,/\,z_0\right]\right\}$$

In these defining equations l represents a mixing length, u_* the friction velocity, z_0 the ground roughness, Δx and Δy the numerical grid intervals, k the von Kárman constant and b the Blackadar constant. The height of the planetary boundary layer η_i is computed following Deardorff's (3) method.

$$\frac{\partial\eta_i}{\partial t} + \frac{u}{\sqrt{g}}\frac{\partial}{\partial x}\left[\sqrt{g}\,\eta_i\right] = \frac{.28u_*}{\sqrt{g}}\left[1 - 3\,\frac{f}{u_*}\,(H + \eta_i\sqrt{g})\right]$$

Above η_i the turbulent exchange vanishes.

The boundary conditions are given by

$$\left.\begin{array}{l} u = v = \dot{\eta} = 0 \\ \dfrac{K_V}{\sqrt{g}}\,\dfrac{\partial|v|}{\partial\eta} = u_*^2\,,\ \dfrac{K_V}{\sqrt{g}}\dfrac{\partial c}{\partial\eta} = 0 \end{array}\right\} \quad \text{at } z = h \leftrightarrow \eta = 1$$

$$\left.\begin{array}{l} \dot{\eta} = 0,\ \dfrac{\partial u}{\partial\eta} = \dfrac{\partial v}{\partial\eta} = 0 \\ \pi\text{- given},\ \dfrac{K_V}{\sqrt{g}}\dfrac{\partial c}{\partial\eta} = 0 \end{array}\right\} \quad \text{at } z = H \leftrightarrow \eta = 0$$

no turbulent fluxes at $x = 0$ and $x = x_{END}$

$$\frac{\partial u}{\partial x} = \frac{\partial v}{\partial x} = \frac{\partial c}{\partial x} = 0 \qquad \text{at the lateral inflow boundary}$$

The initial conditions for $t \leq 0$ are

$$u = u_g\ ,\quad v = v_g\ ,\quad \dot{\eta} = -\frac{\partial h}{\partial x}\,\frac{u_g\eta}{\sqrt{g}}\ ,\quad c = 0$$

The difference mesh is one in which pressure, viscosity coefficients and pollutant concentration are located centrally in the grid system while velocities are staggered one-half grid interval in each respective coordinate direction. The prognostic equations are integrated using forward differencing in time, upstream differencing in space for all advective terms and centered differencing for all other terms.

Numerical Results

The model has been applied to simulate the dispersion process in the Rhine valley north of Karlsruhe. The topography used represents a west-east cross-section through the valley (49° 16.5' N, 8° 04' - 8° 46' E). The x-axis is oriented to the east (across the valley) and the y-axis is aligned to the north (along the valley). The terrain elevation is 600 and 200 m at the boundaries and 100 m in the middle of the valley.

Some parameters have fixed values in all simulations:
$f = 1.1 \times 10^{-4} s^{-1}$, $\theta_0 = 288.15$ K, $p(x = 0, z = 3000) = 720$ mb, $z_0 = 5$ cm.
The horizontal grid intervals Δx and Δy are assumed to be 2000 m, the vertical interval varies between 80 m and 96.7 m. The model height is 3000 m and the time step 60 s.

Starting with the initial field the flow fields reach steady state within 24 hours. In these velocity fields the point - sources are inserted. The flow patterns of the horizontal velocity fields u and v are strongly influenced by the topographic structure of the terrain especially in the lower layers. The lines of constant velocity follow the topography. In the vertical velocity component w upward motions dominates over windward slopes and sinking motions are found over lee slopes.

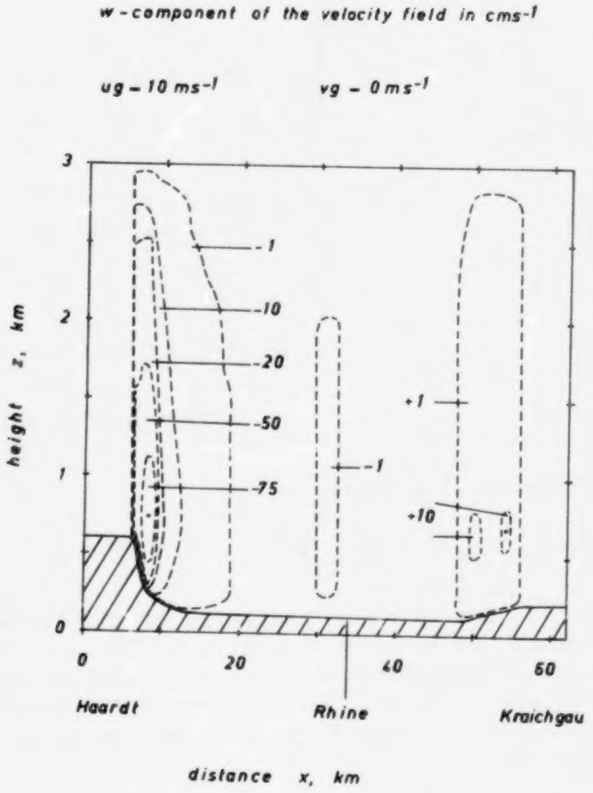

Figure 1. Cross-section of the vertical velocity field.

As an example Fig. 1 shows an x - z cross-section of the vertical velocity field after the model has reached steady state. The geostrophic flow is westerly and its value is 10 m s^{-1}.

The following concentration pattern are x - z cross-sections through the source location after 2 h of integration. The source emits continuously with an emission rate of 1 g s^{-1}. Fig. 2 and 3 show concentration patterns (in g m^{-3}) downwind from an elevated source (h_s = 96.3 m) placed in the middle of the valley for different flow directions.

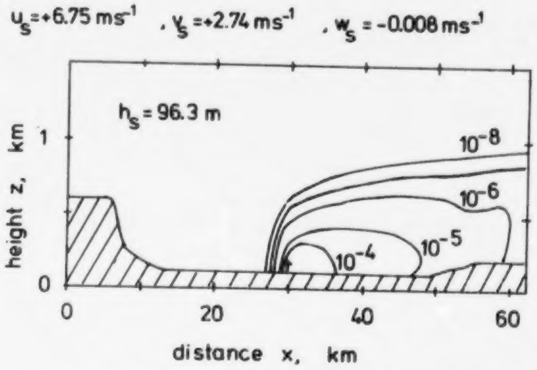

Figure 2. Cross-section of the concentration field for westerly geostrophic wind and source location in the middle of the Rhine valley

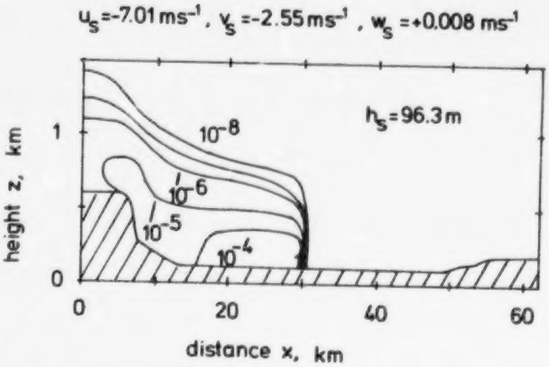

Figure 3. As in Fig. 2 except for easterly geostrophic wind

The synoptic flows ($|v_g|$ = 10 m s^{-1}) are westerly and easterly, the wind direction at the source is SWW and NEE. The influence of the topography is obvious in both cases. Fig. 4 and 5 show the concentration distributions for strong and weak wind conditions. The source (h_s = 80 m) is placed near the maximum slope at the western boundary of the model region. The westerly geostrophic flows are 10 m s^{-1} and 2.5 m s^{-1}. In the case of weak wind the vertical turbulent transport is reduced and the advection effect dominates the dispersion. Comparing Fig. 2 and 4 the influence of different locations is shown.

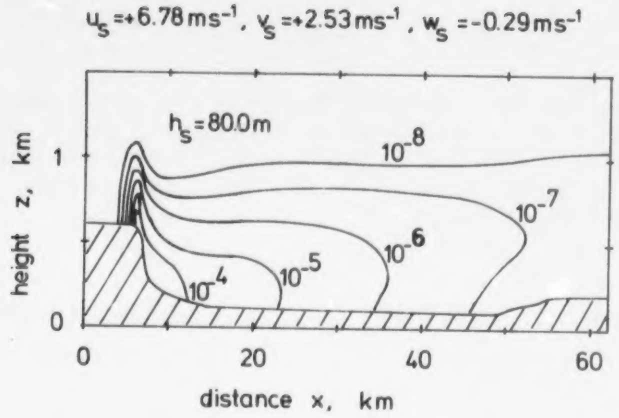

Figure 4. As in Fig. 2 except for source location at the left boundary

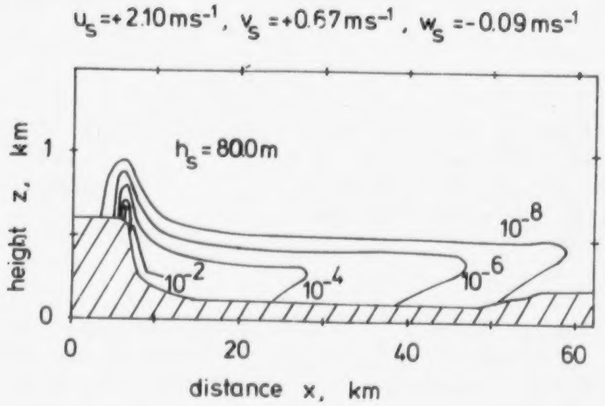

Figure 5. As in Fig. 4 except for weaker geostrophic wind

Conclusions

A numerical model of pollutant dispersion over complex terrain has been presented. The coordinate transformation allows an exact treatment of any kind of topography. The numerical effort is the same as it is in time-dependent two- or three-dimensional models without topography. The use of the hydrostatic approximation restricts the model to mesoscale studies but it increases the practicability because of less numerical effort.

The simulations show the significant influence of the advection on the dispersion process. The pollutant transport by the mean flow over complex terrain modifies the concentration distribution up to more than twice the topographic height.

The model can be improved to include diabatic effects and futher removal processes.

References

1. T.Gal-Chen and R.C.J. Somerville, "On the use of a coordinate transformation for the solution of the Navier-Stokes equations", J.Comp.Phys. 17 (1975), 209 - 228.
2. H.G. Becker, "Eine Hierarchie atmosphärischer Prognosemodelle unter Einschluß orographisch bedingter Einflüsse", Diploma-Thesis, Universität Mainz, 1978.
3. J. Deardorff, "Three-dimensional numerical study of the height and the mean structure of a heated planetary boundary layer", Boundary-Layer Meteor. 7 (1974), 81 - 106.

TEMPERATURE INVERSION DESTRUCTION IN MOUNTAIN VALLEYS-- IMPLICATIONS FOR AIR POLLUTION DISPERSION

by

C. David Whiteman and Thomas B. McKee
Department of Atmospheric Science
Colorado State University
Fort Collins, Colorado 80523 U.S.A.

Abstract. Observations of temperature inversion destruction in Colorado mountain valleys are summarized for undisturbed clear weather periods. Inversions in most valleys break within 5 hours after sunrise in all seasons. In moist or snow-covered valleys inversions take longer to break and may persist all day. Air pollution implications are considered.

Introduction

Some of the most serious air pollution problems in mountain valleys occur during the first several hours following sunrise on undisturbed days when the meteorology of the valley is under local influences[1]. This is the period of the day when the surface-based temperature inversions that have built up during the night undergo destruction. The destruction of these inversions occurs in a fundamentally different manner than the destruction of temperature inversions over flat terrain. It is the purpose of this paper to summarize observations of temperature inversion destruction in valleys of Colorado and to consider the implications of the destruction phenomenon on air pollution dispersion.

Experimental Program

The objectives of the experimental program were to study the structure and evolution of temperature inversions in a number of mountain valleys during different seasons, with the goal of elucidating the physical factors governing the evolution. Experiments were conducted during periods of undisturbed weather with generally clear skies in various valleys in the Colorado Rocky Mountains (Fig. 1). Most observations sites were in valleys on the Western Slope of the Rockies in a region where terrain elevations range from 1500-4000 meters. Here the sunny, dry, continental climate of the region results in frequent temperature inversions. Valleys were chosen for their potential for future development and for their differing topographic characteristics. Characteristics of several of the valleys are given in Table 1.

A commercial tethered balloon data collection system* was the main instrumentation used, and allowed the collection of concurrent temperature, wind, and humidity profiles at approximately 1-hour intervals through a depth of 500-750 meters. An early version of this data collection system has been thoroughly described by Morris et al[2]. Our version differed from the early version mainly in the provision for digital data acquisition. During the period of our field

---

* (Tethersonde ®, A.I.R. Company, Boulder, CO)

Preceding page blank

TABLE 1

VALLEY CHARACTERISTICS

Valley and Site	Latitude	Longitude	Elevation (m MSL)	Drainage Area (km²)	Up-Valley Direction (°True)	Valley Depth (m)	Valley Floor Width (m)	Valley Floor Slope	Sidewall Slope (deg)	Sidewall Aspect (deg True)
Eagle River										
Steve Miller Residence	39° 38' 23"	106° 34' 33"	2222	1061	104	700	1450	.0070	10 21	194 014
Yampa River										
Sombrero Stables	40° 27' 27"	106° 48' 50"	2076	1370	168	450	2580	.0026	9 16	258 078
Horseshoeing School	40° 27' 00"	106° 48' 49"	2070	1370	168	450	2580	.0026	9 16	258 078
Gore River										
Vail Municipal Building	39° 38' 37"	106° 22' 48"	2493	180	93	700	530	.0134	15 16	003 183
Vail Safeway	39° 37' 50"	106° 25' 06"	2426	233	046	600	390	.0174	24 14	136 316

TABLE 2

INVERSION DESTRUCTION DATA

Valley and Site	Date	h_1(m)	γ(°Km^{-1})	t_1(LT)	t_D(LT)	H_D(m)	$\frac{\partial\theta_h}{\partial t}$(°Khr^{-1})	Weather	Along-Valley Winds	700 mb GJT Winds (m sec^{-1})
Eagle River										
Steve Miller Residence	07-09-78	620	.0238	0551	1040	350	.2	Clear → sctd Ac	Strong	250/08
	10-16-77	665	.0269	0721	1125	260	.3	Clear	Strong	235/06
	04-20-78	650	.0182	0527	0945	260	.8	Clear → .8 Ci	Medium	255/06
Yampa River										
Sombrero Stables	02-23-78	530	.0345	0655	INVERSION DID NOT BREAK		.2	Clear, deep snow on ground	Weak	255/05
Horseshoeing School	08-09-78	650	.0187	0615	1045	220	.5	Clear	Weak	185/07
Gore River										
Vail Municipal Building	07-06-78	~750	.0182	0548	1000	260	.3	Clear	Medium	260/02
	10-19-77	585	.0216	0723	1130	235	.3	Clear	Weak	250/06
Vail Safeway	12-10-75	525	.0290	0720	1200	45	-4 to 1	Clear	Very Weak	230/10

observations we occasionally had the use of two such systems, allowing us to make along- and cross-valley profiles or to operate one system in a portable mode from one sidewall while the other system was operated from the valley floor.

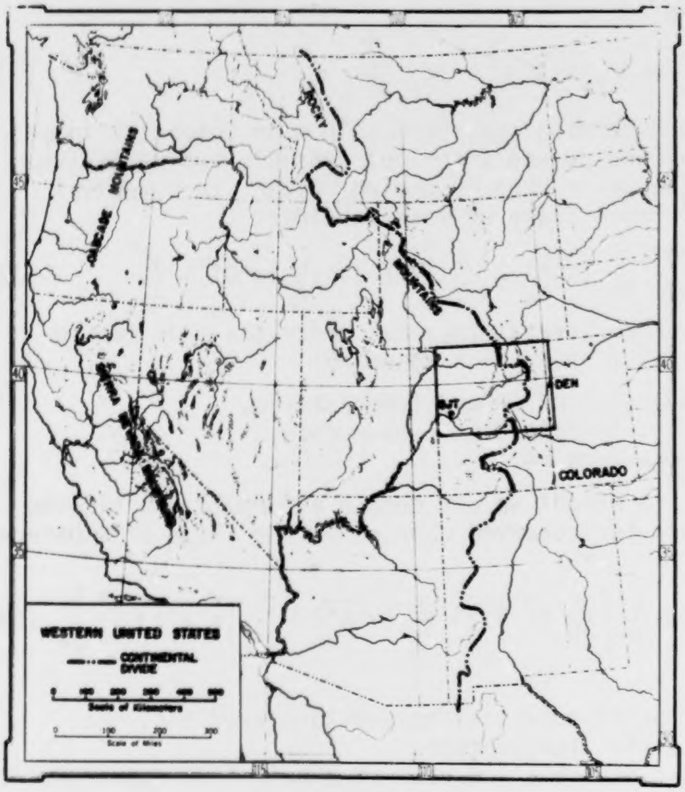

Figure 1. Location of experimental area in Western Colorado. GJT = Grand Junction, DEN = Denver.

Physical Processes Responsible for Changes in Potential Temperature

Sequential samples of the vertical structure of the valley atmosphere will generally reveal point changes in potential temperature, $\frac{\partial\theta}{\partial t}$, and vertical gradient of potential temperature, $\frac{\partial}{\partial t}\left(\frac{\partial\theta}{\partial z}\right)$. It is the purpose of this section to develop a theoretical framework which can be used to understand the physical processes responsible for these changes. We begin by considering that the potential temperature of an unsaturated air parcel can be changed only in the presence of diabatic processes so that we may write

$$\frac{d\theta}{dt} = \frac{\partial\theta}{\partial t} + u\frac{\partial\theta}{\partial x} + v\frac{\partial\theta}{\partial y} + w\frac{\partial\theta}{\partial z} = -\frac{\partial F}{\partial z} \tag{1}$$

where F is the net upward radiative flux. Multiplying the continuity equation by θ

$$\theta\frac{\partial u}{\partial x} + \theta\frac{\partial v}{\partial y} + \theta\frac{\partial w}{\partial z} = 0 \tag{2}$$

and adding it to (1) gives us the flux form of the thermodynamic equation:

$$\frac{\partial\theta}{\partial t} + \frac{\partial}{\partial x}(u\theta) + \frac{\partial}{\partial y}(v\theta) + \frac{\partial}{\partial z}(w\theta) = -\frac{\partial F}{\partial z}$$

By Reynold's averaging of this equation, subtracting the horizontally averaged continuity equation and multiplying both sides by ρc_p, we arrive at a form of the thermodynamic energy equation:

$$\rho c_p \frac{d\bar{\theta}}{dt} = -\rho c_p \nabla \cdot \overline{\mathbb{W}'\theta'} - \rho c_p \frac{\partial \bar{F}}{\partial z} \qquad (3)$$

This equation states that we may determine the changes in mean potential temperature following an air parcel by considering turbulent sensible and radiative heat flux convergences into the parcel. When observing changes in potential temperature from an Eulerian reference frame we must consider:

$$\frac{\partial\bar{\theta}}{\partial t} = -\bar{u}\frac{\partial\bar{\theta}}{\partial x} - \bar{v}\frac{\partial\bar{\theta}}{\partial y} - \bar{w}\frac{\partial\bar{\theta}}{\partial z} - \frac{\partial}{\partial x}(\overline{u'\theta'}) - \frac{\partial}{\partial y}(\overline{v'\theta'}) - \frac{\partial}{\partial z}(\overline{w'\theta'}) - \frac{\partial\bar{F}}{\partial z} \qquad (4)$$

In this general equation we recognize several physical processes that can increase the potential temperature at a point in a sounding:

1) horizontal and/or vertical advection of warmer temperatures,
2) horizontal and/or vertical sensible heat flux convergence,
3) vertical radiative heat flux convergence.

Differentiating (4) with respect to height we can obtain a formula identifying the physical processes responsible for observed changes in the slope of a potential temperature sounding:

$$\frac{\partial}{\partial t}\left(\frac{\partial\bar{\theta}}{\partial z}\right) = \frac{\partial\bar{\gamma}}{\partial t} = -\bar{\mathbb{W}}\cdot\nabla\bar{\gamma} - \frac{\partial\bar{\mathbb{W}}}{\partial z}\cdot\nabla\bar{\theta} - \frac{\partial}{\partial z}\left[\frac{\partial}{\partial x}(\overline{u'\theta'}) + \frac{\partial}{\partial y}(\overline{v'\theta'}) + \frac{\partial}{\partial z}(\overline{w'\theta'}) + \frac{\partial\bar{F}}{\partial z}\right] \qquad (5)$$

These factors include:

1) horizontal or vertical advection of potential temperature gradient,
2) differential advection of potential temperature,
3) vertical gradients of turbulent sensible and radiative heat flux convergences.

It is naturally to be expected that some of the terms in equations (4) and (5) will be more important than others when the equations are applied to atmospheric layers in different situations and the hope is extended that some particularly simple set of reduced equations will be sucessful in describing gross features of potential temperature evolution. Such is the case for the development of a convective boundary layer (c.b.l.) over flat terrain (e.g. Lilly[3]) where equation (5) becomes $\frac{\partial\gamma}{\partial t} = 0$ and equation (4) reduces to $\frac{\partial\bar{\theta}}{\partial t} = -\frac{\partial}{\partial z}(\overline{w'\theta'})$.

Typical Inversion Destruction

The typical evolution of potential temperature and wind profiles for the valleys studied is presented in Fig. 2.

θ-Profiles

Referring to Fig. 2a--at a time near sunrise (t_1) a deep surface-based potential temperature inversion with a near-linear vertical temperature gradient, γ (°km^{-1}), extends from the surface to about the height of the ridgetops (h_1). Successive soundings (at t_2 and t_3) show two main characteristics. First, the height of the top of the inversion, h, continually decreases and, second, a convective boundary layer of height H and potential temperature θ_H develops just above the ground. Despite the lowering top of the inversion and the rising base of the inversion, the lapse rate within the inversion layer (γ) remains nearly constant. A time t_D the rising base and lowering top of the inversion meet to produce an atmosphere of constant potential temperature, θ_D. Typical values of the parameters in Fig. 2a are given for various valleys in Table 2.

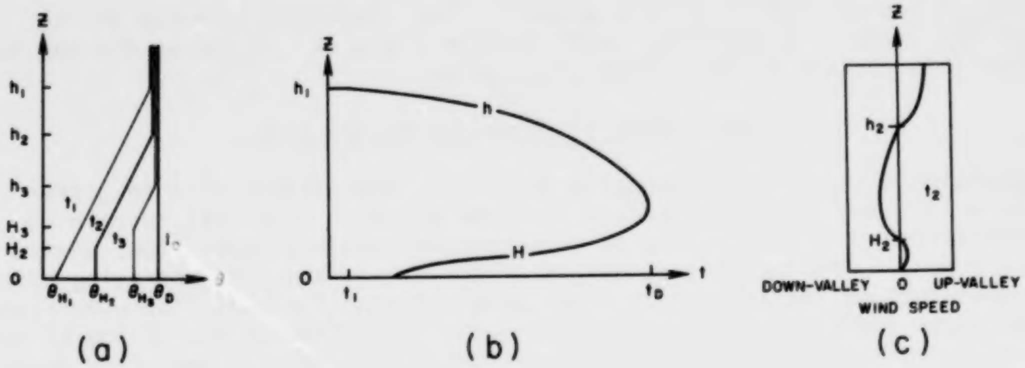

Figure 2. Typical inversion destruction.

h(t), H(t)

In Fig. 2b we present plots of h(t) and H(t) corresponding to Fig. 2a. We should note here that, while this figure presents the typical case, a number of winter observations in different valleys show that the c.b.l. may fail to grow significantly after reaching 25-50 m. Descent of the inversion top, however, is typical of all seasons in the valleys studied.

Wind Structure

In Fig. 2c we summarize the wind structure corresponding to Fig. 2a at time t_2. While the wind structure is much more unsteady in time and space than the temperature structure, it was typical for winds in the neutral layer above the inversion and within the c.b.l. to blow up-valley while the winds in the inversion layer maintained their down-valley flow. Valleys varied greatly in the state of development of their along-valley wind systems. Despite these differences, the potential temperature structures of the different valleys evolved in the same general manner.

Cross-Section

A cross-sectional view of the inversion structure corresponding to Fig. 2 at time t_2 is provided in Fig. 3. Observations from the sidewalls reveal the existence of a growing c.b.l. adjacent to the ground similar to that observed over the valley floor. This neutral stability layer is formed by convective plumes rising from the heated sidewalls. It is, however, an advective boundary layer, carrying mass up the

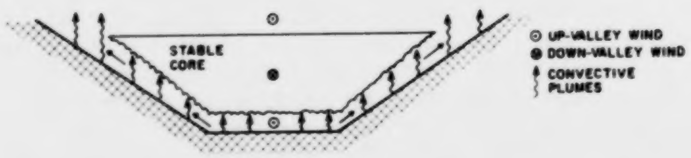

Figure 3. Valley cross-section.

sidewalls at typical speeds of $\sim 1\text{-}2 \text{ m sec}^{-1}$. The indicated increase in the depth of the layer with elevation comes from Moll's work[4], since we did not investigate this feature of the "slope wind system".

An Explanation of Inversion Destruction

Inversion destruction in mountain valleys is immediately seen to differ from the well-known inversion breakup over the plains. Over flat terrain the inversion is broken predominately as a convective boundary layer grows upward from the ground. The increase in height of the c.b.l. and the increasing potential temperature of the layer come from turbulent sensible heat flux convergence into the layer and entrainment of mass into the layer through the action of penetrative convective plumes. The energy available for sensible heat flux depends on solar heat flux and the partitioning of energy in the surface energy budget. The normal growth of the c.b.l. can be retarded by a strong synoptic-scale subsidence field.

In the valley atmosphere the predominant feature in the destruction of the inversion is the descent of the top of the inversion rather than the growth of the c.b.l. In earlier papers we have proposed an explanation for valley inversion destruction, emphasizing that the destruction is caused by the same forcing function active over flat terrain--namely, the input of solar energy into the valley as modified by the surface energy budget to produce sensible heat flux[5,6]. Due to heat flux convergence into the c.b.l. over the elevated sidewalls mass is removed from the valley as individual parcels are moved up the sidewalls in the upslope flows. To satisfy mass continuity the stable core must sink. Successive profiles in the stable core (Fig. 2) are characteristic of a simple downwards advection, being described in equations (4) and (5) by $\frac{\partial\overline{\theta}}{\partial t} = -\overline{w}\frac{\partial\overline{\theta}}{\partial z}$ and $\gamma = \text{constant}$. The potential temperature profile evolution in the advective boundary layers over the sidewalls is described by

$$\frac{\partial\overline{\theta}}{\partial t} = -\overline{v}\frac{\partial\overline{\theta}}{\partial y} - \overline{w}\frac{\partial\overline{\theta}}{\partial z} - \frac{\partial}{\partial z}\left(\overline{w'\theta'}\right) \quad \text{and} \quad \gamma = 0$$

The explanation for the retarded growth of the c.b.l. is the thermally driven divergence of mass from the c.b.l. and the related presence of the locally generated subsidence field at the top of the c.b.l.

Air Pollution Implications

Implications of valley inversion destruction for dispersion of air pollution are investigated by considering that the nocturnal inversion at sunrise contains pollutants emitted from a continuous elevated source. During the night such pollutants would have been carried down the valley in the along-valley wind system, undergoing both vertical and horizontal dispersion. The horizontal dispersion in these flows is known to be much enhanced over horizontal dispersion of pollutants over flat terrain[7]. After sunrise a convective boundary layer forms over the valley floor and sidewalls (Fig. 4a). The subsequent disposition of pollutants in the stable core will be affected by 2 competing processes--the sinking of the stable core and the growth of the c.b.l. We may consider the air pollution implications of the two processes by considering a valley cross-section down-valley from the source at a later time:

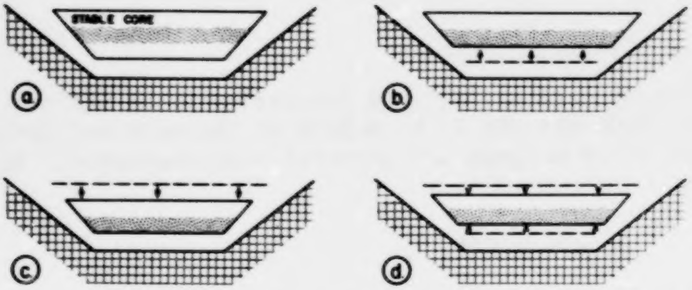

Figure 4. Air Pollution Implications

(1) Growth of convective boundary layer (Fig. 4b): Pure growth of a c.b.l. will result in fumigation[8] of pollutants at the valley floor as the c.b.l. grows upwards into the polluted stable core. This process is favored when the slope flows are ineffective in removing mass from the valley, and thus will occur in very wide or shallow valleys.

(2) Sinking of stable core (Fig. 4c): Failure of the c.b.l. to grow once it has formed over the valley floor and sidewalls results in inversion destruction by sinking of the stable core. Thus the pollutants sink into the top of a shallow mixed layer, producing high concentrations at the ground. The pollutant plume, once entrained into the c.b.l., is advected up the sidewalls and dispersed into the neutral layer aloft[6]. This process is favored for narrow to wide valleys when sensible heat flux is weak.

(3) Combination (Fig. 4d): A combination of c.b.l. growth and stable core descent result in the sinking of pollutants into the top of a growing mixed layer. Pollution concentrations should be intermediate between the previous 2 cases. This case is the most common one in Colorado mountain valleys.

Another process, that of cross-valley advection of the pollutant plume due to differential heating of the valley sidewalls, may be important in determining the cross-valley position of maximum pollutant concentration.

Our observations in snow-free valleys of Colorado show that inversions are typically destroyed within 3-5 hours after sunrise, regardless of season. This weak dependence on season is due to the fact that integrated solar flux on a horizontal surface for the first 4 hours after sunrise is nearly independent of season at Colorado's latitude. Thus, high pollutant concentrations at the ground may be expected in the first 3-5 hours following sunrise in polluted Colorado valleys. But inversions are typically broken every day and, once the inversion is destroyed, good mixing will prevail in an up-valley flow regime that is coupled to flows above the valley.

Moist surface conditions or high albedo due to snow cover may change the surface energy budget components so that sensible heat flux is reduced. In these conditions inversion destruction will be delayed or an inversion may persist all day. In Colorado's snow-covered Yampa Valley on Feb. 23, 1978 the c.b.l. failed to grow deeper than 35 m and the observations were characterized by a slow descent of the stable core. The inversion failed to break during this day although the top of the stable core descended to within 150 m of the ground. In such conditions pollutant residence times may be longer than 24 hours.

Acknowledgements

This research was supported by National Science Foundation Grant ATM76-84405. The contributions of G. Albright and R. B. McBeth of the National Center for Atmospheric Research to the field program are gratefully acknowledged. Ms. O. Panella typed the manuscript.

References

1. Hewson, E.W. and G.C. Gill, 1944: Meteorological Investigations in Columbia River Valley Near Trail, B.C. U.S. Department of Interior. Bureau of Mines Bulletin, 453, 23-228.

2. Morris, A.L., D.B. Call and R.B. McBeth, 1975: A Small Tethered Balloon Sounding System. Bull. Amer. Meteor. Soc., 56, 964-969.

3. Lilly, D.K., 1968: Models of Cloud-Topped Mixed Layers Under A Strong Inversion. Quart. J. Roy. Meteor. Soc., 94, 292-309.

4. Moll, E., 1935: Aerologische untersuchung periodischer Gebirgswinde in V-förmigen Alpentälern. Beitr. Physik fr. Atm., 22, 177-197.

5. Whiteman, C.D. and T.B. McKee, 1977: Observations of Vertical Atmospheric Structure in a Deep Mountain Valley. Arch. Met. Geophys. Biokl., A, 26, 39-50.

6. Whiteman, C.D. and T.B. McKee, 1978: Air Pollution Implications of Inversion Descent in Mountain Valleys. Atmos. Env., 12, 2151-2158.

7. Start, G.E., C.R. Dickson and L.L. Wendell, 1975: Diffusion in a Canyon Within Rough Mountainous Terrain. J. Applied Meteor., 14, 333-346.

8. Bierly, E.W. and E.W. Hewson, 1962: Some Restrictive Meteorological Conditions to be Considered in the Design of Stacks. J. Applied Meteor., 1, 383-390.

TRAJECTORIES UNDER A STRONG TEMPERATURE INVERSION IN A MOUNTAINOUS AREA

by

F. Wippermann and H.J. Koppert
Department of Meteorology
Technical University
Darmstadt, F.R.G.

Abstract. A model is developed which allows the computation of the vertically averaged flow under a strong temperature inversion. Since the hight of this inversion is assumed to be smaller than the highest mountains the flow has to be considered in a multiply connected region.

As an example for a practical application the model has been used to compute the flow in the Rhein-Main-area (central part of the F.R.G.) for 16 different directions of the large-scale wind. It is shown how the trajectories deviate from these directions due to the lateral boundaries and the topographical structure.

1. Introduction: The problem

The most unfavourable weather conditions for an accident of a nuclear power station are given with an anticyclone in winter time accompanied by an (almost stationary) very strong temperature inversion in only a few hundred meters above ground and very weak winds in the layer under the inversion. Such a situation often lasts for a period of several days.
According to the very stable stratification in the layer between the bottom and the inversion the turbulent diffusion in the vertical direction will be here almost zero, in the horizontal directions it will be very weak. That means a radioactive gas released at a power plant will remain concentrated in a cloud with a slowly growing diameter; such a cloud will move slowly advected by the weak winds.

In the case of an accident it would be important to know the way along which the cloud will move; decisions for an evacuation of the population living in an endangered sector should be based on such knowledge.

The way of the cloud can be described by the trajectory of the gravity center of the cloud, or more correct by the projection of this trajectory on the earth surface.
The trajectory can be obtained in a very crude approximation by the direction of the large-scale wind as given by synoptic datas. However the true trajectory is influenced by the topography of the earth surface, since the very stable stratification forces

the flow to go mainly around the topographical obstacles and only to a small portion over them.

The purpose of this paper is the development of a method allowing the computations of trajectories in a mountainous area during the described weather conditions. It is assumed that a very strong temperature inversion exists, which practically decouples the layer under the inversion from the free atmosphere.
The flow in this layer is vertically averaged (v.a.) leading to a 2D-problem; of course, the vertical interval for averaging (from $z = h(x,y)$, the height of the earth surface above sea level, up to $z = H$ the (constant) height of the inversion above s.l.) varies with the horizontal coordinates x and y. The height H of the temperature inversion may be smaller than the maximum height of the mountains; that leads to the consideration of a flow in a multiply connected region.

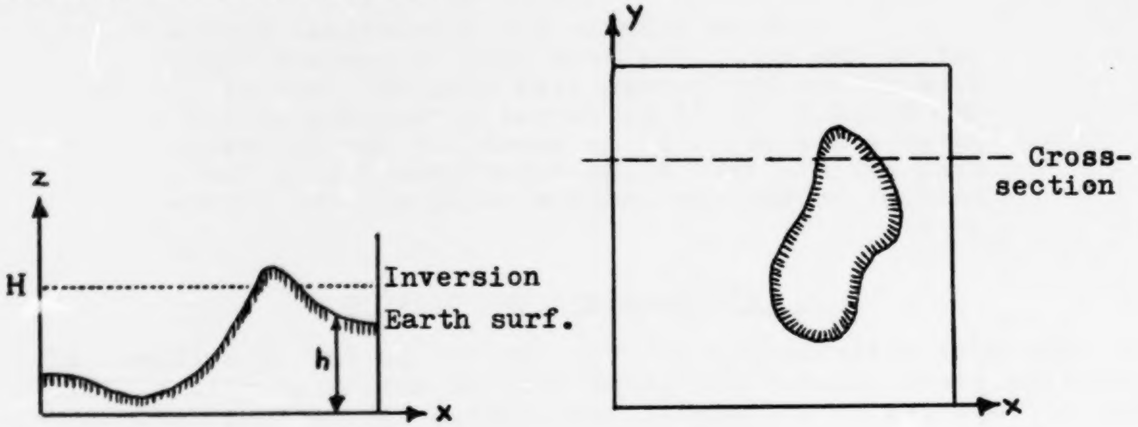

Figure 1. Coordinates, outer and inner boundaries

This involves considerable difficulties in the prescription of the boundary conditions at the inner boundaries.

The area which we consider should be a meso-scale area, let's say $100 \times 100\ \mathrm{km}^2$; the grid-size for the numerical treatment then has to be around $\Delta x = 2000\ \mathrm{m}$. At each grid point (i,j) the topographical value h_{ij} must be given, where this is a height of the earth surface representative of an area $(\Delta x)^2$.

2. The Model

2.1. The Vertical Averaging

In the model the air flow is averaged over the layer from the earth surface $z = h(x,y)$ to the height of the temperature inversion $z = H$, see Fig. 1.; the average is denoted by a circumflex

$$\hat{\mathbf{v}} = \frac{1}{H-h}\int_{h}^{H} \mathbf{v}(z)\,dz \qquad \mathbf{v} := (u,v) \qquad (1)$$

Since the lower boundary depends on the horizontal coordinates one gets for the averaged derivatives

$$\widehat{\nabla\cdot\mathbf{v}} = \nabla\cdot\hat{\mathbf{v}} - \frac{\hat{\mathbf{v}}-\mathbf{v}_h}{H-h}\cdot\nabla h \qquad \widehat{\nabla\times\mathbf{v}} = \nabla\times\hat{\mathbf{v}} + \frac{\hat{\mathbf{v}}-\mathbf{v}_h}{H-h}\times\nabla h \tag{2a}$$

$$\widehat{\nabla^2\zeta} = \nabla^2\hat{\zeta} - \frac{\hat{\zeta}-\zeta_h}{H-h}\nabla^2 h - \frac{2}{H-h}\nabla h\cdot\nabla\{\hat{\zeta}-\zeta_h\} \qquad \zeta := \mathbf{k}\cdot\nabla\times\mathbf{v} \tag{2b}$$

where $\nabla = \mathbf{i}\frac{\partial}{\partial x} + \mathbf{j}\frac{\partial}{\partial y}$ is a horizontal operator.

The velocity $\mathbf{v}$ may be represented by its vertical average and a deviation (denoted by a star)

$$\mathbf{v}(x,y,z) = \hat{\mathbf{v}}(x,y) + \mathbf{v}^*(x,y,z) \qquad \widehat{\mathbf{v}^*} = 0 \tag{3}$$

2.2. Parameterizations

When we average the vorticity equation and the continuity equation according to (1) terms appear, which contain the velocity components (u,v,w) at the upper and the lower boundary (denoted by an index H or h), and others containing correlation products of the kind $\widehat{\mathbf{v}^*\zeta^*}$ and $\widehat{w^*\partial\zeta^*/\partial z}$.

With a slip-condition at the ground the velocity components u_h and v_h should be a certain portion α of the vertically averaged value. Assuming that the wind doesn't turn with height (one of the fundamental model assumptions) this portion is the same for the u- and the v-component.
However this portion α depends on the thickness of the layer, it must $\alpha \longrightarrow 1$ for $h \longrightarrow H$. This dependence is assumed to be linear:

$$\mathbf{v}_h = \alpha\,\hat{\mathbf{v}} \qquad , \qquad \alpha = \alpha_0 + (1-\alpha_0)\frac{h-h_m}{H-h_m} \tag{4}$$

where h_m is the minimum height of the earth surface a.s.l. in the considered area; α ranges $\alpha_0 \leq \alpha \leq 1$, α_0 is of the order 1/10.
The parameterization of the horizontal velocity at the upper border is quite analogous

$$\mathbf{v}_H = \beta\,\hat{\mathbf{v}} \qquad , \qquad \beta = \beta_0 - (\beta_0 - 1)\frac{h-h_m}{H-h_m} \tag{5}$$

where β ranges $1 \leq \beta \leq \beta_0$ with values of β_0 around 6/5.

α and β depend on x and y ; however terms containing the horizontal derivatives of α and β will be neglected as being very small compared with the other terms.

The vertical velocity at the lower boundary is given by the kinematic boundary condition, i.e. for a non-horizontal earth surfave by

$$w_h = \mathbf{v}_h\cdot\nabla h \tag{6a}$$

where $\mathbf{v} = (u,v)$ is the horizontal velocity. At the inversion the vertical velocity should vanish, within the layer w should decrease linearly

$$w(z) = w_h \left\{ 1 - \frac{z-h}{H-h} \right\} \tag{6b}$$

out of which follows

$$\hat{w} = \frac{1}{2} w_h \tag{6c}$$

The correlation products should be parameterized by

$$\widehat{\mathbf{v}^* \zeta^*} = q_1 \hat{\mathbf{v}} \hat{\zeta} \tag{7}$$

$$\widehat{w^* \frac{\partial \zeta^*}{\partial z}} = q_2 \hat{w} \widehat{\frac{\partial \zeta}{\partial z}} \tag{8}$$

where the coefficients have to be determined by experimentation. It has bee found that the results obtained with the model are very insensitive to a variation of the values of q_1 and q_2.

2.3. The Model Equations

The model consists of the steady state vertically averaged (v.a.) vorticity equation, the v.a. continuity equation and the v.a. equation defining the vorticity.
This is a set of three equations for the three variables $\hat{\zeta}$, $\hat{u}$ and $\hat{v}$.

The v.a. vorticity equation reads

$$\begin{aligned}
&(1+q_1)\left\{(\hat{\mathbf{v}}\cdot\nabla)\hat{\zeta} + \hat{\zeta}(\nabla\cdot\hat{\mathbf{v}})\right\} - \\
&\quad - (\hat{\mathbf{v}}\cdot\nabla)h\left\{\frac{\lambda}{H-h}\hat{\zeta} + \frac{\mu}{(H-h)^2}\,\mathbb{k}\cdot\left[\hat{\mathbf{v}}\times\nabla h\right]\right\} - \\
&\quad - K_m\left(\nabla^2\hat{\zeta} - \frac{1-\alpha}{H-h}\left[2\left(\nabla\hat{\zeta}\cdot\nabla h\right) + \hat{\zeta}\,\nabla^2 h\right] - \right. \\
&\qquad\quad - \frac{\alpha(1-\alpha)}{(H-h)^2}\left\{\mathbb{k}\cdot\left[\hat{\mathbf{v}}\times\nabla h\right]\nabla^2 h + \right. \\
&\qquad\qquad\qquad \left. + 2\,\nabla h\cdot\mathbb{k}\times\left[\nabla\times\left[\hat{\mathbf{v}}\times\nabla h\right]\right]\right\} - \\
&\qquad\quad \left. - 2\,\frac{\alpha(1-\alpha)}{(H-h)^3}(\nabla h)^2\,\mathbb{k}\cdot\left[\hat{\mathbf{v}}\times\nabla h\right]\right) = 0
\end{aligned} \tag{9}$$

where K_m is the (horizontal) turbulent diffusion coefficient, which is assumed to be constant. λ and μ are abbreviations

$$\lambda := 1 + q_1 - (1 + q_2)\frac{\alpha}{2}(\beta - \alpha) - \alpha^2 \tag{10a}$$

$$\mu := (1 - \alpha)\left\{(1 + q_2)\frac{\alpha}{2}(\beta - \alpha) + \alpha^2\right\} \tag{10b}$$

The v.a. continuity equation reads

$$(\nabla \cdot \hat{\mathbf{v}}) - \frac{\sigma}{H-h}(\hat{\mathbf{v}} \cdot \nabla h) = 0 \tag{11}$$

where σ stands for

$$\sigma := 1 - \frac{\alpha}{2}\ln(\varrho_H/\varrho_h) \tag{12}$$

with ϱ_H and ϱ_h the densities at the upper and the lower boundary.

In order to derive the v.a. continuity equation in the form (11) it has been assumed that the flow is unelastic and that the density depends only on the vertical coordinate. σ varies with x and y since α and ϱ_h depend on x and y ; however the variation with ϱ_h is neglected.

The third equation is that one defining the v.a. vorticity

$$\hat{\zeta} = \mathbb{k} \cdot [\nabla \times \hat{\mathbf{v}}] + \frac{1-\alpha}{H-h}\mathbb{k} \cdot [\hat{\mathbf{v}} \times \nabla h] \tag{13}$$

2.4. The Boundary Conditions

Since the problem necessitates computations in a multiply connected region one must distinguish outer boundaries and inner boundaries.

For the formulation of the boundary conditions the v.a. velocity should be represented by a stream function $\hat{\psi}$ and a velocity potential $\hat{\varphi}$

$$\hat{\mathbf{v}} = \mathbb{k} \times \nabla\hat{\psi} + \nabla\hat{\varphi} \tag{14}$$

At the inner boundaries the flow should be parallel to the boundary

$$\hat{\mathbf{v}}(\mathbf{x}_{IB}) \cdot \mathbf{n}_\perp = 0 \tag{15a}$$

where $n_\perp$ is a unit-vector perpendicular to an inner boundary. (15a) means

$$\hat{\psi}(x_{IB}) = \text{const.} \quad , \quad \nabla\hat{\varphi}(x_{IB})\cdot n_\perp = 0 \tag{15b}$$

Considerable problems are raised in determining the constant stream functions at the different inner boundaries, mainly when these boundaries are numerous and very irregular. Additional conditions (e.g. vanishing circulation Γ along a boundary, no change of the enstrophy and/or others) are required. We can't deal with these problems here.

For the v.a. vorticity at an inner boundary may be put

$$\hat{\zeta}(x_{IB}) = 0 \tag{15c}$$

At the outer boundaries the inflow into the area under consideration as well as the outflow have to be given

$$\hat{v}(x_{OB})\cdot n_\perp = \text{GIVEN} \tag{16a}$$

It may be desirable to have the flow at the inflow-boundary perpendicular to the boundary; this means that

$$\hat{\psi}(x_{IF}) = \text{GIVEN} \quad , \quad \hat{\varphi}(x_{IF}) = 0 \tag{16b}$$

At the outflow-boundaries the conditions (16c) are used

$$\frac{\partial^2\hat{\psi}}{\partial n^2}(x_{OF}) = 0 \quad , \quad \hat{\varphi}(x_{OF}) = 0 \tag{16c}$$

where $\partial/\partial n = n_\perp\cdot\nabla$ The v.a. vorticity should vanish at the inflow boundary and should have no normal component of the gradient at the outflow-boundary

$$\hat{\zeta}(x_{IF}) = 0 \quad , \quad \frac{\partial\hat{\zeta}}{\partial n}(x_{OF}) = 0 \tag{16d}$$

3. The Solving Procedure

The three equations (9),(11) and (13) have to be solved in order to obtain $\hat{u}(x,y)$, $\hat{v}(x,y)$ and $\hat{\zeta}(x,y)$.

For the sake of simplicity the diffusion part in Eq. (9) should be reduced to $K_m\nabla^2\zeta$; all other terms containing K_m will be neglected as being small compared with the Laplacean of the v.a. vorticity. The neglected terms reflect the influence of the terrain ($\nabla h \neq 0$) on the horizontal friction.

For the solving procedure $\hat{\mathbf{v}} = (\hat{u}, \hat{v})$ will be replaced by $\hat{\psi}$ and $\hat{\varphi}$ given in (14).
The Eqs. (9),(11) and (13) then read

$$\boxed{\begin{aligned}
&\nabla^2\hat{\zeta} - \frac{1+q_1}{K_m}\left\{\mathbf{k}\cdot[\nabla\hat{\psi}\times\nabla\hat{\zeta}] + \nabla\hat{\varphi}\cdot\nabla\hat{\zeta} + \hat{\zeta}\nabla^2\hat{\varphi}\right\} + \frac{1}{K_m}\Big\{\mathbf{k}\cdot[\nabla\hat{\psi}\times\nabla h] + \\
&\quad + (\nabla\hat{\varphi}\cdot\nabla h)\Big\}\left[\frac{\lambda}{H-h}\hat{\zeta} - \frac{\mu}{(H-h)^2}\left\{(\nabla\hat{\psi}\cdot\nabla h) - \mathbf{k}\cdot[\nabla\hat{\varphi}\times\nabla h]\right\}\right] = 0 \qquad (17)\\
&\nabla^2\hat{\varphi} - \frac{\sigma}{H-h}\left\{\mathbf{k}\cdot[\nabla\hat{\psi}\times\nabla h] + \nabla\hat{\varphi}\cdot\nabla h\right\} = 0 \qquad (18)\\
&\nabla^2\hat{\psi} + \frac{1-\alpha}{H-h}\left\{\mathbf{k}\cdot[\nabla\hat{\varphi}\times\nabla h] - \nabla\hat{\psi}\cdot\nabla h\right\} - \hat{\zeta} = 0 \qquad (19)
\end{aligned}}$$

The Eqs. (17),(18),(19) form a complete set of three elliptic differential equations for the variables $\hat{\zeta}$, $\hat{\varphi}$ and $\hat{\psi}$;the boundary conditions are (15b),(15c),(16b),(16c) and (16d).

The solving procedure is an iterative one. Hereby one iteration (denoted by r) consists of three steps. First

$\hat{\psi}^{(r+1)}(x,y)$ is obtained by solving Eq.(19) using $\hat{\varphi}^{(r)}$ and $\hat{\zeta}^{(r)}$

Secondly

$\hat{\varphi}^{(r+1)}(x,y)$ is obtained by solving Eq.(18) using $\hat{\psi}^{(r+1)}$

and thirdly

$\hat{\zeta}^{(r+1)}(x,y)$ is obtained by solving Eq.(17) using $\hat{\psi}^{(r+1)}$and $\hat{\varphi}^{(r+1)}$

The procedure is started with $\hat{\psi}^{(0)} = \hat{\varphi}^{(0)} = \hat{\zeta}^{(0)} = 0$.

4. An Example for a Practical Application

4.1. The Topographical Structure of the Area under Consideration

The area chosen for a practical application is the Rhein - Main - region located in the central part of the F.R.G.

The upper part of Figure 2 gives a perspective view on this region (100 x 100 km^2); it shows the northern part of the Upper Rhein valley. This river enters the area in the middle of the southern edge and turns in the centre of the region to the west. The mountains in the NW form the Taunus range with a maximum height of 878 m above s.l.. In the south-eathern part we have the Odenwald with mountains ranging up to 605 m above s.l. The lowest point in the area is 90 m above s.l.

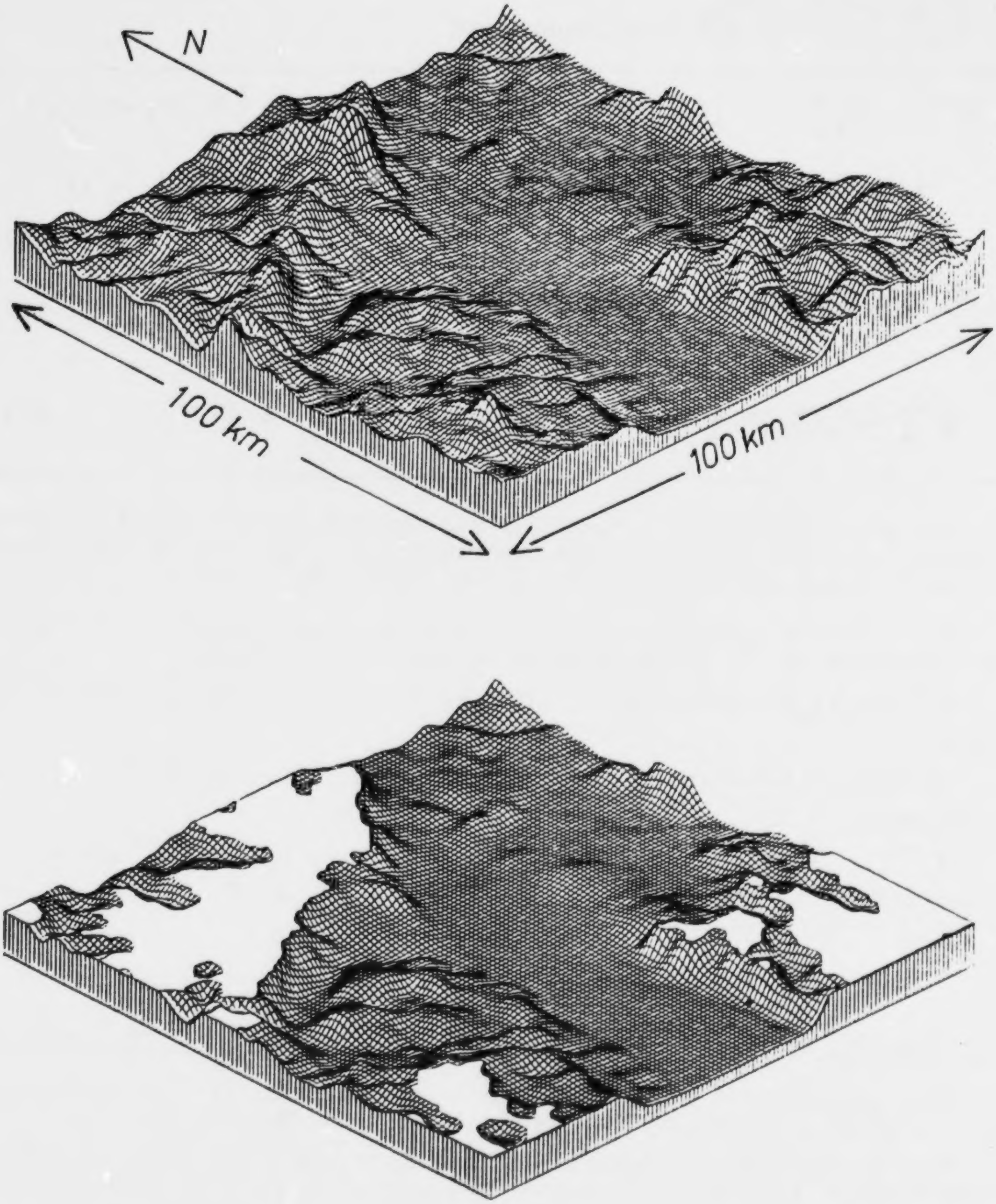

Figure 2. A perspective view on the Rhein-Main-region
Upper part: The topographical structure, see the description in Section 4.1.
Lower part: The remaining area for the flow under an inversion in 300 m above s.l.

4.2. The Input Data

The area is covered by a rectangular grid with a mesh-size of $\Delta x = 2500$ m . For each grid point (i,j) the topographical height according to Figure 2 has to be given.

The height H of the inversion is assumed to be 300 m ab. s.l.. The lower part of Figure 2 shows the same area as in the upper one, but all parts above the inversion are omitted. The borders of these omitted parts have been slightly changed in order to adapt them to the grid.
The remaining area in the NW corner is not connected with the main region, therefore it has been not considered.

The air in the area is subjected to a large-scale pressure gradient producing a (large-scale) velocity, which is assumed to be 2 m/s.
The direction of this velocity is determined by the ratio of the inflow into the area through one boundary section to the inflow going through the other one. The ratio of the outflows through the two boundary sections has to have the same value.

The constants are chosen as follows: $\alpha_o = 0.25$, $\beta_c = 1.20$, $\sigma_o = 1.25$, $q_1 = 0.5$, $q_2 = 0.5$.

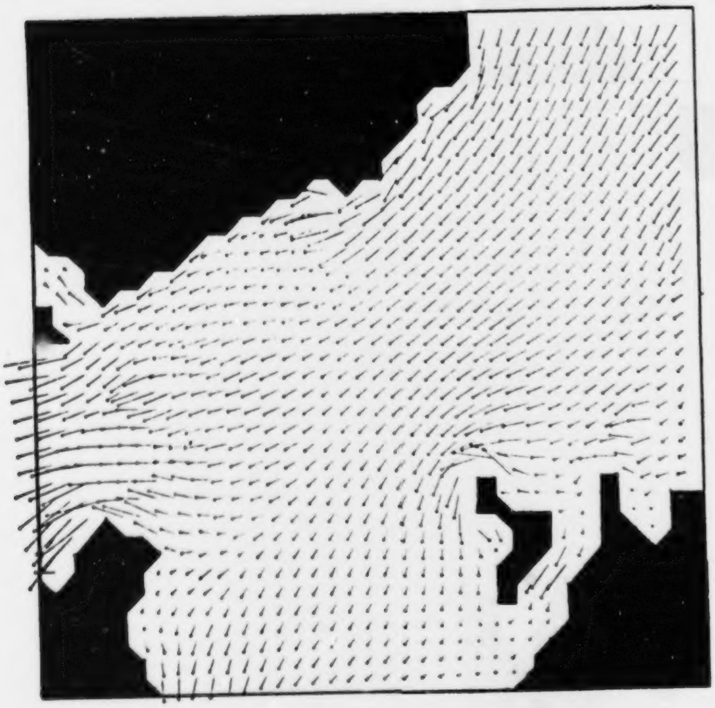

Figure 3.

The flow under the inversion for a (large - scale) wind from NE

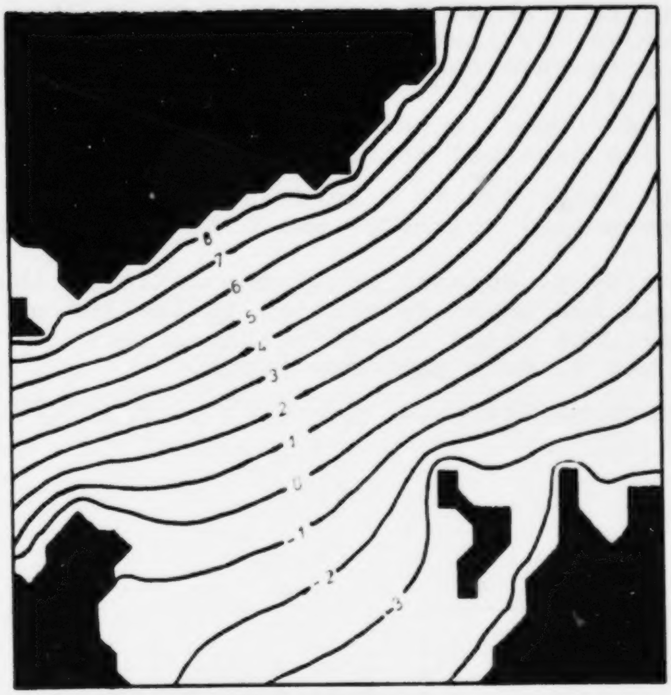

Figure 4a.

The non-divergent part, $\hat{\psi}(x,y)$, of the flow shown in Figure 3

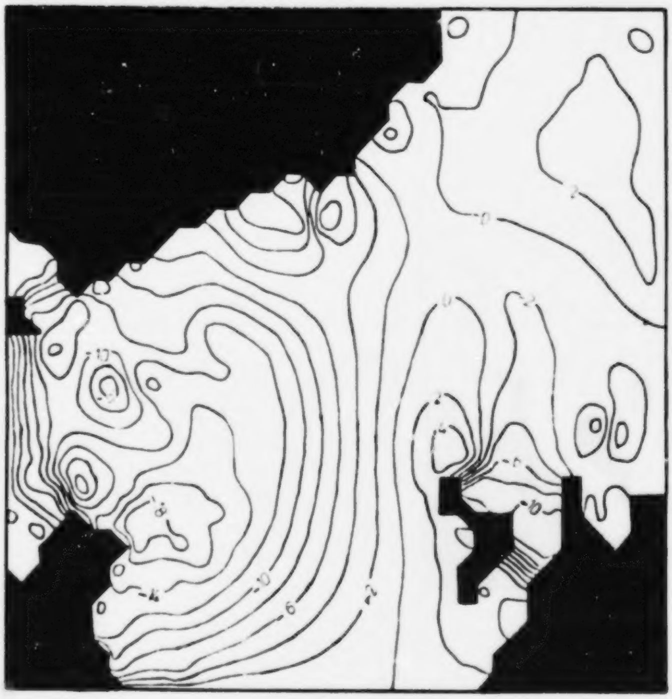

Figure 4b.

The irrotational part, $\hat{\varphi}(x,y)$, of the flow shown in Figure 3

4.3. Results

Computations have been carried out for 16 different directions (every 22.5° ,starting at the North) of the large-scale wind. For one case - the flow from NE - some results are presented here.

Figure 3 shows the flow influenced by the irregular lateral boundaries and by the orographic conditions. For a better understanding the flow is divided in a non-divergent part and in a irrotational one. The first one is shown in Fig. 4a, the second in Fig. 4b, both by isolines.

The computed flow field allows the construction of a trajectory starting at a given point.
For the 16 cases of different directions of the large-scale wind

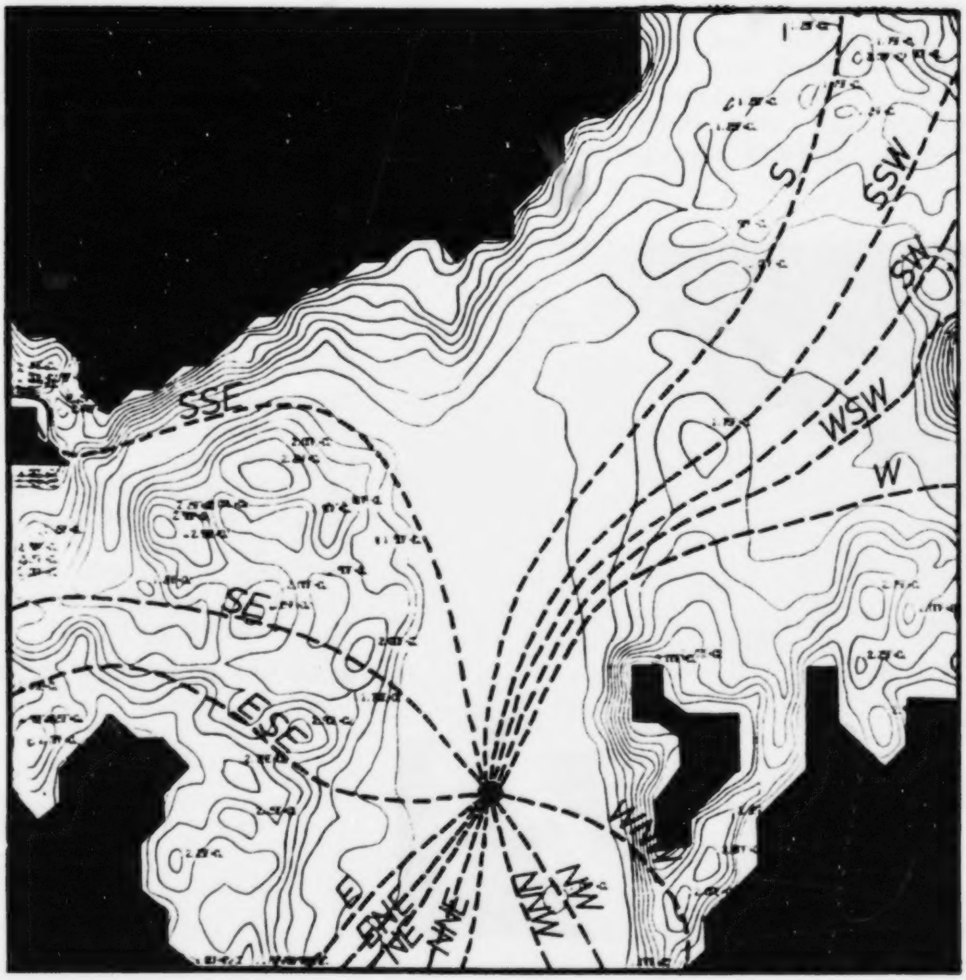

Figure 5. Trajectories (----) for 16 different directions of the large-scale wind. Solid lines are isohypses of the topography of the earth surface, label 25 m .

trajectories have been computed starting at the site of a nuclear power plant (BIBLIS) located on the Rhein river in the southern part of the considered region. Figure 5 shows the trajectories for these 16 cases. One notices that the lateral boundaries as well as the topographic structure cause considerable deviations of the trajectories from the direction of the large-scale wind.

In order to separate these two influences and to study only the influence of the topography a computation has been carried out comparing the trajectories (with a large-scale wind from ESE of 2 m/s) for two different conditions.
The first case is the same as in Figure 5 ,the computation is made regarding the topography h(x,y).
In the second case h(x,y) is put constant, namely the height of the starting point (h = 90 m a.s.l.); in this case the flow in a channel is considered, where the channel has a flat horizontal bottom and irregular solid walls.
Figure 6 shows the two obtained trajectories. The more northern trajectory is that one of the second case; the numbers giving the travel time in hours show that the air moves much faster in this case than in the case with topography. However this may be opposite under different topographic conditions.

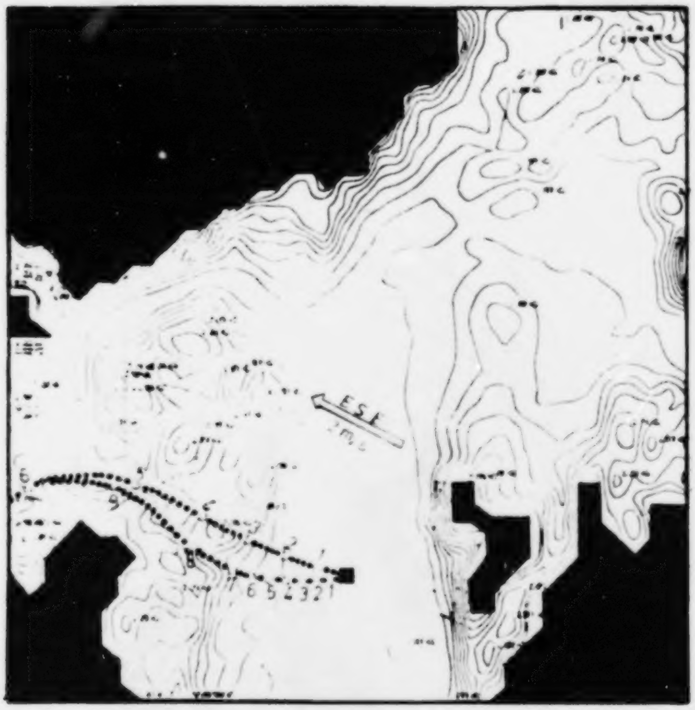

Figure 6.

Trajectories under two different topographical conditions
(a) the southern one: h(x,y) as shown in Fig. 5 by isolines
(b) the northern one: h(x,y) = const. = h of the starting point

Numbers give the travel time in hours

Discussion:

(Rapporteur: A. Braig)

Holzworth:

In your model the trajectories are functions of terrain heights and as showed in your presentation the inversion height is constant. Is there a change of the trajectories when the inversion height is variable?

Wippermann (response):

There is more influence from the wind field on the trajectories.

Nieuwstadt:

Has the model capability of handling varying inversion heights?

Wippermann (response):

The grid-length of the model is 2.500 m.

Because we have no measurements of inversion heights, we used the same height for running the model.

Millàn:

Have you taken into account heat island effect in your model?

Wippermann (response):

Effects of heat island were not considered.

Witheman:

Have you observed cross-valley circulation?

Smith (response):

Have you observed cross-valley circulation? Yes, we have observed cross-valley circulation. But we have seen layers of alternating cross-valley circulations of 0.1 or 0.2 m/s.

Comment of the Chairman:

I would like to comment on observations of the existence of the up-slope flow region. These up-slop flows have often been seen by meteorologists in valleys by means of plumes of vapor that rises from heated slopes.

DEVELOPMENT AND VALIDATION OF AN AIR POLLUTION MODEL FOR COMPLEX TERRAIN APPLICATIONS

by

Michael W. Chan, Sara J. Head, and Savithri Machiraju

Abstract. This paper presents a model that rationally determines the wind field, defines plume transport, and simulates dispersion of pollutants in complex terrain. The wind field is defined by three-dimensional numerical interpolation and extrapolation of measured wind. Transport of the Gaussian plume is treated by segmenting the plume at a given time into a number of time increments. Plume dispersion algorithms utilize measured fluctuations of wind direction and wind meander, and empirical formulations derived from the Lo-Low Altitude Clean Air Turbulence Project (LO-LOCAT).

This model was validated using data obtained in a specially designed tracer experiment conducted in complex terrain in the Rocky Mountains. Validation results show that good agreement exists between observed and predicted concentrations.

Introduction

Air pollutant concentrations at a receptor resulting from a point release are functions of both airflow pattern and turbulent dispersion within this flow. For the simple case of planar terrain, streamlines are well-defined and the assumption of a uniform wind field is not unrealistic. For such a simple case, dispersion properties have been the subject of considerable theoretical and experimental research and are now fairly well-defined in a quantitative fashion. The effect of topographic roughness, adds, on the one hand, an enhancement of the diffusion because of increased mechanical turbulence and wind shear, which is counterbalanced by a possibility of greater pollutant concentrations on rising terrain. In such non-planar terrain the flow trajectories are convoluted by topographic channeling and by thermally induced flows. A model has been developed that rationally determines wind field, defines plume transport, and simulates dispersion of pollutants in complex terrain. This paper describes this model -- AVACTA -- and presents a comparison between data collected in a tracer experiment and model predictions.

A Description of AVACTA

AVACTA is a broad-purpose Gaussian plume model which is able to model transport and diffusion in a spatially inhomogeneous, temporally unsteady wind field in rough terrain. It contains submodels within it for the estimation of wind fields, for the computation of plume rise, for the definition of plume transport, and for the determination of surface-roughness related diffusion.

Wind Field Submodel

The basic concept in this submodel are adapted from the work of Sklarew and Wilson.[1] This submodel first assigns a stability to each grid cell of a three-dimensional grid system defined by the user. This assignment is accomplished by interpolation of input stability data via a $1/r^4$ weighing factor.

The submodel then develops wind flow in the three-dimension grid from all input wind data, topographic data, as well as the calculated stability data. The winds calculated are consistent with any terrain resolved in the three-dimensional grid as well as completely divergence-free.

This wind field development starts with projecting wind data upwards from the point of observation through the portion of the grid without any measurements based on a vertical power law profile of the form

$$u = u_o \ (Z/Z_o)^P \tag{1}$$

for speeds u, and u_o at vertical coordinates Z and Z_o, respectively, with P determined from the following table:

Stability Category	A	B	C	D	E	F	G
P	.15	.17	.20	.26	.39	.48	.54

After the wind speeds are projected upwards, the wind speed and direction are resolved into U and V vector components at every wind site. Then, the entire wind field is developed via a weighted $1/r^2$ interpolation of the vertical profiles for each horizontal plane. Up to this point, terrain has not been considered. Terrain first enters into the wind field determination by shifting the interpolated winds upward to clear the terrain. Following this, the wind fluxes in and out of the boundaries of the computational domain are adjusted such that the flux in equals the flux out.

Atmospheric stability has the effect of varying the relative response to terrain of horizontal and vertical motion. For a neutral or unstable air mass, the flow tends to pass directly over an obstacle, without significant lateral diversion. For a stable airflow, gravitational effects tend to restrict an air parcel from flowing over an obstacle and direct the airstream around the obstacle. This phenomenon is incorporated into the model by assigning transparencies of the horizontal and vertical cell faces based on stability.

The nondivergence of the wind field is imposed by interactive solution based on calculating the divergence such that

$$\nabla \cdot U = \frac{\partial u}{\partial x} + \frac{\partial v}{\partial y} + \frac{\partial w}{\partial z} = 0 \tag{2}$$

and readjusting the velocity to minimize the divergence. A finite difference, iterative scheme is used in the computation. At the completion of the iterative cycle, all residual divergences are swept out of the top of the grid. This completes the generation of a three-dimensional wind for each cell of the grid system.

Plume Rise Submodel

Plume rise calculations are based on Turner's revision[2] of the formulations of Briggs.[3] Meteorological data required for these calculations are those generated by the wind field submodel.

Plume Transport Submodel

For a continuously emitting point source, a trajectory of the plume can be defined, in principle, and is defined in the plume transport submodel by the streak line* of the air flow passing over the source. Once the streak line of the plume is defined, it is broken up into segments. Each segment is represented by a tube with a Gaussian cross-section in the horizontal and vertical direction. The length of each tube is defined by the emissions produced by the source in the time increment of interest (usually from 15 minutes to one hour), and remains constant for the life of the segment. Each successive segment of the plume is a time increment older than the preceding segment if observed by moving downwind along the streak line away from the release point. Each plume segment has a history and has been subjected to aging, various wind speeds, stability classes, terrain roughness, and distance traveled. The history of the plume and its present state are defined by the plume cross-section which is assumed to have a bivariate Gaussian distribution. The cross-section of this distribution is defined by complex terrain algorithms (sigmas) as summarized in the next section, and is updated each hour.

Since this approach is somewhat unusual two examples will help to illustrate this pseudo-steady-state, pseudo-puff concept. First, say that the wind in the study area is uniform spatially, but has erratically shifted from a northwesterly direction to a southwesterly flow in a five-hour period as shown in Figure 1a. The idealized representation of a plan view of the streak line of the plume consisting of hourly plume segments emitted since time t - 4, or five hours ago, is shown in Figure 1b. This is how the plume would appear at time t. An hour later, at time t + 1, the plume would appear as in Figure 1c.

Consider the plume segment between station 3 and station 4 initially at time t. The cross-section of this tube can be completely described if it is assumed to be Gaussian and the σ_y and σ_z are known at every x along the streak line between 3 and 4. An hour later at time t + t, station 3 has moved to 3' and station 4 has moved to 4'. The plume cross-section σ (σ_y or σ_z) changes when moving from 3 to 3' according to the expression

$$\sigma_3' = \sigma_3 + \frac{d\sigma}{dt}\,\Delta t \qquad (3)$$

which can be rewritten

$$\sigma_3' = \sigma_3 + \left.\frac{\partial\sigma}{\partial x}\right|_3 u\,\Delta t + \left.\frac{\partial\sigma}{\partial t}\right|_t \Delta t \qquad (4)$$

where u is the wind speed representative of the hour t to t + Δt

$\frac{\partial\sigma}{\partial x}$ represents the spatial variation of σ

$\frac{\partial\sigma}{\partial t}$ represents the temporal variation.

Because of the pseudo-steady-state assumption, $\frac{\partial\sigma}{\partial t}$ is zero during the interval from t to Δt. The derivatives of σ_y and σ_z with respect to x can easily be evaluated by differentiating the σ equations discussed in the next section, thus allowing calculation of σ'. Concentrations are then calculated by the standard Gaussian plume formulas.

---

* A streak line is defined by connecting, in sequence, all elements of air passing over a point; i.e., the source.

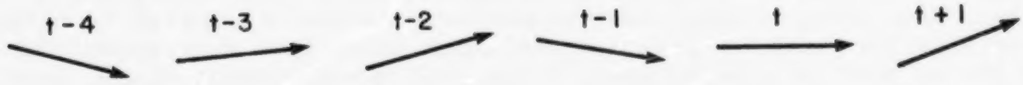
t - 4
t - 3
t - 2
t - 1
t
t + 1

Figure 1a. Wind vectors from time t - 4 to time t + 1.

Figure 1b. Streak line and plume boundaries at time t.

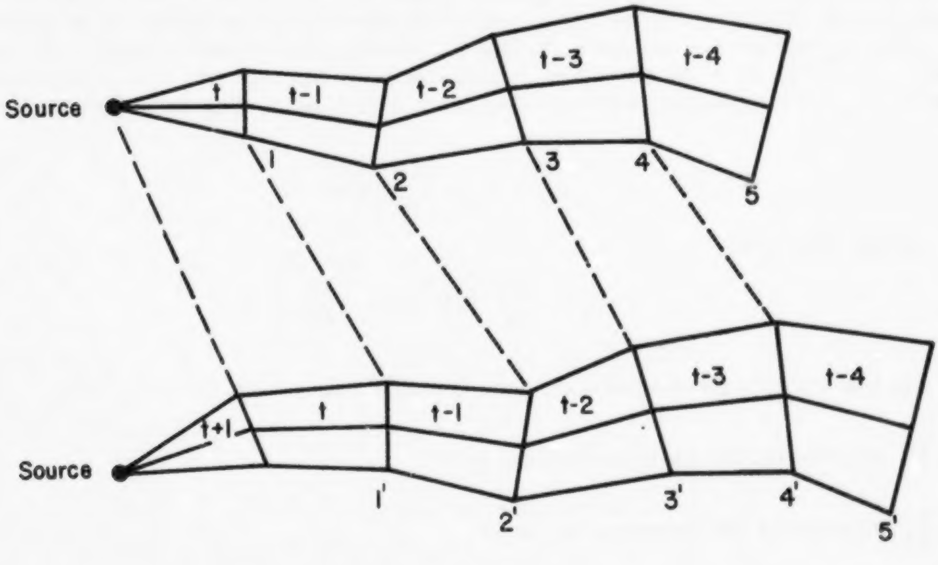
Source
t
t - 1
t - 2
t - 3
t - 4
1
2
3
4
5
Source
t + 1
t
t - 1
t - 2
t - 3
t - 4
1'
2'
3'
4'
5'

Figure 1c. Streak line and plume boundaries at time t + 1.

Consider now a non-homogeneous wind field, i.e., one with turning flow. Figure 2a shows a streamline* passing over a source, with wind vectors at coordinate points S_0, S_1, and S_2. The pseudo-steady-state approach assumes that this streamline would be invariant within a selected time increment, say, one hour. As before, the plume generated during that hour can be simulated by a segment as shown in Figure 2b where the centerline of the plume is defined by the vector $\vec{U}(S_0, t)\ \Delta t$. If this length is small compared to the radius of curvature of the streamline, then the segment will accurately follow the streamline. If this is not the case, and finer time-scale wind data is available, then a better fit is achieved by using a smaller time interval Δt.

At time t + 1 the wind field may be different than before, say as in Figure 2c. In that figure, S_5 is the coordinate location representing the flow to which the front of the initial plume is now subjected. After one hour the result is as shown in Figure 2d, where a new plume segment has been generated with length and direction $\vec{U}(S_0, t+1)\ \Delta t$ and the ends a and b of the prior segment have been transported by an amount $\vec{U}(S_5, t+1)\ \Delta t$ and $\vec{U}(S_0, t+1)\ \Delta t$, respectively, to reach the locations a' and b'.

Diffusion Algorithms Submodel

The AVACTA has a set of diffusion coefficients for complex terrain that relates the diffusion with the measured terrain roughness (σ_{tr}) and with the measured or predicted fluctuation (σ_θ) and meander (Δ_θ) of the wind. A detailed discussion of the derivation of these coefficients appears in a paper by Mullen, et al.[4]

The resulting σ_y and σ_z (horizontal and vertical dispersion coefficients) are defined as:

$$\sigma_y = 0.009\, x \left(\sigma_\theta^{\,2} + \Delta_\theta^{\,2}\right)^{0.5} (1 + 0.0003\, x)^{0.5} \tag{5}$$

and under stability classes A through E:

$$\sigma_z = H_m + 0.45\, \sigma_{tr}^{\,0.13}\, u^{-0.475}\, \sigma_\theta\, x^{0.5} (1 + 0.0003\, x)^{k} \tag{6}$$

where $k = 0.86 - e^{-0.03\,\sigma_\theta}$

whereas, under stability Class F or G:

$$\sigma_z = H_m + 0.46\, \sigma_{tr}^{\,0.21}\, u^{-0.39}\, \sigma_\theta\, x^{0.5} (1 + 0.0003\, x)^{p} \tag{7}$$

where $p = 0.928 - e^{-0.03\,\sigma_\theta}$

Here, x is the downwind distance, u the wind speed, and H_m the initial plume speed. The rest of the symbols have previously been defined.

An approximation for H_m has been empirically derived by examining plume photographs and is equal to 10% of the plume rise at any x.

---

* In contrast to a streak line, a streamline at any moment is defined by the velocity vectors in the flow. The flow is parallel to the streamlines. It does not define the flow trajectory except in steady flow.

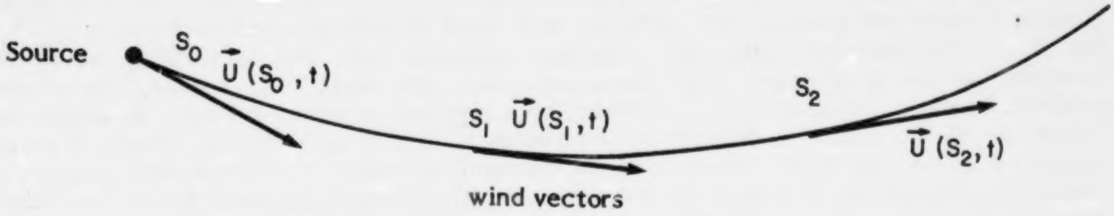
Source
S0
$\vec{U}(S_0, t)$
S1
$\vec{U}(S_1, t)$
S2
$\vec{U}(S_2, t)$
wind vectors

Figure 2a. A steady-state stream line at time t.

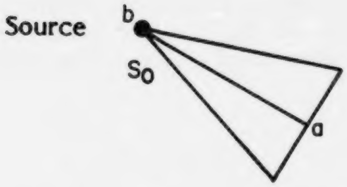
Source
b
S0
a

Figure 2b. Plume generated along this stream line starting at time t.

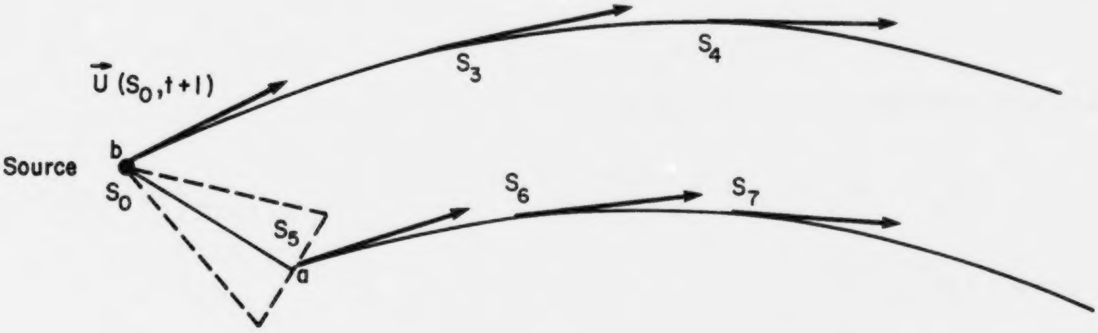
$\vec{U}(S_0, t+1)$
S3
S4
Source
b
S0
S5
a
S6
S7

Figure 2c. Stream lines at time t + a.

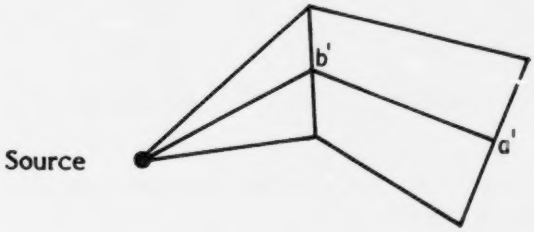

Figure 2d. Plume generated starting at time t plus transport of earlier plume segment by wind between S_0 and S_5.

Validation of AVACTA

This model was validated using data obtained in a specially designed tracer experiment. A description of that experiment appears elsewhere.[6] This experiment involved releasing the SF_6 from a source which was elevated 100 m above the ground by a tethered balloon, measuring meteorological conditions that existed during the experiment and measuring SF_6 concentrations at 23 receptors. Hourly measurements of SF_6 concentrations were made for five consecutive hours on two consecutive days. During the experiment, there were definite wind shifts and changes in atmosphseric stability.

The overall performance of the AVACTA for the two days of simulation is indicated by the linear regression plot of observed versus predicted concentrations in Figure 3. The correlation coefficient was 0.91. The intercept was 0.01 and the slope was 0.87. Such a good fit indicated that the model was able to predict reasonably well the spatial as well as temporal variability of pollutant concentrations under various meteorological conditions.

To test how well the model predicted the spatial distribution for each hour of the experiment, regressions of data sets for each hour were made. Table 1 presents the correlation coefficients, intercepts, and slopes. Good correlations were obtained for all hours. All intercepts were less than 0.5 $\mu g/m^3$, possibly an artifact due to the large numbers of low values, both in the predicted and observed concentrations. The slope gives a better indication on how closely the predictions were to the observations. During one hour the predictions were about 12% lower than observations. One hour gave a slope of 1.00. Six hours gave slopes between .75 and .95, indicating that the model was overpredicting by about 5% to 25%. The remaining two hours showed overpredictions of a factor of two and five. However, the very high overpredictions (a factor of five) occurred in the hour when none of the observations were higher than 0.55 $\mu g/m^3$.

Table 1. Linear regression results for individual hours of predictions versus observations.

Date	Time MDT	Correlation Coefficient	Intercept	Slope
9/14/78	0600-0700	.88	-0.34	.92
	0700-0800	.95	-0.12	1.12
	0800-0900	.89	-0.26	1.00
	0900-1000	.99	0.08	.80
	1000-1100	.91	0.25	.88
9/15/78	0600-0700	1.00	.01	.76
	0700-0800	.99	.01	.76
	0800-0900	.99	.01	.76
	0900-1000	.83	.30	.48
	1000-1100	.72	.04	.22

The ability of the model to predict the temporal variations of SF_6 concentrations is illustrated in Figure 4. Sites 2, 3, and 16 were selected because they were the only sites with observed concentrations greater than 1.5 $\mu g/m^3$. The ability of the model to track the temporal variability of the SF_6 concentrations at affected receptors is obvious.

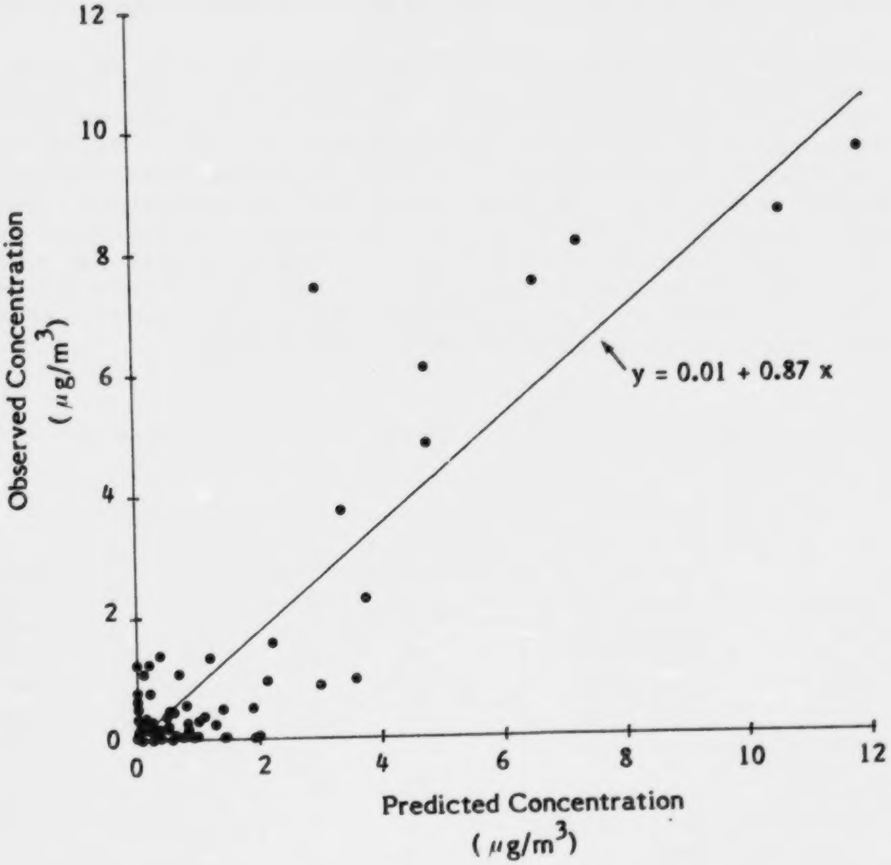

Figure 3. A linear regression plot of observed versus predicted concentrations.

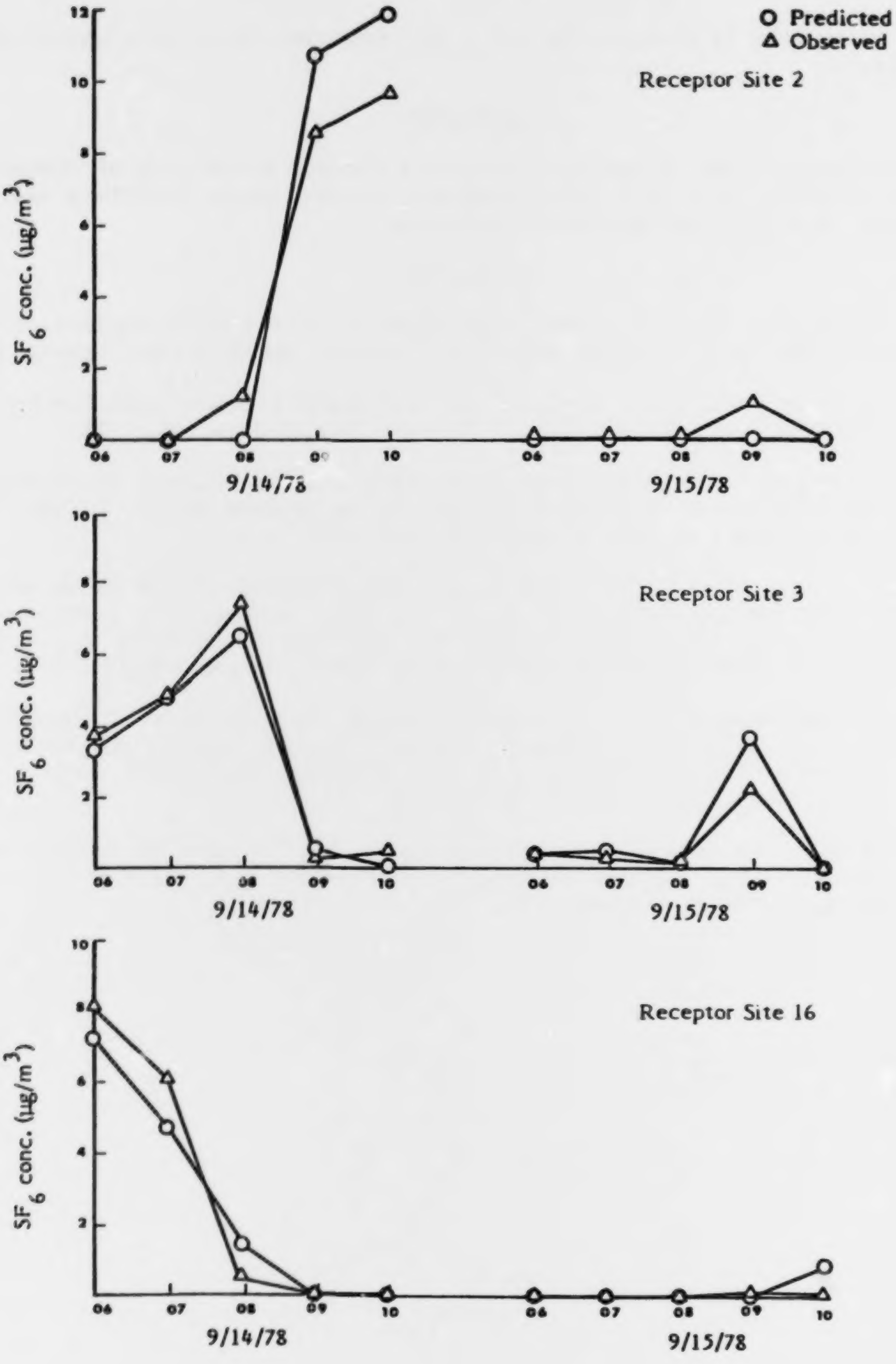

Figure 4. Trend analysis of predicted and observed SF$_6$ concentration at Sites 2, 3, and 16.

It is important to point out that no ad hoc calibration factors were applied to the model results.

Conclusion

AVACTA is a model designed to simulate the transport and diffusion of pollutants in complex terrain. There is a good agreement between model predictions and SF_6 concentrations observed during a tracer experiment.

References

1. R. C. Sklarew, and J. C. Wilson, "Applications of DEPICT to the Garfield, Navajo, and Ormond Beach Air Quality Data Bases," Science Applications Inc. report, 1976.

2. D. B. Turner, "Estimation of Plume Rise. Dispersion Estimate Suggestion No. 2," U.S. EPA, Model Applications Branch, Research Triangle Park, NC., 1973.

3. G. A. Briggs, "Some Recent Analyses of Plume Rise Observation." Proceedings of Second International Clean Air Congress. H. M. Englund and W. T. Bury, eds., Academic Press, New York, NY, pp. 1029-1032, 1971.

4. J. B. Mullen, I. H. Tombach, and M. W. Chan, "Development and Validation of a Model for Diffusion in Complex Terrain," preprint volume, Joint Conference on Applications of Air Pollution Meteorology, November 29-December 2, Salt Lake City, Utah. American Meteorological Society, Boston, MA., pp. 188-191, 1977.

5. P. B. MacCready, Jr., L. B. Baboolal, and P. B. S. Lissaman, "Diffusion and Turbulence Aloft Over Complex Terrain," preprint volume, Symposium on Atmospheric Diffusion and Air Pollution, September 9-13, Santa Barbara, CA. American Meteorological Society, pp. 218-225, 1974.

6. M. W. Chan, "A Tracer Experiment to Determine the Transport and Diffusion of an Elevated Plume in Complex Terrain," paper presented at the 72nd APCA Annual Meeting, June 24-28, Cincinati, OH., 1979.

Discussion:

(Rapporteur: Helga Kolb)

Millàn:

Could you comment whether stationarity and stability were taken into consideration in your experimental design?

Chan (response):

We made sure of steady state conditions by beginning release 3 hrs. before field measurements were made.

Hübschmann:

What computer requirements does your model have in terms of time, core etc.?

Chan (response):

It uses up the total capacity of a UNIVAC 1108 and 1 hr. of dispersion modeling takes up to 5 to 10 minutes CPU-time.

Saab:

Did you use sodar in your study?

Chan (response):

We used sodar to determine inversion structure, but we did not use doppler radar for windfield measurements.

Holzworth:

Does your model account for vertical transport of plume segments?

Chan (response):

Yes.

Jensen:

I have reservations on the approach you took in handling topography in your first submodel.

Chan (response):

I have to admit, that there are imperfections in the wind field submodel. Good agreements between observed concentrations and model predictions were only possible, when a dense network of wind stations was available. Improvements on this submodel are being undertaken.

Vogt:

Can you simulate strong wind direction changes with time with this model?

Chan (response):

Theoretically yes, if the time increments are small enough.

Meroney:

Though visually you only use a dual mountain ridge. I suppose, that in reality you have a whole row of ridges as an effect of the side walls of the tank.

Chan (response):

Only about 1/3 of the tank width was covered by the model, so there will be some effect, but I don't think this critical.

Meroney:

Can you comment on the reliability with respect to separation?

Chan (response):

At the low speed case separation could be important.

Hübschmann:

It is surprising to see the hill and the source moving as a result of the towning, instead of the fluid, that is the atmosphere.

Chan (response):

The important thing is the relative motion - and this can be effected in this manner.

Millàn:

It seems to me, that the air does normally not go as far upstream as your results indicate, that it is going to meet a hill further downstream. Is this an effect of the fluid model?

Chan (response):

No. If the dynamic similarity criteria are correct, there should be no difference.

Meroney:

Wind tunnel experiments with 2- and 3-dimensional hills as well as meteorological data sets indicate the same order of upstream influence of hills.

Portelli:

Is the downdraft on the side of the hills exaggerated in the experiment?

Chan (response):

It might be slightly reduced by turbulences, but otherwise it seems to be real.

PHYSICAL MODELING OF PLUME DISPERSION IN COMPLEX TERRAIN WITH AN ELEVATED INVERSION*

by

H.-T. Liu and J.-T. Lin†
Flow Research Company
Kent, Washington USA

Abstract. Laboratory experiments of plume dispersion in both complex terrain and an elevated inversion were conducted in a stratified towing tank. A stratified fluid with three density layers: a very stable middle layer, a neutral ground layer and a neutral or stable upper layer, was used to simulate the elevated inversion. The physical model was comprised of a smoke stack placed upstream of an idealized, three-dimensional hill. The stack Froude number was about 3; the internal Froude number, based on the ridge height of the hill and the inversion layer's Brunt-Vaisala frequency ranged from 0.68 to 1.85. The plume dispersion and the interaction of the stratified flow with the terrain were investigated by conducting flow visualization experiments, and by measuring the velocity near the stack and the ground concentration in the vicinity of the ridge.

Introduction

During the winter, a ground inversion layer, in which the temperature increases with the height above the ground, usually develops between sunset and sunrise as a result of longwave radiation from the ground. After sunrise, an elevated inversion may evolve from the ground inversion if a convective layer should develop adjacent to the ground and penetrate into the overlying stable layer. Plume dispersion in both ground and elevated inversion layers is of great interest to researchers and engineers because of its important application to air pollution control. By means of physical modeling in a towing tank, plume dispersion in the ground inversion layer has been investigated by the authors and others.[1,2,3] In addition, there have been theoretical and laboratory investigations of stratified flows around idealized, three-dimensional hills.[4,5,6] Therefore, the main objective of the present investigation is to assess the effects of the elevated inversion on plume dispersion in complex terrain since, when an elevated inversion is present in complex terrain, the flow interacts strongly with the topography and further complicates the associated plume dispersion phenomenon.

Experiments were conducted in a towing tank in order to investigate the dispersion characteristics of a plume released from a smoke stack into an elevated inversion in idealized complex terrain. The elevated inversion was simulated by a three-layer fluid consisting of a neutral bottom layer next to the ground; a neutral or stable upper layer high above the ground; and a

---

*This work is sponsored by the U.S. EPA Contract No. 68-02-1293.
†Presently at United Industries Corporation, Bellevue, Washington USA

Preceding page blank

strongly stable layer between the upper and bottom layers. The towing tank experiments were conducted under steady conditions in an idealized terrain model having the essential features of a complex terrain, that is, hilltops, ridges and valleys; in other words, the transient development of the convective layer adjacent to the ground was not simulated. (Laboratory simulation of an elevated plume's fumination during the breakup of a ground inversion has been reported elsewhere by Liu and Lin.[2]) The laboratory experiments included conducting flow visualization of the overall dispersion pattern and measuring the ground concentration and the vertical profiles of the longitudinal velocity component.

In this paper, pertinent literature is briefly reviewed followed by a description of the laboratory facility and experimental methodology. The results of the flow visualization and quantitative measurements are presented subsequently. (The results of the flow visualization were summarized in a 16 mm movie film entitled "Laboratory Simulation of Stratified Flows Over Complex Terrain" by Liu et al.[7]) Finally, a few concluding remarks are made based upon the important findings of the present investigation.

Literature Review

To establish a basis for assessing the effects of an elevated inversion on plume dispersion in complex terrain, a brief review of the essential features of plume dispersion and flows around three-dimensional hills in a fluid of constant density gradient (constant-N fluid) is presented in this section. In a relatively flat terrain, both field and laboratory observations[1,8] have demonstrated that a plume released from a stack in a constant-N ground inversion stays aloft in a thin ribbon formation and makes negligible contribution to the ground concentration.

In the presence of a three-dimensional hill downwind of the stack, the interaction between the stably stratified flow and the topography creates a complex flow field that greatly influences the plume dispersion characteristics. Because the stably stratified flow tends to go around rather than over an obstacle, when the terminal plume height is lower than the hill height, direct impingement of the plume onto the upwind slope of the hill occurs only if the stack is directly upwind of the hill;[1] otherwise, the plume may experience large lateral deflection from its undisturbed course.[2] The stratified flow around an obstacle can be characterized by an internal Froude number defined by $F \equiv U_\infty/2\pi Nh$ where U_∞ is the freestream wind speed, h is the hill height and N is the Brunt-Vaisala frequency,

$$N \equiv (1/2\pi)\sqrt{-\ (g/T_o)(\Gamma - \gamma)}$$

where g is the gravitational acceleration, T_o is a reference absolute temperature, Γ is the aliabatic lapse rate, and γ is the lapse rate. For very small internal Froude numbers $(F << 1)$, the stratified flow around a three-dimensional hill consists of layers of horizontal, two-dimensional flow around the hills contours.[4,5] The numerical solution based upon Drazin's asymptotic theory[9] agrees fairly well with the flow pattern observed over the upstream sides of simple hill models.[4,5] The flow pattern on the downstream side of the hill is affected by the separated wake. Riley et al.[4] have suggested using free streamline potential theory to account for the flow separation. For an axisymmetric, three-dimensional hill of polynomial shape, Hunt et al.[6]

have suggested that impingement of the plume takes place whenever the terminal plume height is lower than the dividing streamline height $H_S = h(1-F)$, where h is the hill height. Laboratory results showed that the ground pollutant concentration is high at the points of impingement and on the slope of the hill along the plume's path as it is being carried around the hill.[1] In the event that the plume goes over the hill, the pollutants in the plume aloft may be brought very close to the surface of the leeward slope of the hill by downslope wind so that high ground pollutant concentration may result. For weakly stratified flows with internal Froude numbers ranging from 0.4 to 1.0, Hunt et al.[4] have demonstrated that the downslope wind tends to suppress flow separation on the lee side of the hill and that an internal hydraulic jump develops some distance downstream of the hill. This may lead to flow channeling phenomenon along valleys in which ground pollutant concentration is greatly increased.[3]

In the presence of an elevated inversion, the flows around a three-dimensional hill and the corresponding dispersion pattern may deviate noticeably from those in a constant-N fluid. The present investigation was specifically designed to address this issue which has not yet received much attention.

Laboratory Facility

Towing Tank

Experiments were performed in a towing tank 18 m long, 1.2 m wide and 0.9 m deep. A detailed description of this apparatus has been given by Liu and Lin.[2] The towing tank's special features that pertinent to this investigation include:

(1) A specially designed filling system which facilitates preparing a density stratified fluid, using salt solution as the working fluid, with any desired neutral or stable stratification.
(2) A carriage (on which the terrain model and instrumentation were mounted) that rides on a film of oil, resulting in a noise level of only about 0.6% of the towing speed in the range of 3 to 6 cm/sec. (This feature allows accurate measurement of the velocity, temperature, and salinity with hot-film, thin-film and/or thermistor, and single-electrode conductivity probes.)
(3) Transparent side walls and bottom that allow flow visualization experiments to be conducted from several directions.
(4) A minicomputer system for direct on-line multiple-channel data acquisition and subsequent statistical analyses.

Terrain Model

The idealized terrain model (see Figure 1 for a contour map) is identical to that used in the earlier plume dispersion experiment by Lin et al.[1] (hereafter referred to as [I]). It had the essential features of a complex terrain, namely, hilltops, ridges, and valleys. The characteristic length scales of the terrain and the stack are summarized in Table Ia.

In the towing tank, the terrain model and the stack were actually mounted upside down on the oil-lubricated carriage. In order to simulate the hot effluent's rising upwards from a stack into an elevated inversion. the

Table I. Experimental Conditions

a. Characteristic Length of the Idealized Terrain Model

Length Scale: 1/2,500

Descriptions	Prototype [m]	Model [cm]
Stack Diameter, D	7.9	0.32
Stack Height, H	127	5.08
Mountain Peaks Height, h_o	610	24.40
Mountain Peaks Separation	941	37.64
Mountain Ridge Height, h	406	16.26

b. Simulation Conditions

Velocity Scale: 1/100

Run Number	U_∞ [cm/s]	K	F_D	Layer	Top of Layer [cm]	N [Hz]	F_h	$\frac{-\partial\bar{\theta}}{\partial z}$ [°C/100m] (prototype)
Ia	3	6.8	3.08	1	9.7	0	∞	-.98
				2	17.8	.20	.92	6.23
				3	40.6	0	∞	-.98
Ib	6	3.4	3.08	1	9.7	0	∞	-.98
				2	17.8	.20	1.85	6.23
				3	40.6	0	∞	-.98
IIa	3	6.8	3.07	1	8.6	0	∞	-.98
				2	19.3	.27	.68	12.22
				3	55.9	.12	1.54	1.59
IIb	6	3.4	3.07	1	8.6	0	∞	-.98
				2	19.3	.27	1.37	12.22
				3	55.9	.12	3.08	1.59

$\rho_s = 1.175$ [gm/cm^3]

effluent, which is heavier than the ambient fluid at the stack exit, was injected downwards from the stack exit into the three-layer fluid. Criteria for laboratory simulation of plume dispersion in a stably stratified atmosphere have been discussed by Snyder[10] and Liu and Lin.[3]

Effluent Injection Device

The effluent was concentrated salt solution, in order to make the plume visible, a blue food color dye was mixed into the effluent. The injection device consisted of a heated flask containing the effluent, a temperature controller (YSI Model 72), a veristaltic pump (Monostat Model 72-895-05) with insulated Tygon tubing, an accumulator, and a heated hose (Technical Heaters, Inc., Model 352) connected to the stack. The effluent was heated to $90^{\circ}C \pm 2^{\circ}C$. To ensure a turbulent plume, a sapphire nozzle of 0.38 mm in diameter was installed about 0.5 cm upstream of the stack exit to trip the plume. The Reynolds number was about 650, based upon the effluent exit speed and the exit diameter.

Methodology

The overall dispersion pattern of the plume was recorded on 35 mm slides and 16 mm color movie films. The movie cameras were mounted on the carriage to provide side and angle views of the plume; during the experiment, they were towed at the same speed as the terrain model. Back diffusive lighting was used to illuminate the plume and the model. A 35 mm camera was also placed under the tank to record the plan view through the transparent bottom.

The density profile of the three-layer fluid was measured with a single-electrode conductivity probe having a 0.025 mm platinum tip together with a conductivity gauge (Flow Research Company, Model 1110). Vertical profiles of the mean and fluctuating longitudinal component of the approaching flow at the stack position were measured with two 10-channel constant-temperature anemometers (Thermo System Inc., Models 1051-10 and 1053B) using 14 concial and cylindrical hot-film probes (TSI Models 1230S and 1290AK). The hot-film probes, which were mounted on a strut, covered a vertical distance of about 30 cm with the space between probes decreasing toward the terrain surface. These probes were calibrated by towing them at five different speeds either before or after each velocity measurement. During calibration, the strut was lowered to a position where no probes were blocked by the terrain model. The calibration data were least-squares fitted by second degree polynomials.

Ground pollutant concentrations on the surface of the terrain model (see Figure 1) were measured with thermistor probes (Fenwal Electronics GC32SM2) using temperature as the tracer. The probe tip was 0.76 mm in diameter and the time constant (3db point) of the thermistor probes in still water was about 0.07 sec. A 10-channel gauge with the thermistor probe as one arm of the wheatstone bridge measured the temperature of the fluid. Typically, the system's sensitivity is about 10 volt/$^{\circ}$C.; but through the use of a signal conditioner, it was amplified by a factor of three. The gauge output fed directly into the minicomputer system for on-line calibration and data acquisition. The noise level was about 1.4×10^{-4} $^{\circ}$C and the thermistor probe had long-term stability (a typical drift of 0.01°C/year). The probes were pre-calibrated against a precision thermometer with 0.01°C divisions (Brooklyn Thermometer Company, Inc.) in a constant-temperature bath. Within the range of temperature differences of interest ($0 \sim 0.5^{\circ}C$), the calibration curves are practically linear;

second-degree polynominals were used to fit the calibration data. Before each experiment, a reference temperature was measured in the towing tank and recorded in the computer. The pre-calibrated curve was then shifted to pass through the point corresponding to the measured reference temperature. For ground concentration measurements, the probes were installed in the terrain model with the probe tips exposed to the ambient fluid at a distance approximately 0.2 cm above the terrain surface.

Experimental Conditions

Table I lists the experimental conditions for all four runs. The free-stream wind speed is denoted by U_∞, and the ratio of the effluent speed W_s to U_∞ is denoted by K. The stack Froude number, F_D, is defined as $F_D = W_s/\sqrt{gD\Delta\rho/\rho_s}$, where D is the stack diameter, $\Delta\rho$ is the difference between the densities of the effluent fluid and the ambient fluid at the stack exit, and g is the gravitational acceleration. The internal Froude number, F_{hi}, is defined as $F_{hi} = U_\infty/N_i h$, where N_i is the Brunt-Vaisala frequency of the i^{th} layer, and h is the height of the ridge between the two hilltops.

The three-layer fluid consisted of a neutral layer near the ground, a neutral layer (Runs Ia and Ib) or stable layer (Runs IIa and IIb) high above the ground, and a strongly stable or inversion layer between the two. The Brunt-Vaisala frequency and the simulated lapse rate in each of the layers can be found in Table Ib. The density profile for Runs IIa and IIb is illustrated in Figure 2. The only difference between Run Ia (IIa) and Run Ib (IIb) was that the towing speed, and therefore the internal Froude number F_{h2}, in Run Ib (IIb) was twice that in Run Ia (IIa).

Discussion of Results

Flow Visualization

Figure 3 shows the side views of the plumes in three-layer stratified flows over the idealized terrain model. The side views (Figures 3a through 3d) indicate that the overall dispersion patterns resemble, to some degree, those observed in the constant-N stratified flows (Figures 15 through 18 in [I]), especially in the region upstream of the hill. In the near field, the turbulent motion in the plume dominates the plume dispersion. The plume released into the bottom neutral layer rises into the middle inversion layer. The distance required for the plume to attain its maximum rise increases with the internal Froude number F_{h2}. This is merely the effect of the ambient stratification as demonstrated in [I]. The bent-over plume overshoots, then relaxes and, finally levels off at its equilibrium level in the inversion layer. In the same stratified fluid, the plume's overshoot is more distinctive for lower F_{h2} (Figures 3a and 3c).

Further downstream, the hill blocks the flow in the inversion layer. For all the cases, the pollutants in the plumes are carried by the wind, at least partially around the hill. Direct impingement of the plume onto the upstream slope of the hill is evident. For the low internal-Froude-number cases (Figures 3a and 3c), the plumes are aloft upstream and downstream of the hill. The wind carries the pollutants around the hill at the same level as those upstream and downstream of the hill. In other words, around the hill, the vertical displacements of the streamlines are small. This provides further eivdence that the strongly stratified flow can be treated as a locally two-dimensional flow around the contour of the three-dimensional hill at the appropriate level.[4] When the internal Froude numbers increase by a factor of two, strong interaction between the stratified flow and the hill occurs and the dispersion patterns change significantly. As the pollutants are being carried around the hill, the flow forces them downward and then upward. As F_{h2} increases, the position at which the subsequent upward motion of the pollutants takes place shifts toward the downstream direction. This complicated pattern results from the vertical pressure gradient developed at the field flows around the hill.[4] The vertical spread of the pollutants increases considerably downstream of the hill. This increase is partly by flow separation around the hill and partly by turbulence generated as the flow around and over (downslope wind) the hill rejoin. Strong vertical mixing of the stratified fluid is clearly observed from the movie records as the result of change in the index of refraction.

For the low F_{h2} case (Figure 3d), the subsequent upward motion has brought the pollutants back to nearly their original levels before flow separation took place (about 80° from the upstream stagnation point[11]). The plume in the flow separation region entrains a large quantity of ambient fluid that has about the same density of the pollutants. Therefore the entrainment merely increases the vertical spread of the pollutants; it does not alter the height of the plume axis. For the high F_{h2} case (Figure 3b), however, the subsequent upward motion has not initiated before flow separation took place. The plume in the flow separation region entrains a large quantity of heavy ambient fluid at the plume level. As a result of the entrainment, the pollutants can recover only a fraction of their original height downstream of the hill.

In the present experiment, lee waves cannot penetrate deeply into the bottom neutral layer; therefore, the strength of the downslope wind that tends to force the pollutants toward the leeward slope of the hill reduces considerably as compared with that in a constat-N ground inversion such as in [I]. Under certain circumstances, for example, if the downslope wind, rather than turbulent transport, should contribute the most to the ground concentration, the ground concentration in the lee of the hill may be lower in the present cases than in the constant-N cases.

Figures 4a through 4d show the plan views of the plumes. The plumes released from the stack (right) were advected toward the hill. The I-shaped, white portion shown in Figure 4d corresponds to the hilltops and the ridge between the hilltops (Figure 1). For all cases, the plan views (Figures 4a through 4d) show that the wind carries the plumes at least partially around the hill. Comparison of Figures 4a and 4c ($K = 6.8$) shows that there was no pollutant carried over the rdige, which indicate that the run with the lower internal Froude number had stronger blocking of the flow. A similar comparision is seen between Figures 4b and 4d.

The two cases with the more stable inversion layer (Figures 4c and 4d) are strikingly different. For the low internal-Froude-number case, the valley just downstream of the mountain ridge is practically free of pollutants (Figure 4c). The pollutants, which are carried by the wind around the hill, are transported downstream along the outside contour of the hill. On the other hand, for the high internal-Froude-number cases (Figure 4d), the valley is filled with pollutants. In this case, a strong reverse flow, which carries pollutants from the sides into the valley, appears to develop in the lee of the hill. As demonstrated in the movie records, a small portion of the pollutants trapped in the downstream valley is contributed to those carried over the ridge of the hill.

Velocity Profile

Hot-film probes in a vertical plane at the stack location measured the mean velocity profile, $\bar{U}(z)$. Figure 5 shows these measurements. The free-stream wind speed or the towing speed was U_∞ = 6 cm/sec. The profile shows several interesting features resulting from the interaction between the stratified flow and the topography. The wind speed in the middle inversion layer, where the flow is blocked by the ridge of the hill, appears to be at a minimum. In the bottom neutral layer, the velocity is higher than that in the middle layer. In the upper stable layer, where no major obstacle blocks the flow, strong overshooting from the mean wind or towing speed was measured; overshooting in the velocity profile is an established characteristics of stably stratified flows.[12,13] The profile displays several regions of high vertical shear, the most pronounced shear region occurring just above the ridge of the hill between the blocked and the overshooting regions. The visualization results (Figure 3 and 4) show that the plume levels off at an elevation slightly below that of the ridge of the hill where the flow is noticeably blocked.

Concentration Measurements

Ten thermistor probes that were installed on the surface of the terrain model measured the ground concentration. Their positions are indicated on the contour map shown in Figure 1. Table 2 summarizes the results of Runs Ia, Ib, IIa and IIb. For Run Ia where $F_{h2} = 0.92$, the wind carries the plume over and around the hill. The maximum ground concentration occurs on the top of the ridge between the peaks (probe 1) and has value as high as 5,700 ppm relative to the effluent concentration. High ground concentration was also measured at other locations on the slope of the hill (probes 4, 5, 9 and 10) along the plume's path over the ridge. These measurements further support the observation in [I], that is, that direct impingement of a plume onto the slope of the hill does occur under stable conditions. The maximum root-mean-square concentration occurred on the ridge (probe 3). This location corresponds to that of the plume edge, where the concentration signal is highly intermittent. When the internal Froude number increases (Run Ib, $F_{h2} = 1.85$), the ground concentration on the ridge of the hill decreases slightly. The measurement of the highest concentration, however, still occurred at probe 1.

In Run IIa, the strongly stable inversion reduces the terminal plume rise which is noticeably below the hill ridge. The wind carries the pollutants around the hill (Figure 4a), and ground concentration on the ridge is low. The vertical spread is so limited that the plume is not in direct contract with any of the probes. When the internal Froude number increases (Run IIb, $F_{h2} = 1.37$), a small portion of the pollutants are carried over the ridge of the hill, resulting in a slightly higher measurement of concentration on the ridge. The vertical spread also increases and high concentration was measured at other locations on the surface of the slope of the hill (probes 2, 4, 7 & 10).

Table II. Data of Ground Concentrations

Thermistor Probe No.	x [cm]	y [cm]	z [cm]	Run Number					
				Ia			Ib		
				$\bar{\theta}$ [°C]	$(\bar{\theta}-\bar{\theta}_a)/(\bar{\theta}_s-\bar{\theta}_a)$	$\sqrt{\overline{\theta^2}}$ [°C]	$\bar{\theta}$ [°C]	$(\bar{\theta}-\bar{\theta}_a)/(\bar{\theta}_s-\bar{\theta}_a)$	$\sqrt{\overline{\theta^2}}$ [°C]
1	61.00	0.00	16.26	20.75	5.74×10^{-3}	3.82×10^{-2}	20.56	4.02×10^{-3}	2.71×10^{-2}
2	57.47	0.00	8.89	20.37	2.87×10^{-4}	1.36×10^{-3}	20.42	2.01×10^{-3}	2.32×10^{-2}
3	61.00	6.35	16.50	20.62	3.87×10^{-3}	1.04×10^{-1}	20.36	1.15×10^{-3}	4.72×10^{-2}
4	57.47	6.35	11.68	20.44	1.29×10^{-3}	4.44×10^{-2}	20.45	2.44×10^{-3}	5.04×10^{-2}
5	67.00	0.00	12.95	20.65	4.31×10^{-3}	1.39×10^{-2}	20.44	2.29×10^{-3}	3.69×10^{-2}
6	64.77	0.00	14.48	20.37	2.87×10^{-4}	5.89×10^{-3}	20.41	1.86×10^{-3}	3.62×10^{-4}
7	36.83	19.69	10.29	20.35	0.0	1.07×10^{-2}	20.28	0.0	1.12×10^{-2}
8	38.74	19.69	12.09	20.37	2.87×10^{-4}	2.82×10^{-2}	20.33	7.17×10^{-4}	4.83×10^{-2}
9	44.45	19.69	14.10	20.48	1.87×10^{-3}	8.06×10^{-2}	20.38	1.43×10^{-4}	5.21×10^{-2}
10	57.47	13.97	13.97	20.42	1.01×10^{-3}	2.31×10^{-2}	20.32	5.74×10^{-4}	1.69×10^{-2}
Ambient Conditions				20.35	-	1.0×10^{-3}	20.28	-	3.0×10^{-4}

Thermistor Probe No.	x [cm]	y [cm]	z [cm]	Run Number					
				IIa			IIb		
				$\bar{\theta}$ [°C]	$(\bar{\theta}-\bar{\theta}_a)/(\bar{\theta}_s-\bar{\theta}_a)$	$\sqrt{\overline{\theta^2}}$ [°C]	$\bar{\theta}$ [°C]	$(\bar{\theta}-\bar{\theta}_a)/(\bar{\theta}_s-\bar{\theta}_a)$	$\sqrt{\overline{\theta^2}}$ [°C]
1	61.00	0.00	16.26	19.93	4.28×10^{-4}	2.65×10^{-3}	20.00	1.43×10^{-3}	7.46×10^{-2}
2	57.47	0.00	8.89	19.91	1.43×10^{-4}	1.70×10^{-3}	20.12	3.14×10^{-3}	5.12×10^{-2}
3	61.00	6.35	16.50	19.92	2.85×10^{-4}	4.42×10^{-3}	19.95	7.13×10^{-4}	8.92×10^{-3}
4	57.47	6.35	11.68	19.90	0.0	4.30×10^{-3}	20.29	5.56×10^{-3}	6.93×10^{-3}
5	67.00	0.00	12.95	19.91	1.43×10^{-4}	2.02×10^{-3}	19.96	8.56×10^{-4}	3.51×10^{-2}
6	64.77	0.00	14.48	19.92	2.85×10^{-4}	1.01×10^{-3}	19.93	4.28×10^{-4}	2.32×10^{-3}
7	36.83	19.69	10.29	19.91	1.43×10^{-4}	3.82×10^{-3}	20.20	4.28×10^{-3}	1.17×10^{-1}
8	38.74	19.69	12.09	19.91	1.43×10^{-4}	2.13×10^{-3}	19.93	4.28×10^{-4}	9.42×10^{-3}
9	44.45	19.69	14.10	19.92	2.85×10^{-5}	4.80×10^{-3}	19.92	3.14×10^{-4}	6.36×10^{-3}
10	57.47	13.97	13.97	20.01	1.57×10^{-3}	5.57×10^{-3}	20.05	2.14×10^{-3}	2.14×10^{-2}
Ambient Conditions				19.90	-	1.0×10^{-3}	19.90	-	1.0×10^{-3}

Effluent Temperature $\bar{\theta}_s = 90 \pm 2^{\circ}C$

Conclusions

The following conclusions are derived from the most important findings obtained in the present investigation.

(a) The bent-over plumes level off and are trapped within the middle inversion layer. For all cases, the wind carries the pollutants in the plume at least partially around the hill; for the cases with a more stable inversion layer, most pollutants are carried entirely around the hill.

(b) Direct impingement of pollutants on the surface of the slope of the hill is evident from both visualization results and probe measurements. For the cases with a less stable inversion layer and a neutral upper layer, the measurement made on the ridge of the hill along the center line of the model has the maximum concentration. For the cases with a more stable inversion layer, ground concentrations on the ridge are low because the terminal plume rise is lower than the ridge and most pollutants are carried around the hill.

(c) For the low internal-Froude-number, F_{h2} , cases, the pollutants remain aloft both upstream and downstream of the hill. The vertical spreads are small. For the high internal-Froude-number cases, the wind forces pollutants downward as it carries them around the hill. Downstream of the hill, the vertical spread of the pollutants increases significantly as a result of the enhanced entrainment introduced by flow separation and by turbulence generated as the flows around and over the hill rejoin.

(d) Downslope wind is not so strong as that in a constant-N ground inversion because the lee wave cannot penetrate into the bottom neutral layer. Under certain circumstances, the ground concentration in the lee of the hill may be lower in the present cases than in the constant-N cases provided that the downslope wind, rather than the turbulent transport, contributes most to the ground concentration.

(e) At the stack location, the velocity profile $\bar{U}(z)$ of Run IIb shows a minimum wind-speed region in the middle inversion layer, where the flow is blocked by the ridge. Pronounced shear regions are present near the interfaces of the layers. Strong overshooting in the velocity profile is observed in the upper layer.

References

1. J.-T. Lin, H.-T. Liu and Y.-H. Pao, "Laboratory Simulation of Plume Dispersion in a Stably Stratified Flow Over a Complex Terrain," EPA Report No. 654/4-74-044, Task I, USEPA, Research Triangle Park, North Carolina, 1974 (Also Paper No. 74-161, Presented at the 67th Annual Meeting of the APCA, Denver, Colorado).
2. H.-T. Liu and J.-T. Lin, "Plume Dispersion in Stably Stratified Flows Over Complex Terrain: Phase 2," EPA-600/4-76-022, 1976.
3. H.-T. Liu and J.-T. Lin, "Laboratory Simulations of Plume Dispersion From a Lead Smelter in Glover, Missouri: Neutral and Stable Atmosphere," EPA-450/3-75-006, 1975.
4. J. J. Riley, E. W. Geller and H.-T. Liu, "A Numerical Model for Stably Stratified Flow Around Complex Terrain," in the Proceedings of the Conference on Environmental Modeling and Simulations, Sponsored by the Environmental Protection Agency, pp. 503-507 (Also EPA-600/4-76-021).

5. P. W. M. Brighton, "Strongly Stratified Flow Past Three-Dimensional Obstacles," *Quart. J. R. Met. Soc.* *104*, pp. 289-307, 1978.
6. J. C. R. Hunt, W. H. Snyder and R. E. Lawson, Jr., "Flow Structure and Turbulent Diffusion Around a Three-Dimensional Hill," Part I, EPA Report No. 600/4-78-041, USEPA, Research Triangle Park, North Carolina, 1978.
7. H.-T. Liu, J.-T. Liu, D. W. Peecher and C. J. Williamson, "Laboratory Simulation of Stratified Flows Over Complex Terrain," Flow Research Film No. 9, May 1975.
8. F. A. Schiermeier and L. E. Niemeyer, "Large Power Plant Effluent Study," (LAPPES), Vol. 1 - Instrumentation, Procedures, and Data Tabulations, National Air Pollution Control Administration Publication No. APTD70-2, 1968.
9. P. G. Drazin, "On the Study Flow of a Fluid of Variable Density Past an Obstacle," *Tullus* *13*, No. 2, pp. 239-251, 1961.
10. W. H. Snyder, "Similarity Criteria for the Application of Fluid Models to the Study of Air Pollution Meteorology," *Boundary-Layer Meteorology* *3*, pp. 113-134, 1972.
11. H. Schlichting, *Boundary Layer Theory*, McGraw Hill, New York, 1960.
12. R. R. Long, "The Motion of Fluids with Density Stratification," *J. Geophys. Res.* *64*, pp. 2151-2163, 1959.
13. Y.-H. Pao, "Laminar Flow of a Stably Stratified Fluid Past a Flat Plate," *J. Fluid Mech.* *34*, pp. 795-808, 1968.

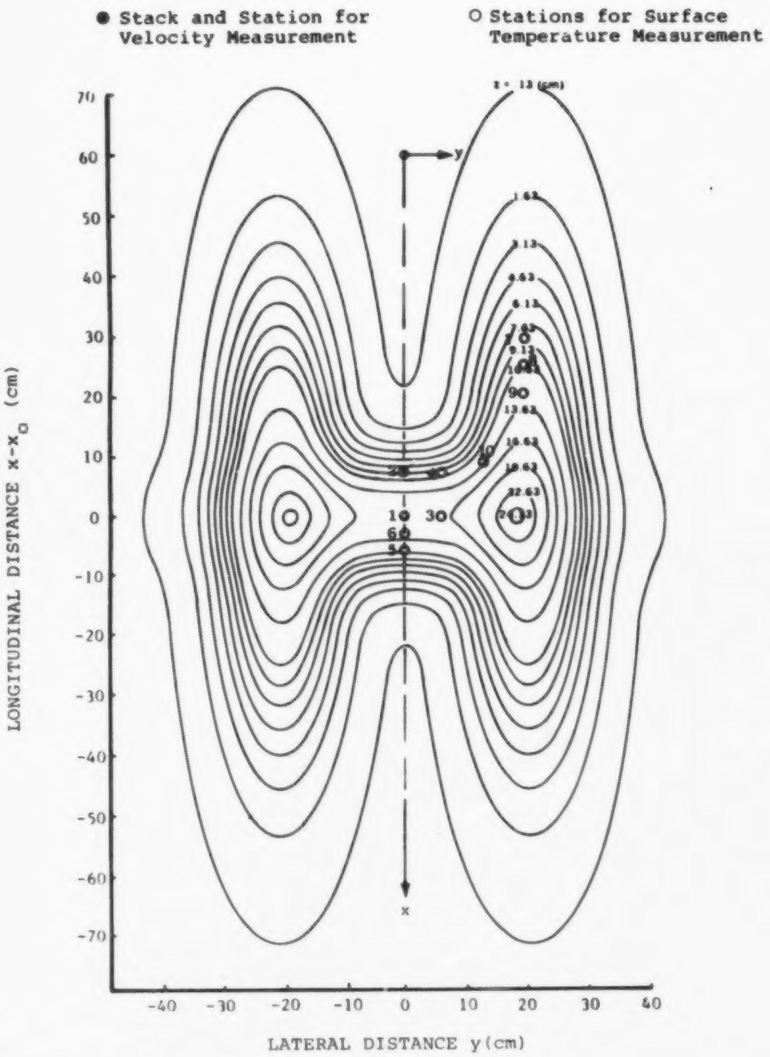
● Stack and Station for Velocity Measurement
○ Stations for Surface Temperature Measurement
z = .13 (cm)
1.63
3.13
4.63
6.13
7.63
9.13
10.63
13.63
16.63
19.63
22.63
24.13
70
90
10
30
20
10
30
60
50
y
x
LONGITUDINAL DISTANCE x-x$_0$ (cm)
70
60
50
40
30
20
10
0
-10
-20
-30
-40
-50
-60
-70
-40
-30
-20
-10
0
10
20
30
40
LATERAL DISTANCE y(cm)

Figure 1. A Contour Map of the Idealized Terrain Model

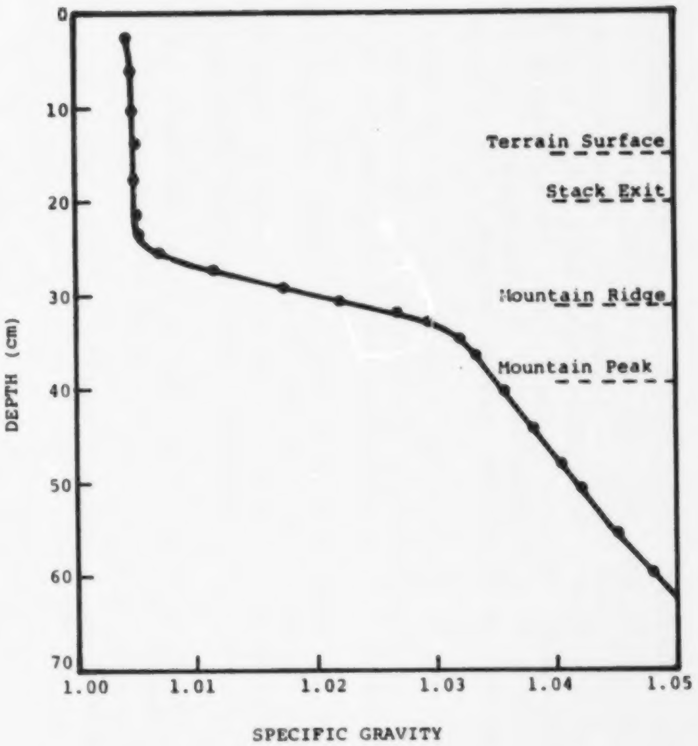

Figure 2. A Typical Three-Layer Stratification Profile (Runs IIa and IIb)

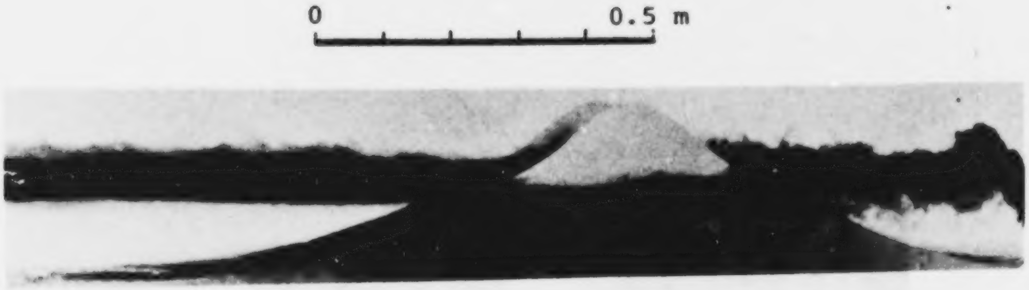

a. Run Ia, U_∞ = 3 cm/s, K = 6.8, F_{h2} = 0.92

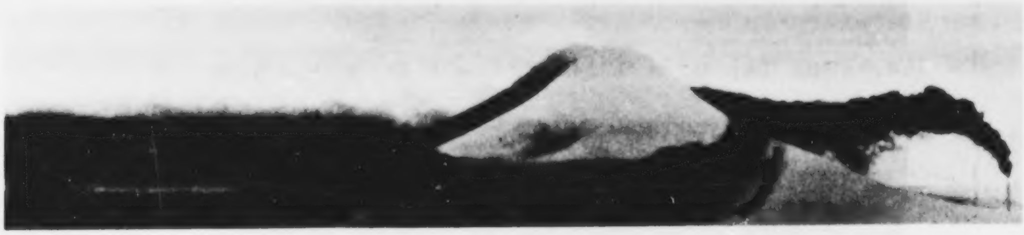

b. Run Ib, U_∞ = 6 cm/s, K = 3.4, F_{h2} = 1.85

c. Run IIa, U_∞ = 3 cm/s, K = 6.8, F_{h2} = 0.68

d. Run IIb, U_∞ = 6 cm/s, K = 3.4, F_{h2} = 1.37

Figure 3. Side Views of the Overall Dispersion Patterns

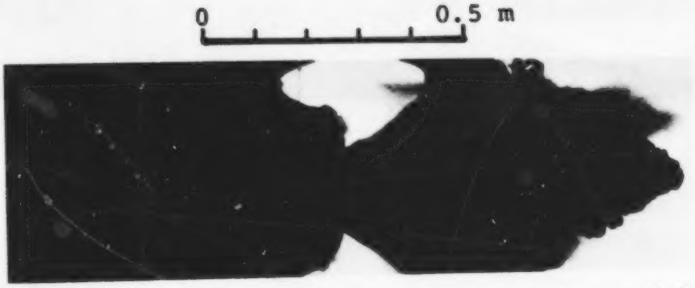

a. Run Ia, $U_\infty = 3$ cm/s, $K = 6.8$, $F_{h2} = 0.92$

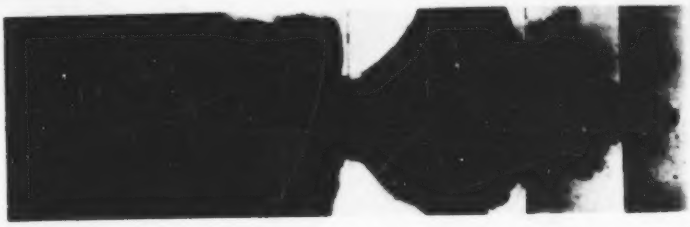

b. Run Ib, $U_\infty = 6$ cm/s, $K = 3.4$, $F_{h2} = 1.85$

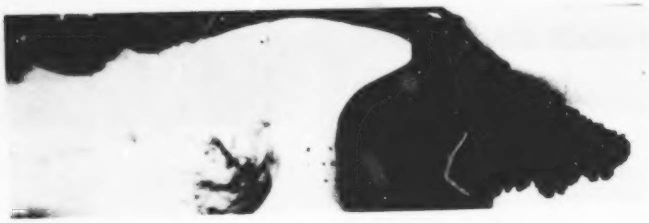

c. Run IIa, $U_\infty = 3$ cm/s, $K = 6.8$, $F_{h2} = 0.68$

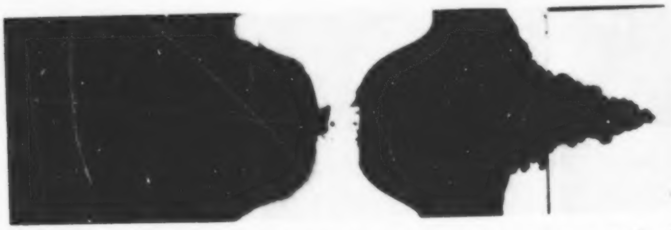

d. Run IIb, $U_\infty = 6$ cm/s, $K = 3.4$, $F_{h2} = 1.37$

Figure 4. Plan Views of the Overall Dispersion Patterns

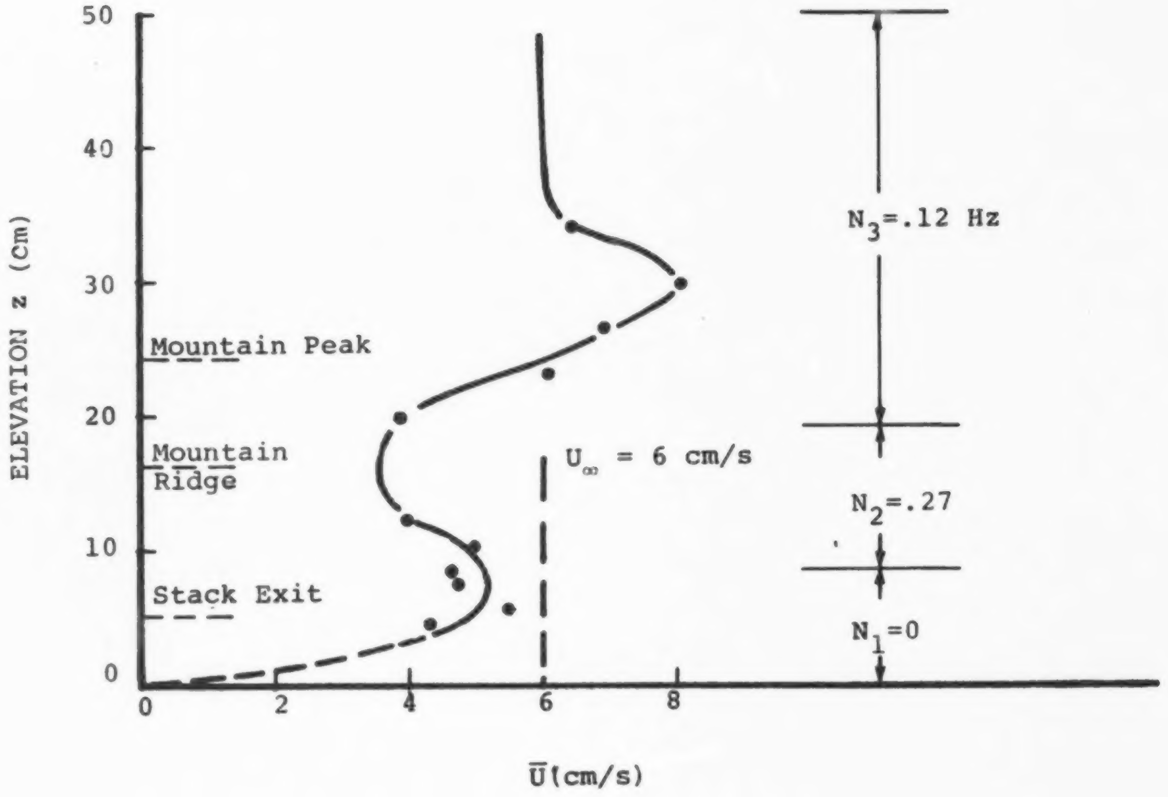

Figure 5. A Typical Velocity Profile for Run IIb at the Stack

A STUDY OF DISPERSION OVER COMPLEX TERRAIN IN THE SOUTHEASTERN UNITED STATES

George C. Holzworth*
Meteorology and Assessment Division
Environmental Sciences Research Laboratory
Environmental Protection Agency
Research Triangle Park, North Carolina 27711 USA

Kenneth E. Pickering and Robert C. Koch
Geomet, Inc.
15 Firstfield Road
Gaithersburg, Maryland 20760 USA

---

*On assignment from the National Oceanic and Atmospheric Administration, Department of Commerce

NATO/CCMS PANEL ON MODELING
October 22 - 26, 1979

Preceding page blank

INTRODUCTION

Recognizing the increasing trend in the United States of power plants and other large sources of pollutants to locate in mountainous regions and recognizing the uncertainties about atmospheric transport and diffusion over complex terrain, the U.S. Environmental Protection Agency in late 1975 initiated a three-phase contract with Geomet, Inc., to:

1. Summarize the current knowledge about dispersion, transformation, and depletion of power plant stack plumes in complex terrain.
2. Conduct an aerometric survey in the vicinity of a large coal-fired power plant located in complex terrain.
3. Analyze and summarize the dispersion characteristics of the power plant stack plume surveyed in 2, above.

Results of the first phase were reported by Koch et al. (1977). The edited measurement data from the second phase have been thoroughly described by Koch et al. (1979a). These data are on a magnetic tape that is available from the U.S. National Technical Information Service (Koch et al., 1979b) The contractor's report on his analyses of these data (Pickering et al., 1979) is nearly complete. The main results pertaining to SO_2 are briefly summarized in this paper.

STUDY SITE

The site chosen for the aerometric survey was the vicinity of the Clinch River Power Plant in southwestern Virginia, about 40 km north of Bristol, Tennessee. This power plant is located in a nonurban, mountainous region, isolated from other major sources of SO_2 but with an extensive network of roads for access to fixed monitoring stations and for deploying a sampling-equipped van. The power plant operators, Appalachian Power Company and American Electric Power Company, provided complete cooperation, which significantly enhanced the field survey. This cooperation is acknowledged with sincere appreciation.

The Clinch River Plant is a baseload plant with a total generating capacity of 712 MW, although its output normally varied diurnally from a daytime maximum of 650 MW to a nighttime low of 400 MW. During the survey the plant burned coal with a sulfur content of about 1 percent. There are three boilers with the effluent emitted through two 138-m stacks which have a separation of 46 m. Stack 1 that serves Boilers 1 and 2 has a diameter of 4.76 m while Stack 2 serves Boiler 3 and has a diameter of 3.81 m.

The plant location is shown in Fig. 1 along with the eight fixed monitoring stations and terrain features. The terrain is characterized by a series of ridges and valleys running southwest-northeast with numerous short valleys perpendicular to the larger ones, creating a truly complex topography. Although many terrain features are inaccessible by auto, roughly one-half of the area is occupied by small farms and rural residences. The plant elevation is 461 m, which puts the stack tops at 599 m. Ridges exceeding 680 m within 5 km of the plant occur in all direction quadrants. Elevations exceeding 870 m occur 8 km to the northwest and 14 km southeast of the plant.

AEROMETRIC MONITORING

In Fig. 1 the eight fixed monitoring stations range in elevation from 451 m at Castle to 792 m at Hockey; Tower is the station closest to the plant at 3.4 km and the most distant is Kent at almost 30 km. All stations measured winds and SO_2 continuously (Monitor Labs Model 8450) and some also measured temperature and NO_x, and collected particulates but this paper is concerned primarily with the analysis of SO_2 concentrations. At Hockey and Tower the wind was measured at 30 m as well as 10 m above station elevation; temperature difference was measured also at Tower. A stack monitor for SO_2 and NO (Environmental Data Corp.) was located in the duct works at the base of the smaller stack that serves the single boiler. Monitoring signals from the eight fixed stations and the stack were telemetered in real time to a central computer for processing, display, and storage.

A van was routinely deployed during daylight hours to monitor SO_2 NO_x, and O_3 in the expected touch-down area of the plume. Typically, after detecting the plume, the van sampled in a stationary mode. A helicopter flew traverses through the plume during two 10-day periods also measuring SO_2, NO_x, and O_3. Vertical profiles of wind and temperature were obtained semi-routinely at the power plant by use of double-theodolite pilot balloons with attached T-sondes.

The overall measurement period was June 1, 1976 through September 30, 1977 but as usual there were some delays in establishing the monitoring network and there were difficulties in maintaining operation at a high level of performance. Also, some monitoring capabilities were added during the project as resources became available. For example, the Lambert and Johnson stations were additions and didn't begin operating routinely until November, 1976; the stack monitor began measuring SO_2 in November, 1976 and NO, one month later. In April, 1977 the Castle station was washed away in a flash flood, which closed down the power plant, causing damage to the stack monitor. In July, 1977 the Lambert station was moved to Castle, which had been the only station downwind of the plant during typical down-valley, nocturnal wind conditions. Each summer the instruments on the tower at the Tower site were damaged by lightning. Pilot balloon soundings were initially taken at the rate of about one per day, but increased to three or four per day before the end of the project. T-sondes were not employed until late in 1976, but their use reached twelve per week before the end of the survey. Independent audits were made of the aerometric monitoring systems and some problems were noted in the air quality data; corrective actions were taken as necessary. That the field sampling was accomplished as well as it was, was due mainly to the dedication and ingenuity of the field crew. Complete details on the aerometric sampling are given by Koch et al. (1979a).

ANALYSES

Statistical Summaries. Typical operating conditions of the power plant are shown in Table 1. The SO_2 emission rates for Boilers 1 and 2 were derived in proportion to generator loads from the stack monitoring data for Boiler 3. For periods when the stack monitor was not operating, a similar relationship was used that included a dependency on sulfur content of the coal. The coal sulfur content was measured when the coal was placed on the stockpile but was estimated for the times when the coal was burned (roughly 1-2 weeks later). Fig. 2 shows hourly average values of typical generator loads for Stacks 1 and 2. Notice the abrupt drop in load at midnight for both stacks, and the increases beginning at 06 EST.

Ambient SO_2 concentrations at the monitoring stations never exceeded the primary U.S. National Standards of 30 ppb, annual average, or 140 ppb, 24-hour average, or the secondary standard of 500 ppb, 3-hour average. As mentioned, the sulfur content of the coal was generally less than 1 percent; it averaged 0.7 percent at the beginning of the survey and began to exceed 1.0 percent near the end. Table 2 shows the SO_2 concentrations for the fixed monitoring stations for the last year of monitoring, when the measurements are considered more reliable. By far, the highest average concentration occurs at Tower, the closest station to the plant, and Tower also had by far the highest percentage of hourly average concentrations 10 ppb or greater. The sensing threshold of the Monitor Labs (flame photometric detection) analyzer was considered to be slightly less than 10 ppb. Thus, the differences of average concentrations among stations in Table 2 should be interpreted as only generally indicative since most measurements were at or below instrument threshold and were highly sensitive to slight errors in calibration.

It should be mentioned that besides the power plant the only known SO_2 source of any significance was a coal preparation plant located 840 m west-northwest of the Tower station. Although at maximum operation this source consumed coal at a rate less than 1 percent of the normal rate of the power plant, it could have contributed to the contentrations at Tower during suitable wind conditions. A frequency distribution of SO_2 concentrations at Tower by Hockey 30-m wind directions (which winds were found to be most indicative of plume transport) shows a slight bulge in the frequency count of SO_2 concentrations greater than 25 $\mu g/m^3$ with northwesterly winds, but the greatest frequency of such SO_2 concentrations was associated with southwesterly winds, the direction of the power plant from Tower. For example, for wind directions from the sector 290-320 degrees the frequency of Tower SO_2 concentrations exceeding 25 $\mu g/m^3$ (10 ppb $SO_2 \simeq 26\ \mu g/m^3$) was 57, while for directions from the sector 210-240 degrees the frequency was 507. Apparently, the coal preparation plant could have had a slight impact on the SO_2 concentrations at Tower. But surprisingly, Munsey, Lambert, and Hockey all had similar slight indications of higher concentrations with winds from the general direction of the coal preparation plant. Furthermore, while all stations showed major impact from the power plant, they also showed some general tendency for slightly higher concentrations with southwesterly winds, suggesting the possibility of a contribution from sources in that general direction.

Greater significance can be placed in individual high SO_2 concentrations than in the overall averages shown in Table 2. Table 3 shows the ten highest SO_2 concentrations measured at each of the eight fixed monitoring stations. Although the highest concentrations clearly occurred at the closest station to the plant, Tower, the lowest concentrations did not occur at the most distant station, Kent, but rather at Lambert, ranked fifth in distance from the plant. Such variations are indicative of terrain effects on plume transport and diffusion. In Table 3 notice that all stations except Hockey had at least one day with at least two of their ten highest hourly concentrations occurring over consecutive hours, indicating that such persistence of relatively high concentrations is not exceptional. Also, notice the high frequency of the ten highest hourly concentrations that occurred during hours ending at 09-13 EST, at least eight such occurrences at each Tower, Lambert, Castle, and Nash. It is hypothesized that these high concentrations typically occurred in association with fumigating plumes as nocturnal inversions were eroded upward from the surface during solar heating. This idea is supported by observations of the field crew and by detailed analysis of periods with high concentrations (Pickering et al., 1979). Further evidence for this hypothesis may be seen in Table 3 in the near simultaneous occurrence (within 1 hour) of high concentrations during 09-13 EST at different stations; e.g., at Lambert and Castle for the hours designated HH, at Lambert and Nash for PP, and at Lambert and Munsey for KK and OO. On the other hand, it is difficult to explain the simultaneous occurrence of high concentrations at 03 EST at such widely separated stations as Hockey and Kent, designated as BB. As a further illustration of diurnal variations in SO_2 concentrations, Fig. 3 shows the hourly frequencies of concentrations exceeding 25 $\mu g/m^3$ at Castle and Johnson, the stations in Table 3 with the most and least concentrations, respectively, occurring during hours ending 09-13 EST. The Castle diurnal variation in Fig. 3 is rather typical of that at Tower, Munsey, and Nash, while the Johnson variation is similar to that at Hockey. The comparatively high frequencies of elevated concentrations during nighttime hours at Johnson and Hockey, both located on ridges, suggests stable plumes from the plant passing near the ridge tops.

The mobile van was highly successful in locating and sampling the power plant plume at ground-level. The van was directed from the headquarters station by radio, largely based on the Hockey 30-m winds which, of the available wind reports, were found to be most indicative of the initial plume transport. A total of 866 hours of sampling was accomplished by the van, 629 hours in the stationary mode and 237 hours while moving. Beginning in March, 1977 all van measurements were made in the stationary mode. Concentrations reported here are averages over about 1 hour. The overall average SO_2 concentration is 32.7 ppb, 37.5 ppb for the stationary mode and 28.8 ppb while moving. Half of the van measurements of SO_2 were 20 ppb or greater, compared to 16.5 percent for Tower, the station with the highest concentrations. In the van, relatively high concentrations were typically measured within 0.5 km of the plant, perhaps resulting from plume downwash in association with air flow over nearby ridges. About 75 percent of the van sampling was done at 3-10 km from the plant; practically all sampling was done between 08 and 16 EST. For sampling at distances greater than 5 km the van was most often in the sector north-northeast to east from the plant, indicating the prevailing daytime southwesterly air flow over the region.

Plume Structure. This section discusses analyses of the SO_2 measurements made by a helicopter flying horizontally across the power plant plume at successively different elevations and in successively opposite directions during July 20-28, 1977. Although the data were corrected for instrument response and transit time from the air intake to the instrument, many of the adjacent-elevation traverses that comprise a cross-section displayed successive back and forth shifts in peak concentrations. Most of the horizontal shifts of the plume center of mass were 100-300 m but some reached 800 m. It was speculated that this shift phenomenon was caused primarily by meander of the winds during successive traverses. This idea is borne out roughly by the range of 2-minute wind directions recorded for the Hockey 30-m sensor (generally near plume elevation) during the time of each complete cross-section (multiple traverses). The range of 2-minute wind directions generally equalled or exceeded the direction range of peak SO_2 concentrations in the individual plume traverses comprising each complete cross-section. In a similar approach the 2-minute vector winds for the Hockey 30-m sensor were successively advected from the power plant to simulate a "pseudo" snapshot of the plume. This was done at successive 2-minute intervals approximately corresponding to times when the helicopter was traversing the plume. When applied to a cross-section based on 18 traverses, the average shift of successive vector-calculated plumes was 290 m, compared to 321 m for the average shift of successive SO_2 peak concentrations. Individual shifts of the vector-calculated plume locations ranged 40-1080 m, compared to 15-850 m for the SO_2 peaks. However, there was no correlation between properly paired shifts.

Of the 24 plume cross-sections obtained by helicopter during July 20-28, 1977, most were within 5 km of the plant. Except for one at 18.2 km, all were within 8.2 km of the plant. All 278 helicopter traverses were accomplished during daytime, none started earlier than 0837 EST and none ended later than 1808 EST.

From the SO_2 cross-sections and pilot balloon winds, the SO_2 mass flux was calculated and compared to the power plant emissions for corresponding hours. The majority of mass flux calculations are considerably less than corresponding emission rates. This appears to be caused in many cases by the full vertical extent of the plume not being sensed by the helicopter. For six cross-sections, each of which consisted of a relatively large number of traverses, there was fair agreement between the calculated SO_2 flux and the plant emission rate. For these six cases the plant SO_2 emission rates ranged roughly 800-1400 g/second and the corresponding calculated flux errors ranged 4-38 percent of the emission rates; all but one were within 24 percent and half were within 16 percent. These errors in mass flux calculations undoubtedly are contributed to by the use of pilot balloon data that are not representative of the plume. This is especially likely for the complex terrain in the vicinity of the Clinch River Power Plant.

Since winds measured at hourly intervals or averaged over 1-hour intervals are often used to depict atmospheric transport, the direction of the SO_2 plume center of mass (as measured by helicopter cross-sections) was compared to the 1-hour average transport vector of the wind measured on the 30-m tower at Hockey. As mentioned, the Hockey 30-m wind had been determined to best represent the plume transport. The comparison for the 24 cross-sections is shown in Table 4. Except for the first three cross-sections, which were based on only three or four traverses, all comparisons are within 59 degrees and 55 percent are within 30 degrees. There is no apparent effect of the distance of the cross-section from the plant or the elevation of the center of mass on the difference between calculated and measured center-of-mass directions. A careful analysis of all available information showed in many cases the likely effects of particular terrain features in diverting the plume from the transport indicated by the Hockey winds. This indicates again the significance of complex terrain effects on plume transport.

The effect of terrain on plume height was analyzed for three cases for which adequate helicopter cross-section data were available. This was done by keeping track of the center-of-mass height of the plume above the terrain at successive downwind cross-sections as the plume encountered elevated terrain. For the three cases studied, the initial plume height above the terrain was reduced by 52, 63, and 71 percent of the terrain elevation increase.

The helicopter cross-sections were also used to calculate plume dimensions. Gaussian diffusion parameters, σ_y and σ_z, were calculated by a method described by Whaley (1974). Horizontal diffusion parameters were calculated for all 24 cross-sections, but data for vertical diffusion parameters were adequate for only seven cases.

Table 5 shows the computed σ_y and σ_z values along with corresponding Pasquill-Turner values (Turner, 1970) and σ_y values calculated as recommended by Pasquill (1976) and as described by Irwin (1979). Pasquill's recommendation uses measured standard deviations of wind direction fluctuations (σ_A, in radians) in the equation

$$\sigma_y = \sigma_A \times f(x)$$

where x is downwind distance in meters.

$$f(x) = \left(1 + 0.0308\ x^{0.4548}\right)^{-1} \quad \text{for } x \leq 10 \text{ km}$$

$$f(x) = 0.333\ (10{,}000/x)^{1/2} \quad \text{for } x > 10 \text{ km}$$

When σ_A is used in Pasquill's method, 11 of 18 cases showed Pasquill-σ_y values less than measured and seven cases showed Pasquill-σ_y values more than measured. For the 18 cases the ratio of values, measured σ_y: Pasquill σ_y, had a mean value of 1.16, indicating favorable comparison for the mostly unstable conditions associated with these data. When Pasquill-Turner σ_y values are compared with measured values, in 18 cases Pasquill-Turner underpredicted, while in six cases they overpredicted. The mean of the ratio, measured σ_y: Pasquill-Turner σ_y, was 1.47 for the 24 cases, indicating an enhancement of flat-terrain σ_y values when applied over complex terrain. In general in Table 5, the measured σ_y values correspond to values for a Pasquill-Turner stability class about one-half class less stable than indicated.

For the seven cases in Table 5 for which σ_z could be calculated, the ratio, measured σ_z: Pasquill-Turner σ_z, averaged 1.04, but the range was 0.56-1.74.

Model Applications. One of the main objectives in conducting the Clinch River Power Plant aerometric study was to collect a long-term (i.e., a year or so), but otherwise unpretentious, set of aerometric data with which to objectively test the reliability of existing dispersion models and modeling concepts. In order to routinely apply models on an hourly basis (i.e., calculate hourly average concentrations) it was necessary to establish methods and criteria for determining values of certain input variables. One such variable is plume height.

The method that was chosen for calculating buoyant plume rise has been described by Briggs (1975) and applied by Holzworth (1978). In this method the vertical variation of temperature and wind speed are used, so it was necessary to determine these values on an hourly basis. This was done by developing empirical relationships for temperature and wind speed based on the continuous measurements of temperature and wind at the various elevations of the aerometric sampling stations, the semi-routine pilot balloon and T-sonde measurements at the power plant, and U.S. National Weather Service rawinsonde observations taken regularly at 12-hour intervals at Charleston, West Virginia and at Greensboro, North Carolina, located 175 km north-northeast and 220 km east-southeast, respectively, of the power plant. Details on the relationships are given by Pickering et al. (1979). The contrived hourly vertical profiles of temperature and wind speed were used in the equations given by Holzworth (1978) to calculate effective stack heights. The necessary plant operating conditions, effluent volume flow rate and temperature at the stack, were supplied routinely by the power plant operators. Table 6 shows a comparison of plume height measurements based on the helicopter traverses, based on the Holzworth-Briggs method, and based on the conventional Briggs method (i.e., using stability classes) as used in the BEH072 subroutine of the U.S. PTMTP model (Turner and Busse, 1973). An average heat emission rate was used for the two Clinch River stacks. The mean absolute error for the Holzworth-Briggs method was 143 m, while for the Briggs BEH072 method it was 321 m. Subsequently, the calculations were done for each stack independently, but with an enhancement factor for multiple stacks (Briggs, 1974) that slightly reduced the error in the Holzworth-Briggs method.

Table 7 presents the diurnal variation in the frequencies of plume center-line heights, calculated by the Holzworth-Briggs method, with respect to the contrived structure of vertical temperature. These data are for the period mid-Oct, 1976-Sep 30, 1977. There is not much difference in the data for the two stacks. Notice that at 04 EST the plume center-lines are estimated to be in an inversion about 60 percent of the time but by 13 EST this value decreases to almost 20 percent, and there is no inversion 11 percent of the time. The data indicate that the plumes were seldom above an inversion, but somewhat more often for Stack 1 (two boilers) than for Stack 2 (one boiler).

Another input variable needed to operate all models is the stability class, e.g., the Pasquill classes as determined by Turner (1964) from sky cover and wind speed. Since cloud observations in the vicinity of the power plant were not taken routinely, another method had to be developed. For a selected period, hourly cloudiness as reported at Bristol, Tennessee (about 25 km south of the power plant) was used with wind speeds at the Tower station to determine Pasquill stability classes for comparison with a bulk Richardson number that was based on routine temperature gradient and wind speed measurements at Tower. From these data a relationship was developed for routinely determining the Pasquill stability class from the bulk Richardson number at Tower.

Lastly, hourly mixing heights were determined by using the contrived hourly temperature profiles that have already been described and the moisture profile of the Charleston or Greensboro rawinsonde. The mixing height was that height where the temperature of a parcel that was lifted dry adiabatically from the surface, pseudoadiabatically above its condensation level, became 1 degree C colder than the temperature profile.

The period that was modeled was from mid-Oct, 1976 through Sep, 1977. The station with the most model-to-measurement comparisons was Munsey, 4410 hours, and Castle had the least, 2392 hours, followed by Johnson with 3466 hours.

The initial model chosen for application was the basic Gaussian, flat terrain PTMTP model (Turner and Busse, 1973), except plume rise was determined from wind speed and temperature profiles, as already described. The model assumes steady state conditions throughout the hour, no terrain or aerodynamic effects, and the Pasquill stability class extends throughout the mixing height. This model is identified as No. 1, Flat Terrain, in Tables 8 and 9. The other thirteen models are the Flat Terrain Model with modifications for plume height due to terrain height differences between the plant and monitoring stations, adjustment of the standard Pasquill values for σ_y and σ_z, and others as described below.

Model No. 2 (Tables 8 and 9), CRSTR H (U.S. Environmental Protection Agency, 1977) decreases the plume height by the full elevation difference between plant base and sampling station for all stability classes.

Model No. 3, NOAA H (Van der Hoven et al., 1972), decreases plume height by the full elevation difference for stable conditions only.

Model No. 4, GEOMET H (Koch, 1978), decreases plume height (H) by a factor (F) of the elevation difference (Z), i.e., by the amount FZ, for stable conditions only. The maximum value of $F = 0.6$ for $Z \leq H$ and $F = 0.6H \div Z$ for $Z \geq H$.

Model No. 5, VALLEY H (Burt 1977), decreases plume height by the full elevation difference for stable conditions only, but the plume is not permitted to come closer than 10 m to the terrain.

Model No. 6, ERT-LAPPES H (Egan, 1975 and Slowik et al., 1977) decreases plume height by half the elevation difference for unstable and neutral conditions and by the amount FZ for stable conditions, where Z is full elevation difference and F = 1 for the plume height (H) above the terrain at the plant when $H \geq 1.7Z$, $F = 0.65$ for $H \leq Z$, and $F = 0.65 + (H-Z) \div 2Z$ for $Z \leq H \leq 1.7Z$.

Model No. 7, GEOMET σ_y IN 6, is Model No. 6, except the standard Pasquill values of σ_y are adjusted for complex terrain by a factor of 3.0 for neutral and stable conditions, and a factor of 2.0 for slightly instability with no adjustment for unstable or very unstable conditions (Koch, 1978).

Model No. 8, LAPPES σ-y IN 6, is Model No. 6, except the standard Pasquill σ_y values are adjusted by a factor of 1.43 for unstable and neutral conditions and for stable conditions by a factor of $1.43 \div (0.4U^{0.3})$, where U is wind speed (Slowik et al., 1977).

Model Nos. 9 and 10 employ modifications already described.

Model No. 11, F. SMITH σ-Z IN 10, is Model No. 10, except the standard Pasquill σ_z values are adjusted according to Smith (1972) by a factor of 1.5 for all stabilities, based on the estimated roughness in the vicinity of the Clinch River Plant.

Model No. 12, PASQ DILUTION IN 10, is Model No. 10, except the standard Pasquill values of σ_z are adjusted for initial plume dilution by the equation

$$\sigma_{z(a)} = (\sigma_{z(s)} + 0.1\Delta H^2)^{1/2}$$

where a and s indicate adjusted and standard, and ΔH is plume rise (Pasquill, 1976).

Model No. 13, WIND EXTRAP IN 10, is Model No. 10, except the routine transport wind speed, the Hockey 30-m measurement which is 361 m above plant elevation (U_{361}), is extrapolated by a power law to the plume elevation above plant elevation (H) by the equation

$$U_H = U_{361} \left(\frac{H}{361}\right)^P$$

The dependence of P on stability has been estimated by Geomet (unpublished) as:

Pasquill Stability	P
A, B, C	0.10
D (day)	0.12
D (night)	0.21
E	0.35
F	0.49

Model No. 14, PASQ σ-Y IN 13, is Model No. 13, except the standard values of σ_y are replaced by values that are a function of the standard deviation of wind directions (σ_A) and downwind distance (x), according to Pasquill's suggestion, $\sigma_y = \sigma_A \times f(x)$, which was discussed earlier.

Model Results. The 14 models described in the foregoing section were applied for the eight fixed monitoring stations, using input data as described. Each calculated hourly average SO_2 concentration was adjusted for a background concentration estimated for each monitoring station as the average of those measured concentrations that were less than one standard deviation above the average for all samples. There were 30,766 model-to-measurement comparisons, which are summarized in Table 8 as the root mean square error (RMSE) and in Table 9 as the correlation. Although some variations in the statistics by stability class were noticed, only the overall summaries for all stabilities are discussed here. However, these summaries are weighted by stable conditions, which occurred in almost seven-tenths of the data, while neutral and unstable occurred in slightly over two-tenths and one tenth, respectively.

In Table 8, the Flat Terrain Model has a surprisingly small RMSE at all stations; it has the smallest RMSE at two stations, but otherwise the smallest RMSE is for Model No. 14. Models Nos. 2, 3, 5, and 6, employing plume height adjustments for terrain, have the highest RMSEs, particularly for stations closer to the plant and at higher elevations. For terrain height adjustments, Model No. 4 is clearly superior. Notice that at Castle, the RMSEs are the same for all plume height adjustments since the elevation at Castle is slightly lower than at the plant. Both adjustments for σ_y in Model Nos. 7-10 produced improvements over the standard values, but it is not clear which one was best. The use in Model No. 10 of enhanced σ_z values did not produce improvement over use of the standard values. However, the use of an enhanced transport wind speed in Model No. 13 and the addition of Pasquill's adjustment of σ_y in Model No. 14 produced improvements. On the basis of RMSE comparisons, Model No. 14, employing the Geomet plume height adjustment, the Pasquill σ_y adjustment and an enhanced transport wind speed, produced the best overall results; Model 13 is judged to be second best. On the basis of the correlations in Table 9, Model No. 14 appears to do best overall and Model No. 13 second best, although there are some comparatively good correlations for other models at individual stations, e.g., Model Nos. 7 and 8 at Hockey and Nos. 9 and 10 at Nash and Kent. The highest correlations are worth mentioning, 0.51 at Lambert, 0.47 at Castle, and 0.41 at Nash, all for Model No. 14.

Table 10 compares the highest and second highest modeled and measured hourly average SO_2 concentrations at each monitoring station. Notice that these are not paired values occurring for the same hours; they are the highest and second highest values modeled and measured for almost 1 year of data. The models are the Flat Terrain (or PTMTP) model without adjustments (Model No. 1 in Table 8) and with the adjustments of Model Nos. 2, 13, and 14. The comparisons are best for Model No. 14 and they are also rather good for Model No. 13. Model No. 2 is the worst by far. All of the models in Table 10 have a tendency to overpredict.

A final comparison of modeled and measured concentrations is presented in Fig. 4 as cumulative frequency distributions plotted on logarithmic-probability scales. The three models are those in Table 10; they correspond to Model Nos. 2, 13, and 14 in Table 8, and are relabeled in Fig. 4 as CRSTR, SSTM, and PASQUILL, respectively. Although cumulative frequency distributions were prepared for all stations, only those for Hockey and Kent are presented here as fairly typical. At both stations the CRSTR model (No. 14) greatly overpredicts high and moderate concentrations. This occurs at all stations except Castle, for which the model makes no plume height adjustment for terrain.

At both stations the SSTM and PASQUILL model curves are quite close together. For low concentrations they are closer to the measured curve at Hockey, but for moderate and high concentrations they are closer to the measured curve for the Kent station. At both stations the SSTM model is slightly better than the PASQUILL model at moderate concentrations, but the reverse is true for very high concentrations.

CONCLUSIONS

This study has shown that a mobile van can be highly successful in detecting and monitoring SO_2 concentrations from a power plant located in complex mountainous terrain. The use of variable profiles of temperature and wind speed in plume rise calculations was superior to the use of a single stability class for the entire layer through which a plume rises. Of those modeling concepts tested, the use of moderate plume height adjustments for terrain and enchanced σ_y values produced the best model-to-measurement comparisons.

While the results reported in this paper have required a very significant effort, a number of possibilities remain for fruitful further analyses. The data are available and in ready form for such studies.

REFERENCES

Briggs, G. A., 1974: Plume rise from multiple sources. ATDL contribution no. 91, Atmospheric Turbulence and Diffusion Laboratory, Oak Ridge, TN 37830, 33 pp.

Briggs, G. A., 1975: Plume rise predictions. Proceedings of AMS workshop on meteorology and environmental assessment, American Meteorological Society, Boston, MA 02108, 296 pp.

Burt, E. W., 1977: Valley model user's guide. USEPA, Office of Air Quality Planning and Standards, EPA-450/2-77-018, Research Triangle Park, NC 27711, 107 pp.

Egan, B. A., 1975: Turbulent diffusion in complex terrain. Proceedings of AMS workshop on meteorology and assessment, American Meteorological Society, Boston, MA 02108, 296 pp.

Holzworth, G. C., 1978: Estimated effective chimney heights based on rawinsonde observations at selected sites in the United States, Journal of Applied Meteorology, 17:153-160.

Irwin, J. S., 1979: Estimating plume dispersion - a recommended generalized scheme. Proceedings of fourth symposium on turbulence, diffusion, and air pollution, American Meteorological Society, Boston, MA 02108, 676 pp.

Koch, R. C., W. G. Biggs, P. H. Hwang, I. Leichter, K. E. Pickering, E. R. Sawdey, and J. L. Swift, 1977: Power plant stack plumes in complex terrain: an appraisal of current research. USEPA, EPA-600/7-77-020, Research Triangle Park, NC 27711, 221 pp.

Koch, R. C., 1978: Use of monitoring data to modify meteorological dispersion models for point sources. To be published in proceedings of 84th national meeting of American Institute of Chemical Engineers.

Koch, R. C., W. G. Biggs, D. Cover, H. Rector, P. F. Stenberg, and K. E. Pickering, 1979a: Power plant stack plumes in complex terrain: description of an aerometric field study. USEPA, EPA-600/7-79-010a, Research Triangle Park, NC 27711, 158 pp.

Koch, R. C., W. G. Biggs, D. Cover, H. Rector, P. F. Stenbert, and K. E. Pickering, 1979b: Power plant stack plumes in complex terrain: data collected during an aerometric field study. USEPA, EPA-600/7-79-010b, magnetic tape, available from National Technical Information Service, Springfield, VA 22151.

Pasquill, F., 1976: Atmospheric dispersion parameters in Gaussian plume modeling, part II. Possible requirements for change in the Turner workbook values. USEPA, EPA-600/4-76-030b, Research Triangle Park, NC 27711, 44 pp.

Pickering, K. E., R. H. Woodward, and R. C. Koch, 1979: Power plant stack plumes in complex terrain: data analysis and characterization of plume behavior. To be published by USEPA, Research Triangle Park, NC 27711.

Slowik, A. A., J. M. Austin, and G. N. Pica, 1977: Plume dispersion modeling in complex terrain under stable atmospheric conditions. Paper No. 77-29.1, presented at 70th annual meeting of Air Pollution Control Association, Toronto, Ontario, 16 pp.

Smith, F. B., 1972: A scheme for estimating the vertical dispersion of a plume from a source near ground level. Proceedings of the third meeting of the expert panel on air pollution modeling, NATO Committee on Challenges of Modern Society, N. 14, Chapt. XVII, 14 pp.

Turner, D. B., 1970: Workbook of atmospheric dispersion estimates, USEPA, Office of Air Programs, Publication No. AP-26, Research Triangle Park, NC 27711, 84 pp.

Turner, D. B., and A. D. Busse, 1973: Users' guide to the interactive versions of three point source dispersion programs: PTMAX, PTDIS, and PTMTP. USEPA, preliminary draft, Meteorology Laboratory, Research Triangle Park, NC 27711, 28 pp.

U.S. Environmental Protection Agency, 1977: User's manual for single-source (CRSTR) model. USEPA, EPA-450/2-77-013, Research Triangle Park, NC 27711, 285 pp.

Van der Hoven, I., G. J. Ferber, P. A. Humphrey, G. C. Holzworth, J. L. Heffter, and R. F. Quiring, 1972: Southwest energy study report of the meteorology work group. NOAA Air Resources Laboratory, Silver Spring, MD.

Whaley, H., 1974: The derivation of plume dispersion parameters from measured three-dimensional data. Atmospheric Environment, 8: 281-290.

TABLE 1. TYPICAL OPERATING CONDITIONS OF THE CLINCH RIVER POWER PLANT

STACK NO.	BOILER NO.	EXHAUST TEMPERATURE (^{o}K)	EXHAUST AIR FLOW (m^3/sec)	GENERATOR LOAD (MW)	SO_2 EMISSIONS (g/sec)
1	1	380-390	320-340	200-225	300-325
1	2	390-400	360-380	225-250	275-300
2	3	380-390	320-340	225-250	275-300

TABLE 2. SO_2 CONCENTRATIONS (ppb), OCT 15, 1976-SEP 30, 1977

STATION	DISTANCE FROM POWER PLANT (km)	TYPE OF TERRAIN	AVERAGE CONCENTRATION (ppb)	CONCENTRATIONS $\geq$ 10 ppb (PER CENT)
Tower	3.4	Plateau	12	25
Munsey	4.2	Valley Side	4	11
Hockey	5.7	Ridge	6	15
Johnson	5.8	Ridge	8	16
Lambert	7.6	Valley Side	3	8
Castle	8.3	Valley	6	16
Nash	10.8	Plateau	2	6
Kent	29.9	Ridge	1	4

TABLE 3. TEN HIGHEST HOURLY AVERAGE CONCENTRATIONS (ppb), ENDING HOUR (HR), AND NEAR SIMULTANEOUS OCCURRENCES (*) DURING OCT 15, 1976-SEP 30, 1977.

	TOWER			MUNSEY			HOCKEY			JOHNSON		
Rank	Conc	Hr	*	Conc	Hr	*	Conc	Hr	*	Conc	Hr	*
1	344	12	A	182	8	II	318	5		246	24	L
2	317	13	A	178	9	II	219	9		199	23	
3	308	10		167	3		215	3		197	3	
4	274	10		135	15		190	3	BB	161	1	M
5	268	11	A	125	16	J	180	24		136	11	
6	261	2	E	119	2	FF	152	9		131	23	L
7	260	11		119	15	J	150	2	FF	127	6	N
8	259	8		111	10	OO	148	8	II	124	5	N
9	252	10		99	11	KK	146	3		110	3	M
10	251	12	L	99	13	K	138	9		109	7	N

	LAMBERT			CASTLE			NASH			KENT		
Rank	Conc	Hr	*	Conc	Hr	*	Conc	Hr	*	Conc	Hr	*
1	77	11	OO	268	9		105	14		200	13	
2	71	11		260	11	G	77	12		180	3	BB
3	70	12	HH	241	11	R	76	10		134	12	
4	68	12	PP	218	10	G	75	11		127	9	C
5	67	10	KK	197	11		71	13	Q	85	6	C
6	57	12	PP	172	12	G	70	12	Q	80	6	D
7	48	11	HH	149	9	R	67	11	PP	75	7	D
8	44	13	HH	141	10	HH	66	11		71	7	C
9	42	17		137	12		66	11		66	5	D
10	33	19		135	12	HH	63	8		61	6	E

* A single letter indicates occurrences on the same date. A double letter indicates occurrences on same date and within 1 hour at different stations. Order of letters has no significance.

TABLE 4. LOCATION OF SO_2 PLUME CENTER OF MASS.

CROSS-SECTION NUMBER	DISTANCE OF X-SECTION FROM PLANT (KM)	ALTITUDE OF CENTER OF MASS ABOVE SEA LEVEL (M)	DIRECTION TOWARD WHICH HOCKEY 30-M WIND TRANSPORTS PLUME (DEGREES)	BEARING OF X-SECTION CENTER OF MASS FROM PLANT (DEGREES)	DIFFERENCES OF CALCULATED & MEASURED CENTER OF MASS (DEGREES)
1	3.0	974	148	7	141
2	3.0	804	148	14	134
3	3.0	795	148	19	129
4	1.8	773	100	49	51
5*	1.8	931	100	55	45
6	3.1	823	33	34	1
7	6.2	902	42	35	7
8	18.2	790	52	54	2
9*	1.8	895	50	54	4
10*	1.8	855	66	57	9
11*	8.2	1055	74	54	20
12	1.8	845	93	54	39
13*	2.3	-	184	221	37
15*	1.6	995	165	175	10
17	5.7	1018	176	179	3
18*	1.7	1212	296-315	333	37-18
20	3.6	1448	277+	325	48
22*	2.5	987	253+	267	14
23	7.6	1146	253+	272	19
24*	7.6	1193	242+	270	28
25*	2.5	1044	198+	257	59
26*	1.8	1266	26+	13	13
28*	5.6	1096	6+	28	22
29*	3.0	1188	46+	19	27

* Cross-sections based on ten or more plume traverses.

+ Based on Hockey 10-m winds.

TABLE 5. PLUME DIMENSIONS AND ASSOCIATED PARAMETERS

CROSS-SECTION NO.	MEASURED IN X-SECTIONS		MEASURED AT HOCKEY	PASQUILL CALCULATED	TURNER STABILITY CLASS	PASQUILL-TURNER VALUES OF	
	σ_Y (M)	σ_Z (M)	σ_A (DEG)	σ_Y* (M)		σ_Y (M)	σ_Z (M)
1	528	-	63.2	1341	A	560	4700
2	869	-	23.4	482	A	550	4400
3	865	-	23.4	482	A	550	4400
4	447	-	67.3	936	A	350	1500
5	479	-	67.3	936	A	350	1500
6	156	-	6.3	136	C	295	175
7	756	-	10.0	410	C	550	325
8	1545	-	13.5	1049	C	1350	880
9	414	179	17.6	243	C	177	103
10	416	131	14.4	339	B-C	220	145
11	932	194	18.0	912	D	465	120
12	310	67	27.9	388	C	180	105
13	837	-	20.9	334	A	440	2550
15	411	-	34.0	457	B	245	190
17	507	-	10.6	401	B	740	740
18	891	212	15.0-62.7	211/851	B/A	285/315	225/1275
20	477	-	missing	-	A	640	5000
22	449	-	"	-	A	470	3100
23	134	-	"	-	C	650	390
24	1182	-	"	-	C	650	390
25	350	124	"	-	C	240	140
26	682	117	"	-	C	270	210
28	799	-	45.8	1710	B	740	740
29	686	-	55.0	1133	B	415	360

* $\sigma_Y = \sigma_A \times f(x)$, see text.

TABLE 6. COMPARISON OF PLUME HEIGHT MEASUREMENTS AND CALCULATIONS

HELICOPTER-MEASURED PLUME CENTER OF MASS HEIGHT ABOVE SEA LEVEL (M)	DEVIATIONS FROM HELICOPTER MEASUREMENTS	
	HOLZWORTH-BRIGGS* CALCULATION (M)	BRIGGS BEH072* CALCULATION (M)
974	-2	+864
804	-4	+690
795	+5	+699
773	+226	+482
931	+68	+324
823	-54	+5
902	-93	-86
790	-40	-6
895	+15	-114
855	+74	-23
1055	-128	-189
845	+76	+220
995	-87	+190
1018	-93	+82
1212	-451	-78
1448	-490	+638
987	-171	+579
1146	-330	+348
1193	-259	+396
1044	-110	+478
1266	MSG DATA	+298
1096	" "	+225
1188	" "	+447

* See text for description of equations.

TABLE 7. FREQUENCY OF CALCULATED CLINCH RIVER PLUME CENTER LINE HEIGHTS RELATIVE TO VERTICAL TEMPERATURE STRUCTURE.

HOUR	% IN INVERSION STACK 1	 STACK 2	% BELOW INVERSION STACK 1	 STACK 2	% ABOVE INVERSION STACK 1	 STACK 2	% NO INVERSIO
1	57	55	32	39	7	2	4
4	61	59	33	39	4	0	2
7	61	59	32	39	6	0	1
10	43	41	46	51	8	4	3
13	21	22	58	61	10	5	11
16	23	25	61	63	8	4	8
19	19	19	71	75	5	2	5
22	47	46	41	45	8	4	4

TABLE 8. ROOT MEAN SQUARE ERROR OF MODEL TO MEASUREMENT SO_2CONCENTRATION DIFFERENCES (PPB) FOR ALL STABILITIES.

STATION: MODELS*	TOWER	MUNSEY	HOCKEY	JOHNSON	LAMBERT	CASTLE	NASH	KENT
1. FLAT TERRAIN	40	23	22	31	12	16	10	8
2. CRSTER H	136	98	370	264	56	16	24	74
3. NOAA H	117	88	365	262	53	16	21	73
4. GEOMET H	40	27	42	48	17	16	12	26
5. VALLEY H	117	88	354	255	53	16	21	73
6. ERT-LAPPES H	93	60	81	65	38	16	23	34
7. GEOMET σ-Y IN 6	57	63	62	61	42	16	16	20
8. LAPPES σ-Y IN 6	70	59	61	57	41	14	18	18
9. LAPPES σ-Y IN 4	33	25	30	41	15	14	10	14
10. GEOMET σ-Y IN 4	37	26	31	49	14	16	10	16
11. F. SMITH σ-Z IN 10	38	34	45	58	29	16	12	18
12. PASQ DILUTION IN 10	36	27	39	52	16	16	10	17
13. WIND EXTRAP IN 10	31	21	23	32	10	14	8	10
14. PASQ σ-Y IN 13	28	19	24	20	9	13	8	10

* See text for description of models.

TABLE 9. CORRELATION OF MODEL TO MEASUREMENT SO_2 CONCENTRATIONS (PPB) FOR ALL STABILITIES.

STATION:	TOWER	MUNSEY	HOCKEY	JOHNSON	LAMBERT	CASTLE	NASH	KENT
MODELS*								
1. FLAT TERRAIN	.15	.16	.15	.08	.32	.27	.35	.29
2. CRSTR H	.20	.04	.03	.14	.07	.27	.18	.03
3. NOAA H	.13	.02	.03	.13	.07	.27	.19	.03
4. GEOMET H	.18	.14	.08	.06	.22	.27	.31	.08
5. VALLEY H	.13	.02	.03	.13	.07	.27	.19	.03
6. ERT-LAPPES H	.26	.08	.05	.07	.11	.27	.18	.06
7. GEOMET σ-Y IN 6	.30	.16	.08	.05	.10	.27	.29	.13
8. LAPPES σ-Y IN 6	.30	.13	.07	.07	.10	.34	.25	.13
9. LAPPES σ-Y IN 4	.20	.15	.10	.06	.25	.34	.38	.17
10. GEOMET σ-Y IN 4	.16	.15	.11	.05	.26	.27	.40	.16
11. F. SMITH σ-Z IN 10	.25	.13	.09	.07	.13	.27	.34	.14
12. PASQ DILUTION IN 10	.17	.15	.09	.07	.23	.27	.40	.14
13. WIND EXTRAP IN 10	.19	.18	.14	.07	.36	.33	.46	.26
14. PASQ σ-Y IN 13	.25	.20	.13	.14	.51	.47	.41	.26

* See text for description of models.

TABLE 10. HIGHEST AND SECOND HIGHEST MEASURED AND MODELED* 1-HOUR SO_2 CONCENTRATIONS (PPB)

	HIGHEST				
STATION	FLAT TERRAIN	CRSTR	GEOMET H & σ-Y WIND EXTRAP	GEOMET H PASQ σ-Y WIND EXTRAP	MEASURED
Tower	1417	4187	1005	381	344
Munsey	599	3228	717	448	182
Hockey	464	13804	463	585	318
Johnson	1396	7532	1141	368	246
Lambert	313	1820	265	223	77
Castle	479	479	355	99	268
Nash	318	653	259	202	105
Kent	123	4200	213	116	200
	SECOND HIGHEST				
Tower	623	2780	476	368	317
Munsey	491	2706	397	383	178
Hockey	411	11337	376	483	219
Johnson	577	6062	981	339	199
Lambert	311	1207	202	186	71
Castle	276	276	114	84	260
Nash	261	390	112	122	94
Kent	84	1049	120	111	180

* See text for description of models.

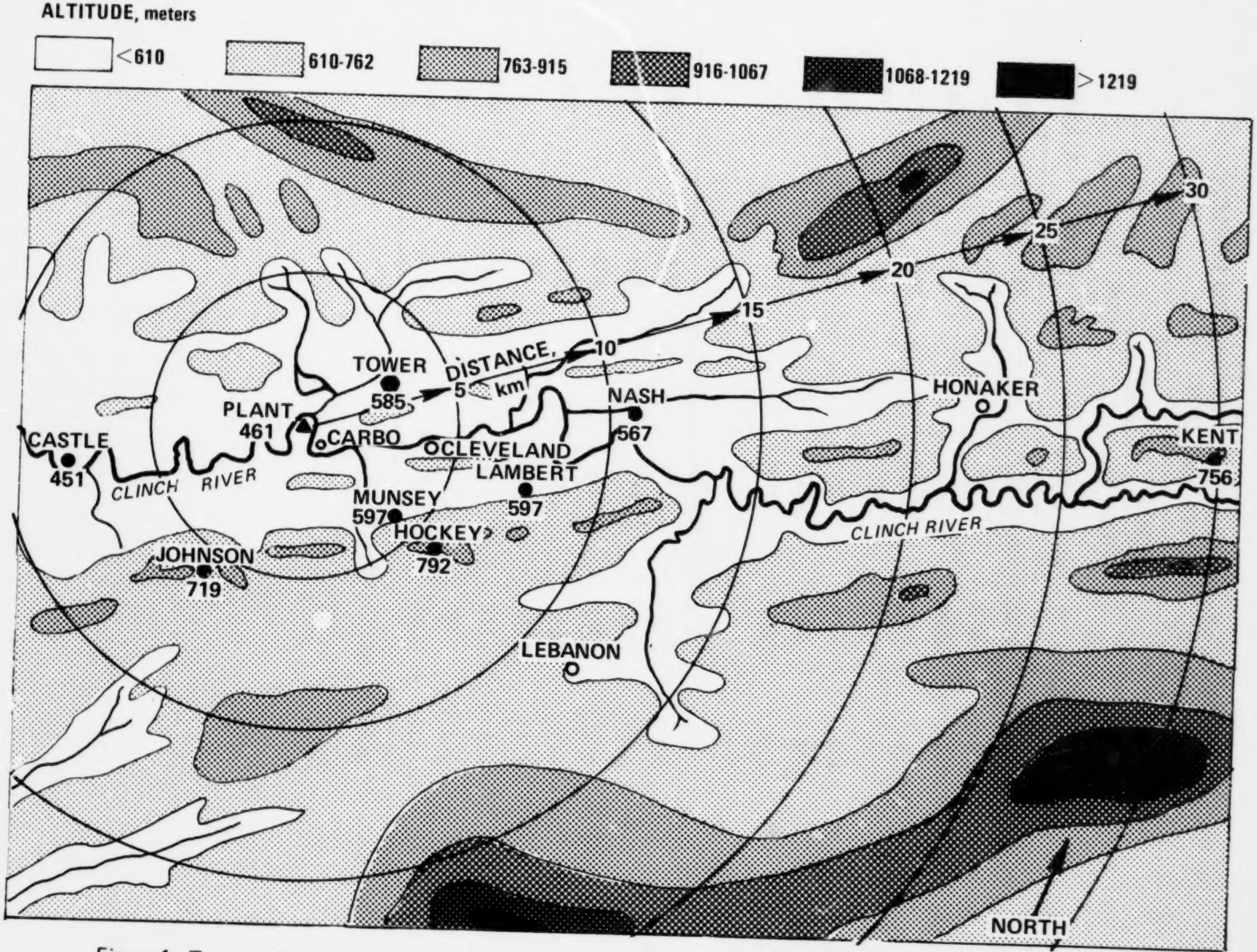
ALTITUDE, meters
<610
610-762
763-915
916-1067
1068-1219
>1219
DISTANCE, km
5
10
15
20
25
30
TOWER
585
PLANT
461
CARBO
CASTLE
451
CLINCH RIVER
OCLEVELAND
LAMBERT
597
MUNSEY
597
HOCKEY
792
JOHNSON
719
NASH
567
HONAKER
KENT
756
LEBANON
CLINCH RIVER
NORTH

Figure 1. Topography (meters above sea level) and monitoring stations in vicinity of Clinch River Power Plant. Names without elevations are villages.

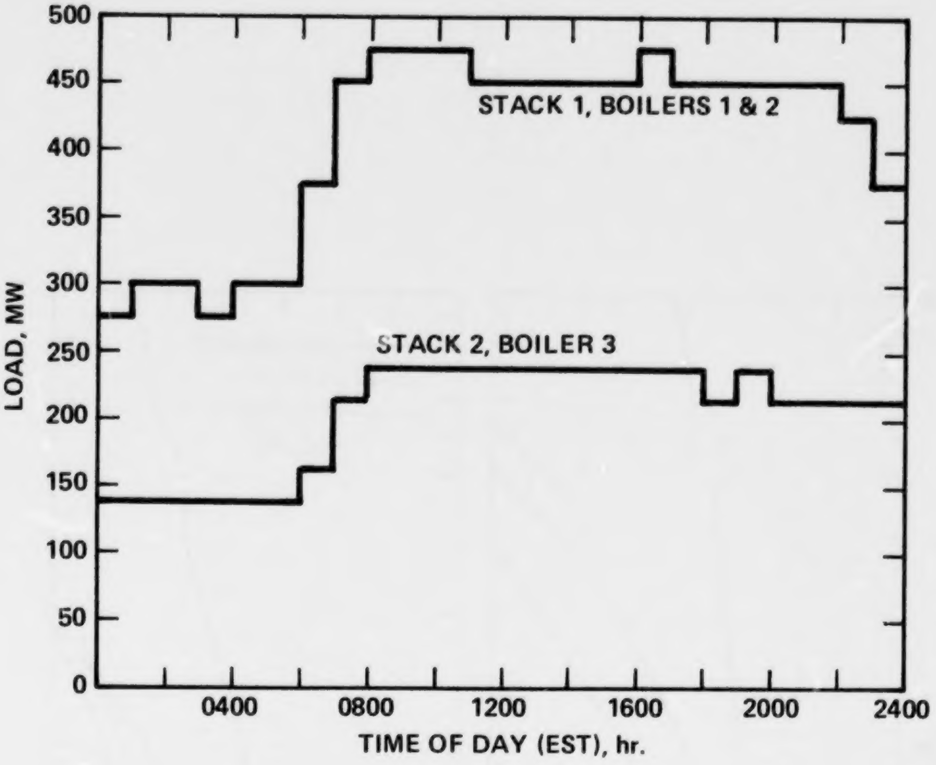

Figure 2. Typical generator loads for Clinch River Plant.

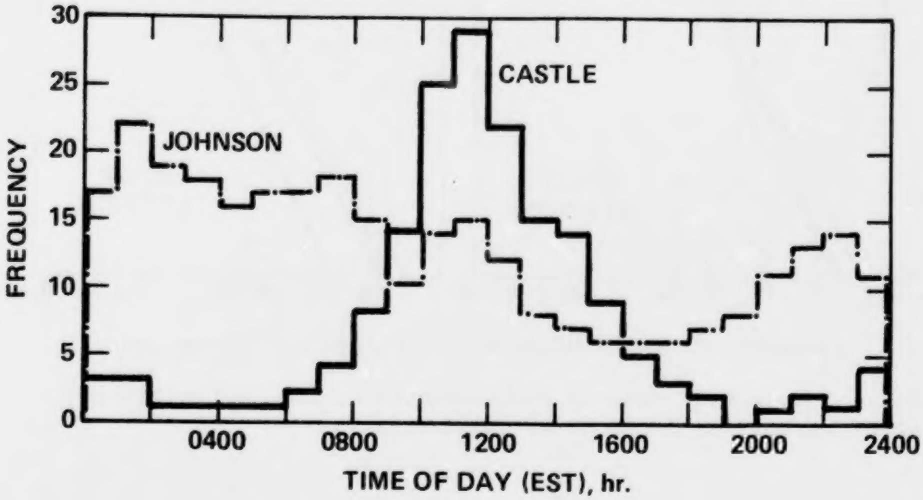

Figure 3. Frequency of SO_2 hourly average concentrations exceeding 25 $\mu g/m^3$ (10 ppb $\approx$ 25 $\mu g/m^3$).

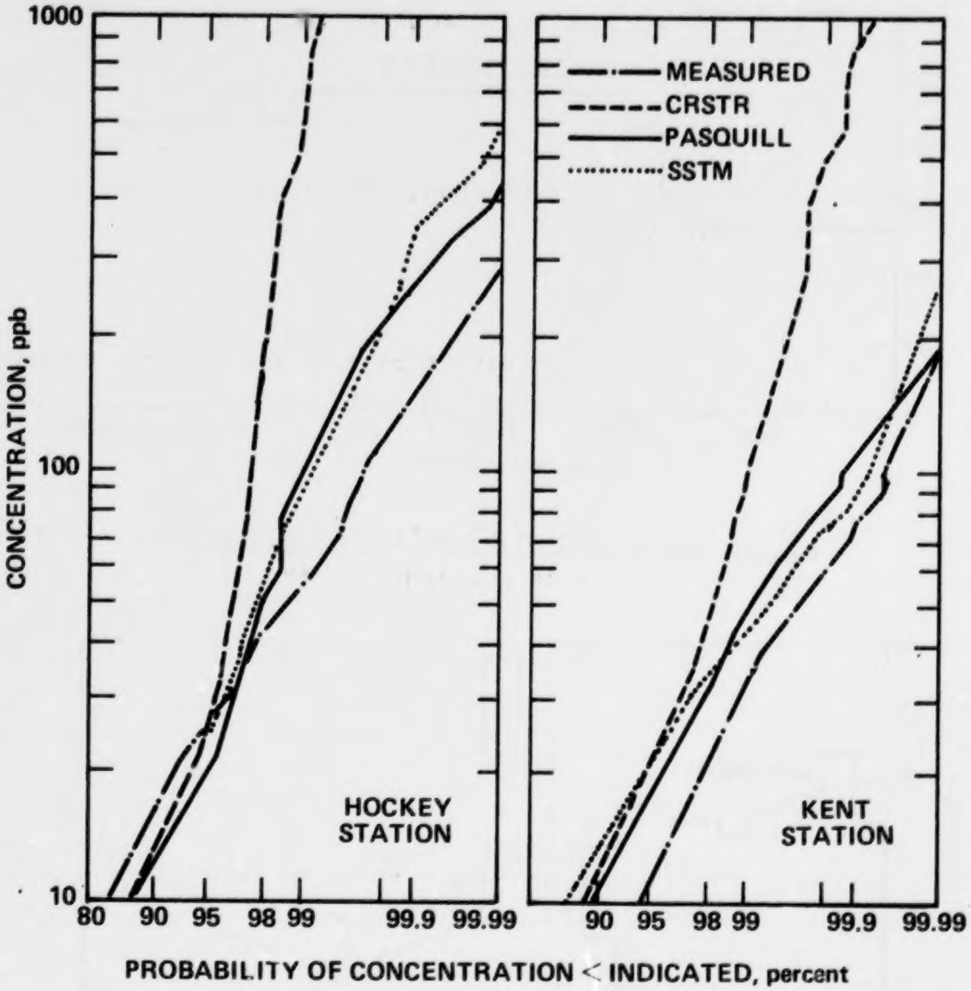

Figure 4. Cumulative frequency distributions for measured and modeled SO_2 concentrations. See text for model identification.

Discussion:

(Rapporteur: D. A. Trout)

Berger:

How many observations did you use for computing your root-mean square errors?

Holzworth (response):

About 24 cross-sections consisting of about 275 helicopter traverses at different altitudes were used.

Berger:

Did you compute the significance levels to determine which of the models are really different?

Holzworth (response):

It is not shown in this paper, but such information will be available in a more complete report that will be published by the US EPA at a later date.

Millàn:

How did you compute σ_y?

Holzworth (response):

We used the method of Whaley, we use the concentrations that were measured by the helicopter and the distance from the mean center value.

Millàn:

Was there any problem in determining the mean center value?

Holzworth (response):

Yes, there were problems in looking at the traverses, the helicopter went through the plume successively in different directions and at different levels. Wehen these data were plotted and corrections were made for the instrument lag and the lag time for the air sample to go through the air sampling line, it was still noted that very often the plume centerline (center of mass for each traverse) was shifting back and forth; this was attributed through an analysis of the wind data so the fluctuation in the wind. The wind fluctuations were determined to be good indication of the plumes dispersion.

Anfossi:

Did you take into consideration the merging of the two plumes, if any, in computing plume rise?

Holzworth (response):

The two chimneys were separated by about 46 m, and visually it appeared that they merged together all the time.

Smith:

Were any of the computed plume heights such that the US EPA Valley Model would predict direct impingement in any cases?

Holzworth (response):

I don't remember, but I really would suspect so because the stacks are only 138 m and expected plume rise would be of the order of only a few hundred meters. Some of the monitors may be within that height so that the Valley model would have suggested impingement.

EXPERIMENTAL DETERMINATION OF DIFFUSION COEFFICIENTS ABOVE AN URBAN AREA

by

L. SANTOMAURO, V. MAESTRO, C. BARBERIS
OSSERVATORIO METEOROLOGICO DI BRERA - MILANO

Abstract. Diffusion coefficients σ_y and σ_z were experimentally evaluated for the urban area of Milan regard to atmospheric adiabatic conditions by the analysis of the fluctuations of Lagrangian velocity components of no-lift balloons. Coefficients were first calculated as function of travel time by the moving-average method and then as function of the downwind distance (up to about 1000 meters) once known the average velocity of the balloons set. Finally the relations $\sigma_i = a_i X^{b_i}$ $i=y, z$ were drawn and the results were analysed and compared with estimates of other authors. We also obtained vertical profiles of wind by pilot balloons released at various points of the urban area.

INTRODUCTION

The urban area which has a noticeably built density and vaste extension, influences, as is known, layers of air above such area. As a matter of fact, the local physical elements, among which radiation, temperature, wind, turbulence, assume special characteristics different than those which can be found above rural areas. This diversity is mainly due to the surface roughness which is different than that of the urban area and that of the rural. Besides it is necessary to remember also the influence of the urban heat island. Consequently, concerning the above-mentioned, we must keep this in mind when we must face the air pollution transport and dispersion problem in the urban boundary layer. This is because we find ourselves in a thermodinamically environment different than that which is above the extra-urban and rural areas. Whenever we want to apply the Gaussian equation of atmospheric diffusion of pollutants in a mathematical model, the σ_y and σ_z diffusion coefficients are different if determinated on an urban area or a rural area[1]. All this because the urban area turbulence is up to 40% higher than that which we could have on a rural area. Therefore, theoretically, the σ_y and σ_z diffusion coefficients values are higher in an urban area.

The Brera Meteorological Observatory has been put in charge of the simulation mathematical model of urban air pollution diffusion. This assignement is a part of the Italian National Research Council about the Environment Quality. Diffusion coefficients which can be found in scientific literature^2 were used in the first edition of this model^3. Successively it was necessary to make plans for researches of the atmosphere in the Milano urban area to determine the local lateral and vertical diffusion coefficients σ_y and σ_z and the vertical profile of mean wind in quasi-adiabatic condition.

THEORETICAL METHOD

There are different experimental methods used to evaluate σ_y and σ_z diffusion coefficients. It is possible to calculate them by analysing stack smoke with optical remote sensing techniques or by using tracers^4. With the use of Lagrangian tracers (i.e. using balanced pilot-balloons^5) it is possible to calculate lateral and vertical dispersion coefficients with different calculation methods.

The σ_y and σ_z coefficients in the Gaussian diffusion formula of a polluted point source show lateral and vertical plume dispersion at every fixed downwind distance x. If we substitute the ensemble average for time averages taken during the path of one particle (ergodic principle), σ_y and σ_z are identified with those of the Taylor turbulence statistic theory. According to this theory the coefficients indicate lateral and vertical dispersion at every fixed time of flight T. If we suppose the validity of the ergodic principle, Taylor coefficients can be calculated with the use of the moving-average method applied to the individual trajectories. Let us consider a reference system in which the X axis shows the mean wind direction; it is understood that the axis is parallel to the soil surface. If we indicate with v_i' $i = y,z$ the deviations from the mean values ($\bar{v}_y = \bar{v}_z = 0$) of the Lagrangian velocity along axis Y and axis Z and we indicate with the simbol $\langle\ \rangle_{\tau,T}$ the moving-average, is:

$$\sigma_i(T) = \left(\overline{\langle v_i' \rangle^2_{\tau,T}} \right)^{\frac{1}{2}} T \qquad i = y, z \tag{1}$$

where τ indicates the sampling-time of every single trajectory and T is the time of flight. The σ_y and σ_z standard deviation values depend on the entire turbulence spectrum filtered by the τ and T parameters. To assure a reasonable statistic stability it is necessary that T is sufficiently lesser than τ. We extended the time of flight T to 30% of τ.

EXPERIMENT DESCRIPTION

Experiments took place for two weeks during the month of March 1978. They consisted of determining:

a) - vertical wind profiles
b) - horizontal wind trajectories
c) - vertical temperature profiles.

In order to determine the vertical wind profiles a pilot-balloon optical tracking technique was used with a theodolite cheching it every 15 seconds. The pilot with a 60 cm diameter were filled with helium. They had an 85 gr vertical buoyant and therefore a rising velocity of 160 m per minute. As for the observation of horizontal wind trajectories is concerned, no lift pilot-balloons were used[6]. The balloon balance was obtained filling them with He and CO_2 proportional mixture. This was to have a density which could be the nearest possible to that of a layer of air. The balanced balloon was let loose at a pre-estblished height.

The vertical temperature and relative humidity measure was obtained using a fast response thermocouple mounted on a 172 Cessna Airplane. This airplane travelled at a speed of about 85 Mph with a steady rising rate of about 200 feet per minute. The vertical profile resolution was about 40 m considering the high response speed of the two dry and wet thermocouples.

Besides a mobile unit was employed for the launching and observation of the pilot and no-lift balloons. A total of 42 no-lift pilot-balloons launchings, 324 pilot-balloons lauchings and 44 dry and wet temperature vertical profiles were made during the entire campaign. A special meteorological briefings were given one before the experiments took place. The briefings concerned the meteorological situations and forecasts for the following day.

DATA PROCESSING

The position and therefore the speed of tha balanced balloon are determined every 15 seconds in respect to a $\hat{X}$ $\hat{Y}$ $\hat{Z}$ reference frame translated in respect to launching base. The trajectory is reconstructed by assuming such dates. In fig. 1 we see the position of the balloon determined every 15 seconds projected on plane $\hat{X}\hat{Y}$. In order to obtain turbulent velocity fluctuations V'_y it is necessary to know the mean flight direction of the balloon on the plane $\hat{X}\hat{Y}$. We were not able to find the mathematical definition of the mean flight direction, at least to our present knowledge.

Having N obervation points on plane $\hat{X}\hat{Y}$ we call

$$\overrightarrow{\Delta r}_i \quad (i = 1,\ldots,N-1)$$

the vector which connects point i with point i + 1.
The total deplacement of the balloon on the plane $\hat{X}\hat{Y}$ is therefore

$$\vec{\Delta r} = \vec{\Delta r}_1 + \vec{\Delta r}_2 + \ldots + \vec{\Delta r}_{N-1}$$

The mean velocity vector is given by:

$$\vec{v} = \frac{1}{N-1} \sum_{i=1}^{N-1} \frac{\vec{\Delta r}_i}{\Delta t} = \frac{1}{(N-1)\,\Delta t} \quad \vec{\Delta r}$$

and is therefore simply proportional to the total deplacement vector. We could define the mean flight direction as the direction of the mean velocity vector $\vec{v}$ but, because Δt = constant, this direction would coincide, as we have seen, with that of the total deplacement vector $\vec{\Delta r}$ which simply connects the first observation point with the last one (fig. 2).

In our opinion the mean flight direction is instead the direction of that straight line that, leaving from the first observation point, interpolates the trajectory in the best way possible. In order to determine this straight line we have first translated the reference frame in which the original observations were made in the first observation point. Then we used a method that, as shown in fig. 3, consists in minimizing the triangles areas sum designed. If ($\bar{x}_i$, $\bar{y}_i$) are the coordinates, in the first quadrant, of the generic point of the trajectory in reference $\bar{X}\bar{Y}$, then the rotation angle ϑ can be shown as being the result of

$$\vartheta = \operatorname{arctg} \sqrt{\frac{\sum_i \bar{y}_i^2}{\sum_i \bar{x}_i^2}}$$

Therefore the method gives a very simple result though appearing to be complex.

It is possible to calculate V'_y once the reference frame is rotated. As for as V'_z are concerned, these are directly calculable from the vertical oscillations.

The vertical profile of the wind mean velocity has been obtained taking in consideration the pilot balloons launching results which took place in various point of the city and at different times of the day.

RESULTS AND DISCUSSION

Only 22 of the 42 no-lift pilot balloons released were utilized in the calculations of the diffusion coefficients So, that is because the remaining 20 launches were too short or else they could not be guaranteed. The time of flight of the utilized lanches was about 10-15 minutes; the altitude of the flights was on average between 120 and 350 m above Milan area (120 m above sea level) and the mean flight speed was 3.4 m s^{-1}.

The atmospheric conditions during the balanced balloons flight period were quasi-adiabatic. Such conditions were the results of thermodinamic soundings carried out by the airplane which explored a layer of air in Milan up to an altitude of 1400 m above sea level.

The calculation of lateral and vertical diffusion coefficients as function of travel time T was made using an electronic calculator applyng equation (1) of moving average to each of the 22 trajectories.

The final equations of the diffusion coefficients are:

$$\sigma_y(T) = 1.921\ T^{0.714} \tag{2}$$

$$\sigma_z(T) = 1.056\ T^{0.872} \tag{3}$$

while, as function of downwind distance, are:

$$\sigma_y(X) = 0.802\ X^{0.714} \tag{4}$$

$$\sigma_z(X) = 0.363\ X^{0.872} \tag{5}$$

The transformation of $\sigma_i(T)$ to $\sigma_i(X)$ was made for the mean flight speed of the no-lift pilot balloons.

The graphics of diffusion coefficients as function of travel time and downwind distance are represented in fig. 4. Values of σ_z are higher than that of σ_y after 150 m downwind in such a way that σ_z is about 40 m hihger than σ_y at a distance of 1000 m.

Some comparisions have been made with the lateral and vertical diffusion coefficients calculated for St. Louis, Missouri[7] and with those re-calculated by Briggs[8] for adiabatic atmospheric conditions. The values with regard to distance are:

McElroy-Pooler $\sigma_y(X) = 0.010\ X^{0.729}$

$\sigma_z(X) = 0.910\ X^{0.702}$

Briggs $\sigma_y(X) = 0.16\ X\ (1+0.0004X)^{-1/2}$

$\sigma_z(X) = 0.14\ X\ (1+0.0003X)^{-1/2}$

The McElroy-Pooler and Briggs coefficients graphic trend for the same downwind distances is shown in fig. 5. Here we can note that, for the same equilibrium conditions, the σ_y and σ_z values calculated for the Milan urban area agree with those of McElroy-Pooler and Briggs. The greater value of σ_z on σ_y is an exception. This may be due to a particular characteristic of the Milan urban area (remarkable number of building per square kilometer and scarse vegetation).

Another coparison was made with the rural areas σ_y and σ_z coefficients determined for the Po Valley[9] (fig. 6). Here we have the results that while there is not appreciable difference concerning the lateral diffusion, there is notable difference in the vertical diffusion. This is a result of the turbulence caused by the urban aspect and local heat island.

To conclude our research, we report also the mean wind vertical profile, established trough launches of pilot-balloons (fig. 7). The equation of wind speed with regard to height is

$$\bar{U}(z) = \bar{U}(z_o)\left(\frac{z}{z_o}\right)^{a}$$

where the coefficient a, obtained from observations, is: a = 0 41. The value of this coefficient obtained for Milan fails within the standard for medium urban areas[10].

ACKNOWLEDGEMENTS

We wish to thank the Italian Air Force Meteorological Service of the Milan-Linate Airport, the Aerological Section of the 3rd Specialist Battery of the 3rd Army Corps and Dr. Gualdi and Dr. Tebaldi of the Milan Provincial Health Laboratory for their valuable assistance during the course of experiments. We also express our appreciation to prof. Oscar Barberis fro the compilation of calculation programs, Mr. R. Cecchini and Mr. C. Costamagna for the elaboration of wind profiles. Futhermore we would like to point out the degree of technical and scientific skill of the Milan Tecno-Geo-Topografia shown during the course of experiments.

These experiments were supported by "Promozione della Qualità dell'Ambiente" Finalized Program grants of the Italian National Research Council.

BIBLIOGRAPHY

1 - F.A. Gifford, "Turbulent Diffusion-Typing Schemes: A Review", Nuclear Safety, vol. 17, n°1, Jannary-February 1976.

2 - M.E. Smith (Ed.), "Reccommended Guide for the Prediction of the Dispersion of Airborne Effluents", 1st ed. American Society of Mechanical Engineers, New York, May 1968.

3 - L. Santomauro, R. Gualdi, G. Tebaldi, "Modello di simulazione della Diffusione Atmosferica Locale (Area Urbana di Milano)", Aa/3/1, Collana del Programma Finalizzato "Programma della Qualità dell'Ambiente, CNR, Roma.

4 - K.J. Vogt, "Empirical Investigations of the Diffusion of Vaste air Plumes in the Atmosphere", Nuclear Technology, Vol. 34, p. 43-57, 1977.

5 - A. Longhetto, D. Anfossi, P. Bacci "Lagrangian Dispersion Parameters determined by Tracking of Balanced Aerological Balloons", Third Symp. Turbulence Diffusion and Air Quality, Raleingh, N.C., A.M.S., pag. 259-263.

6 - A. Longhetto, "Some Improvements in the Balanced Pilot Balloons Technique", Atm. Environ., 5, 327, 1971.

7 - J.L. McElroy, F. Pooler Jr., " St Louis Dispersion Study",vol. II U.S. Dep. of Health, Education and Welfare, December 1968.

8 - G.A. Briggs, "Diffusion Estimates for Small Emission", Environmental Res. Lab., Air Resources Atmos. Turb. and Diff. Lab. 1973 Annual Report, Oak Ridge, 1973.

9 - L. Santomauro, P. Bacci, A. Longhettó, D. Anfossi, R. Richiardone, "Experimental Evaluation of Diffusion Parameters on a Local Scale by Means of No-Lift Balloons", Jour. Appl. Meteor. A.M.S., Vol. 17, Oct. 1978, 1441-1449.

10- T.J. Chandler, "Urban Climatology and its Relevance to Urban Design", Techn. Note n° 149, WMO, n° 438, 1976.

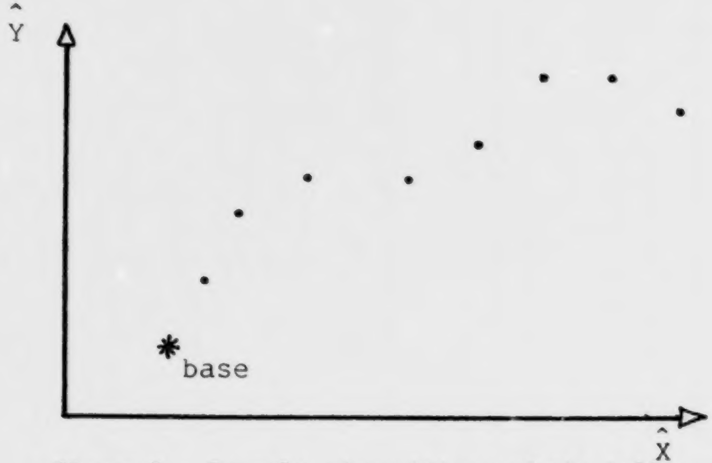
$\hat{Y}$
$\hat{X}$
base

Figure 1. Example of positions of the balloons determined every 15 seconds projected on plane $\hat{X}\hat{Y}$.

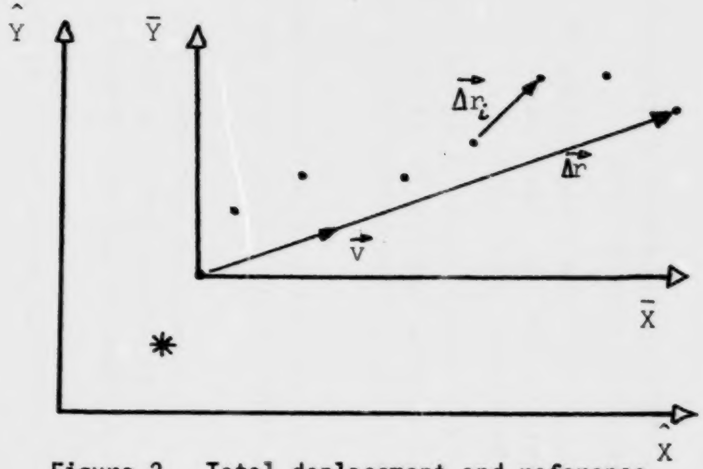
$\hat{Y}$
$\bar{Y}$
$\vec{\Delta r_i}$
$\vec{\Delta r}$
$\vec{v}$
$\bar{X}$
$\hat{X}$

Figure 2. Total deplacement and reference frame used.

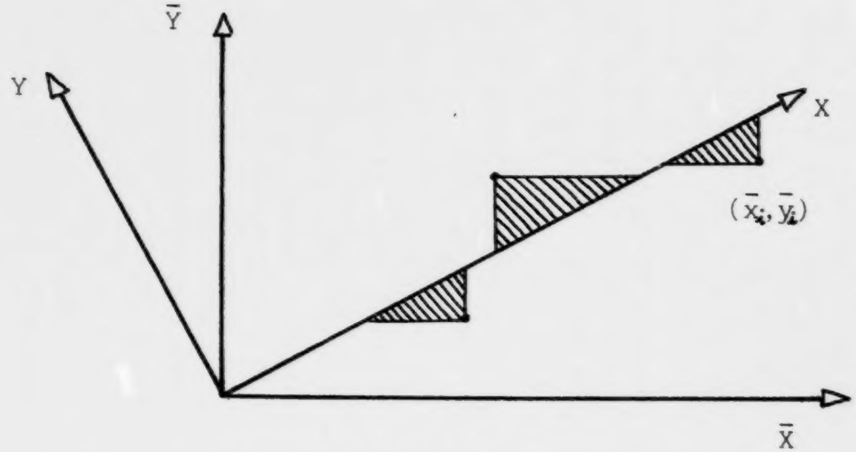
$\bar{Y}$
Y
X
$(\bar{x}_i, \bar{y}_i)$
$\bar{X}$

Figure 3. Method for determining the mean direction.

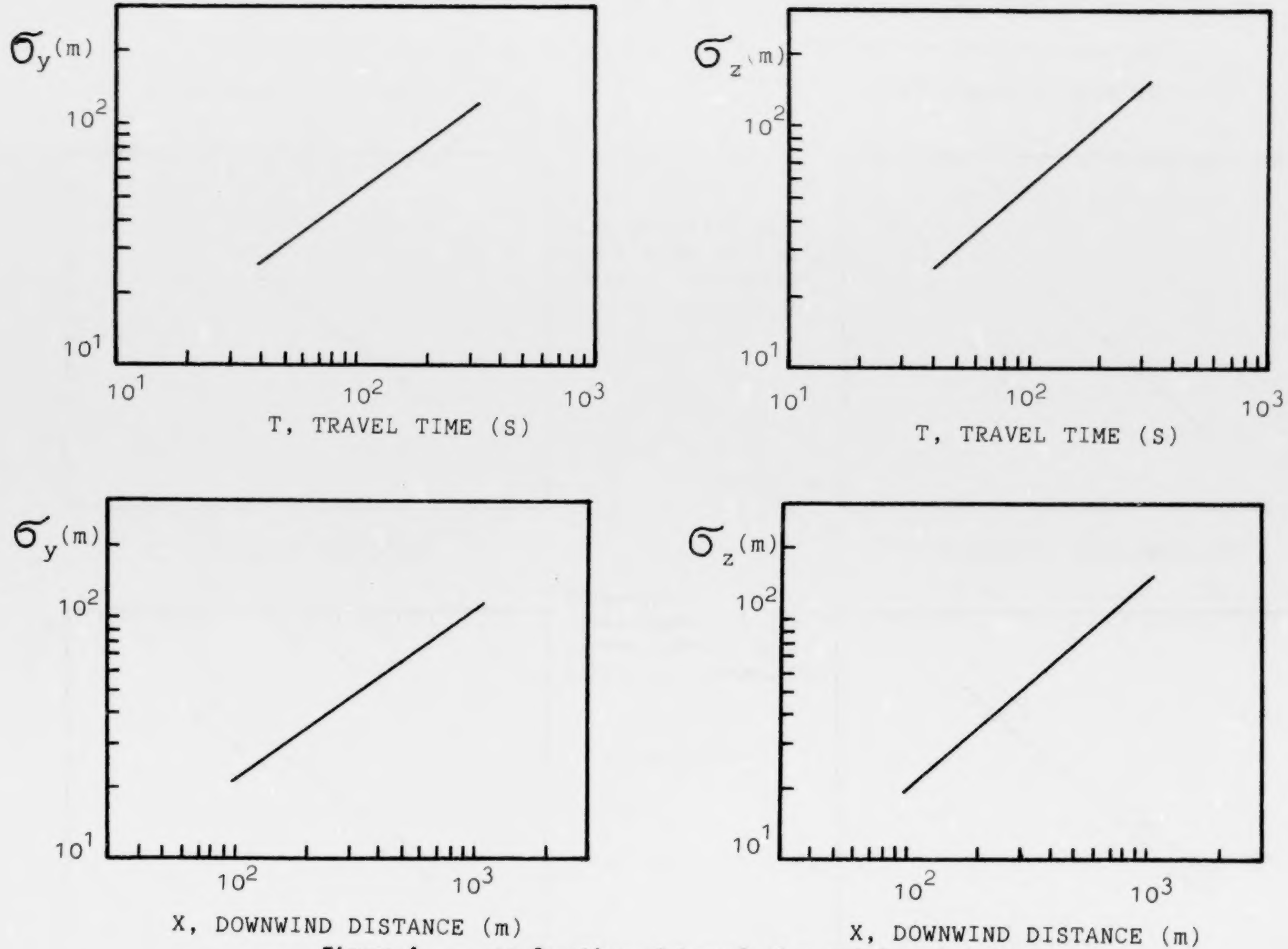

Figure 4. σ_i as function of travel time and downwind distance.

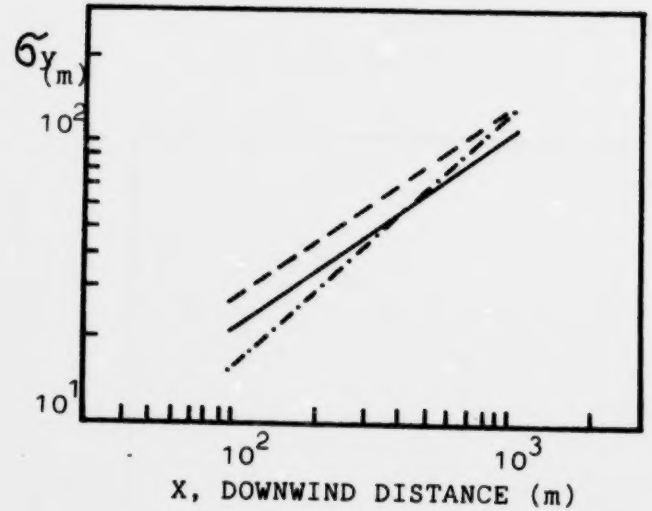

URBAN AREA

Figure 5. Comparison of our results with other urban estimates.

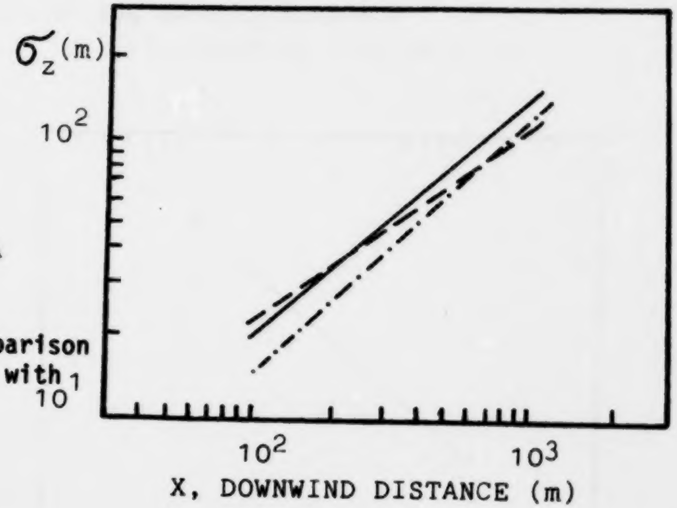

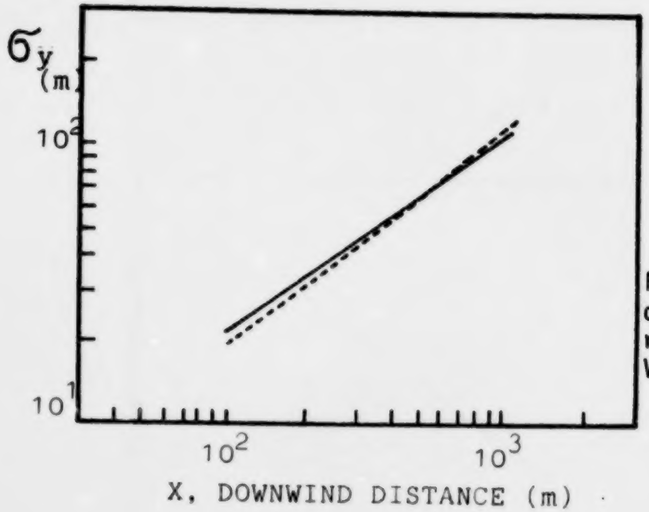

PO VALLEY

Figure 6. Comparison of our urban data with rural estimates in Po Valley.

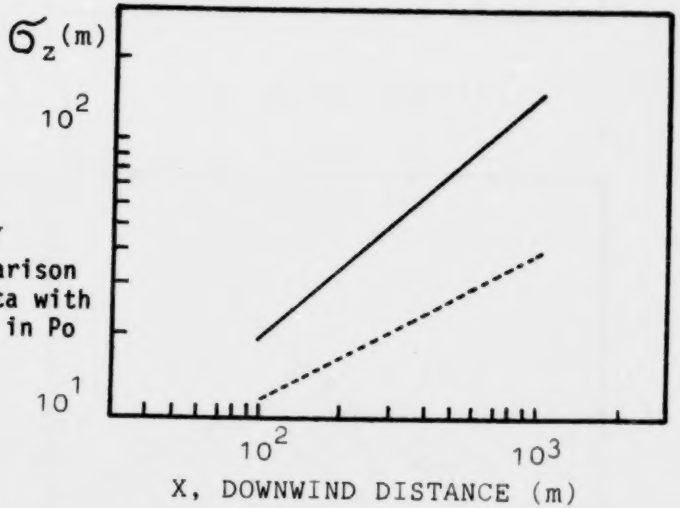

——— Santomauro et al.(1979)

--------- Santomauro et al.(1978)

— — — — McElory-Pooler

-·-·-·- Briggs

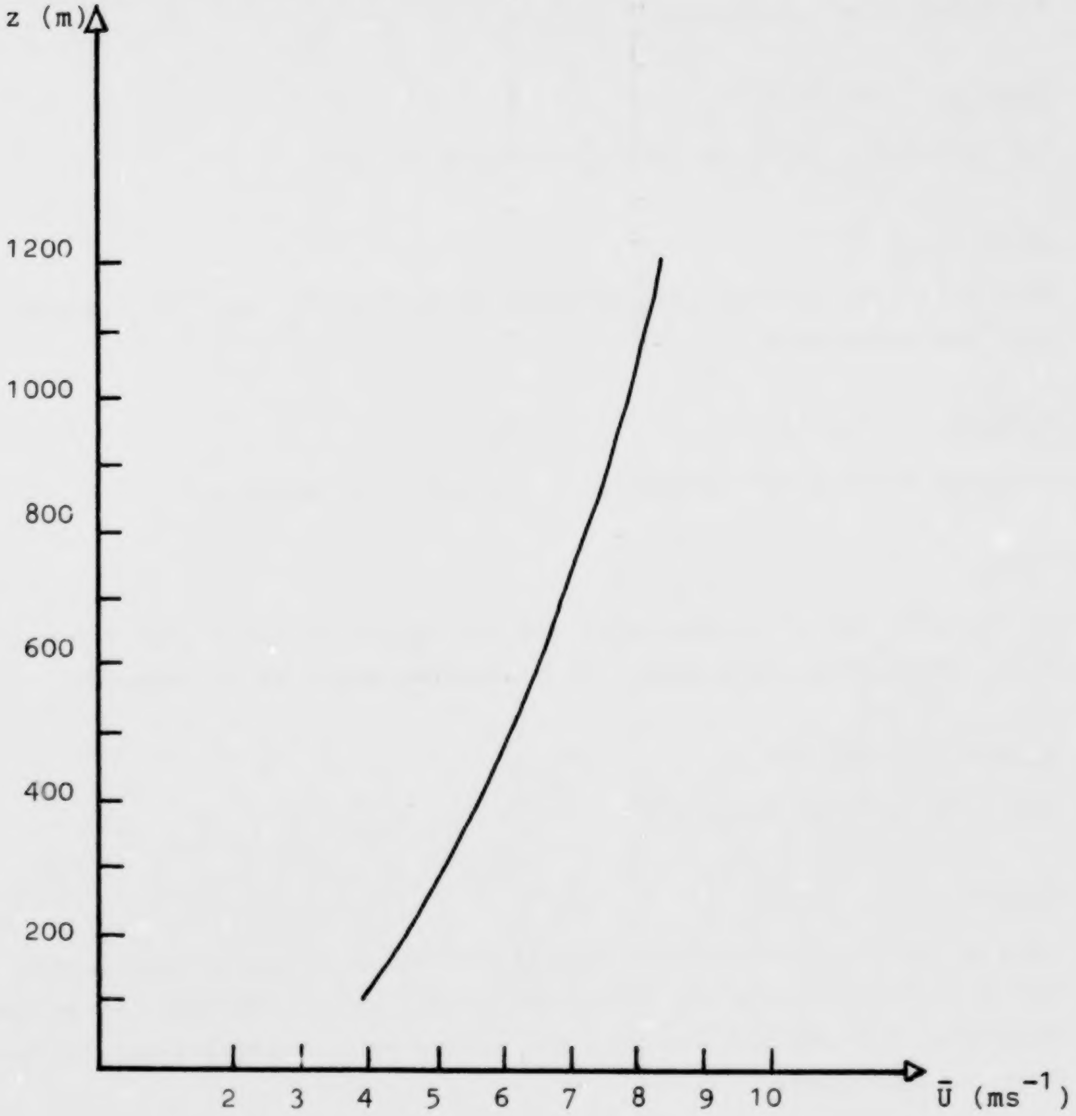

Figure 7. Mean wind vertical profile.

Discussion:

Berger:

Did you apply these new results σ_y and σ_z into Gaussian plume model to evaluate the improvement?

Maestro (response):

Not yet, but it will be done in the near future.

Smith:

What stability classes were represented by the σ_y and σ_z plots that you have presented?

Maestro (response):

The data represented adiabatic (neutral) conditions.

Smith:

In the last set of curves, what was the height of the source for the rural experiments that were from an earlier paper by Santomauro?

Anfossi (response):

100 - 120 m above ground.

Millàn:

Some of the smaller turbulent scales may not be measured due to the finite size of the balloon which cannot respond in the same way as gas molecules. The balloon has drag and aerodynamic characteristic different from air molecules.

Maestro (response):

The 60 cm balloon is a no-lift balloon (neutrally buoyant) and assumed to be a point which does not break the air (moves with the air currents

- no buoyancy or momentum forces are assumed to be associated with the balloon).

Anfossi (response):

We performed comparisons between such balloon data and simultaneous data from a meteorological tower and have found good agreement. We are obviously interested in scales of turbulent dispersion that are larger than the diameter of the balloon (about 60 cm).

A COMPARISON OF SOME INTEGRAL PLUME RISE MODELS WITH FIELD OBSERVATIONS

by

G.A. Davidson, P.R. Slawson
Dept. of Mechanical Engineering
University of Waterloo
Waterloo, Ontario, Canada

and

S.G. Djurfors
Environmental Affairs Dept.
Syncrude Canada Ltd.
Edmonton, Alberta, Canada

Abstract. The performance of three analytical plume rise models is compared against data obtained in a recent field study. For trajectory predictions it is concluded that all three models perform well under uniform wind, constant lapse conditions; that all models can perform reasonably well under windspeed shear conditions, provided that wind profile data is available; and that all models perform relatively poorly under low windspeed conditions. The model developed by Djurfors and Netterville is shown to perform slightly better than the others for wind speed shear conditions. It is also suggested that the buoyancy flux definition used by Briggs leads to superior plume outline predictions due to the fact that it compensates for the Boussinesq approximation.

Introduction

The aim of this paper is to evaluate the performance of three plume rise models by comparing their predictions with field data obtained under various ambient conditions in a recent plume dispersion study.

Plume Rise Models

The models under consideration here may all be classified as integral entrainment models which can be derived as analytical solution of the one-dimensional conservation equations of fluid mechanics:[1,2]

$$\frac{d}{dt}(R^2U) = 2RUv_e \tag{1}$$

$$\frac{dM}{dt} = F \tag{2}$$

$$\frac{dF}{dt} = -MN^2 \tag{3}$$

Equations (1) to (3), which describe respectively conservation of mass, vertical momentum, and energy, apply to a bent-over plume element ($V \cong U$) under the

Preceding page blank

Boussinesq approximation ($\rho_p = \rho_a$ = constant except in those terms involving density differences). The interaction between the plume and its surroundings is described by the entrainment velocity v_e, for which the usual assumption[1,2]

$$V_e = \beta|w| \tag{4}$$

will be made here.

Combining these equations with the kinematic relation

$$\frac{dz}{dt} = w \tag{5}$$

yields four equations for the four unknowns F, M, R, and z as functions of downwind travel time t. The time variable can be related to downwind distance through the relationship

$$\frac{d}{dt} = U\frac{d}{dx} \tag{6}$$

such that the plume centerline trajectory z and radius R can be formulated as functions of downwind distance.

Plume Rise Data

During four seasonal periods in 1977, the dispersion characteristics of the powerhouse plume of the Great Canadian Oil Sands (GCOS) plant in Northern Alberta, Canada were studied. A hot (typically 550°K), visible plume consisting of coke combustion products is discharged from a 106 m high, 5.8 m diameter stack in the GCOS complex. Near the source, plume rise data were collected photographically, while further downwind, sulfur dioxide levels were recorded at various altitudes with an instrumented aircraft. Wind speed, wind direction, and air temperature profiles were continually obtained from pibal flights during each measurement period. Simultaneously, source exit velocity, exit temperature, and sulfur dioxide flow rate were also monitored. Further details of the field program, data abstraction procedure, and resulting data base can be found in References 3, 4, and 5.

To evaluate plume rise models, 37 time-mean-plume data sets have been abstracted from the GCOS measurements. Each set consists of coordinates describing both plume centerline trajectory and visible outlines versus downwind distance, averaged over typically a 40 to 60 minute interval, along with corresponding ambient temperature and wind profiles and source data. Well-established procedures have been applied to correct measured coordinates for camera perspective, and, to minimize measurement errors, care has been taken to eliminate those cases where wind directional shear was significant through the plume rise region.

To aid analysis, it has been found convenient to divide the plume rise data sets into three groups. Group A data, which constitute 12 of the 37 sets, were collected during periods of linear lapse conditions when wind speed and direction were approximately uniform from stack top to the point of maximum plume rise. Group B data (17 cases) were collected during periods of significant wind speed shear, but negligible directional shear. Group C data (8 cases) were collected during periods of low windspeed, with or without speed shear, but with negligible directional shear. Both linear and nonlinear temperature profiles occur in the Group B and C cases.

Model 1

An analytical solution of equations (1) to (6) can be obtained by introducing the further assumptions that U = constant and N^2 = constant[1,2]. During stable conditions ($N^2>0$), the solution becomes

$$R = R_o^* + \beta Z \tag{7}$$

$$Z = \left\{\frac{3}{U\beta^2N^2}\left[F_o^*\left(1-\cos\frac{Nx}{U}\right)+NM_o^*\sin\frac{Nx}{U}\right]+\left(\frac{R_o^*}{\beta}\right)^3\right\}^{1/3}-\frac{R_o^*}{\beta} \tag{8}$$

Following Hanna[6], an initial radius correction

$$R_o^* = R_o\sqrt{w_o/U} \tag{9}$$

has been introduced to match the correct source buoyancy and momentum fluxes to bent-over plume fluxes, such that

$$M_o^* = UR_o^{*2}\,w_o = R_o^2\,w_o^2 \tag{10}$$

$$F_o^* = UR_o^{*2}\,g\,(Tp_o - Ta_o)/Ta_o = w_o\,R_o^2\,g\,(Tp_o - Ta_o)/Ta_o \tag{11}$$

During neutral conditions ($N^2 = 0$), equation (7) remains unchanged, but equation (8) becomes

$$Z = \left\{\frac{3}{2\beta^2}\left[\frac{F_o^*}{U^3}x^2 + 2\frac{M_o^*}{U^2}x\right]+\left(\frac{R_o^*}{\beta}\right)^3\right\}^{1/3}-\frac{R_o^*}{\beta} \tag{12}$$

Note that, if R_o^* and M_o^* terms are neglected, equation (12), and equation (8) with $\frac{Nx}{U} \ll 1$, reduce to

$$Z = \left(\frac{3F_o^*}{2\beta^2U^3}\right)^{1/3} x^{2/3} \tag{13}$$

which is the widely used $\frac{2}{3}$ law of plume rise.

To compare model 1 predictions with GCOS data, the entrainment constant β is first found by applying the procedure of Hoult, Fay, and Forney[7] to Group A cases, those cases which best satisfy the assumptions of the model. Root-mean-square differences between measured and predicted centerline trajectories,

$$\epsilon_{RMS} = \left\{\frac{1}{M}\sum_{i=1}^{M}\left[\frac{Z(X_i)^{model} - Z(X_i)^{obs.}}{Z(X_i)^{obs.}}\right]^2\right\}^{1/2} \tag{14}$$

are computed, as summarized in Table 1 and Figure 1, for various values of β. From Figure 1, the minimum average error of 12.4% occurs with β = 0.88. This error is of the same order as that found in previous studies[7], and is considered reasonable in view of the simplification of the model combined with unavoidable measurement errors in such parameters as windspeed.

Attention is now turned to the application of model 1 with β = 0.88 to Group B data sets, which contain significant windspeed shear. In a first iteration, the model was applied using ambient parameters at stack-top to fix U and N^2.

As was expected, the model performance deteriorated, and the average error for the 17 Group B cases was calculated to be 26.5%. However, following Slawson[8], it was found that a simple averaging procedure leads to improved predictions. The first iteration was used to furnish an initial estimate of plume rise $z_{max}^{(o)}$. Wind speed and temperature lapse were then averaged from stack top to $z_{max}^{(o)}$, and model 1 was reapplied with connected U and N^2 values. In this second iteration, the average error for Group B cases was reduced to 17.3%.

Finally, model 1 with $\beta = 0.88$ was applied to the low windspeed cases of Group C. Using ambient conditions at stack-top for a first iteration, the average error for the 8 Group C data sets was 23.1%. Incorporating the averaging procedure described above to correct U and N^2 in a second iteration, however, did not improve model 1 performance here, and the average error actually increased to 28%. The deterioration in model 1 predictions for Group C cases is attributed mainly to the failure of the bent-over plume assumption.

Model 2

Model 2 is a modified form of model 1 which has been presented by Briggs[2]. It is formally identical to equations (7), (8), and (12) with the R_o*, F_o*, and M_o* parameters replaced respectively by R_o, F_o and M_o. The initial radius correction is neglected, the source buoyancy flux is defined using a Tp_o divisor, such that

$$F_o = F_o^* \, Ta_o/Tp_o \tag{15}$$

and the source momentum flux remains the correct value, such that

$$M_o = M_o^* \tag{16}$$

Note that for the GCOS plume, $F_o \simeq \frac{1}{2} F_o^*$.

Repeating the procedure of the previous section for Group A data sets yields an optimum entrainment constant $\beta = 0.66$ with a corresponding minimum average error of 13%. This β value compares well with Briggs recommendation of $\beta = 0.6$ for the simplified solution, equation (13)[2]. A ten percent increase in β to 0.66 is reasonable for model 2, which retains R_o and M_o terms.

The performance of model 2 with $\beta = 0.66$ deteriorates when it is applied to Group B cases using U and N^2 values at stack top, and an average error of 25.3% results. However, if the averaging procedure is applied from stack-top to $z_{max}^{(o)}$ in a second iteration, the predictions improve, and the average error is reduced to 15.9%.

For the low windspeed cases of Group C, model 2, like model 1, performs relatively poorly. The first iteration using stack top parameters leads to an average error of 21.9%, while the second iteration using average parameters leads to an average error of 28.3%.

It is evident that differences between model 1 and model 2 trajectory predictions are slight. According to model 2, for example, equation (13) becomes

$$Z = \left(\frac{3F_o}{2\beta^2 U^3}\right)^{1/3} x^{2/3} \tag{17}$$

Substituting $\beta = 0.66$ and $F_o \approx \frac{1}{2} F_o^*$ yields

$$Z = 1.20 \; (F_o^* \, x^2/U^3)^{1/3} \tag{18}$$

Similarly, according to model 1, equation (13) with $\beta = 0.88$ reduces to essentially the same result

$$Z = 1.25 \; (F_o^* \, x^2/U^3)^{1/3} \tag{19}$$

The only difference between the two models is their prediction of the growth rate of the plume. Model 1 suggests $\frac{dR}{dz} = 0.88$, while model 2 suggests $\frac{dR}{dz} = 0.66$. This point will be discussed further at the end of this paper.

Model 3

In a recent article[9], Djurfors and Netterville present an analytical solution of equations (1) to (3) under wind shear conditions. Assuming that N^2 = constant and that the wind profile can be described by

$$U = U_o \; (1 + Z/Z_o)^{\gamma} \tag{20}$$

leads to the following solution under stable ($N^2>0$) conditions:

$$R = R_o^* + \beta^* Z \tag{21}$$

$$Z = \left\{ \frac{(3+\gamma) Z_o^{\gamma} \, F_o^*}{U_o \, \beta^{*2} \, N^2} \left[1 - \cos Nt + \frac{N M_o^*}{F_o^*} \sin Nt \right] + \left(\frac{R_o^*}{\beta^*} \right)^{3+\gamma} \right\}^{\frac{1}{3+\gamma}} - \frac{R_o^*}{\beta^*} \tag{22}$$

where

$$\beta^* = \beta / (1 + \tfrac{1}{2} \gamma) \tag{23}$$

$$Z_o = R_o^* / \beta^* \tag{24}$$

The diffusion time is related to downwind distance by the transformation

$$x = \int u(t)dt = U_o \int (1 + Z(t)/Z_o)^{\gamma} \, dt \tag{25}$$

Initial radius and momentum terms are included in this solution along with the source radius correction R_o^* of Hanna. Under neutral conditions, equation (22) becomes

$$Z = \left\{ \frac{(3+\gamma) Z_o^{\gamma} \, F_o^*}{2 U_o \, \beta^{*2}} \left(t^2 + \frac{2 M_o^*}{F_o^*} t \right) + \left(\frac{R_o^*}{\beta^*} \right)^{3+\gamma} \right\}^{\frac{1}{3+\gamma}} - \frac{R_o}{\beta^*} \tag{26}$$

For a uniform windfield, $\gamma = 0$ model 3 becomes identical to model 1. Accordingly, the performance of model 3 against Group A data sets is the same as that of model 1: a minimum average error of 12.4% occurs with an entrainment constant $\beta = 0.88$.

Under shear conditions, equation (20) must be fitted to the measured wind profile by the method of least squares to find the U_o and γ parameters. An initial estimate of plume rise is necessary at this stage, however, to fix the altitude range over which the least squares fit should be made. Just as for model 1, $z_{max}^{(o)}$ is estimated in a first iteration assuming uniform U and N^2

equal to their stack-top values. A least squares fit, such as that illustrated in Figure 2, can then be made and model 3 can be applied in a second iteration. Following this procedure for Group B cases leads to an average root-mean-square error of 13.9%. Model 3 predictions are therefore somewhat better than the second iteration predictions of models 1 and 2 under conditions of windspeed shear.

When model 3 is applied to the low windspeed cases of Group C, however, its performance deteriorates similar to that of models 1 and 2. The average root-mean-square error for the 8 Group C cases increases to 30.9%.

Concluding Remarks

The performance of the three models against measured trajectory data is summarized in Table 2, from which it can be concluded that the performance of all three models is similar. All models perform best under Group A conditions, can still perform well under Group B conditions if sufficient profile data is available, but perform relatively poorly under Group C (low windspeed) conditions.

For dispersion calculations, the final rise height, rather than the detailed plume trajectory, is probably the most important prediction of a plume rise model. In Table 3, final rise predictions of the three models under stable conditions (calculated by solving $\frac{dz}{dx} = 0$ for the maximum point) are compared with aircraft measurements. In these comparisons, the measured final rise height is taken to be the geometrical center of the sulfur dioxide concentration isopleths charted by the aircraft. An example is shown in Figure 3. From Table 3, it can again be concluded that the performance of all three models is comparable. However, it further appears that final rise predictions are generally somewhat better than trajectory predictions. For Group C data, for example, final rise predictions contain an average error of less than 20% whereas trajectory predictions contain average errors of 25 to 30%.

It must be remembered, however, that model 1 and 3 predictions were obtained with $\beta = 0.88$, while model 2 predictions were obtained with $\beta = 0.66$. As is illustrated in Figure 4, model 2 accordingly predicts a lower rate of plume spread. This lower rate of spread is closer to that measured experimentally. The paradox in this result is that model 2 performs better when plume outlines are considered, even though the F_o formulation appears to be less exact than the F_o^* formulation. This question is pursued further in Reference 5, where it is concluded that the Boussinesq approximation is the source of the paradox. The Boussinesq approximation is in serious error for the hot GCOS plume near the source since the true source mass flux is actually far less than that calculated assuming $\rho_p = \rho_a$. Models 1 and 3 therefore need a large value of β to pull predicted trajectories down to measured levels. Model 2, on the other hand, compensates for the Boussinesq approximation by reducing the initial buoyancy flux, such that realistic trajectories can be predicted along with realistic rates of spread. For most industrial plumes, the difference between the two approaches remains small; that is, since $F_o \simeq F_o^*$, predicted rates of spread are also quite similar. The difference between the two approaches becomes significant, however, when very hot plumes are considered.

Table 1. Performance of Model 1 for Group A data sets.

Root-mean-square trajectory errors versus β.

Date		β = 0.70	0.75	0.80	0.85	0.90	0.95
Jan. 25	1138-1235	0.262	0.211	0.168	0.134	0.110	0.097
Apr. 1	0859-1005	0.116	0.090	0.085	0.098	0.119	0.167
July 12	1400-1440	0.244	0.195	0.153	0.120	0.097	0.086
July 20	1935-2026	0.203	0.151	0.107	0.070	0.048	0.069
July 21	1618-1658	0.175	0.157	0.153	0.159	0.171	0.205
July 25	1545-1628	0.377	0.320	0.269	0.226	0.189	0.133
Oct. 18	1602-1634	0.319	0.261	0.209	0.165	0.126	0.071
Oct. 19	1616-1700	0.179	0.135	0.102	0.085	0.085	0.118
Oct. 20	1538-1612	0.449	0.383	0.327	0.276	0.231	0.156
Oct. 24	0930-1002	0.147	0.114	0.097	0.098	0.110	0.151
Oct. 24	1046-1120	0.134	0.098	0.080	0.081	0.098	0.143
Average		0.225	0.181	0.151	0.133	0.125	0.130

Table 2. Comparison of average root-mean-square errors

	Model 1 (β = 0.88)		Model 2 (β = 0.66)		Model 3 (β = 0.88)
	Iteration 1	Iteration 2	Iteration 1	Iteration 2	
Group A	0.124	-	0.130	-	0.124
Group B	0.265	0.173	0.253	0.159	0.139
Group C	0.231	0.280	0.219	0.283	0.309

Table 3. Comparison of final rise errors during stable conditions.

Date		Group	Aircraft Data	Model Predictions (Iteration 2)					
			Height above stack-top(m)	Model 1		Model 2		Model 3	
				Height(m)	Error(%)	Height(m)	Error(%)	Height(m)	Error(%)
July 25	1545	A	575	592	+3.0	577	+0.4	592	+3.0
Oct. 18	1602	A	325	345	+6.2	336	+3.4	345	+6.2
Oct. 19	1616	A	375	332	-11.5	322	-14.1	332	-11.5
Oct. 20	1538	A	450	375	-16.7	356	-20.9	375	-16.7
Jan. 26	1138	B	400	335	-16.3	317	-20.8	340	-15.0
Jan. 26	1316	B	425	380	-10.6	418	-1.7	380	-10.6
Apr. 1	0659	B	325	419	+28.9	401	+23.4	421	+29.5
July 23	2116	B	265	233	-12.1	228	-14.0	239	-9.8
Oct. 17	1548	B	300	319	+6.3	311	+3.7	323	+7.7
Oct. 19	0920	B	152	143	-5.9	139	-8.6	149	-2.0
Oct. 20	0956	B	225	182	-19.1	172	-23.6	184	-18.2
Oct. 25	0958	B	220	248	+12.7	239	+8.6	260	+18.2
Oct. 25	1546	B	350	306	-12.6	264	-24.6	314	-10.3
Oct. 27	1516	B	350	329	-6.0	322	-8.0	336	-4.0
Jan. 25	1418	C	425	364	-14.4	364	-14.4	372	-12.5
Mar. 28	0818	C	250	224	-10.4	217	-13.2	272	+8.8
July 25	1630	C	575	666	+15.8	649	+12.8	663	+15.3
July 26	0615	C	175	117	-33.1	114	-34.9	118	-32.6

References

1. P.R. Slawson, G.T. Csanady (1967): On the mean path of buoyant, bent-over chimney plumes. J. Fluid Mech., 28, 311.

2. G.A. Briggs (1975): Plume rise predictions. Presented at the AMS workshop on Meteorology and Environmental Assessment. Boston, Sept. 29 - Oct. 3, 1975.

3. P.R. Slawson, G.A. Davidson, W. McCormick, G. Raithby (1978): A study of the dispersion characteristics of the GCOS plume. Syncrude Canada Ltd. Report.

4. G.A. Davidson, P.R. Slawson, S.G. Djurfors (1978): A plume dispersion study at Mildred Lake, Alberta. Proc. of the 9th NATO International Technical Meeting on Air Pollution Modelling and its Application. Toronto, Aug. 28-31, 1978.

5. P.R. Slawson, G.A. Davidson, C.S. Maddukuri (1979): Dispersion modelling of the GCOS plume. Syncrude Canada Ltd. Report.

6. S.R. Hanna (1972): Rise and condensation of large cooling tower plumes. J. Appl. Meteorology, 11, 793.

7. D.P. Hoult, J.A. Fay, L.J. Forney (1969): A theory of plume rise compared with field observations. J. Air Pollution Control Assoc., 19, 585.

8. P.R. Slawson (1978): Observations and predictions of natural draft cooling tower plumes at Paradise Steam Plant, Atmos. Environment, 72, 1713.

9. S.G. Djurfors, D. Netterville (1978): Buoyant plume rise in non-uniform wind conditions. J. Air Pollution Control Assoc., 28, 780.

List of Symbols

F	buoyancy flux of plume
g	gravitational acceleration
M	momentum flux of plume
N	Brunt - Vaisala frequency
o	subscript referring to source value
R	plume radius
T_a, T_p	air and plume temperatures
t	downwind travel time
U	windspeed
V_p	plume centerline velocity
v_e	entrainment velocity
w	vertical velocity of plume
x	downwind distance
Z	altitude above stack-top of plume centerline
β	entrainment constant
ϵ_{RMS}	root-mean-square trajectory error
ρ_a, ρ_p	air and plume densities

Note that symbols not appearing in this list are defined in the text.

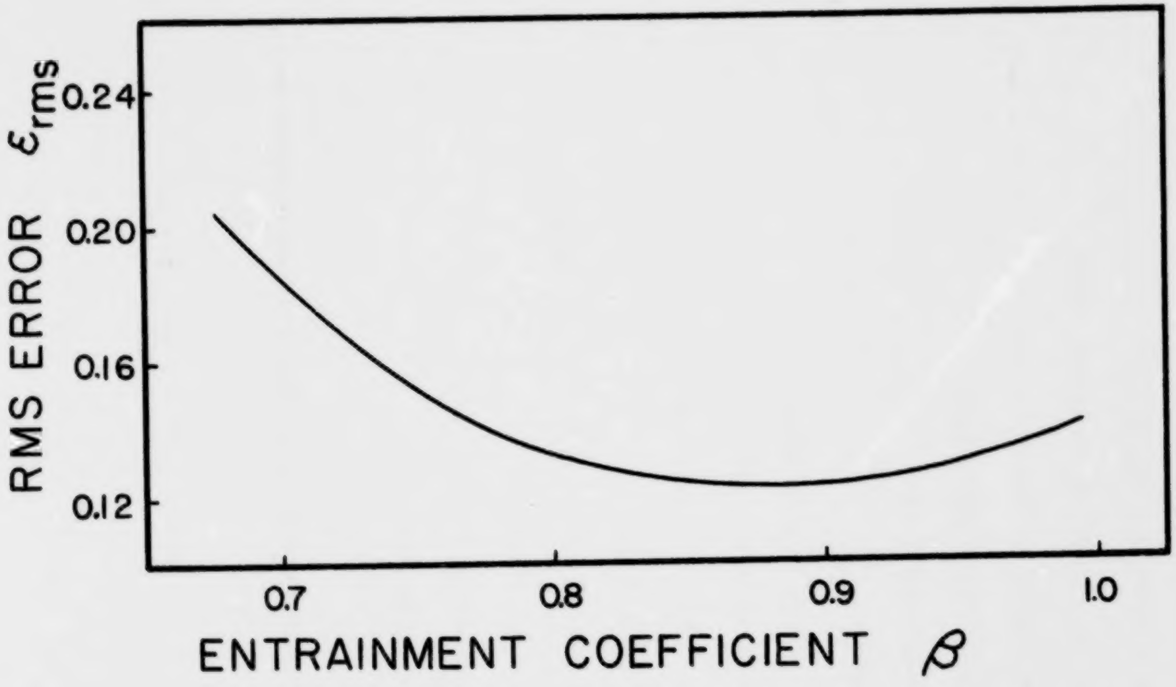

Figure 1. Average root-mean-square error for trajectory fits to Group A data sets versus entrainment constant β. The minimum error of 12.4% occurs at β = 0.88.

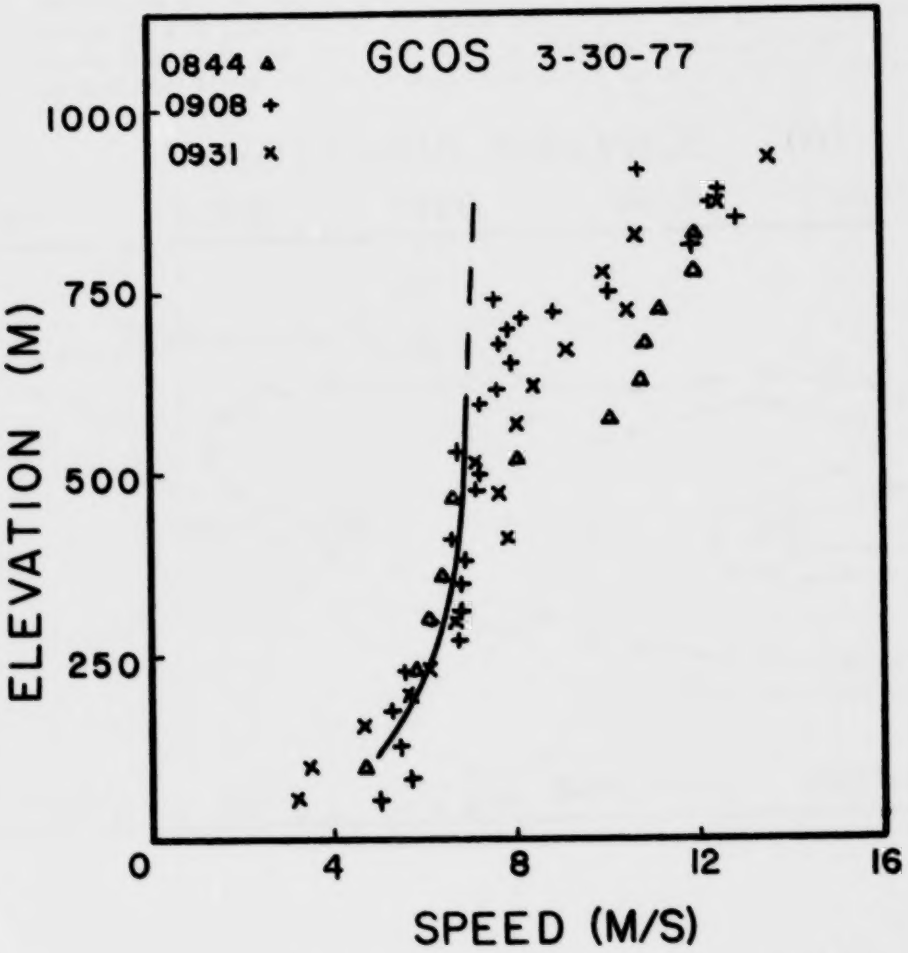

Figure 2. An example wind profile fit for model 3. Pibal data was fit over the range $z = 0$ to $z = z_{max}^{(o)} = 429$ m above stack-top (indicated by S in the figure) to yield the curve shown, which is described by $u = 5.15 (1 + z/6.24)^{0.072}$.

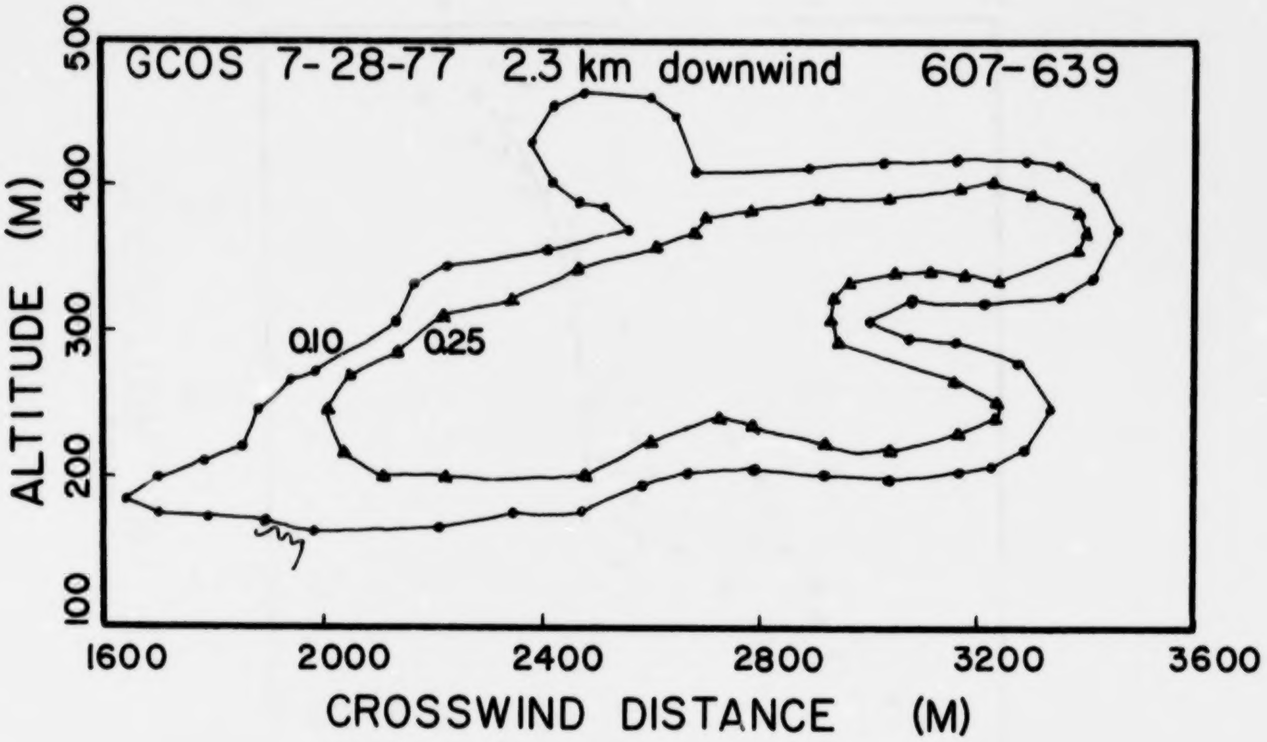

Figure 3. An example plume contour reconstructed from aircraft SO_2 measurements. The outer curve is the isopleth of 10% maximum concentration, while the inner curve is the 25% isopleth. From the figure, the final rise height is estimated to be 300 m above pibal zero, which equals 175 m above stack top.

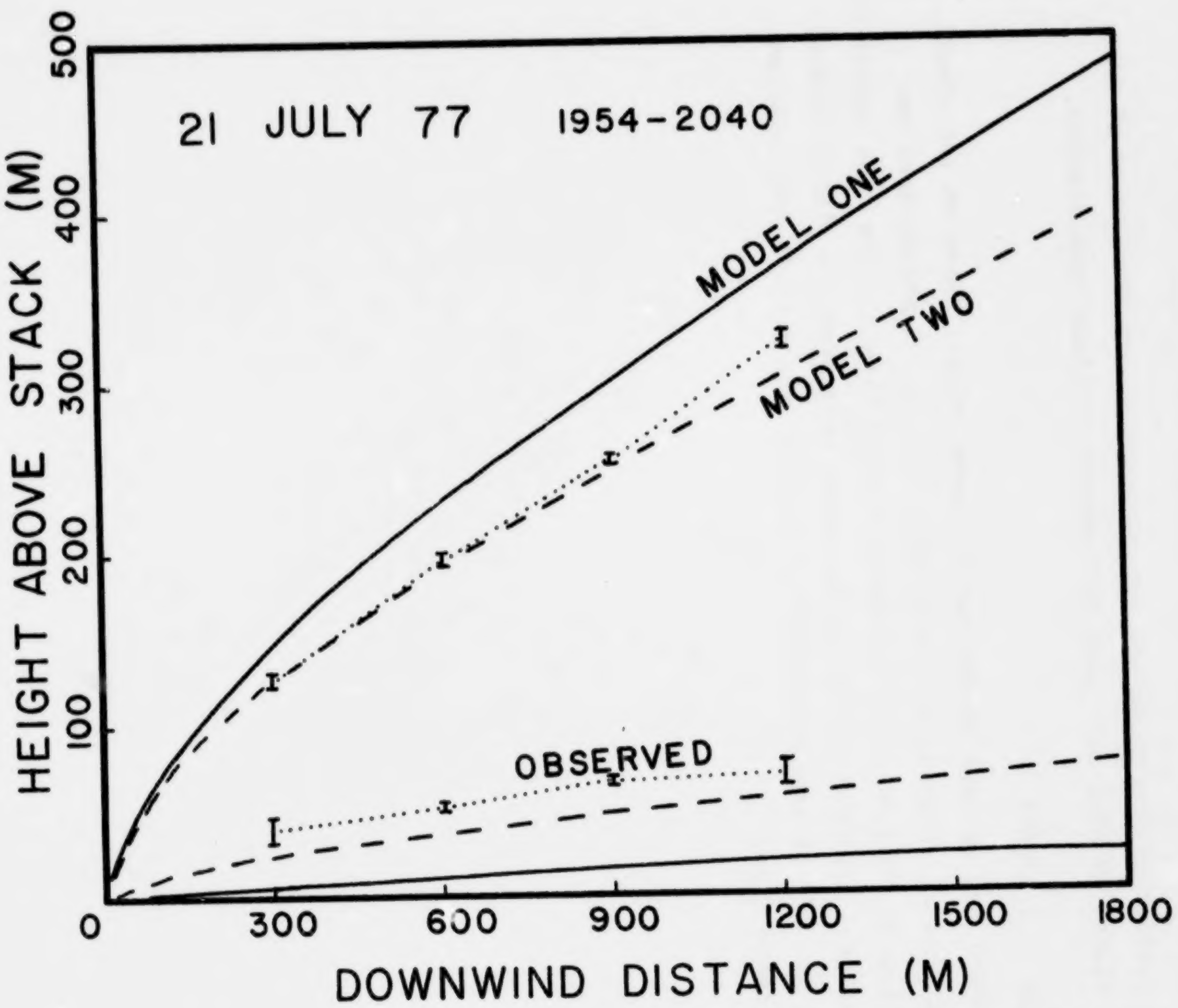

Figure 4. A comparison of measured and predicted plume outlines. The solid line is the model 1 prediction with $\beta = 0.88$, while the dotted line is the model 2 prediction with $\beta = 0.66$. Measurements are indicated by the vertical bars.

Discussion:

Millàn:

The centerline of the plume may not correspond with the center of mass of the plume. We have seen such differences in Lidar measurements.

Djurfors (response):

The centerlines we have determined are geometrical, based on the visual, observations of a number of photographs (e. g. 50 photographs representing 30 minutes yield a geometric centerline). The mass center is not your best indicator of where the plume trajectory is either because very large puff or concentrations in corners may distort the location of the centerline.

ANALYSIS OF SEVERAL LOW WIND SPEED TRACER EXPERIMENTS*

by

R.J. Yamartino**, P.G. Lühring, R.M. Stern***
IVU/Geomet-Berlin
Goethestr. 78
1 Berlin 12, Germany

Abstract. Preliminary results of analysis of several SF_6 tracer experiments performed in the Frankfurt am Main area are reported. These experiments, conducted under the stable, low wind speed conditions which occur frequently in this area, were designed to measure dispersion parameters applicable to this region.

An integrated Gaussian puff model is used in conjunction with an optimization program to determine dispersion rates which yield the best agreement between concentrations predicted by the model and those measured at the 50-station monitoring network. Agreement between predicted and observed average concentration values is usually within a factor of 2.5 at any individual station. The dispersion parameters are found to be in good agreement with previously analyzed Idaho tracer experiments.

Introduction

One portion of the research and development project "Investigation of dispersion under Low Wind Speed Conditions as a Basis for Dispersion Modeling," involves a series of tracer experiments in the Frankfurt am Main Region. The aim of these tracer experiments was to determine dispersion coefficients for the Frankfurt urban area, but initial releases were conducted on gently sloping, open farm fields near Ravolzhausen in order to test equipment, gain insight into optimal receptor placement, and measure dispersion in the absence of urban influences.

Climatology for this area, obtained from the German Weather Service station at Bruchkoebel about 2 km west of the receptor grid, indicates a high probability of low wind, poor dispersion conditions. Winds are generally from the SW or NE due to channeling caused by the orientation of the Rhein-Main basin between the Taunus and Odenwald mountain chains. The annual average wind speed is found to be a low 2.2 m/sec (at 6 m elevation) with wind speeds of less than 1 m/sec occurring 25.2% of the time.

The first four tracer releases were conducted under daytime convective conditions and have not yet been analyzed. Tracer releases five through nine were conducted under stable, nighttime conditions. At night, local downslope flow

---

* Supported by the Bundesminister des Inneren and Hessischer Minister für Landwirtschaft und Umwelt.

** On leave from Argonne National Laboratory, Argonne, Il., USA.

*** Freie Universität Berlin - Institut für Geophysikalische Wissenschaften, Thielallee 50, 1 Berlin 33, Germany.

from the mountains dominates, with the wind direction remaining fairly constant and from the NE. This directional persistence coupled with low wind speeds and stable atmospheric conditions, leads to the extremely low horizontal and vertical dispersion rates observed in these tracer experiments.

These results are then compared with previously analyzed tracer experiments conducted in Idaho and Tennessee and finally discussed in terms of other recent observations and "worst case" dispersion assessments.

The Ravolzhausen Tracer Experiments

Figure 1 shows the arrangement (for experiment 5) of monitors relative to the position of the SF_6 tracer release point. The terrain slopes gently downward from the release point at ≈ 150 m above sea level (3 m above ground level) to the field of receptors, about 1-2.5 km to the southwest, at elevations of 110 to 135 m above sea level (2 m above ground level). The region is populated with sparse low bushes and occasional trees giving a surface roughness estimated to be 10-20 cm. Although somewhat variable between the different tracer experiments, the receptor array consisted basically of a grid with ≈ 200 m spacing about 2 km wide in the crosswind direction and about 1.5 km deep in the alongwind direction.

Wind speed and direction were measured at four points in the receptor network (see Fig. 1) at a height of 2 km and near the release point at a height of 6 m. Unfortunately, the Woelfle cup annemometers available for this study had a fairly high threshold (≈1.0 m/sec). Accompanying these low level wind measurements were hourly, radar-tracked, radiosonde ascents to determine wind and temperature vertical profiles up to ≈ 2000 m. In addition, surface measurements of temperature and relative humidity were obtained and surface observations of cloud cover were recorded. These meteorological data are discussed in detail by Bartels and Keuler[1] and are partially summarized in Table 1.

Each receptor consisted of a set of teflon bags filled sequentially and at a uniform rate over ten minute intervals. In experiments 5-7, each sampler was comprised of six bags filled each alternate 10-minute period, while for experiments 8 and 9, eleven bags were filled during consecutive 10-minute periods. SF_6 concentrations in the bags were measured by personnel of the Hessische Landesanstalt fuer Umwelt using a gas chromatograph with an electron capture detector. A detailed tabulation of these data and associated discussions of errors and thresholds are reported elsewhere.[2]

Each of the experiments considered here consisted of a 30 minute release of SF_6 at a constant (±5%) rate of approximately 1 kg/min. The release point was located ≈ 1.5 km to the northeast of the center of the receptor grid for experiments 5 through 8 (see Figs. 2a-d) and was located at the center of the receptor grid for experiment 9 (see Fig. 2e). Thus, as seen from the source, the receptors covered an angular range of ≈ 60° for releases 5 through 8 and a full 360° for release 9.

Observed concentrations, averaged over all 10-minute samples at a single receptor, divided by the experimental SF_6 threshold, and adjusted radially to a common distance of $r = 2$ km (0.75 km for exp. 9) via the $r^{-1.78}$ theoretical concentration dependence, are displayed as open squares in Figs. 3a-e. We note that the angle given in Fig. 3 is arbitrarily defined in the counter-clockwise sense from the emission point so as to include the entire receptor array. Thus, the range of angle indicates the angular coverage of the receptor network as seen from the source.

Model Development

In the interest of achieving maximal compatibility at finite u with the steady-state Gaussian plume formulation, let us consider the dispersion of a Gaussian puff[3] of pollutant.

$$C(x,y,z,t) = \frac{q \quad e^{-1/2 \left\{ \frac{(X-uT)^2}{\sigma_X^2 (T)} + \frac{Y^2}{\sigma_Y^2 (T)} + \frac{Z^2}{\sigma_Z^2 (T)} \right\}}}{(2\pi)^{3/2} \sigma_X(T) \ \sigma_Y(T) \ \sigma_Z(T)}$$

where u = wind speed

(x,y,z,t) = receptor coordinates
(x', y', z', t') = source coordinates
and q = pollutant mass

$X = x - x'$
$Y = y - y'$
$Z = z - z'$
$T = t - t'$

This expression explicitly satisfies mass conservation and, for $\sigma_X(T)=\sigma_Y(T)= a_h T^{b_h}$ and $\sigma_Z(T)=a_v T^{b_v}$, satisfies the differential equation for diffusion with $D_X = D_Y = b_h \ a_h^2 \ T^{2b_h-1}$ and $D_Z = b_v = b_v a_v^2 T^{2b_v-1}$.

In order to obtain the time averaged concentration one would observe in the case of continuous pollutant emission at rate Q, we must integrate over source time and average over receptor time. Fortunately, the integrand is only a function of $T = t - t'$, so that the two dimensional integral may always be reduced to a sum of at most four one-dimensional integrals. Ignoring momentarily the case $b_v \neq b_h$ (i.e., $b \equiv b_h = b_v$) and introducing the new variable $\phi = \phi(T) = (t_d/T - \eta)$ and additional parameters $t_d \equiv (R/a_h)^{1/b}$, $\varepsilon \equiv \frac{ut_d}{R}$, $\eta \equiv \varepsilon \frac{X}{R}$ where $R \equiv \sqrt{X^2 + Y^2 + Z'^2}$ and $Z' \equiv \frac{a_h}{a_v} Z$, we find that the time average concentration, $\overline{C}$ (x,y,z), for the case of both source and receptor being turned on at time zero and off at time τ is just

$$\overline{C}\ (x,y,z) = \frac{Q\ t_d^{1-3b}}{(2\pi)^{3/2}\ a_h^2\ a_v} \int_{\phi_\tau}^{\infty} d\phi\ (\phi-\phi_\tau)\ (\phi+\eta)^{3b-3} e^{-1/2\ [\phi^2-\eta^2+\varepsilon^2]\ (\phi+\eta)^{2b-2}} \tag{1}$$

where $\phi_\tau \equiv \phi(\tau)$. Combining the results of solving the above integral exactly for $u = 0$ and approximately for all u by setting $b = 1$ in the integrand, we obtain the approximate solution.

$$\overline{C}\,(x,y,z) = \frac{Q\,\Gamma\left(\frac{3b-1}{2b}\right)}{(2\pi)^{3/2}\, a_h^2\, a_v\, (2b)} \left(\frac{2a_h^2}{R^2}\right)^{\frac{3b-1}{2b}} e^{-\frac{\varepsilon^2}{2}(1-X^2/R^2)}\, f(\phi_\tau/\sqrt{2}) \qquad (2)$$

where $f(\xi) \equiv e^{-\xi^2} - \sqrt{\pi}\ \mathrm{erfc}\ \xi.$ (3)

For the case of the source being turned on at time zero and off at time t_e, and the receptors being turned on at time $t_1 > 0$ and off at time t_2, it can be shown that the average concentration $\overline{C}$ is obtained by replacing the term $f(\phi_\tau/\sqrt{2}\,)$ with

$$g(t_e,t_1,t_2) = \frac{t_2\, f\left(\phi'_{t_2}\right) - \left(t_2 - t_e\right) f\left(\phi'_{t_2-t_e}\right) - t_1 f\left(\phi'_{t_1}\right) + \left(t_1 - t_e\right) f\left(\phi'_{t_1-t_e}\right)}{t_2 - t_1}$$

where $f(\xi)$ is given by equation (3) and

where $\phi'_t = \frac{1}{\sqrt{2}}\,\phi(t_2)$, $\phi'_t = \frac{1}{\sqrt{2}}\,\phi(t_1)$,

$\phi'_{t} - t_e = \frac{1}{\sqrt{2}}\,\phi(t_2 - t_e)$, and $\phi'(t_1 - t_e) = \frac{1}{\sqrt{2}}\,\phi(t_1 - t_e)$.

The computation of $g(t_e,t_1,t_2)$ does, however, present certain numerical problems related to computer roundoff, particularly for the case $t_2, t_1 >> t_e$, and full advantage of analytic cancellations must be exploited.

Further theoretical treatment of this low wind speed model is presented in reference 4.

Model Parameter Determination

Optimal determination of the parameters a_h, a_v, and b with respect to existing dispersion curves of Turner[5,6] and with respect to SF_6 tracer experiments in Tennessee[7] and Idaho[8] is described in reference 9 and the resulting optimal values of a_h and a_v are replotted in Fig. 4. The optimal value of $b = 0.9$ from those studies has been assumed for the Frankfurt tracer experiments because the restricted range of downwind distances (i.e., $1.0<x<2.5$ km) does not permit a reliable, independent determination of b from these data.

The basic analysis tactic consisted of considering each release separately and defining the quanties

$$F_{ave} = \frac{1}{N} \sum_{i=1}^{N} \left[\log(\overline{C}_{Ti}/\overline{C}_{0i})\right]^2$$

and

$$F_s = \frac{1}{N} \sum_{i=1}^{N} \frac{1}{n_i} \sum_{j=1}^{n_i} \left[\log(C_{Tij}/C_{0ij})\right]^2$$

where N is the number of stations, n_i is the number of valid samples for the i^{th} station, and C_{Tij} and C_{0ij} are the theoretical and observed concentrations respectively for the j^{th} sample at the i^{th} receptor. The average concentrations at each receptor are given as

$$\overline{C}_{Ti} = \frac{1}{n_i} \sum_{j=1}^{n_i} C_{Tij}$$

for the theoretically predicted concentrations and as

$$\overline{C}_{oi} = \frac{1}{n_i} \sum_{j=1}^{n_i} (C_{0ij} + 0.5\ C_{min})$$

for the observed values. The addition on one-half of the SF_6 detection limit, C_{min}, to the average concentration enables the many below-threshold observations to be utilized as a constraint on the theory. This feature has the potential for introducing some bias into the problem; however, we note the subsidiary conditions

i) if $C_T \le C_{min}$ and $C_0 \le C_{min}$ exclude from the computation of F_{ave} and F_s

ii) if $C_T > C_{min}$ and $C_0 \le C_{min}$ replace the quantity C_T/C_0 with the quantity C_T/C_{min} in the computation of F_{ave} and F_s

greatly limit this potential bias. Determination of the optimal dispersion coefficients is then based on finding those values of a_h and a_v which lead to a minimum in the quantity $F_{tot} = F_{ave} + 0.5\ F_s$, where the factor of 0.5 is introduced to lessen the significance of the 10-minute sample data relative to the time averaged data.

Though the above discussion may appear somewhat overly detailed, it is intended to point out some of the decisions which must be made in interfacing theory and experiment. Had the goodness-of-fit been defined in terms of the magnitude of the concentration differences (i.e., rather than the difference of the logarithms of the concentrations) the question of treatment of below-threshold concentrations would be moot and the resulting dispersion coefficients would be completely determined by the few high concentration samples. This latter approach might, in fact, be preferred by those interested only in dispersion coefficients for "worst case" simulations, but the resulting heavy weighting of a few data points represents non-optimal utilization of the experimental data and, as these tracer experiments lack measurements of the vertical concentration profile and full 360 degree azimuthal coverage (i.e., excepting exp. 9), render the vertical dispersion coefficient a_v more vulnerable to errors introduced by the necessary invocation of mass conservation.

The above mentioned concern regarding mass conservation has further led us to introduce a secondary or wide plume in superposition with the primary, narrow plume. The need for such a secondary plume might be argued on the physical basis that observed pollutant distributions fall off much less rapidly than a Gaussian when more than several standard deviations from the centerline or on the pragmatic basis that incorrect assumption about the fraction of material in the observed primary plume leads to a corresponding error in a_v. Thus the optimization problem increases from a two parameter problem to one involving six parameters: a_h, a_v as before plus a_{h2} for the secondary plume (n.b., $a_{v2} = a_v$), w_1, the fraction of pollutant in the primary plume (n.b., $w_2 = 1-w_1$), and the precise plume headings θ_1 and θ_2, where the last two variables are introduced to partially compensate for the observed curvature of the wind field. Finally, we define the quantities $R_{rms} = \exp(F_{ave})$ and

$$R_{mean} = \exp\left(\frac{1}{N} \sum_{i=1}^{N} \left|\log(\bar{C}_{Ti}/\bar{C}_{Oi})\right|\right)$$

which are given in Table 1 and have the simple interpretation as the root-mean-square and mean values of the fractional deviation. Hence, with perfect agreement between theory and experiment yielding $R_{rms} = R_{mean} = 1.0$, it is seen that all of the tracer experiments yield agreement within a factor of two to three in the mean.

Results and Conclusions

Observed concentrations, averaged over all 10-minute samples at a single receptor, divided by the experimental SF_6 threshold, C_{min}, and adjusted radially to a common distance of r=2 km (0.75 km for exp. 9) via the $r^{-1.78}$ theoretical concentration dependence, are displayed as open squares in Figure 3. The solid line gives the theoretical prediction of equation 2 similarly adjusted for each of the stations. In addition, dotted curves, indicating the predictions of a Gaussian plume model with horizontal dispersion coefficients of 2, 4, 6, 8, and 10 degrees, are drawn so as to pass through the maximum observed concentration and have been added to assist in judging the angular width of the primary plume. We again note that the angle shown in Fig. 3 is arbitrarily defined in the counter-clockwise sense from the emission point so as to include the entire receptor array. Thus, the range of angle indicates the angular coverage of the receptor network as seen from the source. Optimal values of the dispersion coefficients for the primary plume are given in Table 1 and are also plotted in Figure 4 as a function of radiation class. Upon examination of Figure 4 and after comparison with previously fitted tracer experiments, we conclude that:

1) The vertical dispersion rate a_v is directly related to radiation class and thus to the thermal energy available for turbulence.
2) The Ravolzhausen vertical dispersion rates are consistent with the results of tracer experiments conducted in the flat, semi-desert terrain of Idaho[8].
3) The horizontal dispersion parameter is not strongly correlated with radiation class though a lower bound for each radiation class might be defined. Knowledge of the wind directional shear in the lowest layer as well as orographic factors are probably necessary to satisfactorily describe the hotizontal dispersion parameter.
4) Under rather similar, stable conditions, one might observe plume widths comparable to, narrower than (i.e., exp. 7), or broader than (e.g., exp. 8 and especially exp. 9) the sigma theta angular widths for that stability class[10].

Finally, we compare the results of our optimal determination of the vertical dispersion parameter with the more conventional vertical dispersion coefficient, σ_z, computed with the equation $\sigma_z = a_v T^b$ and the diffusivity computed as $K_z = \sigma_z^2/(2T)$, where T is the approximate mean source-receptor travel time.

Exp.	K_z(m^2/sec^2)	σ_z(m)	Klug class/ Vogt σ_z(m)	Turner class/ Turner σ_z(m)*
5	0.64	45	I/43	F/32
6	4.8	80	II/76	E/50
7	16.	187	II/76	E/50
8	1.14	60	I/43	F/32
9	0.48	30	I/24	F/12

Excellent agreement between these σ_z values and those of Vogt are observed except perhaps for exp. 7. However, we note that if some of the SF_6 tracer were present in peaks not observed by the receptor array, values of a_v, K_z, and σ_z would be correspondingly smaller.

---

* Turner σ_z multiplied by 1.46 to correct for averaging time.

References

1. H. Bartels and P.M. Keuler, "Meteorologische Statistiken und Messungen zu den Tracer-Experimenten, in Regionale Forschungsgemeinschaft Untermain, 1. Arbeitsbericht: Untersuchung der Schadstoffausbreitung bei windschwachen Wetterlagen als Grundlage der Ausbreitungsrechnung," Frankfurt, 1978.

2. Hessische Landesanstalt fuer Umwelt, unpublished report, 1979.

3. D. M. Rote, J. W. Gudenas, and L. A. Conley, "Studies of the Argonne Integrated-Puff Model," ANL/ES-9, 1971.

4. R. J. Yamartino, "An Air Quality Dispersion Model Applicable to Calm Conditions," proceedings of the Seventh International Technical Meeting on Air Pollution Modeling and Its Application, September, 1976.

5. D. B. Turner, "Workbook of Atmospheric Dispersion Estimates," U.S. Dept. of Health, Education, and Welfare, PB-191 482, 1970.

6. D. B. Turner, " St. Louis Study," private communication, 1970.

7. R. B. Wilson, G. E. Start, C. R, Dickson, and N. R. Ricks, "Diffusion Under Low Windspeed Conditions Near Oak Ridge, Tennessee," NOAA Technical Memorandum ERL ARL-61, 1976.

8. J. F. Sagendorf and C. R. Dickson, "Diffusion Under Low Windspeed Inversion Condition," NOAA Technical Memorandum ERL ARL-52, 1974.

9. R. J. Yamartino, "A Dispersion Model for Low Wind Speed Conditions: Theory and Experimental Application," APCA-77-58.6, 1977.

10. NRC, "Onsite Meteorological Programs," Regulatory Guide 1.23, U.S. Nuclear Regulatory Commission, 1972.

Table 1. Summary of Ravolzhausen Tracer Experiments

TEST	TIME OF RELEASE (MET)	U* (M/SEC)	θ* (DEGREES)	U** (M/SEC)	θ*** (DEGREES)	$\Delta T/\Delta Z$ (°C/100 M)	CLOUD COVER (EIGHTHS)	RADIATION CLASS	STABILITY TURNER/NRC	PRIMARY PLUME DISPERSION RATES (M/SEC$^{0.9}$)		PERCENT TRACER IN PRIMARY PLUME	R_{RMS}	R_{MEAN}	NO. STATIONS/ NO. SAMPLES
										A_H	A_V				
5	2100-2130	3.8	40°	1.25	71°	3.6	0	-2	F-G/F-G	0.10	0.059	44	3.05	2.37	40/230
6	2100-2130	3.3	70°	3.0	63°	0.70	4	-2/-1	E/E	0.41	0.23	90	2.59	2.01	44/261
7	2100-2130	2.2	60°	1.86	56°	0.50	6	-1	E/E	0.16	0.35	94	3.76	2.68	48/288
8	2100-2130	1.0	50°	1.25	50°	5.4	0	-2	G/G	0.28	0.079	34	2.52	2.07	42/465
9	0200-0230	1.2	90°	0.82	81°	3.5	4	-2/-1	F-G/F	0.89	0.064	91	2.89	2.31	48/524

* MEASURED AT 6 M ELEVATION AT THE SOURCE

** SPACE TIME AVERAGE OF WINDS AT RECEPTOR SITES (Z=2 M) AND AT SOURCE CORRECTED FOR ELEVATION

***BASED ON LOCATION OF OBSERVED CONCENTRATION MAXIMUM

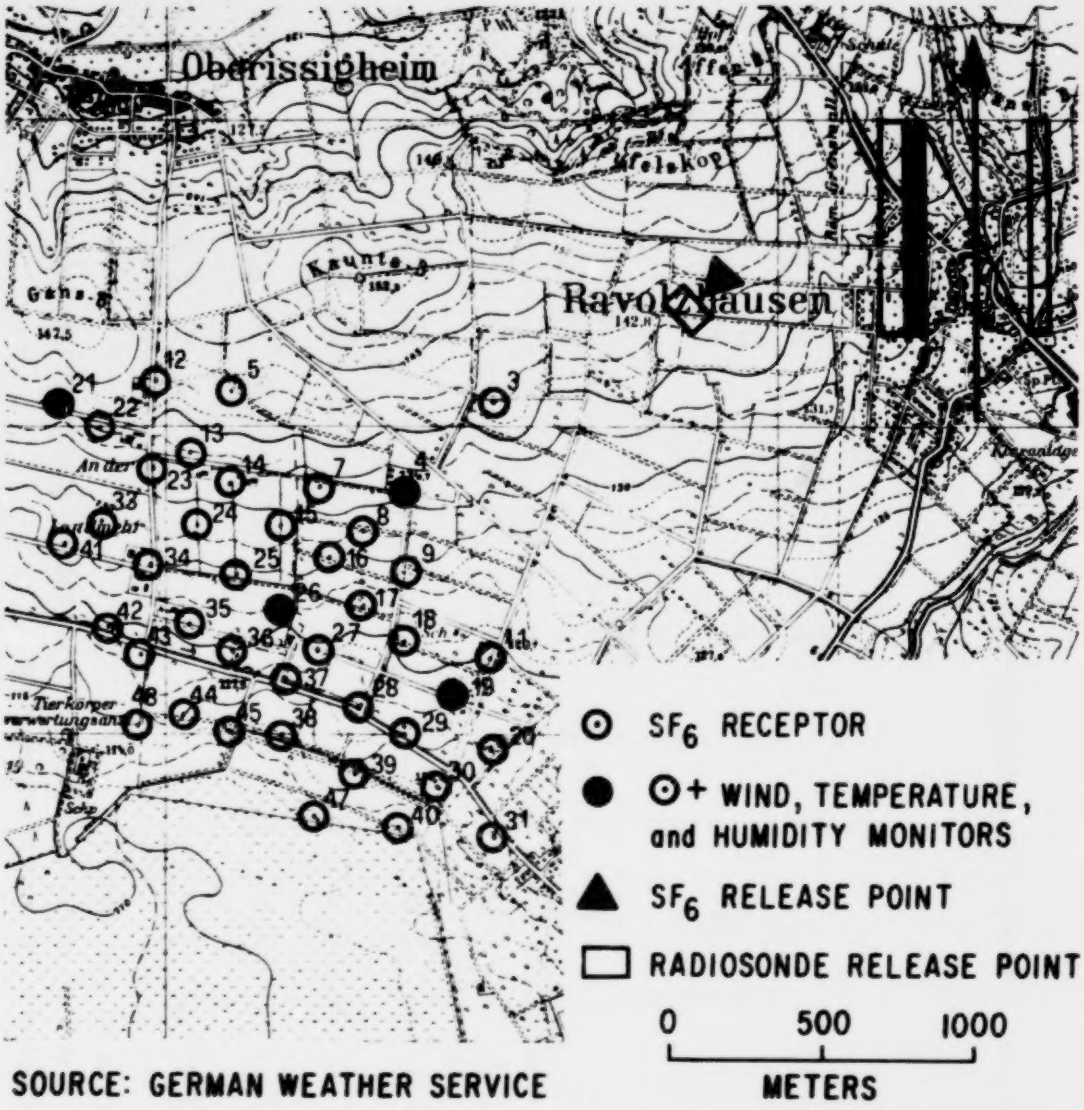
Oberissigheim
Ravolzhausen
Kaunte-B
Gans-B
An der
Tierkörper-verwertungsanst.
1 2 3 4 5 7 8 9 13 14 15 16 17 18 19 20 21 22 23 24 25 26 27 28 29 30 31 33 34 35 36 37 38 39 40 41 42 43 44 45 47 48
⊙ SF_6 RECEPTOR
● ⊙+ WIND, TEMPERATURE, and HUMIDITY MONITORS
▲ SF_6 RELEASE POINT
☐ RADIOSONDE RELEASE POINT
0
500
1000
METERS

SOURCE: GERMAN WEATHER SERVICE

Fig. 1. Map of the Ravolzhausen Experimental Area. Source and receptor locations for Experiment 5 are shown.

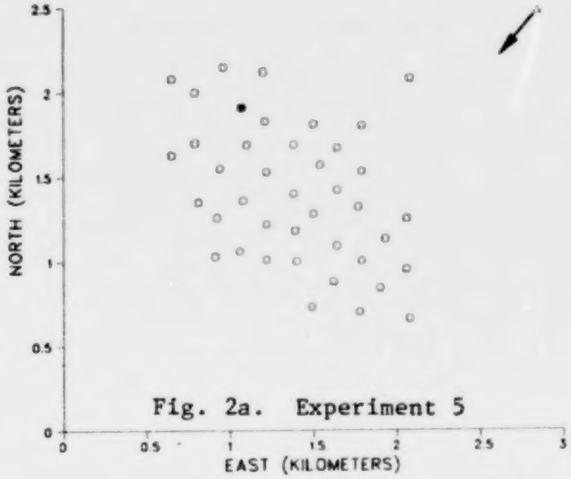

Fig. 2a. Experiment 5

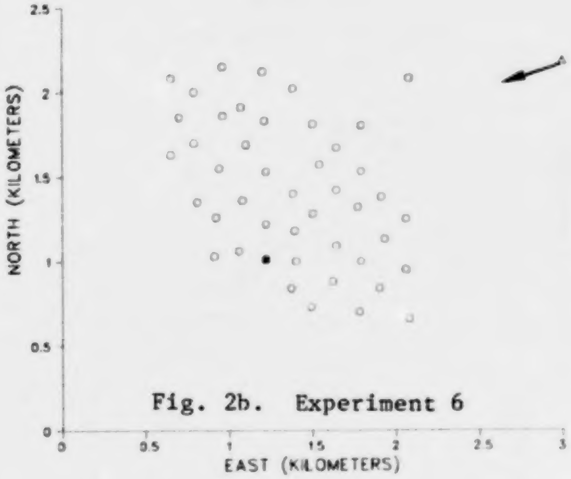

Fig. 2b. Experiment 6

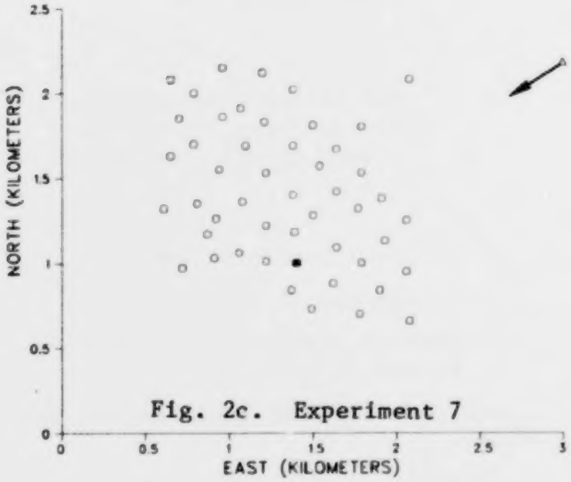

Fig. 2c. Experiment 7

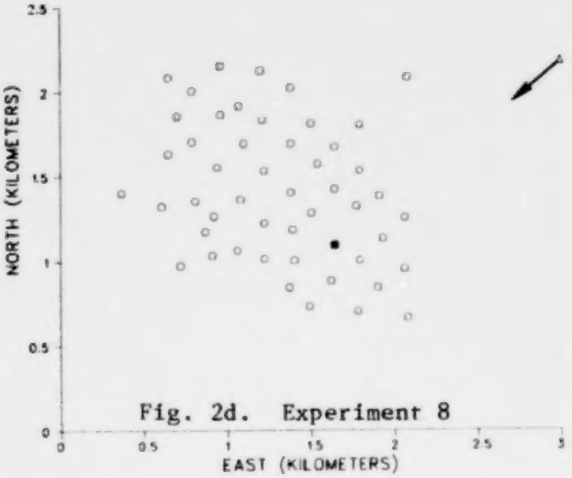

Fig. 2d. Experiment 8

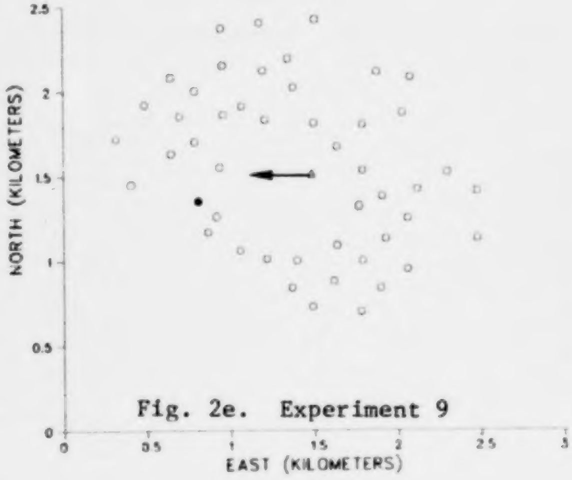

Fig. 2e. Experiment 9

Fig. 2. Source and Receptor Coordinates for Ravolzhausen Tracer Experiments 5-9.

↙ Source and Average Wind Direction at Source

○ Receptor

● Receptor with Peak Concentration

Fig. 3a. Experiment 5

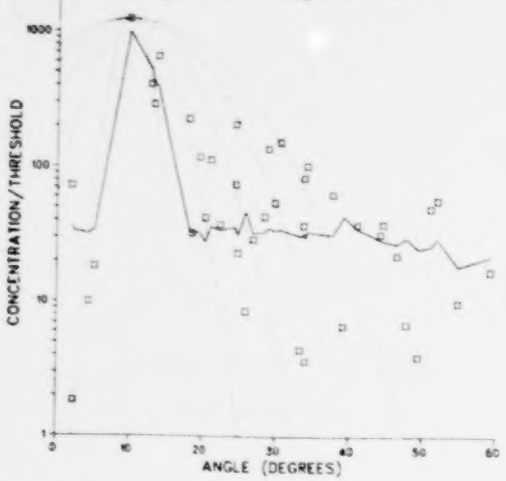

Fig. 3b. Experiment 6

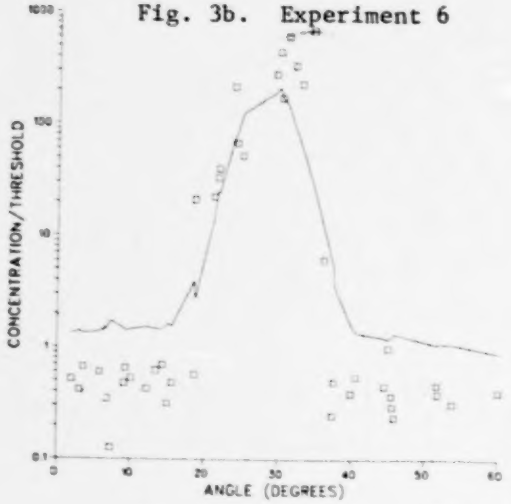

Fig. 3c. Experiment 7

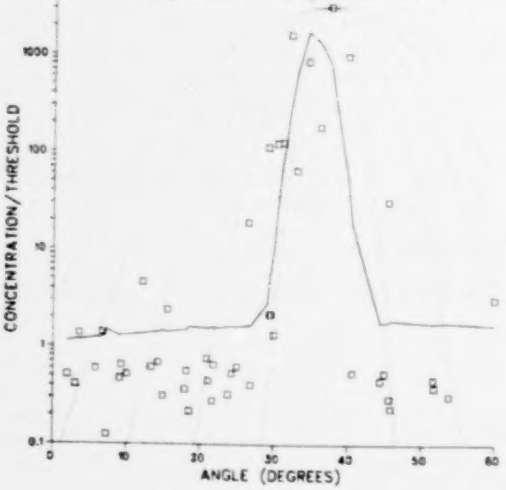

Fig. 3d. Experiment 8

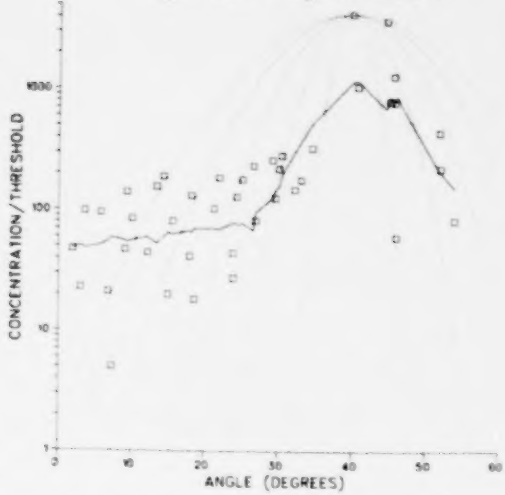

Fig. 3e. Experiment 9

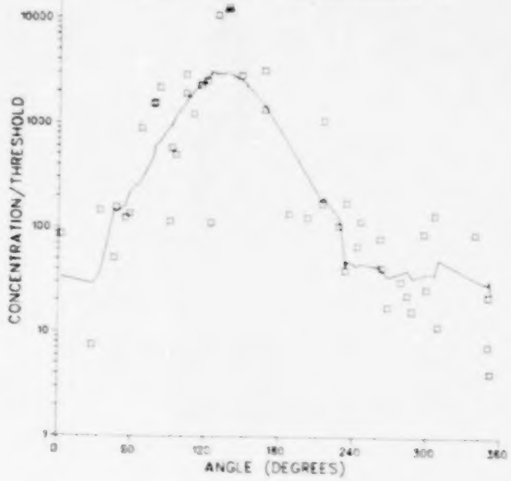

Fig. 3. Normalized Concentration Versus Angle for Ravolzhausen Tracer Experiments 5-9.

□ Observed Concentration

—— Prediction of Equation 2

········ Gaussian Plumes with σ_θ=2,4,6, 8, and 10 degrees.

Symbols are further explained in the text.

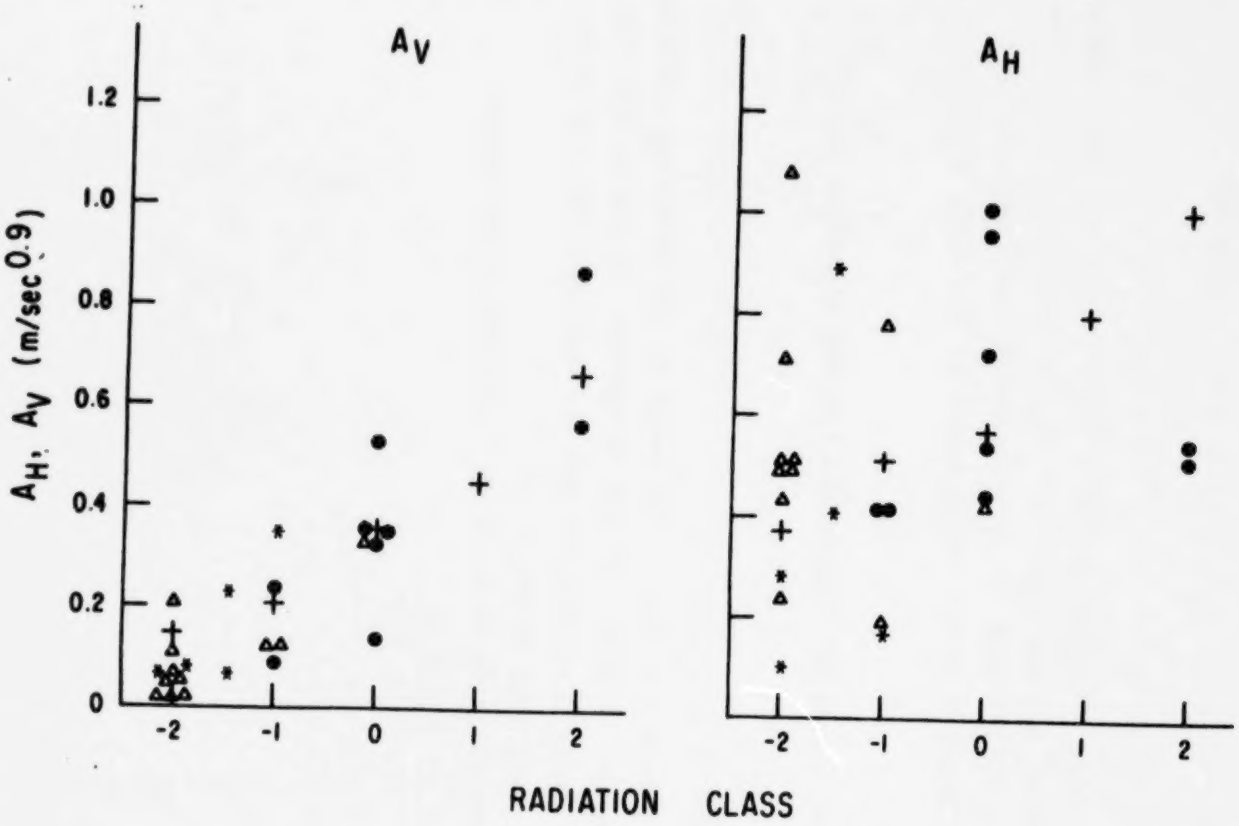

Fig. 4. Vertical and horizontal dispersion coefficients generated by requiring a best fit to low wind speed tracer studies conducted at Ravolzhausen, *, in hilly, wooded terrain of Tennessee[7], ●, and in flat, semidesert terrain of Idaho[8], Δ. The data are shown as a function of radiation class along with the results, +, of a best fit of the model to a Gaussian plume model at $u = 1$ m/sec and $\tau \rightarrow \infty$.

Discussion:

Millàn:

Have strong directional wind shear effects been considered?

Yamartino (response):

There is possibly some directional shear. The releases and the receptors are near ground level and the sigmas of the pollutant cloud are of the order of 10 - 20 m by the time the cloud reaches the receptors, so I guess that wind direction shears could exist in that depth range.

Millàn:

Couldn't such wind shears be responsible for the secondary distribution observed?

Yamartino (response):

We really don't understand what is the cause of the secondary distribution, it could be due to shear, or due to meander, or due to the fact that the eddy velocity distributions are not Gaussian when you go several σ_u or σ_v from the mean value.
Insufficient meteorological data exists to determine the cause.

DIFFUSION OF ATMOSPHERIC POLLUTANTS BEING EMITTED FROM TALL STACKS

W. G. Hübschmann, K. Nester, P. Thomas
Karlsruhe Nuclear Research Center, Safety Department

Abstract. The first series of diffusion experiments carried out at the Karlsruhe Nuclear Research Center with tracers being emitted at heights of 60 and 100 m showed the strong dependence of the resulting diffusion parameters σ_y and σ_z on the surface roughness at the site, being characterised by forest and large buildings. A second series of experiments has been carried out since 1977 with tracers being emitted at heights of 160 and 195 m, covering the diffusion categories A through D. The resulting σ_y- and σ_z-curve families and the normalised diffusion factor curves for an assumed source height of 160 m are shown and the influence of the ground roughness as compared to the lower emission heights is discussed. The long-term diffusion factor for a 160 m high source at the KNRC is evaluatet using both above mentioned σ-curve families and the σ-curves by PASQUILL/GIFFORD. Provided the σ-curve set for 160/195 m gives the best result, the maximum is over- or underestimated both by the factor 1,5 when the non-appropriate σ-curves are applied.

1. Experimental Technique

In the Karlsruhe Nuclear Research Center (KNRC) diffusion experiments have been carried out since 1969 /1/. During the first test series it has been realised, that the widely used diffusion parameters recommended by PASQUILL/ GIFFORD /2/ were not applicable in this area of high surface roughness (high buildings inside, forest outside the research center). The diffusion experiments, therefore have been intensified. Since 1974 chemical tracers are emitted from the 200 m high meteorological tower, mostly at two different levels simultaneously. Chemical tracers (halogenated hydrocarbons) are used, as their concentration in air samples can be measured simultaneously and with high sensitivity.

Evacuated glass bottles are placed at the downwind side of the tower, two bottles each at up to 50 locations in a regular grid. The bottles are opened and closed by an automatically operated valve. During two consecutive 30 minute sampling periods the air is succed into the bottle at a constant rate through a capillary glass tube. The tracer concentration is evaluated by gas-chromatography. A double Gaussian distribution function is fitted to the measured near-ground tracer concentration field by a least squares fit, determining simultaneously the most adequate diffusion parameters σ_y and σ_z. As usual the dependence of these parameters on the source distance x is expressed by a function of the form $\sigma = \sigma_0 x^b$; the method is described in /3/.

2. Results of Diffusion Experiments

The individual σ_y-, σ_z-curves have been used to form combined σ_y- and σ_z-curve families by averaging in a logarithmic scale the σ-curves referring to the same diffusion category.

The evaluation of the diffusion experiments with emission heights of 60 and 100 m resulted in σ_y, σ_z-curve families covering the diffusion categories A through F /3/. These results demonstrated the strong influence of the surface roughness (forest, high buildings) at the research center site on atmospheric diffusion. It was essential to know whether this influence would still be effective at larger emission heights.

Since 1977, diffusion experiments with emission heights of 160 and 195 m have been performed. These experiments cover the range of unstable and neutral diffusion categories (A through D). No experiments with stable categories (E and F) have been performed with emission heights above 100 m, as no measurable tracer concentrations would have been found at ground level. In order to complete the σ-curve families, a method has been developed to extrapolate the σ_y, σ_z-curves referring to emission heights of 160 and 195 m from those derived for 60 and 100 m emission heights. The method is based on the measured maximum concentrations and their distance from the source as a function of the standard deviation σ_ϕ of the vertical wind direction /4/.

Fig. 1 shows the σ_y- and σ_z-curve families evaluated for the emission heights 160 and 195 m. As the number of experiments has been limited and did not represent the normal band width of σ_ϕ values among each of the categories, the original curves derived from the experiments have been shifted in order to represent the average turbulence condition in each diffusion category. The method is described in /4/.

The effect of the larger emission height (160 and 190 m) as compared to the smaller ones (60 and 100 m) can be best demonstrated in fig. 2, showing the normalised diffusion factors (normalised ground level concentrations for 1 m/s wind velocity and unity source strength). Here the two σ_y, σ_z-curve families (60/100 m and 160/195 m) are used to evaluate the diffusion factor for an emission height of 160 m each. The differences can be summarised as follows:

Convective turbulence is even more pronounced at the larger emission height. Therefore the category A and B curve maximum is higher for 160/195 m emission height. The mechanically induced turbulence (effect of ground roughness) decreases with increasing height. For the category D maximum, the effect of the decreased σ_z is compensated by the decreased σ_y. Therefore the maximum is nearly the same for both σ-curve sets. For the stable categories the differences in the concentrations are mainly due to differences of the σ_y.

3. Application of Experimental Results

The three σ-curve families mentioned above have been applied to calculate the long-term diffusion factor (normalized near ground concentration for a unity emission rate) for a 160 m high source at the site of the Karlsruhe Nuclear Research Center. The maximum of this diffusion factor falls into a NE-direction. The long-term diffusion factor $\bar{\chi}_{max}$ has been calculated by the ISOLA-III code /5/, using a 5-year meteorological statistics based on a wind rose divided into 10^0-sectors, see fig. 3. If it is accepted that the Karlsruhe 160/195 m σ-curve set (KNRC 160/195 m) is the most appropriate one for the emission height chosen, then the KNRC 60/100 m σ-curve set delivers a maximum, which is too high by a factor 1,5 at a distance, which is too short by a factor 1,5. These differences are due to the high frequency of the category D (more than 50 %) in the main wind direction sector at the site of the Karlsruhe Nuclear Research Center, and due to the fact, that the σ_z of category D is decreased for the larger emission heights.

The use of the PASQUILL/GIFFORD σ-curve set underestimates the maximum by a factor 1,5. One would expect this, as the diffusion experiments evaluated by PASQUILL have been carried out over a flat terrain of very low roughness (Prairie Grass Experiments).

The following can be concluded from these results: If long-term concentrations of pollutants being emitted from single sources should be estimated with some degree of accuracy it is essential to use diffusion parameters suitable for adequate emission heights and for adequate ground roughness, in order to avoid a large over= or underestimate of long term maximum pollutant concentrations.

References

1. P. Thomas et al.; Experimental Determination of the Atmospheric Dispersion Parameters over Rough Terrain. Part 1, KFK 2285, July 1976.

2. D. H. Slade ed.; Meteorology and Atomic Energy 1968. TID-24 190, May 1969.

3. P. Thomas, K. Nester; Experimental Determination of the Atmospheric Dispersion Parameters over Rough Terrain, Part 2. KfK 2286, June 1976

4. K. Nester, P. Thomas; Im Kernforschungszentrum Karlsruhe experimentell ermittelte Ausbreitungsparameter für Emissionshöhen bis 195 m. Staub-Reinhaltung Luft 39 (1979), 291-295.

5. W. Hübschmann, D. Nagel; ISOLA III, Ein FORTRAN IV-Programm zur Berechnung der langfristigen Dosisverteilung in der Umgebung kerntechnischer Anlagen. KfK 2698, Dez. 1978

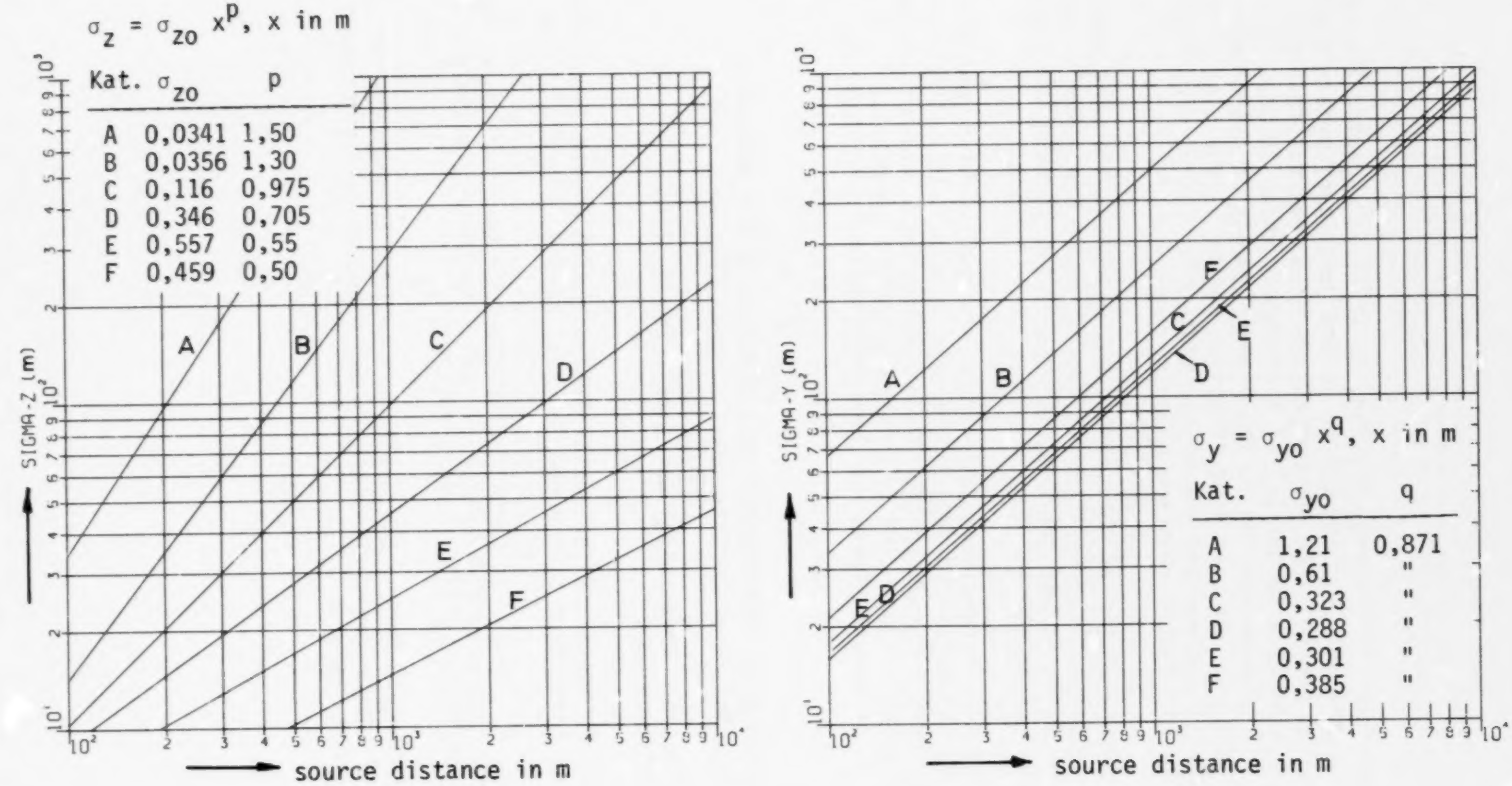

$\sigma_z = \sigma_{zo}\, x^p$, x in m

Kat.	σ_{zo}	p
A	0,0341	1,50
B	0,0356	1,30
C	0,116	0,975
D	0,346	0,705
E	0,557	0,55
F	0,459	0,50

$\sigma_y = \sigma_{yo}\, x^q$, x in m

Kat.	σ_{yo}	q
A	1,21	0,871
B	0,61	"
C	0,323	"
D	0,288	"
E	0,301	"
F	0,385	"

Fig. 1 Diffusion parameters σ_z and σ_y

emission height 160/195 m, KNRC site

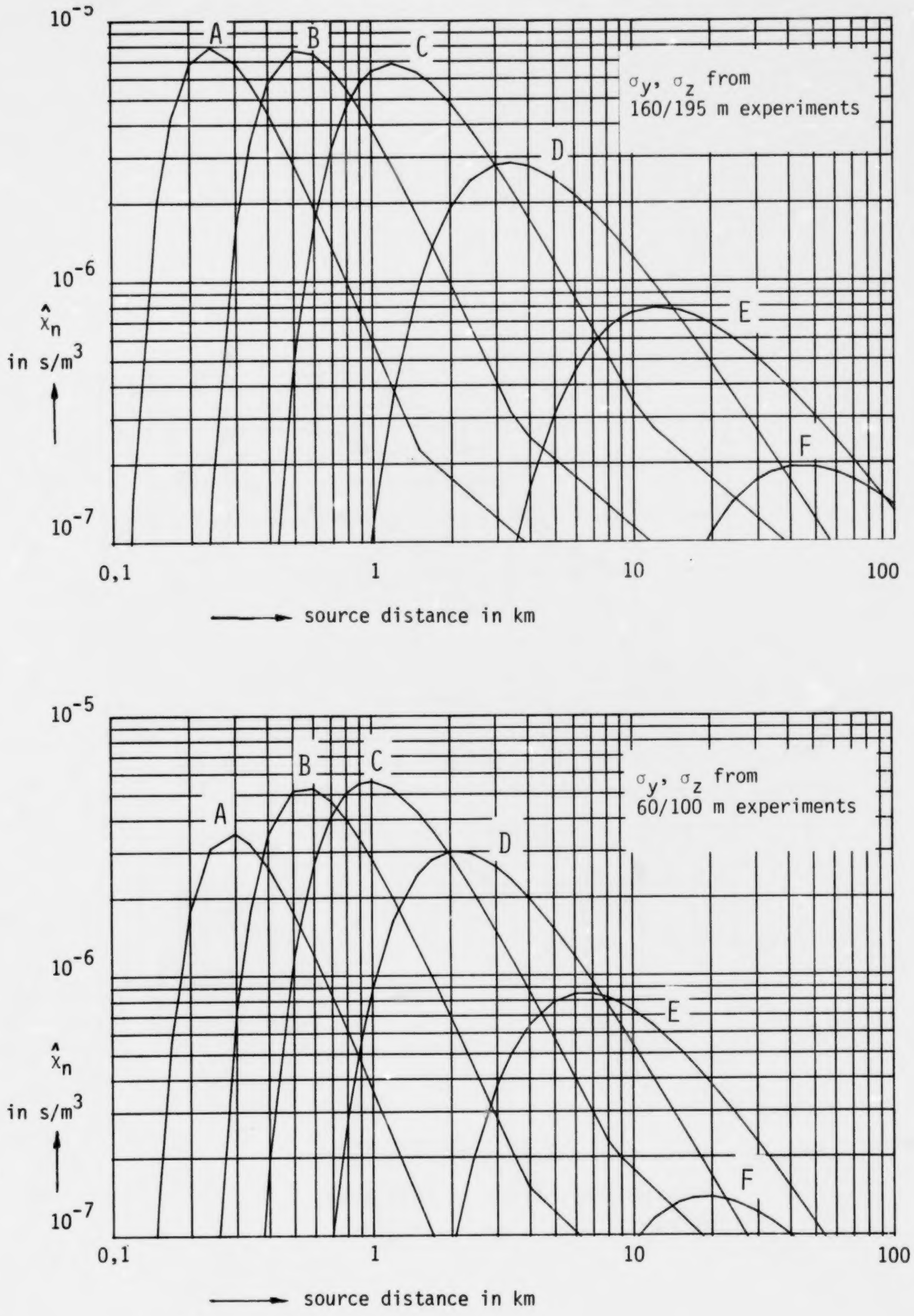

Fig. 2 Normalised diffusion factor $\hat{\chi}_n$ (u = 1 m/s, emission rate 1/s) emission height 160 m, KNRC site

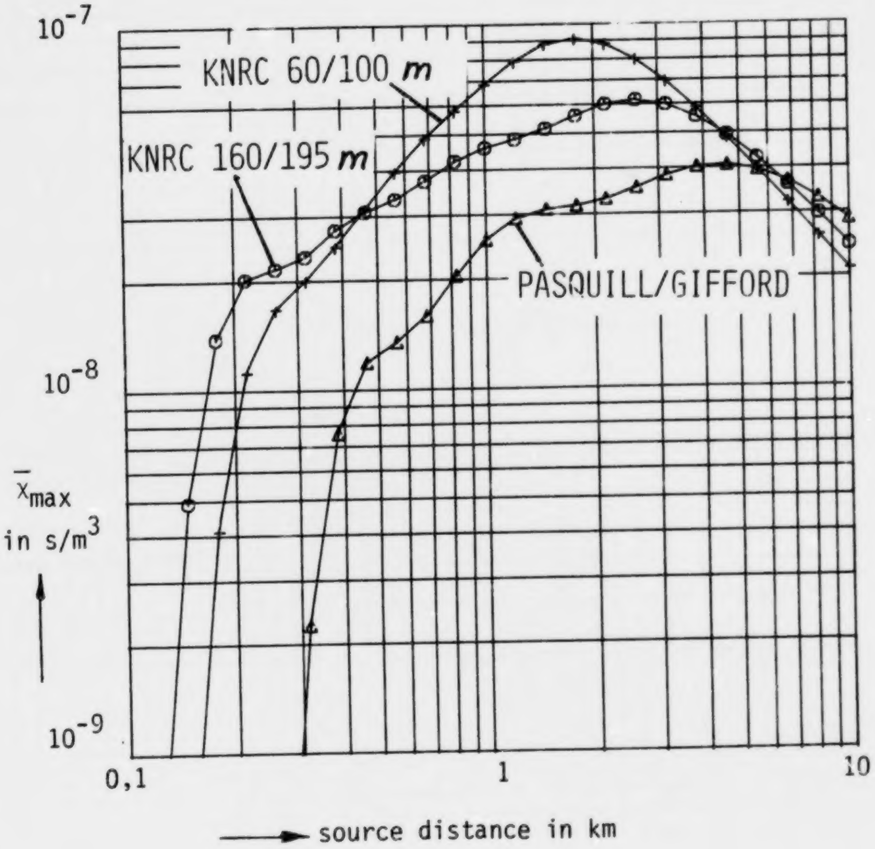

Fig. 3 Maximum long-term diffusion factor $\overline{\chi}_{max}$ emission height 160 m, KNRC site, different σ_y-, σ_z-curve families

Discussion:
(Rapporteur: Henderson-Sellers)

Bultynck:

Is the high slope value for σ_z for categories A and B for releases between 160 and 195 m a result of depletion of material?

Hübschmann (response):

No, the tracer used here is a non-reactive gas CF_2Br_2 and, in a similar way to SF_6, does not suffer such depletion.

Smith:

To what distance from the source did your measurements extend in your evaluation of A and B stability categories?

Hübschmann (response):

This depend upon the distance of the predicted maximum. The data were obtained for A and B stability in a distance of up to 3000m. For C, D and E stability the network extended to greater distances.

Steenkist:

Can you tell me how the stability was defined?

Hübschmann (response):

There are many ways of obtaining an evaluation of the stability e. g. estimates of σ_y, σ_z; the temperature gradient; the wind velocity profile; synoptic observations. These different definitions do not give the same value, then we must take the estimates of σ_z, σ_θ

TESTS ON ATMOSPHERIC DIFFUSION WITH TRACERS IN A URBAN AREA

by

D. Camuffo
CNR Laboratorio Chimica e Tecnologia Radioelementi, Padova (Italy)

M. De Bortoli and P. Gaglione
JRC EURATOM, Chemistry Division, Ispra (Varese, Italy)

Abstract. Some tracer experiments were carried out at Venice during autumn and winter. The release was made both in the centre of the city and a few kilometers offshore. The concentration values inside the city were not homogeneous and pointed out three different behaviours of the airflow depending on the intensity of the local ventilation, as follows:

i) during calm to light air the tracer showed two ways in crossing the city on two separate paths: the first is through a very short path determined by the irregular topography; the second is characterized by a wavy trajectory on a vertical plane when the air is passing over the city;

ii) during light breeze the tracer follows three different paths: the first one, as in the previous case, through the narrowest extension of the city; the second and the third are determined by the meandering of the Grand Canal;

iii) during fresh breeze the paths are initially the same as in the preceding case but afterwards, the channeling of the air masses operated by the Grand Canal causes a strong decrease in the concentration levels.

Introduction

Little is known today about the transport and dispersion of pollutants in the Venetian area and in particular over the Lagoon. In practice there are many indications that the mesoscale circulations are of capital importance in transporting pollutants from nearly located industrial complexes. However the Lagoon cannot be simply considered an intermediate transition zone between land and sea, but is characterized by different roughness and behaves alternatively as a source or a sink of heat, with some spectacular effects, specially during winter when the destabilization of the overflowing air masses is accomplished with the most important pollution episodes in Venice. Some campaigns have been conduced in order to investigate the three dimensional structure of the local circulation, the exchange of heat and moisture, the thermal and dynamical stabilities of the atmosphere and their role in transporting and dispersing pollutants. However, due to the complexity of the site and of the great number of phenomena which may interfere, some situations may be indicated as very typical from the diagnostic point of view; from the prognostic one it seems to be hazardous in forecasting the pollution levels.

The aim of this paper is to present the results of some tracer experiments carried out at Venice during autumn and winter with the SF_6 tracer technique. The releases were made both in the centre of the city, on the top of a building 20 m tall (about twice the height of the environmental bouildings), and a few kilometers offshore from a boat in the Lagoon, according with the two main dominant wind directions. The most important winds in Venice are the northeastern Bora and the southern Scirocco with many variations due to the barrier effect of the Alps. The local circulations and the Scirocco are light or gentle whereas

Preceding page blank

the Bora is generally a fresh to gale wind. However the more frequent winds are due to the barrier effect of the Alps and have the same direction of the Bora, but are weaker. Locally these winds are commonly named "Borino", which literally means "weak Bora". Again, the nocturnal circulation and the sea breeze are almost perpendicular between them and have approximately the same directions as the above named winds. As a consequence the frequency distribution of the wind direction is largely distributed about these two directions. By reason of this situation we decided to carry out the tracer experiments in presence of light winds from these directions and also during fog or haze, since in these conditions the most important pollution episodes are reached. Since we are not interested on the transport of the SF_6 outside of the city, in the following we will deal only with the cloud of the tracer which has crossed the city.

Experimental details and results

The tracer experiments were carried out with sulphur exafluoride (SF_6) for the following characteristics: no toxicity, lack of odour, colour and taste, no fire hazard; high thermal stability (up to 600°C); chemical stability towards hydrolysis, oxidation and photolysis; simple and rapid gas-chromatographic determination down to very low concentrations; low atmosphere background. The release was directly made from a cylinder, by controlling the emission rate with a rotameter. Accurate determinations of the released SF_6 were carried out by weighing the cylinders before and after each release. Air was sampled in different points of a downwind sector (as indicated in the map in Figure 1 and in Tables 1 and 2) into plastic bags (SARAN) by means of small battery (4.5 V) operated pumps and then analyzed by gas-chromatography.

The analytical technique is very sensitive, with a detection limit around 10^{-12} volumes of the tracer per volume of air (about 10 ng/m^3). As the SF_6 background in the region is of the same order, the confidence limit was fixed at 30 ng/m^3. The calibration of the apparatus was performed by means of static mixtures as well as through the exponential dilution technique. The precision of the measurements, in terms of standard deviation, is approximately 1%. The time required for the analysis has no effect on the stability of the SF_6 in the bags, as established by tests described elsewhere[1].

The main data concerning the experiments and the SF_6 concentration levels (CL) measured during each test are reported in Table 1 and in Table 2,respectively. A detailed description of the meteorological conditions during the field tests can be found in refernce[2]. In the following the data of Table 2 will be shown in the Figures relative to each field test. Of course the Figures will suffer of the necessary interpolation in drawing the isolines in order to give a useful aid to their understanding. A more accurate definition of the isolines would require a network with much more sampling points. However the actual network is sufficient in order to point out the main features of the diffusion processes in Venice.

Discussion of the results: October field tests

October 15th, 1974.

Wind direction ENE, light breeze (2.5 m/sec). Cloud cover: 3/8 Sc and 4/8 Ac. Map of the CL in Figure 2.

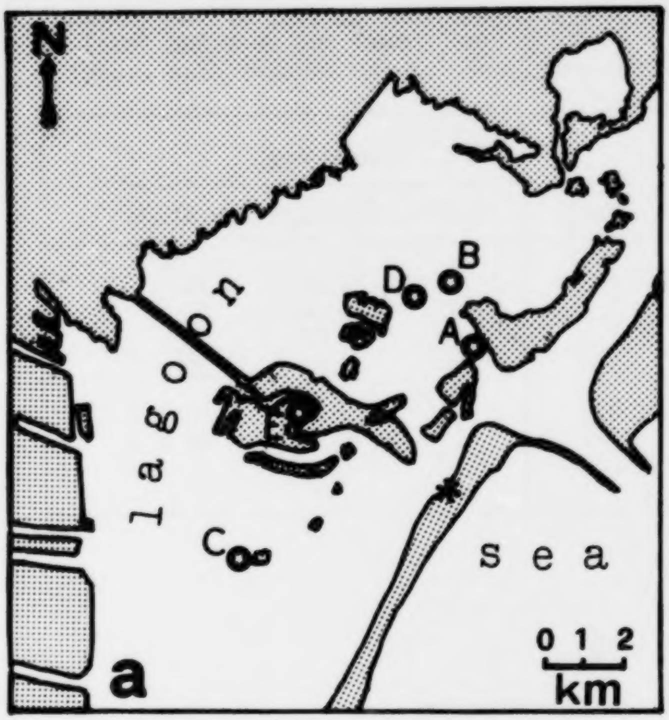
N
B
D
A
E
C
l a g o o n
s e a
0 1 2
km
a

Figure 1 Map of the Venetian area (a). The letters A,B,C,D,E indicate the points where the tracer was released (see Table 1). The sampling network in Venice is evidenced in the magnificated map in the bottom (b). The numbers corresponding to the sampling points are specified in Table 2. The 38th sampling station is external to this map and is shown with an asterisk on the reduced map (a). For the January case studies we will report only the piece of map enclosed in the rectangle in (b).
It should be noted that Venice has a very complicated network of small channels and streets which cannot be represented in this scale.

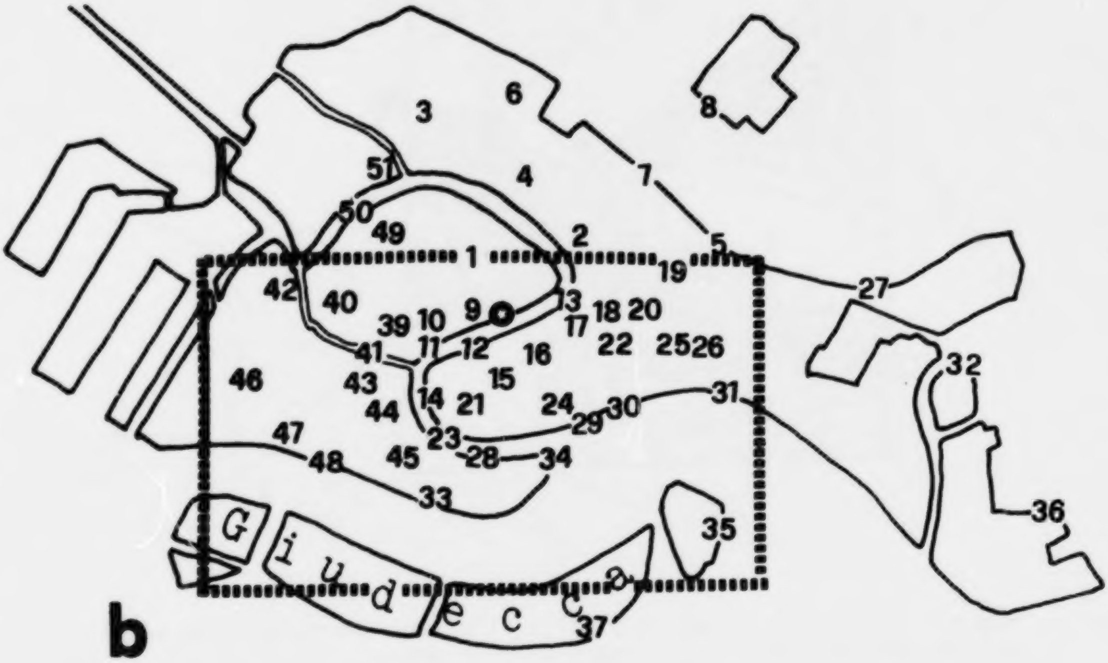
3
6
8
51
4
7
50
49
2
5
1
19
27
42
40
13
18
20
39
10
9
17
41
11
12
16
22
25
26
32
46
43
15
44
14
21
24
29
30
31
47
23
48
45
28
34
33
36
35
G i u d e c c a
37
b

Table 1. SF$_6$ tracer experiments (October 1974 and January 1975). For each field test there are reported: date, site (shown in Figure 1), starting time (hour), duration (min) and emission rate (g/sec) of the release ; number of sampling points, starting time (hour) and duration (min) of the sampling (two consecutive samplings for the January case study).

date	release				sampling		
	site	starting	duration	rate	points	starting	duration
15 Oct	A	14.30	60	2.2	21	15.00	20
16 Oct	B	8.30	55	5.2	20	9.00	20
17 Oct	C	14.00	60	4.7	19	15.00	20
18 Oct	D	8.25	50	5.0	19	9.00	20
14 Jan	E	9.15	45	0.5	17	9.30	15 x 2
15 Jan	E	9.15	45	1.6	23	9.30	15 x 2
16 Jan	E	9.15	45	1.0	22	9.30	15 x 2

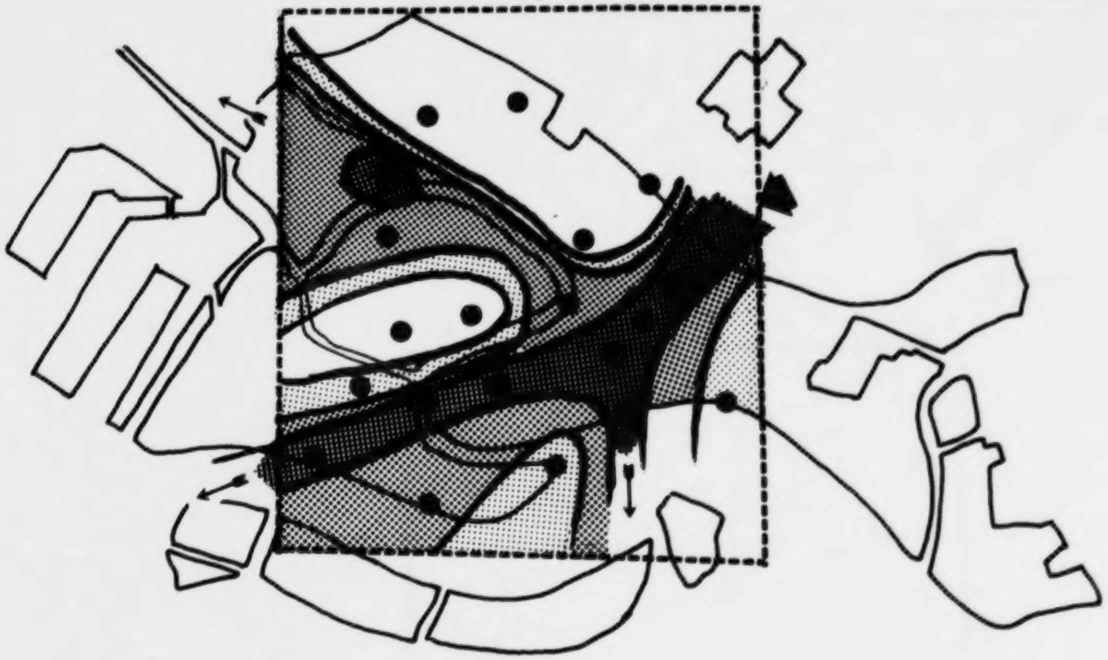

Figure 2. Map of the CL for October 15th,1974. The dots represent the sampling points and the square the limits of the network. The density of the shadings is related to the CL. For the actual values see Table 2. The large arrow shows the wind direction; the smaller ones the three paths.

Table 2. SF_6 concentration levels (CL in $\mu g/m^3$) measured at the sampling points indicated in Figure 1 during the experimental campaigns (Oct 74,Jan 75)

sampling point	date of the experimental campaign							
	15 Oct	16 Oct	17 Oct	18 Oct	14 Jan*	14 Jan**	15 Jan***	16 Jan***
1	-	0.40	-	-	-	-	-	-
2	0.05	0.05	0.40	udl***	-	-	-	-
3	0.25	-	-	-	-	-	-	-
4	-	0.06	-	-	-	-	-	-
5	-	-	-	0.85	-	-	-	-
6	0.17	0.15	-	-	-	-	-	-
7	0.15	0.26	-	0.60	-	-	-	-
8	-	3.8	-	0.11	-	-	-	-
9	0.24	udl	110	0.26	-	-	-	-
10	-	-	-	-	-	-	-	0.27
11	-	-	-	-	-	-	76	161
12	-	-	-	-	0.63	0.63	25	35
13	1.7	1.7	0.40	0.40	7.5	4.1	-	-
14	4.0	0.05	0.23	-	-	-	19	22
15	5.0	0.05	0.25	-	9.0	4.1	40	2.3
16	-	-	-	-	13.5	0.10	3.8	0.20
17	-	-	-	-	1.7	6.6	0.60	-
18	-	-	-	-	0.32	0.25	-	-
19	5.2	0.80	-	0.17	-	-	-	-
20	6.0	0.12	0.46	-	0.70	0.55	-	-
21	-	-	-	-	8.0	0.85	1.7	3.3
22	6.5	0.65	0.07	udl	udl	80	0.26	-
23	-	-	udl	-	-	-	-	28.5
24	-	-	-	-	5.0	0.55	0.47	-
25	-	-	-	-	0.34	udl	2.0	-
26	-	-	0.13	0.60	-	-	-	-
27	-	-	-	0.07	-	-	-	-
28	-	-	-	-	80	1.0	1.4	-
29	-	-	-	-	1.3	0.25	11.6	0.49
30	4.4	1.23	0.10	0.25	2.5	0.10	1.2	0.50
31	0.95	-	4.1	-	0.16	0.10	udl	-
32	-	-	-	udl	-	-	-	-
33	1.8	0.55	2.6	-	0.07	1.0	1.3	25
34	0.85	0.80	0.26	0.26	0.22	0.60	35	9.3
35	-	-	12	-	-	udl	-	-
36	-	-	-	0.09	-	-	-	-
37/a*	-	-	0.55	-	-	-	-	-
37/b*	-	-	28	-	-	-	-	-
37/c*	-	-	0.30	-	-	-	-	-
37/d*	-	-	udl	-	-	-	-	-
38	-	-	-	0.51	-	-	-	-
39	0.24	0.28	2.7	udl	-	-	-	1.1
40	-	-	-	-	-	-	-	8.6
41	-	-	-	-	-	-	-	3.6
42	-	-	0.65	0.78	-	-	-	-
43	0.90	0.11	0.42	2.80	-	-	-	0.10
44	-	-	-	-	-	-	-	0.14
45	-	-	-	-	-	-	0.25	37.2

Table 2 (continued)

point	15 Oct	16 Oct	17 Oct	18 Oct	14 Jan*	14 Jan**	15 Jan***	16 Jan***
46	-	-	-	-	-	-	-	0.10
47	-	-	-	-	-	-	-	0.15
48	4.9	0.05	-	-	-	-	0.09	0.05
49	1.8	0.05	-	-	-	-	-	0.05
50	-	-	0.13	-	-	-	-	-
51	5.4	0.05	-	-	-	-	-	-

Notes to Table 2 :

* CL measured during the first sampling, between 9.30 and 9.45 LT

** CL measured during the second sampling, between 9.45 and 10.00 LT

*** The reported values of CL are the mean of the two consecutive samples

*** udl = under detection limit i.e. 0.03 $\mu g/m^3$

* A vertical profile was performed over the station 37 and the labels a,b,c,d refer to ground level, 50 m, 100 m, 150 m, respectively.

When arrived close to Venice, the cloud was sucked in a very narrow path, located over the line of less resistance in crossing the city. The cloud was then divided by the urban topography into three paths:

i) the first one crossed the city from NNE, utilizing the shortest path;

ii) the second was channeled by the two branches of the Grand Canal, parallel to the actual ENE wind direction. On the two branches two fresh airflows, induced by the reduced roughness, diluted the SF_6 CL and practically limited the lateral expansion of the cloud. This path left Venice through the Giudecca's outlet and may be considered in the actual meteorological conditions as the 2nd line of less resistance through the city;

iii) the third path was due to the suction of the SE branch of the Grand Canal, which flows at NW into the Lagoon with a wide mouth. This path may be considered as both the diffusion of a plume channeled by the Grand Canal, and as the local downdraft associated with the horizontal vortex due to the canyon effect of the Grand Canal on the overlying free stream, almost perpendicular and with a higher concentration of SF_6.

October 16th, 1974.

Wind direction NE, fresh breeze (Borino 9 m/sec). Cloud cover 8/8 Cu. Map of the CL in Figure 3.

The wind, stronger than in the previous day, forced the cloud to enter the city from the same gate, but caused a different behaviour inside the city on three paths:

i) the first and shortest path remained substantially unchanged;

ii) the second seemed to be particularly influenced by the ENE branch of the Grand Canal, in two ways: (a) the Grand Canal appeared to be sucking the cloud through the buildings in the first part of the path; and (b) once over the Grand Canal, the airflow was straightforwardly channeled and the increase in wind speed due to the reduction in roughness caused an abrupt and strong dilution of the tracer;

iii) the third path seemed to follow the behaviour over the 2nd branch of the Grand Canal, due to the increased ventilation and horizontal vortex-type motion.

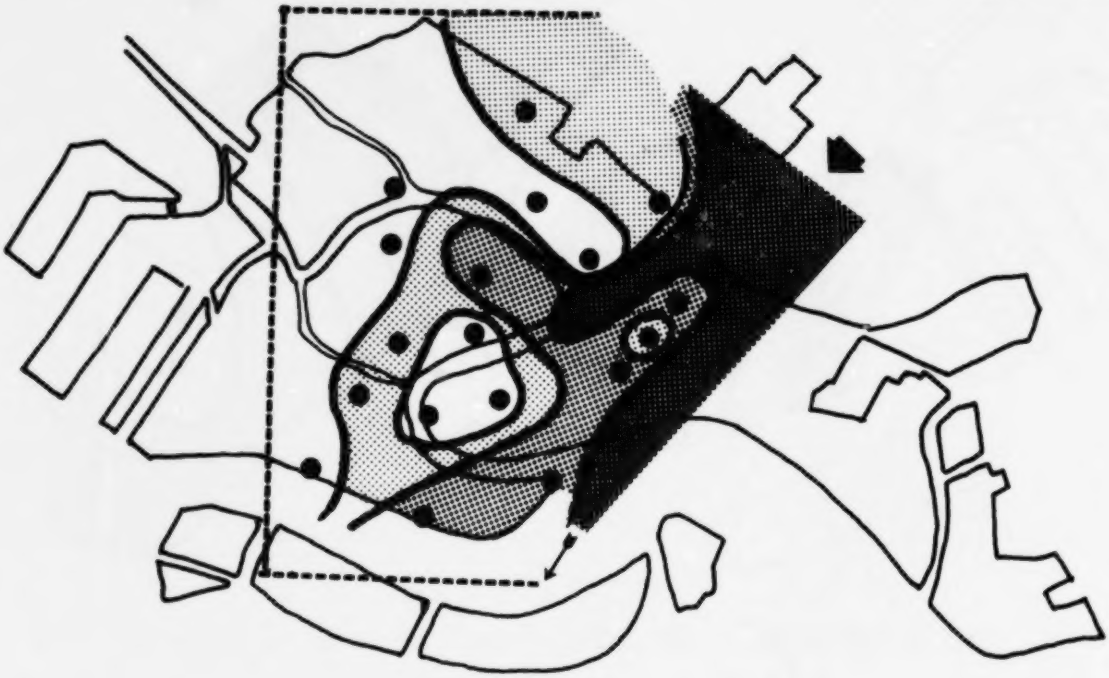

Figure 3. Map of the CL for October 16th, 1974. Symbols as in Figure 2

October 18th, 1974.

Wind direction NE, calm to light air (0 - 1 m/sec). Cloud less sky. Map of the CL in Figure 4.

The ventilation was ranging between calm and light air and the airflow changed character as reported in literature[3] when the wind velocity sinks below 2 m/sec. The cloud entered the city through the same gate which was proved to be dependent only on the wind direction (i.e. this gate is for winds of the 1st Quadrant only) and not on speed.

The first shortest path was unchanged; the direction of the second path still remained but the cloud crossed the city by following a wavy path. It is to be noted that the smallest and widest maximum is in the centre of the city, where the ENE branch of the Grand Canal causes a dilution and a broadening of the CL. The horizontal wave lenght λ (of the order of 1000 m) was determined by the natural subdivision of the Venetian topography, operated by the meandering of the Grand Canal, whose width is about 60 m. A cross section of the CL along the second path is reported in Figure 5 which clearly shows the wavy character of the CL.

This wavy path is recurrent when, as in the 17th, the meteorological conditions favour the formation of some heat islands in a somewhat organized regime over the city which appears as a "heat archipelago". Of course a fresh wind destroys this situation and leads to the diffusion previously described. Further evidence of this wavy diffusion was given by the spectral analysis of SO_2 CL carried out at Venice during similar meteorological situations[4].

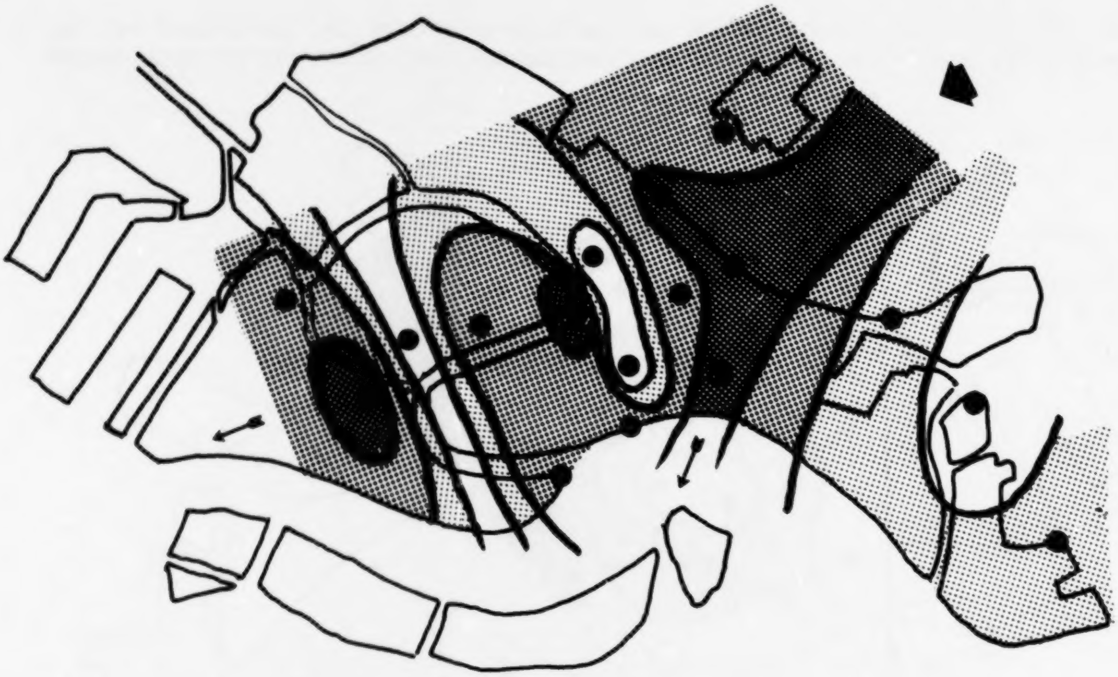

Figure 4. Map of the CL for October 18th, 1974. Symbols as in Figure 2.

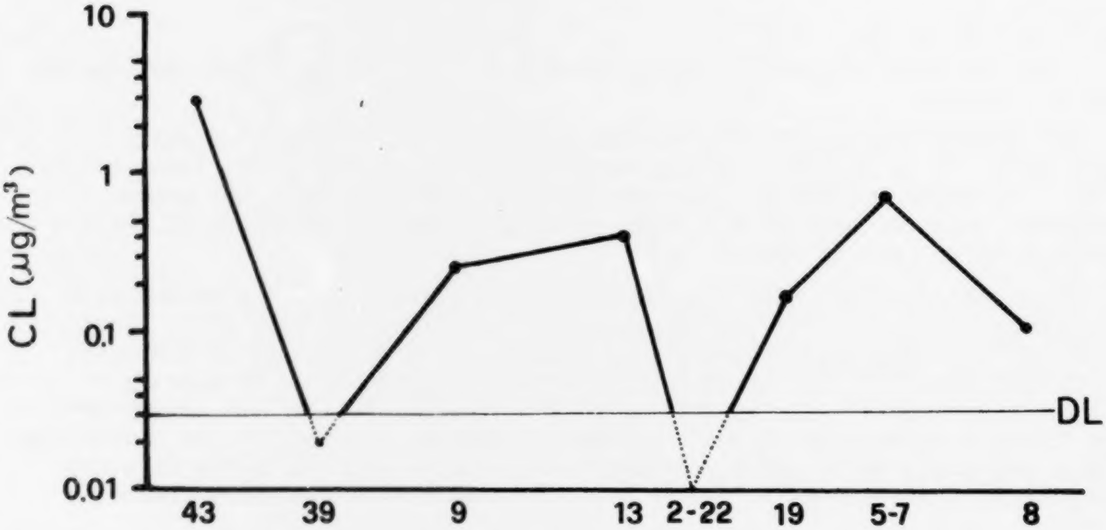

Figure 5. Cross section of the CL (in ordinate, logarithmic scale) along the wavy path over Venice, measured at ground level. The wind is blowing from right like in Figure 4. The numbers in ascissa indicate the sampling stations shown in Figure 1. In this Figure the measured CL are reported : the values under the quoted detection limit DL are indicated with lighter symbols.

In fact in presence of light air and especially during foggy conditions, the spectrum presents three typical periods, namely 15', 25', 45'. The last is due to the fluctuating wind speed. The others to the organized pluming regime over the city. If the frequency of starting of thermals is supposed to be associated with the updrafting velocity, so that a convective cell develops when the preceding one is exausted, the two updrafting velocities $w_1 = 0.22$ and $w_2 = 0.13$ m/sec are obtained.

October 17th, 1974.

Wind direction S, calm to light air (0 - 1 m/sec). Fog just dispersed; cloud cover: 3/8 Ci. Map of the CL in Figure 6.

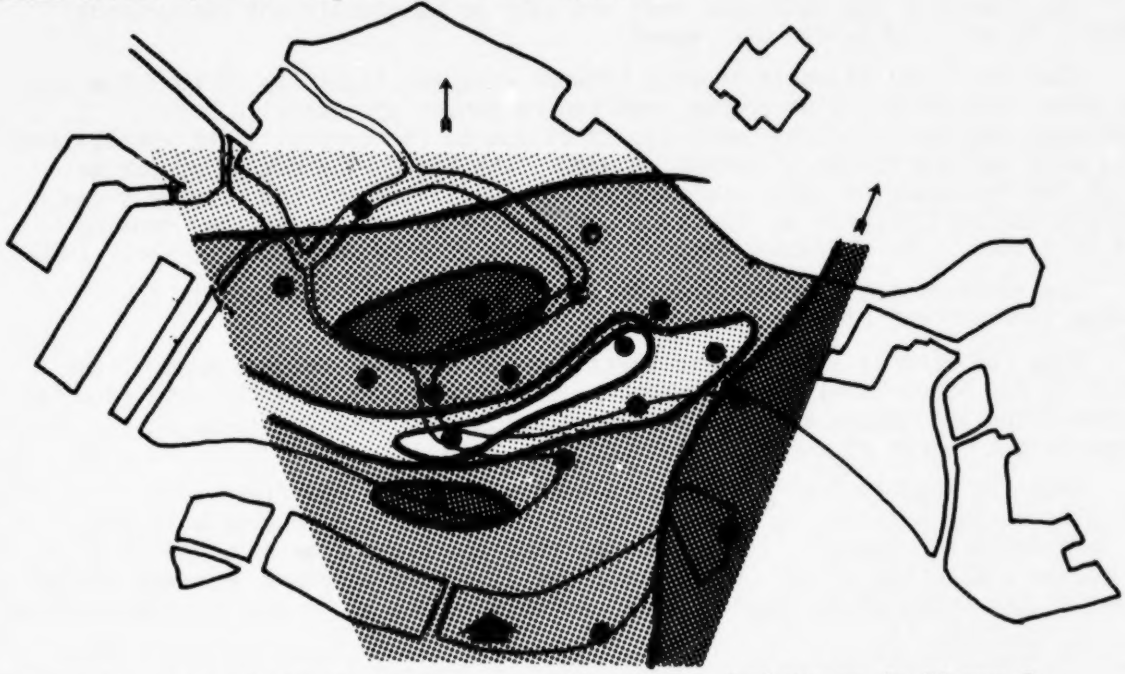

Figure 6. Map of the CL for October 17th, 1974. Symbols as in Figure 2.

In this case study, the transport was due to the southern sea breeze which was very light and retarded, due to the presence of fog in the morning. Of course the pattern with wavy character is the same as in the 18th, except for the direction.

The cloud of SF_6, when facing Giudecca, was divided into two plumes which crossed the city. The first one outflanked the first barrier of islands and entered the city by crossing it directly by way of the shortest path; the second one with wavy character was the result of the transport of the very light ventilation and of the cells over the city.

The three dimensional structure of the wavy character was pointed out by the measurement on the vertical of the SF_6 CL sampled at ground level, 50 m, 100 m and 150 m by means of a captive balloon over the station 37 (see Figure 1 and Table 2). The maximum concentration was at 50 m and not at ground level, as should be required by a mirror reflection on a Gaussian distribution.

The shortest path remained still unchanged, except for the direction.

Unfortunately we could not measure the SF_6 CL on the northern side of the city, where the last oscillation of the CL is expected.

Some remarks on the case studies with release on the Lagoon about 5 Km from Venice (October field tests)

Even if the network could not be satisfactorily extended over all the city and the measurements were carried out only during day (in convective regime), the analysis of the data was able to point out some topics, supported also by different measurements, as follows:

The transport and diffusion over the city is absolutely not homogeneous and occurs as dictated by the wind speed.

When the ventilation is ranging between calm and light air (0 to 1.5 m/sec) the somewhat organized cellar regime over Venice (which appears as a heat archipelago) together with the small transport due to the general light ventilation, cause a wavy pattern of the pollutant CL over the city. The maxima appear as spots at the beginning of each zone, due to the subdivision of the city by urban topography and particularly by the Grand Canal. The minima are at the downwind end of each zone. The characteristic wavelenght λ of this wavy path is about 1 Km.

The shortest path across the city is crossed in this case and in the following, independent of wind speed.

When the wind is light breeze (over 2 m/sec but well below 9 m/sec), the branches of the Grand Canal generate some preferential paths into the city (due to both channeling and canyon effects). We have documented three of these, corresponding to winds of the 1st Quadrant.

When the wind is fresh breeze (9 m/sec in the described field test, practically during Borino), the behaviour outlined in the previous case is still valid in principle. However, if we consider that the flux of mass sucked from above causes a dilution of the CL at ground level, the convergence operated by the branches of the Grand Canal cause a local decrease in CL, as opposed to the previous case.

Discussion of the results: January field tests

January 15th, 1975.

Northern wind direction; calm to light air. Fog. Map of the CL in Figure 7.

During the January case studies the release of SF_6 was made exactly in the center of the city, in order to point out the diffusion of the urban sources. The network was practically limited to the downwind half of the city.

January 15th was characterized by fog and northern light air which are often associated with severe pollution episodes in Venice.

The data analysis outlined two preferential ways for the diffusion:

i) the first one, according to the small channels and streets straightforwardly aligned with the source and the wind direction;

ii) the second one following the cavity of the branch of the Grand Canal, approximately perpendicular to the wind direction, but with an angle slightly greater than 90 deg, caused the air to move with a slow helicoidal motion and with a poor exchange. When this branch bends southward abruptly, becoming aligned with the wind, the increased ventilation causes a sharp decrease in the CL.

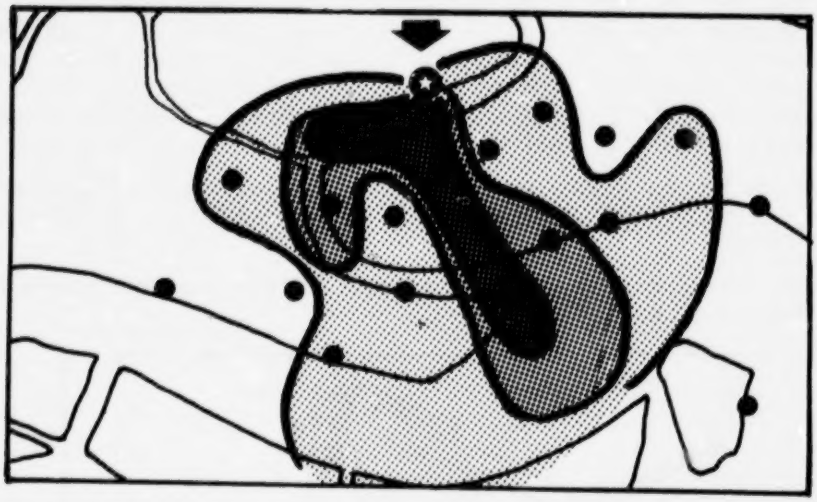

Figure 7. Map of the CL for January 15th, 1975. Symbols as in Figure 2.

January 16th, 1975.

Wind direction from the 1st Quadrant, light breeze (3 m/sec). Fog just dispersed; cloud cover: 6/8 St. Map of the CL in Figure 8.

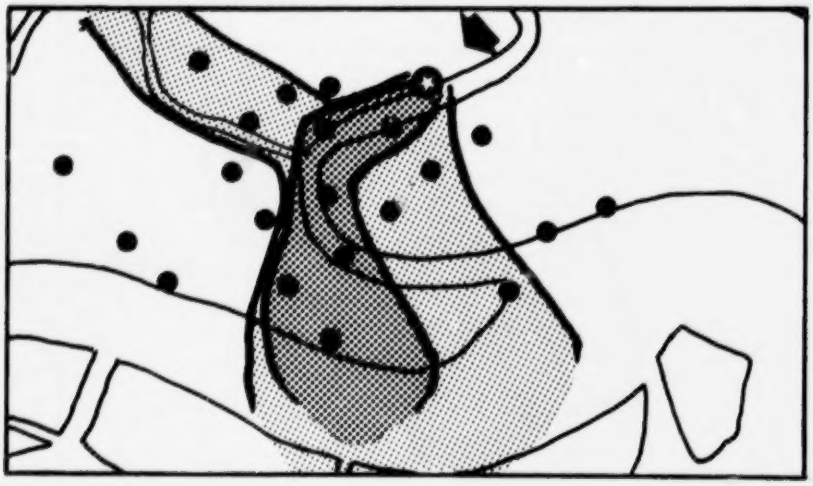

Figure 8. Map of the CL for January 16th, 1975. Symbols as in Figure 2.

The slightly more intense ventilation causes a different pattern for the diffusion, principally due to the different resistance caused by vortexes in the small streets and channels. Thus the aerodynamics seems to allow the diffusion only in the branches of the Grand Canal (where the horizontal vortex type motions assume a greater importance) and ignores the smallest channels and streets, only with a few exceptions for the largest ones.

The cloud follows the approximately perpendicular branch of the Grand Canal but at the named hairpin bend shows a Y shaped path. The first branch begins by following the new branch of the Grand Canal, but ends in some large channels aligned with the wind direction. The second branch, with lower CL, follows some channels which join another branch of the meandering Grand Canal and which allow for a small component of the original wind vector.

This situation presents some analogies to the field test of October 15th.

January 14th, 1975.

Light breeze (0 - 3 m/sec) variable generally from the 3rd Quadrant. Fog. Map of the CL in Figure 9 ab.

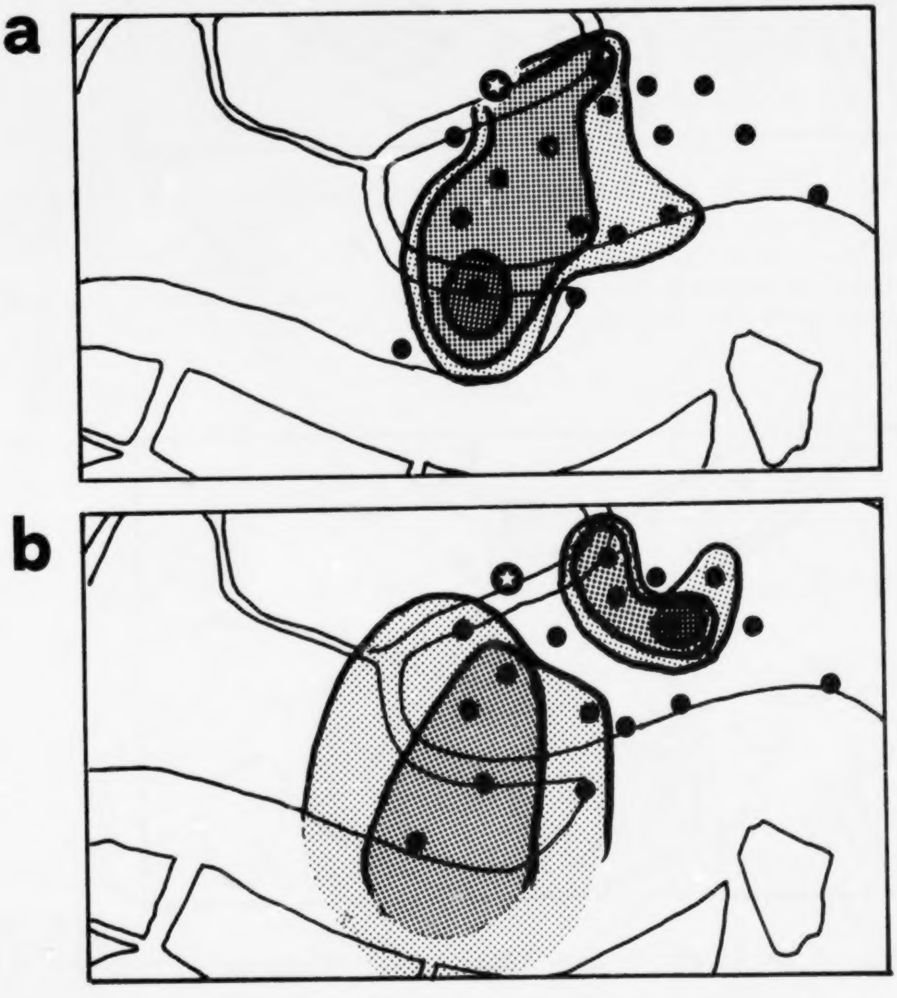

Figure 9. Map of the CL for January 14th, 1975. Symbols as in Figure 2. The figures a, b refer to the two consecutive partial samplings.

The meteorological conditions are typical of the worst pollution episodes from the industrial area. The wind field is irregular and combines with the cellar motions due to the thermal convection over the warm surface of the Lagoon and over the urban heat island. With an acoustic sounder the thermal pluming has been proved to reach 150 - 200 m in the outer fringes of Venice. The result is an alternance of light breeze and short calms, when the cellar effects are more enhanced. This situation leads to the formation of concentrated puffs near the source and results in their subsequent rapid translation and dispersion.

After these remarks, the time history of the tracer can be well understood, as opposed to the overall result of the two samplings (as made for January 15th and 16th), in the sequence of the two consecutive partial samplings (shown in Figure 9a and 9b respectively), whith a sampling period close to that of the cells during fog, namely 15'.

Some remarks on the case studies with release on the centre of the city (January field tests)

The January field tests were characterized by light winds and the fog was present or just dispersed. These conditions are often associated with severe pollution episodes in Venice.

The tracer was released in the centre of the city in order to evidence the behaviour in the urban emissions. In the first two cases the tracer was channeled by the urban topography into two paths with branches depending upon wind speed, due to the different aerodynamic effects of the buildings. In the latter case the tracer appeared as puffs diffused by the combined effect of the rooftop wind speed and thermal convection.

General conclusions

At the end of each experimental campaign we summarized the most outstanding features of the dispersion of the tracer inside the city. The dispersion appears to be chiefly determined by wind speed, urban topography and convective regime over the city. From the qualitative point of view, this may seem an obvious statement and the generally used diffusion equations appear to be deprived of their meaning. However, a quantitative analysis of the data allows to divide the wind speed into classes and to associate to each class a definite behaviour to the dispersion; nevertheless, a detailed forecast of the pollution at Venice seems at now to be comparable to forecast the face on which a dice will fall.

From these measurements it can be noted that the usual models cannot simply be adopted for Venice. In fact this city is characterized by many special effects which must be separately considered. So, further measurements seem to be desirable in order to improve the knowledge of the basic processes and the behaviour of a pollutant inside this peculiar city.

References

1. M. De Bortoli, P. Gaglione and E. Pecchio, "L'esafluoruro di Zolfo come tracciante atmosferico", EUR 5429 i, Ispra, 1975.
2. D. Camuffo, "Fog and related diffusion potentials at Venice: two case studies" Boundary Layer Meteorology (in press).
3. A. Stern, "Air Pollution" 3rd Edit., Vol I, Academic Press, N. Y., 1976.
4. D. Camuffo and L. Cavaleri, "Diffusive processes on offshore cold flows pointed out by spectral analysis of air pollutant concentrations", in preparation.

Discussion:

Steenkist:

A heat island pattern has two cells, yet in your diagram there is only one resulting maximum.
How is this explained?

Camuffo (response):

Venice is not a simple heat island, consisting of many different and interacting heat island effects due to the "fragmented" nature of the city resulting in irregular topography.

Benjamin:

At what height were the samples taken?

Camuffo (response):

At a height of 1.5 m. At only one station were measurements taken at other heights: at 50, 100 and 150 m.

Steenkist:

How is the stability measured?

Hübschmann (response):

The stability is determined with different methods we have ΔT, σ_ϕ, σ_θ etc. When the stability determined with the different methods are not according, we take σ_ϕ.

Steenkist:

A heat island pattern has two cells. In the figure is only one maximum. How can this be explained?

Camuffo (response):

This must be because the pattern over the town is a combination of different heat island effects.

AN EXTENSION OF THE GAUSSIAN PLUME MODEL FOR THE CASE OF CHANGING WEATHER CONDITIONS

by

K.J. Vogt, J. Straka, H. Geiß
Kernforschungsanlage Jülich GmbH

Abstract. The Gaussian normal distribution is widely used for describing the atmospheric diffusion because of its simplicity, although its conventional form can be applied only in case of constant weather conditions. An extension for the case of changing weather conditions during the transport time, will be discussed in this paper. For the case of changing weather conditions a "volume-source-model" for the diffusion of a single puff has been developed yielding a more general Gaussian formula. For continuous releases an "area-source-model" has been introduced for constant wind direction. For the treatment of plumes under changing wind direction the plume has to be subdivided into a number of puffs, each of which follows its own trajectory and can be described by the volume-source-model. Finally a comparison of these generalized models with the conventional Gaussian model has been performed.

1. Diffusion of puffs under changing weather conditions

It has been shown in the literature (1,2) that the concentration distribution in the environment resulting from a puff, i.e. an instantaneous release, from an elevated point source can be described by the Gaussian diffusion equation

$$\chi(x,y,z,t) = \frac{Q}{(2\pi)^{3/2}\sigma_x\sigma_y\sigma_z} \exp\left\{-\frac{(x-\bar{u}t)^2}{2\sigma_x^2} - \frac{y^2}{2\sigma_y^2}\right\} \times \left\{\exp\left[-\frac{(z-H)^2}{2\sigma_z^2}\right] + \exp\left[-\frac{(z+H)^2}{2\sigma_z^2}\right]\right\} \quad (1)$$

σ_i = diffusion parameters, $i=x,y,z$
H = release height
Q = source strength
$\bar{u}$ = average wind velocity
t = travel time

This equation, which on the one hand results from the statistical theory of turbulent diffusion and on the other hand is a solution of the Fickian diffusion equation, has been widely used for environmental exposure modeling because of its simplicity, though there are some theoretical shortcomings. One of the main problems, concerning the correct determination of the diffusion parameters, will be dealt with later.

Evidently eq. (1) is valid only for constant weather conditions, which will generally apply only for local calculations. For regional analyses, because of longer transport times, usually a variation of wind velocity, wind direction and diffusion category has to be considered. In order to extend the conventional diffusion equation eq. (1) to the case of changing weather conditions we have therefore developed a so called "volume-source-model". The principal idea of this model is that, provided that the wind velocity components u_x and u_y and the diffusion parameters σ_x, σ_y and σ_z are known for consecutive time intervals Δt_k (e.g. hours), the concentration distribution in each time interval can be calculated by a superposition of the infinitesimal contributions of all volume elements at the end of the preceding time interval, which are considered as point sources for the diffusion calculation with the new weather conditions. The source strength of these point sources

$$dQ(x_k,y_k,z_k,t_k) = \chi_k(x_k,y_k,z_k,t_k)\,dxdydz \tag{2}$$

resulting from the diffusion calculation in the k-th time interval, has to be inserted into the diffusion equation for the (k+1)-th time interval

$$\begin{aligned} d\chi_{k+1}(x,y,z,t) = {} & \frac{dQ(x_k,y_k,z_k,t_k)}{(2\pi)^{3/2}\sigma_{x,k+1}\sigma_{y,k+1}\sigma_{z,k+1}} \\ & \times \exp\left\{-\frac{[x-x_k-\bar{u}_{x,k+1}(t-t_k)]^2}{2\sigma^2_{x,k+1}} - \frac{[y-y_k-\bar{u}_{y,k+1}(t-t_k)]^2}{2\sigma^2_{y,k+1}}\right\} \\ & \times \left\{\exp\left[-\frac{(z-z_k)^2}{2\sigma^2_{z,k+1}}\right] + \exp\left[-\frac{(z+z_k)^2}{2\sigma^2_{z,k+1}}\right]\right\} \end{aligned} \tag{3}$$

By spatial integration, which can be performed analytically, as we have demonstrated in a previous publication (3), we obtain again a Gaussian normal distribution, which represents the concentration in the puff in the (k+1)-th time interval. As has been demonstrated in detail, beginning with the concentration distribution at the end of the first time interval, after (n-1) iterations of the procedure we get the concentration of the puff in the n-th time interval

$$\begin{aligned} \chi_n(x,y,z,t) = {} & \frac{Q}{(2\pi)^{3/2}\sigma_{x,eff}\sigma_{y,eff}\sigma_{z,eff}} \left\{\exp\left[-\frac{(z-H)^2}{2\sigma^2_{z,eff}}\right] + \exp\left[-\frac{(z+H)^2}{2\sigma^2_{z,eff}}\right]\right\} \\ & \times \exp\left\{-\frac{[x-\bar{u}_{x,n}(t-t_{n-1})-\sum_{k=1}^{n-1}\bar{u}_{x,k}(t_k-t_{k-1})]^2}{2\sigma^2_{x,eff}} - \frac{[y-\bar{u}_{y,n}(t-t_{n-1})-\sum_{k=1}^{n-1}\bar{u}_{y,k}(t_k-t_{k-1})]^2}{2\sigma^2_{y,eff}}\right\} \end{aligned} \tag{4}$$

The effective diffusion parameters $\sigma_{i,eff}$ result from the diffusion parameters $\sigma_{i,k}(t)$ prevailing in the n time intervalls

$$\sigma^2_{i,eff} = \sum_{k=1}^{n} \sigma^2_{i,k} \qquad (i=x,y,z) \tag{5}$$

The time-integrated concentration (sometimes named "dosage"), divided by the source strength Q, is the so called diffusion factor

$$\tilde{\chi}_n(x,y,z) = \frac{1}{Q}\int_{-\infty}^{\infty} \chi_n(x,y,z,t)\,dt$$

$$= \frac{\exp\left[-\frac{(z-H)^2}{2\sigma^2_{z,eff}}\right]+\exp\left[-\frac{(z+H)^2}{2\sigma^2_{z,eff}}\right]}{2\pi\,\sigma_{z,eff}(\bar{u}^2_{x,n}\sigma^2_{y,eff}+\bar{u}^2_{y,n}\sigma^2_{x,eff})^{1/2}} \tag{6}$$

$$\times \exp\left\{\frac{\{\bar{u}_{x,n}[y-\sum_{k=1}^{n-1}\bar{u}_{y,k}(t_k-t_{k-1})]-\bar{u}_{y,n}[x-\sum_{k=1}^{n-1}\bar{u}_{x,k}(t_k-t_{k-1})]\}^2}{2(u_{x,n}\sigma^2_{y,eff}+u_{y,n}\sigma^2_{x,eff})}\right\}$$

This equation has the disadvantage that the diffusion parameter in wind direction σ_x is required, which usually is not known. Therefore we developed an alternative trajectory model in which the wind direction first is kept constant and the diffusion factor is first calculated for the puff's gravity center moving along the x-axis. From eq. (6) then we obtain

$$\hat{\chi}^+_n(x,y,z) = \frac{\exp\left[-\frac{y^2}{2\sigma^2_{y,eff}}\right]\left\{\exp\left[-\frac{(z-H)^2}{2\sigma^2_{z,eff}}\right]+\exp\left[-\frac{(z+H)^2}{2\sigma^2_{z,eff}}\right]\right\}}{2\pi\,\sigma_{y,eff}\sigma_{z,eff}\bar{u}_n} \tag{7}$$

The wind direction changes are then taken into account by bending the originally straigth-line diffusion axis after the end of each time interval into the direction of the real trajectory as demonstrated in Fig. 1. By this procedure, we obtain

$$\hat{\chi}_n(x,y,z) = \frac{\exp\left[-\frac{\eta^2_n}{2\sigma^2_{y,eff}}\right]\left\{\exp\left[-\frac{(z-H)^2}{2\sigma^2_{z,eff}}\right]+\exp\left[-\frac{(z+H)^2}{2\sigma^2_{z,eff}}\right]\right\}}{2\pi\,\sigma_{y,eff}\sigma_{z,eff}\bar{u}_n} \tag{8}$$

where

$$\eta_n = \frac{1}{\bar{u}_n}\left\{\bar{u}_{x,n}\left[y-\sum_{k=1}^{n-1}\bar{u}_{y,k}(t_k-t_{k-1})\right]-\bar{u}_{y,n}\left[x-\sum_{k=1}^{n-1}\bar{u}_{x,k}(t_k-t_{k-1})\right]\right\} \tag{9}$$

is the crosswind distance from the trajectory. By setting $\eta_n=0$, we get the equation describing the trajectory in the n-th time interval

$$y = \frac{\bar{u}_{y,n}}{\bar{u}_{x,n}}\left[x-\sum_{k=1}^{n-1}\bar{u}_{x,k}(t_k-t_{k-1})\right]+\sum_{k=1}^{n-1}\bar{u}_{x,k}(t_k-t_{k-1}) \qquad (10)$$

The diffusion equation for changing weather conditions eq. (8) evidently has a similar form as the conventional diffusion factor resulting from eq. (1), with the exception, that $\bar{u}_n$ is the wind velocity in the n-th time interval and the effective diffusion parameters from eq. (5) have to be applied.

Since the anisotropy of the diffusion process in wind and crosswind direction (e.q. $\sigma_x \neq \sigma_y$) is neglected by rotating the puff into the new wind direction, before calculating the diffusion in the next time interval, as has been demonstrated by Fig. 2, eq. (8) yields only an approximation of the diffusion factor in eq. (6).

It can easily be shown that the relative error in applying the approximation formula eq. (8) instead of the correct formula eq. (6)

$$E = \left|\frac{\tilde{\chi}_n-\hat{\chi}_n}{\hat{\chi}_n}\right| = \left|(\cos^2\alpha_n+p\,\sin^2\alpha_n)^{1/2}-1\right| \qquad (11)$$

(calculated in the vertical plane of the trajectory) depends on the angle of wind direction in the n-th time interval and on the ratio of the horizontal diffusion parameters $p=\sigma_x/\sigma_y$. From Fig. 3, in which the error is shown as a function of α_n and p, it can be seen that for small angles α_n both the equations yield identical results. But even the maximum error, which occurs for $\alpha_n=90^{\circ}$, will not exceed 30%, if σ_x differs from σ_y by not more than a factor of 2. As the results of recent investigations performed by Lamb et al. (4) show that σ_x does not differ considerably from σ_y, the approximative formula eq. (8) can be used without limitation.

Finally the parametrization of the diffusion parameters has to be performed. According to Batchelor (5) the Gaussian normal distribution eq. (1) is a solution of the Fickian diffusion equation under the condition that

$$K_i(t) = \frac{1}{2}\,\frac{d\sigma_i^2(t)}{dt} \qquad (i=x,y,z) \qquad (12)$$

Since the Eddy diffusivities K_i are constant during each time interval with constant weather conditions the integration of eq. (12) yields

$$\sigma^2_{i,k} = \sigma^2_{i,k}(t_k)-\sigma^2_{i,k}(t_{k-1}) \qquad \begin{matrix}(i=x,y,z)\\(k=1,\ldots n)\end{matrix} \qquad (13)$$

That means, the diffusion parameter in the k-th time interval depends solely on the diffusion category and the travel time in this time interval. On the other hand we know that turbulent diffusion cannot be exactly described by the Fickian diffusion equation (6). From Taylor's theorem(7) we expect $\sigma_i \sim t \sim x$ for small travel times t or source distances x and $\sigma_i \sim \sqrt{t} \sim \sqrt{x}$ for long travel times or source distances. Field experiments on the other hand resulted in diffusion parameters being power functions of the source distance (cf. e.g. (8,9).

$$\sigma_{i,k} = p_{i,k}x^{q_{i,k}} = p_{i,k}(\bar{u}\cdot t)^{q_{i,k}} \qquad (i=y,z) \qquad (14)$$

Though these discrepancies are well known, the Gaussian formula eq. (1) is widely used because of its simplicity. This can be justified by the fact, that the empirically determined diffusion parameters, which have been adjusted to the Gaussian equation, compensate the error resulting from application of the Gaussian equation. Thus with the diffusion coefficients from eq. (12) we obtain

$$\sigma^2_{i,k} = p^2_{i,k}\{[\sum_{m=1}^{k}\bar{u}_m(t_m-t_{m-1})]^{2q_{i,k}}-[\sum_{m=1}^{k-1}\bar{u}_m(t_m-t_{m-1})]^{2q_{i,k}}\} \qquad (15)$$

or in the case of constant wind direction

$$\sigma^2_{i,k} = p^2_{i,k}\{x_k^{2q_{i,k}}-x_{k-1}^{2q_{i,k}}\} \qquad (i=y,z) \qquad (16)$$

2. Diffusion of a plume with constant wind direction

If a pollutant is continuously released under constant weather conditions from an elevated point source, the concentration in the plume is usually described by the stationary Gaussian normal distribution

$$\chi_c(x,y,z) = \frac{q\exp[-\frac{y^2}{2\sigma_y^2}]}{2\pi\,\sigma_y(x)\,\sigma_z(x)\,u}\{\exp[-\frac{(z-H)^2}{2\sigma_z^2}]+\exp[-\frac{(z+H)^2}{2\sigma_z^2}]\} \qquad (17)$$

As an extension of this formula for the case of changing wind velocity and diffusion category but constant wind direction we have developed a so called "area-source-model". As discussed in detail in our previous publication (3), in analogy to the "volume-source-model" the fluxes of the pollutant through the infinitesimal elements of a plane perpendicular to the diffusion axis at the end of a time

$$dq_k(x_k,y_k,z_k) = \bar{u}_k\chi_k(x_k,y_k,z_k)\,dydz \qquad (18)$$

are considered as release rates of point sources for the diffusion calculation in the next time interval with different wind velocity and diffusion category. By integration over the resulting contributions

$$d\chi_{k+1}(x,y,z) = \frac{dq_k(x_k,y_k,z_k)}{2\pi\sigma_{y,k+1}\sigma_{z,k+1}\bar{u}_{k+1}}\exp\left[-\frac{(y-y_k)^2}{2\sigma^2_{y,k+1}}\right]$$

$$\times\left\{\exp\left[-\frac{(z-z_k)^2}{2\sigma^2_{z,k+1}}\right]+\exp\left[-\frac{(z+z_k)^2}{2\sigma^2_{z,k+1}}\right]\right\} \qquad (19)$$

to the concentration in the next time interval, beginning with the first time interval, we obtain after n-1 iterations the concentration in the n-th time interval

$$\chi_n(x,y,z) = \frac{q\exp\left[-\frac{y^2}{2\sigma^2_{y,eff}}\right]\left\{\exp\left[-\frac{(z-H)^2}{2\sigma^2_{z,eff}}\right]+\exp\left[-\frac{(z+H)^2}{2\sigma^2_{z,eff}}\right]\right\}}{2\pi\,\sigma_{y,eff}\sigma_{z,eff}\bar{u}_n} \qquad (20)$$

In order to calculate the time-integrated concentration (i.e. the "dosage"), q in eq. (20) has to be replaced by $Q=q\cdot\Delta t$, where Δt is the duration of the time interval. The resulting diffusion factor for the plume, i.e. the concentration divided by the release rate or the "dosage" divided by the source strength, thus is identical with the diffusion factor for the puff given in eq. (7). The effective diffusion parameters can be calculated according to eq. (5) and eq. (16).

3. Diffusion of a plume in case of changing wind direction

In case of changing wind direction a plume along a straight-line diffusion axis will only develop in the first time interval, i.e. before a change of wind direction occurs. At the end of this time interval the plume may be considered as a succession of an infinite number of infinitesimal puffs with individual release times, each puff following the trajectory of the first one. At the end of the first time interval this simple file motion will be terminated, due to the change of the wind direction, and each puff will start to move along its own trajectory, as demonstrated in Fig. 4.

In case of changing wind direction the use of the volume source model for the plume, in contrast to the calculation according to the puff, will not result in an analytical solution for the superposition of the contributions from the infinitesimal point sources, since the diffusion parameters for the single puffs are different, depending on the respective transport times. In order to avoid the necessity of a numerical integration, therefore, the plume may be approximated by a superposition of N succeeding puffs with the source strengths $(\Delta Q)_\ell = Q/N$ and the individual release times

$$t_o^{(\ell)} = t_o + \frac{t_1 - t_o}{N}(\ell-1) \quad (\ell=1,2,\ldots N) \tag{21}$$

From eq. (8) we get the diffusion factor for the ℓ-th puff by substituting t_o by the individual release times $t_o^{(\ell)}$ as given by eq. (21). By multiplying this factor by the individual source strengths $(\Delta Q)_\ell$ and superimposing the contributions from all the N puffs, we obtain the time integral of concentration and, after dividing by Q, the diffusion factor

$$\hat{\chi}_n(x,y,z) = \frac{1}{N}\sum_{\ell=1}^{N} \frac{\exp\left[-\frac{\eta_n^{(\ell)2}}{2\sigma_{y,eff}^{(\ell)2}}\right]}{2\pi\sigma_{y,eff}^{(\ell)}\sigma_{z,eff}^{(\ell)}\bar{u}_n} \left\{\exp\left[-\frac{(z-H)^2}{2\sigma_{z,eff}^{(\ell)2}}\right]+\exp\left[-\frac{(z+H)^2}{2\sigma_{z,eff}^{(\ell)2}}\right]\right\} \tag{22}$$

due to diffusion of a plume in n time intervals with different weather conditions, where

$$\begin{aligned} \eta_n^{(\ell)} = \frac{1}{\bar{u}_n}\Big\{&\bar{u}_{x,n}\Big[y-\sum_{k=2}^{n-1}\bar{u}_{y,k}(t_k-t_{k-1})-\bar{u}_{y,1}(t_1-t_o^{(\ell)})\Big] \\ &-\bar{u}_{y,n}\Big[x-\sum_{k=2}^{n-1}\bar{u}_{x,k}(t_k-t_{k-1})-\bar{u}_{x,1}(t_1-t_o^{(\ell)})\Big]\Big\} \end{aligned} \tag{23}$$

is the crosswind distance from the trajectory in the n-th time interval.

The effective values of the diffusion parameters for the ℓ-th puff

$$\sigma_{i,eff}^{(\ell)2} = \sum_{k=1}^{n}\sigma_{i,k}^{(\ell)2} \quad \begin{matrix}(i=y,z)\\(\ell=1,2,\ldots N)\end{matrix} \tag{24}$$

are obviously functions of its individual release time $t_o^{(\ell)}$ and we get from eq. (15)

$$\sigma_{i,1}^{(\ell)2} = p_{i,1}^2\{\bar{u}_1(t_1-t_o^{(\ell)})\}^{2q_{i,1}} \quad (\ell=1,2,\ldots N) \tag{25}$$

$$\begin{aligned}\sigma_{i,k}^{(\ell)2} = p_{i,k}^2\Big\{&\Big[\sum_{m=2}^{k}u_m(t_m-t_{m-1})+u_1(t_1-t_o^{(\ell)})\Big]^{2q_{i,k}} \\ &-\Big[\sum_{m=2}^{k-1}u_m(t_m-t_{m-1})+u_1(t_1-t_o^{(\ell)})\Big]^{2q_{i,k}}\Big\}\end{aligned} \tag{26}$$

An illustration of this procedure (Fig. 4) shows that the puffs are growing together in course of time so that the simulation of a continuous plume through a finite number of separate puffs becomes more and more realistic with increasing transport time.

The volume source model for the plume so far has dealt with a constant release rate during the first time interval. It is obvious, that the model can be extended for releases with changing release rate. If the release rate is not constant during a time interval with constant weather conditions, the time interval can be subdivided into a number of intervals with approximately constant release rate. If the release covers several time intervals, a superposition of the contributions from the releases in the individual time intervals yields the overall dosage, where evidently the diffusion of each release has to be calculated on the basis of the series of weather conditions following the individual release time.

4. Comparison of the volume-source-model with the conventional model

The influence of changing weather conditions after a release in the first time interval (hour) is demonstrated in Fig. 5. The diffusion factor $\chi(x,0,0)$ (solid curve) resulting from the volume-source-model for a selected exemplary series of successive hourly weather conditions, beginning with diffusion category F in the first hour, is compared with the conventional diffusion factor $\chi_c(x,0,0,)$ (dashed curve) based on eq. (17) with the diffusion category and wind velocity kept constant at the conditions of the first hour. For better interpretation of the course of this functions the diffusion parameters according to the volume-source-model (solid curves) and to the conventional model (dashed curves) are included and the time intervals and diffusion categories can be read at the upper margin. It can be seen, that in this example the dosage in large source distances would be overestimated by the conventional diffusion factor by more than one order of magnitude. This is due to the following effects:
(1) the turbulence increases after the first time interval and
(2) the wind velocity increases.
The short-time irregularities of the diffusion factor according to the volume source model are originated by the changing of wind velocity, which causes corresponding variations of the exposure time of the passing plume.

In Fig. 6 the ratio of the conventional diffusion factor to the diffusion factor according to the volume-source-model is illustrated for three series of weather conditions, beginning with diffusion categories A,D and F respectively. It is demonstrated, that the environmental exposure calculated by the conventional model usually underestimates the realistic values in the case of the starting diffusion category being unstable, while an overestimation is usually connected with a stable category at the beginning. In order to compare the two models under average conditions, 1000 series of weather conditions have been selected statistically from the Jülich hourly meteorological observations and the average diffusion factors according to the two models have been calculated. Curve M shows the deviation of the values resulting from the two models. It becomes manifest, that the conventional model in the case of long-time releases or on the statistics average of short-time tends to an overestimation of the environmental exposure for longer source distances by a factor of two, at least for diffusion statistics typical for Middle Europe. Much more important, however, is the use of the advanced model in cases of single releases (e.g. accidental releases), because in these situations considerable errors are possibly resulting from the use of the conventional model for large source distances.

References

(1) F. Pasquill
Atmospheric diffusion
Ellis Horwood Limited, Chichester (1974)
(2) G.T. Csanady
Turbulent Diffusion in the Environment
D. Reidel Publishing Co., Dordrecht (1973)
(3) J. Straka, H. Geiß, F. Rohloff, K.J. Vogt
Die Ausbreitung von Abluftfahnen bei sich ändernden Wetterbedingungen
PSE-Bericht Nr. 79/5 (1979)
(4) R.G. Lamb, W.H. Chen, J.H. Seinfeld
Numerico-Empirical Analysis of Atmospheric Diffusion Theories
J.Atmos.Sci., 32, 1795-1807 (1975)
(5) G.K. Batchelor
Diffusion in a Field of Homogeneous Turbulence
Australian J.Sci.Res. 2, 437 (1949)
(6) F. Wippermann
Die Ausbreitung luftfremder Stoffe in der Atmosphäre
TH Darmstadt; Skriptum zur Vorlestung im WS 67/68 (1967)
(7) G.J. Taylor
Diffusion by Continuous Movements
Proc. London Math. Soc. A20, 196 (1922)
(8) K.J. Vogt
Empirical Investigations of the Diffusion of Waste Air Plumes in the Atmosphere
Nuclear Technology, 34, 43-57 (1977)
(9) K.J. Vogt, H. Geiß, G. Polster
New Sets of Diffusion Parameters Resulting from Tracer Experiments in 50 and 100 Metres Release Heights
9th International Technical Meeting on Air Pollution Modeling and its Application (NATO/CCMS Air Pollution Pilot Study "Assessment Meteorology and Modeling"), Toronto, 28.-31.8.1978

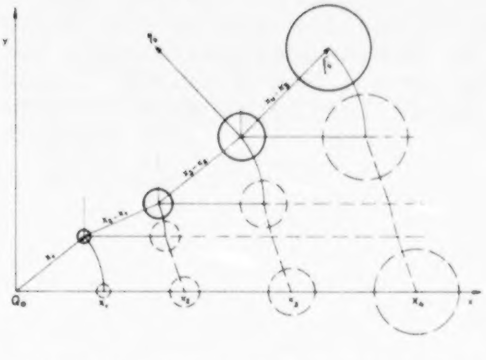

Fig. 1 Scheme of transition from the straight-line Gaussian model to the volume source model, in case of horizontal anisotropy ($\sigma_x \neq \sigma_y$)

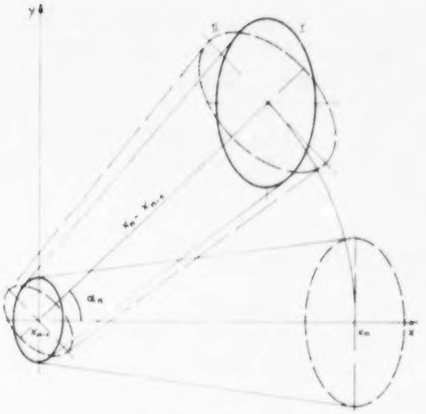

Fig. 2 Shapes of the puffs I and II according to diffusion models represented by eq. (4) and eq. (8) respectively, in case of horizontal anisotropy ($\sigma_x \neq \sigma_y$)

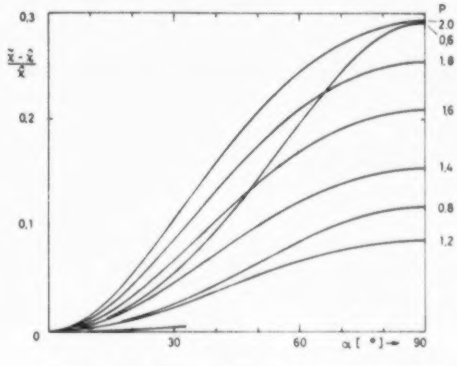

Fig. 3 Error of the approximation depending on the angle between two successive wind directions α and the ratio of the horizontal diffusion parameters $p=\sigma_y/\sigma_x$

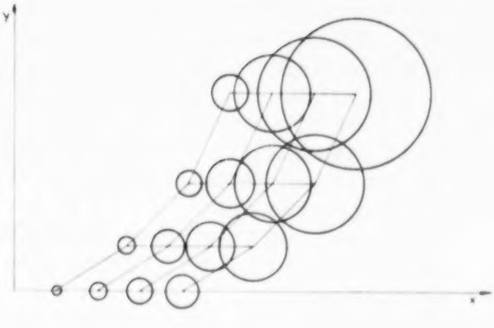

Fig. 4 Scheme of diffusion for a plume, simulated by a finite number of puffs, in case of changing wind direction

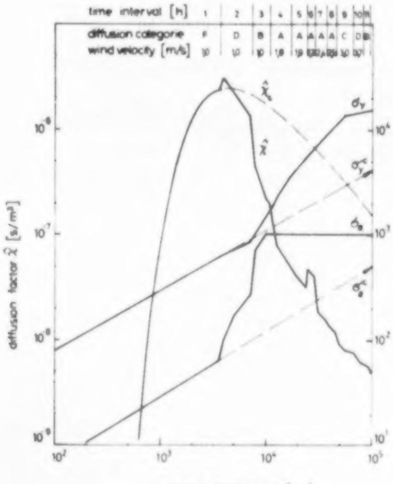

Fig. 5 Diffusion parameters σ and diffusion factors $\hat{\chi}$ for a release height of 100 m corresponding to the conventional Gaussian model (index c) and to the volume source model, considering the change of diffusion parameters and wind velocity

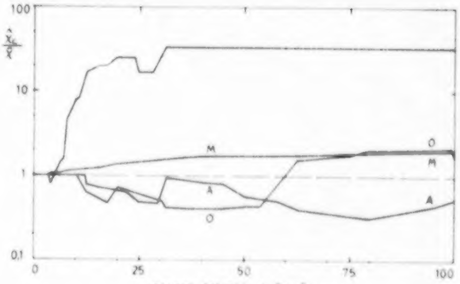

Fig. 6 Relation of the diffusion factor $\hat{\chi}_c$ corresponding to the conventional Gaussian model with persisting diffusion category [illegible] and wind velocity according to the first time interval, and the diffusion factor $\hat{\chi}$ corresponding to volume source model with consideration of the [illegible] weather conditions, for a release height of 100 m

10TH NATO /CCMS INTERNATIONAL TECHNICAL MEETING
ON AIR POLLUTION MODELING AND ITS APPLICATION

TOPIC 3

Multiple Sources

REGIONAL SOURCE QUANTIFICATION MODEL FOR SULPHUR OXIDES IN EUROPE

by

L. P. Prahm, K. Conradsen[+], L. B. Nielsen[+] and A. Eliassen[++]
Danish Air Pollution Laboratory
National Agency for Environmental Protection
Risø National Laboratory, 4000 Roskilde, Denmark

Abstract. An air quality model for estimation of emissions on a regional scale is developed. The model uses measured air concentrations and air trajectory transport calculations to determine the emissions. The optimal emission strength is obtained by a least square approximation between measured and estimated air concentrations of pollutants. The Regional Source Quantification (RSQ) model is used on the European long-range transport data base for sulphur oxides collected by the Norwegian Institute for Air Research. The data base consists of about 60,000 SO_2 and SO_4 air quality samples and four times as many 48-hour back trajectories. The estimated emission strengths based on about 3,500 samples are shown to agree fairly well with the national emission strengths estimated previously from population and industrial density as well as consumption of fuel and raw materials. This is taken as a verification of the RSQ model.

Source Quantification Modelling

Air quality studies can be based on receptor or source oriented meteorological air quality models. Receptor oriented models give estimates on air quality without information on emissions. The source oriented models, which are those most frequently used, relate the estimated air quality to emissions. This is preferable because control of the air quality can be enforced by suitable regulation of the emittents. Emission inventories are required for the source oriented models. The emission survey is usually conducted by estimation of the consumption of raw materials, especially fossil fuel, in different geographical areas.

Obtaining accurate emission inventories is obviously of great importance, and possible alternative procedures for conducting and controlling emission inventories are of interest. This is especially the case for micropollutants where the primary sources might be unknown.

During the OECD study, "Long-Range Transport of Atmospheric Pollutants" (LRTAP), regional transport of sulphur oxides has been demonstrated and quantified. See for example Eliassen (1978), Ottar (1978) and Prahm et al. (1976). These studies are based on emission inventories produced mainly by each participating country, air trajectories and measured SO_2 and SO_4 concentrations. Application of the emission inventory in Eulerian models was demonstrated e.g. by

---

[+]Affiliation: Department of Mathematical Statistics and Operations Research, Technical University of Denmark, 2800 Lyngby, Denmark.
[++]Affiliation: Norwegian Meteorological Institute, P.O. Box 320 Blindern, Oslo 3. Norway.

Preceding page blank

Prahm and Christensen (1977). Regional transport modelling is reviewed by Eliassen (1979).

In the present study, we develop a Regional Source Quantification (RSQ) model for quantification of emission strength on a regional scale by use of air quality measurements and air trajectories. Using the data base from LRTAP, the European sulphur emissions are quantified. Comparison with the national emission inventories reported by LRTAP gives agreement within the estimated accuracy for most areas. This is considered as a verification of the model. In addition, we discuss the disagreements between the LRTAP emission information and the estimated fields which might either be caused by model assumptions, errors in measured concentrations and/or errors in the original emission inventories. Causes of deviations are identified.

Possible application of the RSQ model for planning of future monitoring networks, e.g. for alternative micropollutants, is discussed. The RSQ model is also used for optimalization of SO_2 and SO_4 oxidation and decay parameters by requiring minimum deviation between measured and estimated concentrations.

Source finding studies have been reported earlier for small scales, i.e. up to about 20-30 km, where the advecting wind can be assumed to connect sources with receptors by straight lines. Breuer (1965) presented a method which can be used to establish information on contributions from various point sources to the receptors in a limited urban or rural area. His method is based on short-term averages of measured concentrations. Högström (1975) discussed a procedure for assessing the relative contribution of local point sources to the air pollution observed in a community based on 3-12 measurement stations. His procedure is like Breuer's, but based on 24-hour averages instead of short-term averages. On an even smaller scale, Yamartino and Lamich (1979) presented a source-finding algorithm based on the least square principle like the present study. They used their algorithm on the data base from an airport and found that only the largest sources could be localized.

In the present study, we use the regional European data base and study the relations between number of measured samples, the location of the stations, the number of emission fields and the size of the emission fields which are required to obtain reliable emission estimates. A preliminary presentation of the results has recently been published (Prahm et al., 1979), and a complete presentation is submitted to Atmospheric Environment (Prahm et al., 1980).

Results from the Regional RSQ Model

Location and emission strength of sulphur oxide sources in Europe are estimated by a meteorological air quality model. The model is based on air quality measurements and air trajectories produced for the OECD project, LRTAP. The data base used consists of 24-hour SO_2 and SO_4 measurements from about 45 stations in Europe during the period from 1973 to 1975, and of air trajectories arriving four times a day at each station.

By use of an air trajectory air quality model, a large number of linear equations are produced estimating SO_2 and SO_4 values with emission fields as unknowns. Relating the measured and estimated SO_2 and SO_4 values to each other by a least square method gives an estimate of the emission fields. About 7500 samples and 15,000 trajectories were used.

The estimated fields are compared with information on emissions estimated in the OECD project, LRTAP. Agreement between the LRTAP estimate and the model result is found for most of the emission areas. The emission in some European areas, however, is found to be both overestimated and underestimated compared with LRTAP. Possible reasons for this disagreement are discussed.

The RSQ model presented here is demonstrated to be a useful tool for source estimation on a regional scale. The RSQ model is also found to be valuable for optimal siting of monitoring stations. The decay and oxidation parameters in the air trajectory model are determined by the RSQ model. The decay parameter values agree fairly well with previous estimates, while the oxidation parameters used in the model were found to correspond with a greater initial oxidation than most commonly reported and an insignificantoxidation during transportation.

References

1. W. Breuer, "Die Aussagekraft kontinuerlicher Immissionsmessungen," IWL, Institut für Gewerbliche Wasserwirtschaft und Luftreinhaltung E.V. Forum 65. Band 3. 1965.
2. A. Eliassen, "The OECD Study of Long-Range Transport of Air Pollutants: Long Transport Modelling," Atmospheric Environment, 12, 479-487, 1978.
3. A. Eliassen, "A Review of Long-Range Transport Modelling," Journal of Applied Meteorology, 18, 000-000 (in press), 1979.
4. U. Högström, "Confirming the Local Sources of Observed Air Pollution in Communities," Atmospheric Environment, 9, 929, 1975.
5. B. Ottar, "An Assessment of the OECD Study on Long-Range Transport of Air Pollutants (LRTAP)," Atmospheric Environment, 12, 445-454, 1978.
6. L. P. Prahm, U. Torp and R. M. Stern, "Deposition and Transformation Rates of Sulphur Oxides during Atmospheric Transport over the Atlantic," Tellus, 28, 355-372, 1976.
7. L. P. Prahm and O. Christensen, "Long-Range Transmission of Pollutants Simulated by a Two-Dimensional Pseudospectral Dispersion Model," Journal of Applied Meteorology, 16, 896-910, 1977.
8. L. P. Prahm, K. Conradsen, L. B. Nielsen and A. Eliassen, "Regional Source Quantification Model for Sulphur Oxides in Europe," Proc. WMO Symposium on the Long-Range Transport of Pollutants and its Relation to General Circulation including Stratospheric/Tropospheric Exchange Processes, Sofia, Bulgaria, WMO Report, No. 538, 1979.
9. L. P. Prahm, K. Conradsen and L. B. Nielsen, "Regional Source Quantification Model for Sulphur Oxides in Europe," submitted to Atmospheric Environment, 1980.
10. R. J. Yamartino and D. F. Lamich, "The Formulation of a Source Finding Algorithm," Preprint volume, 4th Symposium on Turbulence, Diffusion and Air Pollution, Reno, January 15-18, 1979, American Meteorological Sociey, Boston, 1979.

Discussion :

(Rapporteur: Yamartino)

Van Egmond:

Did you ensure positive source strength solution values by placing a constraint on the optimization?

Prahm (response):

The negative solutions were allowed but were found not to appear, in agreement with reality.

M. Smith:

You did not mention anything about lateral dispersion in your model. Was this ignored?

Prahm:

Yes! A previous study of ours on long range transport using the pseudo-spectral approach found that lateral dispersion is unimportant on this scale.

AN EXPERIMENTAL AND THEORETICAL INVESTIGATION OF PHOTOCHEMICAL POLLUTION IN TURIN

by

J.H. Weaving & S.F. Benjamin,
BL Advanced Technology Ltd.,
Coventry, England

and

P.P. Gaddo & F. Repetto,
Fiat Engineering, Turin, Italy

Associated with the AQSG
of
Committee of Common Market Automobile Constructors
listed in Appendix

Abstract. The suitability of a mathematical model to simulate photochemical phenomena in European cities is currently being investigated. Model predictions are compared against measurements obtained in the city of Turin during a day when photochemical activity was observed. Helicopter sampling was conducted to establish the pollutant and temperature structure over and across the city. A ground based monitoring network provided data on ground level concentrations and the surface wind field. The performance of the model for this day is discussed.

Introduction

The suitability of a mathematical model to simulate photochemical phenomena in European cities is currently being investigated. It is hoped that such a model can be used to study the effects of various emission control strategies. This paper describes a field experiment conducted by CCMC (Committee of Common Market Automobile Constructors) during the summer of 1979 when measurements were made in the city of Turin during a day when photochemical activity was most probable. Observations are compared against the predictions of the model.

The Mathematical Model

The mathematical model under investigation has been described in detail in a previous paper[1] and so will be discussed only briefly here. It is a Eulerian grid model developed by Systems Applications Inc. in 1973[2] and is a mathematical representation of the transport, diffusion and chemical reactions of pollutants over the city to which it is applied. The chemical kinetic mechanism consists of fifteen reactions involving ten chemical species. Each simulation provides a map of hourly averaged ground cell concentrations over the city from 0500 - 1600 hours for reactive hydrocarbons (HC), NO, NO_2, O_3 and CO. The spatial resolution is determined by the size of the cells of the three dimensional grid over the city in which the governing mathematical equations are solved numerically. The horizontal cell dimensions are 600 x 600 metres. The vertical cell size may vary from hour to hour and is determined by the mixing depth (i.e. the height above the city in which the mixing is assumed to take place). The mixing depth may be divided into as many as six levels and hence typical cell heights vary from about 20 to 200 metres. Hence concentrations represent spatially averaged concentrations over these cells.

As input to the model the wind field, mixing depth and photodissociation rate constant need to be specified for each hour of the simulation period. The initial pollutant field over the city (at 0500 hours) must be specified along with concentrations above the mixing layer. The pollutant fluxes into the city along its upwind boundary must be given for all hours. Mobile and fixed source emissions into each grid square must also be specified for all hours.

Certain model refinements were needed before applying the model to Turin. The vertical diffusivity was modified to incorporate the effect of thermal convection on the mixing processes. Winds are very light in Turin and this type of mixing dominates during sunny summer days in the city. The emissions alogarithms were also modified to allow for the effect of the different driving cycles encountered in the city.

The Measurement Programme

1. Fixed Monitoring Network

Table 1 lists the monitoring stations recording hourly averaged values of pollutant and wind during the experimental day (27.7.79) and Figure 1 shows their locations. In Table 1 the first seven stations are owned by Fiat; the remaining two stations are operated by the municipal authorities in Turin. The sample points were moved, when possible, well away from the kerbside so as to be reasonably clear of local sources of pollution and so as to provide measurements more closely related to the spatially averaged predictions of the mathematical model; the exception was P. Nuova which sampled at the kerbside. All measurements were made within 10 metres of the ground except at Mole Antonelliana, a tall structure, where the sampling point is situated 93 metres above the city. The station at Eremo is situated in the hills to the east of the city about 400 metres above the city itself.

The paucity of wind data was an unfortunate consequence of instrument malfunction at two stations. Supplementary wind data was available from a private source in the city and from the airport (situated about 20 Km. north of the city). Incoming solar radiation is recorded at Lagrange.

Measurements of the wind and temperature aloft are not routinely made in Turin. The nearest radiosonde station is at Milan, about 100 Km. east of Turin.

2. Supplementary Measurements

To assess model performance it is necessary to provide various input data which are not available from the city network. Specifically upwind concentrations are needed as well as a quantification of the vertical pollutant and temperature structure over the city. These latter measurements are needed so as to establish the mixing depth. Measurements of the vertical pollutant profile also test the appropriateness of the values of the turbulent diffusivity coefficients used in the model.

Further, it is anticipated that horizontal gradients of both primary and secondary pollutants exist in the city and that measurements at only a limited number of fixed stations may not adequately reflect a complex pollutant structure over the city, which may or may not be predicted by the model. A need to sample for a limited period over a large section of the city was hence evident.

To fulfil these requirements a helicopter was used to make pollutant and temperature measurements over and across the city. The helicopter was instrumented with a Philips NO/NO_2/NOx analyser and a Philips chemiluminescent O_3 monitor. The NOx and O_3 instruments provided measurements every 60 and 80 seconds respectively. A continuous record of temperature was also obtained during the flights. The sampling point was located ahead of the landing gear at the front of the helicopter.

Results Of Measurements Obtained On 27.7.79.

1. Meteorological Description

In Turin surface winds were light throughout the day. They were of strength about 2 mph during the morning increasing gradually during the day to about 6 mph by mid-afternoon. Being light they were quite variable over the city making it particularly difficult to define accurately the wind field. Both at Mole and Eremo winds were also very light.

The wind field in Turin during the day may be broadly characterised as light N.E. till near noon becoming E/S.E. later in the day; winds being light through the mixing layer. It was very hazy. The maximum temperature at Lagrange was 31°C.

Figure 2 shows the radiosonde data from Milan for 0000 and 1200 GMT. Winds below 700 metres are less than 6 mph. The 1200 GMT sounding shows that below 500 metres winds were generally from the S.E.; above 1000 metres winds are stronger and are from the N.W. The temperature profile at 1200 GMT shows an inversion with base at 1000 metres. It is expected that the principal features of the wind and temperature field aloft may be extended to Turin.

Helicopter soundings were not made until 1300 hours, however examination of the pollutant data from Mole and the surface stations in close proximity suggest that during the early morning mixing was confined to a shallow layer less than 100 metres above ground. The strong insolation on this day suggests that the mixing layer developed quite quickly. By the time of the first helicopter sounding there was a well mixed layer at least up to 500 metres (the highest level sampled by the helicopter). The inversion at 1000 metres at Milan provides an upper limit to the mixing during the afternoon.

2. Monitoring Station Data

Hourly averaged values of the species listed in Table 1 at the various monitoring stations are shown in Figures 3 - 6. Note that the distributions of NOx and CO are not necessarily similar at a monitoring station. Also considerable differences in the distributions for a given pollutant, e.g. CO, are observed over the network.

The variations between stations situated relatively close to each other for a given pollutant may be attributable to several factors amongst which are differences due to local effects of emissions, meteorology, photochemical activity and many other factors. Some of the differences are readily explainable, others are not. However several features of these distributions deserve comment, especially when model performance is to be judged against them.

Figure 1 shows the locations of the monitoring stations. It is convenient to group them geographically. Figure 3a shows the CO values for P. Nuova, Lagrange and Crocetta, all stations within the city centre. Clearly the high values at P. Nuova are a consequence of the sampling point proximity to the kerbside. The values at Lagrange and Crocetta conform more nearly to each other, although there are differences between them which may be attributed to any of the local factors mentioned above and which the model will not be capable of reflecting. Mirafiori is situated adjacent to the large Fiat complex where local heavy traffic is found. Figures 4a and 5a show NO and NO_2 values respectively for the city centre stations. The concentration values at Lagrange are relatively high. This station is situated in an area of narrow streets and tall buildings. It is possible that street canyon effects may be responsible for these higher values.

3. Helicopter Sampling

Two separate flights were made during the afternoon. The flight path for the first flight (1235 - 1407 hours) is shown in Figures 7 and 8. The helicopter base is in the south-west of Turin. In the city the helicopter flew at about 100 metres above ground whereas outside the city it flew at a height of 200 metres. At two locations, A and B, the helicopter executed a slow spiral up to about 500 metres above ground. The excursion on the west boundary of the city was necessitated because of local air traffic problems associated with a small airfield situated close by. The numbers along the flight paths in Figures 7 and 8 denote concentrations (ppb) of NO_2 and O_3 respectively. Numbers in brackets denote times. The measurements obtained in both the ascent and descent part of each of the spirals are shown in Figure 9.

The second flight path (1616 - 1744 hours) is shown in Figures 10 and 11. Again the helicopter flew at about 100 metres above ground in the city whereas outside the city it flew at a height of 200 metres above ground. At locations C and D spirals were executed. The spiral executed at C was limited because of air traffic activity. The numbers along the flight paths in Figures 10 and 11 denote concentrations (ppb) of NO_2 and O_3 respectively. Numbers in brackets denote times. The measurements obtained during the spirals are shown in Figure 12.

Model Predictions And Comparisons With Observations

Predictions for CO

It is convenient to consider the predictions for the inert specie CO separately because this provides a means of examining model performance without the complication of photochemistry.

Figure 3 shows the predicted against measured values for all stations. In Figure 3a predicted values for Lagrange and Crocetta are shown. These stations (see Figure 1) are located in the city centre. Model predictions for the maximum concentrations show fair agreement with observations except at P. Nuova.

This station samples at the kerbside. The correlations on an hour to hour basis between predicted and observed values can be seen to be no worse than the correlations ordinarily encountered between monitoring stations situated in close proximity in a complex urban environment. The model under-predicts at Mirafiori but this is consistent with the expected influence of the local heavy traffic close by.

Predictions for Photochemically Reactive Species

(a) Comparisons with Station Data. Predictions for NO are shown in Figure 4. Figure 4a shows that the model is predicting magnitudes at two of the three city centre locations tolerably well; predictions at Lagrange adequately represent the predictions for the other stations. At Mirafiori the relatively high predicted values are due to the emissions from a power plant situated close to the monitoring station.

The predicted and observed maximum NO_2 concentrations at two of the three city centre stations show fair agreement. As there is some consistency in the observations in the timing of the morning NO_2 peak, this suggests that the predicted NO_2 peak occurs too early. At Mirafiori little NO_2 was observed. The relatively high predicted values are a consequence of the power plant plume plus the effect of the "NO_2 plume" from the city centre sources. This latter plume accounts for about 7 pphm of the predicted value for hour 0800 - 0900.

Predicted and observed O_3 concentrations for Mole are shown in Figure 6c. Ozone was under-predicted at this location during the afternoon.

(b) Comparison with Helicopter Data.

(i) NOx Values. Figure 7 shows that the highest NO_2 concentrations occur near the city centre (3-4 pphm) between 1230 - 1400 hours. By 1600 hours Figure 10 shows that the NO_2 values in the city have fallen to about 1 pphm. This NO_2 reduction is reflected in the station data (see Figure 5a).

The NO_2 predicted values for hours 1100 - 1200, 1200 - 1300, and 1500 - 1600 are shown in Figure 13. Note that the low predicted values for 1500 - 1600 hours are partly due to the advection of the low background concentrations across the eastern boundary of the city as a consequence of the wind direction change occurring around 1300 hours. Because afternoon predicted concentrations are relatively low they will be quite sensitive to background concentrations. For example, higher upwind NO_2 concentrations to the north of the city around noon would increase the predicted city levels. When Figure 13a is compared with Figure 7 the agreement is satisfactory suggesting that the reduction in NO_2 concentrations would appear to have been predicted to occur too early.

The NO predicted values from 1200 hours onwards are 1 pphm or less, in agreement with the helicopter observations.

(ii) O_3 Values. Model simulations for O_3 for hours 1300 - 1400 and 1500 - 1600 are shown in Figure 14. Note the higher concentrations predicted to the west of the city for hour 1300 - 1400. There is evidence in the helicopter data which supports this as seen in Figure 8.

There is a disparity between the high O_3 values observed at Eremo and the helicopter data. Eremo is situated in the Po hills in a heavily vegetated area about 400 metres above the city. Generally it is found that values at Eremo are higher than at Mole (93 metres above the city). It remains to be resolved whether the Eremo concentrations reflect true city values at 400 metres or whether they are subject to local effects.

Conclusions

The predictions of an air pollution mathematical model have been compared against measurements obtained in the city of Turin for a day when photochemical activity was most probable. The conclusions are:

1. Maximum predicted CO concentrations were in satisfactory agreement with observations in the city centre.

2. Maximum predicted NO_2 values during the morning in the city centre gave fair agreement with measured values although the peak was predicted to occur too early.

3. During the afternoon the model broadly predicted the spatial and temporal distribution of NO_2 observed from the helicopter although there is some disparity between the timing of the events.

4. The predicted NO concentrations during the afternoon are 1 pphm or less, in agreement with the helicopter observations.

5. The model predicted higher ozone concentrations in west Turin in the afternoon. There is evidence in the first helicopter flight to support this.

6. A sensitivity analysis would be valuable so as to explore the possible causes of the observed disparities. This analysis should include the effects of the wind field, background concentrations and the photodissociation rate constant.

References

1. J.H. Weaving, S.F. Benjamin, P.P. Gaddo, F. Repetto, "The Application of a Mathematical Model to the Estimation of the Concentration of Pollutants in European Cities", Presented at the NATO/CCMS 9th International Technical Meeting on Air Pollution Modelling and its Application, Toronto, September 1978.

2. S.D. Reynolds, P.M. Roth, J.H. Seinfeld, "Mathematical Modelling of Photochemical Air Pollution - I", Atmospheric Environment Vol.7., pp. 1033 - 1061, 1973.

Appendix

Air Quality Sub Group of CCMC:

Alfa Romeo	Mr. L.M.	Finos
	Mr. A.	Piccone
BL Technology Ltd.	Dr. J.H.	Weaving
BMW	Mr. G.	Straub

Citroen	Mr.	Henriet
Daimler-Benz	Mr.	Haepp
Fiat	Dr. P.P.	Gaddo
Peugeot	Mr. M.	Dupont
Renault	Mme.	Chevrier
Volkswagen	Dr. K.H.	Lies
Porsche	Mr. H.	Spannagel
Rolls Royce	Mr. J.B.H.	Knight

Acknowledgements

We would like to thank Dr. Paolo Natale, Servizio Relevamento Inquinamento Atmosferico Citta di Torino, for supplying the data from the municipal stations.

We would also like to thank the Instituto Di Medicina del Lavoro dell' Universita di Torino - Laboratorio Di Igiene Industriale for supplying the NOx and O_3 instruments used during the helicopter flights.

Table 1. Monitoring Stations. x Denotes Measurement Available for 27.7.79.

Monitoring Station	CO	NOx	NO_2	O_3	THC	CH_4	Wind Speed	Wind Direction
Lagrange	x	x	x		x	x	x	x
Ferriere	x	x						
Mirafiori	x	x	x				x	x
Mole		x	x	x			x	
Eremo		x	x	x			x	
Crocetta	x							
P. Nuova	x							
Consolata		x	x					
Rebaudengo		x						

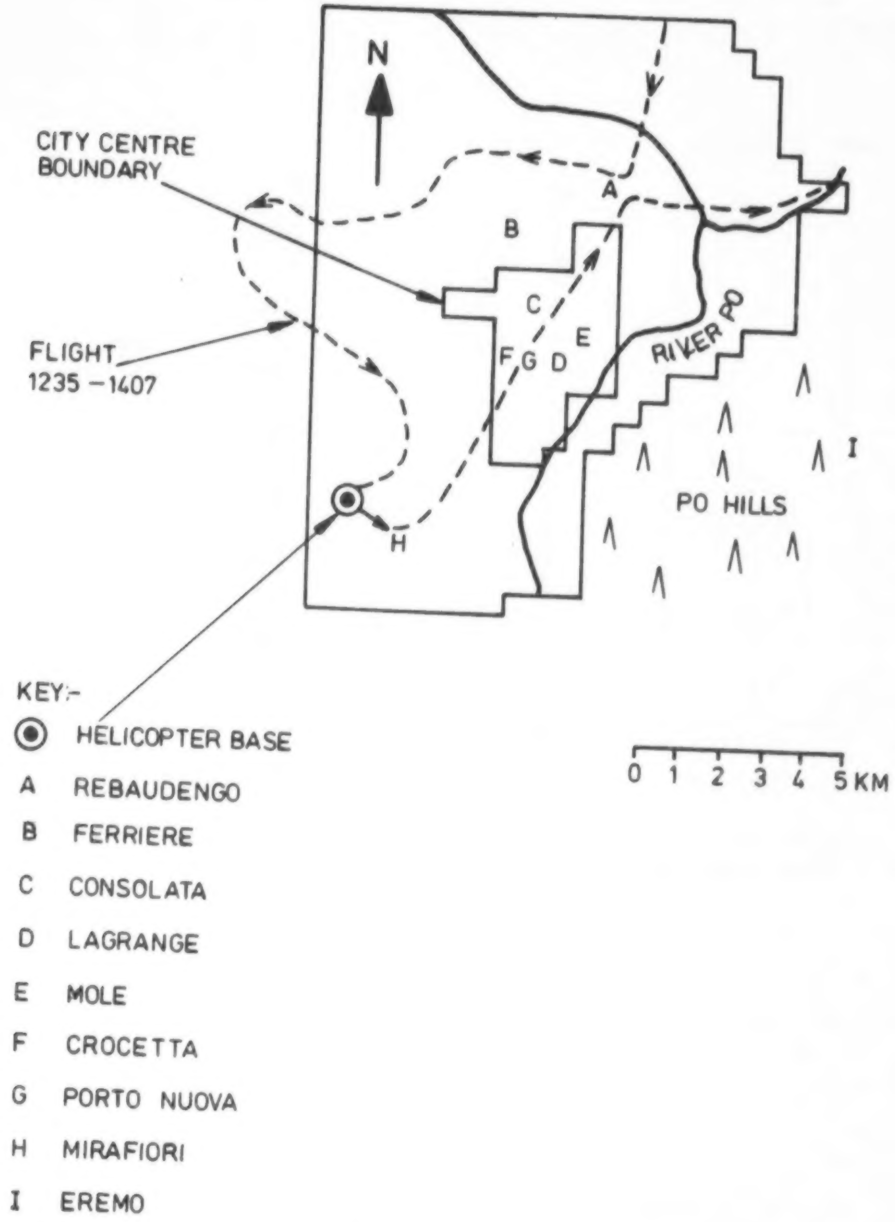
N
CITY CENTRE BOUNDARY
FLIGHT 1235 -1407
A
B
C
E
F G D
RIVER PO
I
PO HILLS
H
KEY:-
HELICOPTER BASE
A REBAUDENGO
B FERRIERE
C CONSOLATA
D LAGRANGE
E MOLE
F CROCETTA
G PORTO NUOVA
H MIRAFIORI
I EREMO
0 1 2 3 4 5 KM

Figure 1. The City of Turin. The Irregular Outer Boundary Delineates the Modelling Region. Monitoring Stations A to I are Indicated. Part of the Helicopter Flight Path for the 1235 - 1407 Flight is Shown.

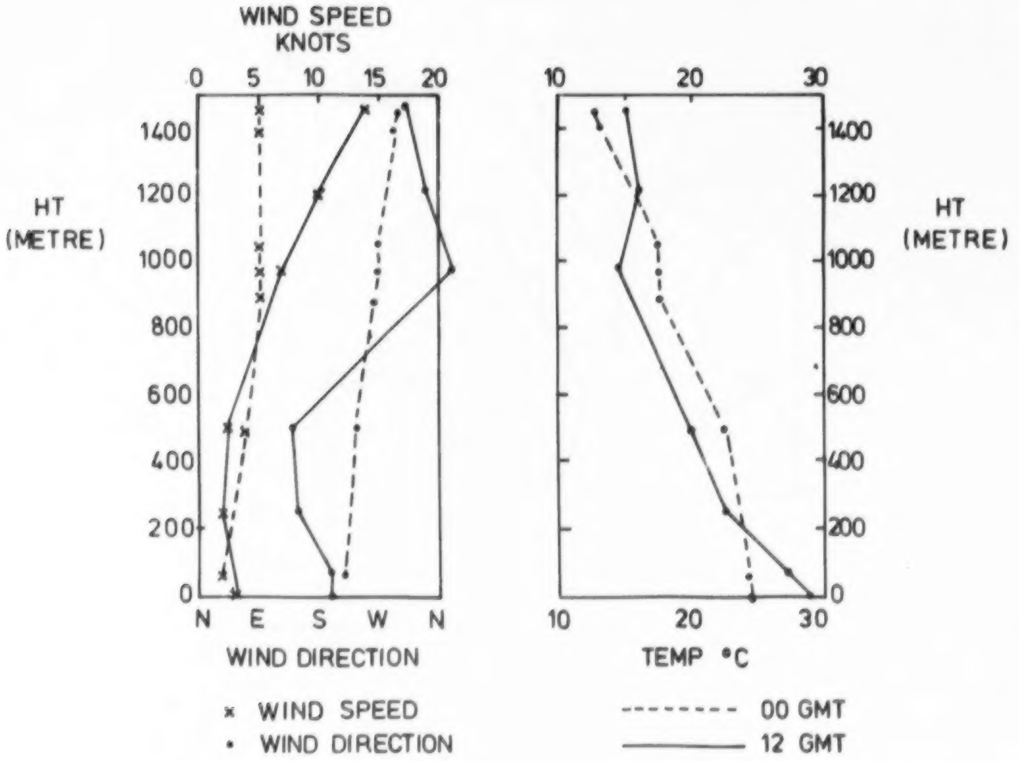

Figure 2. Radiosonde Data from Milan for 27.7.79.

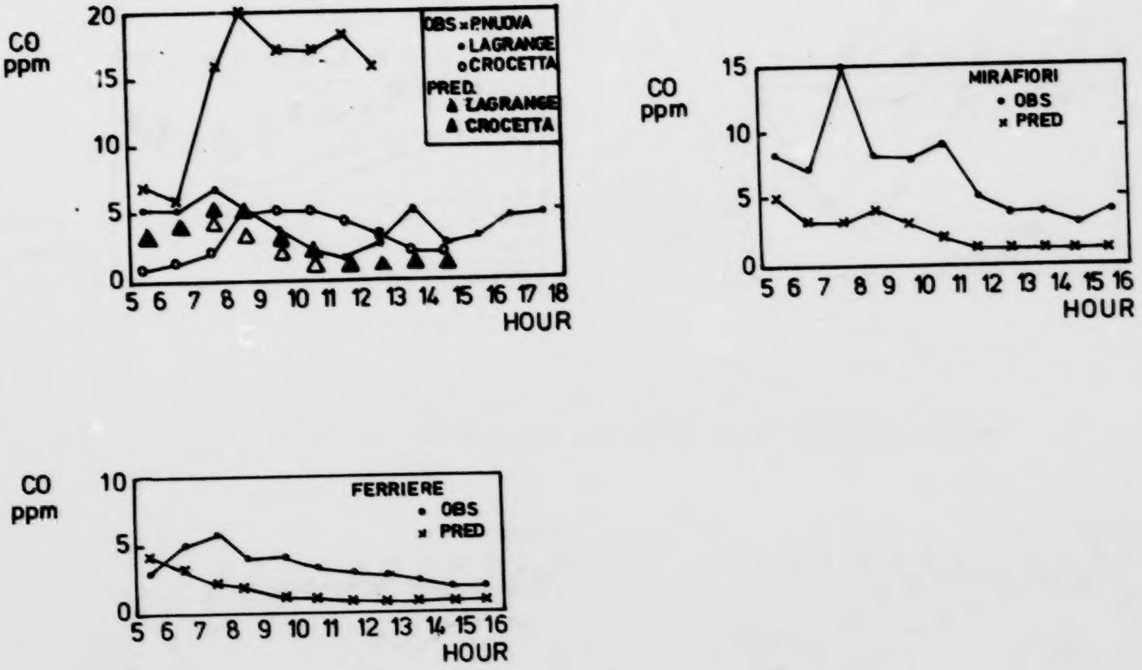

Figure 3. Predicted and Observed CO Concentrations.

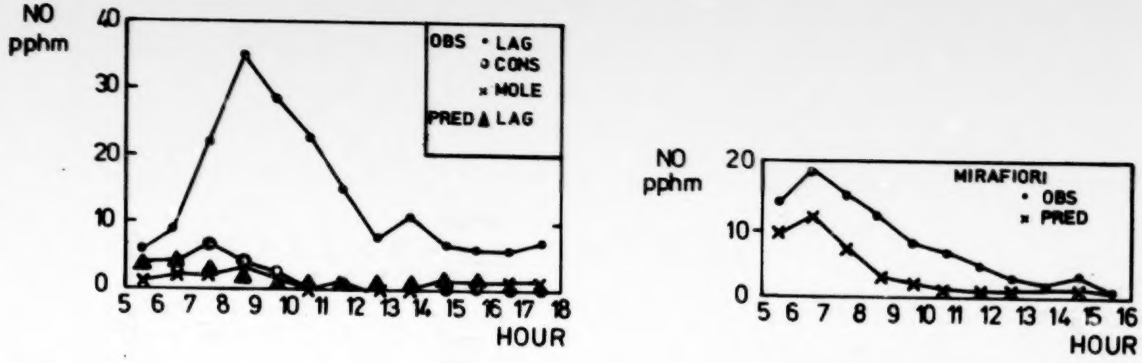

Figure 4. Predicted and Observed NO Concentrations.

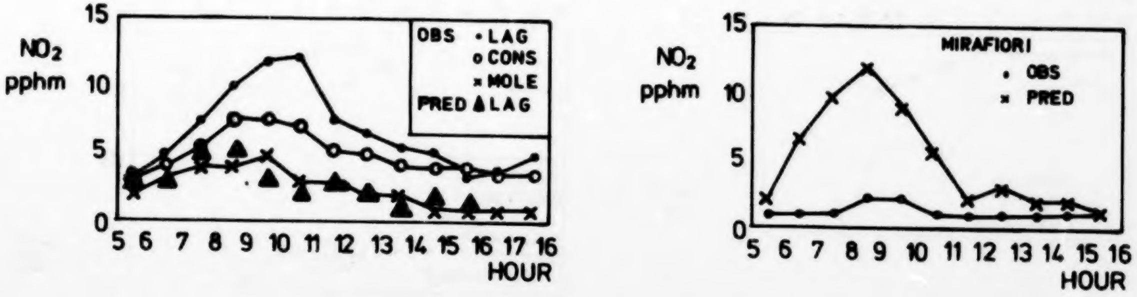

Figure 5. Predicted and Observed NO_2 Concentrations.

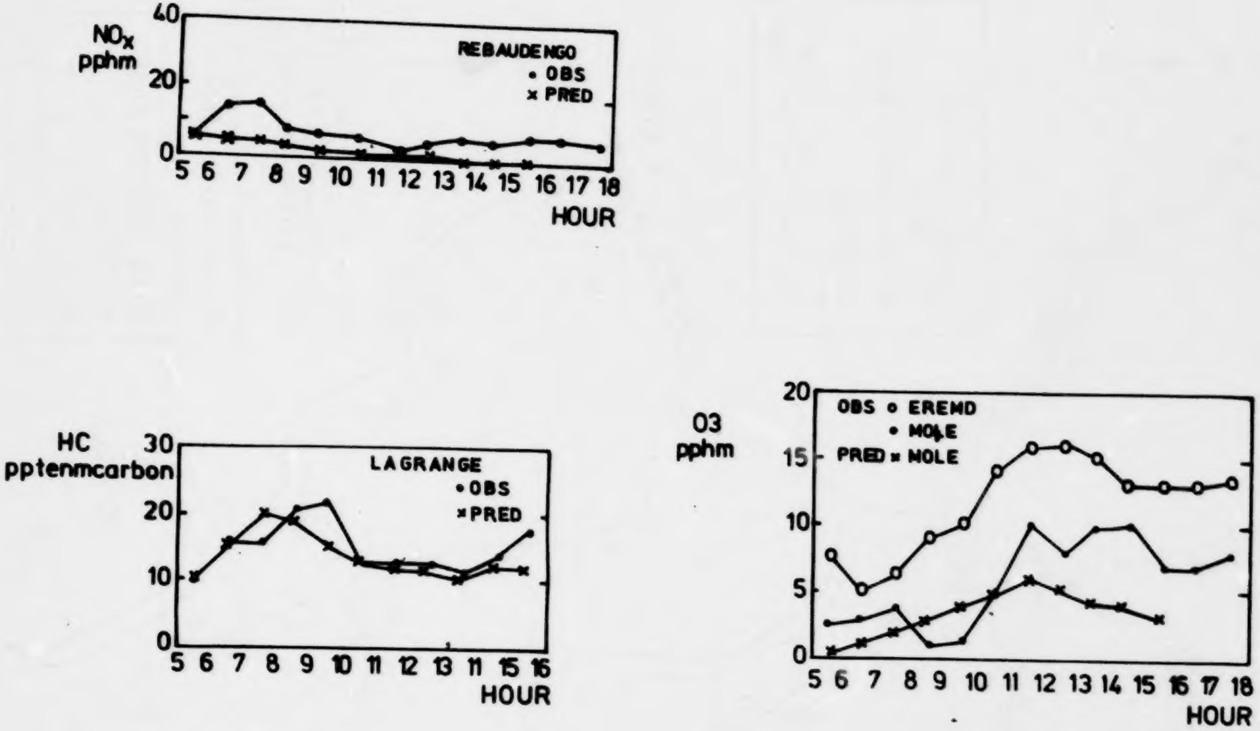

Figure 6. Predicted and Observed NO_x, HC and O_3 Concentrations.

Figure 7. NO_2 Concentrations (ppb) Along the First Flight Path (1235 - 1407 hours).

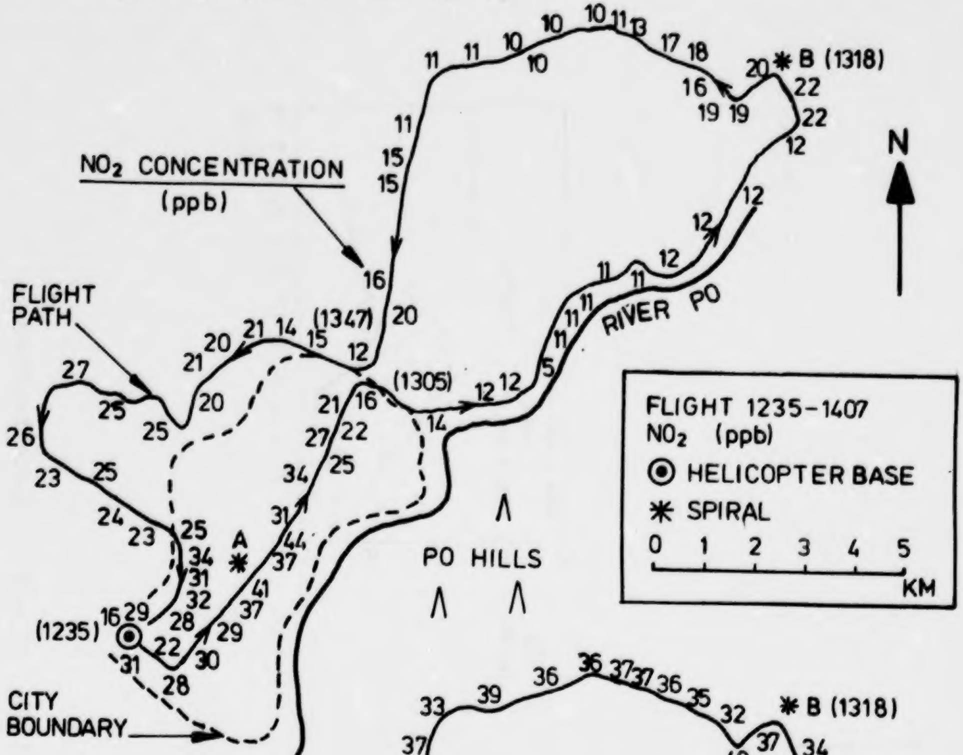
NO₂ CONCENTRATION
(ppb)
FLIGHT PATH
CITY BOUNDARY
RIVER PO
PO HILLS
A
B (1318)
(1235)
(1305)
(1347)
N
FLIGHT 1235-1407
NO₂ (ppb)
HELICOPTER BASE
SPIRAL
0 1 2 3 4 5
KM
11 11 10 10 10 10 11 13 17 18
20 22 22 12
16 19 19
11 15 15 16 20 12
21 20 21 14 15
27 25 25 26 23 25 24 23 25 20
34 31 32 28 29 16 22 31 28 30 29 37 41 37 44 31 34 25 27 22 21 16
14 12 12 5 11 11 11 11 12 12 12

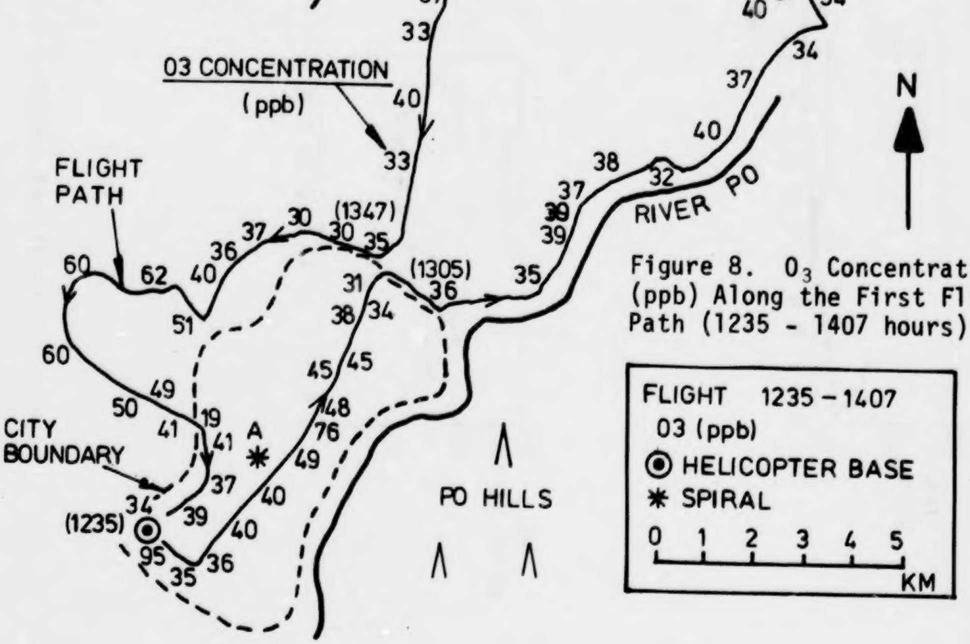
O3 CONCENTRATION
(ppb)
FLIGHT PATH
CITY BOUNDARY
RIVER PO
PO HILLS
A
B (1318)
(1235)
(1305)
(1347)
N
FLIGHT 1235 - 1407
O3 (ppb)
HELICOPTER BASE
SPIRAL
0 1 2 3 4 5
KM
33 39 36 36 37 37 36 35 32
37 34 34 40
37 33 40 33
37 30 30 35 36 40
60 62 51 60 49 50 41 19 41 37 39 34 95 35 36 40 40 49 76 48 45 45 38 34 31 36
35 39 39 37 38 32 40 37

Figure 8. O_3 Concentrations (ppb) Along the First Flight Path (1235 - 1407 hours).

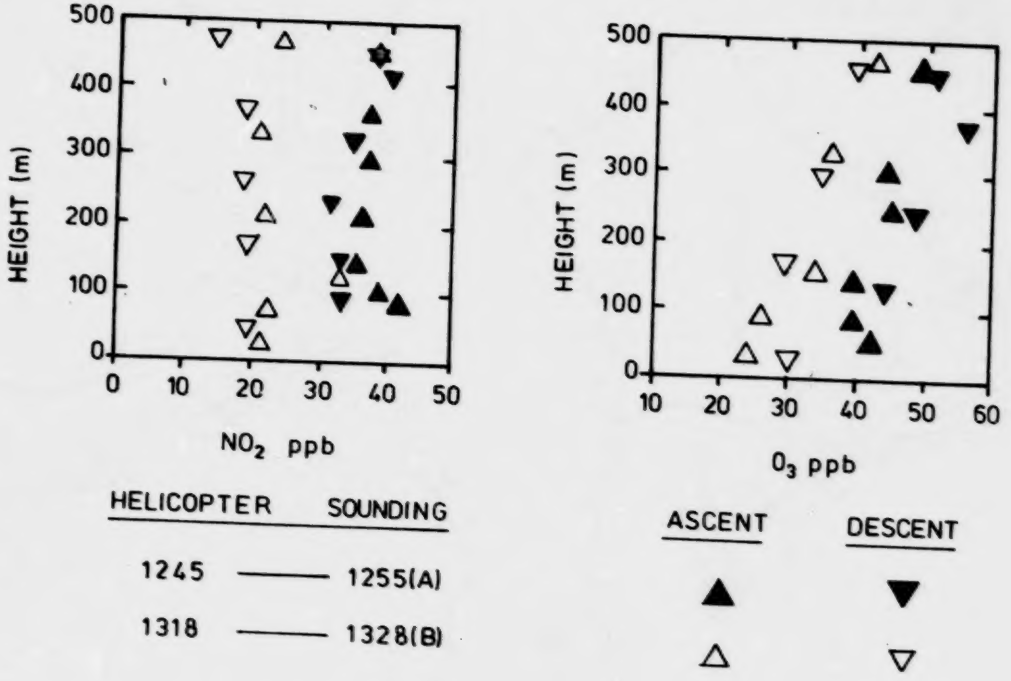

Figure 9. NO_2 and O_3 Concentrations (ppb) for the Spirals Executed During Flight 1235 - 1407.

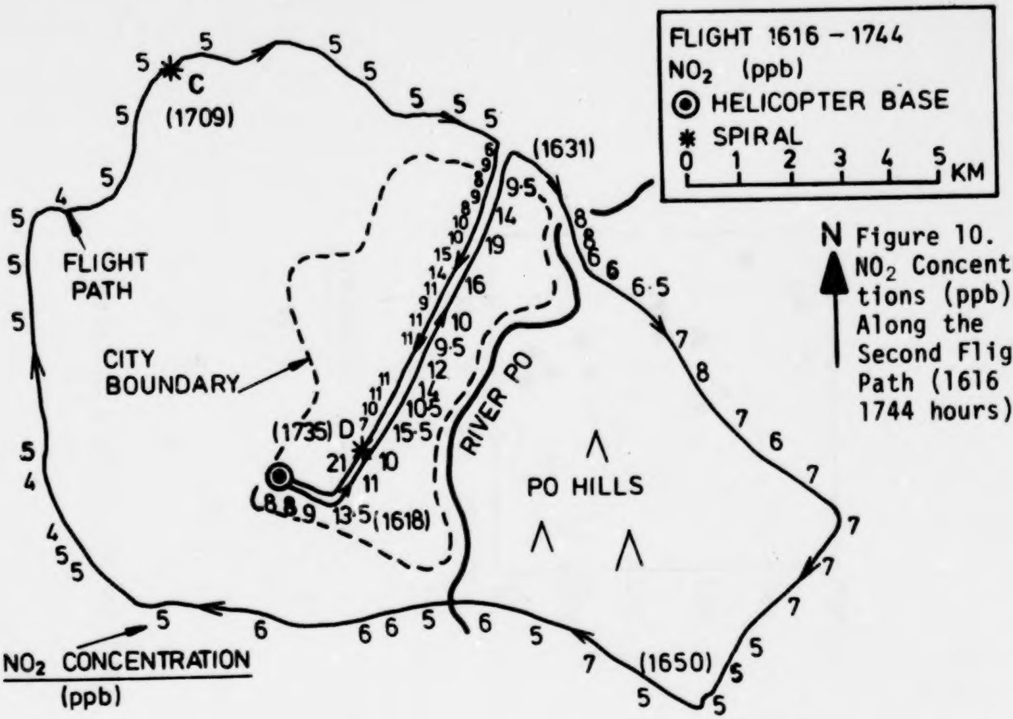
FLIGHT 1616 – 1744
NO_2 (ppb)
HELICOPTER BASE
SPIRAL
0 1 2 3 4 5 KM
N
C (1709)
(1631)
FLIGHT PATH
CITY BOUNDARY
(1735) D
(1618)
RIVER PO
PO HILLS
(1650)
NO_2 CONCENTRATION (ppb)

Figure 10. NO_2 Concentrations (ppb) Along the Second Flight Path (1616 - 1744 hours).

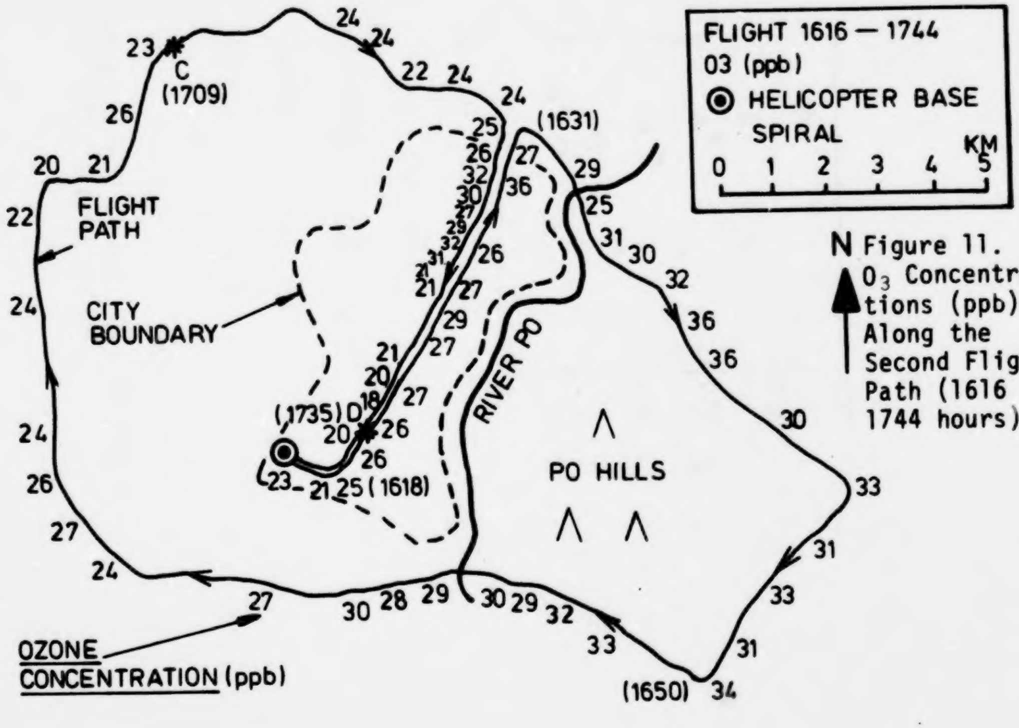
FLIGHT 1616 — 1744
03 (ppb)
HELICOPTER BASE
SPIRAL
0 1 2 3 4 5 KM
N
C (1709)
(1631)
FLIGHT PATH
CITY BOUNDARY
(1735) D
(1618)
RIVER PO
PO HILLS
(1650)
OZONE CONCENTRATION (ppb)

Figure 11. O_3 Concentrations (ppb) Along the Second Flight Path (1616 - 1744 hours).

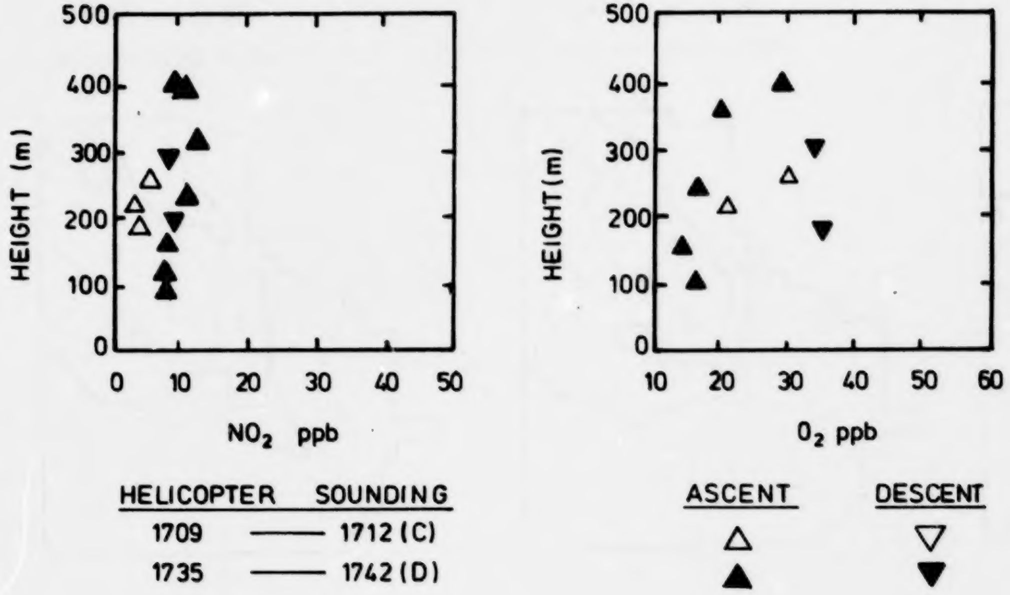

Figure 12. NO_2 and O_3 Concentrations (ppb) for the Spirals Executed During Flight 1616 - 1744.

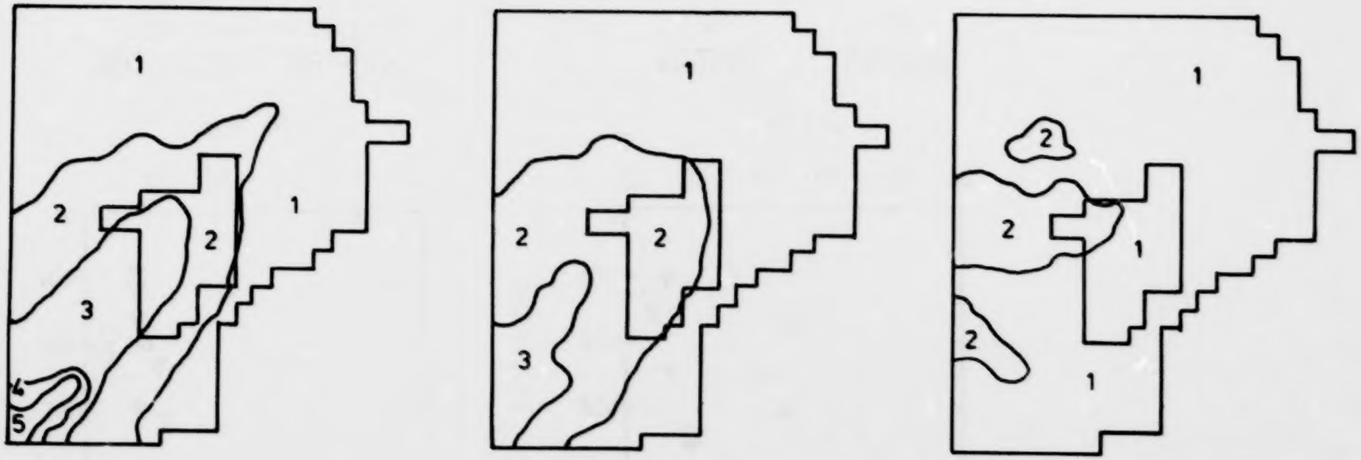
1
2
3
4
5
2
1
1
2
2
3
1
2
2
1
2
1

1100 — 1200 HOUR
NO_2 PPHM

1200 — 1300 HOUR
NO_2 PPHM

1500 — 1600 HOUR
NO_2 PPHM

Figure 13. Predicted NO_2 Concentrations (pphm) for Hours 1100 - 1200, 1200 - 1300, and 1500 - 1600.

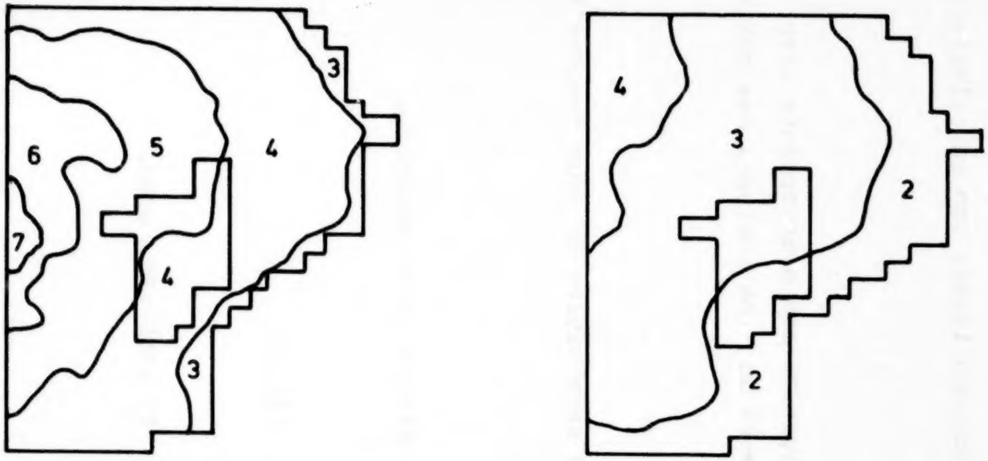

1300 — 1400 HOUR
OZONE PPHM

1500 — 1600 HOUR
OZONE PPHM

Figure 14. Predicted O_3 Concentrations (pphm) for Hours 1300 - 1400 and 1500 - 1600.

Discussion:

Van den Hout:

How did you accout for the effect of upwind hydrocarbons on the ozone levels? In Europe these hydrocarbon levels can be relatively high and therefore very important.

Benjamin (response):

Unfortunately no continuous hydrocarbon measurements were taken outside the city. Bag samples were taken but the analysis has not yet been completed.

Van den Hout

Do you have a feeling for the sensitivity of your results to the hydrocarbon levels?

Benjamin (response):

The results would be quite sensitive to hydrocarbons.

Anfossi:

How did you choose the diffusivities?

Benjamin (response):

The diffusivity profiles given by Lamb were used.

MULTIVARIATE REAL TIME PREDICTORS OF SULPHUR DIOXIDE CONCENTRATIONS IN MILAN CITY (*)

by

D. Barbieri, M. Baroni, G. Finzi

Istituto di Elettrotecnica ed Elettronica
Centro Teoria dei Sistemi C.N.R.
Politecnico of Milan
Italy

Abstract. A multivariate ARX type stochastic model of SO_2 pollution in Milan city is illustrated. The model describes the dynamics of a vector of three variables taken as representative of pollution (the vector of daily Dosage Area Products or DAPs in three sectors of the area under consideration). Precisely, the DAP vector in each day is expressed in the model as a function of the DAP vector in the previous day, of wind speed and of temperature (which is assumed to account indirectly for the emission term). A separate meteorological wind speed predictor is also set up. The one day ahead forecast performance of the DAP model has been tested in correspondence with two heating seasons data and has turned out rather satisfactory both in medium pollution situations and in episodes.

1. Introduction

In the last few years stochastic mathematical models such as ARIMA (Auto Regressive Integrated Moving Average) or seasonal ARIMA have been largely used in order to fit time series of pollutant concentrations[1-4]. Moreover, real-time predictors have been derived from such models[5], that is, recursive relationships supplying, at the beginning of each time interval, the optimal forecast of future concentrations on the basis of concentrations data recorded during the previous intervals. The problem concerning ARIMA models is that no physical cause of the phenomenon (meteorology and emissions) is pointed out as input to the model, but the effect of such causes on pollutant concentrations is represented only by the random terms. So, the derived predictors are unable to give a satisfactory forecast performance in presence of pollution episodes. In fact, such rapid increases and subsequent decreases of pollutant concentrations can be explained only bu putting into evidence the existence of a particular me-

---

(*) Research supported by C.N.R. - Progetto Finalizzato "Promozione della Qualità dell'Ambiente".

teorological and/or emission situation.

Therefore, a better real-time predictor can be derived by the so-called ARIMAX (ARIMA with eXogenous inputs) stochastic mathematical representations [5-6]. In such models, the average concentration in a certain interval is expressed as a linear combination of past average concentrations, plus linear combinations of present and past physical inputs, plus the noise term[7-9].

The present paper illustrates a multivariate ARX (Auto Regressive with eXogenous inputs) stochastic model and predictor of daily SO_2 concentration in Milan (Northern Italy) during the heating season. More specifically, such model describes the dynamics of a vector of three variables, taken as representative of pollution (the vector of daily Dosage Area Products or DAPs [10] in three sectors of the area under consideration).

The paper is organized as follows. The basic characteristics (meteorology, emissions, data set,...) of the pollution modelling problem in the area under consideration are illustrated in the next section. The definition of the three-component DAP vector is given in the 3rd section. Then the stochastic model describing the dynamics of the DAPs is illustrated together with a separate wind speed model, based on forecast synoptic meteorology. Finally, the one-day-ahead forecast performance of the pollution predictor is examined.

2. Description of the area and data set

The city of Milan is shown in Figure 1 together with the network of ten SO_2 monitoring stations, each supplying hourly averages. Specifically the regions under consideration are R_1, R_2, R_3, that is three sectors of a circular region R.

The city is situated in the Po Valley, a completely flat area without any orographic effect.

Hourly wind speed and direction are measured by one meteorological station in the center of region R. The station also records average hourly and daily temperatures, as well as daily maxima and minima.

Particularly in the heating season, Milan is affected by a very weak circulation[11] (average daily wind speed = 2 m sec^{-1}). Moreover in such season there are often many days of calm and inversion, which lead to high accumulation of pollutant (hourly averages not unfrequently over 1 ppm).

The frequencies of wind direction in the time periods analyzed in this study are shown by the wind rose of Figure 2, which is rather similar from year to year. Wind direction is rather highly correlated to wind speed; in particular the most frequent winds (S-SE) correspond in most cases to a weak circulation in the range 0,5 $msec^{-1}$ - 1,5 $msec^{-1}$.

As for emissions, in winter time pollution in R is practically due only to residential heating, since there are neither significant industrial sources in R nor significant transport from external industrial zones. In particular, the industrialized area of Sesto is located in the north-east, the direction which corresponds to the most unfrequent wind. By looking at the figures of population density in R, it is reasonable to assume slight disuniformities in the emission spatial pattern. This pattern has been the main factor which has influenced the subdivision of R into the three sectors shown in Figure 1. In particular R_1 is the "most polluting" zone. Because day-by-day emission rates are non measured, emission is only indirectly taken into account in the model (See 4th section).

3. The dosage area product vector

From SO_2 hourly averages it is straightforward to derive the daily dosages in the ten stations; in order to obtain the time series of the variables taken as pollution representative, such data have been manipulated as follows.

Consider a coordinate system with the origin in the center of region R, the X-axis and the Y-axis directed towards the east and the north respectively. The Dosage Area Product over the j-th sector of the region R in the k-th day is defined as

$$DAP_j(k) = \frac{1}{A_j\Delta} \int_{R_j} \int_{k\Delta}^{(k+1)\Delta} c(x,y,t)\,dt\,dx\,dy \qquad j=1,2,3 \qquad (1)$$

where

Δ = 1day

A_j = area of R_j

$c(x,y,t)$ = pollutant concentration at time t at point (x,y).

Formula (1) differs from the original DAP formula[10] because of the scale factor $A_j\Delta$.

If $D(x,y,k)$ denotes the k-th day dosage at point (x,y), then eq.(1) can also be written in the form

$$DAP_j(k) = \frac{1}{A_j} \int_{R_j} D(x,y,k)\,dx\,dy \qquad j=1,2,3 \qquad (2)$$

Let (x_i,y_i), $i=1,2,\ldots,10$, be the coordinate of the i-th station and let $D_i(k) = D(x_i,y_i,k)$, denote the daily dosage in the i-th station. An approximate evaluation of the integral in eq. (2) by means of the measured variables $D_1(k)$, $D_2(k)\ldots,D_{10}(k)$ can be obtained through the socalled polygons method. The method consists of :

i) subdividing R by a thick grid;

ii) assuming that in each square of the grid the dosage is the same as in the station nearest to the square (i.e. giving each station a polygonal "area of influence").
There turns out an approximation of the type

$$DAP_j(k) = \frac{1}{A_j} \sum_{i=1}^{10} a_i^j D_i(k) \qquad (2')$$

where

a_i^j = area of the surface common to sector R_j and to the polygon covering the grid squares near station i.

By considering the daily dosage data recorded in the periods (October 16th, 1975 - March 30th, 1976), (October 16th, 1976 - March 30th 1977) in the ten monitoring stations and by applying eq. (2') to such data, a time series of the vector of interest $DAP(k) = |DAP_1(k), DAP_2(k), DAP_3(k)|'$ ('= vector transposition symbol) has been obtained. Such time series, from now onwards called "historical DAP series", together with the series recorded by the meteorological station in the same period, has allowed to estimate the parameters of the model of the DAP vector described in the next sections.

4. A Multivariate ARX model of the DAP vector

First, the "historical DAP time series" mentioned above has been assumed to be a (finite) realization of a three variate stationary random process $\{DAP(k)\}_k$, whose main statistics are shown in Table 1a).

The stationarity hypothesis means to postulate that the random process is not affected by cycles or trends. It is a reasonable assumption, since only daily DAP in the heating season is considered, so that the process $\{DAP(k)\}_k$ is a priori not affected by daily and seasonal astronomical and emission cycles. Moreover, the habits in the use of residential heating do not suggest the presence of a weekly emission cycle. As for trends, there is no reason to presume their existence in the period under consideration.

Then, it has been assumed that the DAP process can be represented by the following three variate ARX(p) (Auto Regressive of order p with eXogenous inputs) models class :

$$DAP(k+1) = \sum_{l=1}^{p} \alpha_l DAP(k-l+1) + \sum_{i=1}^{r} \beta_i u_i(k+1) + \varepsilon(k+1) \qquad (3)$$

where

α_l = 3x3 matrices of model parameters.

Table 1. a) DAP means and standard deviations
b) "Episodes" means and standard deviations.

J	1	2	3
μ_j [ppm]	.208	.183	.168
σ_j [ppm]	.115	.101	.089

a)

J	1	2	3
μ_J^E [ppm]	.420	.357	.340
σ_J^E [ppm]	.105	.087	.081

b)

β_i = three component vectors of model parameters.

$\{\varepsilon(k)\}_k$ = three variate, purely random zero mean process (white noise).

$\{u_i(k)\}_k$ = emission and/or meteorological exogenous input.

p = order of the autoregressive part of the model.

Eq. (3) can be interpreted in the following way. The DAP value in the (k+1)-th day is expressed as a linear combination of previous DAP values (Auto Regressive part of the model), plus external inputs contribution, plus a random fluctuation (stochastic part of the model).

Because day-by-day emission from each residential heating source is not obviously recorded, it has been assumed that overall emission in the (k+1)-th day can be somehow taken into account by introducing the average temperatures T(k) and T(k-1) of the two previous days as model inputs. Precisely the emission in (k+1)-th day over the j-th sector has been represented as follows:

$$u_{1J}(k+1) = a_J.f(T(k)) + b_J.f(T(k-1)) \qquad J=1,2,3 \qquad (4)$$

where

$$f(T(k)) = \frac{1}{c+T(k)} \qquad (5)$$

This assumption is equivalent to postulate a one day delay in the reaction of people to temperature changes. Moreover, such reaction may be different depending on the temperature gradient from day to day. Such arguments have proved reasonable a posteriori, since the use of T(k) and T(k-1), instead of T(k+1) and T(k) has given a better forecast performance.

As for (5), the choice of an hyperbolic function is arbitrary, but, again, a posteriori the use of form (5) has given a better forecast quality than the use of other decreasing functions of T(k).

Moreover, average daily wind speed has been introduced into the model as meteorological input taking

$$u_{2J}(k+1) = m_J v(k+1) + q_J \qquad J = 1,2,3 \qquad (6)$$

In view of (4), (5) and (6), taking p=1, the multivariate ARX model turns out to be :

$$DAP(k+1) = \alpha DAP(k) + \beta_i u_1(k+1) + \beta_2 u_2(k+1) + \varepsilon(k+1) \qquad (7)$$

that is equivalently :

$$DAP(k+1) = \alpha DAP(k) + a' \frac{1}{c+T(k)} + b' \frac{1}{c+T(k-1)} + m'v(k+1) + q' + \\ + \varepsilon(k+1) \qquad (7')$$

The estimation of the parameters of the model has been carried out from the historical DAP time series of 1975/76 heating season. In particular, the model is non linear with respect to the c parameter. Hence, standard least squares fitting techniques[12] cannot be applied. So, a simple iterative parameter estimation procedure has been set up, based on the consideration that model (7') is linear with respect to α, a', b', m', and q'. The general step of such procedure consists of the following operations:

i) a value of c is given by the previous step; in correspondence with such given value of c, optimal estimates of the other parameters are found through standard least squares fitting;

ii) in correspondence with such values, c is changed in accordance with a gradient technique[13] in order to improve fitting.

Operations i) and ii) are iterated untill the estimates of all the parameters converge.

The predictor derived by model (7') simply consists of setting $\varepsilon(k+1)$ to its expected value, namely zero. Precisely, the forecast of the (k+1)-th day DAP vector, made at the end of the k-th day is given by the realtionship

$$\hat{DAP}(k+1) = \alpha\ DAP(k) + a' \frac{1}{c+T(k)} + b' \frac{1}{c+T(k-1)} + m'v(k+1) + q' \qquad (8)$$

But, clearly, v(k+1) is not an available datum at the end of k-th day. To overcome such difficulty, it is necessary to set up a separate meteorological model and predictor of wind speed and subsequently introduce day-by-day wind speed forecasts as inputs for the DAP predictor (8).

5. A wind speed predictor

A simple real-time wind speed predictor has been used:

$$\hat{v}(k+1) = \phi\ (s(k+1))\ v(k) + \zeta(s(k+1)) \qquad (9)$$

where $s(k+1)$ is a meteorological binary category defined on the basis of forecast synoptic tables, that is an information about the expected general atmospheric circulation. More precisely two meteorological classes are defined in this way :

i) First class: anticyclonic conditions on Northern Italy
ii) Second class: cyclonic conditions on Northern Italy.

So, the parameters estimates change in accordance with the prediction of the meteorological class. Such prediction is an available datum because it is regularly supplied by the Italian Air Force Meteorological Service.

6. Real Time DAP predictor

By introducing $\hat{v}(k+1)$ given by eq. (9), the DAP predictor takes the form :

$$\hat{DAP}(k+1) = \alpha\ DAP(k) + a'\ \frac{1}{c+T(k)} + b'\ \frac{1}{c+T(k-1)} + m'\hat{v}(k+1)+q' \qquad (8')$$

Predictor (8') has been tested on a computer in correspondence with the heating season 1976/77, that is a different period from the one used for estimating the parameters of the predictors.

Component by component, the forecast performance of the DAP predictor (8') has been measured by the following indexes:

θ_j = correlation between predicted and observed DAP_j
θ_j^E = correlation between predicted and observed DAP_j during episodes;
$\sigma_j^\varepsilon/\mu_j$ = ratio between the standard deviation of the forecast error $\varepsilon_j(k) = DAP_j(k) - \hat{DAP}_j(k)$ and the mean of $\{DAP_j(k)\}_k$;
η_j^E/μ_j^E = ratio between the mean square error of the forecast and the mean of $\{DAP_j(k)\}_k$ during episodes.

Specifically an episode has been defined as a time interval characterized by $DAP_j(k) > \mu_j + \sigma_j$ (means and standard deviations of episodes process are reported in Tab. 1b).

The forecast performance is summarized in Table 2 (top part) and is quite satisfactory, mainly in episode situations.

Moreover, day-by-day behaviour of DAP forecast is reported in Figure 3. Precisely, Figure 3 reports the pairs ($DAP_2(k)$, $\hat{DAP}_2(k)$) in the two heating seasons considered.

To measure the effectiveness of the meteorological predictor (9), the pollution predictor (8) has also been run introducing the future true value of v(k+1) at each forecast step. The result is summarized in Table 2 (bottom part) and shows the loss due to imperfect wind speed forecast. The loss, however, is not so high as one might have feared by the gross nature of meteorological predictor.

Table 2. Forecast performance of predictors.

Meteorological inputs to ARX predictors	J	θ_j	θ^E_j	$\sigma^\varepsilon_J/\mu_j$	$\eta^\varepsilon_J/\mu^E_j$
T(k),T(k-1) v(k),s(k+1)	1	.80	.64	.35	.33
	2	.82	.71	.33	.28
	3	.80	.51	.34	.31
T(k),T(k-1) v(k+1)	1	.85	.69	.31	.29
	2	.85	.73	.31	.27
	3	.84	.53	.31	.28

7. Concluding remarks

An ARX multivariate stochastic model and predictor of a pollution index vector(the daily Dosage Area Product vector) has been tested on Milan SO_2 concentration data.Inputs to such model are mean daily temperatures of the two previous days(as representative of overall emissions) and mean daily wind speed of next day. So, while the temperature inputs are available data at the same time when the prediction is made, the wind speed input requires a separate meteorological predictor. Such predictor is a very simple one, based on the analysis of past measurements and on the definition of two gross synoptic meteorological categories (cyclonic or anticyclonic circulation on Northern Italy). The forecast performance of the resulting DAP predictor is rather satisfactory and encourages the authors to carry on the study of possible utilizations of synoptic meteorology forecast in pollution predictors.

Acknowledgment

The authors thank Prof. L. Santomauro, Director of the "Osservatorio Meteorologico di Brera" (Milan), and Dr. R. Gualdi and Dr. G.C. Tebaldi of the "Laboratorio Provinciale di Igiene e Profilassi" (Milan) for their collaboration and useful criticism.

References

1. P.H. Merz, L.Y. Painter, P.R. Ryason, "Aerometric data analysis. Time series analysis and forecast and an atmospheric smog diagram", Atmospheric Environment 6: 319, 1972.
2. D.P. Chock, T.R. Terrel, S.B. Levitt, "Time-series analysis of Riverside, California air quality data", Atmospheric Environment 9:978, 1975.
3. G.M. Mc Collister, K.R. Wilson, "Linear stochastic models for forecasting daily maxima and hourly concentrations of air pollutants", Atmospheric Environment 9:417, 1975.
4. G.C. Tiao, G.E.P. Box, W.J. Hamming,"A statistical analysis of the Los Angeles ambient carbon monoxide data 1958-1972", J. Air Pollut. Contr. Ass. 25:1129, 1975.
5. G.E.P. Box, G.M. Jenkins, "Time Series Analysis, Forecasting and Control". Holden-Day, San Francisco, 1970.
6. P. Young, P. Whitehead, "A recursive approach to time series analysis for multivariable systems", Int. J. Control, 25:457, 1977.
7. G. Finzi, G. Fronza and S. Rinaldi "Stochastic modelling and forecast of the dosage area product", Atmospheric Environment, 12:831, 1978
8. G. Finzi, P. Zannetti, G. Fronza, S. Rinaldi: "Real time prediction of SO_2 concentration in the Venetian Lagoon area", Atmospheric Environment, 13:1249, 1979.
9. G. Finzi, G. Fronza, S. Rinaldi, A. Spirito, "Prediction and Real-time Control of SO_2 Pollution from a Power Plant", Air Pollution Control Association Annual Meeting - Houston, 1978.

10. S. Duckworth, and E. Kupchanko, "Air analysis: the standard dosage area product", J. Air Pollut. Control Ass. 17:379, 1967

11. L. Santomauro, R. Gualdi, G. Tebaldi, "Modello di simulazione della diffusione atmosferica locale (Area Urbana di Milano)"CNR-AQ/3/1. Coll. del Prog. Fin. "Promozione della Qualità dell'Ambiente", 1978.

12. K.Y. Åstrom, P. Eykhoff, "System identification: a survey", Automatica 7:123, 1971

13. D.G. Luenberger, "An introduction to linear and non linear programming", Addison-Wesley, Reading-Mass, 1973.

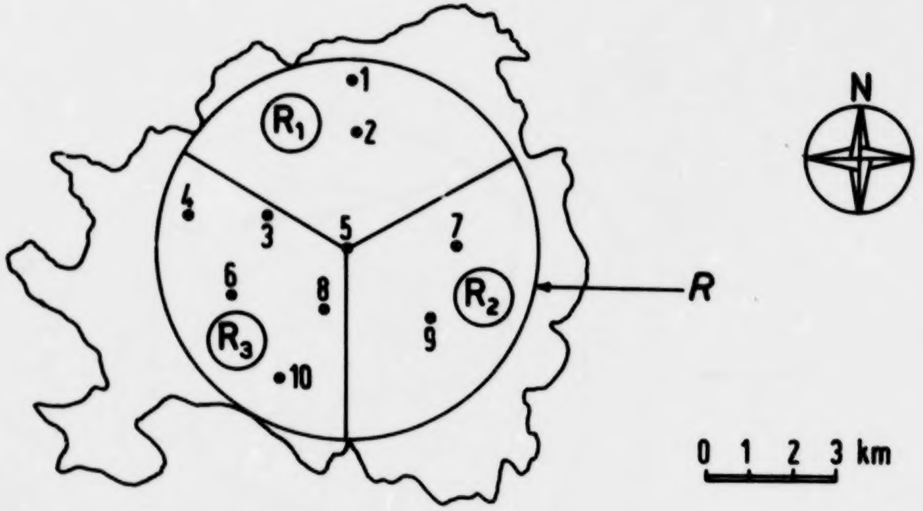
N
R
R1
R2
R3
1
2
3
4
5
6
7
8
9
10
0 1 2 3 km

Figure 1. The region under consideration, the three sectors and the SO_2 monitoring network.

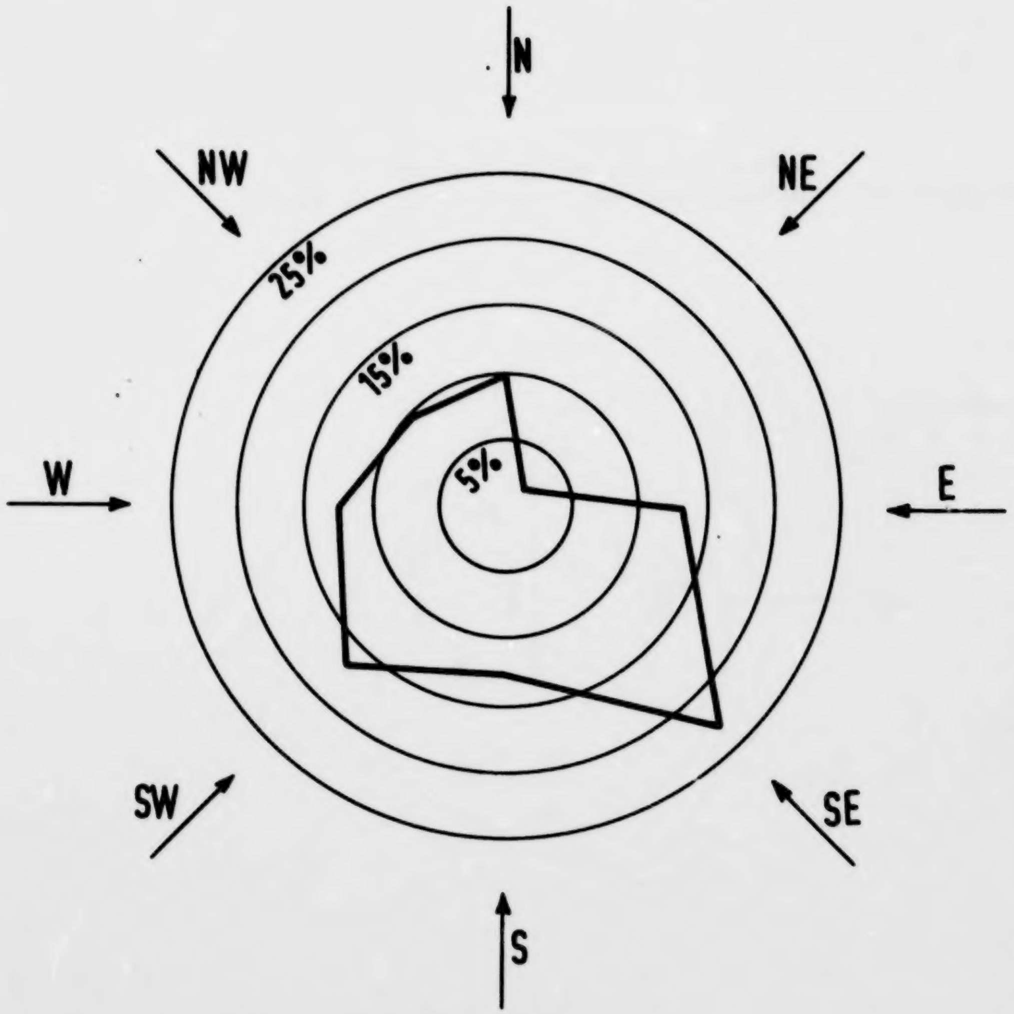

Figure 2. Wind rose in the heating season.

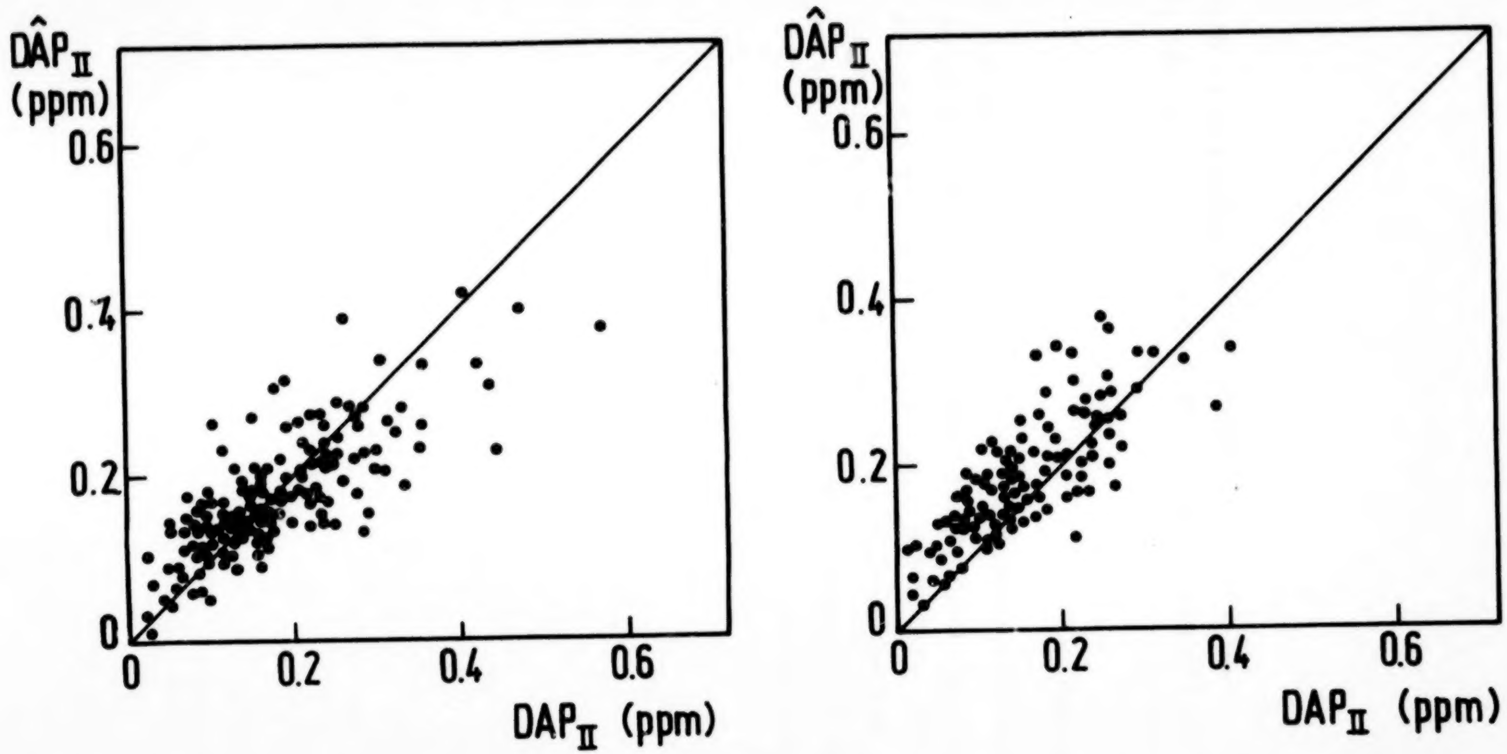

Figure 3. Forecast versus observed DAP_2 ((a) 1975-76 heating season; (b) 1976-77 heating season).

Discussion:

Barrett:

Is there an important contribution to the pollution in Milan from sources outside, for example other cities in Northern Italy, and if so, how do you allow for it?

Finzi (response):

We have primarily considered the SO_2 from winter heating. There is a large industrial zone to the north of Milan but a study of the wind rose indicates that wintertime winds from this sector are quite infrequent. Therefore, the assumption of no outside sources appears to be reasonable. Examination of the wind rose also served as a basis for selection of the three sectors used.

SOME COMMENTS ON THE VALIDATION OR VERIFICATION OF MULTIPLE SOURCE MODELS FOR IMPACT ASSESSMENT

by

J.G. Kretzschmar
Nuclear Energy Research Centre
B2400 Mol, Belgium

Abstract. Validation or verification of whatever mathematical model is a "conditio sine qua non" for the proper use of that model, especially when impact assessment studies, and the corresponding air quality management are based on the results of the model. Based on a critical review of the existing validation procedures some hints for the validation of multiple source models for impact assessment are formulated. The importance of validation in time and in space is stressed, and practical examples illustrate the feasibility of the approach.

Introduction

Whatever mathematical dispersion model, simple or complex, naive or sophisticated, is useless for practical applications, especially in Air Quality Management, if no proofs can be given of the fundamental correctness of the model formulation on one side and if the accuracy, this is the ability of the model to replicate known conditions, has not been assessed and illustrated by means of practical examples on the other side. These statements seem to be rather trivial, but their practical application is not trivial nor straightforward at all. At least two recent papers, respectively by D. Bruce Turner and by K.E. Bencala and J.H. Seinfeld, are surely worthwhile to be read in this context.[1,2] Having finished the lecture of these papers, the interested reader could start the reading of at least one thousand other scientific papers, reports and books which deal in one way or another, directly or indirectly, with the above mentionned problems of correctness of model formulations and accuracy of model calculations. The impressiveness of this large amount of available information illustrates very well the already mentionned non-triviality of what's normally called model validation or model verification.

Validation or verification

Although not based on the one thousand available publications in the open and the grey litterature, this paper will try to review and discuss some of the commonly used techniques to verify the accuracy of the results of multiple source models, with the accent on models for impact assessment studies. This is clearly an engineer's point of view and not the approach of a physicist, being possibly more interested in the fundamental correctness of the model formulation, although it must be emphasized that for the multiple source problem the latter approach seems to be too complicated anyway.

In what follows the terms validation and verification are used as synonyms, both implying that a mathematical analysis was performed either on a data set consisting of measured concentrations and modeled estimates for the same locations and times, or on an ensemble of measured and calculated statistical quantities derived from the previous data sets over a specified period of time.

While it is certainly true that the advisable validation procedure for a specific model is biased by the objectives of the model, it is also a fact that oversimplifications, such as reducing the entire validation procedure to the verification of the end results of the model, e.g. the arithmetic means over one year in a multiple source region, must be avoided because they lead sometimes to rather naive assumptions concerning the real validity and applicability of the model.

Validation procedures are not only functions of the output and objectives of a model, but maybe even more of the available input data and their quality. Using complicated or sophisticated mathematical techniques on the output of models with poor input data is merely a waste of time. If for example the model calculations are based on joint frequency tables over one year for the meteorological input, how could one ever hope to compare calculated and measured values for a specific day or even hour ? Although calculated and measured cumulative frequency distributions could be compared here, one could seriously question the soundness of the conclusions of such a comparison.

Analysis of Residuals

The systematic comparison over a given period of time of the successively calculated and measured short-term (t_{av} = 30 min to 24 h) concentration values for a given pollutant in a specific site is by far the most straightforward, and possibly also the most objective way for assessing the accuracy of model calculations. Such an analysis of residuals is normally based on the ensembles of the absolute differences between observed and calculated concentrations, although relative residuals, with respect to the observed values, could give specific information as well. The results of the analysis are normally presented as summary statistics for a given averaging time over the period T. For each site are given the mean error, the root mean square error centered at the mean, the error range or error band, a complete histogram of the residuals and a residual plot or scatter diagram [2,4,5,6].

Instead of analyzing the residuals on the individual concentration values, quite a lot of validations are limited to the analysis of the residuals on certain specific statistical parameters such as arithmetic- or geometric averages, geometric standard deviations, some specific percentiles or certain extreme values, such as second highest or highest concentration values for a given averaging time and period over which the calculations and observations were done. It is obvious that those checks have to be done, especially when the impact model has to be used in context with an Air Quality Standard specifying one or more of these statistical parameters.

It is nevertheless quite true that a good agreement between calculated and observed values on this level does not at all imply a proper control of the validity of the model as quite different distributions could have the same overall statistics. Summarizing one could state that controls of this type are necessary but not sufficient, especially not when the so-called validated model will be used for Air Quality Management implying a selective emission reduction strategy.

Correlation and Regression Techniques

Not only in air pollution modelling, but in almost all air pollution problems and studies, the correlation and regression techniques are very popular. For model verifications the correlation technique tries to show that there exists a systematic relationship between observations and calculations, while the regression technique tries to find the proper equation for that relation. It must be emphasized once again that these techniques must be applied to the basic elements of simulation namely the short-term averages (t_{av} = 30 min to 24 h). The best guarantee for building a good house is to start with the control of the bricks and the concrete. This does not imply that the house as a whole has not to be controlled.

The results of these correlation and regression techniques must be reported in a concise but complete way. Statements such as "A significant correlation was found" or "The correlation coefficient was high, namely 0.7" are too general and obscure. For each site where a set of calculated and simultaneously observed short-term concentrations were obtained one shall report the following information : type of correlation and regression technique (linear, power low, parabolic ...), number of elements or pairs of simultaneous calculation and observation (n), together with the averaging time (t_{av}),correlation coefficient (r), coefficients of the regression equation (a,b...), standard error of estimates (S_y, S_x) or confidence limits and preferentially also a scatter diagram showing the dispersion of calculated and measured values with respect to the regression curve [3,6,8,9,10,11,12].

Quite a lot of validation exercises reported in the open litterature restrict themselves to the calculation of the linear correlation coefficient and the linear regression line for long-term averages in the same site or in different sites e.g. monthly means, 3 monthly means, seasonal means or yearly means. Although this approach is quite interesting, especially from the point of view of the reproducibility of these long-term averages in time and space, it must be stressed that it is a very dangereous approach if this is the only verification whereon the further use of the model will be based.

It is also quite surprising that everybody uses linear regression techniques without any proof that this approach gives the highest correlation. It is not because a good model should show a linear relation between calculated and observed values, that a linear regression always gives the best fit for the output of whatever model. As the specific form of the best fit could be quite revealing for the properties of the model, it is maybe worthwhile to give sufficient attention to this point.

Before ending this paragraph on correlation it is interesting to remember that the statistician can only help out the specialist in the field, not replace him and that at no point statistical methods are more of a sausage machine than in correlation analysis [13].

Time Series Analysis

Instead of comparing measured and calculated short-term concentrations by a statistical analysis of the residuals it is mostly interesting to plot both quantities as a function of time. The variability of the residuals as a function of time appears now, together with information concerning the possible existence and proper simulation of cycles (diurnal, weekly, seasonly and/or yearly) [3,5,6,10]. It is clear that a time plot of the residuals yields good complementary information here. Especially for multisource models such a time series could give some indication of the proper simulation of the different groups of sources (industry, space heating, traffic). These plots not only clearly identify the largest deviations between calculated and observed values, but also inform the modellist when they occur and if there is a systematic in their occurrence.

Regrouping calculated and measured values as a function of time over a long period e.g. as a function of the time of the day, the day of the week or the month of the year leads to a comparison between the average calculated and observed cycles. Such summaries are sometimes revealing, although the normally not given variances or standard deviations on the individual data points (arithmetic averages) could damp certain too optimistic conclusions.

When long-term trends over many years are observed in measured data, calculations must be repeated for different years in that period. The availability of the required input data could be the restricting factor for this kind of analysis.

Cumulative Frequency Distributions

In an indirect way many Air Quality Standards are in fact specifying a cumulative frequency distribution (CFD), and it is common use to compare CFD's of measured concentrations with the Air Quality Standard CFD in order to check the actual air pollution situation in a given region [14]. When the desired air quality is specified by a CFD it is possible to define the impact of an existing or future source, or group of sources, as its expected influence upon the actually existing cumulative frequency distribution.

Models applied for this purpose should first of all be able to reproduce the CFD's of the existing air-quality, and appropriate tests for this have to be included in a validation procedure [3,5,6,15,16,17,18]. Comparisons between calculated and measured CFD's are very useful for instance to detect overall under- or overestimations. Seasonal CFD's, subdivided into CFD's for the different source categories (point, line, area), sometimes bring more light in the darkness of the global statistics.

A check on the CFD's is a control on the properties of the statistical ensembles of measured and calculated air pollution levels. As such it is a must, but it is neither a guarantee for the individual values nor a proof for the ability to simulate the share of a specific source within the multiple source configuration. A validated model is nevertheless quite often intended to control specific sources or categories of sources.

Spatial Analysis

Increasing the number of receptor points or grid points where series of successive concentration values, or summary statistics, have to be calculated over a specified period of time is only a matter of slightly increasing the CPU time for most operational models. This means that spatial concentration patterns, as well for short-term as for long-term levels, are easily obtained. The verification of these patterns on the contrary is not at all easy. Model validation is normally not the principal purpose of a monitoring network and this results into an insufficient number of monitoring stations when the simulated pollution pattern has to be verified. As a consequence spatial verification or validation is usually restricted to some of the previously mentioned tests in a limited number of receptor points. This seems to be quite sufficient for smoothly varying concentration patterns, but has to be checked by supplementary measurements as soon as rather important gradients are noticed in the calculated or measured patterns.

More qualitative evaluations, such as comparing patterns of calculated and measured isolines, have to be handled with great care as the former are based on a freely chosen and not restricted grid point density, while the latter are mostly interpolations based on a very limited and unevenly distributed number of monitoring sites.

Analysis with respect to the input parameters

The analysis with respect to the input parameters aims at the discovery of possible systematic errors in the model results with respect to the input parameters [7]. Such an analysis is normally based on the variation of average computed and observed concentrations as a function of time, e.g. time of the day, day of the week, month of the year, as a function of certain meteorological input data, e.g. wind speed, wind direction, stability, mixing height or as a function of the emission strength of all sources or groups or categories of sources. Some typical examples of such an analysis are given in references 5 and 6.

A particular application of the analysis of the output with respect to the input is the comparison of calculated and observed air pollution roses on a site by site basis. Even in a multisource configuration measured air pollution roses sometimes clearly show the influence of a specific source on one or more monitoring sites. If properly simulated the same influences must appear in the calculated pollution roses.

A combination of measured air pollution roses in different sites, together with the spatial distribution of the emission strengths used as input for the model, quite often reveals if there is a wind direction dependent background level, which could never been explained by the source distribution actually used in the model. All calculated or measured values have to be corrected once the wind direction dependent background levels are determined. For further analysis especially in the single source case, it is advisable to correct the measured values and not the calculated ones, as the latter procedure could completely falsify certain statistical analyses e.g. a correlation between average observed and calculated values does not make much sense when the majority of the calculated values are artificially introduced background levels which by definition equal the observed values.

Conclusions

A unique or ideal validation or verification procedure does not exist and is not very likely to appear in the near future. Many different mathematical techniques have been applied in different contexts and for varying purposes. Each of them has advantages and shortcomings, so that a combination of different techniques seems to be a reasonable approach. Therefore a statement regarding validation or verification should include information as to what statistics were used to analize what data base.

The user of statistical techniques must be aware of averaging out effects and the possibility for error compensation. Verification of the individual portions of the model, analysis of the output as a function of the input parameters and comparison of the properties of the calculated and observed short-term averages are highly recommended for an objective evaluation of the model performance. It is always desirable to confirm whatever conclusion by means of second independent procedure. The findings for a specific test over a limited period of time should be confirmed by a second test over a different period of time.

Although regulatory specifications heavily bias the ultimate (mostly simple) output and use of a specific impact assessment model, the verification of such a model should not be restricted to the parameters specified by the regulatory purposes. Too complex or sophisticated validation procedures must be avoided on the other hand especially when the quality of the input data and the available measured air quality data is rather poor. What is lost in physics is never recuperated in statistics.

References

[1] D.B. Turner, "Atmospheric Dispersion Models. A Critical Review", J. Air Poll. Control Assoc. 29:502 (1979).

[2] K.E. Bencala and J.H. Seinfeld, "An Air Quality Model Performance Assessment Package", Atmos. Env. 13:1181 (1979).

[3] J.G. Kretschmar, G. De Baere and J. Vandervee, "Validation of the IFDM in the region of Antwerpen, Belgium", Proceedings of the Seventh International Technical Meeting on Air Pollution Modeling and Its Application; 1976, Airlie, U.S.A. NATO Committee on the Challenges of Modern Society. Publ. No.51. Brussels, Belgium, 1976 (Also available from NTIS PB 270-799).

[4] K.E. Noll, "A Comparison of three Highway Line Source Dispersion Models", Atm. Env. 12:1323 (1978).

[5] S. Okamoto and K. Shiozawa, "Validation of an Air Pollution Model for the Keihin Area", Atm. Env. 12:2139 (1978).

[6] G.L. Marziano, C.C. Shir, L.J. Shieh, A. Sutera, L. Gianolio and M. Ciprian, "Study of the SO_2 Distribution in Venice by means of an Air Quality Simulation Model", Atm. Env. 13:477 (1979).

[7] L.J. Shieh and C.C. Shir, "Analysis of Input Parameters and Results of Urban Air Pollution Computation", Proc. 3rd Symp. on Atmos. Turbulence, Diff. and Air Quality, AMS, Boston, MA, U.S.A., pp. 374-381 (1976).

[8] L.V. Gibson and L.K. Peters, "A Short-Term Air Quality Model for Sulfur Dioxide in Louisville, Kentucky", J. Air Poll. Control Assoc. 27:218 (1977).

[9] D.C. Guzewich, "Validation of the EPA-PTMTP Short-Term Gaussian Dispersion Model", J.Air Poll. Control Assoc. 27:540 (1977).

[10] M.C. MacCracken et al., "The livermore Regional Air Quality Model : I. Concept and Development and II. Verification and Sample Application in the San Francisco Bay Area", Journal of Applied Meteorology 17:254 (1978).

[11] T.S. Wong, K. Heidorn and D. Yap, "Modelling Sulphur Dioxide Levels in the Sarnia Area", Water, Air and Soil Pollution 5:407 (1976).

[12] R.E. De Mandel et al., "Comparisons of EPA Rollback, Empirical /Kinetic, and Physicochemical Oxidant Prediction Relationships in the San Francisco Bay Area", J. Air Poll. Control Assoc. 29:352 (1979).

[13] M.J. Moroney, "Facts From Figures", Pelican Books A236, Penguin Books Ltd, Harmondsworth, Middlesex, GB.

[14] L.J. Brasser, "Presentation of Air Pollution Measuring Data in Relation to Air Quality Standards", Proceedings of the Fourth International Clean Air Congress, Tokyo (1977).

[15] H.G. Fortak, "Numerical Simulation of Temporal and Spatial Distributions of Urban Air Pollution Concentration", Proceedings of Symposium on Multiple Source Urban Diffusion Models, A.C. Stern, Ed. U.S. EPA, Pub. No. AP-86 (1970).

[16] D.B. Turner, "Air Quality Frequency Distributions from Dispersion Models compared with Measurements". Proceedings on the Symposium on Statistical Aspects of Air Quality Data, U.S. EPA, Pub. No.EPA-650/4-74-038 (1974).

[17] P.H. Guldberg and C.W. Kern, "A Comparative Validation of the RAM and PTMTP Models for Short-Term SO_2-Concentrations in Two Urban Areas". J. Air Poll. Control Assoc. 28:207 (1978).

[18] R.H. Kummler et al., "A Comparative Validation of the RAM and modified SAI Models for Short-Term SO_2-Concentrations in Detroit", J. Air Poll. Control Assoc. 28:907 (1978).

Discussion:

Yamartino:

I agree that one must be careful in doing background substractions. An approach we have used is substraction of the isotropic, or network average, value of theory and experiment from the theoretical and observed concentrations respectively.

The resulting model minus observation residuals reflect only the interstation concentration differences. These residuals are smaller than the full concentration residuals but this factor is compensated by a reduction in the number of degrees of freedom.

Kretzschmar (response):

I would prefer to see a set of background stations surrounding the region where the validation is being done especially in certain European configurations where different source regions possibly influence each other.

Venkatram:

Models always predict an ensemble average while observations represent particular values within the ensemble; thus you can have substantial residuals even if the model is perfect.

Kretzschmar (response):

I cannot agree with that because impact models are quite often used to impose emission limits on specific sources within an ensemble of sources.

Runca:

I think it is important in model validation studies to consider the model performance for situations having the same meteorological characteristics. I mean to analyze the model results separately for all the cases having a certain stability, for example, then for all the cases having another stability, and so on for all the other parameters which can be relevant.

Kretzschmar (response):

I agree.

COMPARISON OF FINITE DIFFERENCE AND GALERKIN TECHNIQUES APPLIED TO NUMERICAL TREATMENT OF ADVECTION AND DIFFUSION OF AIR POLLUTANTS.

by

E. Runca and P. Melli
IBM Italy Scientific Center
Via del Giorgione, 129
00147 Roma, Italy.

Abstract. In the application of K-models to simulate air pollutant dispersion great attention has been paid to the numerical treatment of pure advection while a few studies deal with the case in which both advection and diffusion are relevant. In order to provide some further enlightening on the latter subject this paper discusses the numerical solution both by finite difference and Galerkin techniques of the two dimensional time dependent advection-diffusion equation describing air pollutants dispersion downwind from a line source. Comparison of the different algorithms considered in this article is discussed with reference both to the time evolution of the concentration field and to its steady state. Moreover a sensitivity analysis of the model to inaccuracies in the eddy diffusivity profile is also presented.

Introduction

The classical Eulerian way of simulating air pollutant dispersion consists of computing the time variation of the pollutant concentration at a given point as the combined result of the fluxes due to the mean flow, the turbulent motion, the sources, and deposition and transformation processes. By analogy with molecular diffusion, Prandtl (see e.g. Leslie (1)) proposed to model the turbulent flux as the product of an eddy diffusivity coefficient and the gradient of the mean concentration. Other approaches have been more recently proposed (see e.g., Lumley and Khajeh-Nouri(2); Lewellen and Teske(3); Berkowicz and Prahm(4)), but due to theoretical and computational difficulties they are not yet of common use. Thus, in practice, most of the Eulerian models, in accordance with Prandtl's theory, reduce to the integration of the classical diffusion-advection equation. They are generally named gradient-transfer theory models. Limitation of these models are discussed, e.g. by Corrsin (5) and Lamb (6).

Neglecting removal processes the advection-diffusion equation of a gradient transfer model has the general form:

Preceding page blank

$$\frac{\partial C}{\partial t} + \underline{\nabla}\cdot(\underline{u}C) = \underline{\nabla}\cdot(\overline{\overline{K}}\cdot\underline{\nabla}C) + S(\underline{x},t) \tag{1}$$

In Eq. (1) C is the concentration, $\underline{u}$ is the velocity vector, $\overline{\overline{K}}$ is the diffusivity tensor and S is the source term.

In the numerical treatment of Eq. (1) attention was principally given to the approximation of the advective terms, in other words to the solution of the transport equation:

$$\frac{\partial C}{\partial t} + \underline{\nabla}\cdot(\underline{u}C) = S(\underline{x},t) \tag{2}$$

A summary of the numerical methods applied to Eq. (2) and of their accuracy can be found in Christensen and Prahm (7). The origin of the interest in the numerical solution of Eq. (2) is due to the amplitude and phase errors which might occur when it is attempted to simulate numerically the transport by a velocity field of a Fourier component of the concentration. Since, in general, both diffusion and advection contribute to the dilution of the pollutant, the numerical analysis has to be extended to the solution of Eq. (1). This study which is at a preliminary stage has two main objectives. First of all it aims to contributing to the definition of a numerical algorithm to be used in the application of a gradient transfer theory model to problems of air pollution; secondly it aims to performing a sensitivity analysis of the gradient transfer model with respect to relevant parameters. The latter investigation is useful in order to establish the accuracy needed in parameters evaluation studies.

At the stage so far reached results are here presented concerning comparison of finite difference and finite element type algorithms defined for Eq. (1) in the case of dispersion of pollutants downwind from a line source in an atmosphere vertically limited by an inversion layer. In addition a sensitivity analysis of the ground concentration to different approximations of an exponential diffusivity profile is presented.

Reference solution.

Comparison of finite difference and finite element type algorithms implemented in this study is obtained by evaluating them with respect to a reference solution. The choosen reference case corresponds to dispersion of air pollutants downwind from a line source in an atmosphere limited vertically by an inversion layer.

By taking the reference frame with the x axis along the wind direction and by assuming ground and inversion layer as totally reflecting barriers the model derived from Eq. (1) takes the form:

$$\frac{\partial C}{\partial t} + u(z)\frac{\partial C}{\partial x} = K_x\frac{\partial^2 C}{\partial x^2} + \frac{\partial}{\partial z}\left(K_z(z)\frac{\partial C}{\partial z}\right) + Q\,\delta(z-h_s)\,\delta(x-x_s) \tag{3}$$

$$K_z\frac{\partial C}{\partial z} = 0 \quad ; \quad z = 0, H \tag{3.a}$$

$$C(x,z,t)=0 \quad ; \quad x=\pm\infty \tag{3.b}$$

$$C(x,z,t)=0 \quad ; \quad t=0 \tag{3.c}$$

where H is the inversion layer height, Q the emission rate and source has been located at $(x_s,\ 0,\ h_s)$. In the case described by Eqs. (3)-(3c) the additional assumption of : region unpolluted at time t=0, constant horizontal diffusivity , and wind and vertical diffusivity only function of vertical coordinate have been made.

To generalize the problem described by Eqs. (3)-(3c) the variables and parameters x, z, t, u, K_z, K_x, C have been made dimensionless by scaling them respectively to the following factors: $H^2\,u(H)/K\,(H)$; H; $H^2/K\,(H)$; u(H); $K_z(H)$; $H^2u^2(H)/K_z(H)$; $Q/(u(H)\cdot H)$. Use of these factors leaves Eqs. (3)-(3c) formally unchanged, except for the emission rate and the inversion layer height which take the dimensionless value of one.

Integration of the boundary value problem given by Eqs. (3)-(3c) requires the definition of wind and vertical eddy diffusivity. Consistently with previous studies (8,9) they were expressed in dimensionless form as follows:

$$U=Z^{0.5} \quad ; \quad K_Z=Z \tag{4}$$

The choosen wind and vertical diffusivity profiles describe dispersion in a case of very strong wind shear joint to a diffusivity whose intensitf grows linearly up to the mixing height. This last assumption is unrealistic, as in general turbulence intensity increases up to a certain height from the ground and then decreases. However, it was not modified, first of all because it is consistent with previously mentioned numerical studies in which this assumption allowed to derive analytical solutions of a boundary value problem similar to the one described by Eq. (3)-(3c), secondly because it is not relevant to this study whose main objective is the analysis of numerical methods, not the simulation of a real situation.

For the case described by Eqs. (3)-(3c) and (4), solution has to be derived numerically. In order to get solutions to be used in the following analysis as reference solutions, Eqs. (3)-(3c) were integrated in the region:

$$0 \leq x \leq 0.056$$
$$0 \leq z \leq 1.$$

by using a very refined mesh consisting of 505 points in the horizontal corresponding to a $\Delta x=10^{-3}/9$ and 161 points in the vertical corresponding to a $\Delta z=1./160$. A correspondingly small time step equal to $10^{-3}/9$ was taken. Solutions were derived for source heights $h_s=1/4$ and $h_s=1/9$. In both cases the source was located at

x_s=0.0075.

The numerical scheme used to compute the reference solution was devised according to a fractional step procedure (8,9,10) according to which the advection-diffusion process of Eqs. (3)-(3c) is fractioned into the four processes of emission, advection, horizontal diffusion and vertical diffusion described by the equations:

$$\frac{\partial c}{\partial t} = \delta(z-h_s)\delta(x-x_s) \tag{5.a}$$

$$\frac{\partial c}{\partial t} = -U\frac{\partial c}{\partial x} \tag{5.b}$$

$$\frac{\partial c}{\partial t} = K_x\frac{\partial^2 c}{\partial x^2} \tag{5.c}$$

$$\frac{\partial c}{\partial t} = \frac{\partial}{\partial z}\left(K_z\frac{\partial c}{\partial z}\right) \tag{5.d}$$

In reality the four processes (5a)-(5d) occur simultaneously, in the numerical procedure they occur in sequence; one after the other Eqs. (5a)-(5d) are integrated by taking as initial concentration field of each step the one obtained at the end of the previous step. The concentration field generated after the integration of Eq. (5d) is an approximation of the solution at time t+Δt (note that the concentration at time t was the initial condition for Eq. (5a)). In other words, the processes (5a)- (5d) are considered to occur separately at each time step. Reduction to zero of the integration time step reduces to zero the error introduced by the fractional step procedure (5a)-(5d).

The numerical algorithms used to solve Eqs. (5a)-(5d) in order to generate the reference solutions were defined according to classical finite difference schemes. More specifically advection was approximated by means of Lax-Wendroff scheme and diffusion by means of Crank-Nicolson scheme(11). The latter was choosen since, being unconditionally stable, allows to be very flexible in the definition of a variable vertical grid geometry which is needed in the case of a mixing height changing with time (see e.g. Shir and Shieh, (12)). Variable grid spacing might also be used to increase the resolution of the mesh in the region where the maximum concentration gradients occur (10).

Numerical schemes.

A finite difference and a finite element type scheme have been considered. The finite difference scheme is identical to the one used to to generate the reference solutions, but it is applied to two less refined grid geometries respectively consisting of 57×41 and 57×21 points. Thus the horizontal grid spacing is 9 times larger than that used in the reference solution, while the vertical grid sizes are respectively 4 and 8 times larger. Accordingly with the increased horizontal grid size the time step is 9 times larger than the one used in the reference solution.

The finite element scheme used to solve the boundary value problem (3)- (3c) was derived from the Galerkin method.

The finite element scheme here discussed is an extension of the one studied by Melli(13) from which it differs in that the grid here used is a rectangular one and moreover horizontal diffusion is considered. In the finite element scheme here implemented the same number of points as in the above discussed finite difference scheme is introduced, and the considered region is divided into triangular elements whose vertices are coincident with the grid points used in the finite difference application. Concentration is expressed as a linear combination of the set of linear piecewise functions Φ (pyramidal functions) assuming a value of one at a grid point and zero at the surrounding points:

$$C^t \simeq \sum_{j=1}^{N} c_j^t \phi_j \tag{6}$$

where N will be in the following equal to 57×41 or to 57×21, and c_j^t are given by the solution of the following system of ordinary linear differential equations:

$$\begin{aligned}&\sum_{j=1}^{N}\left[\iint_\Omega \phi_i\phi_j\,dx\,dz\right]\frac{dc_j}{dt} + \sum_{j=1}^{N}\left[\iint_\Omega U\phi_i\frac{\partial\phi_j}{\partial x}\,dx\,dz\right]c_j + \\ &+\sum_{j=1}^{N}\left[\iint_\Omega K_x\frac{\partial\phi_i}{\partial x}\frac{\partial\phi_j}{\partial z}\,dx\,dz + \iint_\Omega K_z\frac{\partial\phi_i}{\partial z}\frac{\partial\phi_j}{\partial z}\,dx\,dz\right]c_j + \\ &+\sum_{j=1}^{N}\left[\int_\Gamma K_x\phi_i\frac{\partial\phi_j}{\partial x}\cos\widehat{x\underline{n}}\,ds\right]c_j = \phi_i(x_s,h_s)\ ;\ i=1,2,\dots,N\end{aligned} \tag{7}$$

where Ω is the region of integration, Γ is its boundary, s is the curvilinear coordinate along Γ and $\underline{n}$ is the inward vector normal to Γ. Discretization of the time derivative by means of the Crank-Nicolson scheme leads to a system of linear equations which has been solved by means of Seidel iterative technique.

Comparison with reference solution.

Accuracy of the two methods is compared in fig. 1 and 2 which report the isolines of the percent error:

$$\varepsilon = |C - C_{ref}| \times 100/C_{ref} \tag{8}$$

for both the cases hs=1/9 and hs=1/4 (41 vertical points). In each figure the left side refers to finite element method and the right one to finite difference.

The plots indicate that as the pollutant moves away from the source the error decreases for both methods. The Galerkin method shows areas of small errors larger than the finite difference

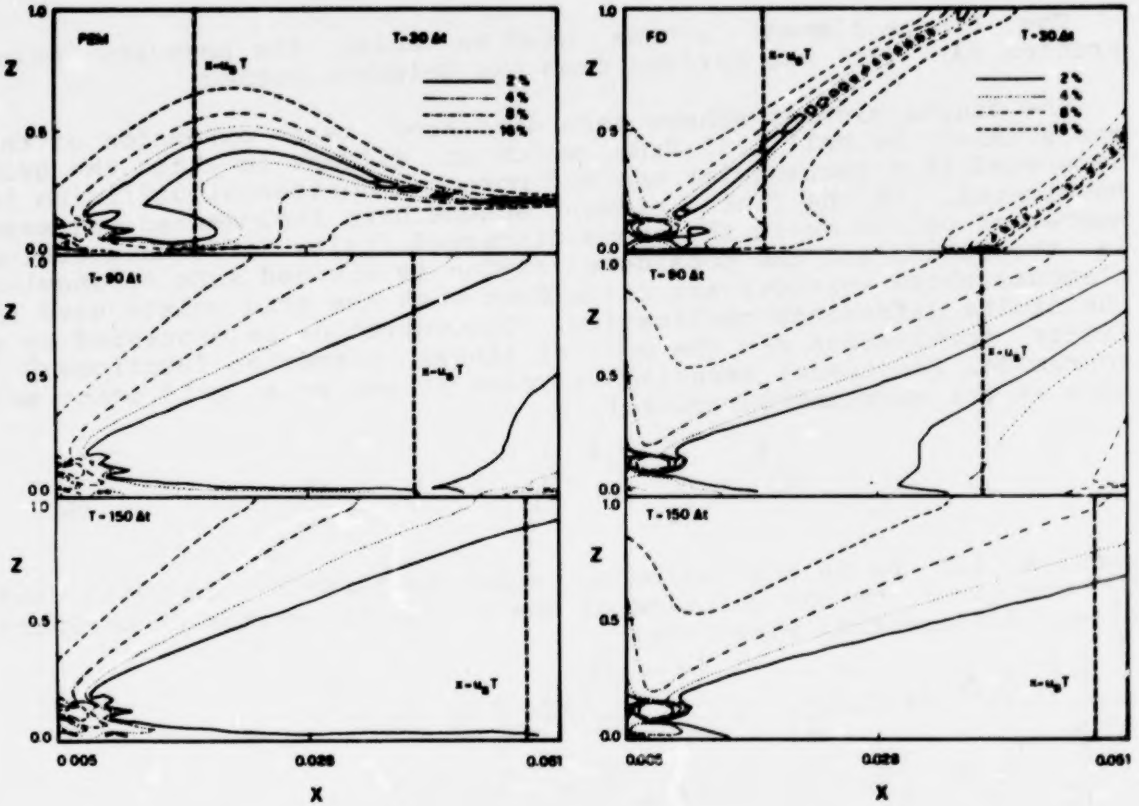

Fig.1 - Time sequences of percent error distribution for $h_s=1/9$ and vertical grid size $\Delta z=0.025$ (41 grid points in the vertical); u_s is the wind speed at source height.

schemes at any time steps. In other words, the Galerkin technique approximates better than the finite difference scheme the evolution in time of the concentration field. However, as the steady state is approached the two methods become comparable. Reduction in the numerical error as the steady state is approached can be noticed locally at every time step in the region between the source and the vertical dashed lines, which represent the average distance travelled by a particle released at source height. Roughly in this region concentration is close to the steady state and the areas of minimum error are the largest ones.

Mainly in air quality control the maximum relevance is given to the ground level concentration. Analysis of fig. 1-2 indicates that both methods are inaccurate close to the ground, and in general close to the boundaries. Comparison of ground concentration values reported in fig. 3 shows that finite difference is superior to finite element both for 21 and 41 vertical points.

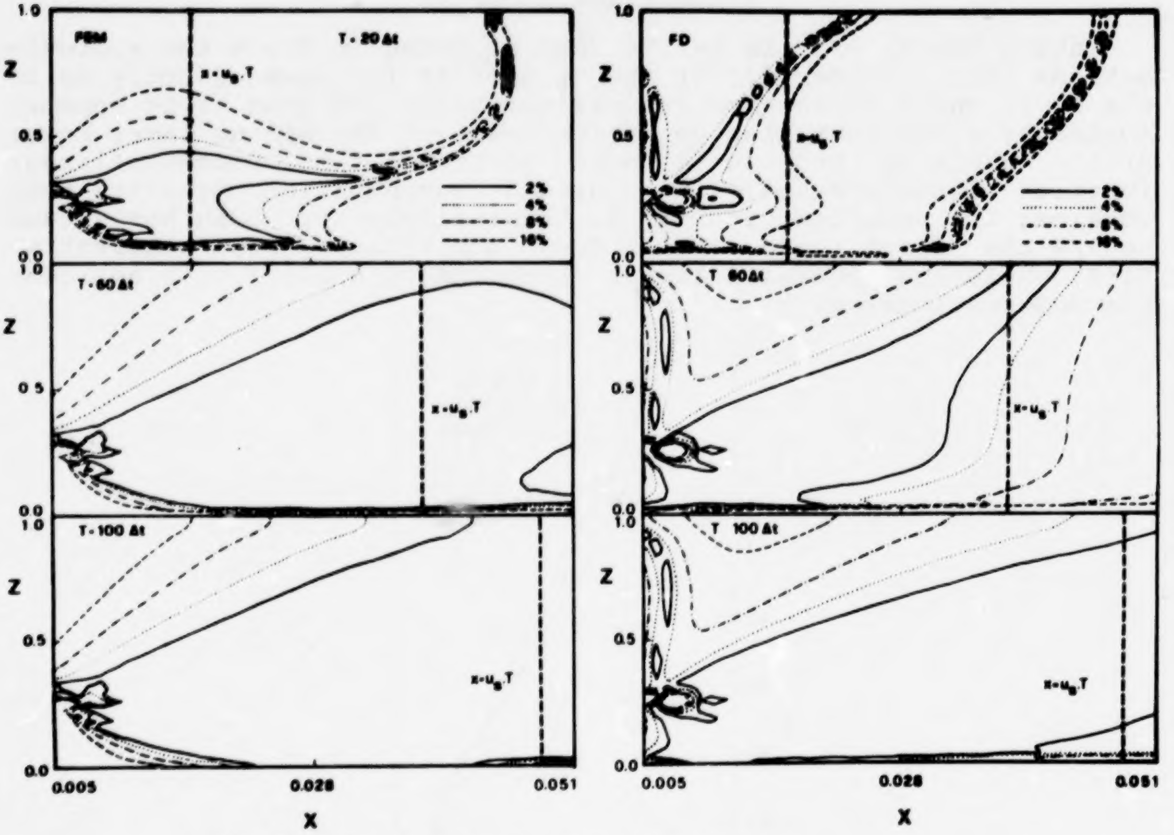

Fig.2 - As in fig.1, but for $h_s=1/4$.

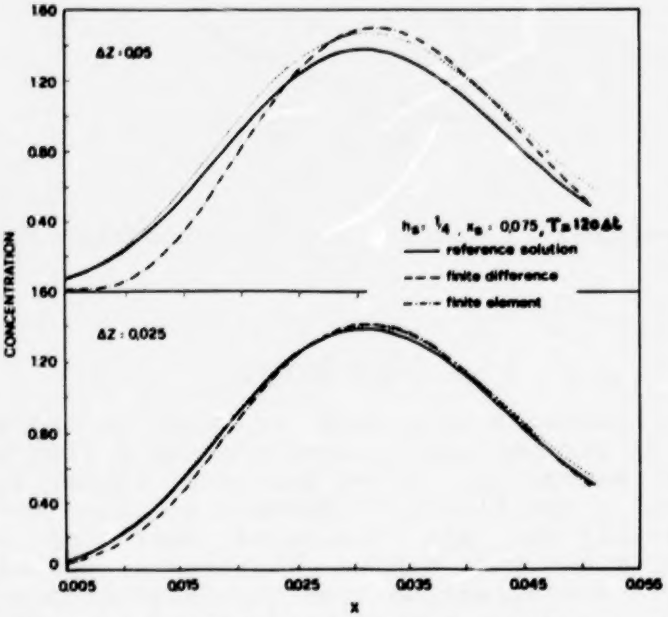

Fig.3 - Comparison of ground concentration values for 21($\Delta z=0.05$) and 41 ($\Delta z=0.025$) vertical grid points.

Sensitivity analysis.

Taking the K_z profile as the one reported in fig.4 two approximations were considered: 1) the K_z profile is known exactly up to the level where it reaches its maximum value and then it is approximated by a straight line up to its value at the mixing layer base; 2) the whole K_z profile is known in form of a piecewise linear function (dotted-dashed line). Ground concentration profiles thus obtained are reported in fig. 5. Surprisingly for both hs=1/9 and hs=1/4 the first approximation does not affect ground concentration, while the piecewise linear approximation leads to a noticeable underestimation.

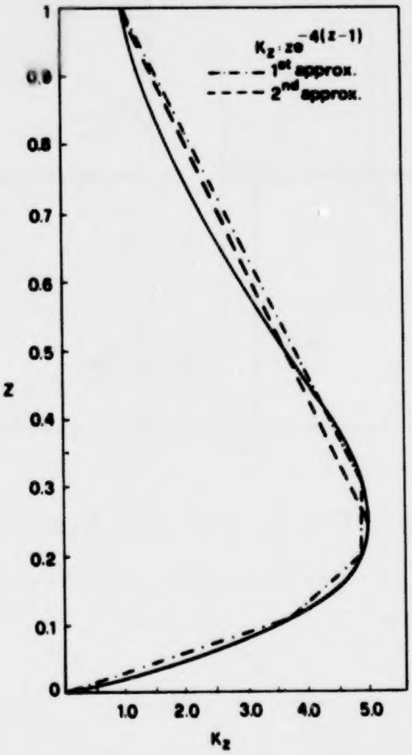

Fig.4 - Exponential K_z profile and approximating functions.

Conclusion.

Comparison against a reference solution of the advection-diffusion process of air pollutants simulated by a finite difference and Galerkin type method has shown that the latter is globally more accurate. Locally the finite difference solution may result superior. Specifically for the considered test case and the related boundary conditions the finite difference solution provides at ground a better approximation than the Galerkin one.

Analysis of concentration evolution in time has shown that the Galerkin solution is superior at any time step to the finite difference one. This greater accuracy is found both close and far from the source. However, as the steady state is approached not immediately close to the source the two methods become comparable. Superiority of the Galerkin method remains very close to the source also when the steady state is reached.

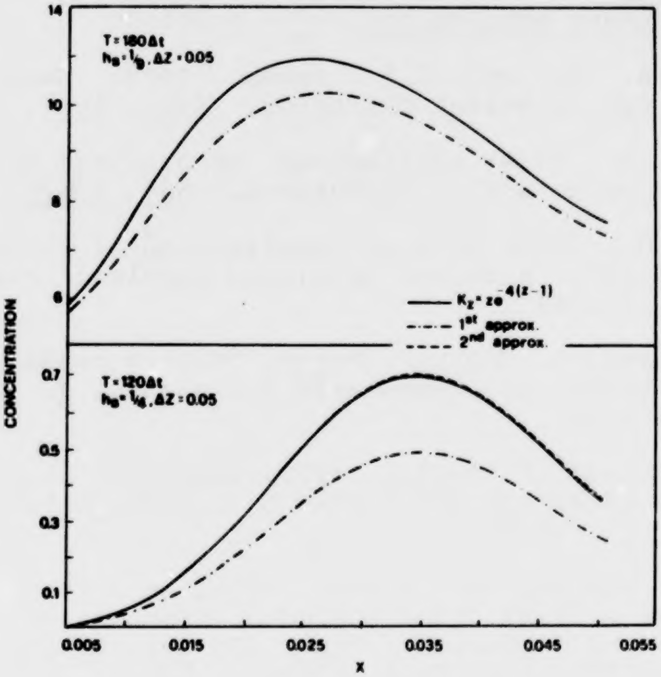

Fig.5 - Ground concentration values corresponding to K_z profiles of fig.4 for both $h_s=1/9$ and $h_s=1/4$.

Analysis of the influence of inaccuracies in the estimation of eddy dispersion profiles have shown that in a strong wind shear situation ($u= z^{0.5}$) the K_z profile must be determined with great accuracy in the lower part of the PBL. Above its maximum value it might be approximated by a straight line. However this conclusion is very preliminary and needs further analysis.

ACKNOWLEDGEMENTS

The authors are grateful to dr. F. Sardei (Max Planck-Institut, Garching bei Munchen) for many enlightening discussions.

References

1. Leslie, D.C., 1973: *Developments in the theory of turbulence*. Clarendon Press-London. pp. 300-311.

2. Lumley, J.L. and B. Khajeh-Nouri, 1974: Computational modeling of turbulent transport. *Adv. Geoph.*, *18A*.

3. Lewellen, W.S. and M.E. Teske,1976: Second-order closure modelling of diffusion in the atmospheric boundary layer. *Boundary Layer Meteorology*, *10* , pp.69-90.

4. Berkowicz, R. and L.P. Prahm, 1979: Generalization of K-theory for turbulent diffusion. *Jour. Appl. Meteor.*, *18*

5. Corrsin, S., 1974: Limitations of gradient transport models in random walks and in turbulence. *Adv. Geoph.*, *18A*.

6. Lamb, R.G., 1973: Note on application of K-theory to turbulent diffusion problems involving chemical reaction, *Atmos. Environ.*, *7* ,235.

7. Christensen, O. and L.P. Prahm, 1976: A pseudospectral model for dispersion of atmospheric pollutants, *J. Appl. Meteor.*, *15* , 1284-1294.

8. Runca, E. and F. Sardei, 1975: Numerical treatment of time dependent advection and diffusion of air pollutants. *Atmos. Environ.*, *9* , 69-80.

9. Sardei, F., and E. Runca, 1976: An efficient numerical scheme for solving time dependent problems of air pollution advection and diffusion, *Proc. IBM Seminar on Air Pollution Modelling*, IBM Italy Techn. Report, Roma.

10. Runca, E., P. Melli and A. Spirito, 1979: Real time prediction of SO$_2$ pollution in Venice lagoon area; Part I: The advection-diffusion model. *IIASA Research Report* (in press), IIASA, Laxenburg, Austria.

11. Richtmyer, R.D. and K.W. Morton, 1967: *Difference methods for initial-value problems*. Interscience, New York.

12. Shir, C.C., and L.J. Shieh, 1974: A generalized urban air pollution model and its application to the study of SO distributions in the St. Louis Metropolitan Area. *J. Appl. Meteor.*, *13* , 185-204.

13. Melli, P., 1976: An application of the Galerkin method to the Eulerian-Lagrangian treatment of time dependent advection and diffusion of air pollutants. *Proc. Int. Conf. in Finite Elements for Water Resources*, (Princeton), Pentech Press, Plymouth, England.

Discussion:

Klug:

What is the difference in computation time between the finite difference and Galerkin techniques?

Runca (response):

In the numerical tests we did the Galerkin technique took three times more computer time than the finite difference method.

Weil:

Are you applying this technique to unstable conditions? If so, the work of Willis and Deardorff have shown that both negative and positive diffusivities are needed to satisfactorily deal with this situation.

Runca (response):

Yes I am aware of this, but this work investigates numerical methods to solve the advection-diffusion equation. For the cases where this equation is applicable, we try to provide understanding of the performance of different numerical schemes.

10TH NATO /CCMS INTERNATIONAL TECHNICAL MEETING ON AIR POLLUTION MODELING AND ITS APPLICATION

TOPIC 4

Mesoscale Diffusion

THE DEVELOPMENT AND APPLICATION OF A MATHEMATICAL MODEL FOR THE MESOSCALE DIFFUSION OF ATMOSPHERIC POLLUTANTS

by

Donald Henderson*
U.S. Environmental Protection Agency
1860 Lincoln Street
Denver, Colorado 80295

Michael Wojcik
and
Mei-Kao Liu
Systems Applications, Incorporated
950 Northgate Drive
San Rafael, California 94903

Abstract

A mathematical model based on the numerical solution of the diffusion equation has been developed to simulate the transport and diffusion of atmospheric pollutants over horizontal distances on the order of several hundred kilometers. This model has been applied to the Northern Great Plains area in the United States to assess the sulfate and visibility problems as a result of sulfur dioxide emissions from multiple point sources.

Introduction

Serious issues have recently been raised concerning the transport of atmospheric pollutants over long distances. A mathematical model of mesoscale diffusion was developed and applied to the Northern Great Plains region in the United States to assess the air quality impact of emissions from existing and proposed energy developments in that area.

This model is based primarily on the solution of the atmospheric diffusion equations for multiple species. The model is composed of two interconnected submodels: a mixing-layer model and a surface-layer model. The mixing-layer model is designed to treat transport and diffusion above the surface. The model of the surface layer, embedded in the mixing layer, is designed to calculate pollutant fluxes to the ground. Pollutants are removed from the atmosphere by their diffusion through the surface layer to the ground and their absorption or adsorption at the ground. A unique feature of the surface-layer model is its ability to incorporate the diurnal variation in surface temperature that results from daytime heating and nighttime cooling of the ground. Although only the pseudo-first order reaction between SO_2 and sulfate was considered in the early version of this model, extensions have been made to include nonlinear gas phase reactions and aerosol formation.

---

* Currently with the U.S. National Park Service, Denver, Colorado, 80225.

Preceding page blank

This model was applied to the Northern Great Plains and exercised for all combinations of two emissions inventories--for the year of 1976 and 1986--and three meteorological scenarios--a strong-wind winter case, a stagnation spring case, and a moderate-wind summer case. The mesoscale diffusion model can also be used to study environmental problems such as visibility degradation and acid rains caused by the long distance transport of SO_2 and its derivative, sulfate. In this context, the sensitivity of computed sulfate concentrations to SO_2-to-sulfate conversion rates was also examined in this study. A low SO_2 to sulfate conversion rate of 0.3 percent per hour and a one percent per hour conversion rate were used in the model to compute the sulfate buildup. Using empirical formulae relating sulfate concentration and visibility, isopleths for visual ranges can be generated.

Description of the Model

The model equation is based on the time-dependent multiple-species atmospheric diffusion equation in two dimensions, which can be expressed as follows:

$$\frac{\partial c_i}{\partial t} + u \frac{\partial c_i}{\partial x} + v \frac{\partial c_i}{\partial y} = \frac{\partial}{\partial x}\left(K_x \frac{\partial c_i}{\partial x}\right) + \frac{\partial}{\partial y}\left(K_y \frac{\partial c_i}{\partial y}\right) + D\, f(D) + R_i + S_i \quad , \quad (1)$$

$$i = 1, 2, \ldots, N \quad ,$$

where c_i is the vertically averaged concentration of species i in the mixing layer, u, v, K_x, and K_y are wind velocities and turbulent diffusivities in the x and y directions, respectively, D is the two-dimensional divergence (= du/dx + dv/dy), R_i and S_i are chemical reaction and volumetric source terms, respectively, and

$$f(D) = \begin{cases} c_i & D < 0 \quad , \\ c_{iA} & D > 0 \quad , \end{cases}$$

where c_{iA} is the concentration of species i aloft. Although this study considered only SO_2 and sulfate formed through a first-order reaction, the regional model can be extended to handle multiple reactive species.

The main feature of this model equation is that the pollutant distribution has been assumed to be nearly uniform in the vertical direction. With this assumption, the model equation can be formally derived from the more general atmospheric diffusion equation. The compelling reason for this assumption is that the vertical diffusion term is about 100 times greater than the transport ter, and the horizontal diffusion term is only a fraction of the transport term (ref. 1). Because of the relatively large spatial scale, artificial diffusion associated with the numerical solution of the atmospheric diffusion equation can be overwhelming. An accurate finite difference formula to represent the advection term must be used. The SHASTA method has thus been selected for this purpose, and a detailed description of this scheme can be found in Ref. 1.

The importance of dry deposition of SO_2 and sulfate in long range transport problems necessitates treatment of this process in the model. For pollutants originating from either elevated or distant ground-level sources, most of the pollutant mass is contained in the mixing layer. The removal processes consist of the diffusion of the pollutants through the surface layer to the ground, followed by absorption or adsorption at the atmospheric-ground interface. A unique feature of the surface layer is its diurnal variation in temperature, which is a result of daytime heating and nighttime cooling of the surface. This variation affects the vertical pollutant distribution through atmospheric stabilities and, consequently, the rate of surface uptake of pollutants.

The surface layer can be viewed as two layers: the turbulent layer and the viscous sublayer. With this simplification, the pollutant flux to the ground surface due to dry deposition, F, can be obtained through the following equation:

$$I \cdot F + \gamma^{-1/a} \cdot F^{1/a} - c = 0 \quad , \tag{2}$$

where

$$I \equiv \frac{1}{\beta u_*} + \int_{z_0}^{h} \frac{\phi(z)}{k u_* z}\, dz \quad , \tag{3}$$

and where k is the von Karman constant, u_* is the frictional velocity, β is the Stantion number, ϕ is the dimensionless wind shear (ref. 2), and z_0 and h are the surface roughness and the height of the surface layer, respectively, for the uptake of air pollutants by chemical reaction or catalytic decomposition at the ground surface. For a = 1, 2, and 3, closed-form solutions can be found for F:

$$F = \begin{cases} \dfrac{c}{I + \dfrac{1}{\gamma}} \quad , & a = 1 \quad , \\[2ex] \dfrac{-\dfrac{1}{\sqrt{\gamma}} + \left(\dfrac{1}{\gamma} + 4Ic\right)^{1/2}}{2I} \quad , & a = 2 \quad , \\[2ex] (A_+ + A_-)^3 \quad , & a = 3 \quad , \end{cases} \tag{4}$$

where

$$A_{\pm} = 3\left\{\frac{c}{I} \pm \left[\left(\frac{c}{2I}\right)^2 + \frac{1}{27\gamma I^3}\right]^{1/2}\right\}^{1/2} \quad . \tag{5}$$

These formulas reduce to that of Thom (ref. 2) for the special case of a first-order surface reaction and a neutrally stratified atmosphere.

Prescription of the Meteorological Parameters

In urban-scale air quality modeling, generally, wind data are collected and then interpolated to generate the wind field. Since the horizontal component of the wind is a two-dimensional vector, it is difficult to find an interpolation scheme that produces a field that is satisfactorily smooth. The horizontal components of the wind in a mesoscale modeling study can be, however, calculated from the gradient of geopotential height, Z, on a constant pressure surface using the geostropohic wind relationship:

$$u = -\frac{g}{f}\left(\frac{\partial Z}{\partial y}\right)_p \quad , \tag{6}$$

$$v = \frac{g}{f}\left(\frac{\partial Z}{\partial x}\right)_p \quad , \tag{7}$$

where g is the gravitational constant and f is the Coriolis parameter. Geopotential height data are readily available from weather maps. Since geopotential height is a scalar quantity, one needs, therefore, to smooth only a scalar instead of a vector. In the present study, a bicubic spline fitting technique has been chosen to interpolate the geopotential heights (ref. 3). Mathematically, the bicubic spline fit is a piecewise third order polynomial passing through all data points and having continuous first and second derivatives. The spline functions can be viewed as a set of cubic equations, one equation for each interval between successive data points. The coefficients of the cubic equations are such that at any data point the equation for the left interval will yield the same values for the first and second derivatives, respectively, as will the equation for the right interval.

Based on a review of pertinent observational and theoretical studies on mesoscale diffusion, the horizontal eddy diffusivity, K_H, appears to be both scale and shear dependent (refs. 4 and 5). To realistically parameterize K_H, one must, therefore, take both of these effects into consideration. The present prescription for K_H is first proposed by Smagorinsky (ref. 7), who showed that nonlinear lateral diffusion can be formulated on the basis of the Heisenberg (ref. 8) similarity theory for turbulence in the equilibrium range. Assuming that density variations can be ignored, the horizontal eddy diffusivity coefficient can be derived as:

$$K_H = \frac{5}{4} \cdot (\alpha\Delta)^2 \cdot |\mathrm{Def}| \quad , \tag{8}$$

where Δ is the grid spacing and |Def| is the magnitude of the velocity deformation tensor,

$$|\mathrm{Def}| = \left[\left(\frac{\partial v}{\partial x} + \frac{\partial u}{\partial y}\right)^2 + \left(\frac{\partial u}{\partial x} - \frac{\partial v}{\partial y}\right)^2\right]^{1/2} \quad . \tag{9}$$

The empirical coefficient, α, was estimated to be 0.28 based on gobal-scale modeling studies. A series of numerical experiments were performed to test the prescription for horizontal diffusivities, the values ranging from 10^3 m/sec to 10^4 m^2/sec, seems to be reasonable when compared with observational data (ref. 5), as well as numerical experiment on the dispersion of a cluster of particles (refs. 4 and 6).

Analysis of the Results

The mesoscale model was applied to the Northern Great Plains and exercised for all combinations of two emissions inventories--for the year of 1976 and 1986--and three meteorological scenarios--a strong-wind winter case (27-31 January, 1976), a stagnation spring case (4-7 April, 1976), and a moderate-wind summer case (9-11 July, 1975). The predicted SO_2 concentrations are generally highest in the stagnant spring case, intermediate in the strong-wind winter case, and lowest in the moderate-wind summer case. Figure 1 shows the computed 3-hour average SO_2 concentration after 48 hours of simulation.

The mesoscale diffusion model can be used to study environmental problems such as visibility degradation and acid rains caused by the long distance transport of SO_2 and its derivative, sulfate. In this context, the sensitivity of computed sulfate concentrations to SO_2-to-sulfate conversion rates was also examined in this study. A low conversion rate, 0.3 percent per hour, was used in Figure 1 and generated negligible sulfate concentrations above the background. However, when a one percent per hour conversion rate was used, moderate sulfate buildup was found as shown in Figure 2, with maximum concentrations reaching 6 $\mu g/m^{-3}$.

For a homogeneous medium, visual range is linearly related to the scattering coefficient of the atmosphere (ref. 9): $VR = 3.91/b_{scat}$. In contrast, light scattering depends on the mass concentration, chemical composition, and size distribution of atmospheric aerosols. Recent studies have shown, however, that the scattering coefficient correlates poorly with the total aerosol mass, but reasonably well with sulfate (refs. 10, 11). Using a least-squares fit of Los Angeles data, White (ref. 9) obtained the following relationship, which was used in the present study:

$$b_{scat} = 7.6\ m^2g^{-1}[\text{Sulfate}] + 2.4\ m^2g^{-1}[\text{Nonsulfate Aerosol}] \quad . \qquad (10)$$

Using these empirical formulae relating sulfate concentration to visibility, isopleths for visual ranges can be generated as shown in Figure 2. The numbers in the bracket indicate visual ranges in kilometers.

Summary and Conclusions

A mathematical model based on the numerical solution of the diffusion equation for simulating mesoscale transport and diffusion of atmospheric pollutants over horizontal distances has been described. This model can be used to address regional air quality problems related to emissions of sulfur dioxide from various sources. In this paper, the application of this model to the Northern Great Plains area in the United States to assess the sulfate and visibility problems as a result of sulfur dioxide emissions from a multiple of point sources has been discussed. This model should also be useful for examining the acid precipitation problem in the Western Europe as a result of long range transport of air pollutants (ref. 12).

Acknowledgment

This work was supported in part by the U.S. Environmental Protection Agency under Contract 68-01-3951.

References

1. M. K. Liu and D. Durran, "The Development of a Regional Air Pollution Model and Its Application to Northern Great Plains," EPA-908/1-77/001, Systems Applications, Incorporated, San Rafael, California, 1976.

2. A. S. Thom, Quart. J. Roy. Meteor. Soc., Vol. 98, pp. 124-134, 1872.

3. M. K. Liu and M. Wojcik, "Further Studies of Regional Diffusion Modeling in the Northern Great Plains," EPA-9-8/1-78/005, Systems Applications, Incorporated, San Rafael, California, 1979.

4. R. J. Murgatroyd, "The Dispersion of Pollutants in the Free Atmosphere by the Large Scale Wind Systems," Trans. Roy. Soc. Lond. A., Vol. 265, pp. 273-294, 1969.

5. D. Randerson, "Temporal Changes in Horizontal Diffusion Parameters of a Single Nuclear Debris Cloud," J. Appl. Meteor., Vol. 11, pp. 670-673, 1972.

6. S. K. Kao and D. Henderson, "Large-Scale Dispersion of Clusters of Particles in Various Flow Patterns," J. Geophys. Res., Vol. 75, pp. 3104-3113, 1970.

7. J. Smagorinsky, "General Circulation Experiments with the Primitive Equation: I. The Basic Experiment," Mon. Wea. Review, Vol. 91, pp. 99-164, 1963.

8. W. Heisenberg, "Zur Statistischen Theorie der Turbulenz," Z. Phys., Vol. 124, p. 614, 1948.

9. W.E.K. Middleton, "Vision Through the Atmosphere, University of Toronto Press, Toronto, Canada, 1952.

10. W. H. White, Nature, Vol. 264, pp. 735-736, 1976.

11. G. M. Hidy, et al., "Characterization of Aerosols in California," Final Report, California Air Resources Board, Sacramento, California, 1974.

12. B. Ottar, "An Assessment of the OECD Study on Long Range Transport of Air Pollutants (LRTAP)," Atmos. Environ., Vol. 12, p. 445, 1978.

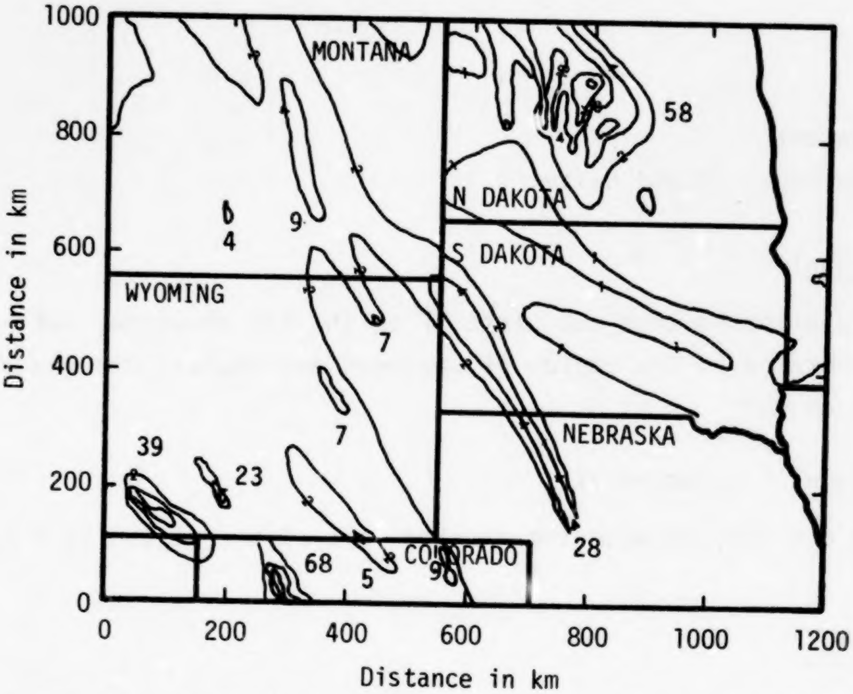
1000
800
600
400
200
0
Distance in km
0
200
400
600
800
1000
1200
Distance in km
MONTANA
N DAKOTA
S DAKOTA
WYOMING
NEBRASKA
COLORADO
58
9
4
7
7
39
23
68
5
9
28

Figure 1. Predicted SO_2 concentration fields in $\mu g/m^{-3}$ for 800 to 1100 MST on 6 April 1976

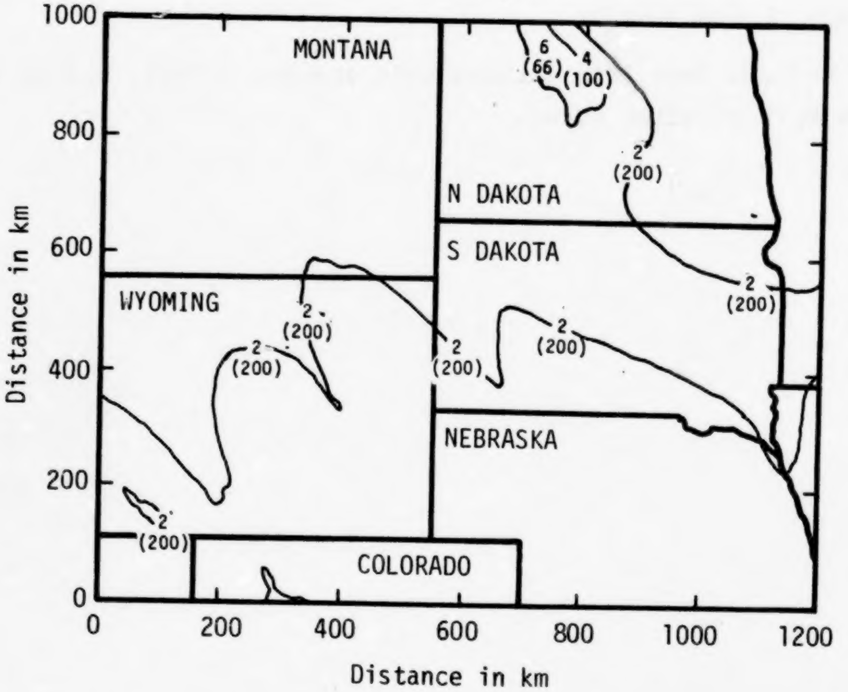
1000
800
600
400
200
0
Distance in km
0
200
400
600
800
1000
1200
Distance in km
MONTANA
N DAKOTA
S DAKOTA
WYOMING
NEBRASKA
COLORADO
6 (66)
4 (100)
2 (200)
2 (200)
2 (200)
2 (200)
2 (200)
2 (200)
2 (200)

Figure 2. Predicted sulfate concentration fields in $\mu g/m^{-3}$ for 800 to 1100 MST on 6 April 1976

Discussion:

(Rapporteur: Klaus Herrmann)

van Ulden:

The trajectories were calculated from the 850 mb-winds, but some of the mountains in the region of interest are higher. Did you take this into account?

Henderson (response):

No, we did not, because the greater part of the region is relatively flat.

van Ulden:

You assumed equally distributed pollutants in the vertical; this cannot be true if a nocturnal inversion would occur.

Henderson (response):

We did not yet take into account this special effect, but we are developing a more detailed model.

APPLICATION OF THE MESO-SCALE DIFFUSION MODELS MESOS AND TALD TO ACCIDENTAL RELEASES OF RADIOACTIVITY

by

H. ApSimon and J. Wrigley
Imperial College, London (MESOS)

and

J. Le Grand and A. Després
Commissariat à l'Energie Atomique,
Fontenay-aux-Roses (TALD)

Paper presented by H. Bultynck
Studiecentrum voor Kernenergie
Centre d'Etude de l'Energie Nucléaire, Mol.

Abstract Two models, MESOS and TALD, used by the European Communities to evaluate over a long distance the possible consequences of an accidental radioactive release, are reviewed. An example of calculation is given in order to illustrate the performance of both models.

INTRODUCTION

A working group of the European Communities has undertaken a study for determining the possible consequences over a meso-scale range of an accidental release of radioactive nuclides originating from an European site. The group has made use of existing models for treating diffusion on a meso-scale as developed by the Imperial College of Science and Technology, London, and by the Commissariat à l'Energie Atomique, Fontenay-aux-Roses. The performance of these meso-scale diffusion models is enlightened by a few examples of calculation and a brief description of the methodology is given.

THE MESOS MODEL

A prototype version of the MESOS model for predicting the dispersal of radioactive releases over distances up to a thousand kilometres or more has been described at an earlier NATO/CCMS meeting in AIRLIE, Virginia in 1976[1]. The model is applicable to releases of 3 hours duration or longer, and is currently being used in conjunction with a data base giving data from synoptic stations and ships over Europe at 3 hourly intervals throughout most of a year from March 1973 to February 1974. This data base is used to supply realistic meteorological conditions along the trajectories of specimen puffs released at 3 hourly intervals from a specified source, and to compute the trajectories themselves from the surface pressure fields[4].

Each of these tracked puffs is treated as a column of polluted air expanding vertically and horizontally according to local conditions along the trajectory allowing for depletion by natural decay, dry deposition and wet deposition. These changing local conditions include the underlying surface of land or sea, the windspeed, observations of present weather and rainfall, current Pasquill category and turbulence, and depth of the mixing layer. The deduction of these parameters from the synoptic data is described in references 2 and 3. Using the detailed histories of the tracked puffs released every 3 hours for unit releases of a few selected nuclides, predicted exposure patterns can be built up, assuming that a continuous release behaves like an assembly of intermediate puffs fanning out between the tracked puffs and with intermediate dispersion and depletion found by interpolation. The exposure patterns are produced at regular grid points over the area between latitudes 44°N and 62°N and longitudes 10°W to 20°E.

The model is currently being applied to small routine continuous releases, and has been used to produce statistics on the likelihood of different degrees of exposure in hypothetical accident studies. In the latter context it is felt to be particularly apt. Firstly it is a trajectory model. Trajectories play an important role in lateral dispersion on the synoptic scale and in the fanning out of puffs as they pass across the map area. This means that the duration of a release has a considerable effect on the probable consequences of a postulated accident and the area exposed.

In MESOS it is assumed that each expanding puff column is advected with a mean wind based on the geostrophic wind, but backed and reduced in strength according to the likely wind profile over the vertical extent of the puff. Still more sophistication is possible in the MESOS model. Such trajectories may well be in considerable error in specific instances but are sufficient for statistical application over many different release periods ; it should be mentioned that in any particular situation the consequences can be very sensitive to the exact trajectories as illustrated by the application of the MESOS model to the Windscale release of 1957[3].

Changes in the mixing layer depth and Pasquill category are also important in the possible consequences of an accident. Detailed development of the vertical dispersion over the first 12 to 14 hours of travel can produce differences of orders of magnitude in the flux of depositing nuclides which still survives to give contamination later on[2]. The underlying surface is also important. When material passes out over the sea the diurnal cycle is relatively weak. The most important consideration is whether the air is warmer than the sea as it leaves the land, in which case a surface inversion is likely, reducing dry deposition and depletion over the sea, and maintaining the flux and concentration levels when the trajectory next reaches land.

Wet deposition of some nuclides may frequently be the most critical factor in possible accident consequences. In this context it is important to allow for the spatial and temporal occurrence of rain on a realistic basis for example orographic rain. The data base used with MESOS gives a rain index every 3 hours in each grid square of the map, based on observations of present weather and thus reflects the intensity and type of rainfall.

As an illustration of the application of the model to possible accident consequences Figures 2 to 4 show some of the preliminary results obtained using the atmospheric dispersion model MESOS for hypothetical releases of ^{131}I from MOL. In each of these figures there are 16 histograms corresponding to 16 exposure points (Figure 1). These are in the directions due North, East, South and West of the source at distances of approximately 100 km, 300 km, 500 km and 800 km, except to the South where the outermost point is only 700 km away to remain within the map limits.

The figures give the probability distributions of different exposures for 253 unit releases of 1 Ci each spread over a day ; each day's release was built up as eight consecutive 3 hourly releases each of 1/8 Curie.

For each site the histograms give in each of a series of consecutive intervals of exposure the number of days leading to estimated exposure at the exposure point within that range of exposure ; the intervals of exposure are logarithmic with two intervals for each consecutive power of 10, so that within each interval exposure varies by a factor of approximately 3. A value of 0.3 cm/s was assumed for the basic dry deposition velocity, and a washout coefficient

$$\Lambda = 1.6\times10^{-4}\ J^{0.8}$$

where J is the rainfall rate in mm/h[5].

It is immediately apparent that the prevailing westerly winds and tendency of weather systems to translate eastwards lead to a higher probability of exposure of sites to the east of the source. Many of the histograms are quite skew with the most probable exposure within one or two orders of magnitude of the maximum exposure, and show a slow decrease over several orders of magnitude towards lower exposures. Dry deposition in Figure 3 follows a similar pattern to the integrated concentrations in air in Figure 2, but in Figure 4 the wet deposition is considerably greater to the North and East and much lower to the South and West. Summing over the 253 days represented, the ratio of the total wet deposition to the total dry deposition varies by an order of magnitude from 0.4 to 5 at the different exposure points, and reflects the rainfall patterns, being greater where orographic rain is likely. There is less likelihood of rain in trajectories to the South and West which are most frequently anticyclonic. However, although the probability of exposure at any site from wet deposition, is less than that from dry deposition (since it only rains a fraction of the time) the maximum exposures from wet deposition in the histograms of Figure 4 are generally an order of magnitude greater than the corresponding maximum values for dry deposition in Figure 3. Thus realistic prediction of wet deposition would seem to be particularly important in estimating possible accident consequences.

THE TALD MODEL

The mathematical model TALD ("Transfert Atmosphérique à Longues Distances") is used to determine the air concentrations over Western Europe following a continuous release with a constant output of radioactive gases or aerosols from a site anywhere in Europe.

Method

Two successive steps are taken :

- the determination of trajectories of the pollutant, based on real meteorological data ;
- the calculation of the air concentration in the cloud associated with the trajectories. The diffusion model is a plume model.

The release is decomposed in elementary releases with a duration of 12 hours. Each release is characterized by one trajectory ; one admits that it is representative of the family of the individual trajectories over the twelve hours of release.

If the meteorological data are available over a long period of time, it is possible to deduce a great number of trajectories and in this way a statistical sample is obtained, for a release point and a receptor point both of them situated in Western Europe, allowing for :

- the determination of the distribution of air concentrations as a consequence of a release of a duration of twelve hours ;
- the determination of the integrated air concentration, by adding the contributions of each elementary release, for a continuous release with a constant output, over a long period (one or two years).

The distribution of the air concentrations in a receptor point for a release of twelve hours is determined by gathering the calculated values in classes. The distribution can then be presented as histograms of frequencies of concentrations giving the crude results of the calculation or further under the form of cumulative probabilities, in the actual case that the receptor point is reached by the plume, corresponding with a fixed value of the concentration. The results can also be presented in the way of histograms of frequencies of concentrations for different classes of wind directions occuring at the release point.

The integrated air concentration resulting from a continuous release with a constant rate over a long period is calculated in a great number of grid-points, covering Western Europe. With these calculated values it is possible to draw isolines of integrated concentrations over the period of release around the source.

Trajectories

The trajectories are constructed with real meteorological data. For 1975 and 1976, the windspeed and winddirection, averaged between the pressure levels 850 and 1000 mb, at 00h00 and 12h00 GMT, in 400 gridpoints of the meteorological forecast area are provided by the "Météorologie Nationale". The grid covers nearly an area situated between the latitudes 30°N to 65°N and the longitudes 20°W to 20°E.

In order to avoid sudden changes by taking meteorological situations every twelve hours and to approach the reality of a continuous variation between the two meteorological observations, intermediate situations at 06h00 and 18h00 have been established by interpolation between the data of 00h00 and 12h00.

Further the windspeed and direction at the point of release during the years 1975 and 1976 have to be known. Nine classes of winds are considered, the first eight are related with winddirection, the ninth comprises calm winds with ill defined directions.

The trajectories are constructed by segments, adopting constant meteorological conditions over 6 hours. During the first three hours, the windvector at the point of release is used, later on one considers the windvector, averaged between 800 and 1000 mb, as provided by the "Météorologie Nationale".

Calculation of concentrations

A certain number of hypothesises allows for the adoption of a gaussian plume. The most relevant ones can be stated as follows :

- the release occurs over a sufficient period of time so that the longitudinal diffusion can be neglected with respect to the transport action by the wind ;
- the windvector remains constant during 6 hours.

A further hypothesis concerns the thickness of the mixing layer : a constant height of 1000 m has been adopted over Western Europe. The release is assimulated with a ground release.

From these hypothesises it follows that the air concentration is calculated in two different ways depending on the travel time. For travel times shorter than twenty hours, the air concentration at ground level, in a point (xy), is calculated by means of a bigaussian diffusion model applied to a ground release, taking into account the reflexion by the surface. For travel times longer than twenty hours, the distribution of the emitted material is uniformally distributed along the vertical and only the lateral diffusion in a horizontal plane obeys a gaussian distribution law.

The standard deviations, σ_y and σ_z, of the distribution of the concentrations in a perpendicular plane to the axis of transport, are generally expressed by :

$$\sigma = (At)^k$$

with t : traval time

A and k are parameters depending on the travel time.

The impoverishment of the plume, due to dry deposition and radioactive decay is taken into account. Deposition due to washout by rain is disregarded.

Calculation programme

The TALD programme is divided in two distinct subprogrammes : TRAJEC and CONCEN.

TRAJEC produces a file of the trajectories starting from the point of release during the considered period of time. The input are the meteorological data issued by the "Météorologie Nationale", the windspeeds and winddirections at the point of release and the coordinates of this point. The output on magnetic tape includes the coordinates of the points of the trajectory, the coordinates of the outskirts of the plume defined by 2.15 σ_y and the average windspeed at those points. The trajectories are identified in the file in function of the nine classes of winddirections at the point of release ; a programme allows for a classification in chronological order.

CONCEN calculates the concentrations for a specified nuclide. The input data are :

- the listing of the trajectories established by TRAJEC ;
- the parameters characterizing the radionuclide (deposition velocity, radioactive decay) ;
- the geographic coordinates of the points where the calculation of the concentration is wanted.

The output concerns :

- for each trajectory, the integrated concentrations calculated in its vicinity ;
- for each receptor point the histogram of frequencies of air concentrations over the considered period and over each class of winddirection

related to the release point as well as the integrated air concentration over the considered point.

Example of calculation

The programme TALD has been applied for the sites of SACLAY and MOL over the years 1975 and 1976. Over these two years, a file of trajectories starting from these two points of release has been established. The file of SACLAY comprises 670 trajectories for 1975 and 689 for 1976 ; the file of MOL comprises 680 and 692 trajectories for the two years respectively.

To illustrate the kind of answer that one can get from TALD, releases of three different radionuclides were considered from a source situated at SACLAY, releasing 1 Ci in 12 hours somewhere in 1975 :

- Krypton-85 : long half-life and no deposition ;
- Plutonium-239 : long half-life and dry deposition ;
- Iodine-131 : relative short half-life and dry deposition.

An equal deposition velocity of 5×10^{-3} $m.s^{-1}$ has been adopted for Iodine-131 and Plutonium-239.

The receptor point is situated in the vicinity of MUNICH, at a distance of nearly 600 km from the point of release.

Figure 5 represents the cumulative probability P that a given concentration is smaller than or equal to a given quantity, if the receptor is located within the plume, for each of the considered radionuclides.

The relative importance of the difference between Krypton-85 and the two other radionuclides shows the relevance of the impoverishment of the plume due to dry deposition. On the contrary, the travel time is not generally sufficiently long so that the radioactive decay of Iodine-131 should play an important role.

In the course of 1975, the probability α that the plume reaches the receptor is equal to 0.11 (the receptor is reached by the plume if the distance between the receptor and the trajectory is smaller than $2.15\ \sigma_y$).

The probability that a given value of the concentration has been exceeded at the receptor point, for an emission of 1 Ci during 12 hours in the course of the considered year is given by :

$$Pr = \alpha\ (1 - P)$$

REFERENCES

1. H. ApSimon and A.J.H. Goddard, "Modelling the Atmospheric Dispersal of Radioactive Pollutants beyond the First Few Hours of Travel," Proc. 7th NATO/CCMS, Int. Tech. Mtg. on Air Pollution Modelling and its Applications, Airlie, Va., 1976.

2. H. ApSimon, D. Earnshaw, A.J.H. Goddard, J. Wrigley, "On the Importance of the Vertical Structure of the Boundary Layer in Modelling the Long Range Transport Following an Accidental Release of Pollutant," Proc. W.M.O. Symposium on Boundary Layer Physics Applied to Specific Problems of Air Pollution, Norrköping, Sweden, June,19 - 23,1978.

3. H. ApSimon, D. Earnshaw, A.J.H. Goddard, J. Wrigley, "Modelling of Mesoscale Atmospheric Dispersion and the Application of the MESOS Model to the 1957 Windscale Release," October 1978, Final Contract Report, SAF 013.

4. J. Wrigley, H. ApSimon, A.J.H. Goddard, "Meteorological Data and the MESOS Model for the Long Range Transport of Pollutants," Proc. W.M.O. Symposium on the Long Range Transport of Pollutants and its Relation to General Circulation Including Stratospheric/Tropospheric Exchange Processes," Bulgaria, October 1979.

5. R.J. Engelmann, "Precipitation Scavenging," Proc. of Symposium Richland, Wash., 1970, 2 - 4 June, AEC Symp. Series No. 22.

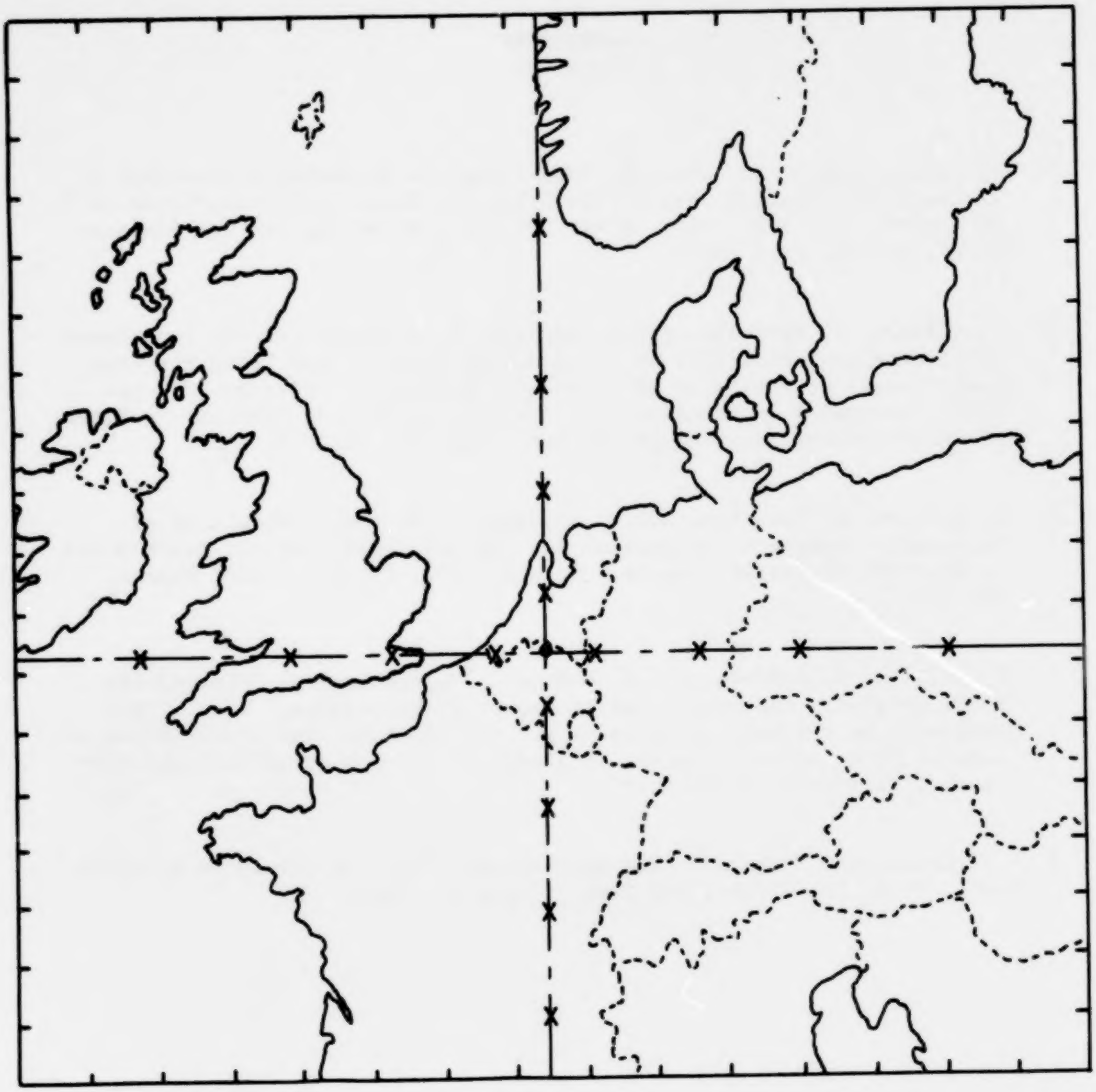

Figure 1. Selected Exposure Points

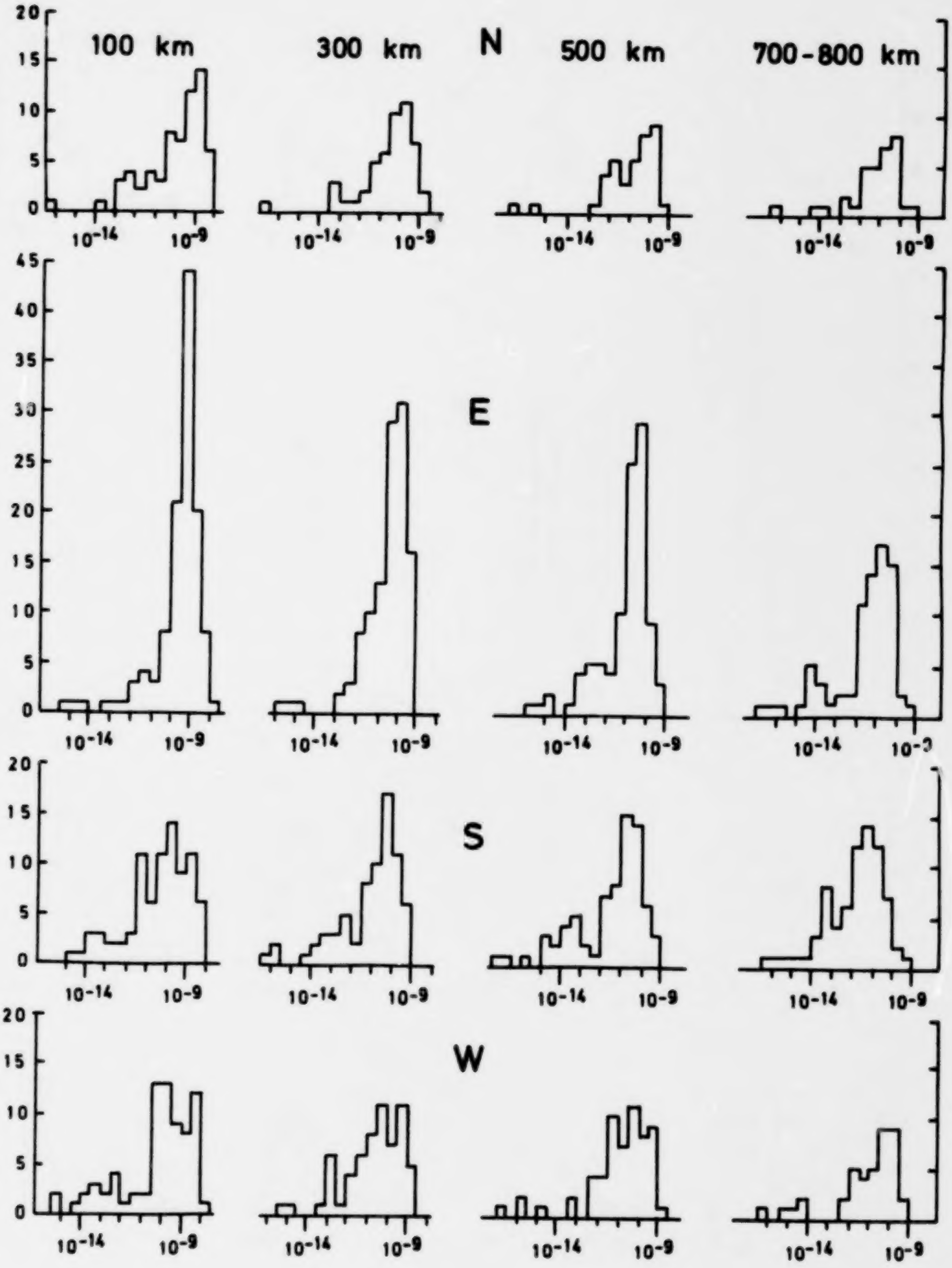

Figure 2. Integrated atmospheric concentrations for releases of 1 Ci over 24 hours of ^{131}I (Ci. s/m^3)

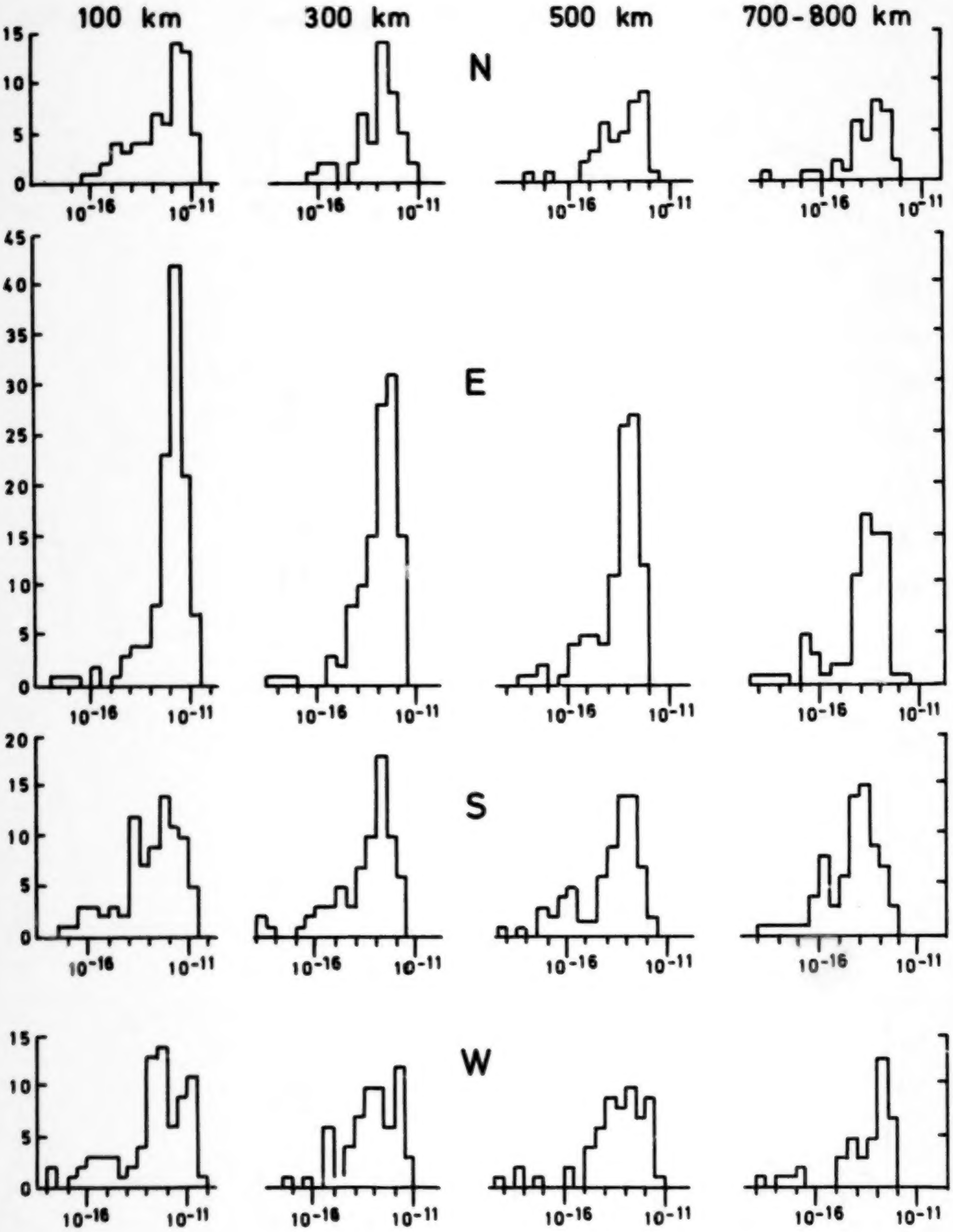

Figure 3. Dry deposition for releases of 1 Ci over 24 hours of ^{131}I (Ci / m^2)

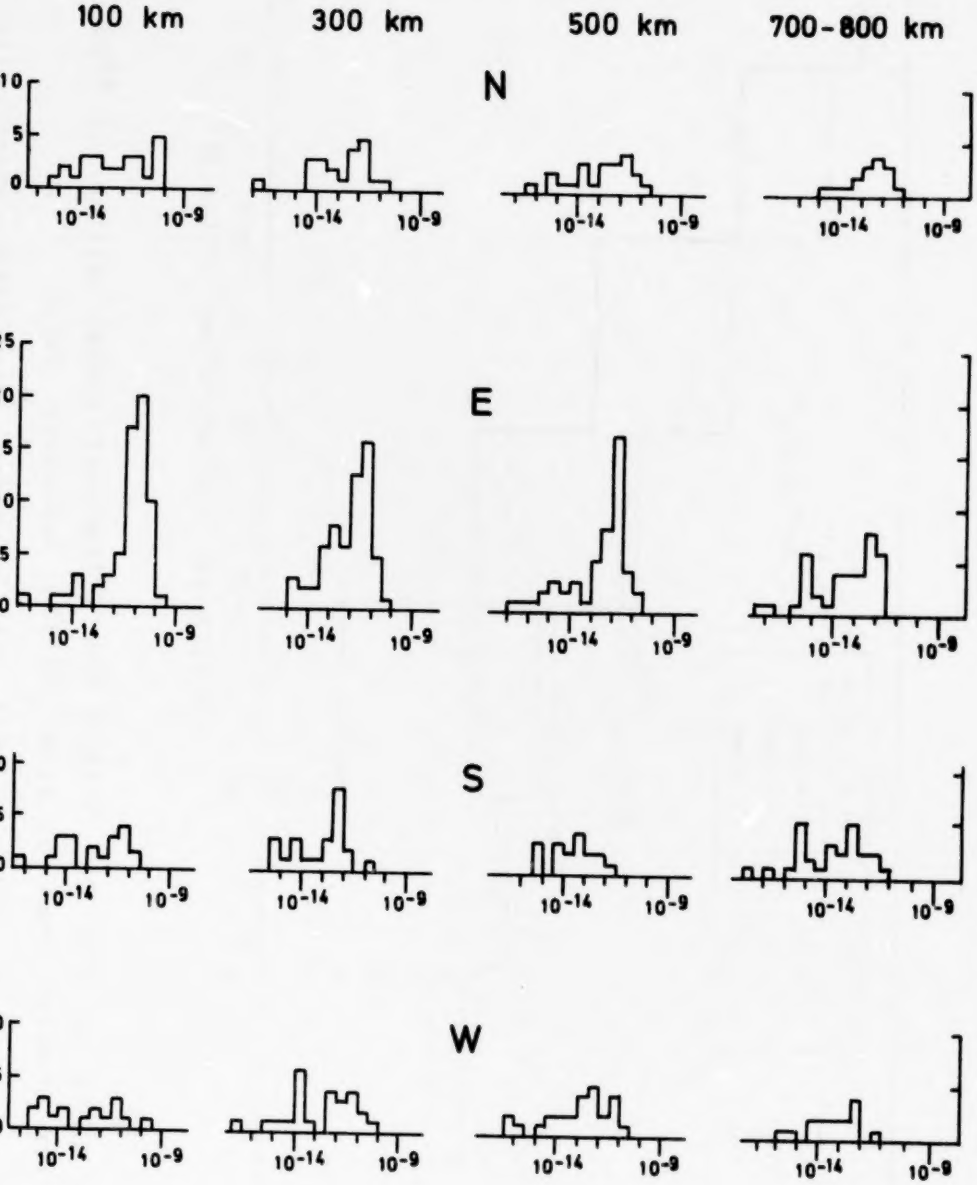

Figure 4. Wet deposition for releases of 1 Ci over 24 hours of ^{131}I (Ci/m^2)

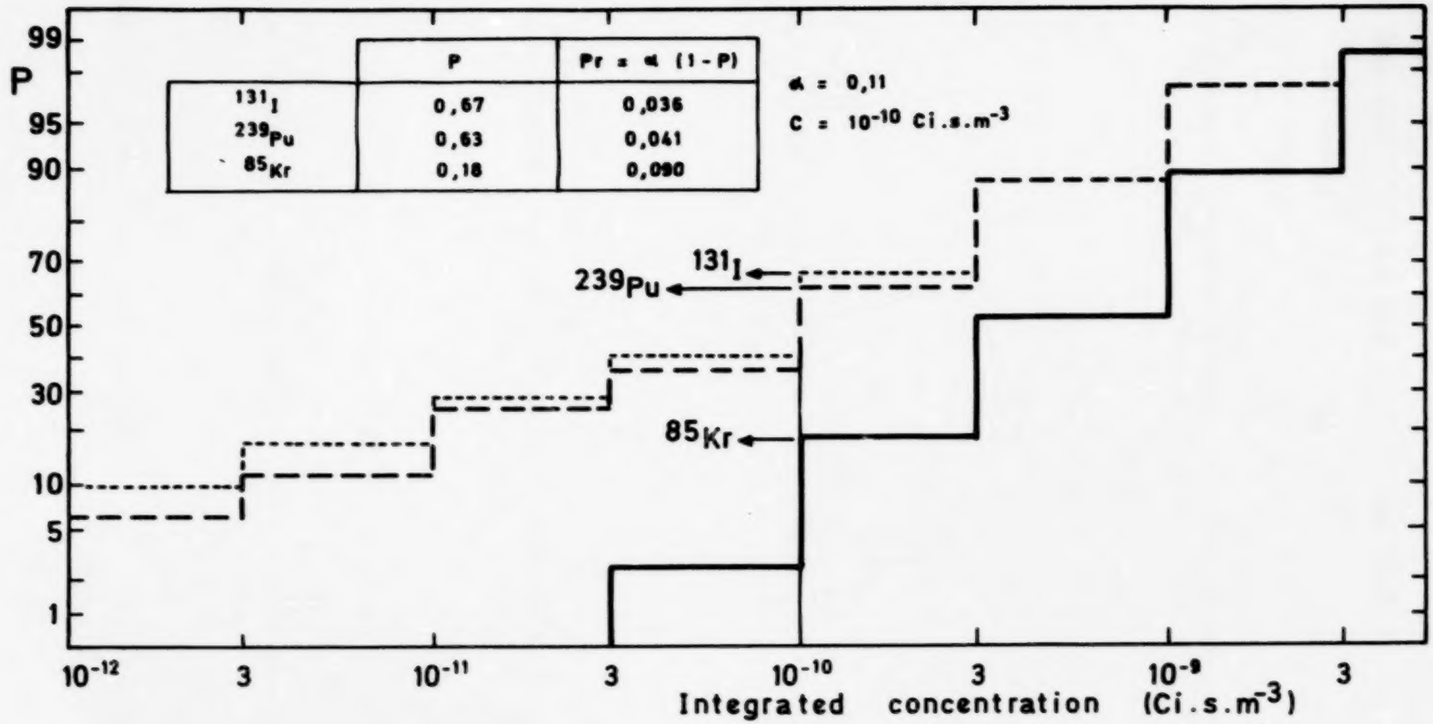

	P	Pr = α (1 - P)
^{131}I	0,67	0,036
^{239}Pu	0,63	0,041
^{85}Kr	0,18	0,090

Figure 5. - Cumulative probability P that the integrated concentrations of ^{85}Kr, ^{239}Pu, ^{131}I are smaller than or equal to the indicated value

- Cumulative probability Pr that the indicated integrated concentration has been exceeded
- α, probability that the plume reaches the receptor

Discussion:

Klug:

Did you compare the two models MESOS and TALD with respect to their simplicity? May the simple model (TALD) give realistic results too?

Bultynk (response):

We applied both models to the Winscaleaccident, but the results were not satisfying. At the present time we try to get realistic results from the complicated model, and after that we will simplify the method.

Runca:

Do you apply the model as a real time procedure?

Bultynk (response):

The model was created for climatological purposes to give guidelines for the planning of new nuclear power plants.

Hübschmann:

In my opinion trajectories over distances of 600 km do not say anything about the risks of nuclear plants; the problem is to find out, what could happen in the neighbourhood of the plant.

VARIATION OF ACID RAIN CONCENTRATIONS WITH SUMMER PRECIPITATION EVENTS IN THE SCHEFFERVILLE, QUEBEC AREA

by

John E. Lewis and Bohdan Hrebenyk
Department of Geography
McGill University
Montreal, Quebec

Abstract. A pilot study was conducted to measure the chemical constituents of precipitation in the Schefferville area of Nouveau Quebec during July and August 1978. Sampling was performed on a storm event basis where a total of five storms were analyzed. Two of the five storms had pH less than 5. One of the storms had sulphate value of 1.6 ppm and a pH of ≃ 4.6; all the remaining storms had sulphate values below detectable limits. Preliminary evidence indicated that a certain combination of synoptic weather conditions must exist to produce acid rain events in Nouveau Quebec during the summer season.

Introduction

A ubiquitous environmental ingredient of continuing industrialization is acid rain. Through the mechanism of long range atmospheric transport and the wet/dry deposition, pollutant loadings are occurring in remote areas with increased frequencies. The concern voiced for this problem and the effect on different ecosystems is well-documented (Beamish, 1976; Braekke, 1976; and Seliga and Dochinger, 1976).[1,2,3]

Though the influence of acid rain on the ecology of a region is as yet imperfectly understood, increasing interest in the subject has spurred the Canadian government through the offices of Atmospheric Environment Service (AES) to establish the Canadian Network for Sampling Precipitation (CANSAP). While CANSAP includes some stations in northern Quebec, it is felt that the approach taken by AES tends to minimize information on the mechanism of pollutant transport. Specifically, the collection of rain is carried out over a period of approximately one month and then is analyzed as a single sample. While this may provide useful standards on which to base comparisons of total pollutant loading on the environment, the data collected in this manner will not serve to demonstrate the origins of the various chemical elements of the rainfall. Furthermore, studies conducted in the OECD pollution program (OECD, 1977) indicate that infrequent meteorological events are often associated with the episodic deposition of pollutants (5% of the wet days in sections of Scandinavia accounted for 30% of total wet sulphate deposits).[4] It was felt that a program designed to study the interstorm variability of pollutant deposition would serve as an important contribution to the better understanding of acid rain phenomena in eastern subarctic Canada and would better aid in the evaluation of the CANSAP data. A pilot study was conducted to measure chemical constituents of precipitation and to describe the synoptic events which generated the rainfall for the Schefferville area of Nouveau Quebec during July and August 1978.

Preceding page blank

Methodology

Precipitation was collected in 9 in. diameter plastic rain gauges at two primary locations around Schefferville, (1) at the McGill Subarctic Research Station and (2) on Dolly Ridge, 3 miles east of the McGill Station. In addition, intermittent samples were collected at Iron Arm, approximately 12 miles east of the Station. During some storms, a sequence of precipitation samples were collected. The process of collection was rather tedious during this period because a wet/dry collector was not available; however, this situation has been remedied now.

The following procedures were maintained throughout the experiment:

(1) the rain gauges were washed with a weak acid solution and then thoroughly rinsed with distilled H_2O after which the gauges were sealed.

(2) when a storm was forecast and the initial precipitation occurred, the rain gauges were set out for collection.

(3) as soon as precipitation ceased, a 250 ml sample was collected; the gauges returned to the laboratory where they were washed and sealed to await the next storm.

The precipitation samples were filtered and then the pH measured. The samples were stored at $4^{o}C$ until the end of the summer at which time they were shipped to Montreal for further chemical analyses. Atomic absorption spectrophotometry was used to obtain concentrations of Na^+, Fe^{++}, Ca^{++}, and Mg^{++}, whereas nitrate (NO_3^-) and sulphate ($SO_4^=$) concentrations were measured with an automated calorimetric method (Technicon Auto-Analyzer).

Precipitation Analysis

Between July 1 and August 14, seven major storms occurred in the Schefferville region; however, due to various problems only five storms were analyzed - July 8, 16, 20, 27 and August 5-6. These five storms constituted ≈ 73% of the total precipitation during the study period.

In only two of the five storms (July 16 and 27) was the pH less than 5. Table 1 is a list of the storm events and the precipitation chemistry. The storm of July 16 had a pH of ≈ 4.8 while on the 27th the pH was ≈ 4.6. Only the latter storm had values of sulphate concentrations above detectable limits of < 0.5 ppm. A comparison for the July 27th storm between the McGill Station site and Dolly Ridge shows sulphate concentrations of 1.6 ppm with 10.6 mm total precipitation for the Station to 1.8 ppm and 8.8 mm for Dolly Ridge. Nitrate concentrations had their highest values for these two storms with .16 ppm for July 16th and .3 ppm for the first part of the July 27th storm and .16 ppm for the second. Positive ions (Na^+, Ca^{++}, Mg^{++}, and Fe^{++}) generally displayed small concentrations for the five storms monitored. An ionic balance could not be calculated because of our failure to measure ammonium (NH_4^+) during this period.

Synoptic Storm Characteristics

Utilizing some of the early work of Barry (1959) for the Labrador region, we developed a preliminary synoptic classification of summer rain events for Schefferville.[5] Ten years (1965-1974) of summer weather events were typed into four groups. From this synoptic classification, we isolated three important storm parameters which we felt related to potential pollutant deposition episodes:

(1) the position of the cyclonic storm track in association with 850 mb back trajectories;

(2) antecedent synoptic conditions in middle and eastern North America; that is, 2 or more days of anticyclonic weather existing for this region;

(3) the number of hours the rain was occurring within the storm before it arrived at Schefferville.

These parameters are more distinctive for eastern Canada than the two main synoptic conditions which produce episodic wet deposition in northwestern Europe (Smith and Hunt, 1978).[6]

Discussion

Figure 1 displays the storm tracks with their predominant SW-NE movement. The location of these storm tracks will impart an overall characteristic to the storm but each storm should be inspected in conjunction with air trajectories. For each of the storms, 850 mb back trajectories (Petterssen, 1956) were calculated as shown in Figure 2.[7] Most readers appreciate the assumptions and possible errors incorporated in the calculation of trajectories (Pack et al., 1978), but for this study the trajectories serve as a qualitative geographical indication of general source regions.[8] The first trajectory segment is for 6 hours based on four surrounding stations, whereas succeeding segments are for 12 hours and the number of synoptic stations used in the calculations increase markedly towards the south.

The storm of July 16th developed farther east and the movement had a more northerly component than the 27th storm which proceeded slowly along a track from western Ontario across James Bay into middle Quebec. However, the 850 mb trajectories are very similar. Both these 850 mb trajectories have geographical approximation to two major point sources - Sudbury with emission over one million tons of sulfur a year (3500 tons/day) (Luis and Wiebe, 1976) and Noranda with 600 thousand tons of sulfur emitted a year.[9] In addition, there are many possible point and area source contributions of SO_2 from the entire Great Lakes region.

The discriminating feature for these two storms as to the production of acid rain is their precipitation pattern. Precipitation for the 27th storm was confined to a more northerly location and the rain commenced only 30 hours before it reached Schefferville. This is contrasted with July 16th storm where rainfall occurred over a wide region of southern Quebec and the precipitation started > 48 hours before arriving at Schefferville. Figures 3 and 4 display the synoptic weather maps for these two storms.

For the other sotrms, either the 850 mb trajectories were too far north, taking the air flow outside possible emission source regions, or antecedent synoptic conditions were not favourable for the build-up of sulphate concentrations.

Based on this preliminary evidence, there appears to be a particular combination of atmospheric conditions which produce individual synoptic events that increase the incidence of acid rain at Schefferville as well as other areas of Nouveau Quebec. A CANSAP station, 250 km south of Schefferville, recorded a July 1978 pH of 4.8, sulphate loading of 1.1 mg/l and a total rainfall catch of 172 mm. In contrast, it may be the specific, infrequent event which yields above normal values of rain acidity as indicated by Schefferville data. Such episodes should be identified on a case-by-case basis as they occur. With further work, it may be possible to develop a synoptic classification of these events to determine their frequency of occurrence.

Acknowledgement

We greatly appreciate the financial support received from the Department of Indian and Northern Affairs through McGill's Centre for Northern Studies and Research, The Atmospheric Environment Service of Canada, and the Natural Sciences and Engineering Research Council of Canada.

References

1. R.G. Beamish, Acidification of lakes in Canada by acid precipitation and resulting effects on fishes. J. Wat. Air Soil Pollut. 6, 501-514, 1976.
2. F.H. Braekke (ed.), Impact of Acid Precipitation on Forest and Freshwater Ecosystems in Norway, SNSF Project, Research Report FR/76, Oslo, 1976.
3. T.A. Seliqa and L.S. Dochinger (ed.), Proceedings of the First International Symposium on Acid Precipitation and the Forest Ecosystem, USDA Forest Service, General Technical Report, NE-23, 1976.
4. OECD, The OECD Programme on Long Range Transport of Air Pollutants. OECD, Paris, 1977.
5. R. Barry, Synoptic Climatology of Labrador-Ungava, M.Sc. Thesis, Department of Geography, McGill University, 1959.
6. F.B. Smith and R.D. Hunt, Meteorological aspects of the transport of pollution over long distances, Atmospheric Environment, 12, 461-477, 1978.
7. S. Petterssen, Weather Analysis and Forecasting, McGraw-Hill, N.Y., 1956.
8. D.H. Pack et al., Meteorology of long-range transport, Atmospheric Environment, 12, 425-444, 1978.
9. M.A. Luis and H.A. Wiebe, The rate of oxidation of sulfur dioxide in the plume of a nickel smelter stack, Atmospheric Environment, 10, 793-798, 1976.

Table 1. Precipitation chemistry for rainfall collected during July-August 1978

Class		Nitrate ppm	Sulfate ppm	pH(1)	Ca ppm	Na ppm	Fe ppm	Mg ppm	Total Precipitation mm
A-03 8/7	DR	0.05	<0.5	5.5	nd	.005	.02	.022	13.5
A-04 8/7	IA	0.02	<0.5	5.4	nd	nd	--	.005	
A-05 8/7	S	0.036	<0.5	5.5	nd	.010	.05	.003	11.0
A-06 16/7	DR	0.165	<0.5	4.8	nd	.15	.05	.011	16.0
A-07 16/7	IA	0.070	<0.5	4.7	nd	.025	.025	.006	
B-22 20/7	S^{1st}	0.014	<0.5	5.2	nd	.089	.07	.015	15.0
B-23 20/7	S^{2nd}	0.012	<0.5	5.1	nd	.013	.035	.006	
B-24 20-21/7	S Total	0.013	<0.5	5.8	nd	nd	.03	.018	14.5
B-25 20/7	DR	0.130	0.8	5.0	nd	.011	.05	.003	
B-26 20/7	IA	<0.001	<0.5	5.2	nd	.016	.06	.013	
C-02 27/7	S^{1st}	0.3	<0.5	4.5	nd	.01	.02	.006	10.6
C-03 27/7	S^{2nd}	0.16	1.6	4.8	nd	.013	nd	.014	
C-04 27/7	DR	0.008	1.8	4.9	nd	.01	.015	.010	8.1
D-18 5/8	S	0.008	<0.5	5.6	nd	.04	.02	.01	12.8
D-19 5-6/8	S	<0.001	<0.5	4.9	nd	nd	nd	.007	
D-20 5-6/8	DR	<0.001	<0.5	5.4	--	nd	nd	--	13.5
E-01 21-23/7	LS	<0.001	<0.5	6.0	--	--	--	--	
E-02 23/7	DR	<0.001	<0.5	5.6	--	--	--	--	
Distilled H_2O C-00 26/7		<0.001	<0.5	5.7	nd	nd	.02	nd	

S = Schefferville (Lab.)
DR = Dolly Ridge
IA = Iron Arm
LS = Laurentian Shield

nd = non-detectable

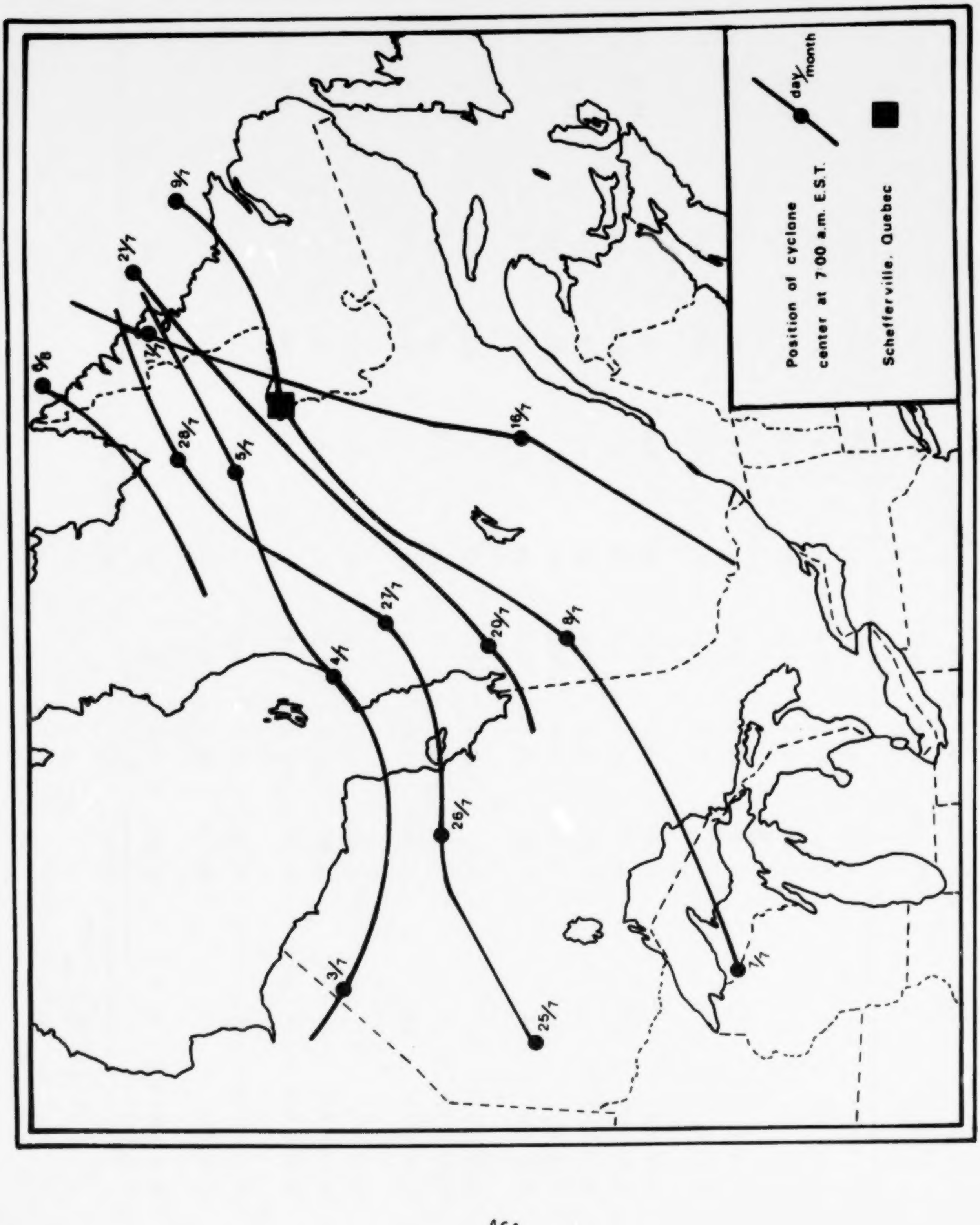

9/8
9/1
21/1
17/1
28/1
5/1
16/1
27/1
29/1
8/1
4/1
26/1
3/1
25/1
7/1
day/month
Position of cyclone center at 7:00 a.m. E.S.T.
Schefferville, Quebec

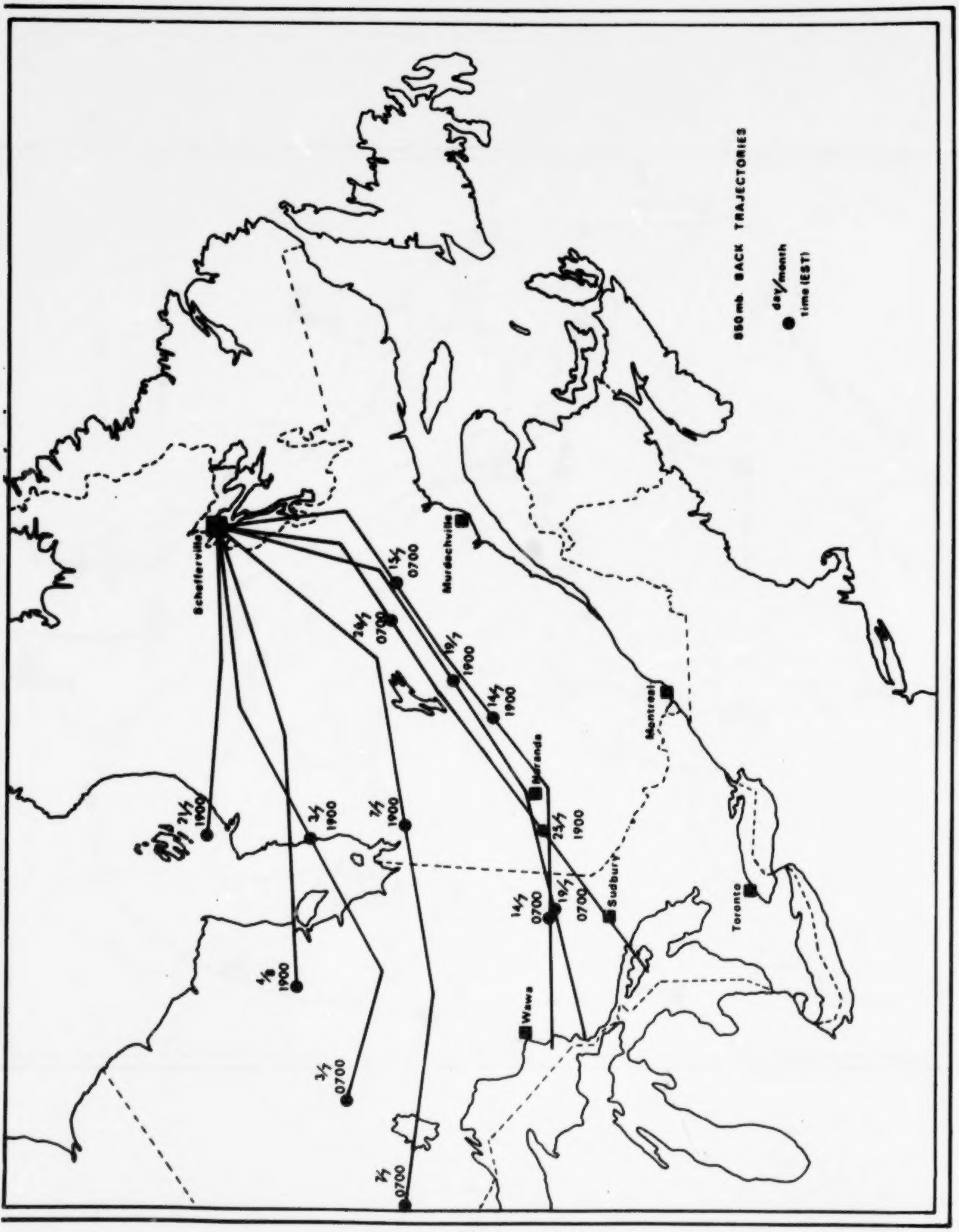
850mb BACK TRAJECTORIES
day/month
time (EST)
Schefferville
Murdochville
Noranda
Montreal
Sudbury
Toronto
Wawa
15/7 0700
26/7 0700
19/7 1900
14/7 1900
21/7 1900
3/7 1900
7/7 1900
23/7 1900
14/7 0700
19/7 0700
4/8 1900
3/7 0700
7/7 0700

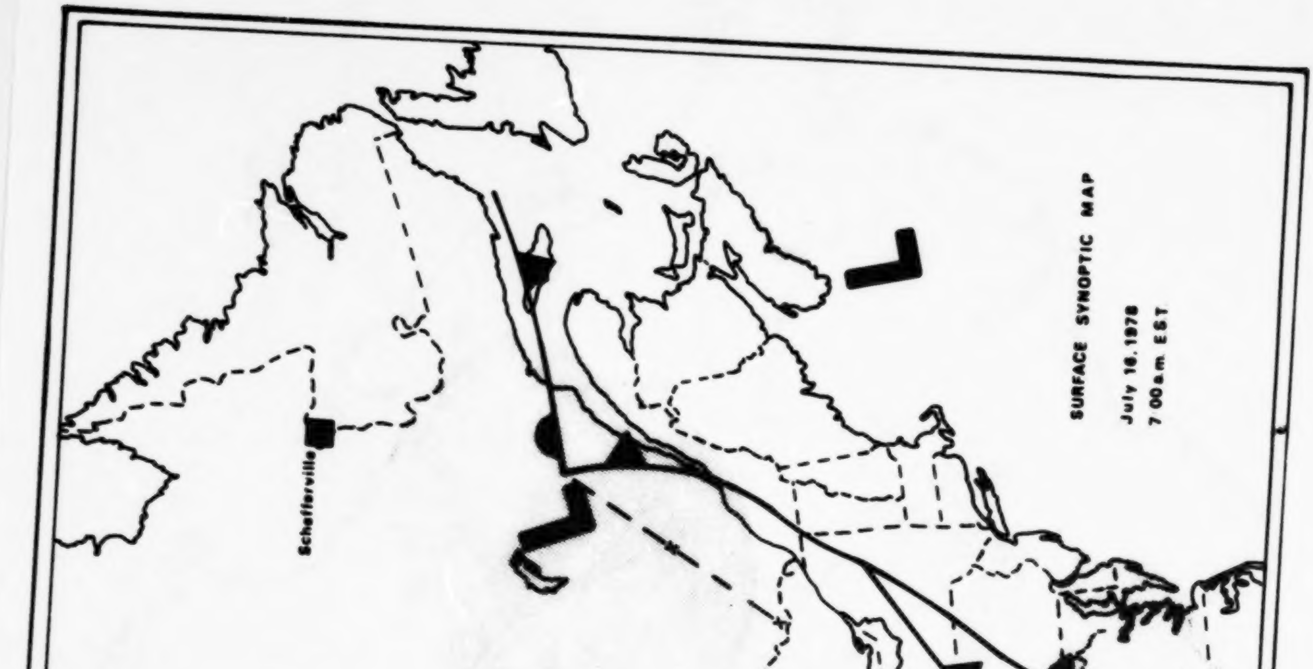
Schefferville
L
L
L
H
SURFACE SYNOPTIC MAP
July 16, 1978
7:00a.m. EST

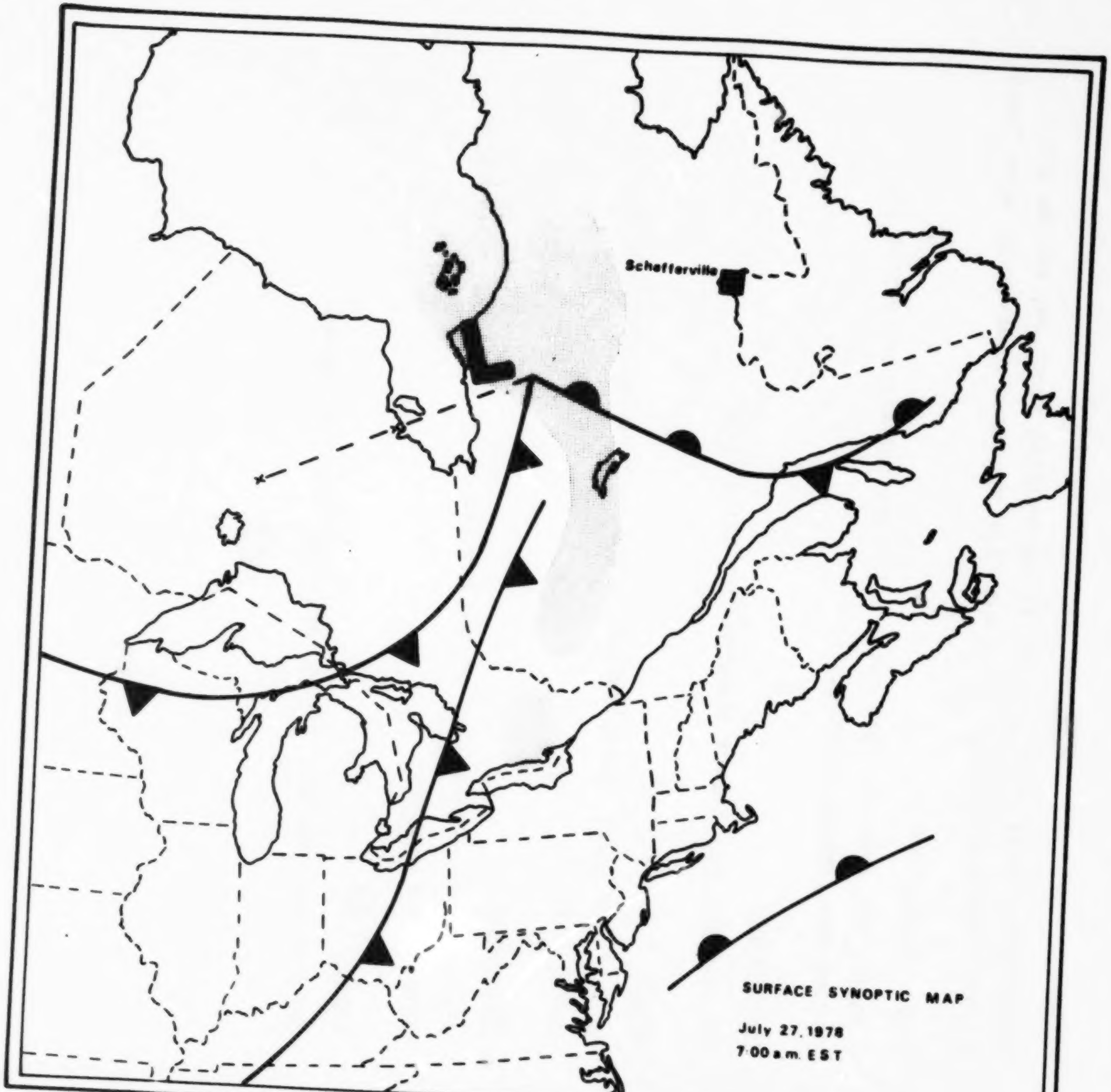

Schefferville

SURFACE SYNOPTIC MAP

July 27, 1978
7:00 a.m. EST

Discussion:

Davis:

Trajectories under conditions of an approaching front may not be calculated from the pressure field but from the three dimensional wind field.

Lewis (response):

I agree, but then you need data, which are not available from the routine measurement service.

Hübschmann:

Why did you only select thunderstorm situations?

Lewis (response):

90 % of the total precipitation in our test region occurred under these conditions.

Venkatram:

Did you measure pH-values of the precipitation along the whole travel path of the storms?

Lewis:

Only at one position 150 km away from our test region.

THE USE OF TIME AVERAGED PRECIPITATION FOR WET REMOVAL IN A REGIONAL AIR POLLUTION ASSESSMENT MODEL

by

W. E. Davis and W. J. Eadie
Pacific Northwest Laboratory
Richland, Washington USA

Abstract. Results are presented of the test of a regional scale assessment model using four modes of precipitation hourly, six hourly, averaged turned on and off with the natural frequency and average precipitation. The test cases were carried out for a release of SO_2 with transformation to SO_4 at three different sites in the United States for July 1974. The results indicated that the use of average precipitation turned on and off with the natural frequency could be used instead of hourly precipitation for long-term assessments.

Introduction

One of the problems that confronts regional scale computer modelers is how to incorporate precipitation into a model with precipitation removal. In particular, one problem is what kind of average precipitation data should be used. A number of different approaches to this problem in the regional scale assessments have been used in the past. In Johnson et al.[1], six-hour precipitation was used for an assessment. In Eliassen[2], six- and twelve-hour precipitation was used in an assessment for 1974. In Slinn[3], a recommendation was made that researchers use a constant wet deposition velocity based on the average annual precipitation. At Pacific Northwest Laboratory (PNL), hourly precipitation is used for most assessments[4,5].

The production of hourly precipitation tapes is long and costly. A computer program developed by Fox and Wendell[6] takes station file data from more than 3,000 reporting stations in the United States (Fig. 1) and converts it to synoptic file data. This data in turn was gridded to be used in an assessment. The time, effort, and expense to produce this data can cause severe limitations for regional scale assessments produced on a limited budget. With this in mind, an alternative approach was considered.

A study by Wendell, Powell and McNaughton[7] demonstrated that the use of average precipitation would cause an overestimate of the amount of SO_4 deposited in a regional study when compared to results using hourly precipitation. This prompted a paper by Davis[8] that showed that increasing the averaging times increased the amount of deposition for washout ratios greater than 5×10^4. It was also shown in this paper that when the average precipitation, corrected to the average intensity during wet periods, was turned on and off with the average frequency and for the average duration of naturally occurring precipitation that the mass balance was approximately the same as when hourly precipitation was used. However, this work was done with an idealized pollutant that neither dry deposited or underwent chemical transformation. It is the purpose of this paper to test whether or not this approach can be extended to an assessment using SO_2 and SO_4.

The Pacific Northwest Laboratory Assessment Model

A number of regional assessment models exist at PNL. The one described here[9] was originally developed by Wendell, et al.[10] and was adapted for use in the western United States by Renee, et al.[11] and Sandusky, et al.[12]. Sensitivity and verification studies with the model have been conducted by Powell, et al.[4] and McNaughton[5] for SO_2 and SO_4 air concentrations and depositions in the northeastern United States.

The model, as used in this study, assumes hourly puffs. The puffs are advected in hourly steps using gridded layer averaged wind (100 m - 1000 m). The vertical component of the wind is assumed to be zero. The following assumptions are made on atmospheric diffusion:

1. Horizontal diffusion is a function of synoptic scale wind variation only. Tennekes[13], Bolin and Persson[14], and Prahm and Christensen[15] support this assumption. All state that either horizontal turbulent diffusion about the plume centerline is relatively unimportant or that it is less important than plume meandering.
2. The vertical-turbulent diffusion parameterization is a function of stability in a specified diurnal cycle for all plume elements within the daytime mixed layer or the nocturnal stable layer.
3. The depth of the daytime mixed layer is represented by a diurnal cycle in which a daytime layer increased from a minimum depth at sunrise to a maximum depth in the afternoon. A nocturnal layer builds to a lower depth.
4. Depth of the boundary layer (mixed layer in daytime or nocturnal layer) for each hour determines which of two vertical dispersion regimes - mixed layer or above mixed layer - will be applied to a given plume element. Those elements released within the depth of the layer expand according to the stability of the hour. Those released above the current depth of the layer expand as if the atmosphere were extremely stable. An exception to this method occurs when releases have expanded to the maximum depth of the mixed layer during the previous day; in this case, their expansion continues according to a fixed function of travel time independent of stability or layer depth.
5. Depth of the mixed layer provides a vertical constraint for releases at heights within this layer. The depth of the nocturnal boundary does not serve as an analogous constraint. Carson[16] supports this assumption by depicting the mixed-layer depth as a function that increases during the daytime, then loses its definition. This picture is in relative agreement with modeling results by Venkatram and Viskanta[17] and with experiment results by Kaimal et al.[18] who find that about one hour before sunset, the convective layer disintegrates rather abruptly, although remnants of the capping inversion persist through the development of the nocturnal boundary layer.
6. At the present stage of model development, terrain effects are neglected.

For additional information, the reader is referred to Eadie and Davis[9] for a complete description of the model.

Precipitation Frequency

There are at least two recent papers which treat precipitation frequency: on a single station basis[19], and on a regional basis[20]. They have computed the duration of wet and dry periods. The former for a single station in Europe using a year's data while Henmi and Reiter[20] produced an analysis of the United States east of 105°W longitude based on records for 61 stations for 1974. One can apply their results, or as has been done for one of the studies in this paper, examine the weather maps for the month's data to be used and hand compute a mean dry period and a mean duration of precipitation.

Case Study

Three sites were selected (Fig. 2) with two in the western United States and one in the eastern United States for July 1974. Figure 3 shows the distribution of precipitation. The reader might note that the western sites were relatively dry while the eastern site was in a fairly intense precipitation zone.

From the distribution of precipitation, one would suspect that both the average dry period and the average duration of precipitation would vary from east to west. For the two sites in the west, the same values were used. The average duration of precipitation of three hours was selected for every 120 hours. These values were chosen based on a rough average of values presented by Henmi and Reiter[20]. A different set of averages was used in the east with six hours of precipitation for every 60 hours. These values were roughly estimated on the basis of a hand analysis of surface reports in the east.

The PNL model was run in four precipitation modes for each of these sites for hourly, six-hourly, average precipitation turned on and off (on/off) and average precipitation. The coefficients used in this study for SO_2 and SO_4 are shown in Table 1. These were obtained from Sandusky et al.[21]. An example of the air concentrations and depositions produced by the PNL model for July 1974, are shown in Figures 4-11 for a source near Anaconda, Montana.

Results

The results of the mass balance comparison (Table 2) using the average (on/off), average, and the six-hourly precipitation with the hourly precipitation results show very good agreement for all three sites. Also the air concentration patterns for SO_2 show good agreement for all techniques (Fig.4-7).

However, when the deposition patterns using the average precipitation (Fig. 11) and the average precipitation (on/off) (Fig. 10) are compared to the pattern produced using the hourly precipitation (Fig. 8), a wide variance appears. Even using six hourly precipitation (Fig. 9) can cause large differences in deposition when compared to the deposition from using hourly precipitation.

The widest variance cccurs in SO_4 wet, the amount deposited by washout, whereas increasing the averaging time increases the amount in wet deposition.

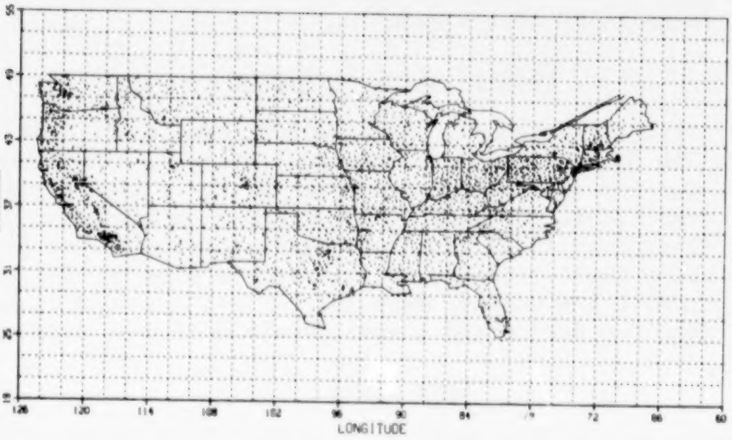
LATITUDE
55
49
43
37
31
25
19
126
120
114
108
102
96
90
84
78
72
66
60
LONGITUDE

Figure 1. Hourly reporting precipitation stations.

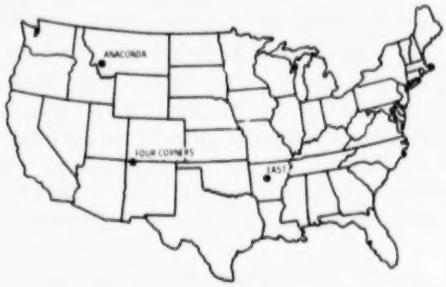
ANACONDA
FOUR CORNERS
EAST

Figure 2. Stations used in this study.

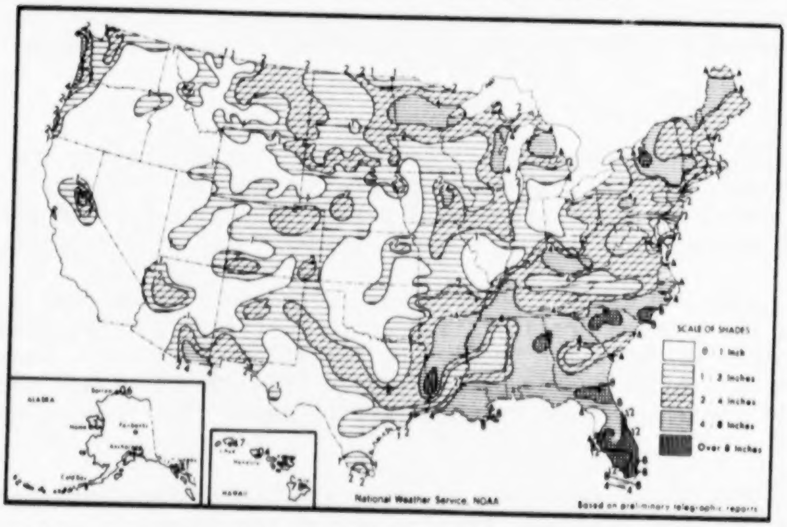
SCALE OF SHADES
0 - 1 inch
1 - 2 inches
2 - 4 inches
4 - 8 inches
Over 8 inches
ALASKA
HAWAII
National Weather Service, NOAA
Based on preliminary telegraphic reports

Figure 3. Total precipitation (inches) July 1974.

Table 1. Model Input Data

Time period for meteorological data	1-31 July, 1974
Advection grid spacing (35°N latitude)	321 Km
Grid spacing for precipitation data, and sampling of results (35°N latitude)	32 Km
Effective stack height	200 m
Mixing height	Variable
Stability	Variable
Dry deposition velocities:	
SO_2	1.4 cm/sec
Sulfates	0.23 cm/sec
Wet removal coefficients[a]:	
SO_2	0.058 P/hr
Sulfates	$.38\ P^{.73}$/hr
Transformation rate of SO_2 to sulfates	0.005/hr
Percentage of emissions as primary sulfates	0.02 (2% of emission)

---

[a] P=rainfall rates mm/hr.

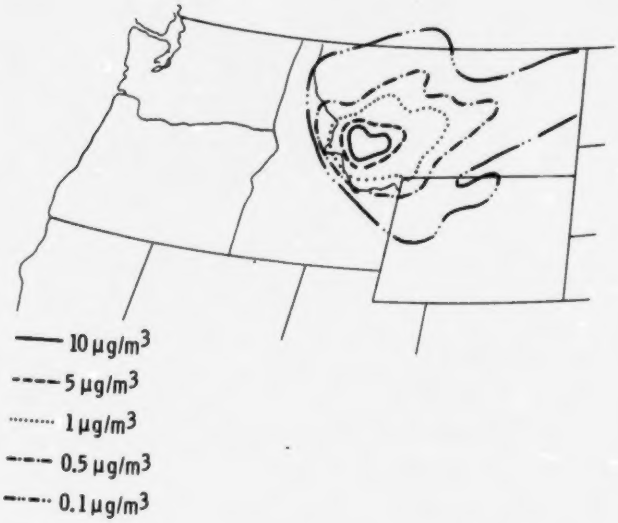

Figure 5. Six hour precipitation, SO_2 air concentration, July 1974.

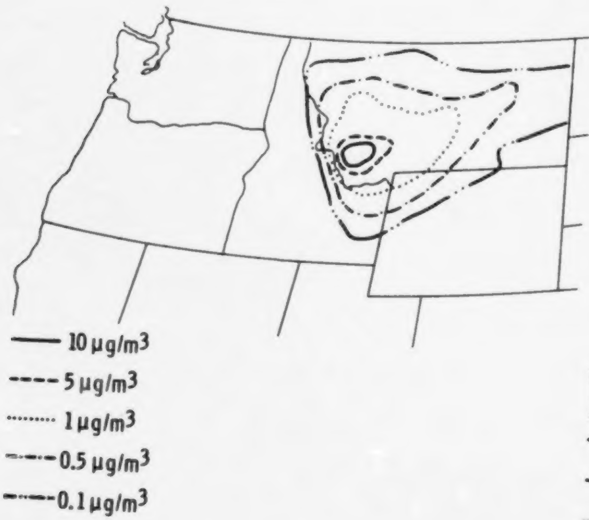

Figure 4. Hourly precipitation, SO_2 air concentrations, July 1974.

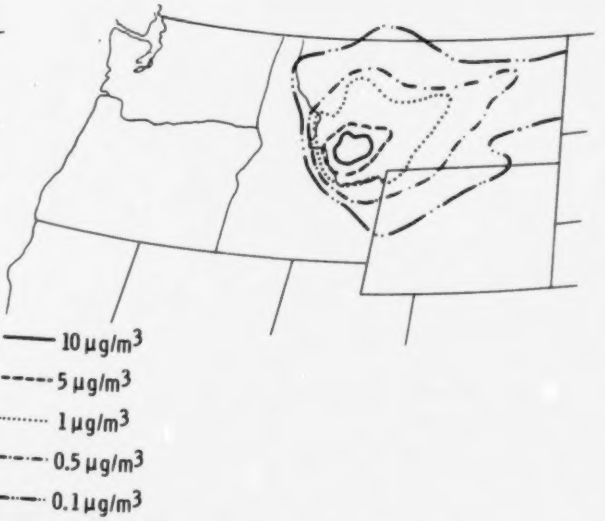

Figure 6. Time averaged precipitation (3 hr on/120 hr off), SO_2 air concentrations, July 1974.

For example, in the East where the percent wet deposited by the use of hourly precipitation was 7.85%, by the use of six-hourly precipitation was 8.74%, and by the use of average monthly precipitation was 10.28%. These results compare favorably with the results found by Davis[8] (Table 3). The average (on/off) generally compares favorably with the values arrived at using the hourly precipitation in all categories.

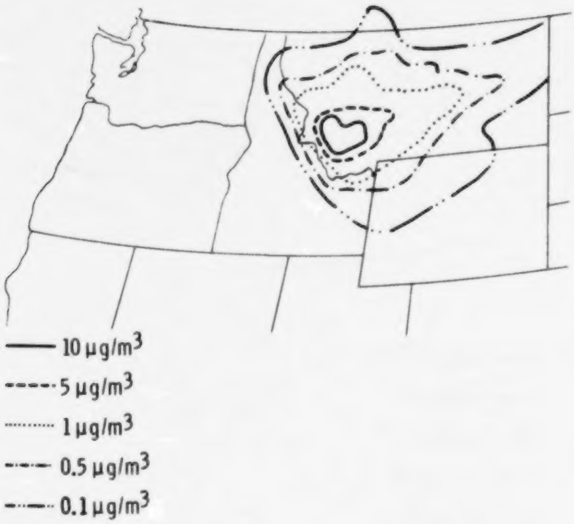
10 μg/m³
5 μg/m³
1 μg/m³
0.5 μg/m³
0.1 μg/m³

Figure 7. Time averaged precipitation, SO_2 air concentrations, July 1974.

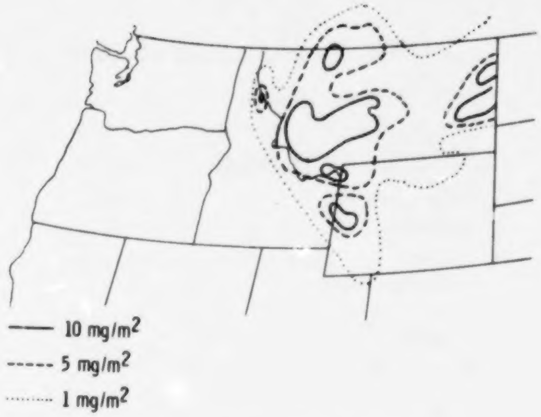
10 mg/m²
5 mg/m²
1 mg/m²

Figure 9. Six hour precipitation, SO_4 deposition, July 1974.

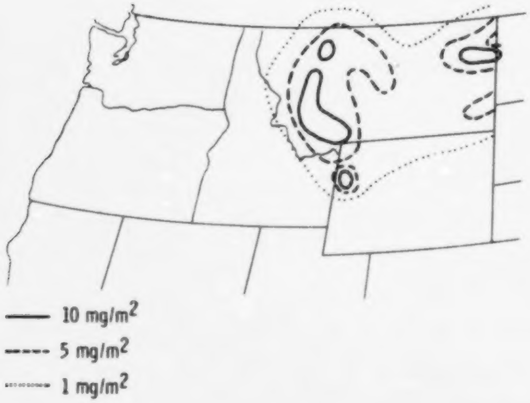
10 mg/m²
5 mg/m²
1 mg/m²

Figure 8. Hourly precipitation, SO_4 deposition, July 1974.

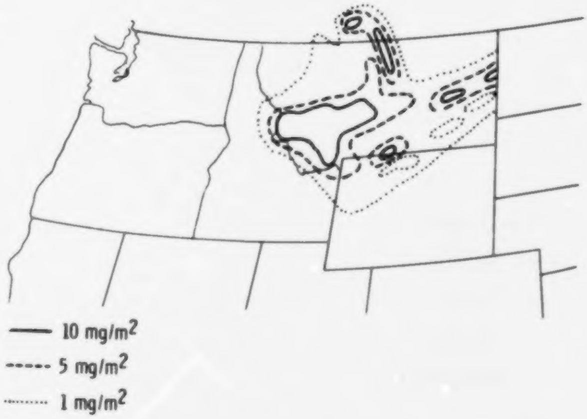
10 mg/m²
5 mg/m²
1 mg/m²

Figure 10. Time averaged precipitation (3 hr on/120 hr off), SO_4 deposition, July 1974.

The reader should also note in Table 3 that results are also presented of another PNL model with eight layers and vertical motions[22]. Also, the 10% represents seven hours duration of precipitation for every 72 hours.

Basically, the results confirm earlier findings by Davis[8]. That is, when the average precipitation is turned on and off at approximately the same frequency that occurs and for the same intensity in the area of interest, the mass balance is approximately the same. Also, the same result was found that the

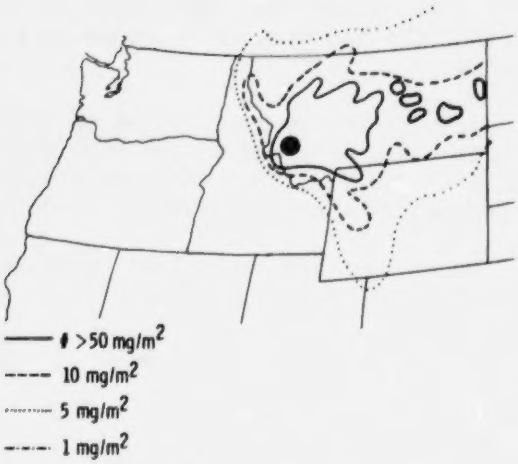

Figure 11. Time averaged precipitation, SO_4 deposition, July 1974.

Table 2. Mass Balance (% of Release).

STATION	TYPE PRECIPITATION	SO_2 Air	SO_4 Air	SO_2 Deposit (SO_2 Wet)	SO_4 Deposit (SO_4 Wet)	SO_2 Off	SO_4 Off	SO_2 Drop	SO_4 Drop
Anaconda Montana	Hourly	3.12	1.70	84.31 (4.15)	8.95 (5.60)	.15	.33	.16	1.47
	6-Hourly	3.13	1.57	84.42 (4.84)	9.60 (6.96)	.13	.24	.14	.76
	Average (on/off)	3.2	1.84	84.06 (3.23)	8.93 (5.72)	.22	.84	.13	.78
	Average	3.08	.60	84.29 (3.95)	11.30 (9.64)	.21	.23	.13	.16
Four Corners Southwest U.S.	Hourly	3.16	1.16	34.69 (6.46)	9.39 (6.64)	0	0	.16	1.43
	6-Hourly	3.19	1.19	84.65 (6.75)	9.40 (6.83)	0	0	.18	1.39
	Average (on/off)	3.21	1.65	84.51 (5.75)	9.32 (6.41)	0	0	.19	1.13
	Average	2.87	.28	85.11 (7.70)	11.46 (10.30)	0	0	.16	.11
East Central Arkansas	Hourly	2.93	.71	84.81 (6.99)	10.46 (7.85)	.35	.27	.10	.37
	6-Hourly	2.74	.30	85.27 (8.8)	10.99 (8.74)	.28	.15	.09	.18
	Average (on/off)	3.26	1.14	84.65 (7.52)	10.41 (8.48)	.27	.15	.08	.05
	Average	2.73	.18	85.25 (8.92)	11.33 (10.28)	.32	.06	.07	.01

deposition patterns were quite different for the deposition calculated using hourly precipitation versus the deposition calculated using average precipitation (on/off) and average precipitation. This points out the importance of using hourly precipitation when considering episodal cases. The reason for the difference is that precipitation events are relatively infrequent and by using the time averaged precipitation turning it off and on from 7 to 12 times a month will cause the deposition pattern to be heavily influenced as to when the precipitation is turned off and on. However, for long-term assessments where a year's data is used, it is expected that these differences will probably average out and that the patterns will become more similar. This will have to be investigated.

The use of average precipitation is discouraged in that the pattern doesn't tend to average out. This is based on the high deposition near the source due to scavenging of all puffs. When the rain is turned on and off with the approximate natural frequency, a better estimate of deposition is obtained.

Table 3. Total Deposition (in percent of total released) Using Different Averaging Times

Type of Model	W	Averaging Times	Total Deposited
(Period 1, April 1-15, 1974)			
Single Layer	5×10^5	Hour	52
Single Layer	5×10^5	Six Hours	56.6
Single Layer	5×10^5	360 Hours	75
Eight Layer	5×10^5	Hour	41.6
Eight Layer	5×10^5	Six Hours	44.3
Eight Layer	5×10^5	12 Hours	47.4
Eight Layer	5×10^5	24 Hours	51
Eight Layer	5×10^5	360 Hours	64.2
(Period 2, January 1-31, 1975)			
Single Layer	5×10^4	Hour	29.9
Single Layer	5×10^4	744 Hours	23.8
Single Layer	5×10^4	10%**	25.7
Single Layer	5×10^5	Hour	52
Single Layer	5×10^5	Six Hours	57.1
Single Layer	5×10^5	744 Hours	82
Single Layer	5×10^5	10%**	51.5
Single Layer	5×10^6	Hour	61.1
Single Layer	5×10^6	744 Hours	99.9
Single Layer	5×10^6	10%**	53.6

W - Washout ratio

** Seven hours of 10x average precipitation every 72 hours.

Conclusions and Recommendations

PNL regional scale model results from using average precipitation turned off and on at approximately the same frequency of naturally occurring rain in the region has yielded mass balances which compared favorably with model results using hourly and six-hourly precipitation for SO_2 and SO_4 for three sites in the United States for July 1974. These results confirm earlier results by Davis[8] which first presented the technique of turning off and on the average precipitation in a regional scale model. The earlier work was performed with an idealized situation with no dry deposition or chemical transformations.

This technique of turning on and off the precipitation as well as using six-hourly or longer average precipitation should not be used for episodal studies where both air concentrations and deposition are important. Although the air concentration patterns are quite similar for the month of study, the deposition patterns are quite dissimilar.

The technique of turning on and off the precipitation presented is recommended for annual assessments in order to allow for enough rain events to occur to average out the deposition patterns. However, additional comparisons should be made for an annual assessment to validate whether the proper averaging of the deposition pattern will take place. The other technique of using six-hourly precipitation also yielded comparable results with results using hourly precipitation. This technique can also be utilized for long-term assessments.

References

1. W. B. Johnson, D. E. Wolf and R. L. Mancuso, "Long-Term Regional Patterns and Transfrontier Exchanges of Airborne Sulfur Pollution in Europe," Atmos. Environ., 12, Nos. 1-3, 1978.
2. A. Eliassen, "The OCED Study of Long-Range Transport of Air Pollutants: Long-Range Transport Modelling," Atmos. Environ., 12, 1-3, 1978.
3. W. G. N. Slinn, "Parameterization for Resuspension and for Wet and Dry Deposition of Particles and Gases for Use in Radiation Dose Calculations," Nuclear Safety, 19(2), March-April 1978, 205-219.
4. D. C. Powell, D. J. McNaughton, L. L. Wendell and R. L. Drake, A Variable Trajectory Model for Regional Assessments of Air Pollution from Sulfur Compounds, PNL-2734, Battelle, Pacific Northwest Laboratories, Richland, WA., 1979.
5. D. J. McNaughton, "Initial Comparisons of SURE/MAP3S Sulfur Oxide Observations with Long-Term Regional Model Predictions." Submitted to Atmos. Environ., 1979.
6. T. D. Fox and L. L. Wendell, "Precipitation Data Base Manipulation for Use in Regional Transport and Removal Models," Pacific Northwest Laboratory Annual Report for 1976 to ERDA, BNWL-2100, Part 3, UC-11, Part 3: Atmospheric Sciences, 1977.
7. L. L. Wendell, D. C. Powell and D. J. McNaughton, "A Multi-Source Comparison of Real Time Versus Time Average Precipitation Data on SO_2 and Sulfate Particulate Removal in a Regional Assessment Model." Joint Conference on Applications of Air Pollution Meteorology, November 29 - December 2, 1977. Salt Lake City, Utah.
8. W. E. Davis, "The Effect of Using Time Averaged Precipitation for the Estimation of Wet Deposition in a Regional Scale Model", Fourth Symposium on Turbulence, Diffusion, and Air Pollution, Reno, Nevada, January 15-18, 1979.
9. W. J. Eadie and W. E. Davis, "The Development of a National Interregional Transport Matrix for Respirable Particulates," PNL-RAP-37, (in print).

10. L. L. Wendell, D. C. Powell and R. L. Drake, "A Regional Scale Model for Computing Deposition and Ground Level Air Concentration of SO_2 and SO_4 from Elevated and Ground Sources," Third Symposium on Atmospheric Turbulence, Diffusion and Air Quality, Raleigh, NC, Amer. Meteor. Soc., 1976.

11. D. S. Renne, W. J. Eadie and D. L. Elliott, "Air Quality Impacts," The Impact of Increased Coal Consumption in the Pacific Northwest. Richland, WA., Pacific Northwest Laboratory, BNWL-RAP-21, 1978.

12. W. F. Sandusky, W. J. Eadie and D. R. Drewes, Long-Range Transport of Sulfur in the Western United States. Richland, WA., Pacific Northwest Laboratory, PNL-RAP-26, 1979.

13. H. Tennekes, "The Atmospheric Boundary Layer," Physics Today, 52-63, 1974.

14. B. Bolin and C. Persson, "Regional Dispersion and Deposition of Atmospheric Pollutants with Particular Application to Sulfur Pollution over Western Europe," Tellus XXVII, 3:281-310, 1975.

15. L. R. Prahm and O. Christensen, "Long-Range Transmission of Pollutants Simulated by the 2-D Pseudospectral Dispersion Model," J.A.M., 16:696-910, 1977.

16. D. J. Carson, "The Development of a Dry Inversion-Capped Convectively Unstable Boundary Layer," Quart. J. G. Met. Soc., 99:450-467, 1973.

17. A. Venkatram and R. Viskanta, Radiative Effects of Pollutants on the Planetary Boundary Layer, Research Triangle Park, NC, Office of Research and Development, U.S. Environmental Protection Agency Report EPA-600/4-76-039, 1976.

18. J. C. Kaimal, J. C. Wyngaard, D. A. Haugen, O. R. Cote, Y. Izumi, S. J. Caughey and C. J. Readings, "Turbulence Structure in Convective Boundary Layer." J. of the Atm. Sci., 33:2152-2169, 1976.

19. H. Rodhe and J. Grandell, "On the Removal Time of Aerosol Particles from the Atmosphere by Precipitation Scavenging" Tellus., 24(5):442-454, 1972.

20. T. Henmi and E. R. Reiter, "Regional Residence Time of Sulfur Dioxide over the Eastern United States," Atmos. Environ., 12:1489-1495, 1978.

21. W. F. Sandusky, W. J. Eadie and D. R. Drewes,"Long-Range Transport of Pollutants in the Pacific Northwest." 25th. Annual Meeting of the Institute of Environmental Sciences, Seattle, WA., April 20-May 3, 1979.

22. W. E. Davis, "Comparison of the Results of an Eight-Layer Regional Model Versus a Single Layer Regional Model for a Short-Term Assessment," World Meteorological Organization Symposium on Long-Range Transport of Pollutants, Sophia, Bulgaria, 1979b.

SPECTRAL TURBULENT DIFFUSIVITY THEORY APPLIED FOR POINT SOURCE DISPERSION

by

Ruwim Berkowicz
Danish Meteorological Institute
100 Lyngbyvej, DK-2100 Copenhagen

Lars P. Prahm
National Agency for Environmental Protection
Air Pollution Laboratory, Risø National Laboratory
DK-4000 Roskilde, Denmark

Abstract. Turbulent diffusion is, in general, a scale-dependent process. Dispersion with a scale-dependent diffusivity can be described by a model based on the Spectral Turbulent Diffusivity (STD) theory. Diffusivity is related to Fourier coefficients of the concentration distribution and is a function of the wave number. The resulting equation is an Eulerian integro-differential equation. The local K-model appears as a special case of the more general STD-theory. The spectral diffusivity coefficients can be expressed in terms of the turbulent energy spectra. The rate of growth of a plume or a puff predicted by the STD-theory is in agreement with prediction from statistical dispersion theories.

Introduction

In spite of more than a 50-year history, the problem of diffusion in a field of turbulent motion still does not have any unique solution. Even in the most simple case of homogeneous and stationary turbulence, the problem is far from a trivial one. Theoretical analyses of the diffusion of material in a turbulent flow have devoloped along two main lines: the statistical theory and the gradient-transfer (K-theory) approach.

The statistical theory, as formulated by Taylor[1], is based on statistical treatment of particle motion in a turbulent flow. It gives answers in terms of standard deviation of particle displacement. Many of the properties of turbulent diffusion can be resolved by this statistical approach; however, difficulties arise when modelling of turbulent dispersion under more general conditions is attempted.

Studies of transport of atmospheric pollutants often require treatment of non-homogeneous and non-stationary flows. Also emission from several sources and physical and chemical transformations must be accounted for. Such problems are difficult or even impossible to model in terms of Taylor's statistical theory, and description based on an Eulerian model is more suitable.

The aim of our research was to formulate a theory of turbulent diffusion for practical applications in air pollution modelling, a theory which reveals the essential features of turbulent diffusion, but which as far as possible preserves the simplicity and flexibility of the K-theory formulation.

In terms of K-theory, the transport of pollutant concentration is given by the continuity equation

$$\frac{\partial c}{\partial t} = -\mathrm{div}(\underline{v}\cdot c) + \mathrm{div}(\overline{K}\cdot \mathrm{grad}\cdot c) + S + Q \ , \tag{1}$$

where $\underline{v}$ is the vector of the mean flow velocity, $\overline{K}$ the eddy diffusivity tensor and S and Q are terms describing sinks and sources, including physical and chemical processes.

The second term on the r.h.s. of (1) describes the turbulent diffusion and results from the so-called gradient-transfer approximation. The gradient-transfer approximation is based on the hypothesis of a turbulent flux proportional to the gradient of the concentration. The earliest attempts to use the gradient-transfer approximation for atmospheric diffusion are due to Schmidt[2] and since then, numerous studies have been undertaken (for a review, see e.g. Pasquill[3]).

Because of its flexibility, the K-theory approach is widely used for modelling atmospheric dispersion. The use of the K-theory, however, is limited by serious restrictions. The theory is based on the analogy of turbulent diffusion to molecular diffusion (Fick's law); this analogy is, in fact, a very poor one. Molecular diffusion is caused by microscale motion. Turbulent diffusion, on the other hand, is produced by eddies of usually a broad range of sizes. If the size of the turbulent eddies responsible for the diffusion is small compared with the length scale of the diffusing distribution, the K-theory approximation is appropriate. In the case of eddy diffusion in the atmospheric boundary layer, horizontal motions with a length scale of 100 m to 1000 m can dominate the diffusion process and use of the K-theory approach for a narrow distribution is not valid.

The Spectral Turbulent Diffusivity Concept

The main problem arising in the modelling of turbulent diffusion is the proper description of scale dependence of the diffusion process. In two recent papers (Berkowicz and Prahm[4] ; Prahm et al.[5]), a new theory has been formulated, the spectral turbulent diffusivity (STD) theory, which makes it possible to apply the diffusivity formulation for turbulent diffusion taking the scale dependence into account, but without losing the Eulerian properties. The theory has been formulated on the basis of a phenomenological understanding of the physics of turbulent diffusion. Derivation of STD-theory from a physical description of the turbulent mixing is presented in Berkowicz and Prahm[6]. Here, only a short resume of the most important findings of the theory will be given. For more details, the reader is referred to the original publications.

Taking only the diffusion term of (1) and considering a one-dimensional and homogeneous case, we have

$$\frac{\partial c}{\partial t} = K\cdot\frac{\partial^2 c}{\partial y^2} \ . \tag{2}$$

The Fourier transform of (2) is

$$\frac{\partial \tilde{c}(k,t)}{\partial t} = -k^2 K \tilde{c}(k,t) \ , \tag{3}$$

where $\tilde{c}(k,t)$ is the amplitude of the Fourier mode with wave number k. The scale dependence of the turbulent diffusivity results from the varying size of eddies which are effective in the diffusion process in relationship to changes in the size of the concentration distribution. Only small eddies are effective for diffusion of a narrow distribution, while larger eddies become active when the distribution becomes broader. The scale of the concentration distribution depends on the relative strength of Fourier modes of different wave numbers. A narrow distribution is characterized by all modes, also those with high wave numbers, while a broad distribution can be described by Fourier modes only with relatively small k-values. In order to account for the scale dependence of the turbulent diffusivity, we have postulated that the eddy diffusivity K in (3) is different for different Fourier modes of the concentration distribution. We have introduced the spectral turbulent diffusivity coefficient K(k). The equation corresponding to (3) is now

$$\frac{\partial \tilde{c}}{\partial t}(k,t) = -k^2 K(k)\tilde{c}(k,t) \ . \tag{4}$$

The STD-coefficient K(k) is a physical parameter as it depends only on the state of the turbulent flow. Eq. (4) can be converted to real space, resulting in an integro-differential equation,

$$\frac{\partial c}{\partial t}(y,t) = \frac{\partial}{\partial y} \int_{-\infty}^{\infty} D(y-y') \frac{\partial c}{\partial y'}(y',t)dy' \ , \tag{5}$$

where the Turbulent Diffusivity Transfer (TDT) function is given by

$$D(y-y') = \frac{1}{2\pi} \int_{-\infty}^{\infty} K(k)\exp(ik(y-y'))dk \ . \tag{6}$$

In contradiction to the gradient-transfer formulation as given by (2), (5) describes a process which is non-local in space. This is a characteristic property of turbulent transport caused by the finite size of the turbulent eddies.

Derivation of the Spectral Turbulent Diffusivity

Derivation of the STD—coefficient is given in detail by Berkowicz and Prahm[6]. The procedure presented there is, to some extent, similar to that applied by Prandtl[7] when he formulated his famous "mixing length" concept. Further development of his procedure, avoiding some essential simplifications, leads directly to the concept of the spectral turbulent diffusivity.

Considering the turbulent mixing as a process arising from a linear superposition of action of eddies of different size, the rate of change of the concentration with time is given by

$$\frac{\partial c}{\partial t} = \int_0^{\infty} \frac{v(\ell)F(\ell)}{\ell} \left[c(y+\ell) - c(y) + c(y-\ell) - c(y)\right] d\ell \ , \tag{7}$$

where $F(\ell)$ is the probability density of occurrence of an eddy of length ℓ and $v(\ell)$ is the characteristic transport velocity of this eddy.

The Fourier transform of (7) is

$$\frac{\partial \tilde{c}(k)}{\partial t} = -k^2 \left[\int_0^{\infty} v(\ell)\ell F(\ell) \frac{\sin^2 \frac{k\ell}{2}}{(\frac{k\ell}{2})^2} d\ell \right] \tilde{c}(k) \ . \tag{8}$$

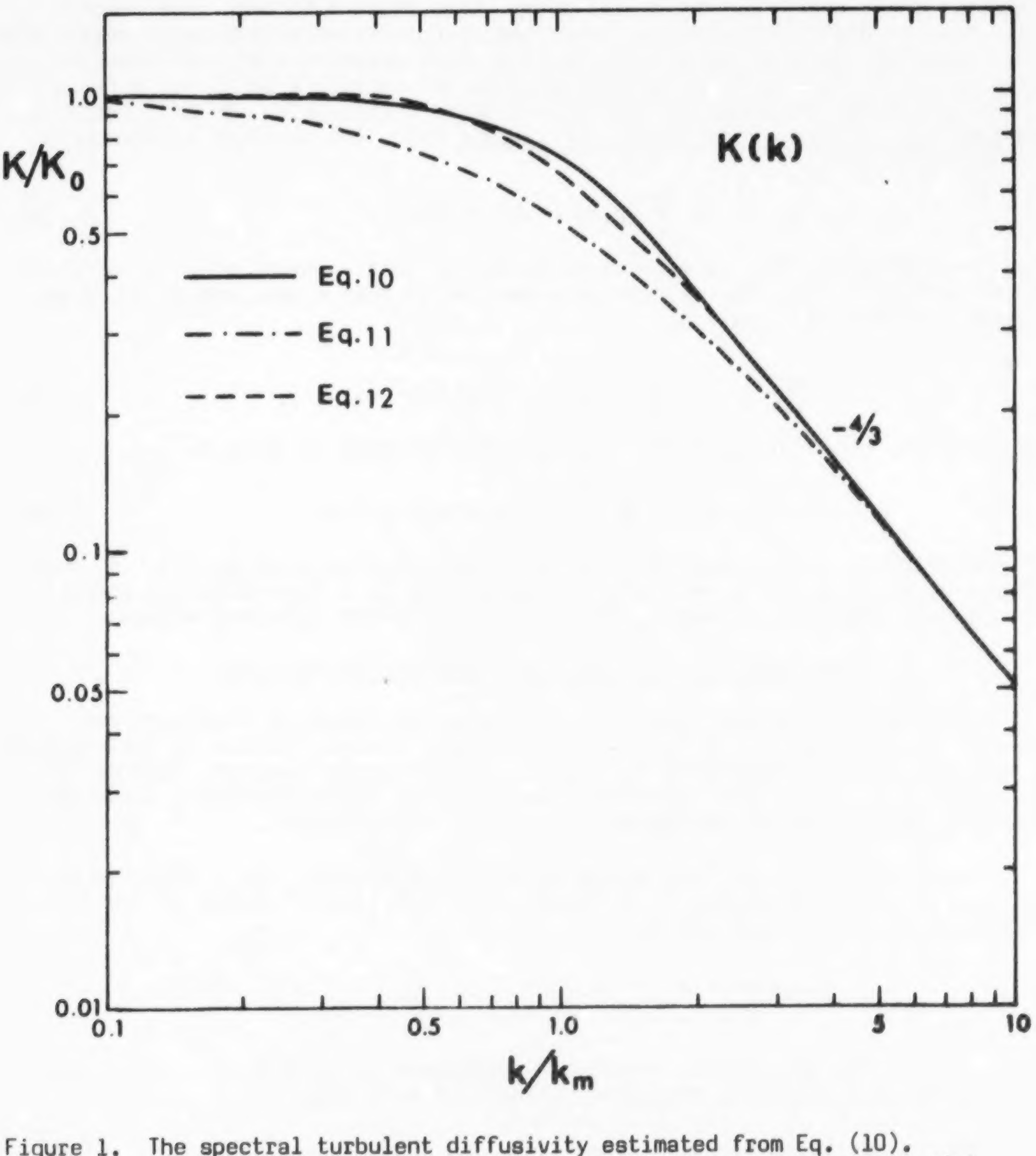

Figure 1. The spectral turbulent diffusivity estimated from Eq. (10). Also curves given by (11) and (12) are presented. Note that K(k) exhibits the shape of $k^{-4/3}$ for large values of k.

One can see that (8) is now identical with (4) if

$$K(k) = \int_0^\infty v(\ell)\ell F(\ell) \left(\frac{\sin\frac{k\ell}{2}}{\frac{k\ell}{2}}\right)^2 d\ell \; . \tag{9}$$

We have evaluated $F(\ell)$ and $v(\ell)$ using the energy spectrum of the inertial subrange and a linear Lagrangian correlation function[6] We obtain the following expression for $K(k)$:

$$K(k) = \frac{2}{3\pi}\,\sigma_v \ell_m^{-1/3} \int_0^{\ell_m} \ell^{1/3} \left(\frac{\sin\frac{k\ell}{2}}{\frac{k\ell}{2}}\right)^2 d\ell \tag{10}$$

where σ_v is the standard deviation of the wind velocity fluctuation and ℓ_m is the length of the largest eddies. $K(k)$ computed from (10) is shown in Fig. 1. Note that in this figure $k_m=\pi/\ell_m$ is the wave number associated with the eddies of the length ℓ_m. The most important feature of the STD-function presented here is that it exhibits a shape of $k^{-4/3}$ for large k-values. It has been shown by Prahm et al.[5] that this form of $K(k)$ gives the correct growth of a puff in accordance with statistical theories.

In Figure 1, two other curves are plotted according to simple formulas which approximate the expression (10). They are:

$$K(k) = \frac{K_0}{1+0.87(k/k_m)^{4/3}} \tag{11}$$

$$K(k) = K_0\left[1-\exp\left[-(k_m/k)^{4/3}/0.87\right]\right] \; . \tag{12}$$

Application for Plume Dispersion

The application of the STD-theory for plume dispersion was treated by Prahm et al.[5]. In order to model a time-averaged concentration in a plume, one has to take into account the "meandering" of the plume due to action of eddies larger than the size of the plume. Such an effect can be ascribed to phase fluctuation of Fourier modes of the transversal cross-section of the plume.

From (4), it is easy to write an expression for a linear plume in the field of homogeneous turbulence if the plume is considered as a superposition of virtual puffs:

$$c(x,y) = \frac{Q}{\pi u}\int_0^\infty \cos(ky)\, \exp\left[-k^2K(k)(x/u)\right] dk \tag{13}$$

where u is the mean wind velocity and Q is the continuous source strength. Meandering of the plume can be accounted for if we introduce the shift of the center line of the plume.

For a meandering plume, we can write

$$c(x,y,t) = \frac{Q}{\pi u}\int_0^\infty \cos\left[k(y-y_0)\right] \exp\left[-k^2K(k)(x/u)\right] dk \tag{14}$$

where $y_o = y_o(x,t)$ is the displacement of the plume axis at the distance x from the source and at a time t. Thus $y_o(x,t)$ fluctuates both in time and space. This results in the broadening of a time-averaged plume cross-section.

Considering again the Fourier components of the plume cross-section, we put forward the hypothesis that y_o is also a function of k. This means that the plume not only is shifted as a whole, but that it is also deformed due to action of eddies of different size. Furthermore, we assume that the standard deviation of the fluctuations of y_o for each Fourier mode of the concentration distribution can be given by

$$\sigma_{y_o}^2(k,t) = 2K_p(k)\cdot t \ . \qquad (15)$$

We have introduced here a spectral phase diffusivity coefficient $K_p(k)$ which governs the time-averaged "diffusion" of phases of Fourier modes of concentration distribution. Note that the puff diffusivity discussed previously governs the decay of amplitudes of the Fourier modes. With the spectral phase diffusivity introduced in (15), a plume can be modelled in a way analogous to puff, i.e. by using the spectral advection-diffusion equation.

We will not discuss here the derivation and the form of $K_p(k)$. For details, the reader is referred to Prahm et al.[5] The asymptotic behavior of $K_p(k)$ is

$$k \to o \ , \quad K_p(k) \to o \qquad (16)$$

$$k \to \infty \ , \quad K_p(k) \sim k^{-1} \ . \qquad (17)$$

It is shown in Prahm et al.[5] that (17) gives the proper, i.e. linear, rate of growth of a plume close to the source.

Diffusion in a Non-homogeneous Turbulent Flow

The STD-theory was derived under assumption of homogenity of the turbulent field. The results, however, can be reformulated in order to account for the non-homogenity[5]. Considering for example vertical diffusion, we can write:

$$\frac{\partial}{\partial t}\tilde{c}(k,t) = -k\int_{-\infty}^{\infty} k'\tilde{K}(k-k',k')\,\tilde{c}(k',t)\,dk' \ . \qquad (18)$$

Here, $\tilde{K}(k-k',k')$ is the Fourier transform of the space dependent spectral diffusivity, i.e.

$$\tilde{K}(\kappa,k) = \frac{1}{\pi}\int_{0}^{\infty} K(z,k)\,e^{-i\kappa z}\,dz \ . \qquad (19)$$

It appears that $K(z,k)$ is in general a complex quantity. However, the imaginary part can be related to a k-dependent vertical velocity. A more detailed presentation of the non-homogeneous case is under preparation. The preliminary results show that some special features, not explainable in terms of the K-theory, can be explained when the spectral formulation is used. The STD-theory is especially relevant for modelling vertical diffusion from elevated sources in the planetary boundery layer. The theory has been applied to model transport of pollutants on a global scale in a two-dimensional meridional troposphere-stratosphere model[6].

References

1. G. I. Taylor (1921), Diffusion by continuous movements. Proc. London Math.Soc., Ser. 2, 20, 196-211.

2. W. Schmidt (1925), Der Massehaustausch in freier Luft und Verwandte Erscheinungen, Probleme der Kosmischen Physic. Hamburg, Verlag Von Henri Grand.

3. F. Pasquill (1974), Atmospheric Diffusion, 2nd ed. Chichester, Ellis Norwood Ltd.; New York, John Wiley and Sons.

4. R. Berkowicz and L. P. Prahm (1979), Generalization of K-theory for turbulent diffusion. Part I. Spectral turbulent diffusivity concept. J.Appl. Meteor., 18, 266-272.

5. L. P. Prahm, R. Berkowicz and O. Christensen (1979), Generalization of K-theory for turbulent diffusion. Part II. Spectral diffusivity model for plume dispersion. J.Appl.Meteor., 18, 273-282.

6. R. Berkowicz and L.P. Prahm (1979), On the spectral turbulent diffusivity theory for homogeneous turbulence. J.Fluid Mech. (to be published).

7. L. Prandtl (1925), Bericht über Untersuchungen zur ausgebildeten Turbulenz. Zs.angew.Math.Mech., 5, 136-139.

8. R. Berkowicz, L.P. Prahm and J.-F. Louis (1979), Global 2-D spectral dispersion model. Proc. WMO Symposium on the Long-Range Transport of Pollutants and its Relation to General Circulation including Stratospheric-Tropospheric Exchange Processes, Sofia, 1-5 October, 1979. WMO Report No. 538.

Discussion:

(Rapporteur: Ch. M. Bhumralkar)

Van den Hout:

Can the author comment whether his spectral turbulent diffusivity theory can be extended to include chemical reactions?

Berkowicz (response):

It is not easy because there are numerical problems. I would not recommend it also because it is time consuming.

Venkatram:

How does -4/3 law apply to large scale?

Jost:

Is it possible to introduce your theory in large scale diffusion?

Berkowicz (response):

The theory can be used for any scale larger than eddy size.

Fiocco:

Is your approach applicable to Boundary Layer Theory?

Berkowicz (response):

No, due to feedback effects.

MODELLING DRIFT OF FOREST PESTICIDE SPRAY USING THE MONTE CARLO METHOD

by

John D. Reid
Boundary Layer Research Division
Atmospheric Environment Service, Canada

Abstract. Pesticide spraying to kill the Spruce Budworm larve has been conducted in New Brunswick forests for more than 25 years. It is now evident that some spray may escape the target and drift considerable distances to other very different environments.

In order to focus research for better understanding, computations were made for a specific spray scenario. For the conditions considered about 0.12% of the original insecticide mass was still airborne 80 km downwind of spraying. The original spray droplet mass weighted spectrum mode diameter of $\sim$104 μm shifted to $\sim$21 μm by 80 km downwind. Results are strongly influenced by the form of the initial droplet spectrum, droplet evaporative behavior and effective source height.

Introduction

Pesticide spraying to reduce the impacts of the Spruce Budworm moth has now been conducted in New Brunswick forests for 25 years. Such spraying is designed to kill the larvae in the immediate spray area. Recently concern has grown that an important fraction of the toxic spray escapes the target forest area and drifts considerable distances to very different environments.

An evaluation of the potential for such long-range drift using a Monte Carlo predictive modelling approach is reported. The technique is that of tracing the trajectories of typical spray droplets under the influence of the different processes acting. The primary objective was to identify areas of poor understanding which cause important errors in assessment.

In order to focus the discussion of this problem a spray scenario was formulated. In the following section the spray scenario is detailed. Then the basis for the representation of each process, and potential errors are discussed. This is followed by a brief consideration of the model computational procedure and detailed discussion of model results and conclusions. This paper considers the airborne insecticide mass budget and evolution of the airborne droplet size spectrum. For a discussion of concentrations of spray interested readers are referred to Reid (1979 a).

The Spray Scenario

For the purposes of this study the influences of topography are neglected. The area is assumed uniformly covered by forest with a tree height of 12 metres.

Aerial spraying takes place by three TBM tankers, each with 600 U.S. gallons capacity. They are assumed to spray in formation back and forth along a 2 mile (3.2 km) line normal to the wind, spraying at 1 U.S. gallon per minute through each of 24 nozzles. Composition of the spray is, by volume: 11% Fenitrothion; 1.5% Dowanol Solvent; 1.5% Atlox Emulsifer; 86% water. The Fenitrothion and Atlox are found not to evaporate perceptably so the vapour pressure for spray evaporation is taken to be that for pure water down to 12.5% of the original volume.

The droplets initially produced are assumed to have a Gamma distribution with mass mean diameter 82 μm. The cumulative number and mass distributions are shown in Figure 1. Density of the Fenitrothion residual is 1.33 g cm^{-3}. The effective spray emission height above tree top level is 6 metres. This accounts for the effects aircraft trailing vortices on the initial spray motion and any bulk sedimentation effects. This simplification for vortex effects is quite severe. For a detailed treatment see Trayford and Welch (1977).

Meteorologically there is assumed to be a neutral stability layer from the surface to 400 metres above ground, where there the layer is capped by an inversion. Winds are assumed from the west, with friction velocity 0.3 m s^{-1}, roughness length 1 metre and displacement height 90% of tree height or 11 metres. This gives a wind speed of 2 m s^{-1} at 10 m above tree-top and ~5 m s^{-1} near inversion base. Ambient relative humidity is 60%.

Finally, and to avoid the problems of dealing with in-canopy transport processes, any droplets which move beneath tree-top level are treated as trapped and not considered further.

Physical Processes

Numerous interacting physical processes pertain to the fate of aerial sprays. Their relative importance depends upon the specific spray in question (e.g. chemical composition, spectrum of drop sizes), and the conditions of spraying (e.g. spray height, meteorological conditions). A good general treatment allowing for all possible processes and interactions is far beyond the bounds of current knowledge. In this model, transport by the mean wind, vertical turbulent motion, sedimentation, evaporation and surface deposition are considered in detail.

Transport by the Mean Wind

Over homogeneous surfaces, such as grass prairie, observations show logarithmic or log-linear wind speed increase with height in the lowest few tens of metres, depending on atmospheric stability, with constant wind direction. According to Mukammal (personal communication) profiles measured over forests do not tend to show such regularity, probably owing to surface inhomogenities. Forest profiles do not appear to have been systematized. This being the case it is reasonable to maintain a rather simple approach and assume a logarithmic wind profile

$$u(z) = \frac{u_*}{k} \ln \left(\frac{z-d}{z_0}\right) \qquad (1)$$

where z_0 is roughness length (1 m), d is displacement height (11 m), u_* is friction velocity (0.3 m s^{-1}) and k is von Karman's constant (0.35).

Above the lowest few tens of metres wind speeds usually continue to increase and direction often varies consistently from that at the surface. Observational data become indispensable where trajectories pass into this region. For this scenario calculation there is probably little better alternative than to assume a continuation of the surface layer profile.

Vertical Turbulent Motion

Particles move vertically owing to the action of vertical turbulent air motion. The trajectory approach to non-buoyant particle dispersion has been investigated by Reid (1978, 1979) using Monte Carlo techniques, the discussion will not be repeated here. The parameters characterizing the turbulent motion are σ_w, the standard deviation of the turbulent vertical velocity, and T_L, the Lagrangian time scale.

In this study σ_w is assumed given by its surface layer value

$$\sigma_w = 1.25\ u_* \tag{2}$$

throughout the sub-inversion layer depth. Deardorff (1972) suggests that σ_w decreases slowly with height in neutral conditions above the surface layer, but the vertical variation is not well established and the assumption of invariance is not unreasonable.

Even less certainty exists about the variation of Lagrangian time scale. Reid (1979) argues for a relationship

$$T_L = 0.4\ \frac{z}{u_*} \tag{3}$$

for the neutral surface layer which gives good agreement between dispersion simulations and observations. Neumann (1978) suggests $T_L \sim 70$s for the neutral boundary layer. In this study Reid's expression is modified to

$$T_L = 0.4\ \frac{(z-d)}{u_*} \exp\left(-\ 3\frac{(z-d)}{h}\right) \tag{4}$$

where h is inversion height and d is incorporated to account for displacement height effects. Thus T_L has a maximum at $\sim$1/3 inversion height giving an asymptotic vertical eddy diffusivity profile, $K_w = \sigma_w{}^2 T_L$, with conventional behavior. For the parameters of this scenario, $u_* = 0.3$ m s^{-1}, h = 400 m, the maximum T_L is $\sim$65s and average $T_L \sim 45$s.

In calculating trajectories for particles with non-zero settling velocities the effect of particles falling through the turbulence field, rather than being completely advected along with it need to be accounted for. Csanady (1963) considered this trajectory crossing effect and showed that it is not important for small settling velocities. Since only small droplets having small terminal velocities are able to remain in the atmosphere to the downwind distances of interest here, this effect is not incorporated in these calculations.

Sedimentation

Gravitational settling of spray droplets is treated as fall at the terminal velocity appropriate to a sphere of the same density. Approximate calculations show that even the slowest responding droplets reach terminal velocity in a fraction of a second. The effects of non-sphericity also seem to be insignificant judging by data of Berry and Pranger (1974). An efficient method for computing terminal velocity which accounts for deviations from Stokes law drag is to calculate the Best number (X), the product of the drag coefficient and Reynolds number squared, which is related to droplet mass (m), air density (ρ_a) and dynamic viscosity (η_d) by

$$X = \frac{8}{\pi} \frac{mg\rho_a}{\eta_d^2} \tag{5}$$

The Best number is a monotonic function of Reynolds number, over the range of concern, and empirically given by a polynomial

$$Re = a_{11}X + a_{12}X^2 + a_{13}X^3 + a_{14}X^4. \tag{6}$$

Following Berry and Pranger (1974) the values

$$\begin{aligned} a_{11} &= 0.412657 \times 10^{-1} \\ a_{12} &= -0.150074 \times 10^{-3} \\ a_{13} &= 0.758804 \times 10^{-6} \\ a_{14} &= -0.168841 \times 10^{-8} \end{aligned} \tag{7}$$

good for the range of Reynolds number encountered, are applied. The terminal velocity is computed from

$$V_T = \frac{\eta_d R_e}{2r\rho_a} . \tag{8}$$

Figure 2 shows terminal velocity as a function of droplet diameter.

With only the water component of the droplets evaporating, the bulk density of a droplet increases as it evaporates. The effect on terminal velocity is shown in Figure 2.

Evaporation

A preliminary calculation for droplet evaporation using the method of Goering et al (1972) at 60% ambient relative humidity determined that droplets evaporated very quickly down to half their original diameter (12½% original volume). For example, an original 128 μm diameter droplet evaporated to 64 μm in ∿12 seconds. Smaller droplets evaporate even more rapidly. By the assumptions of this scenario no evaporation of Fenitrothion residual is allowed. It was decided that for this scenario evaporation could be considered to occur instantaneously after spraying without incurring any appreciable error.

Evaporated water vapour is of no further interest. Figure 3 shows the effect on the mass distribution of spray droplets. The curve labelled "Original Spray" is just the derivative of the curve labelled "Mass" in Figure 1. The mode of this distribution is at ∿104 μm with the ordinate normalized to unity at the mode. The evaporated spray droplet distribution has a mode of ∿52 μm. However, because of the shape of the spectrum and greater density of evaporated droplets there is actually greater mass of droplets smaller than ∿45 μm than originally. In fact, for all droplets smaller than 2 μm diameter the mass has increased from ∿0.007 g to ∿0.067 g, for droplets from 2 to 25 μm diameter the increase is from 10.53 to 40.79 kg, and for 25 to 50 μm diameter droplets the increase is from 242.2 to 354.5 kg. Only for droplets larger than 50 μm does the mass decrease, from 6765. to 737.5 kg.

Deposition

A full treatment of this spray situation would require accounting for flow, dispersion and deposition effects within the forest canopy. Understanding of these processes in the forest is poor and their treatment must be regarded as beyond the scope of this study. As a great simplification the problem is circumvented by specifying that any droplet or vapour molecule which moves below tree-top level is deposited.

Chamberlain (1975) gives a good review of vapour and droplet deposition. Generally large particles and moist particles are efficiently deposited but small particles and vapours are less efficiently deposited. Deposition is greater to moist and sticky surfaces. The perfect deposit efficiency assumed in this study will tend to overestimate deposition of vapour and small droplets, but as these contain only a small proportion of the mass this will not likely constitute a serious error.

One further process which is neglected, but is certainly likely to be significant, is evaporation of deposited insecticide. This will act as a distributed secondary vapour source of low intensity but prolonged duration. Insecticides with long chemical half-lives will be the most important.

Computational Procedures

Separate computations were performed for representative droplet sizes across the spectrum of sizes for evaporated spray at 0 km (Figure 3). In each of these computations droplet trajectories are calculated for small time steps under the influence of vertical turbulent motion, gravitational settling and mean horizontal winds with the assumption that each of these influences remains constant for the course of one time step. Time steps of 20% of the Lagrangian time scale are adopted except near the surface where a lower limit of 1s is established. Numerous tests showed that results were not systematically adversely influenced by the choice of time step here.

In this type of computation it is always necessary to specify the fate of a droplet which encounters an upper or lower boundary. The assumption of complete deposition at tree-top level has already been explained. For the upper boundary, which is an inversion at 400 m in this computation, a perfect reflection condition is assumed. If a particle is above the inversion at the end of a time step it is moved an equal distance below and the sign of its turbulent velocity is reversed.

Computations of fraction of droplets remaining in the atmosphere were made by noting the passage of droplets past each 1/2 km distance from the source. The number of droplets still airborne as a fraction of the total number released is the appropriate fraction for that particular size and distance. Up to 10,000 initial droplets were followed. Surface deposition is found from continuity since the difference in airborne fraction between two downwind distances can only be accounted for by deposition.

Different droplet sizes are examined, for example, 0 μm, 5 μm, 15 μm, 25 μm, 40 μm and 60 μm diameter droplets were taken for one series of computations. The downwind airborne mass fraction computed is plotted against diameter and interpolation used to derive values for intermediate diameters. By weighting with the mass in the original distribution spectrum (after evaporation) and using numerical integration the mass for the whole spectrum of droplet sizes is computed.

Results and Conclusions

Figure 4 shows some results of these calculations in terms of percent of droplets, of various terminal velocities, remaining in the atmosphere for downwind distances to 100 km. Terminal velocities may be related to droplet diameter by referring to Figure 2. Two features of the evolution are of particular note:

(i) The initial deposition is large. Detailed calculations show that ∿82% of residual Fenitrothion mass is deposited within 500 m of spraying. Only about 50% of the smallest droplets are deposited in this target region. Subsiduary calculations show that the effective spray height has a strong influence on target area deposition of small droplets.

(ii) The fraction of droplets deposited declines markedly downwind, particularly for the larger droplets. For example, at 9.5 to 10 km downwind the percent deposition of vapour is ∿10% of its value for the first 500 m, whereas for 10 cm s^{-1} fall velocity it is only ∿0.1%. Altogether only ∿0.1% of the Fenitrothion mass at spraying is deposited between 9.5 and 10 km.

Figure 5 shows the spectrum of airborne droplets at 80 km, produced by applying the percentages at 80 km in Figure 4 to the ordinate values for the evaporated spectrum in Figure 3. Note the expanded ordinate scale in Figure 5. The airborne spectrum mode has shifted to 21 μm with larger droplets having had a preferential tendency for deposition. A little over 1 kg of insecticide residual is in the 2-25 μm class and about 1/3 kg in the 25-50 μm class. This represents about 0.12% of the original insecticide mass.

In considering the implications of the results of this study it is important to appreciate that certain conditions of the scenario may not be necessarily very representative of actual spraying conditions. Best guesses were made for conditions and parameterizations where these are not yet well defined by measurements. As a consequence not too much attention should be paid to absolute values reported. The simulations are much more useful in defining trends and the relative importance of the interacting processes.

The computation results are strongly influenced by the form of the initial droplet spectrum and droplet evaporative behavior. In general, the greater the mass sprayed, or evaporated rapidly into the smallest droplet sizes (and vapour), the greater the long distance drift will be. Current lack of knowledge of the mass distribution within the lowest 30 μm droplet diameter range is a significantly limiting factor for fidelity in simulation. Likewise, effective emission height is important in governing the time available until droplets impact on the surface. Neglect of evaporation from deposited spray is another important limitation of this simulation. A regional survey by Yule et al (1971) showed elevated background phosphorus* levels in the New Brunswick atmosphere during the spray season which suggest the importance of this secondary source.

Of meteorological factors, wind direction is critical where impact at a specific location is of concern. This is particularly so because of its wide diurnal and spatial variations. Finally, stability variations, resulting in turbulence variations, also need to be well defined. Specifically, the assumption of low-level neutral stratification here is not likely very representative of a more typical variation from stable during spraying, through neutral, to unstable later in the morning.

References

Berry, E.X. and M.R. Pranger, "Equations for Calculating the Terminal Velocity of Water Drops," J. Appl. Meteor. 13, 108-113. 1974.

Chamberlin, A.C., "The Movement of Particles in Plant Communities." In Vegetation and the Atmosphere (J.L. Monteith, ed) Vol. 1, 155-203, Academic Press, 1975.

Csanady, G.T., "Turbulent Diffusion of Heavy Particles in the Atmosphere." J. Atmos. Sci., 20, 201-208. 1963.

Deardorff, J.W., "Numerical Investigation of Neutral and Unstable Planetary Boundary Layers". J. Atmos. Sci., 29, 91-115. 1972.

Georing, C.E., L.E. Bode and M.R. Gebhardt, "Mathematical Modelling of Spray, Droplet Deceleration and Evaporation." Trans. of the ASAE, 15, 220-225. 1972.

Neumann, J., "Some Observations on the Simple Exponential Function as a Lagrangian Velocity Correlation Function in Turbulent Diffusion", Atmospheric Environment, 12, 1965-1968. 1978.

---

* Phosphorus is a component of Fenitrothion

Reid, J.D., "Experiments with a Markov Chain Dispersion Model Applied to Vertical Dispersion in the Surface Layer." Proc. NATO/CCMS 9th Intl. Technical Meeting on Air Pollution Modelling and its Application, August 28-31, Toronto, Ontario, 1978.

Reid, J.D., "Markov Chain Simulations of Vertical Dispersion in the Neutral Surface Layer for Surface and Elevated Releases." Boundary Layer Meteor., 16, 3-22. 1979.

Reid, J.D., "Some Computations of Long-Distance Drift of Aerial Sprays." Atmospheric Environment Service Internal Report, ARQL 2/79, 31 pp. 1979 a.

Trayford, R.S. and L.W. Welch, "Aerial Spraying: A Simulation of Factors Influencing the Distribution and Recovery of Liquid Drops." J. Agric. Engng. Res., 22, 183-196. 1977.

Yule, W.N., A.F.W. Cole, I. Hoffman, "A Survey for Atmospheric Contamination following Forest Spraying with Fenitrothion." Bulletin of Environmental Contamination & Toxicology, 6, 289-296. 1971.

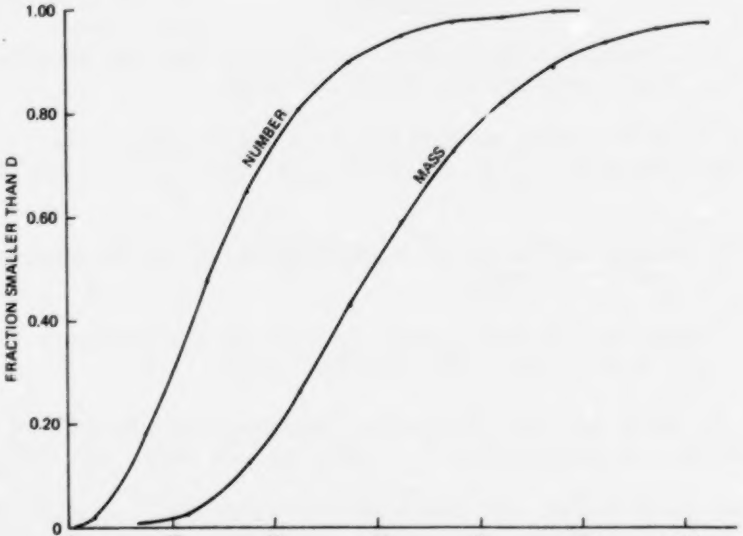

Figure 1: Cumulative Number and Mass Distributions for Initial Spray Droplets

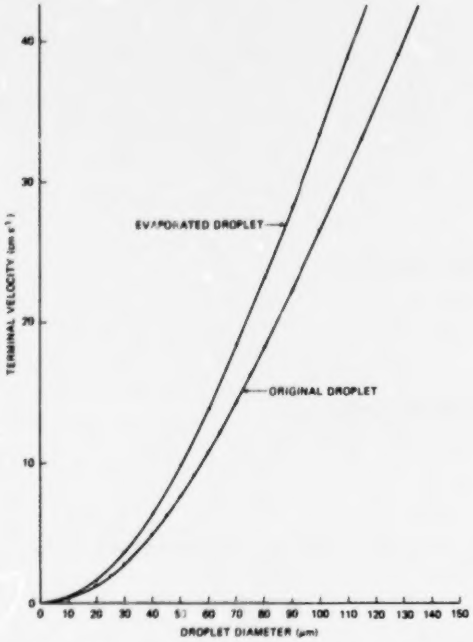

Figure 2: Droplet Terminal Velocities as a Function of Diameter

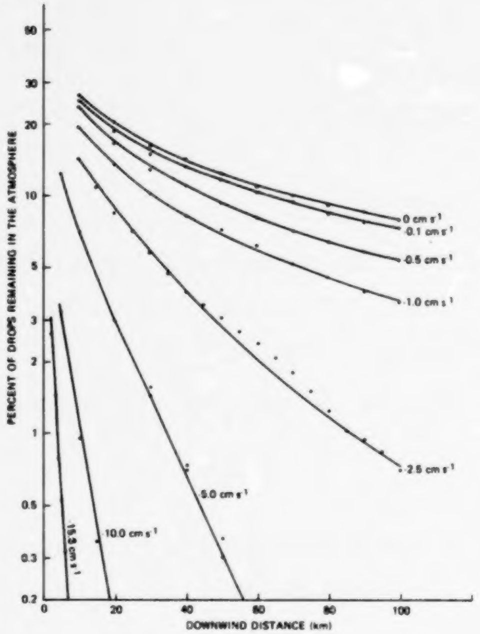

Figure 4: Airborne Residual as a Function of Downwind Distance for Various Droplet Terminal Velocities

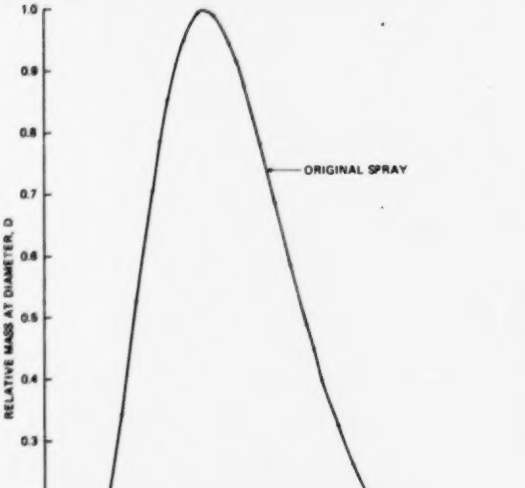

Figure 3: Mass Distribution of Droplets Before and After Evaporation

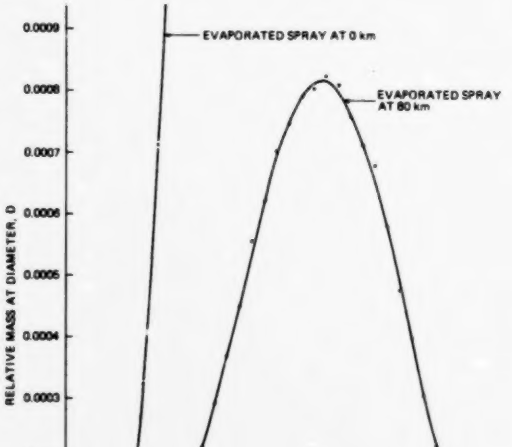

Figure 5: Mass Distributions of Evaporated Droplets at 0 and 80 km

Discussion:

Yamartino:

Have you considered the material in the canopy?

Young (response):

No, it is not taken into account in this model

Smith:

After the pesticide droplets enter the canopy, is it important how they are distributed within the forest?

Young (response):

It is very important, but our objective was to define the behaviour of the droplets in the free air above the canopy and their entry into it.

A STATISTICAL STUDY OF AIR TRAJECTORIES IN CONNEXION WITH THE OBSERVED LEVEL OF MESO-SCALE POLLUTION

A. Berger, G. Deman, Cl. Demuth, P. Hecq
Catholic University of Louvain
Institute of Astronomy and Geophysics
2, Chemin du Cyclotron
B-1348 Louvain-la-Neuve
Belgium

Abstract. The problem which is developped here is related to the study of the origin of the high concentration level of SO_2 observed in a region where no significant source exists in the close vicinity. In order to determine the origin of the observed pollutants, simple trajectory methods have been tested and compared. On the basis of such methods : (1) a meso-scale climatological map of the trajectories ending in Louvain-la-Neuve has been drawn and the importance of the contribution from non local urban and industrial sources to the general pollution level in Louvain-la-Neuve is pointed out and (2) the origin of the pollutants has been located in specific cases of episodes.

Introduction

In air pollution dispersion problems, it happens that the simultaneous occurence of particular meteorological situations, large emissions and specific topography induce high pollution level far away from the source. In situations where the pollutants released in the atmosphere diffuse very slowly over meso-scale distances, analysis of the local conditions is not suffisant and a more general study must be done to detect the direction from which the pollutants have been issued.

The problem developped here is related to the origin of high SO_2-concentration levels observed in a region where no significant sources exist in the immediate vicinity. For this purpose, simple trajectory methods have been developped, tested and compared. A climatology of these trajectories has also been settled. In this paper, one example will illustrate each chapter, all detailed results being available in Berger et al. (1979).[12]

The trajectory methods

Fundamentally, the equation of motion, the equation of continuity, the equation of state, the thermodynamic law and the humidity equation are required to constitue a closed system allowing to determine the wind, temperature, pressure, density and humidity fields. Unfortunately, solutions applicable to the trajectory problems are not easy to obtain.

Approximate trajectories can, however, be obtained from time series of meteorological observations like wind, pressure ..., observed at a discrete limited number of stations.[1,2,3] There are at least three different ways to compute such air trajectories. The first one carries out the trajectory computation involving the estimation of wind from meteorological maps (interpolation method) ; the second is based on radiosonde measurements of pressure, temperature, humidity, horizontal components of the wind and uses entropy, density or pressure as the vertical coordinate ; the last one is entirely based upon numerical integration using the velocity fields obtained from numerical weather models.

In this paper, only methods based on the wind field analysis will be considered. First, it will be shown how a graphical method based on the synoptic wind data allow : (1) to draw rather easily a meso-scale climatological map of trajectories ending in Louvain-la-Neuve (Belgium) and (2) to locate, in specific cases of "episode", the origin of the pollutants.

Next, we shall briefly compare this method to numerical methods based on more accurate techniques of wind field analysis.

The climatology of trajectories in Belgium

1. Selection of the method [4,5]

The objective was to select a method which was rather accurate, not too expensive and which could be applied systematicaly, namely for tracing the origin of episode in an open non-polluted country. It seems, from practical experiences, that the graphical method by Gustafsön is a good compromise between all these requirements.

This method requires first to plot isogones and isotachs from synoptic wind data ; from these charts, stream-lines are then computed and finally, a modified Gustafsön method is used to build up the trajectories. In fact, the Gustafsön method has been prefered because it allows to trace the origin of pollutants detected in a specific area like Louvain-la-Neuve : instead of starting from the emission points, the computation is done backward from the ending point of the air mass trajectories.

Figure 1 illustrates the comparison between three similar methods : Gustafsön, Pettersen, DD-FF (the so called "DD-FF" method is an even more simple method in which wind direction and wind speed are maintained constant during each time step between observations).

2. Numerical computation of trajectories

The method which has been used above is largely subjective. The geostrophic wind has to be assessed from a meteorological map and,namely in light wind conditions, this can be very difficult. Nevertheless, a subjective computation allows personal judgment to be used and can thus takes some account of streamline curvature and time dependence. A numerical method is perhaps less able to represent the effects of frontal system since the discontinuities are often smoothed by the numerical analysis used ; however, the machine-calculated trajectories is less time consuming than a graphical one.

In a first time, we will use an accurate technique of 2-D interpolation of the wind data to provide the wind field over the region concerned.

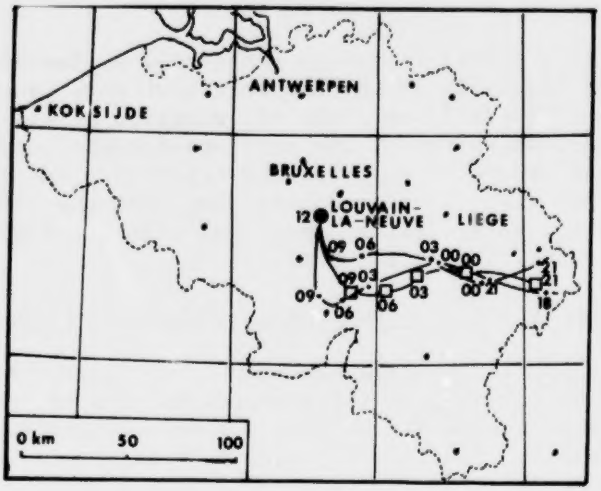
KOKSIJDE
ANTWERPEN
BRUXELLES
LOUVAIN-LA-NEUVE
LIEGE
12
09
06
03
00
21
18
0 km
50
100

Figure 1. Comparison between three methods of trajectory computation. For each method, the positions of air masses at successive time steps have been plotted (the numbers along the trajectories are the hours (UT) considered in the computation). The analysed period starts from November 5, 1974 at 21·00 (UT) till November 6 at noon (UT). (- □ - : Gustafsön, - × - : Pettersen, - · - : DD-FF).

In a second step we will show that an objective analysis of the wind field may be introduced.

a) *interpolation*. Two techniques of interpolation for irregular spaced data have been developped and compared ; one method is based on a double Fourier series analysis [6] and the other uses a technique based on isoparametric meshes [7]. We simply present the results in one case in Fig. 2.

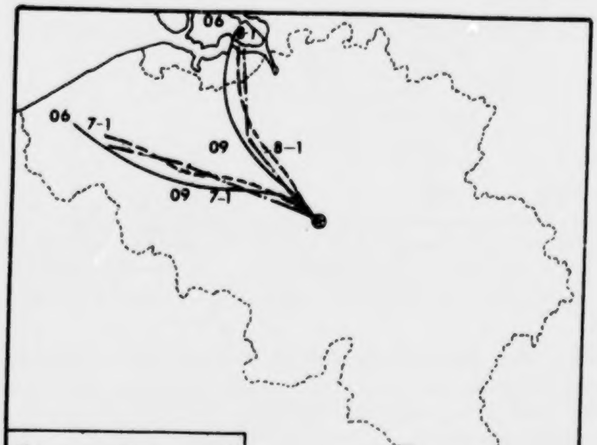
06
06
7-1
09
8-1
09
7-1
0km
50
100

Figure 2. Computed trajectories for January 7 and 8 from interpolated synoptic data. (The starting hour is 06.00 UT or 09.00 UT, the end is at 12.00 UT) (——— : subjective interpolation ; - - - - - - : mathematical interpolation ; - . - . : objective analysis)

b) Objective analysis. This technique introduced by Sasaki (1958-1970) [8,9] and developped specially in the Lawrence Livermore Laboratory by Sherman [10], Dickerson and others [11] uses the minimisation of the difference between computed and observed values of the wind speed components. Fig. 2 shows in the same case as above, the shape of the trajectory deduced from the computed wind field components. These examples show that the differences between the three trajectories are rather small and that the Gustafsön method gives results which are sufficiently accurate.

3. Frequency distribution of trajectories ending in Louvain-la-Neuve

The period under study starts from November 1, 1974, till March 31, 1975, mainly because it is a period during which domestic heating is very intense and the higher levels of pollution are usually observed. Meteorological informations were available every 3 hours at 15 synoptic stations distributed over Belgium.

After having drawn the daily trajectòries for all the period considered, the results have been analysed month by month. Figure 3 is a typical example showing, for January 1975, the localisation, at different times of the day, of all the air masses arriving at 12.00 UT in Louvain-la-Neuve.

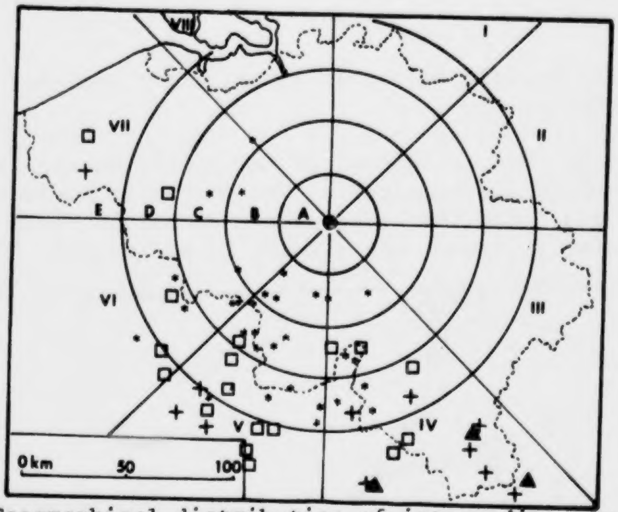

Figure 3. Geographical distribution of intermediate positions at 09.00 UT (*), 06.00 UT (□), 03.00 UT (+), 00.00 UT (▲) of air masses arriving daily in Louvain-la-Neuve (January 1975) at noon.

From such results, the frequency distribution for intermediate positions and origin (*) of the trajectories has been built using distance and direction criteria, the area centered in Louvain-la-Neuve being divided into five concentric rings (radius ranging from 25 up to 125 km) and into eight angular sectors.

(*) origin means the farthest position of the air mass from Louvain-la-Neuve which is still in the frame of the figure at one of the selected synoptic hour.

Figure 4 shows the frequency distribution for all sectors and it is particularly significant to note the differences with the wind rose built over the same period. Although the most frequent wind direction changes from month to month, the S-W sector seems to be generally the most important, except in February where the East direction is the most frequent (this is mainly due to the high pressure system located over Scandinavia and S-E Europa at that time). It must also be pointed out that the direction of the maximum frequencies for wind and trajectories differs by as much as 45°. This expected result, due to the non-stationarity of the wind field in space and time has to be kept in mind before drawing any conclusion in air pollution problem when using only wind data from one single meteorological station.

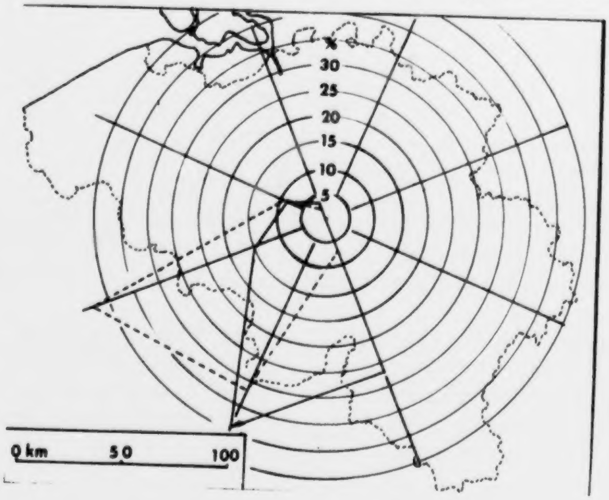

Figure 4. Frequency distribution of origins (January). For each sector, the radius is proportional to the number of case where an intermediate position or an origin of air masses arriving at Louvain-la-Neuve at 12.00 UT was found inside this sector (——— : trajectory, - - - : wind speed).

For practical purpose, it could also be useful to have the mean length of all these trajectories. Figure 5 provides such a result : for each sector, the mean position at 3,6,9 hours, of the air masses ending in Louvain-la-Neuve at noon has been represented.

From the results for the whole period (Fig. 6 and 7), the following conclusions may be drawn :

(1) most of the trajectories have their origin in the SSW direction ;
(2) on the average, trajectories from NE and NNW are shorter : wind is weaker in these directions and higher level of pollution has to be expected ;
(3) when the location of the most important industrial sources and the distribution of the population density are considered (Fig. 8), it appears that the main sources of pollution for Louvain-la-Neuve are in the NW,E and SW sectors.

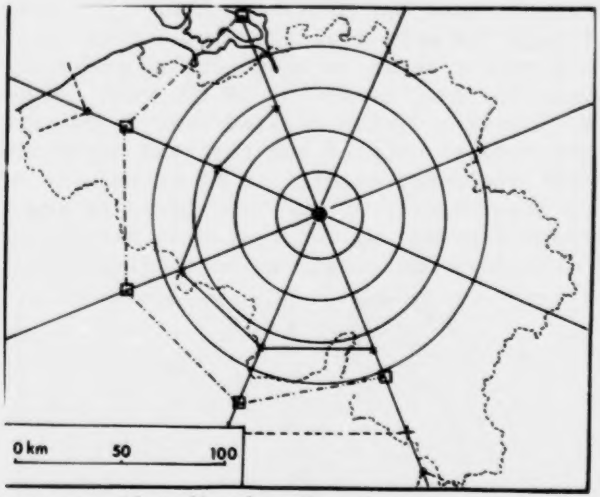

Figure 5. Frequency distribution for January of the "trajectories mean length", respectively at 09.00 UT (*), 06.00 UT (□), 03.00 UT (+), for the air masses arriving in Louvain-la-Neuve at 12.00 UT.

From the trajectories statistics, it is thus possible to conclude, with a reasonable confidence, that non-local urban and industrial area would have a non-negligible potential influence on the pollution background in Louvain-la-Neuve area. This is well confirmed through the study of episodes observed in Louvain-la-Neuve, as presented in the next section.

Specific cases of pollution episode

In this section, two specific cases will be analysed briefly to show how the computation of the trajectories can allow to locate the origin of the pollutants.

The first case concerns January 1975. Fig. 9 shows the evolution of the daily concentration in SO_2[*] and of the mean wind speed recorded in Louvain-la-Neuve. For each period under episode conditions, Fig. 10 and 11 show the computed trajectories :

January 1-6 (Episode) : origin of the trajectories is located in the S-SW sector. The air masses cross over industrial areas and trajectories are rather short (light wind). On the 5th and 6th, the wind speed increases and dispersion becomes to be stronger.

January 7-8 (Episode) : the origin is now W and N-W, but air masses cross now over urban polluted areas ; the wind speed is greater, allowing a more efficient atmospheric dilution.

January 11-14 (no-episode) : trajectories are from S and are rather long (strong wind except on the 13th) ; dispersion is much stronger with a consequently low concentration level.

(*) In our non-polluted area, an episode has been defined when the daily mean concentration is greater than 50 $\mu g/m^3$. This arbitrary level does not bias our conclusions at all.

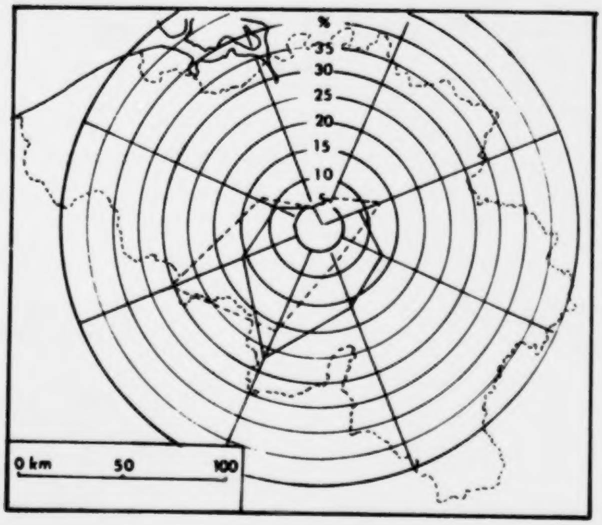
%
35
30
25
20
15
10
5
0 km
50
100

Figure 6. Frequency distribution of origins (same as in Figure 4 but for all the period studied: November 1974 → March 1975).

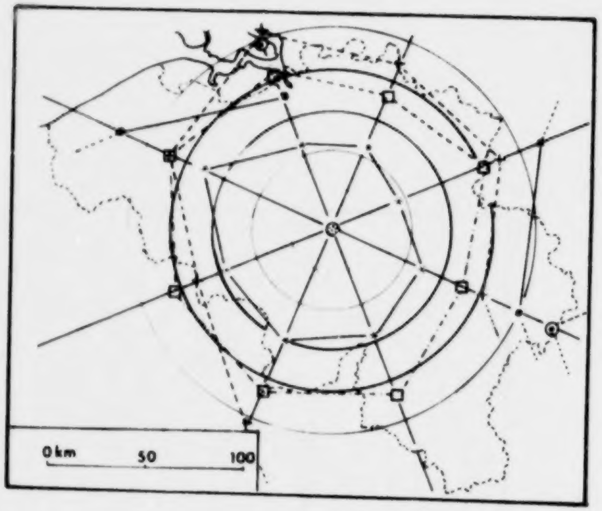

Figure 7. Frequency distribution of "trajectories mean length" (same as in Figure 5 but for all the period). 09.00 UT (※), 06.00 UT (□), 03.00 UT (+) 00.00 UT (.), 21.00 UT (⊙).

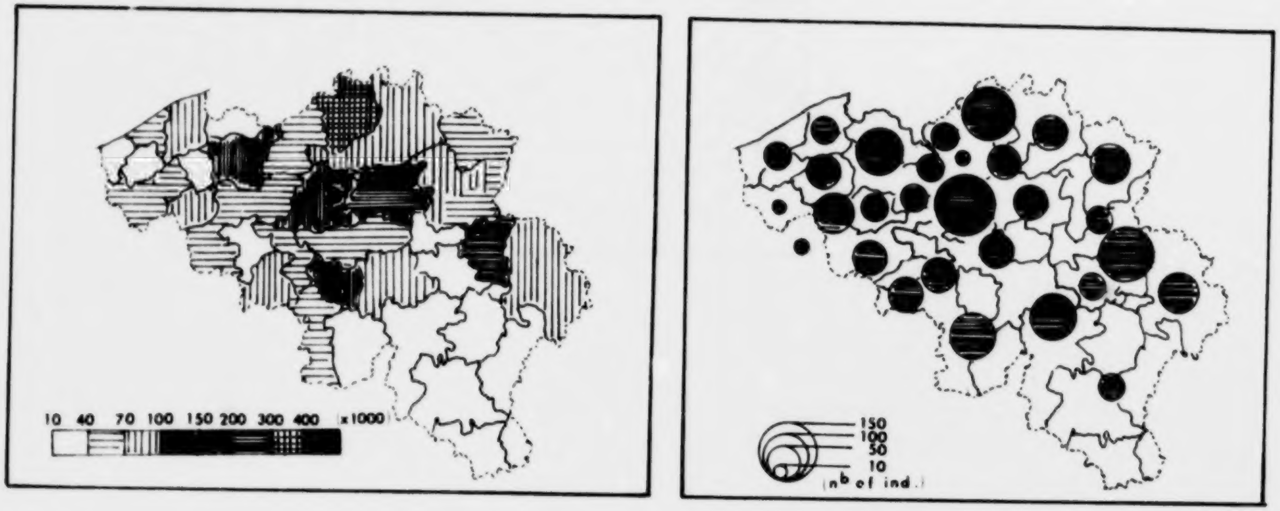
10
40
70
100
150
200
300
400
(x1000)
150
100
50
10
(n° of ind.)

Figure 8. Gross distribution of industrial areas (A) and population density (B).

January 15-18 (no-episode) : the situation is the same as before except for the 18th : this day, the wind speed decreases and the trajectory is more meandering, which may account for the slight increase in the concentration level.

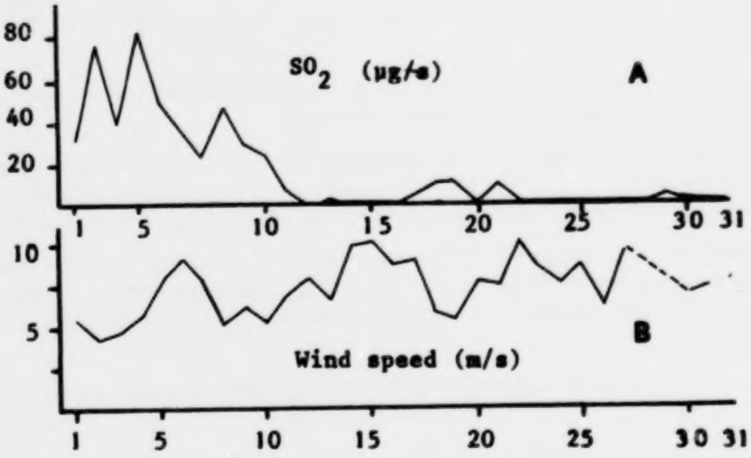

Figure 9. Daily concentration in SO_2 (A) and wind speed (B) for January 1975.

The second case is relative to a period extending from January 27 to the February 5, 1976. During this period, a very important episode of pollution, occurs with concentration of the order of 360 $\mu g/m^3$ and the meteorological situation was caracterised by the existence of a persisting inversion. For each day, the hourly concentration of SO_2 was related to the relevent trajectories and it has been shown that, in the limit of the accuracy of the method, nearly all high concentration levels occured when the trajectories cross over polluted area such as Liège (29 January) and the Ruhr (31 January).

Conclusion

All results presented here show that the trajectory method is an easy and accurate way to explain the general level of pollution at the meso-scale in an open-country free of local pollution sources. No inconsistancy have been found between air masses trajectories and observed levels of pollution.

The analysis of meteorological factors like air stability or inversion even stresses the results obtained from the trajectories alone. To our point of view, this method has to be taken into account in all problems where background pollution has to be determined.

References

1. S. Petterssen, "Weather Analysis and Forecasting", 2 vol., 2nd Ed., Mac Graw-Hill, New York, 1956.

2. E.F. Danielsen, "Trajectories : Isobaric, isentropic and actual", J. Meteorol., vol. 18, p. 479-486, 1961.

3. E.F. Danielsen, "Review of trajectory methods", Advances in Geophysics, vol. 18B, Academic Press, New York, p. 73-94, 1974.

4. D. Djuric, "On the accuracy of air trajectory computation", J. Meteorol., vol. 18, p. 597-605, 1961.

5. C.S. Durst and N.E. Davis, "Accuracy of geostrophic trajectories", Meteorol. Magaz., vol. 86, p. 138-141, 1957.

6. P. Hecq, A. Berger, Cl. Demuth, "Interpolation par un développement en double série de Fourier", Catholic University of Louvain-la-Neuve, Institute of Astronomy and Geophysics, Scientific Report 1978/8.1.

7. P. Hecq, Cl. Demuth, A. Berger, "Une technique d'interpolation basée sur l'emploi de mèches isoparamétriques", Catholic University of Louvain-la-Neuve, Institute of Astronomy and Geophysics, Scientific Report 1979/3. (to be published)

8. Y. Sasaki, "An objective analysis based on the variational method", J. of the Meteorological Society of Japan, vol. 36, 3, p. 77-82, 1958.

9. Y. Sasaki, "Some basic formalism in numerical variational analysis", Monthly Weather Review, vol. 98, 12, p. 875-883, 1970.

10. C. Sherman, "A mass-consistant model for wind fields over complex terrain", Lawrence Livermore Laboratory, University of California, Livermore, California 94550, preprint UCRL, 76171, 1976.

11. M.M. Dickerson, "Mascon. A mass-consistent atmospheric flux model for regions with complex terrain", J. of Applied Meteorology, vol. 17, 3, p. 241-253, 1978.

12. A. Berger, G. Deman, Cl. Demuth, P. Hecq, "Climatology of air trajectories in connexion with meso-scale pollution", Institute of Astronomy and Geophysics, Catholic University of Louvain-la-Neuve. Contribution n° 20.

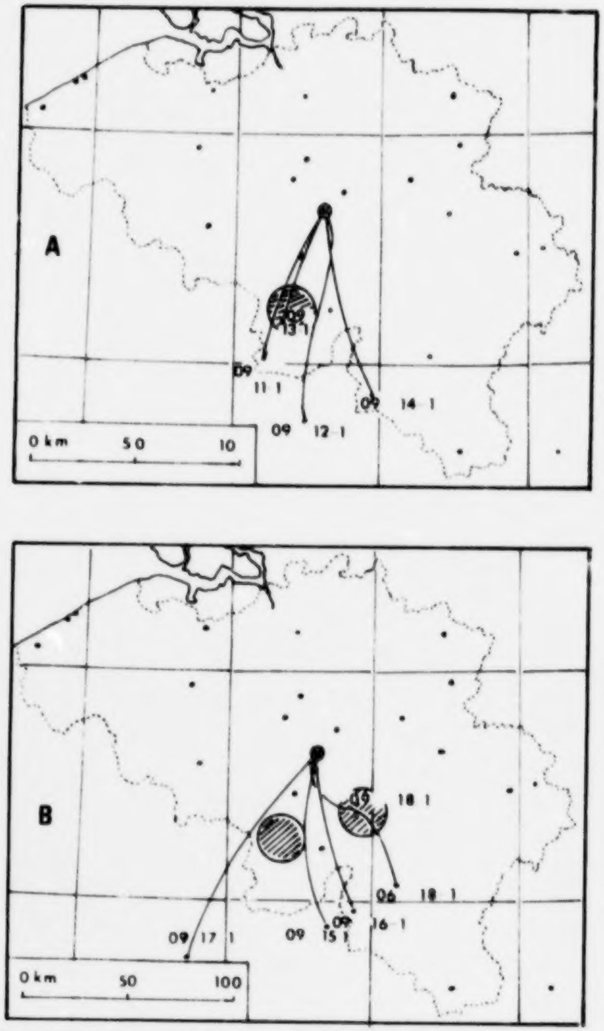
A
09
11 1
09 12 1
09 14 1
0 km 50 10
B
09 17 1
09 15 1
09 16 1
06 18 1
18 1
0 km 50 100

Figure 10. Evolution of trajectories (January 1975). Period: 1-6 January (A), 7-9 January (B).

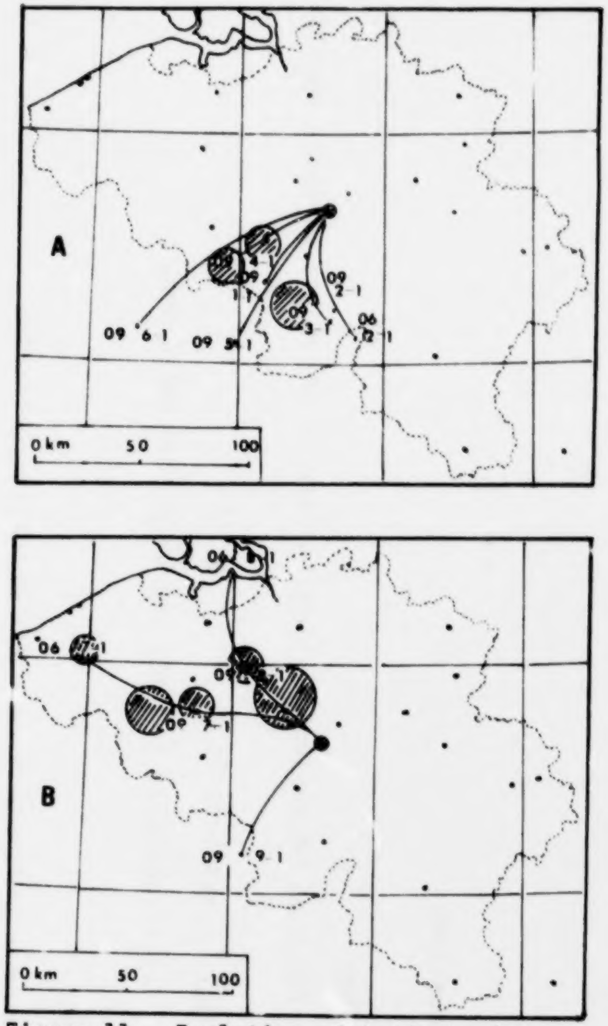
A
09 6 1
09 5 1
09 2 1
09 3 1
06 12 1
0 km 50 100
B
06
09 9 1
09 7 1
0 km 50 100

Figure 11. Evolution of trajectories (January 1975). Period: 11-14 January (A), 15-18 January (B).

Discussion:

Fiocco:

Can the idea of trajectory rose be used to the treat chemical aspects?

Berger (response):

Yes, it is possible to show the origin of emissions.

Saab:

How many points were used for objective analysis?

Berger (response):

50 points.

THE MATHEMATICAL MODELLING OF THE MESO-SCALE AND LONG-RANGE TRANSPORT OF SULPHUR COMPOUNDS.

by

P.R. Maul
Central Electricity Generating Board,
Scientific Services Department,
Ratcliffe-on-Soar,
Nottingham NGII OEE, England.

Abstract. Methods have been developed to describe the atmospheric transport of sulphur compounds based on analytical solutions of the diffusion equation. A steady state model is suitable for the meso-scale transport of pollutant plumes and has been applied to measurements of sulphur dioxide in the East Midlands of England. Calculations suggest that the measurements are consistent with a large scale deposition velocity of 8mm s^{-1} for this gas. For long-range transport a time dependent model is used which follows individual puffs of pollution. Calculations of transport and deposition on chosen days in 1973/4 compare well with daily measurements of sulphur in air and rainwater made in Southern Norway.

Introduction

Figure 1 shows the important physical processes that are involved in the transport of sulphur compounds. The primary pollutant, sulphur dioxide, is transported in the vertical to the surface and the top of the mixing layer by turbulent diffusion and large scale vertical velocities may be important for long travel times. Chemical conversion produces the secondary pollutant, particulate sulphate, and material can be lost by dry deposition to the surface and by precipitation scavenging. The variation in depth of the mixing layer can result in material being isolated from the surface for long periods.

For meso-scale transport (~ 100 km) it is often a good approximation to take the mixing layer to be in a steady state. It is then possible to consider pollutant plumes as described in the first model below. The steady state assumption is clearly not appropriate for long-range transport (~ 1000 km) and it is then necessary to consider instantaneously released puffs of pollution. The time dependent model allows the mixing layer to change in a step-wise manner to simulate its development with time. Concentrations at a receptor point are then calculated by summing over a number of separate puffs.

Both models describe the vertical spreading of material using the diffusion equation. This has the advantage of being able to incorporate the effect of source height and dry deposition at the surface directly. The use of analytical solutions based on Green's functions considerably reduces the computing time required. The applications described in this paper are examples of how the use of these models can help improve one's understanding of the physical processes involved in the transport of sulphur compounds so that a fuller knowledge of the dispersion and ultimate fate of anthropogenic sulphur is possible.

The Steady State Model

Model Description

Figure 2 gives details of the model which is a development of the long-range transport model of Scriven and Fisher[1]. Each source is represented by an effective height of emission h and the pollutant is assumed to disperse in a mixing layer of constant depth a. The steady state two-dimensional diffusion equation is solved in this region with both wind speed and diffusivity profiles decreasing within a surface layer of depth s. The advecting wind is taken in the direction of the x-axis and this will depend upon source-receptor separation[2]. Deposition to the surface is represented by a deposition velocity v_d defined at a height z_d above the surface. Other loss mechanisms can be included by incorporating appropriate sink terms in the diffusion equation.

The concentration of the pollutant at any point (x, y, z) is given by

$$C = \sum_i q_i \ \Gamma_i \ Y_i \tag{1}$$

where the summation is over all sources under consideration and q_i is the source emission rate of source i. The functions Y_i defining the crosswind spread are taken to be Gaussian for point sources. For line sources they can be expressed in terms of error functions. Γ_i is the Green's function for the diffusion equation.

The profiles used for the diffusivity and windspeed are chosen to enable analytic solutions to be employed and to represent the surface layer reasonably accurately. It is important to allow the profiles to reduce towards the surface especially when one is concerned with ground level measurements, but little is gained by incorporating completely general profiles which would necessitate a numerical solution[3].

Application to Measurements of Sulphur Dioxide by a Measuring Network

The network is situated in the rural East Midlands of England and consists of ten measurement sites away from nearby major sources of sulphur dioxide measuring concentrations of the gas continuously[4]. These concentrations have contributions from transport from sources over a wide range of travel distances. This means that interpretation of measured data can only be made satisfactorily using a model of the type described above. The periods for model calculations were restricted to those without significant rainfall, because although the scavenging of sulphur dioxide by rain can be included in the model, periods with rainfall are seldom sufficiently steady for the application of the model to be useful and the amount of precipitation can vary greatly over the region of interest.

The model can only be used when the mixing layer is close to a steady state for the whole period of transport from each source to the measurement site. Two sets of periods were used, in the day and night. The daytime periods were defined between noon and 4 p.m. on days when the wind was 'steady' from 4 a.m..

Similarly, the night-time periods were between midnight and 4 a.m. with a steady wind from 4 p.m. the previous day. These restrictions ensured that for most sources the transport was entirely in the daytime or nocturnal mixing layers. In addition only those wind directions were considered for which transport was primarily meso-scale and not long-range from other European sources.

A detailed source inventory for sulphur dioxide is required by the model and this was drawn up for low level and elevated emissions for the central U.K.[4] Daytime mixing layers were split up into stable, near neutral and convective classes with mixing layer depth and diffusivity profile assigned accordingly. Nocturnal mixing layers were assumed to be stable. From the two-and-a-half years available data only about 10% could be compared with model calculations, but this is not surprising in view of the many restrictions imposed. The comparisons were generally good, with most of the calculations being within a factor of two of the measurements for individual periods, and with average values being within a few $\mu g\ m^{-3}$. Table 1 gives details of the average measurements and calculations for the four classes of mixing layer for two different values of the deposition velocity for sulphur dioxide.

For all the classes the mean difference between calculations and measurements was smaller with $v_d=10\ mm\ s^{-1}$ than $5\ mm\ s^{-1}$. The comparisons clearly suggest that the large scale average deposition velocity lies between the two values and closer to the larger figure. This is consistent with the widely used value of $8\ mm\ s^{-1}$ [5,6].

Table 1. Averaged Comparisons between Measurements and Calculations of the Steady State Model.

Mixing Layer	Number of data points	Measured average concentration ($\mu g\ m^{-3}$)	Calculated average concentrations ($\mu g\ m^{-3}$)	
			$v_d=10mm\ s^{-1}$	$v_d=5mm\ s^{-1}$
Stable	114	41	39	57
Near Neutral	544	31	28	33
Convective	121	30	28	34
Nocturnal	710	27	28	40

The Time Dependent Model

Model Description

For long range transport the assumption of steady state conditions is not valid and one has to consider instantaneously released puffs of pollution rather than continuous plumes. By considering a series of puffs released at different times T one can calculate the resulting concentration at the receptor by summing over all those puffs which pass over it. The concentration of sulphur dioxide at any point (x, y, z) at time t is given by

$$C = \sum_i \int_T q_i \, G_i H_i \qquad (2)$$

As before the summation is over all the sources under consideration, whilst the integration is over all puff release times. In practice the integration is replaced by a summation when puff releases at regular intervals are used and the emission rate q is replaced by the total emission Q during the interval. G is the Green's function for the one-dimensional time dependent diffusion equation and H is the term describing the puff's position and spread in the horizontal plane. There are corresponding equations for the atmospheric concentration of particulate sulphate and the wet deposition of sulphur at the receptor.

Figure 3 illustrates how the model approximates the time dependence of the transport processes. The equation for G which governs the vertical diffusion and removal of sulphur dioxide is solved in a step-wise manner with the pollutant profile at the end of one step being the initial profile for the next. The figure illustrates the mass balance that is carried out for each time step. The flux of material entering the mixing layer from the previous mixing layer (F_1) together with the material entrained from above it (E) equals the flux of material entering the next layer (F_2) combined with the material lost to dry deposition (D), precipitation scavening (W), chemical conversion (S) and material lost from the top of the mixing layer (L). A similar mass balance is undertaken for particulate sulphate.

Surface pressure measurements are used to enable the trajectory of the centre of mass of the puff to be calculated[7]. The development of the mixing layer along the trajectory is determined by windspeed, incoming solar radiation, surface roughness and other external factors.

Example of Model Calculations

The easiest way to understand the methods used by the model is to look at an example calculation for a single puff. Figure 4 shows three synoptic charts at twelve hour intervals between noon on the 11th and noon on the 12th of January 1974. On the first chart there is an occluded front passing over Europe with a region of slack pressure gradient behind it over the North Sea. A depression crosses the U.K. and Scandinavia on the following day. Figure 5 shows the calculated trajectory of the centre of mass of a puff released from (1^{0}W, 52^{0}N) at noon on the 11th with the times shown being measured from the beginning of that day. The puff travels eastwards for about twelve hours behind the occluded front until early on the 12th when it begins to move northwards ahead of the approaching warm front. Figure 6 gives details of the calculated development of the puff in the vertical plane. The puff is released in a strong wind deep mechanical mixing layer, but the wind speed gradually drops as the puff enters the region of slack pressure gradients with diverging air. Early on the 12th the wind speed begins to increase again as the warm front approaches and the puff experiences the large scale vertical motion associated with the frontal region. From about 19h on the 12th rain fell as the puff travelled across Sweden.

Table 2 illustrates the mass balance procedure for the puff just before and just after the rainfall at the end of the trajectory in terms of fractions of the emitted sulphur. The model parameters used in this example to describe the transformation and removal of the pollutants were as follows; the transformation rate of sulphur dioxide to sulphate away from the source was $3X10^{-6}\ s^{-1}$, the scavenging coefficients for sulphur dioxide and sulphate were $3X10^{-5}\ R\ s^{-1}$ where R is the rainfall rate in mm h^{-1}, the deposition velocity for sulphur dioxide was 8 mm s^{-1}, and 5% of the emitted sulphur dioxide was assumed to be converted to sulphate in the immediate vicinity of the source.

Table 2. Mass Balances for the Example Model Calculation.

Time	SO_2 in mixing layer (F)	SO_2 above mixing layer (L)	Loss to dry deposition (D)	Sulphate (S)	Loss to wet deposition (W)
41h	16%	19%	41%	24%	0%
47h	16%	3%	43%	16%	22%

Application to O.E.C.D. Measurements in South Norway

Several periods have been chosen between August 1973 and February 1974 to investigate in detail examples of the long-range transport of sulphur compounds from north-west Europe to South Norway. Model calculations have been compared with daily measurements of atmospheric sulphur dioxide and sulphate and sulphur in rainwater made at ten O.E.C.D. measurement sites[5]. A data base of surface pressure and other meteorological measurements was used for trajectory analysis calculations, the description of mixing layer development and the estimation of rainfall[8]. The source inventory that was employed is based on that drawn up by the O.E.C.D.[9]. So far nineteen days have been studied and comparisons between measurements and calculations are good. Table 3 summarises these comparisons for the same set of model parameters used in the example calculation above.

Table 3. Averaged Comparisons between Measurements and Calculations of the Time Dependent Model.

	Rainfall (mm)	Wet Deposition (mg SO_4 m^{-2})	Conc. S in rainwater (mg SO_4 l^{-1})	Sulphate in air ($\mu g\ m^{-3}$)	SO_2 in air ($\mu g\ m^{-3}$)
Measured Average	15	26	1.8	3.9	6.4
Calculated Average	12	22	1.9	4.0	4.1

It should be emphasised that these days do not represent a typical average picture as they were specially selected. The method used to estimate rainfall from routine meteorological measurements results in a slight underestimation on average and this produces a similar small underestimation of wet deposited sulphur. The measured and calculated weighted mean concentrations of sulphur in rainwater are, however, very close as are the measured and calculated values of sulphate in air. This is not the case for the sulphur dioxide concentrations, however, where examination of the measurements suggests the influence of local sources on several days.

It is not possible to describe in detail the model comparisons, but some of the main conclusions to be drawn can be summarised. The time dependent model appears to compare better with individual daily measurements than constant mixing layer models, but long term averages are not very different. In addition, wet deposition calculations in particular are not very sensitive to the choice of model parameters. This gives added confidence to the long term average calculations of deposition in Europe by other authors [5,10].

Acknowledgments

The author wishes to acknowledge valuable discussions with Dr. H.M. ApSimon of the Environmental Safety Group of the Mechanical Engineering Department, Imperial College, London and to express his appreciation for access to the data base held by that group which was used in the time dependent model calculations. This work is published with the permission of the Central Electricity Generating Board.

References

1. R.A. Scriven and B.E.A. Fisher, "The Long Range Transport of Air-Borne Material and its Removal by Deposition and Washout, II The Effect of Turbulent Diffusion", Atmos. Env. 9, 56-68, 1975.

2. P.R. Maul, "The Effect of the Turning of the Wind Vector with Height on the Ground Level Trajectory of a Diffusing Cloud", Atmos. Env. 12, 1045-50, 1978.

3. P.R. Maul, "The Mathematical Modelling of the Meso-Scale Transport of Gaseous Pollutants", Atmos. Env. 11, 1191-95, 1977

4. P.R. Maul, F.R. Barber and A. Martin, "Some Observations of the Meso-Scale Transport of Sulphur Compounds", Atmos. Env. (In press).

5. O.E.C.D., "The Long Range Transport of Air Pollutants, Final Report", 1977

6. F.B. Smith and R.D..Hunt, "The Dispersion of Sulphur Pollutants over Western Europe", Phil. Trans. R. Soc. Lond. A 290, 523-542, 1979.

7. P.R. Maul, "Trajectory Analysis and Associated Techniques for Use in Conjunction with Models for the Long Range Transport of Atmospheric Pollutants", C.E.G.B. Internal Report SSD/MID/N63/78, 1978

8. H.M. ApSimon, D. Earnshaw, A.J.H. Goddard and J. Wrigley, "Atmospheric Transport of Radioisotopes and the Assessment of Population Doses on a European Scale", Progress Report, Imperial College, London, June 1978.

9. O.E.C.D., "The LRTAP Emission Survey", LRTAP 2/74, 1974.

10. B.E.A. Fisher, "The Calculation of the Long Term Sulphur Deposition in Europe", Atmos. Env. 12, 489-501, 1978.

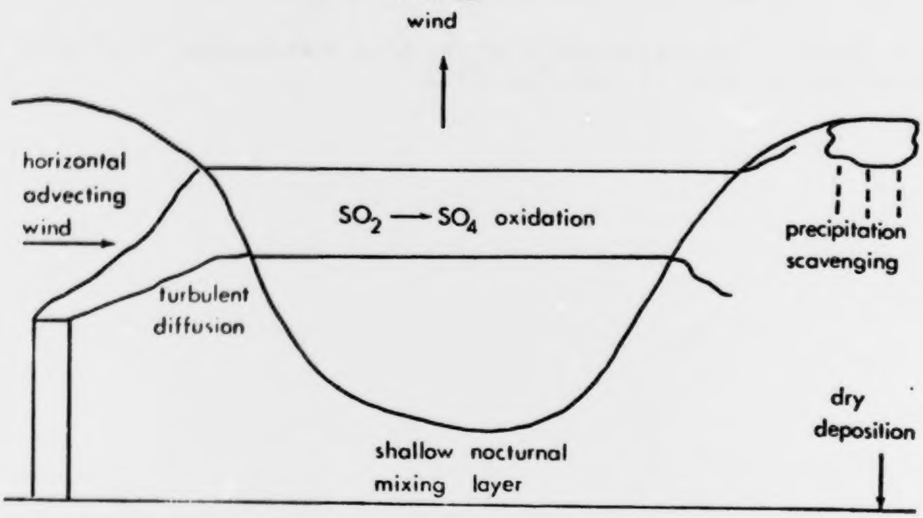
vertical
wind
horizontal
advecting
wind
$SO_2 \rightarrow SO_4$ oxidation
precipitation
scavenging
turbulent
diffusion
dry
deposition
shallow nocturnal
mixing layer

Figure 1. Important processes in the transport of sulphur compounds.

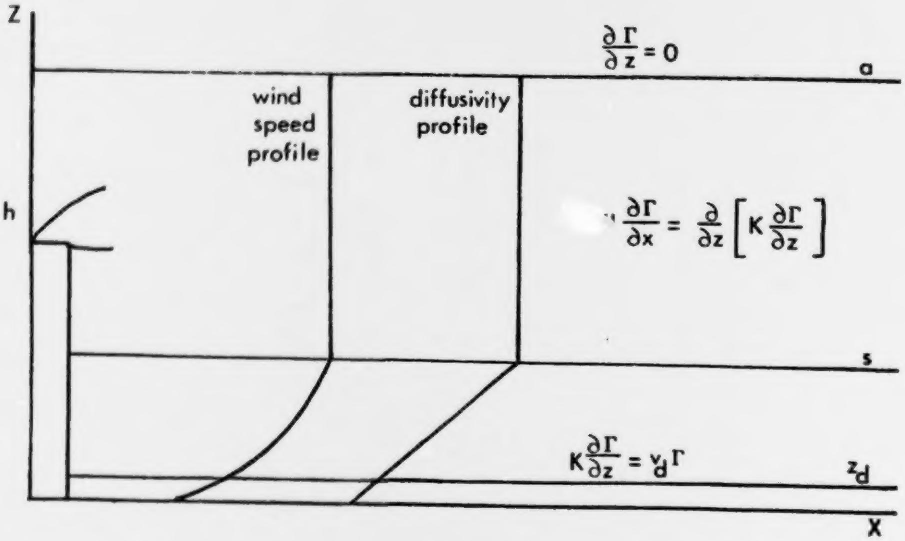
Z
$\frac{\partial \Gamma}{\partial z} = 0$
a
wind
speed
profile
diffusivity
profile
h
$\frac{\partial \Gamma}{\partial x} = \frac{\partial}{\partial z}\left[K \frac{\partial \Gamma}{\partial z}\right]$
s
$K\frac{\partial \Gamma}{\partial z} = v_d \Gamma$
z_d
X

Figure 2. Details of the steady state model.

$$F_1 + E = F_2 + L + D + W + S$$

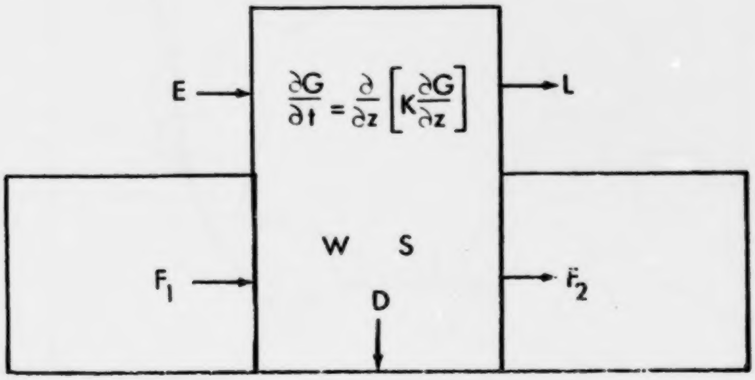
E
$\frac{\partial G}{\partial t} = \frac{\partial}{\partial z}\left[K\frac{\partial G}{\partial z}\right]$
L
W S
F_1
D
F_2

Figure 3. The step-wise mass balance procedure.

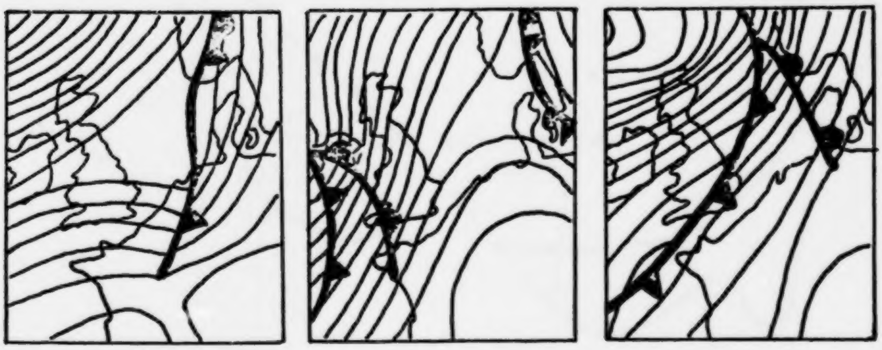

12.00 11th 0.00 12th 12.00 12th

Figure 4. Three synoptic charts in January 1974.

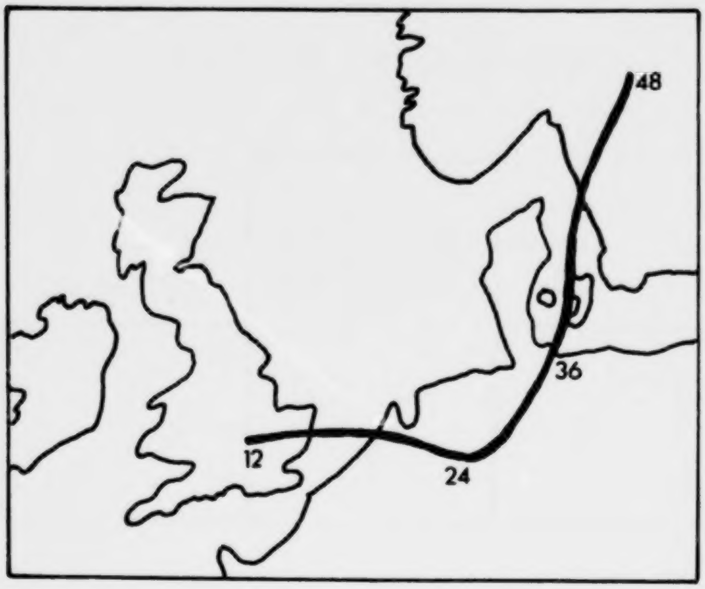

Figure 5. The trajectory for the example puff calculations.

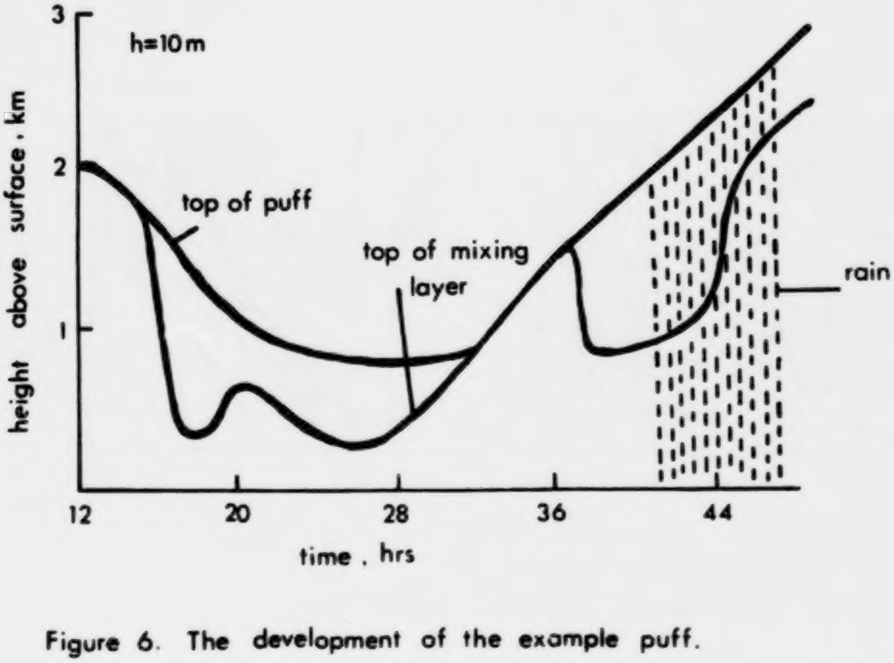

Figure 6. The development of the example puff.

Discussion:

Kretzschmar:

I did not quite understand how numerical values are linked to the trajectory. How many days'data has been used for averaging?

Maul (response):

Average is based on data for 19 specific days for which data base is available.

Prahm:

How sensitive is the model to the diffusive properties of your method?

Maul (response):

Not very dependent. There is zero diffusivity above mixing layer and constant diffusivity below it. Model is arranged such that material is left above the mixed layer.

Hübschmann:

Is there a discrepancy between calculated and measured rainfall?

Maul (response):

Yes, due to the method of calculating rainfall from measured 3-hourly data.

Nieuwstadt:

How do you determine height of mixing layer for night?

Maul (response):

It is quite complicated. For day time I use the 'Carson' method.

Van den Hout:

How does mixing height rise rapidly?

Maul (response):

Due to increased wind speed.

MODELLING INTERREGIONAL TRANSPORT OF SO_2

by

Klaus Herrmann
BASF - Aktiengesellschaft
Ludwigshafen, FRG

Abstract. A three dimensional time dependent transport and diffusion model is used to simulate SO_2 transport over distances up to 200 km. Various sensitivity analyses and comparisons between calculated and measured ground level concentrations allow to describe the effects, which are important for mesoscale diffusion.

Introduction

Between 1974 and 1977 a Dutch-German project was carried out to study interregional transport in the atmosphere, which means transport over distances up to 200 km.[1] One part of this project consisted in setting up and applying a transport and diffusion model based on the extensive data basis measured and evaluated by seven various working groups; figure 1 shows the region, in which SO_2 concentrations as well as meteorological parameters were measured. The main sources are located in the south-eastern part, the so called Rhein-Ruhr area; for this industrial region an emission inventory is available. So we were especially interested in weather situations connected with winds from south-east leading to a transport of air pollutants from the main source region into the so far little affected agricultural region of East- and North-East-Netherland.

45 ground level SO_2-stations and 17 ground level wind stations allowed us to define so called episodes, meaning weather situations under which interregional transport occured, and to initiate more detailed measurements, as for example profile measurements of temperature and wind or SO_2 aircraft samplings. Eight episodes were observed alltogether between 1974 and 1977 and these observations spent the data basis for the application of the model.

Application of the Model

We used a three dimensional time dependent box model taking into account advection and diffusion along the three Cartesian coordinate directions, limited vertical mixing, and either chemical decay of SO_2 or deposition at the surface[2]. Along the horizontal axes the model region was subdivided into 10 by 10 km^2-grids, while along the vertical the grid distance ranged from 20 m near the surface up to 100 m near the top of the mixing layer. The latter is given by the observed height of the inversion, which was found between 500 and 800 m during all episodes.

The continuously measured data and the emission rates were given as hourly mean values and so the model calculations had to go forward in time hour by hour (see figure 2). The concentrations at time Zero were chosen as Zero in the whole area. Each one hour step is subdivided into several numerical time steps, the length of which varies between 1 and 15 minutes depending on the actual set of transport parameters. After having finished the calculations for one hour the model input parameters and following from this the numerical time step have to be changed.

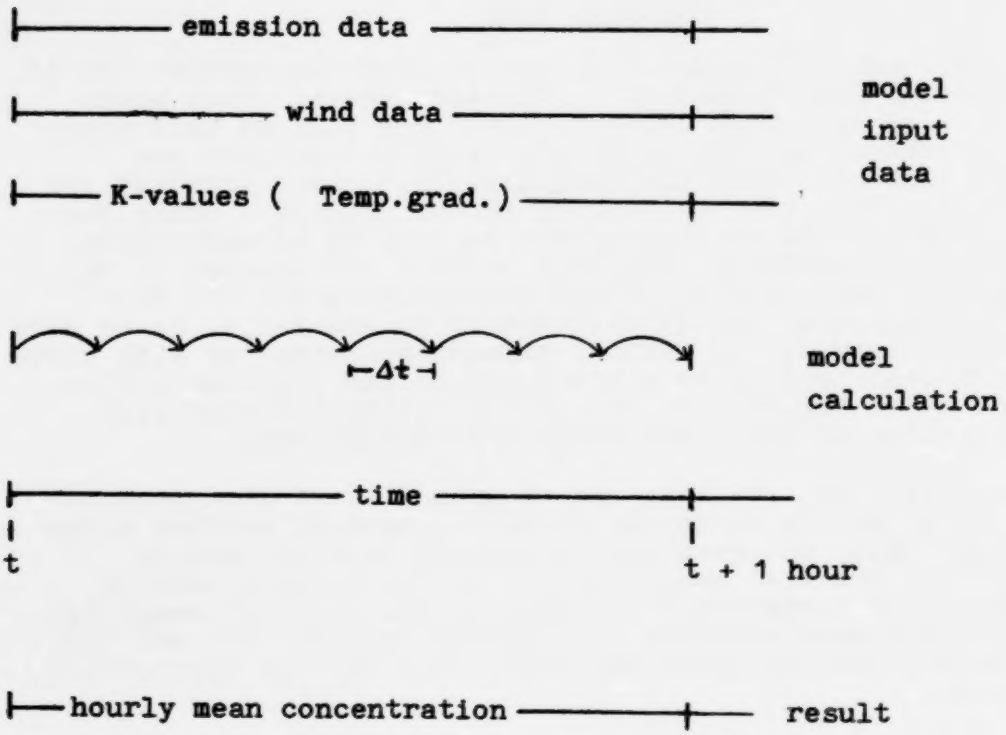
emission data
wind data
K-values (Temp.grad.)
model input data
Δt
model calculation
time
t
t + 1 hour
hourly mean concentration
result

Figure 2: Time scheme for the model calculations.

The model input data were determined as follows:

1. The emission inventory allows the simulation of the hourly, daily, and monthly variations of the emission rate of each source. So for each hour the actual source distribution has to be calculated.
2. The wind speed components near the ground were determined by using an interpolation scheme, which takes into account the three measurements located nearest to the grid point of interest. At higher levels only the data from a 200 m meteorological tower and from hourly pilote balloon soundings carried out near the Dutch German border were available (see figure 1). Therefore for heights above 200 m a constant wind speed and direction had to be used, while for heights between 20 m and 200 m the model wind continuously turns from the ground level value into the 200 m value.
3. The thermal stratification - determined as temperature gradients from the temperature data of the balloon soundings and the tower measurements - varies arbitrarily with time and height; an example is given in figure 3. These complicated conditions cannot be described in the model by a mean value of the stratification, as we learned from a greater number of sensitivity analyses. Therefore we used K-values in the model, which were calculated for each grid level as a function of the temperature gradient at the corresponding height (see figure 4). The two parameters were connected by combining a measured frequency distribution of temperature gradients and stability classes and the well known σ-values of the Gaussian plume formula. Doing so we were able to model the variation of the stratification with time and height, which is one of the most important effects observed during the transport episodes.

About that there is no need for changing the vertical spacing of the grid system to fulfill the upper boundary condition if the inversion height has changed. A strongly stable stratification implies very small K-values and following from this a neglectable turbulent flux across the upper boundary.

Results of the observations and modeling calculations

The most important results of the observations and a greater number of modelling calculations can be summarized as follows:

1. Relatively high concentrations in greater source distances only occure as long as the depth of the mixing layer is limited to a few hundred meters by a marked inversion.

2. Diffusion along both horizontal axes gives an unimportant contribution to the transport and can therefore be neglected.

3. The ground level concentration field is rather sensitive to the fixing of the height of the area sources including the domestic heating and other small sources, which cannot be treated individually in the model and in the emission inventory. Nearly the whole region is covered by such area sources; they contribute to the ground level concentration at a rate of about 20 - 60 %, while their emission only reaches 5 - 20 % of the total. The height of the area sources is not given in the inventory and so we used a mean value of at last 10 m.

4. The source heights of the great point sources and the intensity of vertical mixing determine the mean concentration level in the whole field, but not the position and strength of the ground level maximum. The latter is more influenced by the magnitude of the deposition velocity - as long as the sink of SO_2 is treated as deposition - and the variation of the stratification with time.

5. The sinks of SO_2 were simulated either by a chemical decay rate or a deposition velocity, both determined from mass balance measurements. Satisfying results of the model calculations could only be reached by simulating deposition at the surface with deposition velocities between 1 and 2 cm/s. These values agree with the measured ones.

There is no need to take into account rain out, because all observed transport episodes occured under weather counditions without any precipitation. Meanwhile a new project has been set up to study also the effects of rain out and wash out as a part of interregional transport of SO_2.

References

1. W. Klug, T. Schneider e.al.,"Interregional Transport of Air Pollutants, Results of he Final Scientific Session." Edited by Umweltbundesamt, Berlin, 1978.

2. K. Herrmann, "Zur Simulation Interregionaler Transportvorgänge in der Atmosphäre." Dissertation an der Techn. Hochschule, Darmstadt, 1978.

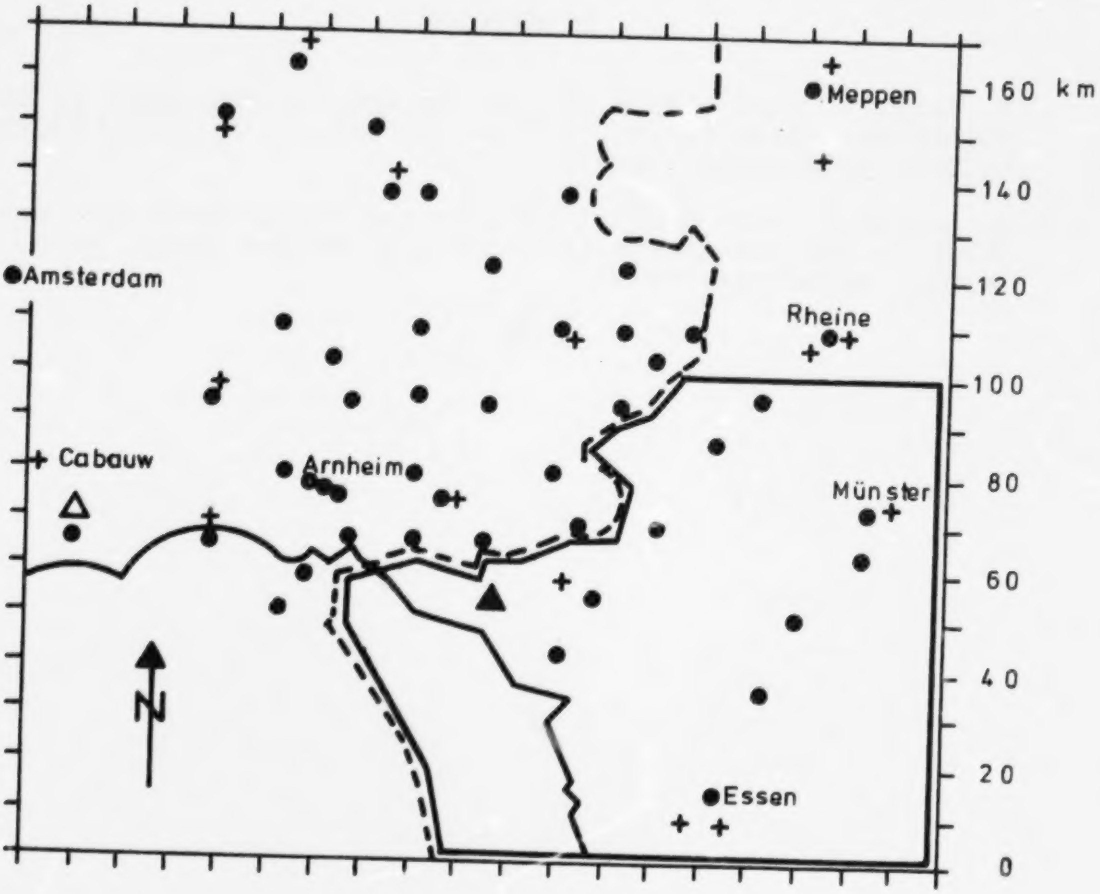
Meppen
Amsterdam
Rheine
Cabauw
Arnheim
Münster
Essen
N
160 km
140
120
100
80
60
40
20
0

Figure 1. Region of North-West Germany and East-Netherland, where the measurements were carried out.

--- Dutch-German border

___ Rhein

● SO_2 ground level measurements

+ ground level measurements of wind speed and direction

Δ 200 m meteorological tower

▲ Pilot ballon soundings (hourly)

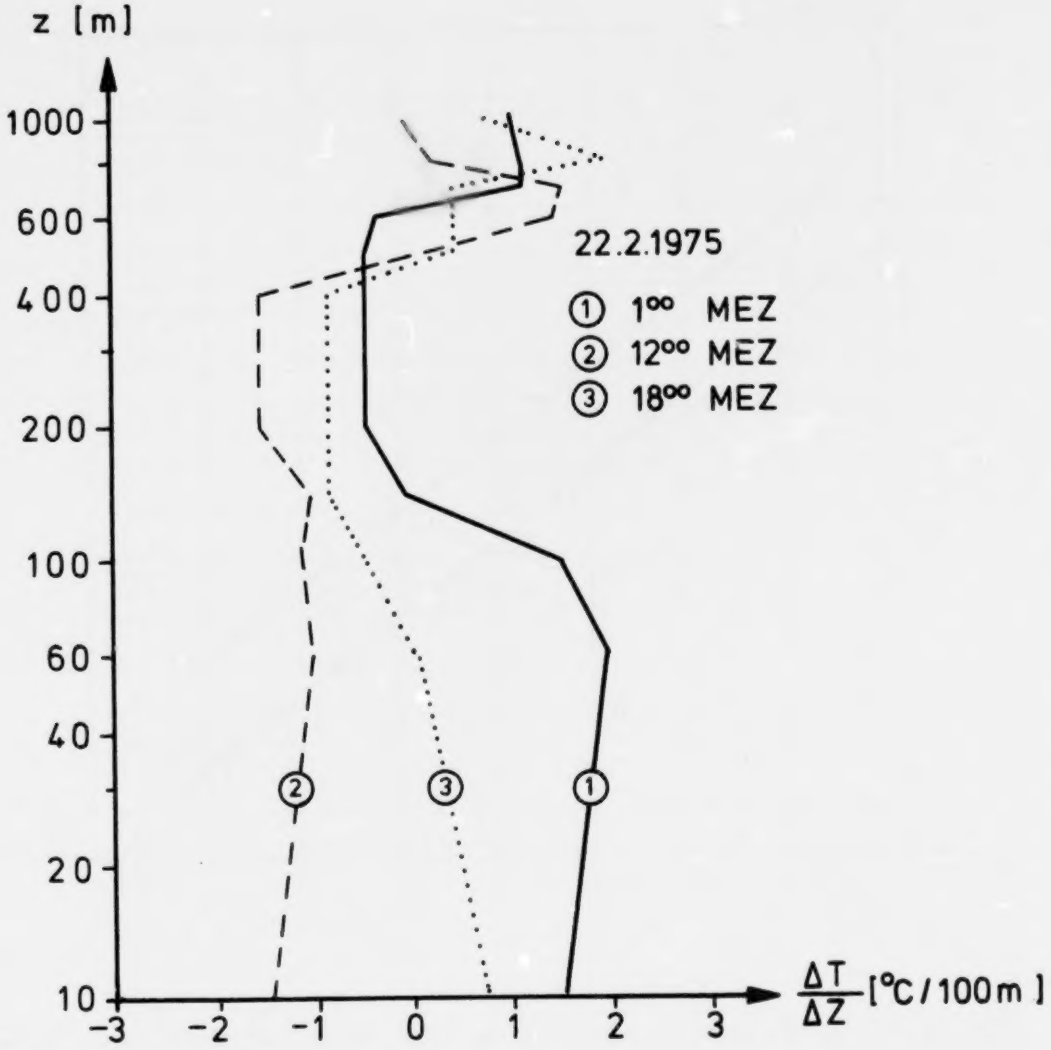

Figure 3. Temperature gradients as a function of height measured during an observed transport episode.

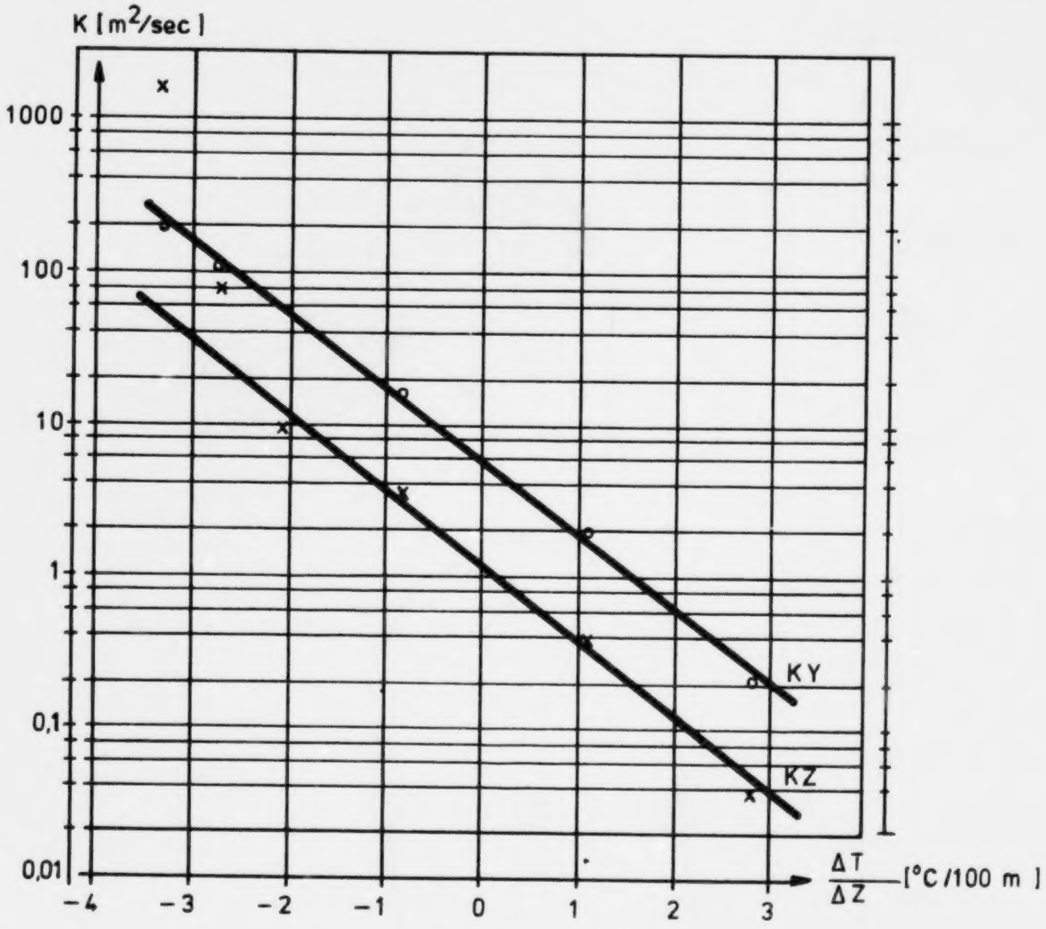

Figure 4. Diffusion coefficients for vertical (KZ) and lateral (KY) diffusion as a function of the temperature gradient

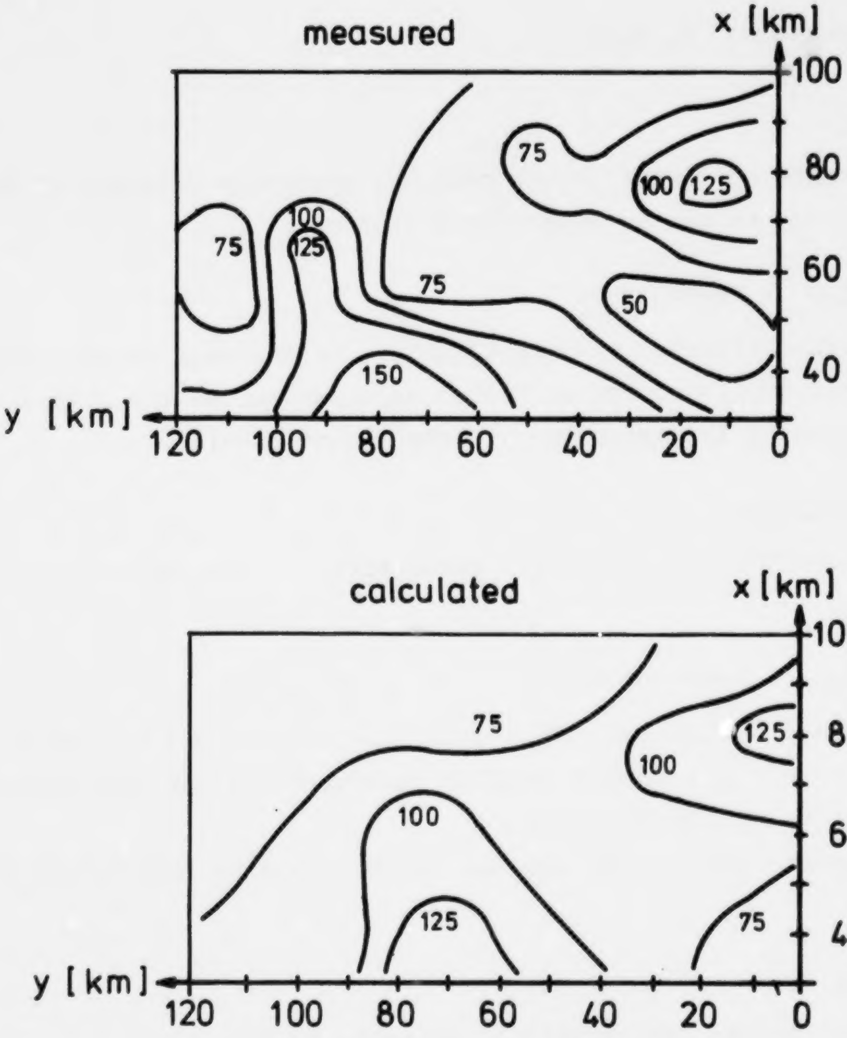

Figure 5. 24 hour mean values of the measured and calculated ground level concentration field. The numbers at the isolines give the concentration in $\mu g/m^3$.

Discussion:

(Rapporteur: D. Jost)

Prahm:

The smoothing effect in the calculations shown relative to the measured values may be due to numerical diffusion.

Herrmann (response):

Numerical diffusion is only important in the case of advection but less with this multi source diffusion model at all as the diffusion within the first (the emission-) grid is not handled.

Kretzschmar:

What were the dry deposition velocities in this paper and in that one by Maul.

Herrmann (response):

The values derived from this study are between 0.5 t 9 cm/sec. Reasonable concentration results have been reached with deposition velocities of 1 to 2 cm/sec.
The number used by Maul was 0.8 cm/sec. as also used in the OECD-LRTAP-Study.

Steenkist:

Did you measure the deposition velocity in the night?

Herrmann (response):

No, we measure it during the night. In literature values are found between 0.5 - 9 cm/sec.

Steenkist:

The difficulty in measuring the deposition velocity during the night is defining the situation of the ground. It gives large differences whether the ground is (by dew) or dry.

Herrmann (response):

We tried in the model which value of V_g gave the best results and found V_g = 1 - 2 cm/sec. the best.

EVALUATION OF A MESO-SCALE MODEL OF THE DISPERSION OF SULPHUR DIOXIDE

by

N.D. van Egmond,
RIV, Bilthoven, The Netherlands

and

C. Huygen
IMG-TNO, Delft, The Netherlands

Abstract. The time-averaged SO_2-concentration at about 10000 grid points in the Netherlands was calculated from the emission of the same number of domestic and foreign sources. The performance of the dispersion model was evaluated by comparison with measurement results of about 200 measuring stations.

By analyzing the measuring results the contributions of ten main source areas were found. These were used in the testing of the long distance part of the model.

The short distance part was tested by means of regression analysis of measuring results and the calculated contribution of high and low sources.

The agreement was quite good for yearly averages. Seasonal variation in both vertical mixing and SO_2 loss appeared to be larger than predicted by the model.

Introduction

As part of a contract between the Dutch Ministry of Public Health and Environmental Hygiene and TNO, a study was carried out to predict the development of the air quality as dependent on possible economic developments and proposed government actions. An integrated economic development/air quality model has been and is being developed. The SO_2 dispersion module of this model was used to calculate ground-level concentrations for seventy-five different emission situations in the future. Confidence in the predictions might be increased by evaluation of the performance of the dispersion model for a reference year, chosen to be 1977. Inasmuch as the model was adjusted to fit the situation of that year it could be said that its function is to extrapolate the known situation of 1977 to the years 1980-2000.

The evaluation was facilitated by the results of a method developed at the National Institute of Public Health to derive the contribution of different source areas to ground level concentrations from measurement results.

This paper describes that method and the results of the performance evaluation.

The emission inventory

A detailed inventory of all major air pollutant emissions in the Netherlands is now in progress. The results for 1977 were not completely available and had to be supplemented with those of a special inventory of the larger SO_2 sources. In this way the individual characteristics of these larger, in general industrial, sources within the Netherlands were known. The more diffuse emission resulting

Preceding page blank

from space heating, traffic and small scale industrial activities was allocated to aera sources. They were assumed to have a uniform effective height of 20 m.

The emission of the aera sources was attributed to 5x5 km grid squares except for a number of density populated districts, where 1x1 km squares were used. The uncertainty in the total emission per grid square (table 1) was of course larger, but not much larger than in the total emission of the country.

Table 1. Emissions (1977) and estimated maximum errors in the emission per 5x5 km grid square.

ECONOMIC SECTOR	EMISSION (10^6 KG/Y)	MAX. ERROR (PERCENT)
INDUSTRY (POINT SOURCES)	343	10
INDUSTRY (AREA SOURCES)	30	30
SPACE HEATING	39	30
ROAD TRAFFIC	14	> 50
INLAND NAVIGATION	8	20
SEA-GOING VESSELS	27	30
AGRICULTURE	7	20
OTHER	1	-
TOTALS	470	10

The estimation of the emissions of foreign countries - Belgium, northern part of France, Germany, Luxembourg - was based on the LRTAP report[4] and a number of German reports [5,6,7,8]. The total foreign emission was estimated at 6.2 x 10^9 kg/y, distributed over either 5x5 km or 25x25 km squares. The area sources formed in this way were given an effective height of either 250 m (60% of the emission) or 35 m (40%). In total the emission of about 700 point sources and about 9000 area sources was determined.

Short description of the dispersion model

Three main parts were distinguished in the model respectively describing the contribution of distant sources (25 - 450 km), of (low) area sources at small distances (< 25 km) and of (high) point sources at small distances.
The distinction is more or less artificial, but useful for the performance evaluation.

The short distance part of the model was essentially identical to a model presented earlier by Nieuwstadt et al [1,2]. It is a gaussian plume model for the calculation of long term concentration averages, using frequencies of meteorological conditions. For low sources Pasquill's set of vertical dispersion coefficients is used, for high sources (> 100 m) that proposed by Singer-Smith. At a later stage the model was modified. Pasquill's coefficients were then used throughout.
At a distance of at most 75 km the short distance Gaussian plume model has gradually changed into a box model, but does not contain loss terms. The influence of

SO_2 losses, through chemical transformation and wet and dry deposition, on the surface concentration was built into the long distance model in a relatively simple manner. The admissability of the simplifications was tested by means of sensitivity analysis. At distances larger than 75 km, a dry deposition velocity of 0.8 cm/sec was chosen for low sources and of 0.4 cm/sec for high sources. The losses through chemical reaction and wet deposition together were taken to be 2% per hour. For source receptor distances between 25 and 75 km a transitional model was constructed. A more detailed description is to be found in several reports.[3] Based on the model a system of computer programmes was built to calculate ground level concentrations on the 4000 nodes of a 5x5 km grid comprising the whole country. A finer grid (1x1 km) was used in a number of interesting areas. The number of grid points was 8400.

The network of measuring stations

The results of three networks were used:

- the RIV network (National Institute for Public Health), using Philips coulometric instruments (figure 1, figure 2);
- the Rijnmond network, using the same monitors (figure 2);
- the network of the province of South-Holland using the hydrogen peroxide method (figure 2).

The measuring results of about half of the stations of first network were used in the investigation of the long distance part of the model. The selected stations were evenly distributed over the country. The rest is concentrated in specially interesting areas. Twenty-two stations were used together with those of the local networks, thirty-two stations of the Rijnmond network, sixty of the South-Holland network. Estimations of the reliability of the measuring methods are given in table 2.

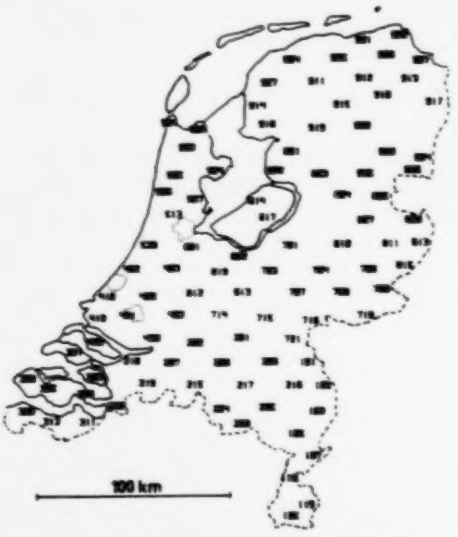

Positions of the measuring stations used in the testing of the long distance part of the model

Figure 1.

Positions of the measuring stations used in the testing of the short distance part of the model

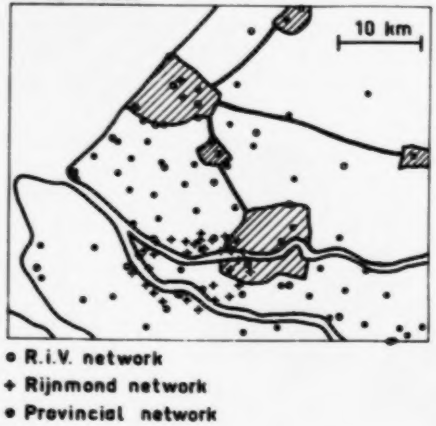

Figure 2.

Table 2. Estimated precision of the measuring methods, expressed as the root mean square of the difference between the measured and the "true" value of a long term average.

RIV NETWORK	5 µG/M^3 + 5% OF TRUE VALUE;
RIJNMOND NETWORK	10 µG/M^3 + 5% OF TRUE VALUE;
SOUTH HOLLAND NETWORK	20 µG/M^3 + 15% OF TRUE VALUE.

Testing the long distance part of the model

Analysis of the measuring results

Graphical presentations of concentration fields derived from hourly measuring results (figure 3) strongly suggest that the long distance dispersion of SO_2 may be described by a simple Gaussian plume model. Also the possibility presents itself that the contribution of different source areas to long term averages of ground level concentrations may be determined by fitting this model to the hourly data.
Such a procedure was used earlier for the analysis of data of air pollution in urban areas (e.g. Heimbach and Sasaki[9]).
The Gaussian model was simplified by assuming complete vertical mixing, an unknown but constant relative SO_2 loss per unit of time and a dependence of the horizontal dispersion coefficient σ_y on the distance x as given by: $\sigma_y = p\, x^{0.89}$.

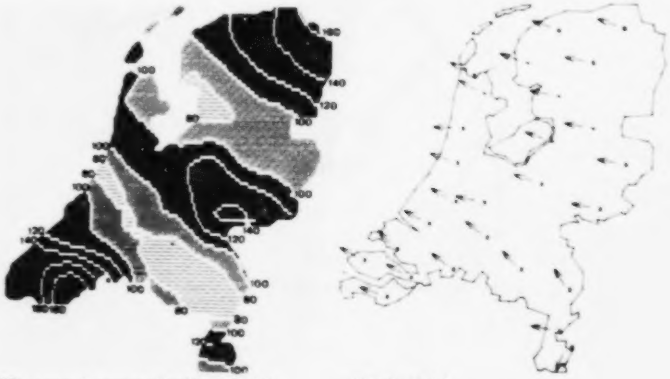

Measured concentration field Wind field

Figure 3.

Large scale plumes

The parameters p and the rate of loss are varied to obtain the best fit. As wind speed and of course wind direction enter into the model, observations of the hundred evenly spread stations were sorted out in four wind speed classes and twelve wind direction classes. Optimization of the parameters was done by using a trial-and-error least square method per wind class. The corresponding contributions to the long term average concentrations of the chosen source areas were averaged.

The frequencies of occurrence of the wind classes were used as weights in the averaging procedure. A detailed description is given by Van Egmond et al.[10] It appeared that with this method it was possible to distinguish ten main source areas (figure 4). As the method relies on recognition of the plume shape, distant sources cannot be individually distinguished. Their presence shows up in a uniform decrease of the concentration levels in the wind direction. By analysing these decreases, their contributions were estimated. They were largest in the direction of known distant sources. The remainder was attributed to more or less uniformly distributed local sources.

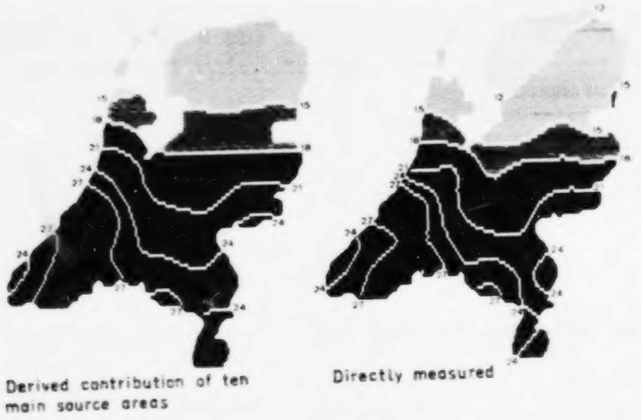
Derived contribution of ten main source areas

Directly measured

Yearly average of SO_2-concentrations

Figure 5.

Finally, about 80% of the total spatial variability could be "explained" by this method. Accordingly, the calculated and observed concentration fields agreed well (figure 5). Of course the main purpose was, however, the determination of the origins of the SO_2 pollution.

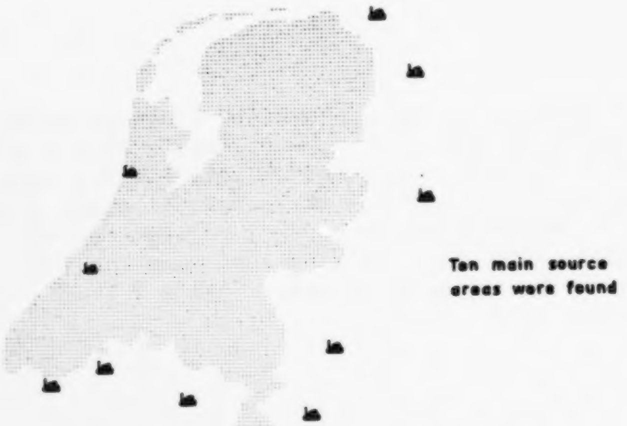

Figure 4.

Comparison of "measured" and calculated contribution of distant sources

In this paragraph the values derived from measurements with the method described in the previous paragraph will be called "measured" values. Calculations of the contribution to the long term average from known sources is trivial. The contribution from unknown distant (> 450 km) sources can only be estimated as a difference between measured and calculated values. It proved to be difficult to obtain complete agreement between those values in relatively clean areas with reasonable adjustments of the model. It was therefore assumed that distant foreign sources contributed about 5 $\mu g/m^3$ to the yearly average in all locations. Applications of the model to sources in the United Kingdom, eastern Europe and the south of Germany indicated that this assumption is not unreasonable. The amount is included in the calculated other foreign sources row in table 3.

Table 3. Contributions to the average yearly concentrations ($\mu g\ SO_2/m^3$) in 1977) of selected measuring stations. Comparison between calculated values and those derived from measurements.

	station no. 911		613		409		217	
SOURCE	MEAS	CALC	MEAS	CALC	MEAS	CALC	MEAS	CALC
BELGIUM	0	0.5	3	5.1	4	6.2	7	9.1
GERMANY	3	2.5	5	4.9	2	2.6	6	5.9
OTHER FOREIGN	5	5	7	5	7	5	8	5
DUTCH	6	3.3	6	9.8	14	8.9	5	14.2
TOTAL	13	11.3	21	24.8	27	28.9	26	34.2

The extend of agreement between calculation and measurement is encouraging. The ground level concentration averaged over the whole country (about 40.000 km^2) and the year 1977 was about 20 $\mu g/m^3$. Both measurement and calculation indicate that about a third resulted from domestic emissions and the remainder about equally from near (< 200 km) and distant (> 200 km from the border) foreign sources. In polluted areas these ratios are quite different. Calculations were carried out not only for the year 1977 but also for its quarter years. Table 4 shows that for this case the agreement is less good.

Table 4. Comparison between measured and calculated concentrations. Quarterly averages over all measuring stations (µg SO_2/m^3).

QUARTER OF THE YEAR 1977	MEASURED	CALCULATED
1	34	26
2	16	19
3	15	19
4	33	26

Apparently the contribution from foreign sources, especially the distant sources are underestimated during the winter. The simplest explanation would be that considerable seasonal variations in the rate of SO_2 loss may occur.

Testing the short distance part of the model

A first confrontation of calculated and measured results required an adjustment of the model. Contrary to what one would expect for an unbiased model, the difference between measured and calculated values appeared to be strongly dependent on the magnitude of the calculated contribution of the higher (point) sources (figure 6). This contribution appeared to be overestimated several times, at least when it was large. Rather arbitrarily, Singer-Smith's set of vertical dispersion coefficients was replaced by Pasquill 's to obtain better agreement between measured and calculated values (figure 7).
A certain tendency to overestimate both the contributions of low (area) and high (point) sources remained.

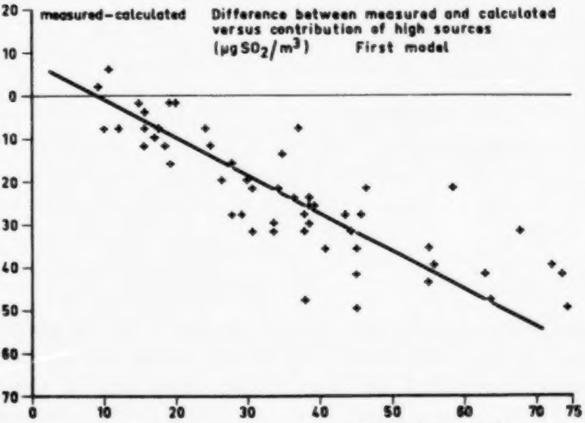

Figure 6.

Figure 7.

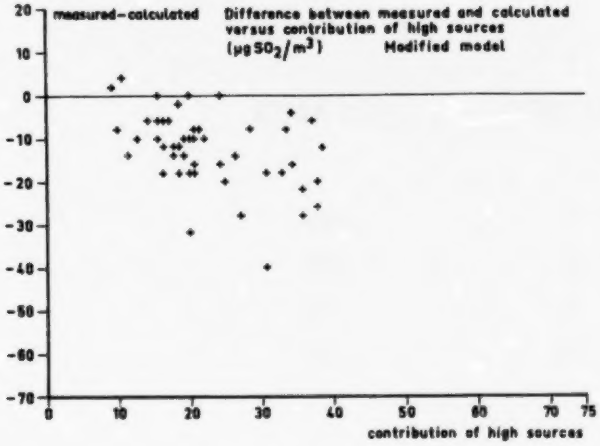

Linear regression analysis of quarterly results was carried out (table 5). The values of the 95% confidence interval should be taken as indicative only.

Table 5. Regression analysis of quarterly results of the contributions from different source types.

MEASURED - FOREIGN = A X (HIGH SOURCE) + B X (LOW SOURCE)

SEASON	A	95% INTERVAL FOR A	B	95% INTERVAL FOR B
1	0.21	-0.13 TO 0.55	1.16	0.80 TO 1.51
2	0.63	0.42 TO 0.55	0.61	0.36 TO 0.85
3	0.64	0.39 TO 0.89	0.38	0.10 TO 0.65
4	-0.06	-0.38 TO 0.25	1.24	0.88 TO 1.61

As indicated earlier a season dependent error may exist in the calculated contribution of foreign sources. In the relatively more polluted area under consideration, this error should not be more than 10% of the total. One would therefore expect a value of 1 for both a and b if the model was unbiased. The apparent overestimation of the high source contribution in winter and the low source contribution in summer points to underestimation of the seasonal variation in the intensity of vertical diffusion by the model.

Nevertheless the results for the yearly averages are reasonably accurate and the model appears to be able to serve its purpose: extrapolation of known data to the future.

In fact, so far as the correlation of the calculated and measured values is better for one measuring method than for another, it may be stated that the calculation is more precise than at least one of the measuring methods (figure 8, figure 9).

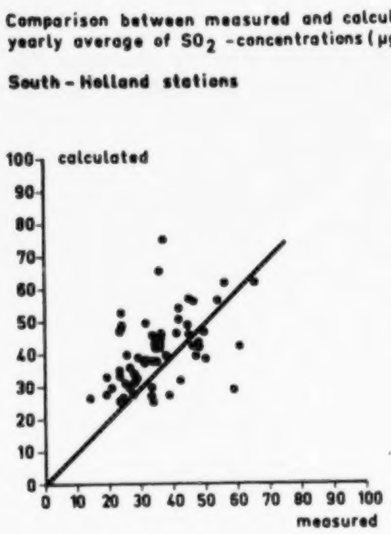

Figure 8.

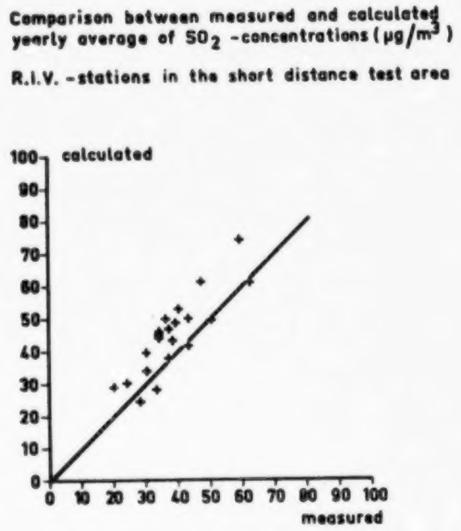

Figure 9.

References

1. F.T.M. Nieuwstadt, C.M. Verheul and J. Addicks.
The validation of the Gaussian dispersion model for long term average ground level concentrations in the Rijnmond area.
Proc. 7th Meeting on Air Pollution Modelling NATO-CCMS.
2. Modellen voor de berekening van de verspreiding van luchtverontreiniging inclusief aanbevelingen voor de waarden van parameters in het langetermijnmodel (Models for the calculation of the dispersion of air pollution including recommendations for the values of parameters in the long term model.)
Staatsuitgeverij, The Hague, April 1976.
3. Reports on the project "Berekenen Luchtkwaliteit" ("Calculation of air quality").
CMP-TNO, Delft, THe Netherlands, 1978, 1979.
4. The OECD programme on long range transport of air pollutants.
OECD, Paris,1977.

5. Raumliche Erfassung der Emissionen ausgewählter Luftverunreinigung der Stoffe aus Industrie, Haushalt und Verkehr in der Bundesrepublik Deutschland 1960-1980, Bundesministerium des Innern.
6. Interregionaler Transport von Luftverunreinigungen, 10. Arbeitsbericht des Deutsch-Niederländischen Zusammenarbeit auf dem Gebiet der Luftreinhaltung.
7. Materialien zum Immissionensschutzbericht 1977 der Bundesregierung an den Deutschen Bundestag; Umweltbundesamt.
8. Luftreinhalteplan Rheinschiene Süd (Köln) 1977-1981, Ministerium für Arbeit Gesundheit und Soziales des Landes Nordrhein-Westfalen, 1976.
9. J.A. Heimbach and Y. Sasaki.
   A variational technique for meso-scale objective analysis of air pollution.
   J. Appl. Meteor., 14 (1975) 194-203.
10. N.D. van Egmond, O. Tissing and H. Kerseboom.
    Estimating contributions of source areas to the measured yearly average SO_2 concentration field in the Netherlands by dispersion model parameter optimization.
    Atm. Environment (in press).

Discussion:

Hübschmann:

This is a further indication that tall stacks can not solve air pollution problems for larger areas. The legislation should take care of this.

AIR POLLUTION MODEL FOR CALCULATING SHORT-TERM (DAILY) REGIONAL PATTERNS AND TRANSFRONTIER EXCHANGES OF AIRBORNE SULFUR IN EUROPE

by

Chandrakant M. Bhumralkar, Warren B. Johnson
Robert L. Mancuso, and Daniel E. Wolf
SRI International
Menlo Park, California USA

and

Jürgen Pankrath
Umweltbundesamt, Berlin FRG

Abstract. An air pollution model, EURMAP-2, has been developed to simulate and assess the effects of daily variation in sulfur emissions, over large regions, on short-term (daily) air quality in central and western Europe. The model has been used to calculate concentrations, depositions, and transfrontier/international exchanges of SO_2 and $SO_4^=$ during the episodes of 25-26 August and 14-16 September 1974. A comparison between model-calculated and measured concentrations of SO_2 and $SO_4^=$ shows a good agreement over large portion of the model grid, although calculated concentrations are lower than measured values in the eastern portion. Calculated patterns for dry SO_2 deposition show strong correlation with emissions; patterns for wet deposition correspond closely to natural inhomogeneities in precipitation.

Introduction

In recent years, special attention has been given to problems resulting from long-range transport of air pollutants over large regional- or continental-scale areas. In many studies, theoretical models have been developed to simulate the transport, diffusion, transformation, and removal of SO_x released into the atmosphere from the multitude of sources located within a given region (Ottar, 1978; Pack, 1977; Hidy, et al., 1979).[1,2,3]

SRI has developed a model called EURMAP-2 as part of a study (sponsored by Umweltbundesamt, Federal Republic of Germany) to develop, evaluate, and apply a practical, quantitative technique (model) for assessing the effects of air-pollution emissions in each country in central and western Europe on both the long-term (annual, seasonal, and monthly) as well as short-term (daily) air quality in each of the other countries.

The SRI study initially resulted in the development of a long-term model, European Regional Model of Air Pollution, designated as EURMAP-1 (Johnson et al.; 1977, 1978).[4,5] The performance and sensitivity of EURMAP-1 were evaluated by determining the values of various parameters that gave optimum correspondence

Preceding page blank

between calculated and measured values of the pollutants considered by the model (Mancuso et al., 1978).[6]

The basic design of the short term model EURMAP-2, is the same as that of the long-term model EURMAP-1. The principle of operation of the EURMAP-2 model is shown in Figure 1. The model calculates 24-hour average values and thus is useful for application to study short-term air pollution "episodes" on a regional scale.

Design of the EURMAP-2 Model

The EURMAP-1 and EURMAP-2 models share several distinctive features and are designed for minimum computing requirements (and thus for economical use), yet also achieve acceptable realism in simulating the important processes in the transfrontier pollution problem. However, the long-term model was based on certain implicit assumptions which are inappropriate for the calculation of values for short-term (daily) episodes. Table 1 lists the fundamental differences between EURMAP-1 and EURMAP-2 (in the treatment of pollution puffs and averaging times). Table 2 lists the treatment of some important physical elements in EURMAP-1 (long-term) and EURMAP-2 (short-term). For comparison, we have included corresponding characteristics of NILU trajectory model developed by Norwegian Institute for Air Research in Tables 1 and 2.

Formulation of the EURMAP-2 Model

Pollutant Emissions Data

The sulfur emissions data used in EURMAP-2 are from the most recent OECD-Long Range Transport of Air Pollutants (LRTAP) study (OECD, 1977),[7] which consists of emissions data from the countries listed in Table 3. The emissions are divided into two components--continuous and variable. The continuous emissions (E_c), which are principally industrial, are assumed to be the same throughout the year, and the variable emissions (E_v), which are principally household emissions, are assumed to have a temperature dependence.

Table 1. Fundamental Differences Between EURMAP-1 and EURMAP-2.

Model	Emission Puff Frequency (hours)	Puff-Tracking Frequency (hours)	Minimum Averaging Time for Concentrations and Deposition
EURMAP-1	12	3	1 month
EURMAP-2	6	1	1 day
NILU	6	2	1 day

Mixing Height

The mixing height is allowed to vary diurnally in EURMAP-2. The maximum and minimum values of mixing-height for a given day are calculated by using the upper-air sounding data for 0000 and 1200 GMT and hourly values for that day are

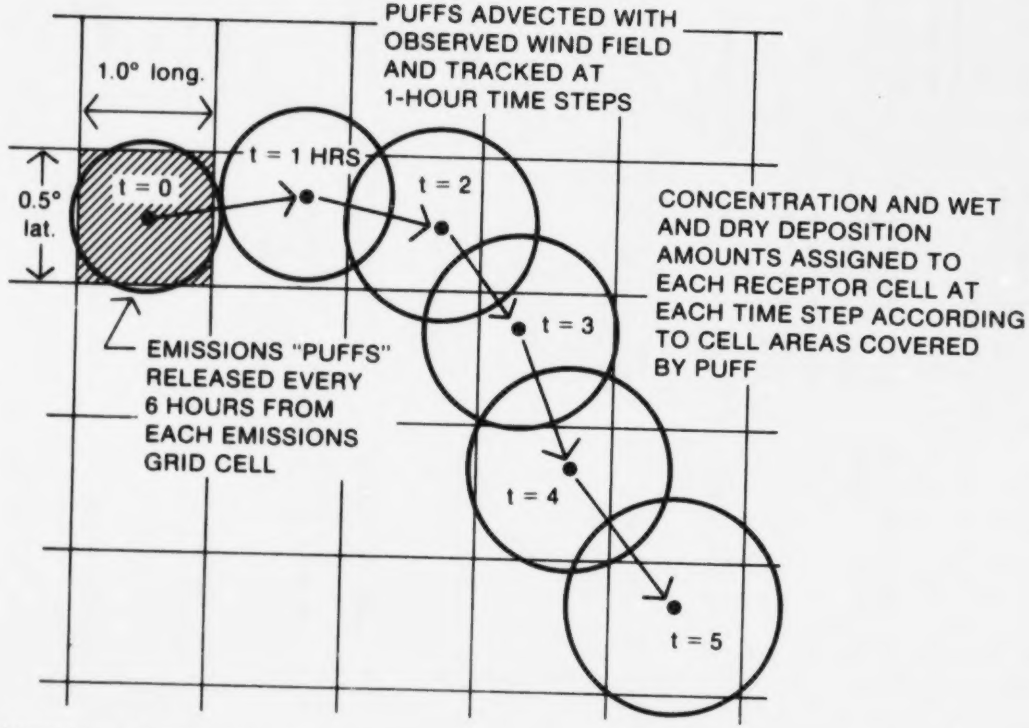
PUFFS ADVECTED WITH
OBSERVED WIND FIELD
AND TRACKED AT
1-HOUR TIME STEPS
1.0° long.
0.5°
lat.
t = 0
t = 1 HRS
t = 2
t = 3
t = 4
t = 5
CONCENTRATION AND WET
AND DRY DEPOSITION
AMOUNTS ASSIGNED TO
EACH RECEPTOR CELL AT
EACH TIME STEP ACCORDING
TO CELL AREAS COVERED
BY PUFF
EMISSIONS "PUFFS"
RELEASED EVERY
6 HOURS FROM
EACH EMISSIONS
GRID CELL

Adapted from Johnson et al (1978)

Figure 1. Emissions puff advection in EURMAP-2.

Table 2. Differences in the treatment of some physical elements between EURMAP-1, EURMAP-2, and NILU.

Element	Model		
	EURMAP-1	EURMAP-2	NILU
Emission data	For 13 countries SO_2 amount constant and based on annual total	For 19 countries; includes emissions from all countries within grid SO_2 amount consists of constant and variable components Variable component is based on degree days	For polar stereographic grid covering Europe (emission from southeast section excluded) SO_2 amount constant and based on annual total
Mixing height (h)	Constant at 1 km	Varies diurnally	Constant at 1 km
Transport wind (V_T)	$V_T = 0.75\ V_{850}$ $\theta = \theta_{850} - 15°$	Based on surface and 850-mb winds and a power law of the form $\frac{V_2}{V_1} = \left(\frac{Z_2}{Z_1}\right)^p$	$V_T = V_{850}$ $\theta = \theta_{850}$
Horizontal diffusion	Fickian diffusion	Based on horizontal deformation of wind field	None stated
Vertical diffusion	Immediate uniform mixing in vertical Limited up to mixing height	Not instantaneous Puff is allowed to penetrate beyond mixing height	Immediate uniform mixing in vertical
Decay rates (% per hour)	Dry deposition 2.9 for SO_2 0.7 for $SO_4^=$ Wet deposition[*] 21.6 · R for SO_2 7.0 · R for $SO_4^=$ Transformation 1.0 for $SO_2 \rightarrow SO_4^=$	Dry deposition[†] $2.9/Z_p$ for SO_2 $0.7/Z_p$ for $SO_4^=$ Wet deposition[‡] 21.6 · R for SO_2 7.0 · R for $SO_4^=$ Transformation[‡] 1.0 for $SO_2 \rightarrow SO_4^=$	Decay rate 5.4 for SO_2 1.44 for $SO_4^=$ Transformation 0.72 for $SO_2 \rightarrow SO_4^=$

[*] R is rainfall rate in mm/hr

[†] Z_p is the height of the top of the puff in km

[‡] Same as EURMAP-1

Table 3. Countries Whose SO_2 Emissions Data Have Been Used in EURMAP-2.

Austria	Luxemburg
Belgium	Norway
Czechoslovakia	Poland
Denmark	Romania
Federal Republic of Germany (FRG)	Spain
France	Sweden
Germany Democratic Republic (GDR)	Switzerland
Hungary	United Kingdom
Italy	U.S.S.R.
	Yugoslavia

then obtained by interpolating between the maximum and minimum values.

Pollutant Transport Wind

In EURMAP-2, transport wind is divided into upper-layer wind, from h_s to 850 mb (~1500 m), and surface-layer wind, from surface (10 m) to h_s where h_s, the height of the surface layer, is set at 300 m. The pollutant puff is transported by using the wind given by the formula

$$V_T = \frac{h_s \cdot V_s + (Z_p - h_s)V_u}{Z_p} , \qquad (1)$$

where h_s is height of surface layer, V_T is the transport wind speed. V_s and V_u are respectively the average wind speeds in the surface and upper layers calculated by using a power law.

Equation (1) shows that the transport wind used in EURMAP-2 depends on the puff height Z_p. For example, for a puff located at or below h_s, the transport wind will be V_s or a fraction thereof, and for a puff above h_s, V_T is a weighted mean between surface- and upper-layer winds.

Horizontal Diffusion

In EURMAP-2, the horizontal diffusion of the material in the puff is calculated by using the formula

$$A = A_O + K_H t ,$$

where A_O is the initial area of the puff, and K_H is the horizontal diffusion coefficient. K_H is estimated by using a nonlinear formulation following Keyser and Anthes (1977):[8]

$$K_H \; \alpha \; (DS)^2 \; D \; ,$$

where DS is a grid length, and D is deformation in horizontal wind, given by

$$D = \left[\left(\frac{\partial u}{\partial x} - \frac{\partial v}{\partial y} \right)^2 + \left(\frac{\partial v}{\partial x} + \frac{\partial u}{\partial y} \right)^2 \right]^{\frac{1}{2}}$$

Vertical Diffusion of Pollutants Puffs

In EURMAP-2, the puff initially extends from the surface to a height of 400 m, following Fisher (1975)[9] who has indicated that about half of the sulfur emissions are from sources whose effective height in summer could be as high as 400 m. The maximum height of puff in EURMAP-2 is prescribed to be 1.5 km. On the basis of curves drawn by Turner (1970)[10] this corresponds to a horizontal travel distance of 1000 km when the puff is either off the model domain or is so depleted that its contribution is relatively small.

Decay Coefficients for SO_2 and $SO_4^=$

The wet deposition (k_w) and transformation (k_T) coefficients in both EURMAP-1 and EURMAP-2 are the same. However, in EURMAP-2, the dry deposition coefficient is calculated from the formula

$$k_d = w/Z_p \; , \tag{2}$$

where

k_d = dry deposition coefficient (percent per hour)

w = constant deposition velocity (km per hour)

Z_p = puff height (km)

Equation (2) implies that the decay of pollutant due to dry deposition is proportional to concentration. Thus, more pollutant material is lost during the initial life of the puff, when Z_p is small. The values of k_w, k_T, and other parameters used in calculating decay rate are as given in Table 2.

Results of EURMAP-2 Calculations

EURMAP-2 calculations were performed for two selected episodes in 1974: 25-26 August and 14-16 September. Detailed description of EURMAP-2 calculations for these episodes are given by Bhumralkar et al. (1979).[11] In this paper the results of September episode only are discussed.

Input Data and Initialization

Figure 2 shows the annual sulfur emissions (from the countries listed in Table 3) used as input with EURMAP-2; the highest emissions lie in a broad band extending from the central United Kingdom east-southeastward to southwestern

Poland encompassing most of the heavily industrialized regions in the study area. The input parameters for EURMAP-2, such as mixing depth, transport wind, horizontal diffusion coefficient, temperature, atmospheric stability, and rainfall rate were derived from the upper-air and the surface data reporting stations over Europe for 1974. The daily rainfall patterns for the two episodes were computed from rainfall data recorded at three-hour intervals at meteorological measuring stations situated within the model domain. Because no rainfall measurements were available over the North Sea, these were approximated by distance-weighted averaging of the rainfall measurements at surrounding land stations.

EURMAP-2 is initialized by performing the model calculations for five days preceding the first day of the episode which has been determined by performing several tests.

Comparison Between Calculated Results and Measurements

Figures 3 and 4 show calculated and measured concentrations for SO_2 and $SO_4^=$ respectively (measured values of SO_2 and $SO_4^=$ are in circles).

A comparison of computer-run results with measured values of SO_2 concentrations shows that the model results agree satisfactorily with measurements in the United Kingdom area. For example, on 14 September, a contour line representing 16 $\mu g/m^3$ of SO_2 concentration encompasses measured values of 21 and 17 $\mu g/m^3$. On 15 September, measured values of 20 and 29 $\mu g/m^3$ are close to the calculated contour value for 32 $\mu g/m^3$.

The comparison between calculated and measured $SO_4^=$ concentrations (Fig. 4) shows reasonable agreement in the United Kingdom and Netherlands/northern FRG areas. However, in the Denmark/southern Sweden region, the model-calculated values for 16 September are much lower than those measured on this date.

This discrepancy arises because unlike the situation of real world the model puffs do not incorporate any emissions from the eastern European regions, and the calculated transport winds are relatively stronger than the observed wind. Figure 5 shows a scatter diagram of calculated vs. measured $SO_4^=$ concentrations on 14-16 September 1974. The correlation coefficients (r) and root-mean-square errors (rmse) are also shown. The figure shows that for this episode EURMAP-2 generally underestimates $SO_4^=$ concentrations. We believe this to be a result of the use of a transformation rate of 1 percent per hour, which appears to be lower (by a factor of 2 to 3) than some recently observed transformation rates.

Deposition Results

Calculated results (not shown) indicate that SO_2 dry depositions are strongly influenced by the emissions (and therefore concentration) distribution, with maxima generally corresponding to the emissions field and the wet deposition patterns correspond closely to the natural inhomogeneities in precipitation.

International/Transfrontier Exchanges

[In this paper, the terms "International" and "transfrontier" are taken to have the same meaning]. Table 4 shows the total sulfur depositions (in tons) that came from emissions from each of the total countries during the three-day

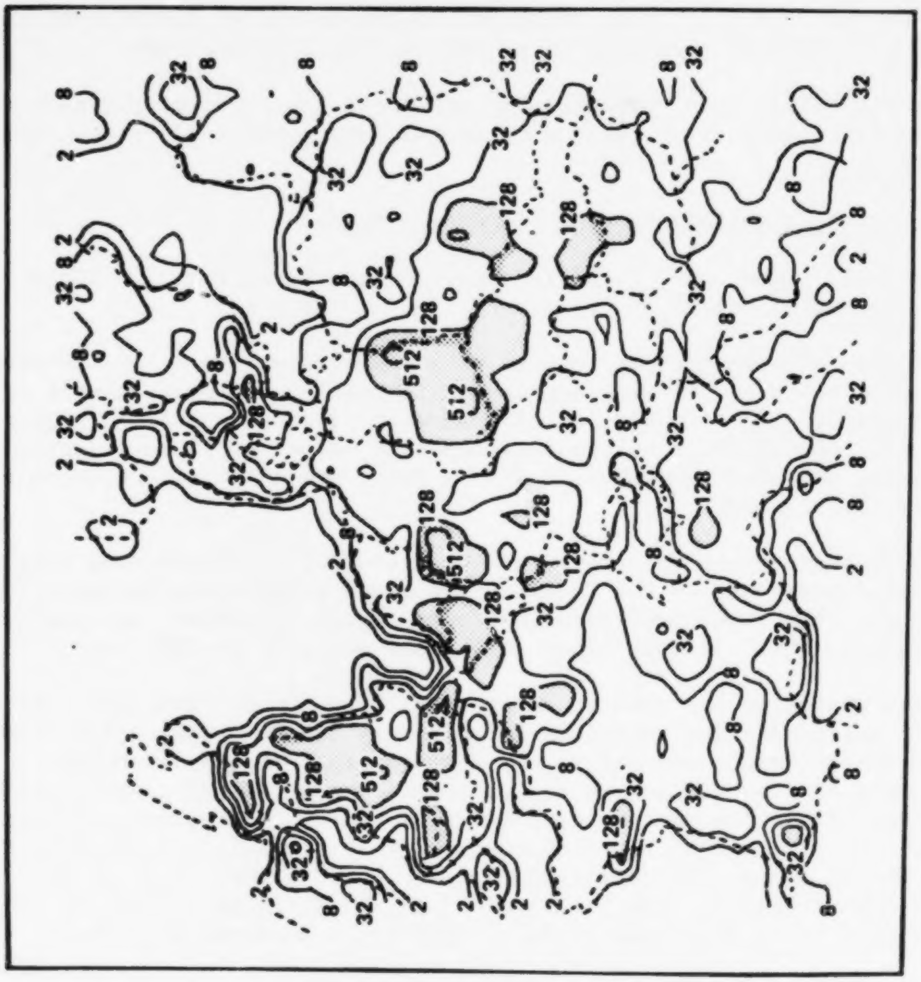
2
8
32
128
512

Figure 2. Annual emissions of sulfur over Europe for 1973 (10^{-1} ton S/km^2).

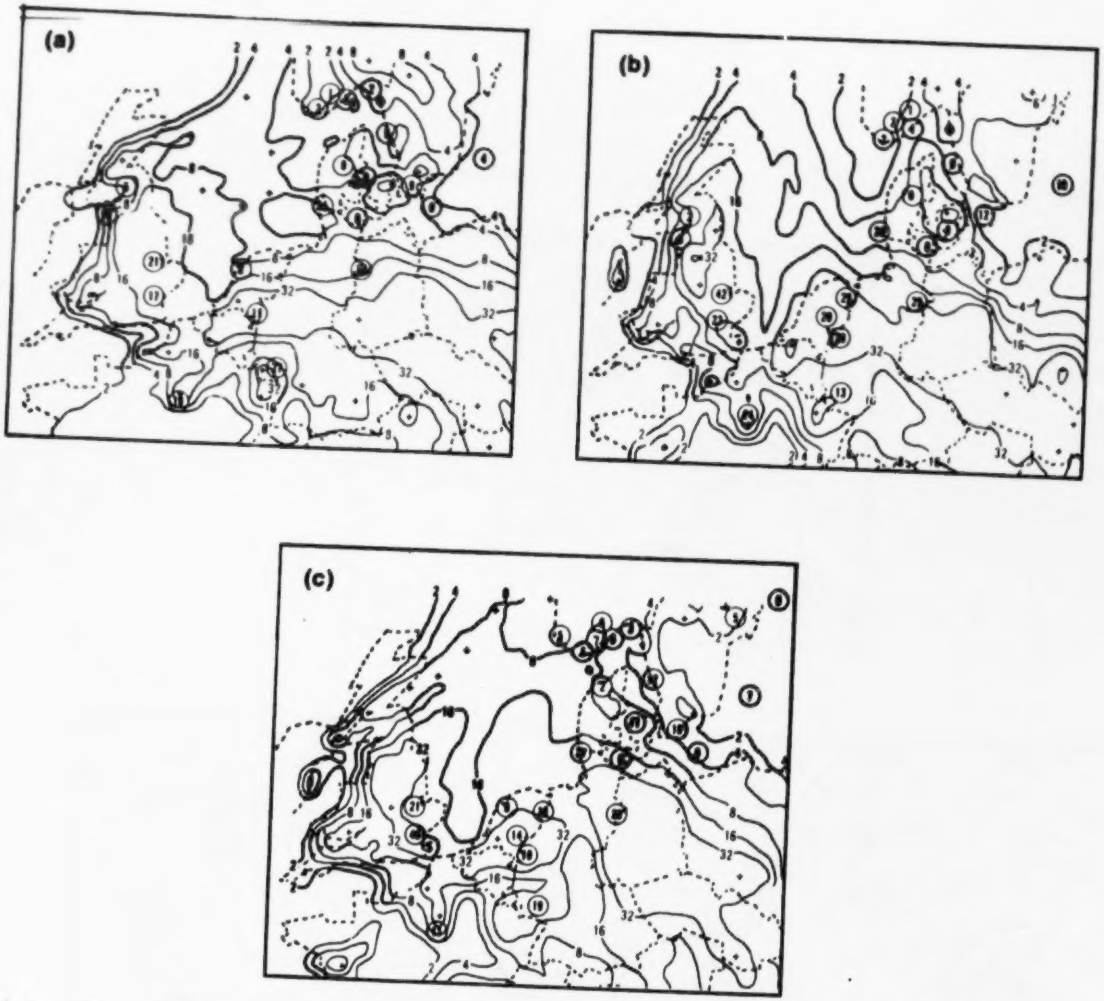

Figure 3. Calculated and measured concentrations of SO_2 for 14 to 16 September 1974 ($\mu g/m^3$). (a) 14 September 1974; (b) 15 September 1974; (c) 16 September 1974.

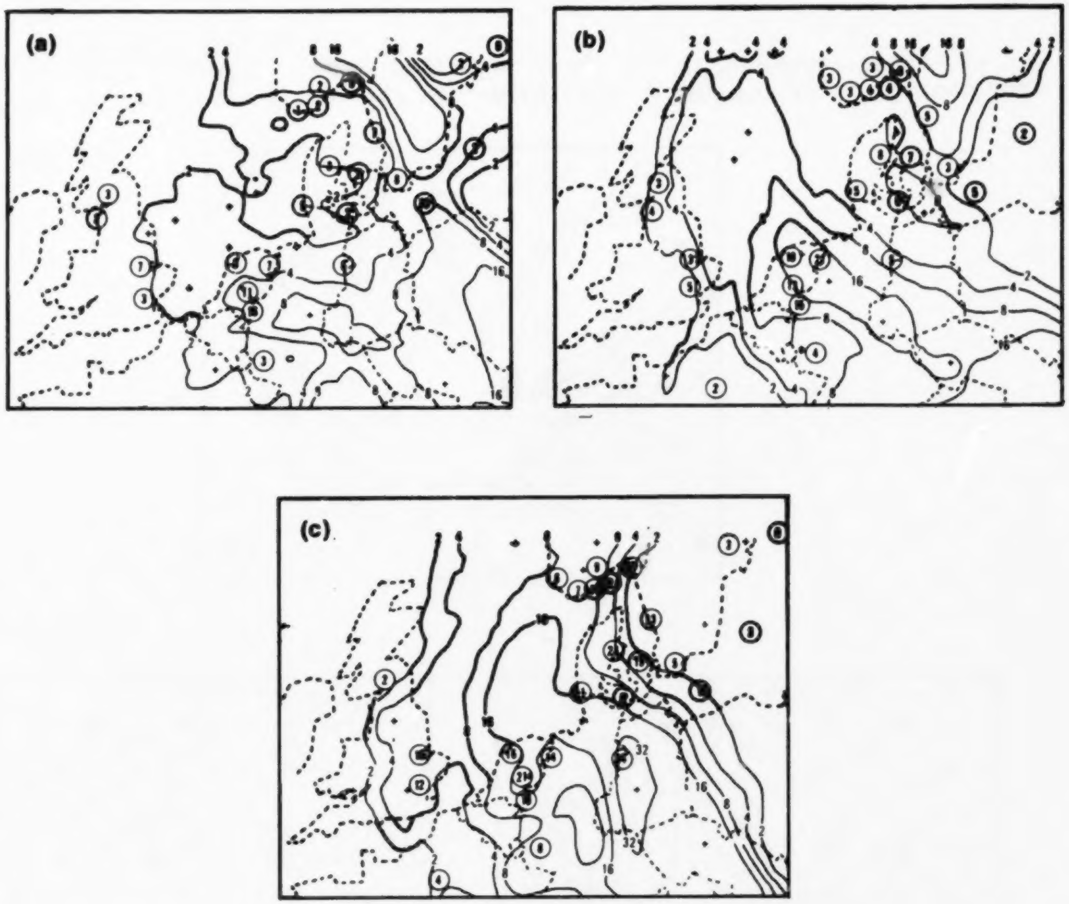

Figure 4. Calculated and measured concentrations of $SO_4^=$ for 14 to 16 September 1974 ($\mu g/m^3$). (a) 14 September 1974; (b) 15 September 1974; (c) 16 September 1974.

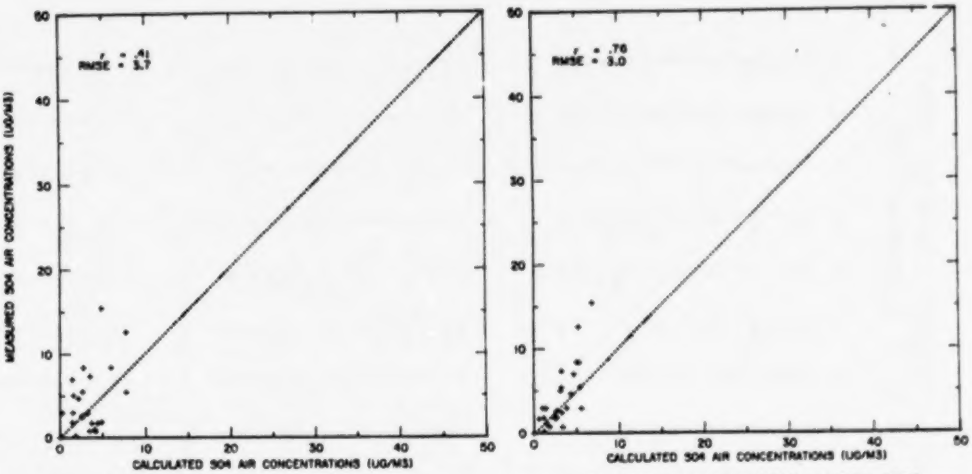

(a) EURMAP-2, 14 SEP. 1974 (b) NILU (TRAJECTORY), 14 SEP. 1974

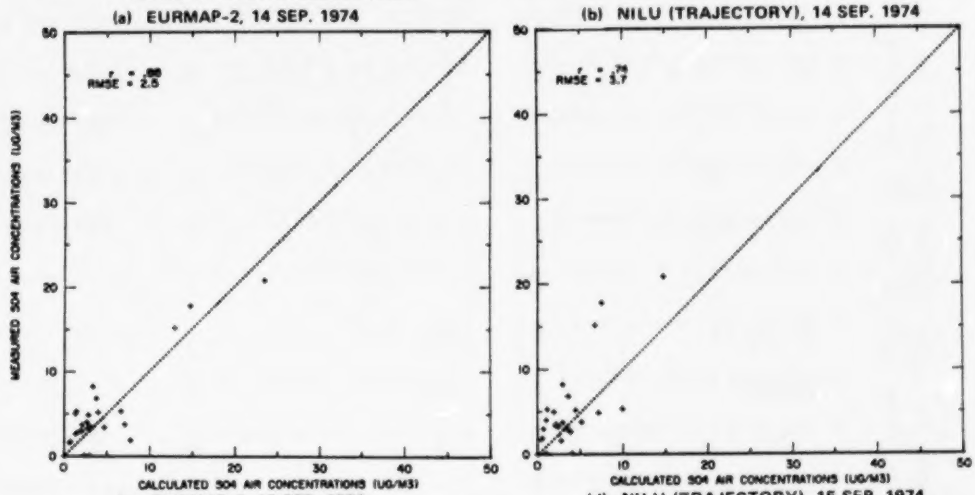

(c) EURMAP-2, 15 SEP. 1974 (d) NILU (TRAJECTORY), 15 SEP. 1974

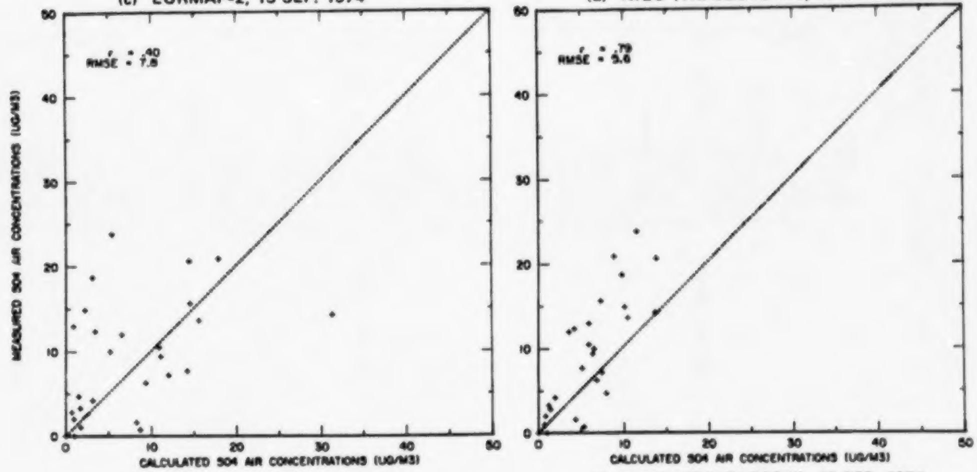

(e) EURMAP-2, 16 SEP. 1974 (f) NILU (TRAJECTORY), 16 SEP. 1974

Figure 5. Scatter diagrams showing comparison between calculated and measured $SO_4^{=}$ concentrations for 14 to 16 September 1974.

Table 4. Contributions to total sulfur depositions within receptor countries based on emissions from each of the 19 countries on 14 to 16 September 1974.

	EMITTOR COUNTRY	1	2	3	4	5	6	7	8	9	10	11	12	13	14	15	16	17	18	19
	1 FRG	1409	261	26	504	198	12	15	8	0	46	70	79	11	30	23	20	0	7	0
	2 GDR	68	583	0	1058	443	0	0	0	0	157	208	17	0	38	9	16	0	46	2
	3 FRANCE	301	58	1120	204	78	9	11	99	0	3	41	17	23	6	4	1	22	0	0
	4 POLAND	0	11	0	1852	148	0	0	0	0	121	91	0	0	24	0	1	0	388	20
	5 CZECHOSLOVAKIA	11	5	1	261	1020	0	8	0	0	10	35	120	0	553	29	129	0	74	48
	6 DENMARK	0	2	0	8	0	92	0	0	0	34	30	0	0	0	0	0	0	19	0
	7 HOLLAND	74	37	0	28	10	4	95	4	0	7	18	0	0	0	0	0	0	1	0
	8 BELGIUM	154	55	5	64	36	2	67	150	0	1	18	1	0	0	0	0	0	0	0
SEP 14, 1974	9 U. K. + IRELAND	140	76	6	21	1	61	104	15	1011	106	102	0	0	0	0	0	0	8	0
	10 S. SWEDEN	0	0	0	0	0	0	0	0	0	2	75	0	0	0	0	0	0	0	0
	11 S. NORWAY	0	0	0	0	0	1	0	0	0	205	110	0	0	0	0	0	0	3	0
	12 AUSTRIA	8	0	2	0	4	0	0	0	0	0	0	148	1	48	58	114	0	0	1
	13 SWITZERLAND	11	0	13	4	1	0	0	0	0	0	0	6	44	0	7	0	0	0	0
	14 HUNGARY	0	0	0	0	15	0	0	0	0	0	0	9	0	487	28	290	0	13	93
	15 N. ITALY	19	0	348	0	0	0	0	0	0	0	0	11	82	0	640	0	0	0	0
	16 YUGOSLAVIA	0	0	3	0	0	0	0	0	0	0	0	2	0	17	80	750	0	0	18
	17 N. SPAIN	0	0	3	1	0	0	0	0	0	0	1	0	0	0	0	0	18	0	0
	18 W. RUSSIA	0	0	0	4	2	0	0	0	0	1	0	0	0	4	0	1	0	187	22
	19 ROMANIA	0	0	0	0	0	0	0	0	0	0	0	0	0	22	0	100	0	3	183
	TOTAL (TONS S)	2243	1089	1526	4006	1957	182	292	276	1012	684	794	410	131	1231	1074	1421	38	722	384
	1 FRG	1734	104	84	51	162	11	349	68	0	29	10	85	15	62	31	43	0	8	11
	2 GDR	408	1286	4	102	479	7	1	0	0	42	28	91	0	156	13	49	0	82	78
	3 FRANCE	255	12	2091	18	66	0	74	212	34	2	3	28	19	40	3	14	10	2	2
	4 POLAND	15	141	0	1006	453	1	0	0	0	72	20	6	0	130	0	16	0	172	269
	5 CZECHOSLOVAKIA	108	75	8	48	930	0	0	0	0	4	1	225	0	321	34	475	0	20	178
	6 DENMARK	1	5	0	7	0	117	0	0	0	25	19	0	0	0	0	0	0	8	0
	7 HOLLAND	36	7	0	3	27	0	122	8	0	1	2	3	0	2	0	0	0	1	1
	8 BELGIUM	88	5	12	5	55	0	188	207	0	0	0	10	0	9	0	1	0	0	0
SEP 15, 1974	9 U. K. + IRELAND	68	60	4	11	18	36	22	0	1803	99	59	0	0	0	0	0	0	1	0
	10 S. SWEDEN	0	0	0	0	0	0	0	0	0	1	27	0	0	0	0	0	0	0	0
	11 S. NORWAY	0	0	0	1	0	1	0	0	0	165	35	0	0	0	0	0	0	1	0
	12 AUSTRIA	31	0	8	0	1	0	0	0	0	0	0	207	2	4	115	48	0	0	0
	13 SWITZERLAND	11	0	39	0	1	0	0	0	0	0	0	3	44	1	3	1	0	0	0
	14 HUNGARY	0	0	2	0	8	0	0	0	0	0	0	18	0	264	63	480	0	1	78
	15 N. ITALY	16	0	609	0	0	0	0	0	0	0	0	4	57	0	738	0	0	0	0
	16 YUGOSLAVIA	0	0	13	0	0	0	0	0	0	0	0	6	0	4	112	568	0	0	5
	17 N. SPAIN	0	0	22	0	1	0	0	0	0	0	0	0	0	0	0	0	12	0	0
	18 W. RUSSIA	0	0	0	28	2	0	0	0	0	7	0	0	0	7	0	6	0	118	43
	19 ROMANIA	0	0	0	0	0	0	0	0	0	0	0	0	0	1	1	178	0	0	104
	TOTAL (TONS S)	2771	1895	2875	1275	2202	173	756	495	1837	448	205	688	136	1022	1118	1853	21	387	787
	1 FRG	1631	80	63	8	71	35	356	91	0	0	204	32	10	25	16	41	0	0	5
	2 GDR	628	1283	19	23	95	135	5	0	0	1	37	29	1	34	12	160	0	0	38
	3 FRANCE	112	14	1929	2	24	1	49	147	64	0	51	11	10	20	2	28	25	0	2
	4 POLAND	55	409	0	1143	230	41	0	0	0	28	7	11	0	55	1	230	0	8	80
	5 CZECHOSLOVAKIA	172	514	48	152	811	0	0	0	0	0	1	119	3	86	47	351	0	0	14
	6 DENMARK	0	1	0	1	1	63	0	0	0	11	150	0	0	1	0	0	0	0	0
	7 HOLLAND	19	9	0	0	7	1	160	9	0	0	66	1	0	1	0	1	0	0	0
	8 BELGIUM	31	12	19	1	16	0	165	250	0	0	76	6	0	2	0	3	0	0	0
SEP 16, 1974	9 U. K. + IRELAND	10	18	4	1	0	11	0	0	1466	3	192	0	0	0	0	0	0	0	0
	10 S. SWEDEN	0	0	0	0	0	0	0	0	0	0	15	0	0	0	0	0	0	0	0
	11 S. NORWAY	0	0	0	1	0	0	0	0	0	90	26	0	0	0	0	0	0	0	0
	12 AUSTRIA	119	2	58	0	47	0	0	0	0	0	0	178	12	1	58	8	0	0	0
	13 SWITZERLAND	10	0	52	0	0	0	0	0	0	0	0	1	31	0	1	1	0	0	0
	14 HUNGARY	2	0	17	0	51	0	0	0	0	0	0	86	2	329	72	281	0	1	11
	15 N. ITALY	12	0	1267	0	0	0	0	0	0	0	0	8	107	0	832	0	0	0	0
	16 YUGOSLAVIA	2	0	69	0	0	0	0	0	0	0	0	22	4	8	88	538	0	0	5
	17 N. SPAIN	0	0	28	0	0	0	0	0	0	0	0	0	0	0	0	0	22	0	0
	18 W. RUSSIA	0	0	0	46	11	0	0	0	0	8	0	0	0	32	0	24	0	100	28
	19 ROMANIA	0	0	0	0	0	0	0	0	0	0	0	0	0	8	2	134	0	0	83
	TOTAL (TONS S)	2804	2341	3574	1376	1366	288	735	497	1531	142	826	499	180	599	1130	1799	48	107	288

September episode. The values along the diagonal of the matrix represent the amounts emitted by each country and the amount deposited within the country itself. For example, 1852 tons of total sulfur deposition within Poland came from emissions from Poland itself. Similarly, FRG received from itself 1409 tons of total sulfur deposition. The table also shows the amount received by each country from a given emitter country. For example, on September 14 Poland received 4006 tons of total sulfur deposition from all the 19 emittor countries (including itself) combined. Out of this, Poland received 1852 tons (ie. 46%) from itself, 1058 tons (26%) from GDR, 504 tons (13%) from FRG and so on.

Comparison Between EURMAP-2 and NILU (Trajectory) Model Results

Table 2 shows the differences in the treatment of some important elements between long-term EURMAP-1, short-term EURMAP-2, and NILU Trajectory models. It shows that there are some significant differences between the characteristics of short-term EURMAP-2 and NILU. EURMAP-2 is being developed to simulate short-term (daily) episodic conditions, and therefore incorporates various physical characteristics that are necessary for simulating daily conditions but that can be simplified for long-term simulations. For example, there are differences in the treatment of mixing depth and horizontal and vertical diffusion. Therefore, we believe that it is perhaps not meaningful to make a comparison between the performances of EURMAP-2 and NILU.

However, since NILU is the only trajectory model that has been extensively applied to simulate sulfur pollution, patterns over western and central Europe, a comparison between the results of EURMAP-2 and those of NILU is presented below.

Figures 5(b), (d), and (f) show scatter diagrams of measured and calculated $SO_4^=$ concentrations on September 14 to 16, 1974 for NILU (trajectory) model results.

The scatter diagrams for NILU-model results have been obtained by using the calculated and measured values given by Eliassen et al. (1976).[12] For purposes of comparison with EURMAP-2 results, certain portions of the NILU-model domain that fell outside the EURMAP-2 model domain have been excluded. This accounts for the differences between the r values shown in Figures 5(b), (d), and (f) and those listed in Tables C-4 through C-6 of the paper by Eliassen et al. (1976).[12] EURMAP-2 calculates higher $SO_4^=$ concentrations than those calculated by NILU. This is perhaps due to a higher rate of transformation (1 percent per hour) used by EURMAP-2 than the one used by NILU (0.7 percent per hour).

Table 5 shows a comparison between correlation coefficients and RMSE for SO_2 concentrations for EURMAP-2 and NILU. It shows that whereas r values for EURMAP-2 on September 14 and 15 are smaller than those for NILU, on September 16 EURMAP-2 has higher r than NILU.

However, we wish to emphasize that, for the reasons stated above, a comparison between EURMAP-2 and NILU is perhaps not meaningful.

Table 5. SO_2 Concentrations for September 14 to 16, 1974, Calculated by EURMAP-2 and NILU

Model	September 14		September 15		September 16	
	r*	RMSE†	r	RMSE	r	RMSE
EURMAP-2	0.54	10.5	0.50	20.4	0.61	16.6
NILU	0.70	6.5	0.74	8.2	0.56	9.5

*r = correlation coefficients

†RMSE = root-mean-square errors

Conclusions

The regional air pollution model EURMAP-2 is capable of describing short-term (daily) patterns of airborne sulfur over central and western Europe. This paper has presented a comparison between calculated and measured daily concentration of SO_2 and $SO_4^=$. The comparison shows that the model calculated concentrations are generally in reasonable agreement with the measurements over most of the model region.

However, there are significant differences between calculated and measured concentrations in the eastern part of the region, which may be partly attributable to nonavailability of emissions from the eastern boundary of the model domain. The discrepancy between model results and measurements can also occur because the model in its present form does not incorporate the effect of complex terrain on transport and dry deposition processes. Other limitations of the model that can influence its performance pertain to the treatment of vertical diffusion, tranformation rate, wet and dry deposition rates, rainfall over the North Sea.

The continued development of the EURMAP-2 model is now directed to obviate these limitations.

Acknowledgments

This study has been conducted under a contract from the Federal Environmental Agency (Umweltbundesamt) of the Federal Republic of Germany (FRG), under the supervision of Dr. D. Jost and Dr. J. Pankrath of that Agency and E. Weber of the Federal Ministry of the Interior (FRG). We acknowledge the assistance of Russell Trudeau and Dorothy Sevela of SRI International in the preparation of this paper.

References

1. Ottar, B. 1978. The OECD study on long range transport of air pollutants (LRTP). Atmos. Environ., 12, 445-454.

2. Pack, D.H. 1977. Meteorology of long range transport. International Symposium on Sulfur in the Atmosphere 7-14, Dubrovnik, Yugoslavia, 42 pp.

3. Hidy, G.M., Meuller, P.K., Dez, V. and Detore, K.C. 1979. Design and implementation of the sulfate regional experiment (SURE). Fourth Symposium on Turbulence, Diffusion, and Air Pollution. Am. Met. Soc., 15-18 January 1979, Reno, Nevada, 314-321.

4. Johnson, W.B., Wolf, D.E. and Mancuso, R.L. 1977. Long term regional distributions and transfrontier exchanges of airborne sulfur pollution in Europe. Final Report, SRI Project 4797, Contract LUP 411 515/IIIA315 SRI International, Menlo Park, California.

5. Johnson, W.B., Wolf, D.E. and Mancuso, R.L. 1978. Long term regional patterns and transfrontier exchanges of airborne sulfur pollution in Europe. Atmos. Environ. 12, 511-527.

6. Mancuso, R.L., Bhumralkar, C.M., Wolf, D.E. and Johnson, W.B. 1978. Evaluation and sensitivity analysis of the European Regional Model of Air Pollution (EURMAP-1). Progress Report, SRI Project 4797, Contract LUP 411 515/III A 315 SRI International, Menlo Park, California.

7. OECD, 1977. The OECD program on long-range transport of air pollutants: Measurements and findings. Organization for Economic Cooperation and Development (OECD), Dir. of Inf. OECD, Paris, France.

8. Keyser, D. and Anthes, R.A. 1977. The applicability of a mixed layer model for the planetary boundary layer to real data forecasting. Mon. Weath. Rev. 105, 1351-1371.

9. Fisher, B.E.A. 1975. The long range transport of sulfur dioxide. Atmos. Environ., 9, 1063-1070.

10. Turner, D.B. 1970. Workbook of Atmospheric Diffusion Estimates. Publication No. AP-26 Office of Air Programs, U.S. Environmental Protection Agency. Triangle Park, North Carolina, 89 pp.

11. Bhumralkar, C.M., Johnson, W.B., Mancuso, R.L., Wolf, D.E. 1979. Regional patterns and transfrontier exchanges of airborne sulfur pollution in Europe. Final Report, SRI Project 4797. FRG contract No. LUP 411 515/III A 315 SRI International, Menlo Park, California, 43 pp. and Appendices A to D.

12. Eliassen, A., Jensen, O. and Saltbones, J. 1976. Model comparison using selected test-results with NILU (trajectory) model. Report EMP 3/76 (Nov.) Norwegian Institute for Air Research, Lillestrom, Norway.

10TH NATO /CCMS INTERNATIONAL TECHNICAL MEETING
ON AIR POLLUTION MODELING AND ITS APPLICATION

TOPIC 5

Regulatory Applications

Preceding page blank

THE CHANGING REGULATORY ENVIRONMENT: AN APPRAISAL OF MODEL NEEDS IN THE ANALYSIS AND EXAMINATION OF POTENTIAL AIR QUALITY IMPACTS OF NO_x EMISSIONS FROM LARGE POINT SOURCES

by

S. R. Hayes

Systems Applications, Incorporated
950 Northgate Drive
San Rafael, California 94903, USA

Abstract. Regulations concerning nitrogen dioxide are currently undergoing substantial revision in the United States. When promulgated, these new regulations and others pertaining to visibility impairment will have a considerable effect on the need for and the capabilities required of the models that are used to review applications for the construction of large, NO_x-emitting point sources (like power plants). This paper appraises NO_2 and visibility modeling needs for such sources first by mapping models and the regulatory issues requiring examination by a series of decision trees, and then assessing the current needs for model development that are suggested by the associations of issues and models portrayed by the decision trees.

Introduction

The regulatory environment in the United States, insofar as NO_x-related air quality impacts are concerned, is undergoing substantial change. The Clean Air Act Amendments, as enacted by the U.S. Congress in 1977, established a legislative basis for formulating standards for short term ambient concentrations of NO_2 and for visibility, and possibly including NO_2 in the Prevention of Significant Deterioration (PSD) program. When in place, these will supplement a long-standing, annually averaged NO_2 standard.

These regulatory changes will place new demands on air quality modeling capability. Because of this, it is timely to conduct an evaluation of current modeling approaches and to determine whether they are adequate for use. A number of analytic approaches are currently available, many of which already have a record of use in considering other pollutants.

Ideally, such a modeling assessment should be comprehensive, systematically and definitively examining the adequacy of model performance, theoretical soundness, and reliability. However, in practice, to conduct such an assessment would be premature for two reasons: 1) The modeling community has had limited experience employing models to estimate short term NO_2 levels and visibility impairment, and

Preceding page blank

2) "test-bed" data sets have not yet been assembled specifically for the purpose of conducting meaningful performance evaluations for NO_2 and visibility models.

To overcome these problems, a major committment of both time and resources will be required. While it is not immediately possible to draw definitive conclusions about current modeling capability, it is nonetheless possible to take a stride in the proper direction: One can assess, at least in a preliminary way, whether model types exist that are capable of addressing all NO_x-derivative air quality issues. Structural inadequacies in modeling capability and needs for new model development may thereby be identified.

In this paper, such an assessment is described for models used to certify large, NO_x-emitting point sources like power plants. A set of model-selection decision trees is employed to associate currently available types of models with the NO_x-related regulatory issues that will require examination. By using the decision trees, the ability of current models to fulfill the requirements of federal law can be assessed. Taking the shortcomings revealed by the decision trees into account, one can infer some areas for future model development.

A Perspective on the Reported Work

For the applicant seeking permission to construct a large, NO_x-emitting point source, it is of great importance to choose a modeling approach that is technically sound, no more costly than necessary, and compatible with regulatory agency needs and preferences. Mindful of this and desiring a broad understanding of the implications of the anticipated federal NO_2 and visibility regulations, the Electric Power Research Institute (EPRI) contracted with Systems Applications, Incorporated (SAI) to assess the needs and options of the electric power industry in the United States that derive from NO_x-related regulations. As a part of this much broader study, a comprehensive, multivolume reference set is currently being prepared by SAI, comprising separate volumes dealing with laws, regulations, and the permitting process; the physical and photochemical processes influencing NO_2 formation and transport in the atmosphere; the mathematical modeling of atmospheric NO_2 and visibility impairment; the types and costs of NO_x emissions control alternatives; and the design of suitable NO_2 modeling strategies. While preparing this reference set, the modeling appraisal that is being discussed in this paper was conducted.

The Regulatory Setting in the United States

To secure approval for the construction and operation of a large point source in the United States, an applicant must successfully complete several procedural steps, satisfying the permitting agencies that a new or modified source will comply with federal and local regulations concerning emissions, control technology choice, and plant configuration, and will not produce unacceptable impacts downwind of the source. For NO_2, such impacts either have already been, or are in the process of being, defined by statutes and regulations to include maximum ground-level concentrations, incremental additions to concentrations in certain downwind areas, and visibility impairment.

The United States has been subdivided into 247 Air Quality Control Regions (AQCRs), with the air quality in each area designated for each federally regulated pollutant as being either in attainment or nonattainment of the federal standards. The air quality issues that must be addressed by an applicant depend on the site attainment status. Specifically, the emissions from the proposed source must not result in, or exacerbate, an exceedance of the federal or state ambient air quality standards, either in the vicinity of the source, or downwind in a distant nonattainment area. Neither can its incremental impact in an attainment area, near the site, if so located, or downwind in a distant attainment area, exceed that allowed by Prevention of Significant Deterioration regulations, nor can visibility impairment result in certain pristine PSD areas. Should any of the aforementioned impacts be projected to occur, some of the applicant's options could include reducing the size of the source, increasing emissions controls, resiting to a location farther from sensitive downwind areas, or acquiring emissions offsets by retiring existing sources and, thus, reducing the siting area inventory by an amount greater than the emissions from the proposed source. NO_2 is not currently included in the PSD program--only SO_2 and TSP are. However, it is expected that NO_2 will be included in the near future. Similarly, while no formal visibility standards have yet been promulgated, they are anticipated.

Associating the Air Quality Issues with the NO_x Models: The Decision Tree Approach

To gain a perspective on the match between the air quality issues that must be addressed and the types of models that are currently available, a set of model-selection decision trees can be employed. The selection of a model for estimating the air quality impacts of a large, NO_x-emitting point source is by no means a simple process, amenable to being reduced to "cookbook" procedures guaranteed to work each time they are used. Rather, the choice of a suitable approach depends on many factors, including, especially, the following: First, the choice will be influenced by the selection of the site, that is, the character of surrounding terrain; the proximity of large lakes, rivers, or oceans; the geographic setting; the flow of local and synoptic winds; and the presence and the configuration of receptors and upwind and nearby emissions sources. Second, model choice will depend on the form of the standard being considered, that is, the measure of impact and averaging time. Third, the choice will vary depending on the intended level of analysis, that is, a screening or a refined level. Fourth, model choice may be influenced by pragmatic factors such as data and resource availability or the modeling practices and preferences of the permitting agencies. Because of the complexities involved in each new situation, the circumstances particular to any proposed application should be examined carefully, and the final selection of models should be made only by individuals experienced in air quality modeling use.

Nevertheless, there are several advantages to being able to associate, at least in a general way, the air quality issues an applicant will be asked to consider with a type of model that is likely to be suitable for use. Such mapping can offer general guidance, helping to highlight major decisions to be made in the model selection process. Also, it can provide an overall perspective, facilitating the viewing of the choice of a particular model as part of an integrated modeling strategy. Most importantly for the purposes of this paper, by associating issues and models, one can assess, at least in a preliminary sense, current needs in modeling.

Model Nesting and Chaining: Two Important Concepts

In modeling the NO_2 impact of a large point source, a range of spatial scales may have to be considered. Long range transport may affect the background into which the point source plume will mix. Emissions from nearby sources, both upwind and downwind, may significantly affect the behavior of the plume. Further, the receptor area may not only be well downwind of the planned source, but also may itself require explicit modeling. Because of the scale over which cause-and-effect relationships could range, occasionally more than one model will be required to address a single regulatory issue. The linkage between these models can be provided through the transfer of boundary conditions from one model to another.

Using one model to generate boundary conditions for another is referred to here as nesting if the modeling regions lie one within another, and chaining if they abut each other. Specifically, the two terms denote the practice of using one model to drive the boundary conditions of another model, whose results may, in turn, be used to drive still another model. It must be emphasized that such techniques are technically valid only to the extent that "decoupling" can be assumed, that is, the results of the model providing boundary conditions do not themselves depend on the results of the model to which they are supplied.

An extreme case is illustrated in Figure 1, in which a three-tiered model nest is shown. In this figure, a regional model must simulate long range transport from upwind Cities B and C to City A, providing boundary conditions to an urban model, which then must do likewise for the plume model. Employing the notation used in the decision trees, the model nest can be denoted as "regional model/urban model/plume model."

Elements of the Decision Trees

The Air Quality Issues. Throughout this paper, the air quality issues are abbreviated as follows: AAQS--compliance with the ambient air quality standards, OSR--emissions offset rules, DAA--impact in distant attainment areas, PSD--prevention of significant deterioration, VIS--visibility impairment, and DNA--impact on distant nonattainment areas. Although in any given example, any of the above mentioned issues may have to be addressed, for convenience they may be associated with the site attainment designation with which they most often occur: nonattainment areas--AAQS, OSR, and DAA; attainment areas--AAQS, PSD, VIS and DNA.

The NO_x Models. Plume models can be distinguished by means of their ability to account for plume photochemistry. Gaussian short term (G/ST) and long term (G/ST) models[1] cannot explicitly consider the photochemical conversion of NO to NO_2, but must rely on assumptions about such conversions (for example, the highly conservative assumption that all NO_x is emitted as NO_2). When the plume is unlikely to contain or entrain a significant amount of reactive hydrocarbons (RHC), post-release conversion of NO to NO_2 will occur only through the interaction of NO with background ozone. Coupling the description of this conversion, using the so-called equilibrium/steady-state relationship, to a Gaussian model would result in what might be termed an equilibrium plume model (EPM).[2] When RHC is likely to be entrained by the plume, a reactive plume model (RPM) should be employed to consider a fuller range of photochemistry reactions. Several such models have been used to examine NO_2 and ozone formation in power plant plumes.[3,4]

Other dispersion models referenced in the decision tree include a trajectory (TRAJ) model, an urban scale grid model (USGM), and a regional scale grid model (RSGM). Also, model nests or chains, though seldom likely to be required in practice, have occasionally been used to consider the impact of a power plant on a downwind urban area (for instance, the Conjoint Model developed at SAI,[5] a model chain which links an RPM to a USGM). Types of visibility models considered are a plume visibility model (PVM) and a regional visibility model (RVM)--see Ref. 6 for an example of such models. Though subject to broad uncertainty, some rough estimates of the ranges of typical modeling costs and duration, by model type, are shown in Table 1. These estimates, which do not include the often substantial costs of data gathering, are included only to illustrate the order-of-magnitude cost differences among models.

Averaging Time of the Standard. For NO_2, the long term standard is an annually averaged value. The hourly averaged standard that is expected to be promulgated soon by the EPA represents the short term value of interest. Because these two time scales are so disparate, widely different types of models are required for the two alternatives.

Entrainment of Reactive Hydrocarbons (RHC). The importance of photochemistry within an effluent plume depends on the level of fresh reactive material (principally hydrocarbons) that is either in the plume or entrained by it. Since power plants, for example, do not emit significant levels of RHC, entrainment is the principal mechanism for introducing fresh reactive material into power plant plumes. This material may be transported from upwind, or it may be emitted from downwind sources passed over by the plume. The presence of fresh reactive material requires that the chosen model(s) be able to account for atmospheric photochemistry.

Availability of Boundary Conditions Information. Boundary conditions for a model can be estimated in one of two ways: they can be based on best-guess engineering judgment or determined through the use of another model by means of nesting or chaining. In practice, limitations on the availability of data may be such that there is no alternative to a best-guess estimation. However, when possible, and where sensitivity analyses indicate that model results are strongly sensitive to uncertainties in estimated values, generating boundary conditions through modeling should be considered.

Long Range Transport from Upwind. In certain areas of the country, like the urbanized northeastern United States, many point source sites are located downwind of large cities. Prevailing winds blow material from these cities considerable distances, thus contributing to the background pollutant levels in the ambient air into which the plume is injected. The proper design of a model nest or chain depends on the presence of absence of upwind transport.

Suitability of Trajectory-Type Modeling. In some areas, wind patterns are relatively simple in the vicinity of, and downwind from, the point source site. Such might be the case, for example, when no wind flow convergence or divergence is present. If in addition, downwind emissions are uniformly or homogeneously distributed, and if only short-distance, daytime transport is to be simulated, then a trajectory-type model might be considered for use in place of a broader scale model, such as a grid model. The use of a trajectory-type model may often be less costly.

The Decision Trees

Two sets of decision trees are employed here to associate air quality issues and types of NO_x models, one set for each attainment site designation (see Figures 2 and 3 for the first set and Figures 4 and 5 for the second). A major distinction is drawn between screening and the refined usage of models. A screening analysis is usually performed prior to undertaking a refined examination of a site. The primary purpose of the screening is to identify the need for further analysis. Thus, the models chosen for use must be conservative, that is, they must not indicate that there is no need for further study when, in fact, there is. In an attempt to ensure conservatism, it is typically assumed that all NO_x is either emitted as, or converted to, NO_2 before the plume reaches the ground. As a practical matter, such screening analyses may often suffice and a refined analysis would be conducted only when the screening indicated that a more precise examination of a plant's impact was warranted. Models employed for refined usage are generally more complex than are screening models, treating atmospheric processes with greater completeness, and therefore, their data needs, as well as their expense, are usually greater.

Several important qualifications apply to the decision trees:

> The decision trees consider only NO_2-related impacts and are specific to large point sources such as power plants. They should not be applied to other pollutants or to dissimilar types of sources.

> The decision trees apply only where the terrain and meteorology are simple or moderately complex. In highly complex terrain, model selection can be considerably more difficult, and in some cases may not be possible.

> The decision trees consider only general model classes, not specific model codes (that is, the individual computer programs actually used).

> The decisions to be made at each branch of the tree are qualitatively expressed. The advice of an experienced analyst may be required to make a final determination of the proper choice.

An Assessment of Current Needs in NO_x-Related Modeling

While there are certianly exceptions to their use, the decision trees in Figures 2 through 5 apply to many situations of practical interest that involve large, NO_x-emitting point sources. To the extent that these decision trees represent the range of possibilities, an important conclusion may be reached: For applications involving simple or moderately complex terrain or meteorology, types of models that appear suitable for use in most circumstances are currently available.

This conclusion suggests that attention should be turned to evaluating and improving current models rather than developing new models, except in areas where no adequate model exists. Specifically, the conclusion underscores the importance of 1) conducting a comprehensive program that would evaluate the performance of currently available models and would include the gathering of requisite observational data; and 2) sponsoring continuing efforts that would technically improve these models and provide a better understanding of their fundamental theoretical limitations. Technical improvements might be made in such areas as plume rise, dispersion characterization and atmospheric chemistry; an example of a limitation that should be recognized might include the breakdown of K-theory when used to represent near-source plume dispersion.

The decision trees also suggest that there are shortcomings in the capabilities of current models. Efforts toward development of new or better models, some of which are already underway, might focus on the following needs:

> A model capable of estimating long term NO_2 averages for refined analyses should be developed.

> Additional development of visibility models should be undertaken, with efforts focused on four key areas: The development of a plume visibility model for use when plume or ambient reactivity is important; a continuing attempt to develop improved regional visibility models; the development of visibility models for use in moderately to highly complex terrain; and the identification of screening methods for visibility analysis.

> The development of models for use in complex terrain should continue for both refined and screening usages.

Related to the decision trees, but not directly revealed by them, are other developmental needs:

> Models that overcome the limitations introduced by coupling (see the earlier discussion) should be developed to improve upon the concept of model nesting and chaining.

> Better screening models are needed to conduct the preliminary analyses that precede more refined analysis efforts.

> Model development should continue in supplementary areas, including sulfate and nitrate particulate formation, complex three-dimensional winds specification, inversion formation and destruction, acid rain, and surface deposition.

Acknowledgments

The author wishes to express his thanks to Dr. Philip M. Roth, whose insightful comments and constructive suggestions were most helpful.

References

1. D. B. Turner, "Workbook of Atmospheric Dispersion Estimates," AP-26, U.S. Environmental Protection Agency, Research Triangle Park, North Carolina, 1969.

2. M. A. Yocke, M. K. Liu, P. M. Roth, C. S. Burton, "An Examination of Candidate Methods for Predicting One-Hour-Average NO_2 Ground Level Concentrations Produced in Point Source Emissions," EF76-77, Systems Applications, Incorporated, for the U.S. Environmental Protection Agency, Research Triangle Park, North Carolina, 1976.

3. J. M. Hales, D. C. Powell, T. D. Fox, "STRAM--An Air Pollution Model Incorporating Nonlinear Chemistry, Variable Trajectories, and Plume Segment Diffusion," Contract 68-02-1982, Battelle Pacific Northwest Laboratories, for the U.S. Environmental Protection Agency, Research Triangle Park, North Carolina, 1977.

4. M. K. Liu, D. A. Stewart, P. M. Roth, "An Improved Version of the Reactive Plume Model (RPM-II)," NATO/CCMS Ninth International Technical Meeting on Air Pollution Modeling, Toronto, Canada, 1978.

5. M. K. Liu, et al., "The Development and Application of a Conjoint Model to Study Plume-City Interaction," to be submitted for publication, 1979.

6. D. A. Latimer, et al. "The Development of Mathematical Models for the Prediction of Anthropogenic Visibility Impairment," EF78-63A and B, Systems Applications, Incorporated, for the U.S. Environmental Protection Agency, Washington, D.C., 1978.

7. M. A. Yocke, "Techniques for Predicting Short Term Ground-Level Concentrations for Stationary Point Sources," EI79-92, Draft report, Systems Applications, Incorporated, for the U.S. Environmental Protection Agency, Research Triangle Park, North Carolina, 1979.

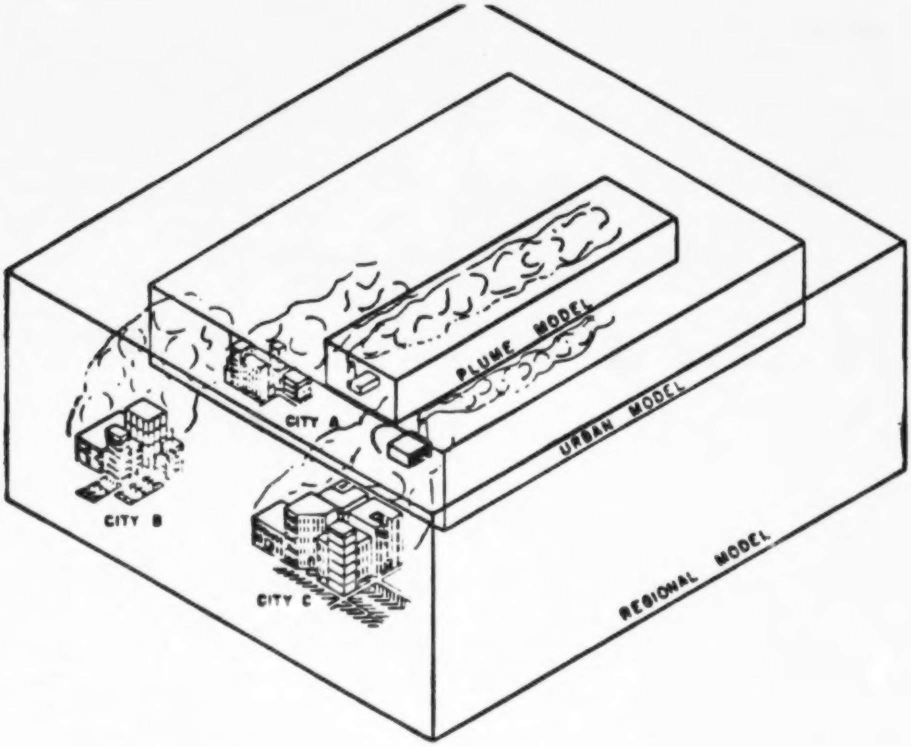
PLUME MODEL
URBAN MODEL
REGIONAL MODEL
CITY A
CITY B
CITY C

Figure 1. Relationship of Nested Plume Model, Urban Model, and Regional Model (Power Plant Construction in an Urban Area).

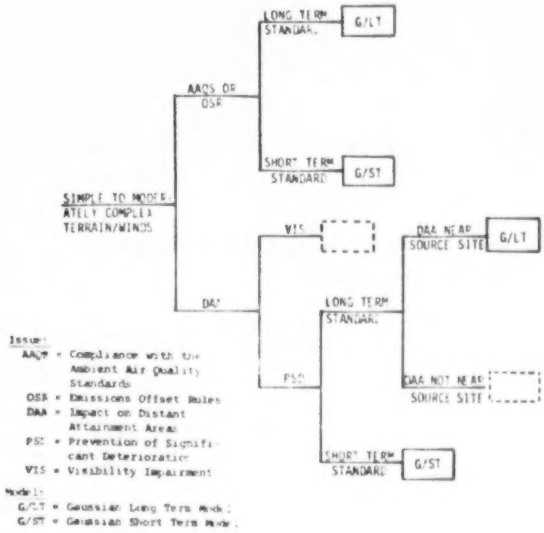
LONG TERM STANDARD
G/LT
AAQS OR OSR
SHORT TERM STANDARD
G/ST
SIMPLE TO MODERATELY COMPLEX TERRAIN/WINDS
VIS
DAA NEAR SOURCE SITE
G/LT
DAA
LONG TERM STANDARD
PSD
DAA NOT NEAR SOURCE SITE
SHORT TERM STANDARD
G/ST
Issues
AAQS = Compliance with the Ambient Air Quality Standards
OSR = Emissions Offset Rules
DAA = Impact on Distant Attainment Areas
PSD = Prevention of Significant Deterioration
VIS = Visibility Impairment
Models
G/LT = Gaussian Long Term Model
G/ST = Gaussian Short Term Model

Figure 2. Decision Trees for Screening Usage in Nonattainment Areas.

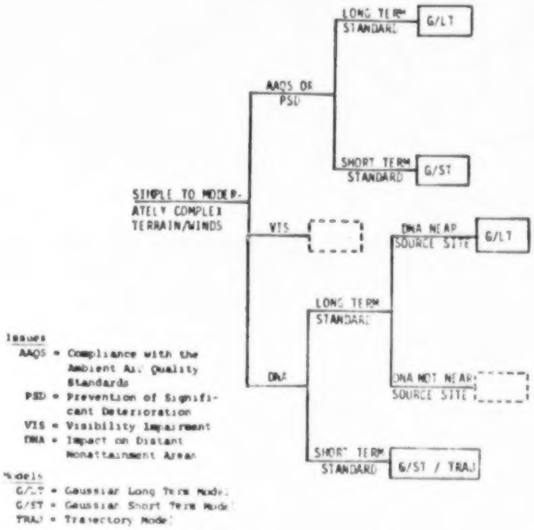
LONG TERM STANDARD
G/LT
AAQS OR PSD
SHORT TERM STANDARD
G/ST
SIMPLE TO MODERATELY COMPLEX TERRAIN/WINDS
VIS
DNA NEAR SOURCE SITE
G/LT
LONG TERM STANDARD
DNA
DNA NOT NEAR SOURCE SITE
SHORT TERM STANDARD
G/ST / TRAJ
Issues
AAQS = Compliance with the Ambient Air Quality Standards
PSD = Prevention of Significant Deterioration
VIS = Visibility Impairment
DNA = Impact on Distant Nonattainment Areas
Models
G/LT = Gaussian Long Term Model
G/ST = Gaussian Short Term Model
TRAJ = Trajectory Model

Figure 3. Decision Trees for Screening Usage in Attainment Areas.

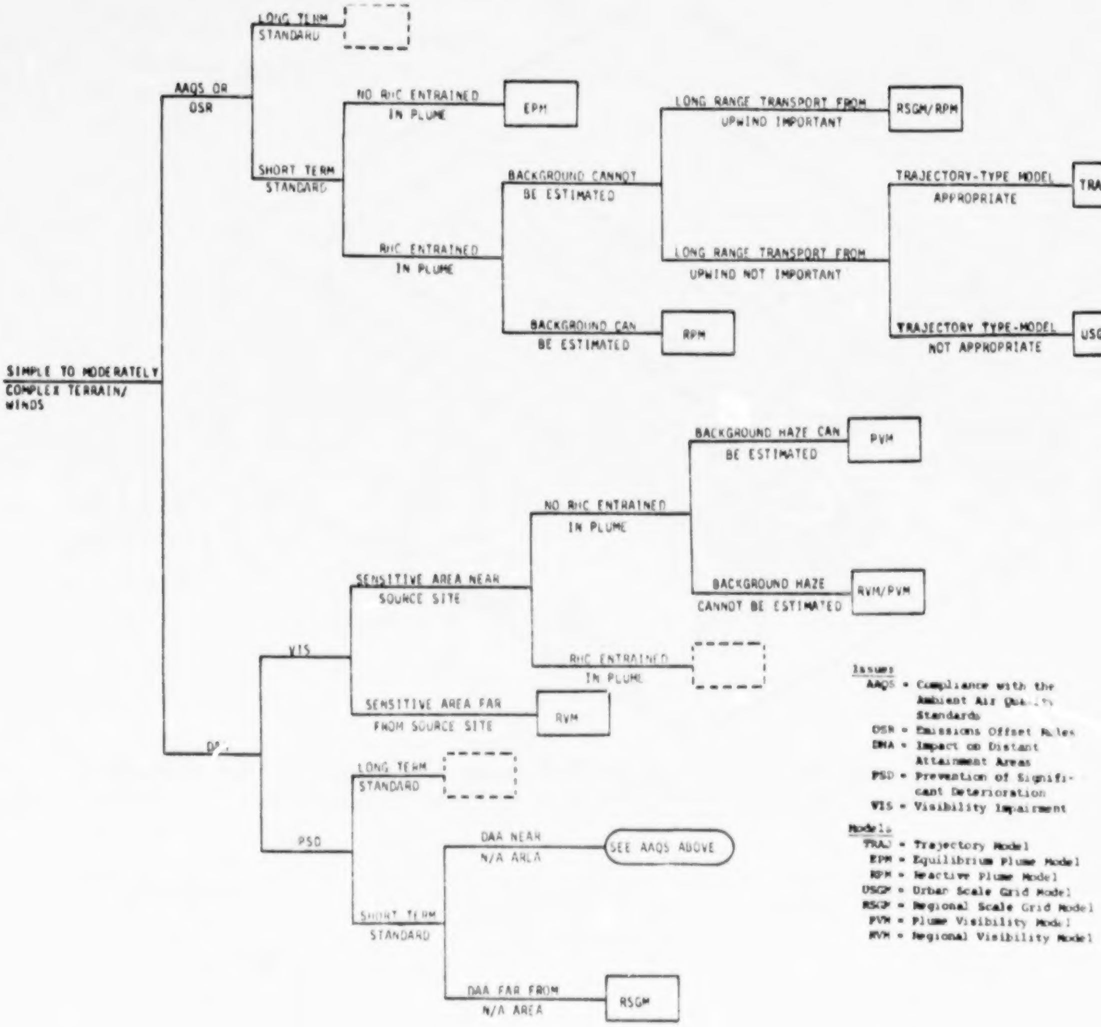
SIMPLE TO MODERATELY COMPLEX TERRAIN/ WINDS
AAQS OR OSR
LONG TERM STANDARD
SHORT TERM STANDARD
NO RHC ENTRAINED IN PLUME
EPM
RHC ENTRAINED IN PLUME
BACKGROUND CANNOT BE ESTIMATED
BACKGROUND CAN BE ESTIMATED
RPM
LONG RANGE TRANSPORT FROM UPWIND IMPORTANT
RSGM/RPM
LONG RANGE TRANSPORT FROM UPWIND NOT IMPORTANT
TRAJECTORY-TYPE MODEL APPROPRIATE
TRAJ/RPM
TRAJECTORY TYPE-MODEL NOT APPROPRIATE
USGM/RPM
DAA
VIS
SENSITIVE AREA NEAR SOURCE SITE
NO RHC ENTRAINED IN PLUME
BACKGROUND HAZE CAN BE ESTIMATED
PVM
BACKGROUND HAZE CANNOT BE ESTIMATED
RVM/PVM
RHC ENTRAINED IN PLUME
SENSITIVE AREA FAR FROM SOURCE SITE
RVM
PSD
LONG TERM STANDARD
SHORT TERM STANDARD
DAA NEAR N/A AREA
SEE AAQS ABOVE
DAA FAR FROM N/A AREA
RSGM
Issues
AAQS = Compliance with the Ambient Air Quality Standards
OSR = Emissions Offset Rules
DAA = Impact on Distant Attainment Areas
PSD = Prevention of Significant Deterioration
VIS = Visibility Impairment
Models
TRAJ = Trajectory Model
EPM = Equilibrium Plume Model
RPM = Reactive Plume Model
USGM = Urban Scale Grid Model
RSGM = Regional Scale Grid Model
PVM = Plume Visibility Model
RVM = Regional Visibility Model

Figure 4. Decision Tree for the Refined Usage of Models in Assessing The Impacts of Large Point Sources of NO_x Sited in Nonattainment Areas.

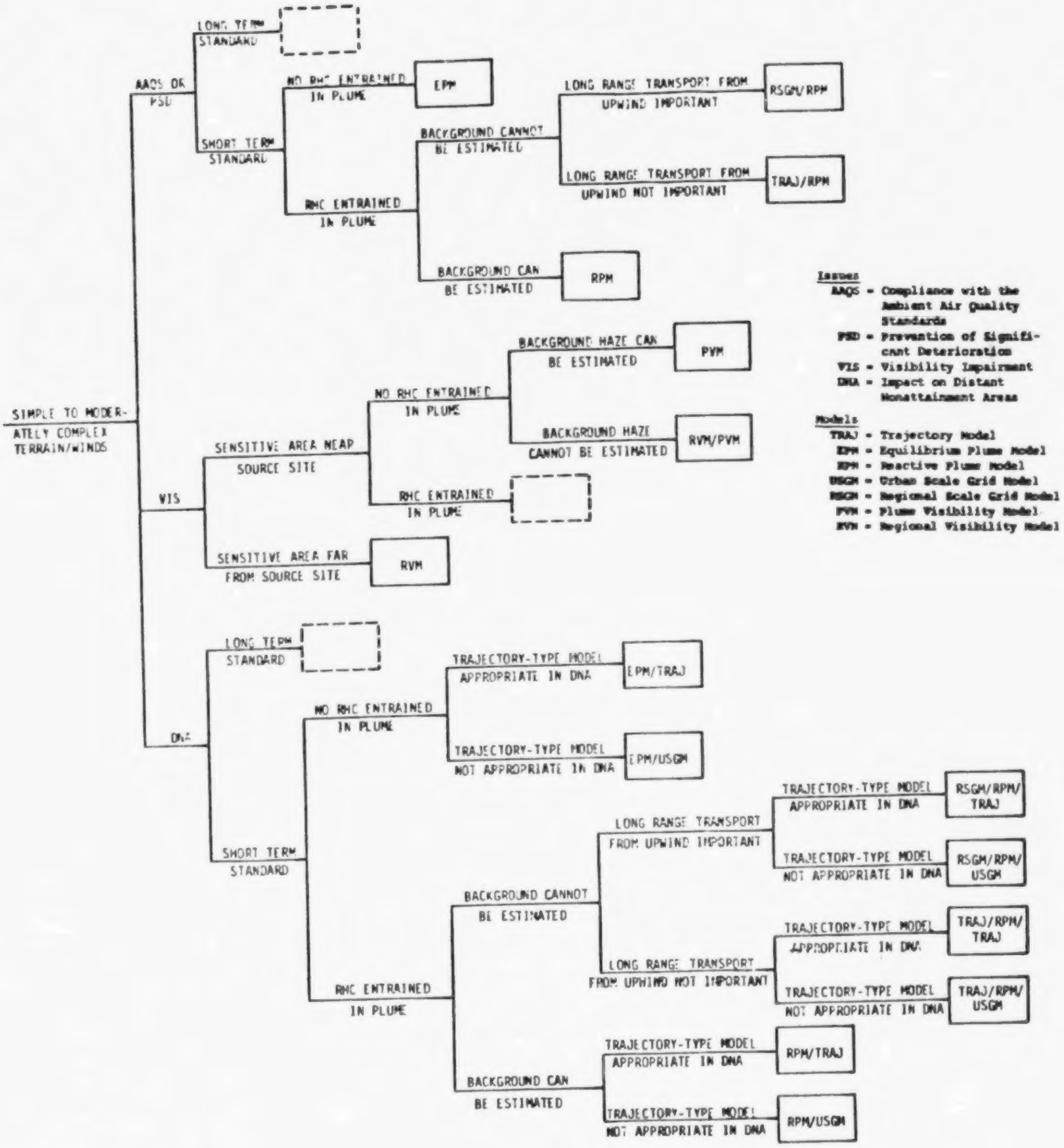
SIMPLE TO MODERATELY COMPLEX TERRAIN/WINDS
AAQS OR PSD
LONG TERM STANDARD
SHORT TERM STANDARD
NO RHC ENTRAINED IN PLUME
EPM
RHC ENTRAINED IN PLUME
BACKGROUND CANNOT BE ESTIMATED
LONG RANGE TRANSPORT FROM UPWIND IMPORTANT
RSGM/RPM
LONG RANGE TRANSPORT FROM UPWIND NOT IMPORTANT
TRAJ/RPM
BACKGROUND CAN BE ESTIMATED
RPM
VIS
SENSITIVE AREA NEAR SOURCE SITE
NO RHC ENTRAINED IN PLUME
BACKGROUND HAZE CAN BE ESTIMATED
PVM
BACKGROUND HAZE CANNOT BE ESTIMATED
RVM/PVM
RHC ENTRAINED IN PLUME
SENSITIVE AREA FAR FROM SOURCE SITE
RVM
DNA
LONG TERM STANDARD
SHORT TERM STANDARD
NO RHC ENTRAINED IN PLUME
TRAJECTORY-TYPE MODEL APPROPRIATE IN DNA
EPM/TRAJ
TRAJECTORY-TYPE MODEL NOT APPROPRIATE IN DNA
EPM/USGM
RHC ENTRAINED IN PLUME
BACKGROUND CANNOT BE ESTIMATED
LONG RANGE TRANSPORT FROM UPWIND IMPORTANT
TRAJECTORY-TYPE MODEL APPROPRIATE IN DNA
RSGM/RPM/TRAJ
TRAJECTORY-TYPE MODEL NOT APPROPRIATE IN DNA
RSGM/RPM/USGM
LONG RANGE TRANSPORT FROM UPWIND NOT IMPORTANT
TRAJECTORY-TYPE MODEL APPROPRIATE IN DNA
TRAJ/RPM/TRAJ
TRAJECTORY-TYPE MODEL NOT APPROPRIATE IN DNA
TRAJ/RPM/USGM
BACKGROUND CAN BE ESTIMATED
TRAJECTORY-TYPE MODEL APPROPRIATE IN DNA
RPM/TRAJ
TRAJECTORY-TYPE MODEL NOT APPROPRIATE IN DNA
RPM/USGM
Issues
AAQS = Compliance with the Ambient Air Quality Standards
PSD = Prevention of Significant Deterioration
VIS = Visibility Impairment
DNA = Impact on Distant Nonattainment Areas
Models
TRAJ = Trajectory Model
EPM = Equilibrium Plume Model
RPM = Reactive Plume Model
USGM = Urban Scale Grid Model
RSGM = Regional Scale Grid Model
PVM = Plume Visibility Model
RVM = Regional Visibility Model

Figure 5. Decision Tree for the Refined Usage of Models in Assessing the Impacts of Large Point Sources of NO_x Sited in Attainment Areas.

Table 1. APPROXIMATE COSTS OF APPLYING DIFFERENT NO_2 AND VISIBILITY MODELS

Model Type	Typical Cost Range for Input Data Preparation (per simulation)	Typical Cost Range for Actual Computing (per simulation)	Total Cost Range for Typical Project	Typical Project Duration
Class I models:				
Gaussian Short-Term Model (G/ST)	$ 100-2,000	$ 0-100	$ 500-10,000	1 week - 3 months
Gaussian Long-Term Model (G/LT)				
Equilibrium Plume Model (EPM)				
Class II models:				
Plume Visibility Model (PVM)	500-4,000	25-100	5,000-50,000	1 month - 6 years
Trajectory Model (TRAJ)*				
Reactive Plume Model (RPM)*				
Class III models:				
Urban Scale Grid Model (USGM)†	50,000-400,000	500-2,000	50,000-500,000	3 months - 2 years
Regional Scale Grid Model (RSGM)†				
Regional Visibility Model (RVM)†				
Class IV models:				
Conjoint Models† (Two-tiered model chain employing a reactive plume model to drive an urban scale grid model--RPM/USGM)	50,000-400,000	500-2,500	50,000-500,000	6 months - 2 years

---

Adapted from: Yocke, (1979)[8]

* One simulation--along 6 hour trajectory pathway

† One simulation--24 hours long

Discussion:

Hübschmann:

I found your point that visibility is the subject of legislation an interesting one. I think it would be difficult to trace a reduction in visibility back to the source of pollution. How do you propose that this should be done, since meteorological factors will combine with the emission to reduce visibility?

Hayes (response):

This is true. But in a number of circumstances, for example in dry areas where the air is very clear, it is possible. The motivation for visibility legislation came from legislators for those areas who were concerned to maintain the natural vistas of regions. In Eastern US, there would undoubtedly be difficulties due to meteorological factors which influence visibility.

THE CURRENT ROLE OF TALL STACKS IN THE UNITED STATES

TECHNOLOGY VERSUS POLITICS

by

Maynard E. Smith, President
Meteorological Evaluation Services, Inc.
Amityville, New York, USA

Abstract

After two decades of intensive study and development of tall-stack technology, the United States is now systematically denying itself the advantages of such stacks by refusing to recognize their existence in regulatory proceedings, and by ignoring ambient monitoring data. Analysis of these governmental procedures has revealed a number of interesting and important deficiencies in the management and diffusion modeling of tall-stack sources. These are examined, and suggestions are made for avoiding these regulatory inconsistencies. The most important remedy would be to match the procedures to the goals.

Introduction

In 1966, at the Third National Conference on Air Pollution in the United States, I presented a survey paper on the advantages and disadvantages of tall stacks. In the opening sentence of that paper[1], I said:

> *"In the past fifteen years the high stack has become almost symbolic of good industrial air pollution practice, and its use as an effective and economical device for reducing ground-level air pollution has become widespread."*

In that same paper, after recounting an extensive list of positive benefits associated with dispersion from tall stacks, I also noted that:

> *"The fact of the matter is, of course, that stacks possess no magic power to eliminate a pollutant. They do not reduce by one gram the total amount of pollutant released to the atmosphere."*

Preceding page blank

I had no way of knowing at that time that the two viewpoints presented in these quotations would become the focus of a serious controversy. For in the succeeding ten years, industry and the electric utilities continued to see the tall stack as the most practical and economical means of alleviating undesirable local ground-level pollutant concentrations, while some U.S. regulatory agencies, particularly the Federal Environmental Protection Agency (EPA), became firmly opposed to tall stacks because they do not reduce the overall pollutant burden in the atmosphere.

EPA, anxious to reduce emissions but apparently unable to prove that serious health effects were associated with low concentrations of various pollutants, chose to downgrade the importance of tall stacks. The Agency has succeeded, to the point at which the United States now has regulatory procedures which virtually ignore the existence of such stacks. In my view, this has led to a truly incredible regulatory mess, in which excellent technology is being ignored in favor of unrealistic, complex, immensely costly, and unfair procedures.

It is important to say that my reason for presenting criticisms of our regulatory system to this international audience is not an attempt to carry an internal American problem to a larger forum. I am aware that many of the European countries, individually and collectively, are facing similar regulatory problems, and I sincerely hope that this presentation may influence others to avoid duplication of American mistakes.

I also admit that there may be valid reasons for reducing the overall level of emissions of some pollutants. We know that the Canadians would be happy to see a reduction of U.S. SO_2 emissions, and the Scandinavians have made it clear that they would prefer similar reductions from their industrial neighbors to the west and south. The United States is trying to accomplish such reductions for completely new sources with the New Source Performance Standards, but its treatment of older sources is difficult to understand.

U.S. Regulatory System Involving Tall Stacks

It is impossible in this short presentation to review all of the details of the individual U.S. regulatory documents pertaining to this problem. Instead I shall simply list them and then summarize the key provisions. Beginning in 1970 with the Clean Air Act[2], the United States has developed a series of rules relating to tall stacks and their use. The most important of these are the 1977 Amendments to the Clean Air Act[3], the regulations for the Prevention of Significant Deterioration[4,5], the diffusion modeling guideline[6], the proposed "good engineering practice" regulation[7], and the technical support document explaining how fluid modeling tests should be developed[8].

The important provisions of these documents are not apparent to the casual reader; one must actually apply them to specific cases to understand their implications. However, I have tried to summarize the key points below.

GEP Stack Height

A stack height greater than that given by a simple downwash formula (similar to the 2-1/2 times building height rule) may not be used in analyzing the concentrations derived from any new or altered source. This is the so-called good engineering practice (GEP) stack height rule. It means, for example, that a stack having an actual height of 300 meters may be treated in diffusion calculations as though it were only 125 meters high.

Downwash and Fluid Modeling

Stacks higher than GEP in the above definition may be used in diffusion calculations, but only after an elaborate fluid modeling or field study has proven that a greater height is needed to offset adverse aerodynamic effects produced by the terrain or by building structures.

Diffusion Modeling

Diffusion modeling is established as the sole method of determining the suitability and emission limitations for either a new or altered source, often using fictitious stack heights as defined above. A specific set of EPA diffusion models is "recommended" for these evaluations, which means that they must be used unless an elaborate proof is offered of the validity of some other model.

Multiple Sources

In regulatory analyses, not only the source in question, but other sources in the area are modeled in a multi-source computer program as though they had GEP stacks. These analyses may therefore contain a strange mixture of actual stack heights and artificially short stack heights. The results of these calculations are to be carried forward into future analyses.

Air Quality Data

Air quality data are officially recognized as important in tempering the results of modeling, but in practice the field data are ignored completely in most cases.

Consequences of the System

The result of this multiplicity of regulations is a system which effectively denies the technological advantages of the tall stack, and creates almost unbelievable inaccuracy and confusion in its application. The typical industrial applicant has almost no idea what the regulations mean, nor does he know how to apply them. He may also find that he is treated quite differently in terms of the solution of his problem depending upon which side of a regional boundary his plant may fall. Specifically, the system has the following drawbacks:

Conservatism

The official diffusion models are conservative, especially when used to represent tall stacks. The models typically overpredict the maximum short-term concentrations by factors of 2 to 3, even when actual tall stacks are modeled. In extreme cases, one of the models may overpredict by a factor of 100. This conservatism is greatly compounded when the fictitious, short, GEP stack heights are used in a multisource evaluation.

Furthermore, the problems will become worse as unrealistic concentration estimates for new facilities in each region are added to the unrealistic predictions already documented for earlier construction. The conservatism and other weaknesses of the EPA models have been documented in two papers by Smith and his associates[9,10].

Inconsistencies

As Martin[11] has pointed out, the current EPA models are inconsistent among themselves, one model giving concentration estimates quite different from another when applied to the same problem. These inconsistencies are further complicated by different applications by the various regional offices of EPA.

Inflexibility

The system has already become remarkably inflexible. It is very difficult, for example, to induce EPA to temper its conclusions on the basis of monitoring data. The typical retort on the part of the Agency is that the data were not taken in the right places, or at the right times, or that they were not of acceptable quality.

Exhorbitant Cost

Despite the fact that the United States is disturbed about monetary inflation, there seems to be little concern or even appreciation of the enormous costs involved in this regulatory program. Although I cannot possibly provide you with accurate estimates of the legal, engineering and equipment costs involved in meeting the requirements, I can give you realistic estimates of the meteorological evaluations which are required. An air quality analysis of a new facility for three pollutants, sulfur dioxide, suspended particulates and nitrogen oxides, would cost a prospective client approximately $300,000. This price would include the computer calculations, preconstruction pollution monitoring, meteorological analysis, meetings and hearings, as well as review of the study by an independent "third party." If the study should require fluid modeling to obtain credit for a taller stack in rough terrain, the total cost could reach $800,000.

Injustice

Because of the complexity and cost of the procedures, the small industrial or utility applicant is penalized to the point at which he often cannot afford to make additions or changes to his facility. Consider, for example, the small company requiring approval for a new stack having a construction price of $500,000. If this facility should be in rough terrain, he would have to spend $1,300,000 to obtain credit for his stack and build it.

Recommendations

It is always easier to criticize than to organize and administrate, but it seems to me that the types of problems created by the American system of air pollution regulation could be remedied by a little clear thinking.

The most important problem, by far, involves matching the procedures to the goals. In the U.S. system, we are trying to achieve reduction of overall emissions, presumably to eliminate long range effects on other regions and countries. For new sources, we are insisting on direct reduction of emissions. For older sources, however, we are obviously trying to achieve goals of regional and international significance by using regulations dealing with short-term, local concentrations. If one can prove the necessity for limiting overall emissions because of acid rainfall or other large-scale effects, one should establish achievable emission limitations by a direct process. If local concentrations are actually the problem, one does not need very expensive studies to establish proper stack heights.

Second, in our assessment of goals we should avoid what Comar[12] has called "bad science." The tendency to draw hard conclusions from inadequate data, and to base regulatory policies and procedures on such conclusions, is much too widespread. It would be far better to direct some of the countless millions of dollars now wasted on misguided regulatory procedures into improving scientific understanding of long range transport and atmospheric chemistry.

Third, it is ridiculous to establish a regulatory system based entirely on diffusion modeling, especially when fictitious stacks are used. I have been personally involved in model development for many years, and I know the weaknesses of models; so does this audience, I am sure.

Air quality data should always be used as the primary guide, with modeling as an aid in filling out the details. Where a model clearly predicts values different from those observed, the model should be suspect, not just the data.

Fourth, regulatory procedures should be as simple as possible, not made deliberately complex. In a recent criticism[13] of the U.S. guideline on the application of fluid modeling to derive GEP stack heights, my colleagues and I described the procedures as "an excellent outline for a doctoral dissertation"... "far beyond the financial and technical reach of a large number of applicants..." This certainly should not be true of a practical regulation. Regulations must be reasonable and simple. If not, they will either fail, or become embroiled in endless litigation, as has happened in the United States.

References

1. Smith M.E., "Reduction of Ambient Air Concentrations of Pollutants by Dispersion From High Stacks", Proceedings, Third National Conference on Air Pollution, Washington, D.C., 1966.
2. U.S. Congress, "Clean Air Act", Public Law 74-70, 1970.
3. U.S. Congress, "Clean Air Act Amendments of 1977", Public Law 95-95, 91 Stat 685, 1977.
4. U.S. Environmental Protection Agency, "Prevention of Significant Deterioration", 40 CFR 52.21, 1977.
5. U.S. Environmental Protection Agency, "Prevention of Significant Deterioration, Proposed Rules", FRL 981-2, 1979.
6. U.S. Environmental Protection Agency, "Interim Guideline on Air Quality Models", U.S. EPA OAQPS No 1.2-080, 1977.
7. U.S. Environmental Protection Agency, "1977 Clean Air Act Amendments for Stack Heights, Proposed Regulatory Revisions", 40 CFR 51, 1979.
8. U.S. Environmental Protection Agency, "Draft Guideline For Use of Fluid Modeling to Determine Good Engineering Practice Stack Height", EPA-450/4-79-015, 1979.
9. Smith M.E., Martin J.R., Kramer M.L., Calby R.H., Butler M.J., "Review of the EPA CRSTER Diffusion Model", Journal, American Institute of Chemical Engineering, (in press).

10. Smith M.E., Kramer M.L., Martin J.R., "Comments on FRL 1053-7, Reconsideration of the Use of Pasquill-Gifford Dispersion Coefficients for Stability Class A in Setting Emission Limitations for Four Ohio Power Plants," Meteorological Evaluation Services, Inc., 1979.

11. Martin J.R., "Critical Inconsistencies Between the Official U.S. EPA Rural Versions of the CRSTER and RAM Diffusion Models, Presented, Air Pollution Control Association, 1979.

12. Comar C., "Bad Science and Social Penalties," Science, V. 200, No. 4347, 1978.

13. Smith M.E., Kramer M.L., Dupuis L.R., "Comments on Draft Guideline for Use of Fluid Modeling to Determine Good Engineering Practice Stack Height," Meteorological Evaluation Services, Inc., 1979.

Discussion:
(Rapporteur: McQuaid):

Holzworth:

Mr. Chairman: I would like to make a statement. We in the US-EPA are pleased to have the comments of Mr. Smith for we recognize that some scientific aspects of our air pollution control regulations are in need of refinements. But I believe we should view the level of science in air pollution control today in perspective of the progress that has been made. When air pollution controls were just beginning in the US, 25 - 30 years ago, it was by the jurisdiction of individual communities and there was great diversity in the approaches that were used. That range of variability may be viewed as the base of a pyramid, which at the present time is coming somewhere towards the top point of the pyramid. Obviously, there is yet some ways to go. Both within and outside the EPA we are striving for valid scientific methodologies. And the EPA has large research projects underway. I should like to point out also that while some groups feel strongly that the regulations are not severe enough. I thank you.

Smith (response):

I agree, of course, that there is great diversity of opinion about the necessity for severe emission restrictions, and it may well be that there is need for restrictions more severe than the present regulations require. My concern is more with the use of very complex procedures to achieve the results.

Tikvart:

Two points should be clarified. One is that the use of air quality data has not been replaced by models. Models must be used to determine what air quality increment will be used by a new source. Since the source does not yet exist, no air quality data is available for this purpose. Thus only a model can be used.

Tikvart (continue):

The second point concerns the Valley Model.
This model attempts to mathematically simulate the impact of a plume on elevated terrain features as was demonstrated by Dr. Liu in water channel experiments. The model has been shown to estimate concentrations quite well in some circumstances. Thus there is no basis for contentions made by some that this model systematically overestimates concentrations.

Venkatram:

Could you elaborate on the use of air quality data rather than modeling in the formulation of regulations?

Smith (response):

One can always say that data for any particular area are inadequate. But it has been the practice in the United States to assume that models are always accurate in preference to data; I strongly object to this. Take, for example, the VALLEY model. At a particular source in Utah, the VALLEY model predicted very high concentrations of SO_2. However, monitoring stations set up at these receptor points showed that the model was inaccurate by a factor of 100.

Hübschmann:

I agree with your general statements relating to tall stacks. I would stress the fact that in Europe this is an international problem and action will have to be formulated on an international basis.

Smith (response):

I agree.

SENSITIVITY OF MODEL CALCULATIONS ON THE METEOROLOGICAL DATA AND ITS RELEVANCE TO REGULATORY ASPECTS[+)]

by

Lothar Kropp and Wolfram Bahmann
Technischer Überwachungs-Verein Rheinland
Köln, Federal Republic of Germany

Abstract. The German regulations to perform air quality simulations ask for joint frequency distributions over periods of several years. A daily or monthly or seasonal variation of the meteorological data is not taken into account. This paper investigates the influence of these effects.

Due to the choice of joint frequency distributions

- over 1, 5, 10 or 20 years model calculation results may deviate by about 20 %,
- for the whole year, for the seasons or the months model calculation results may differ by 70 % (seasons) or even 130 % (months) against the annual values,
- for day or night time the differences in the results may be more than a factor of 2.

Further to this investigation the significance with respect to licensing procedures is discussed.

Introduction

The German air quality policy asks for measurements of the actual air quality situation on the one hand and for air pollution simulation calculations on the other in order to develop measures for the reduction of air pollution caused by existing or new sources of pollutants.

Within the licensing procedure comprehensive air quality forecasts are requested, i. e. (1) a determination of the actual situation, (2) a simulation of expected additional air pollution due to new plants or plant parts and (3) a superposition of measured basic load (1) and calculated pollution increase (2).

Clean air plans which have to be established for polluted areas request (1) also a determination of the actual air quality situation, (2) an analysis of the main sources responsible for the air pollution being present, (3) measures to reduce air pollution

---

+) The investigations were financially supported by the Umweltbundesamt, Berlin.

Preceding page blank

and (4) the calculation of the future air quality situation if all measures were performed as a simulation of the expectable success.

The German regulations /1,2/ in general ask for measurements during a time period of one year; however, this time period can be reduced to only two months when conclusions with respect to the annual air pollution situation can be drawn i. e. either the air pollution situation is not subject to seasonal changes or these changes can be estimated via calculations. Furthermore, the measurements are mostly performed during the day times (esp. working hours) only.

In order to decide upon the possibility of performing such conclusions it was investigated how the calculated concentration pattern and the representative concentration data are influenced by the choice of the frequency distributions of joint meteorological data (wind direction, wind speed and turbulence situation). In detail, the influence of meteorological turbulence statistics for different time periods (1, 5, 10 and 20 years), for different seasons and months and for different day times (day and night time statistics) was analysed.

Model Calculations

The investigations were performed employing the Gaußian plume model with the following parameters:
- dispersion parameters of Singer and Smith /3/,
- plume rise formula of Moses and Carson (neutral) /4/,
- turbulence classification of Klug and Manier /5/,
- meteorological statistics of the Düsseldorf and Köln airports,

and the following source data:

source height	100 m	flue gas flow	365000 m^3/h
source strength	270 kg/h	flue gas exit speed	15 m/s
operating time	8760 h/a	flue gas temperature	140 °C

The results of the air quality calculations are given as average concentration values and as 95-percent sum frequency concentration values (95-percentiles).

The intention of the calculations was to outline relative changes of the ground level concentrations; therefore no verification taking into account measurements was tried.

Model Results

1-, 5-, 10-, 20-Years Statistics

Model calculations were performed for the joint meteorological statistics of the Düsseldorf airport taken during the following time periods: one year period 1965
five years period 1962 - 66

ten years periods 1951 - 60 and 1961 - 70
twenty years period 1951 - 70.

The calculated concentration patterns for the different averaging time periods are displayed in figs. 1 (average concentrations) and 2 (95-percentiles). The shaded areas represent the concentration values for the ten years period of 1951 - 60 which is normally used as reference time period in Germany. The dashed curves reflect the results for the corresponding other time periods.

Slight changes in the patterns for the different time periods are perceptible. The maximum displacements against the standard time period 1951 - 60 of the e. g. 2 μg/m³ isolines in the case of the average concentrations and of the 10 μg/m³ isolines of the 95-percentiles are about 2 to 2,5 kilometers.

The relative changes of the concentration values at the maxima north-west and east of the source are given in table 1.

If the highest concentration values for the standard time period 1951 - 60 are set 100 % the highest average concentrations of the other time periods correspond to 93 to 100 % and the 95-percentiles are between 86 and 95 % whereby the location of the maximum shifts from NW to E of the source. Setting the highest concentration values of the 20 years time period as 100 % the concentrations of the other time periods amount to 100 up to 107 % for the average values and from 100 to 116 % for the 95-percentiles.

The following conclusion can be drawn from this investigation:

Taking into account the overall uncertainty of dispersion model calculations the use of the standard time period 1951 - 60 seems acceptable for air pollution simulations within licensing procedures. However, for analyses of the main source within clean air plans the use of the same time period as of the measurements (mostly a one year period) is strongly recommended.

Annual, Seasonal and Monthly Statistics

Air quality model calculations were performed for the joint meteorological statistics of the Köln/Bonn airport which were collected during the time period of 1951 - 60 and evaluated for the whole year, for the four seasons and for the twelve months.

The results of the calculations for the year and the seasons are displayed in figs. 3 and 4 as average concentration values (fig. 3) and 95-percentiles (fig. 4). The concentration patterns differ strongly from season to season (except fall and winter) and against the annual values. In summer a dominant maximum arises east of the source, while in fall and winter the dominant maximum is north-west of the source.

The highest values of average concentrations and 95-percentiles for the different seasons are summarized in table 2. These results show the following characteristics for the Köln meteorological statistics in comparison to the annual values: (a) significant higher fall and winter values NW of the source (130 to 150 %), (b) much higher summer values east of the source (160 to 170 %).

The following conclusion may be drawn form these results:

If the air quality situation is determined (measured or calculated) during the seasons, only, the average concentrations as well as the 95-percentile values may be overestimated with respect to the annual concentration values at certain locations around the source. Within licensing procedures that would mean a too conservative judgement. Within clean air plan procedures of analysing relevant pollution sources, however, the evaluation may lead to incorrect consequenses.

Further to the seasonal averaging monthly evaluations were done for the 1951 - 60 time period. The annual dependence of average concentrations and the 95-percentiles are displayed in fig. 5. The aforementioned results for the seasons can be seen from this graph, too. The solid lines represent the highest values NW of the source and the dashed lines those for the maximum in the east. As is to be expected the monthly values show a much stronger dependence than the seasonal values: (a) 50 % higher average concentrations in november and december NW of the source than the annual average, (b) 70 to 80 % higher average concentrations in june and july east of the source and (c) twice as high 95-percentiles in november NW and in july E of the source than the annual 95-percentiles.

The graph reflects the significant meteorological situation of the Köln area, i. e. westerly winds during spring and summer and dominant south-easterly winds in fall and winter.

As a conclusion it can be outlined:

Though the investigation was performed for the Köln area, only, a judgement of the annual concentration values (averages or 95-percentiles) does not seem possible from monthly determinations (calculations as well as measurements).

Day and Night Time Statistics

Air quality model calculations were performed for day time and night time meteorological statistics of the Köln/Bonn airport during a period of 10 years (1951 - 60).

The corresponding results displayed in figs. 6 and 7 show strong differences in the day and night time concentration patterns and their absolute values (see table 3): (a) the dominant maximum of the annual averages and the 95-percentiles are NW of the source, (b) the values of day time averages and day time 95-percentiles are generally higher than the annual values with as high maxima NW and E of the source and (c) the maximum night time values are half as high as the maximum day time average concentration or even only 40 % of the day-time 95-percentile.

The conclusion to be deduced from these results should be:

Calculations performed for the whole day joint meteorological statistic i. e. for 8760 hours per year will significantly differ from corresponding measurements of the same pollutant performed only during the day time hours (e. g. normal working hours). Such measurements thus being done for licensing procedures as well as for clean air plans may therefore lead to wrong statements.

Conclusion

Though this investigation was performed for only one source, one meteorological site and via model calculations, only, a judgement on the annual air quality situation on the basis of seasonal measurements during day time seems possible. However, a thorough and comprehensive calculation would be necessary, i. e. an extrapolation of the - say for instance - day time measurements during a few months. Further investigations for an ensemble of several sources is necessary. If the results tend to be similar, it is much more recommended - as it is mentioned in the new draft /5/ of the German regulation - "the technical guideline for assessing air quality", to perform measurements at all hours of the day, at all days of the week and at all seasons.

References

/1/ Bundesminister des Innern (BMI), Technische Anleitung zur Reinhaltung der Luft (TAL) vom 28.08.1974, GMBL Nr. 24 (1974) 425.

/2/ Bundesminister des Innern (BMI) 4. BImSchVwV Ermittlung von Immissionen in Belastungsgebieten (Determination of Air Quality in Loaded Areas) 08.04.1975.

/3/ Cited in Minister für Arbeit, Gesundheit und Soziales (MAGS), RdErl. III B4/III B6 - 8856.4 (III Nr. 13/1975) vom 14.04.1975.

/4/ H. Moses, G. H. Strom, J. E. Carson, Effects of Meteorological and Engineering Factors on Stack Plume Rise, Nucl. Safety 6 (1971) 1.

/5/ Bundesratsdrucksache 420/78 vom 08.09.1978 Entwurf der Techn. Anleitung zur Reinhaltung der Luft (Draft of the Guideline for Assessment of the Air Quality).

Table 1: Results for different time periods (1 - 20 years averages)

Time period	Average wind speed m/s	Average concentration				95-percentile			
		1		2		1		2	
		µg/m³	%	µg/m³	%	µg/m³	%	µg/m³	%
1 year (1965) +)	3,9	2,5	86	2,9	100	17	77	21	95
5 years (1962 - 66) +)	3,8	2,4	83	2,8	97	15	68	20	91
10 years (1961 - 70) +)	3,8	2,4	83	2,8	97	16	73	19	86
10 years (1951 - 60) +)	3,8	2,9	100	2,6	90	22	100	18	82
20 years (1951 - 70) +)	3,8	2,6	90	2,7	93	19	86	19	86
1 year (1965) ++)	3,9	2,5	93	2,9	107	17	89	21	110
5 years (1962 - 66) ++)	3,8	2,4	89	2,8	104	15	79	20	105
10 years (1961 - 70) ++)	3,8	2,4	89	2,8	104	16	84	19	100
10 years (1951 - 60) ++)	3,8	2,9	107	2,6	96	22	116	18	95
20 years (1951 - 70) ++)	3,8	2,6	96	2,7	100	19	100	19	100

+) (1951 - 60) values set as 100 %

++) (1951 - 70) values set as 100 %

1 = maximum NW of the source

2 = maximum E of the source

Table 2: Results for different seasons (time period 1951 - 60)

Season	Average wind speed m/s	Average concentration				95-percentile			
		1		2		1		2	
		µg/m³	%	µg/m³	%	µg/m³	%	µg/m³	%
years	3,2	2,7	100	2,3	87	19	100	12	61
spring	3,3	2,3	87	2,6	98	13	68	17	90
summer	2,7	2,5	94	4,3	160	11	58	33	170
fall	3,0	3,3	125	1,8	68	27	142	5	26
winter	3,7	3,4	130	1,8	68	28	147	3	16

1 = maximum NW of the source

2 = maximum E of the source

Table 3: Results for different day times (time period 1951 - 60)

Time	Average wind speed m/s	Average concentration				95-percentile			
		1		2		1		2	
		µg/m³	%	µg/m³	%	µg/m³	%	µg/m³	%
whole day	3,2	3,2	100	2,7	83	19	100	12	63
day time	3,5	3,8	119	3,8	119	31	160	30	160
night time	2,7	2,1	66	1,0	31	12	63	0	0

1 = maximum NW of the source

2 = maximum E of the source

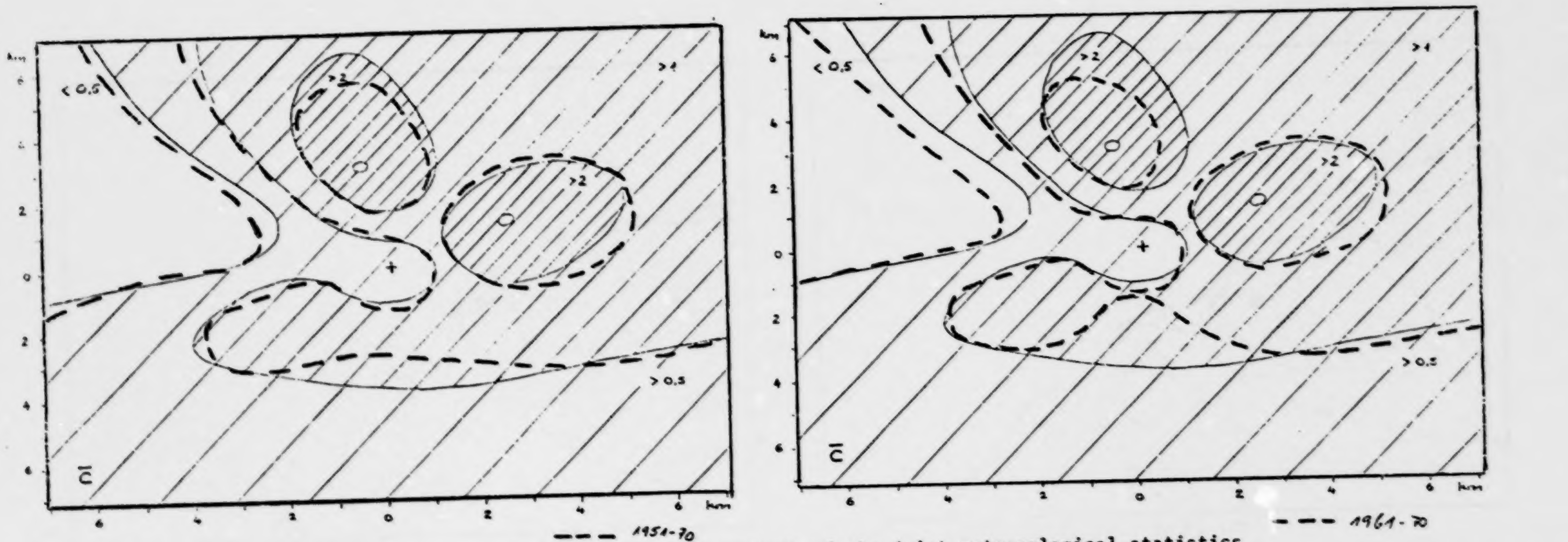
km
6
4
2
0
2
4
6
< 0,5
>2
>2
>4
> 0,5
C̄
6
4
2
0
2
4
6
km
1951-70
km
6
4
2
0
2
4
6
< 0,5
>2
>2
>4
> 0,5
C̄
6
4
2
0
2
4
6
km
1961-70

Figure 1. Average concentration pattern for different time periods of the joint meteorological statistics.

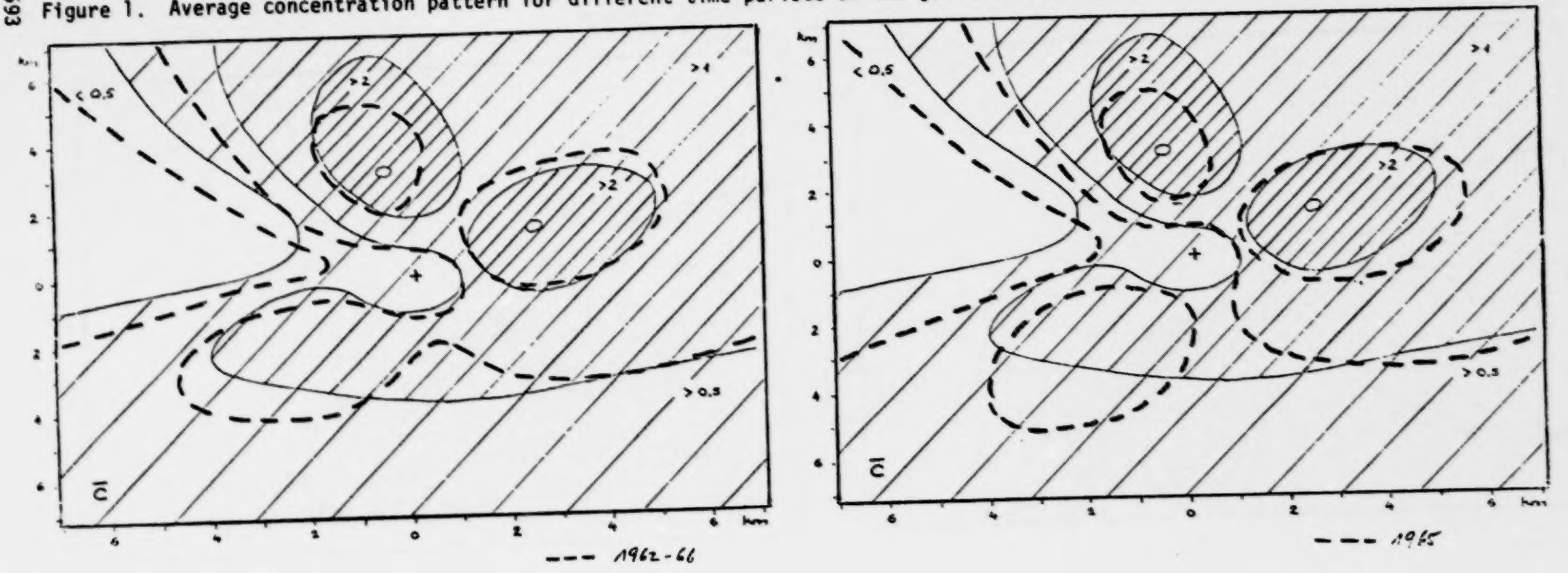
km
6
4
2
0
2
4
6
< 0,5
>2
>2
>4
> 0,5
C̄
6
4
2
0
2
4
6
km
1962-66
km
6
4
2
0
2
4
6
< 0,5
>2
>2
>4
> 0,5
C̄
6
4
2
0
2
4
6
km
1965

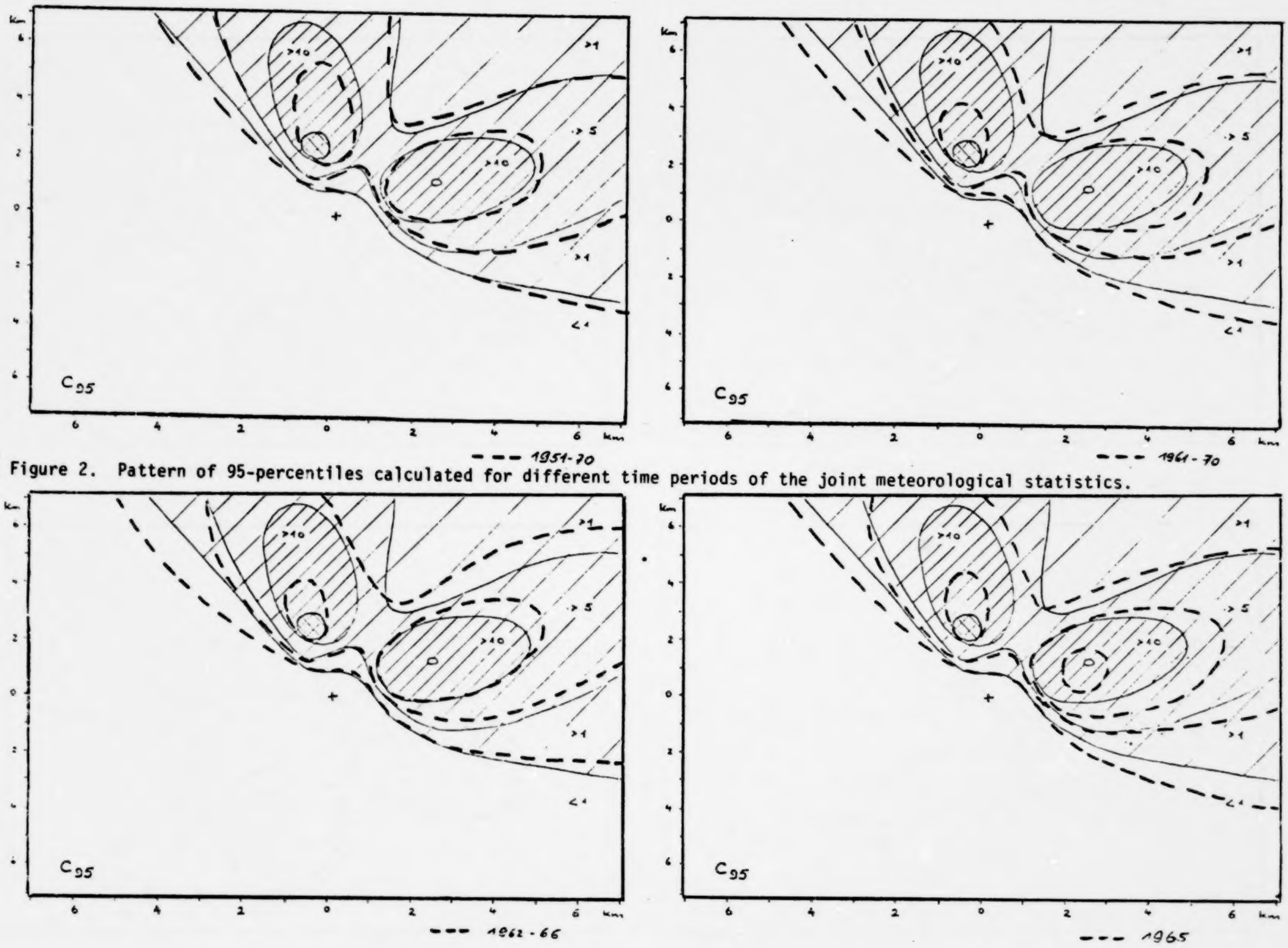

Figure 2. Pattern of 95-percentiles calculated for different time periods of the joint meteorological statistics.

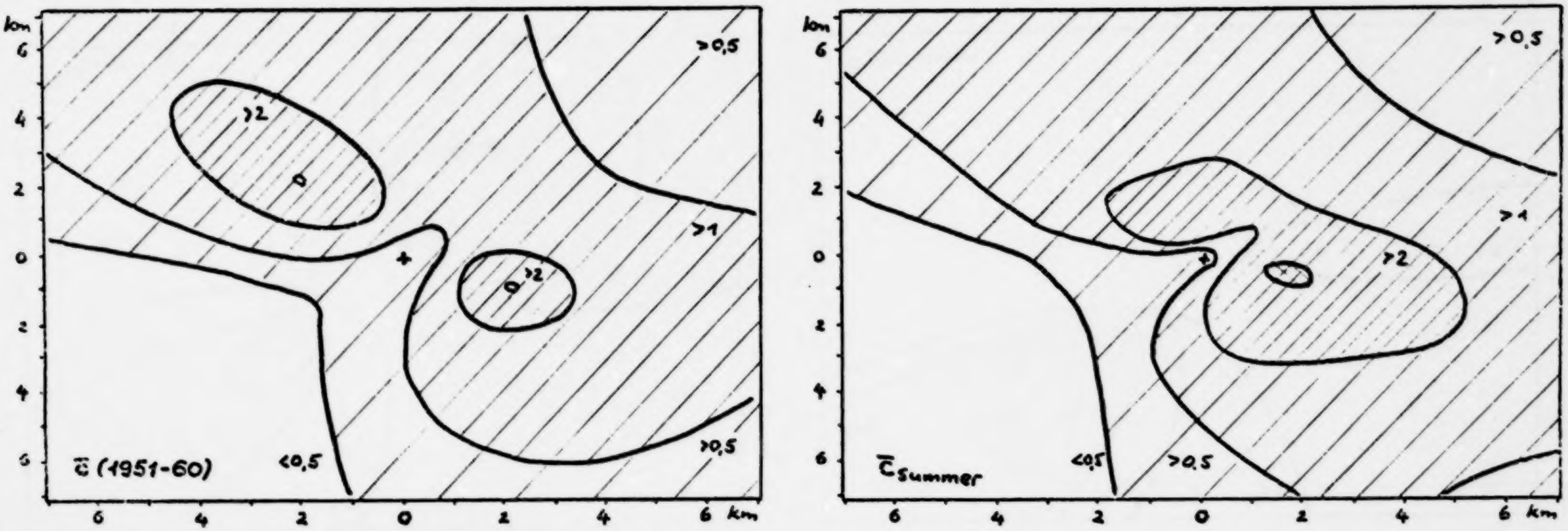

Figure 3. Average concentration pattern for joint meteorological statistics of different seasons.

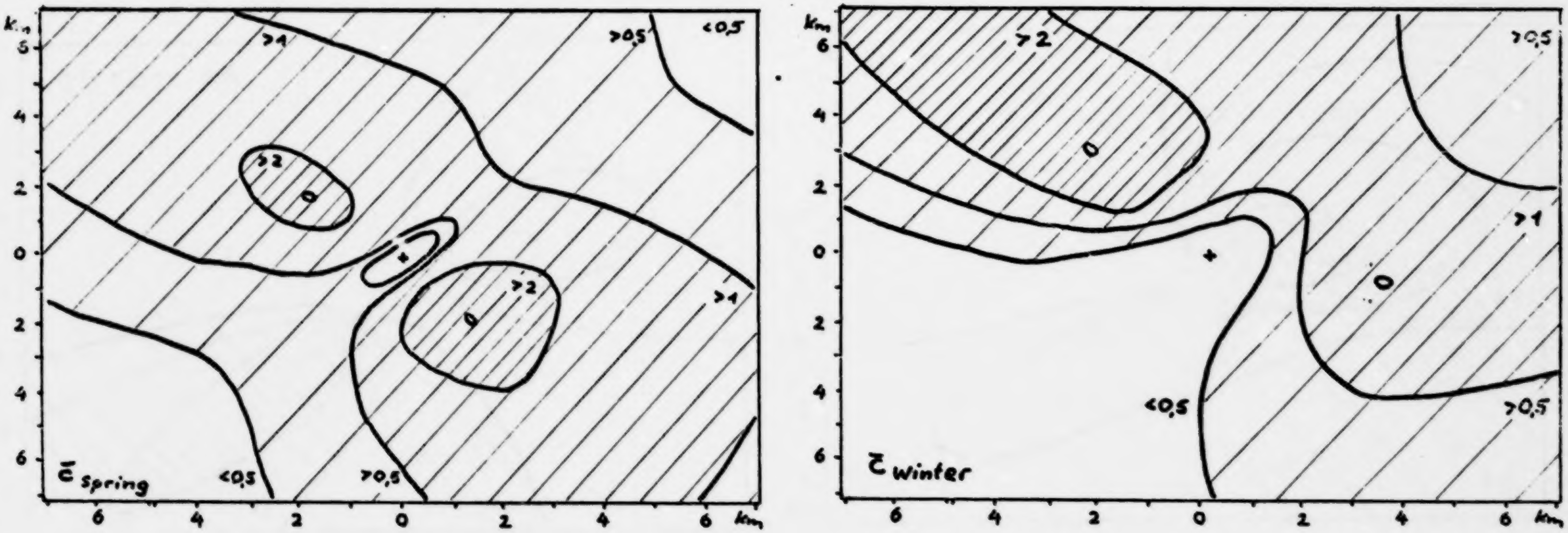

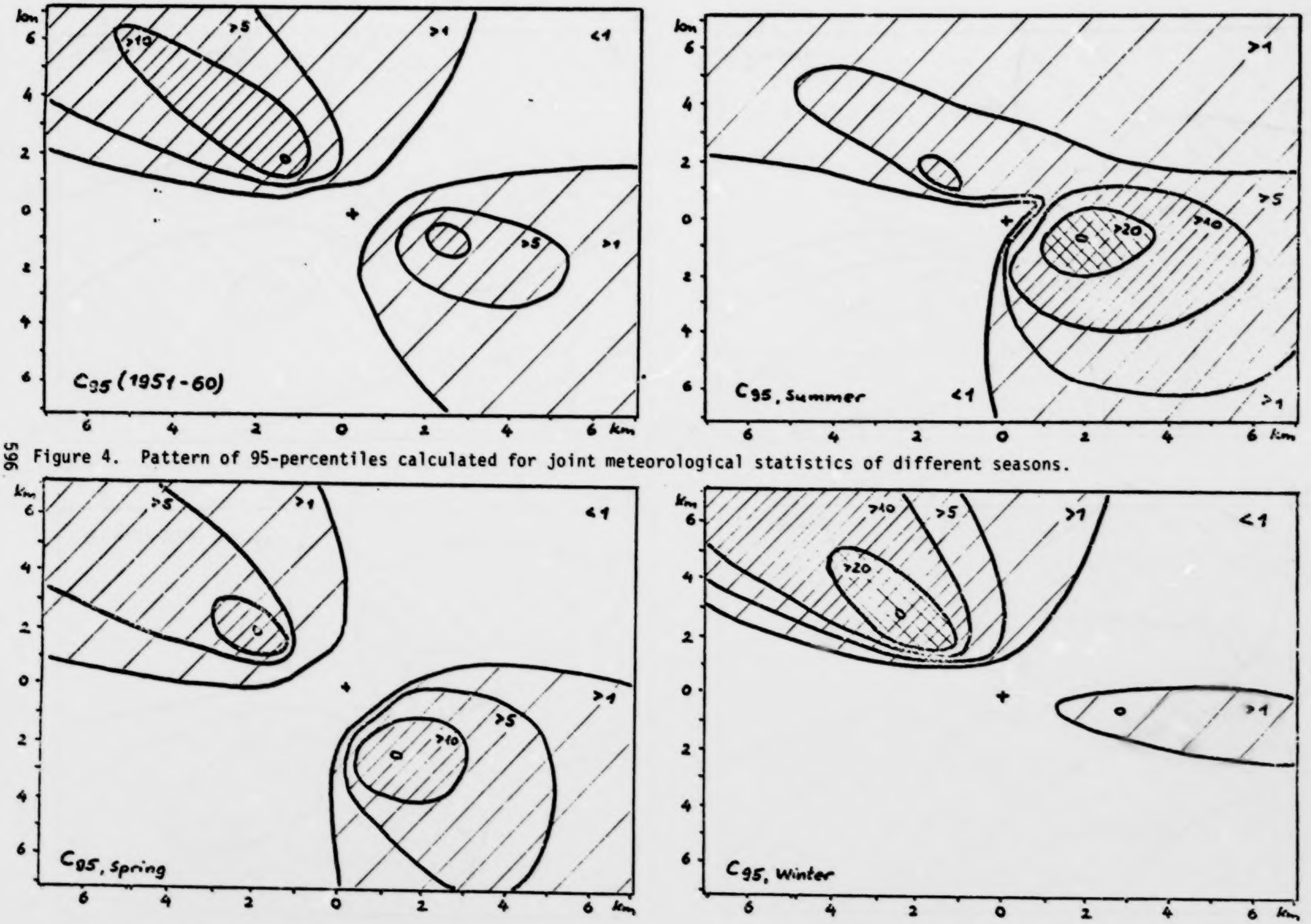

Figure 4. Pattern of 95-percentiles calculated for joint meteorological statistics of different seasons.

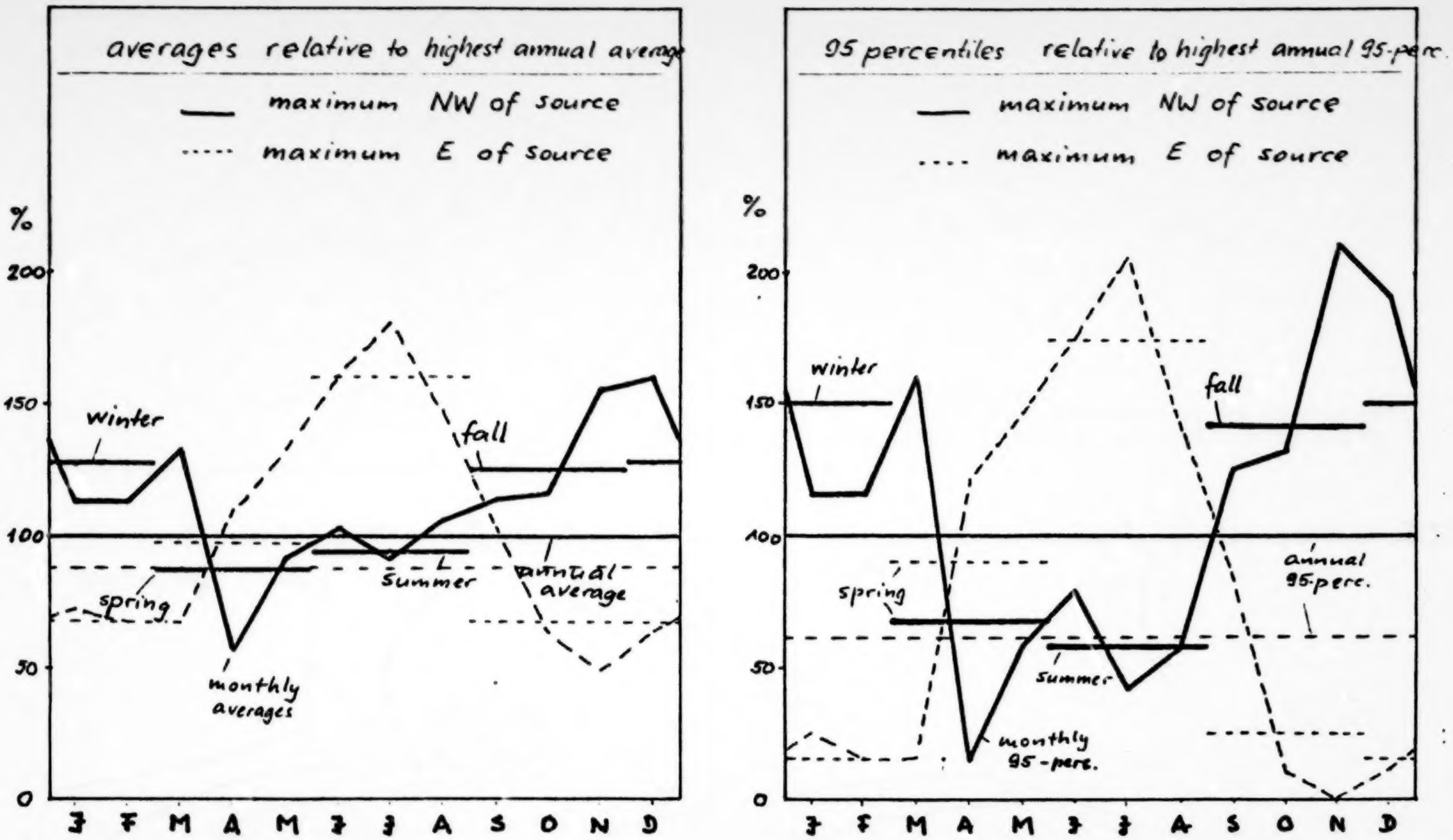

Fig. 5: Seasonal and monthly dependence of maximum calculated averages and 95-percentiles.

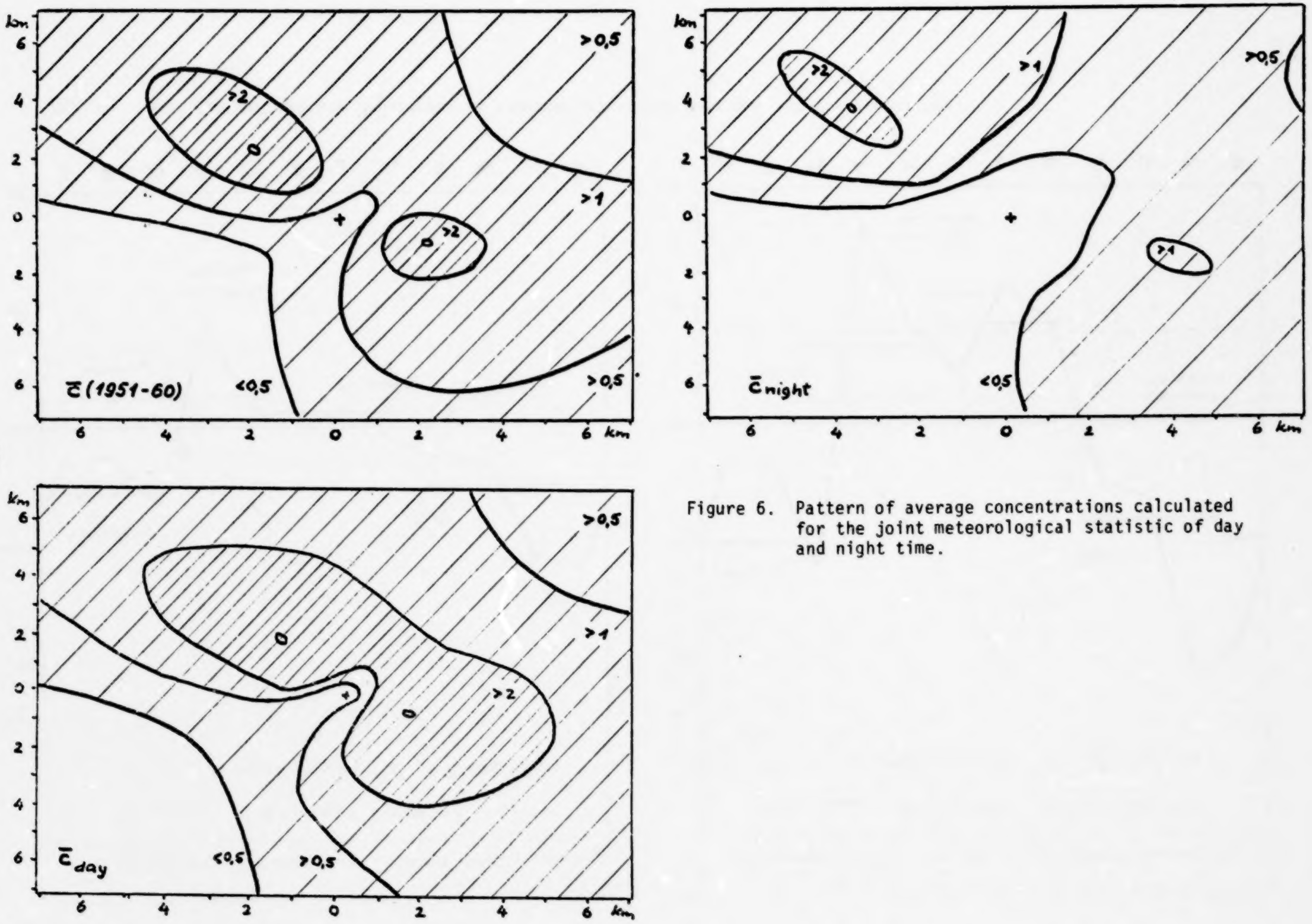
km
6
4
2
0
2
4
6
6
4
2
0
2
4
6 km
$\bar{c}$ (1951-60)
>2
0
>0,5
>1
<0,5
>0,5
$\bar{c}_{night}$
>2
0
>1
>0,5
>1
<0,5
$\bar{c}_{day}$
0
>2
0
>0,5
>1
<0,5
>0,5

Figure 6. Pattern of average concentrations calculated for the joint meteorological statistic of day and night time.

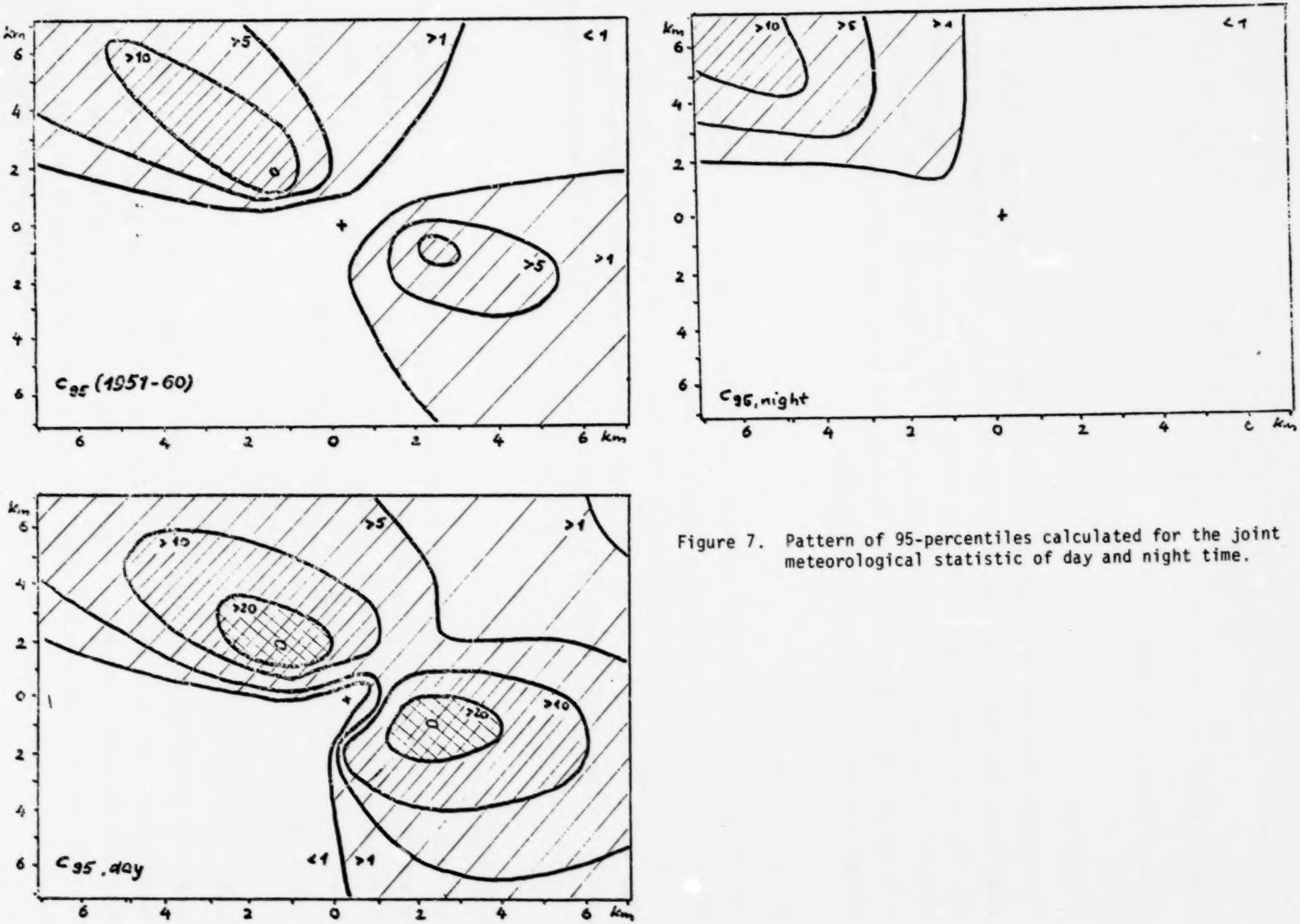

Figure 7. Pattern of 95-percentiles calculated for the joint meteorological statistic of day and night time.

Discussion:

(Rapporteur: McQuaid)

Herrmann:

You showed how the calculated concentration field of a single source depend on the length of the time period during which the basic meteorological data were measured. From these results you cannot draw any conclusion, how the real or measured actual concentration field, which is influenced by a great number of sources with various emission heights, depend on the period of measurements.

Kropp (response):

The original intention of my paper was to investigate the influence of meteorology on the calculated ground level concentrations. You are certainly right that varying emission heights will affect other results. But this investigation in my opinion gives already hints to a strong dependence on meteorology superposed of course by an influence of emission data (height and activity with respect to time).

Hübschmann:

You stated that under some circumstances daytime measurements alone would be sufficient. Would that statement not depend on the emission height, since ground level inversion layers are formed mainly during night and these would influence ground level and elevated source emissions in different ways?

Kropp (response):

It should be possible to extrapolate from daytime measurements to annual values. But that is a theoretical exercise. Ideally, we should have measurements over the whole year. Our intention was to stick to a fixed emission and a fixed stack height and to show the influence of meteorology alone. One should do much more investigation on the measurement side.

Kretzschmar:

In the EEC directive, there is a recommendation on SO_2 which specifies medium for yearly periods as for the heating season do the results of your research imply that for impact studies the calculations of the median values will have to be done for a number of different years?

Kropp (response):

The German regulations speak of annual 95 percentiles. If we do have seasonal limit values, we would have to do calculations for those seasons, too. But our calculations are only the tip of the iceberg. We should do much more investigations in this direction.

TOTAL ENVIRONMENTAL PREDICTION - AIR QUALITY COMPONENT

by

James W.S. Young
Atmospheric Environment Service
Downsview, Ontario

Abstract. There are environmental parameters which have socio-economic significance and which change primarily due to the march of meteorological events. Those items in this group of parameters that are amenable to diagnosis and real-time prediction form the set for total environmental prediction.

This paper presents one approach to real time air quality forecasting in a maritime environment and preliminary tests of its accuracy and ease of use. The paper discusses both the technical and non-technical (public and government response) aspects of the total environmental prediction concept as it applies to air quality.

Introduction

The ultimate goals of air pollution modelling are the complete understanding, prediction and preservation of our environment. It is becoming evident that meteorological services have an important responsibility in responding to man's requirements for total environmental prediction because the prediction of environmental parameters must be based on meteorological observations and predictions and must be available in real-time.

Total environment prediction will encompass those parameters which have socio-economic significance and may include:

(a) ice prediction,
(b) air quality prediction,
(c) prediction of the movement of oil on water
(d) wind-wave predicton,
(e) storm surge prediction,
(f) stream and flood prediction,
(g) prediction support for forestry operations and forest-fire control, and
(h) prediction support for agriculture.

This paper will examine in some detail the air quality prediction parameter because of its potential impact on the population as shown in Figure 1.

Preceding page blank

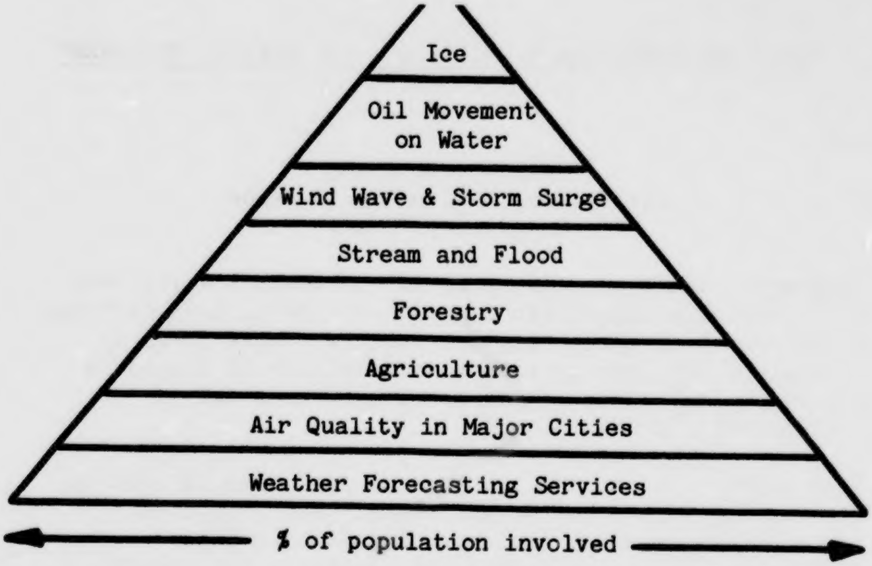
Ice
Oil Movement on Water
Wind Wave & Storm Surge
Stream and Flood
Forestry
Agriculture
Air Quality in Major Cities
Weather Forecasting Services
% of population involved

Figure 1. Population Impact of Various Parameters

Air Quality Prediction

Ideally this capability should provide real-time predictions in the same way as meteorological predictions are obtained. They should provide predictions over a range of scales from local variability, with a spatial resolution of a few kilometres within large urban areas, to regional scale air quality prediction (spatial resolution of about 100 km) and finally to large scale background air pollution prediction (including long-range transport of air pollutants).

For the purposes of this study, a detailed examination is presented for the fine scale within an urban area.

Some attributes that these models must have are:

- must permit re-evaluation of a given scenario for various control agency responses
- must be usable for alerts and warnings of critical or hazardous conditions
- must permit the assessment of future meteorological conditions
- must be able to address local phenomena such as wind variability, channelling, sea-breeze circulations, etc.

The major components of a comprehensive air quality prediction scheme are:

(1) conventional meteorological observations and predictions;

(2) a pollutant source inventory; and

(3) data from an air quality monitoring network.

The design phase of the model can take place in either an integrated or a segmented manner. Table 1 gives some of the characteristics of these two design methods.

There is, however, a need for both segmented and integrated air quality prediction models at the local scale.

Table 1. Design Method Characteristics

	Method	
Characteristic	**Integrated**	**Segmented**
Use	Real-time	Non Real-time
Feedback Interactions with Atmospheric Processes	Yes	No
Computer Power	Large	Small
Alternative Scenarios	No	Yes
Example	Climate Model	Urban Air Management Model
Jurisdiction	National	Local

For example, a local air pollution control agency would like a weather service forecast of meteorology that is likely to produce an episode. Once the episode is confirmed, the agency has a need to know the air quality impact of that meteorological scenario and what effect various abatement options will have for their episode control plan. In this example, the original episode forecast (or potential) is likely to use the integrated approach in that it would be run by the weather service with the forecast model, whereas the air management strategy options would be run locally (segmented) with real-time inputs (source strengths, and monitored concentrations).

This paper deals with a local segmented approach for a maritime environment.

The Maritime Episode Model

The Maritime Episode Model (MEM) forecasts short term (30 to 60 minute average) concentrations at ground level for stable pollutants. The output is a 10 x 10 kilometre grid with a spacing of 1 kilometre and the model uses a multiple point source inventory. This model was developed for urban areas in a maritime climate and is used in an interactive mode. The emission inventory and the forecast (or observed) meteorology are used to simulate the dispersion of airborne pollutants within the mixing layer. The model allows specification of the location of the output grid as well as its topographical features.

The dispersion is simulated using the limited mixing Gaussian plume hypothesis with several enhancements. These include the treatment of the wind field, the change of wind speed with height and a stack downwash correction.

The programme uses an inverse distance relationship to calculate the surface wind direction (DO) and speed (UO) at each source and receptor given several meteorological observing stations. In the Figure 2 below, the wind direction and speed at output point A is assumed to be a function of the wind at the observation stations.

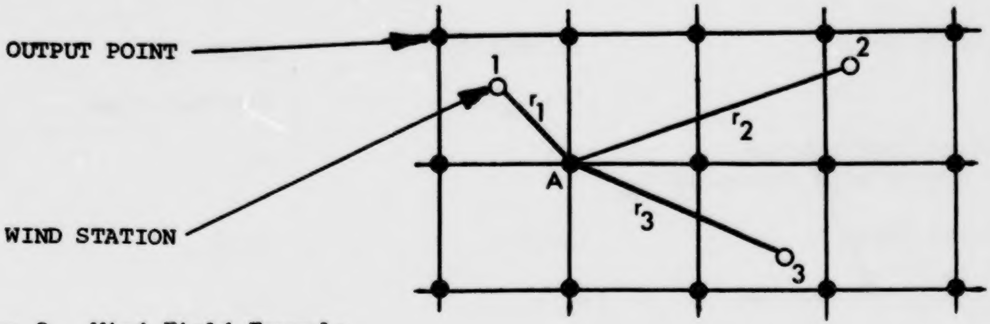

Figure 2. Wind Field Example

The functional relationship assumed in this example with three wind stations is:

$$W_A = \left(\frac{W_1}{r_1} + \frac{W_2}{r_2} + \frac{W_3}{r_3}\right) \Bigg/ \left(\frac{1}{r_1} + \frac{1}{r_2} + \frac{1}{r_3}\right) \qquad (1)$$

where W = wind component of interest (either D = direction or S = speed) and r = distance between point A and the point at which the wind observation is made. The programme ensures that the discontinuity between 359 and 0 degrees is taken into account before equation (1) is used.

The wind speed at stack top (UH) is then calculated using:

$$UH = UO\ (HS/10)^{P} \qquad (2)$$

where P is a function of stability category as outlined in the RAM model[1].

When downwash occurs, the following correction[2] (DH) is subtracted from the actual stack height (HS):

$$DH = 2\ (1.5 - VS/UH)*DS \qquad (3)$$

where VS = exit gas velocity (m/s)
DS = stack diameter (m)

The Briggs Urban[2] relationships are used for the dispersion coefficients (σ_y and σ_z) and the Briggs equations[3,4,5] for hot, buoyant plumes are used to estimate plume rise.

Complete details of this model can be found in the user's guide[6].

The model can be used to analyze (1) single or multiple point sources to determine their impact, (2) episodes and the optimum control strategy and (3) monitor site effectiveness.

Preliminary Validation Runs

The model exists in draft (Version 795) form at the present time and has not been extensively tested and/or validated. The example presented here is a simulation of a 24 hour period during which an episode occurred in August of 1978 in Saint John, New Brunswick. Data were averaged into 3 hour periods in an attempt to smooth out wind direction which was only available to 16 compass points and had a variation, therefore, of ± 22.5°. The general layout of the modelled area and the six wind stations is shown in Figure 3.

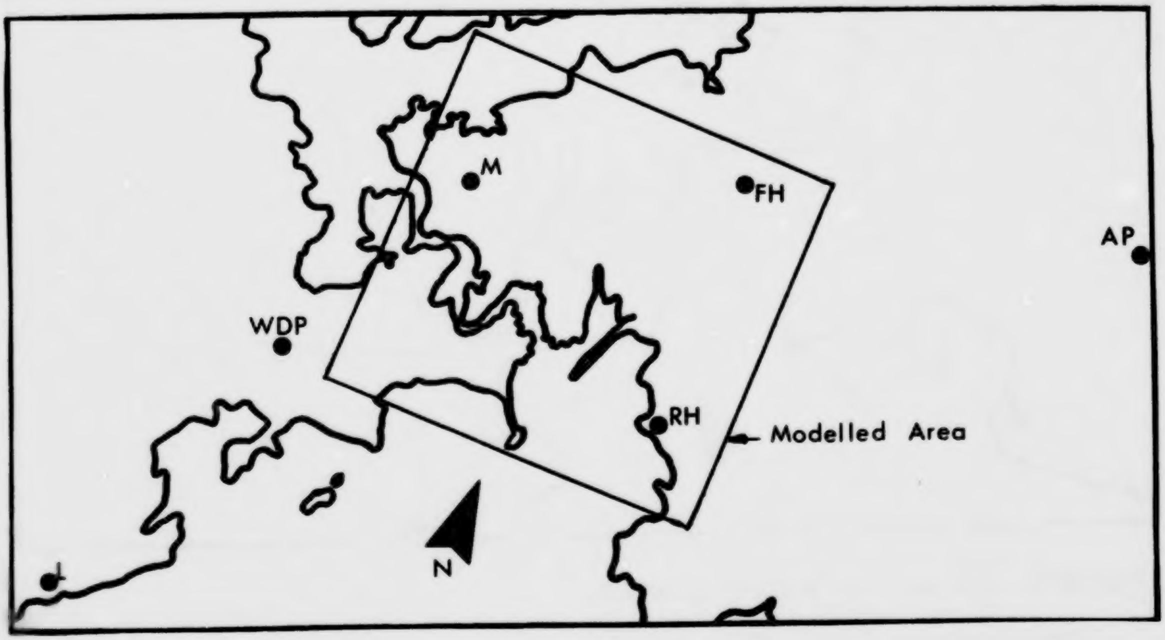

Figure 3. Wind Station Locations.

Temperature was taken as the average value over the modelled area and the mixing depth was estimated to be 250 m. The input meteorological data are summarized in Table 2.

Figure 4 shows the locations of the air quality monitoring stations that were measuring sulphur dioxide during the period of the episode. During the 24 hour period of the simulation 14 point sources were emitting 2991 g/s of sulphur dioxide of which 1980 g/s were due to a single thermal plume which was lofting above the inversion.

Table 2. Input Meteorological Data

Time	Temperature (°C)	Wind Station - Direction (°)/Speed (m/s)					
		AP	FH	RH	M	WDP	L
0000-0200	15	180/5	203/4	180/5	180/2	180/3	285/4
0300-0500	15	188/5	203/3	180/5	180/3	180/3	270/3
0600-0800	15	203/5	203/5	180/5	180/3	180/4	285/4
0900-1100	15	203/6	203/5	180/5	180/2	180/4	285/3
1200-1400	16	203/7	203/6	180/6	180/3	180/4	270/3
1500-1700	16	203/7	203/7	180/6	180/3	180/4	270/3
1800-2000	16	218/7	203/5	180/4	225/2	210/5	300/4
2100-2300	16	203/5	195/3	180/4	180/2	195/2	315/2

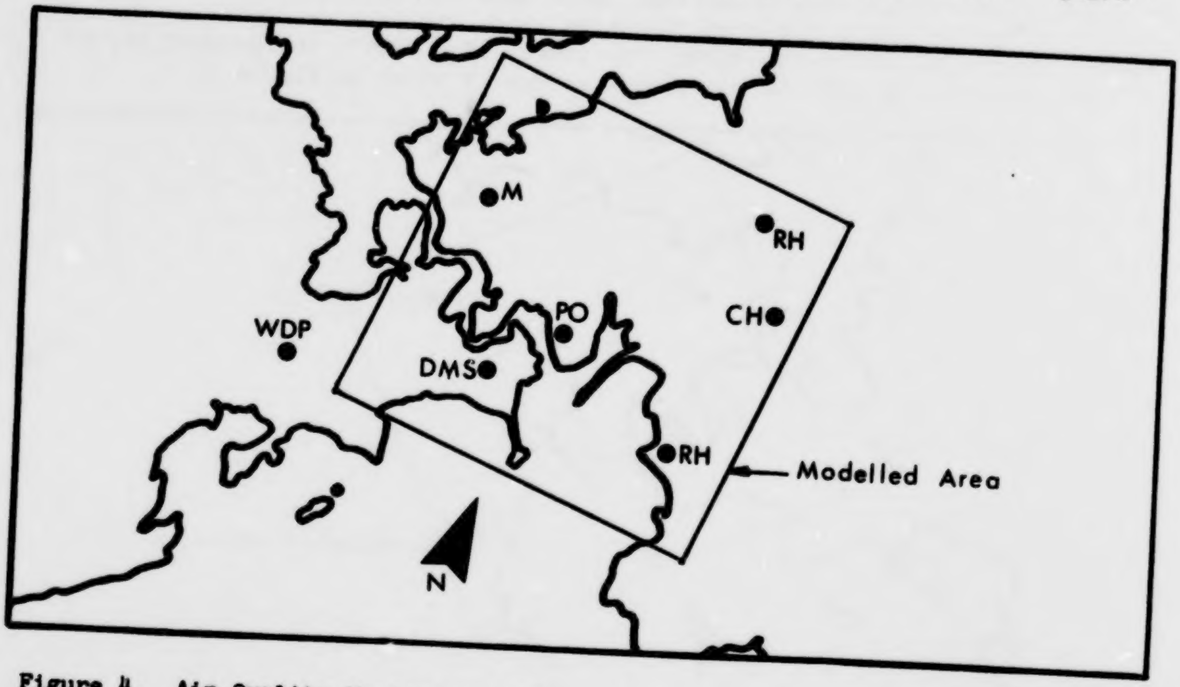

Figure 4. Air Quality Monitor Location.

Table 3 gives a comparison of model calculations against measured data for sulphur dioxide for each three hour period. The correlation coefficient between measured and calculated values is 0.884 when all data points are included and 0.853 with all 0/0 removed. The mean value of the 56 observations was 48 μg/m^3, with a standard deviation of 102 μg/m^3, while the mean calculated value was 32 μg/m^3, with a standard deviation of 65 μg/m^3. The data set indicates a systematic under-prediction of observed 3-hourly average values which may be partially due to a lack of background levels (no area sources included). The poorest prediction of a 3-hour period was 1800-2000 hours which was probably due to a wind shift of approximately 10 degrees. Complete sensitivity and validation testing is currently in progress.

Table 3. Comparison of Calculated Against Observed Sulphur Dioxide Data

	Monitoring Station - CALC/OBS ($\mu g/m^3$)						
Time	FH	RH	M	WDP	PO	DMS	CH
0000-0200	221/372	0/0	0/27	0/0	0/0	0/0	22/0
0300-0500	226/292	0/0	0/27	0/0	0/0	0/27	22/0
0600-0800	202/239	0/0	0/27	0/0	0/0	0/27	43/0
0900-1100	209/398	0/0	0/53	0/0	0/0	0/0	43/0
1200-1400	176/265	0/0	0/53	0/27	0/0	0/0	29/0
1500-1700	168/239	0/0	0/53	0/27	0/0	0/0	28/0
1800-2000	59/239	0/0	0/0	0/0	6/0	0/0	149/0
2100-2300	112/239	0/0	0/27	0/27	0/0	0/0	48/0

Technical Aspects

The range of possibilities for the technical details of the air quality component of total environmental prediction is immense. The extreme ends of the scale, from local to synoptic, have been studied in great detail. The objective of future research is to determine the minimum useful scale for an integrated design (see Table 1). This phase of the work will be started by 1981.

Non-Technical Aspects

In Canada, we have a shared jurisdiction for atmospheric environmental matters. The Federal government is responsible for hazards to health and providing meteorological services whereas the Provincial governments are responsible for the control and abatement of air pollution. The detailed segmented approach outlined in this paper is very useful at the local level and requires a detailed local emission inventory.

If an integrated Federal approach were to provide an indication of air quality with the daily weather forecasts, public pressure to control local problems could cause jurisdictional wrangling and strain Federal/Provincial relations. The approach being taken is to work with the Provincial agencies to develop the kinds of products (predictions) that they require and at the same time produce forecasts of poor air quality potential so that those periods may be simulated in detail at the local level with local information.

References

1. EPA, "User's Guide for RAM Volume 1 - Algorithm Description and Use", EPA-600/8-780016a, 70 pp, 1978.

2. Briggs, G.A., "Diffusion Estimation for Small Emissions", In the Environmental Research Laboratories, Air Resources Atmospheric Turbulence and Diffusion Laboratory 1973 Annual Report. USAEC Report ATDl-106. NOAA, December 1974

3. Briggs, G.A., "Plume Rise", USAEC Critical Review Series TID-25075, NTIS, Springfield, Virginia, 22151, 1969.

4. Briggs, G.A., "Some Recent Analyses of Plume Rise Observations", Proceedings of the Second International Clean Air Congress, edited by H.M. England and W.T. Berry. Academic Press, New York, pp 1029-2032, 1971.

5. Briggs, G.A., "Discussion on Chimney Plumes in Neutral and Stable Surroundings,", Atmos. Environ., 6, 507-510, 1972.

6. Young, J.W.S., "User's Guide for the Maritime Episode Model", in draft form at the Atmospheric Environment Service, Downsview, Ontario, August 1979.

Discussion:

Runca:

Your prediction takes account of topography. I did not understand how this was done?

Young (response):

The model uses MSL as the datum and all topography, source heights and effective plume heights are with respect to that datum. The plumes are assumed to flow parallel to the datum after final rise so that they impact on topography that is higher than the respective effective stack heights.

THE USE OF GOOD ENGINEERING PRACTICE STACK HEIGHTS IN AIR POLLUTION CONTROL

by

Alan H. Huber and Joseph A. Tikvart
Monitoring and Data Analysis Division
Office of Air Quality Planning and Standards
U. S. Environmental Protection Agency
Research Triangle Park, North Carolina USA

Abstract. In the United States the Clean Air Act directly addresses the use of tall stacks as a control measure. The Act indicates that a new source should not receive credit for atmospheric dilution associated with stack heights greater than "good engineering practice." Good engineering practice (GEP) stack height is defined as that height necessary to avoid wakes, eddies and downwash caused by nearby buildings and terrain features. The technical basis used for determining GEP stack height is summarized. Mathematical and physical modeling procedures for determining this height are reviewed. A brief example of problems associated with determining GEP heights controlled by building-induced turbulence is provided.

Introduction

In the United States the Clean Air Act requires that constant emission controls should be the primary basis for limiting the amount of pollutants emitted to the atmosphere.[1,2] Increased stack heights and other dispersion techniques, such as intermittent control systems (ICS), can be used only in limited circumstances. The reason is that dispersion techniques generally do not reduce total pollutant emissions to the atmosphere on a continuous basis. Rather, emissions are dispersed over a wider geographic area by use of a stack. Also, the rate of emission is varied according to atmospheric conditions by use of an ICS. Thus, while ambient concentrations of a pollutant may be reduced in the vicinity of a source, the amount of pollution entering the atmosphere is not reduced by use of a tall stack and is reduced only on an intermittent basis by use of an ICS.

To limit the use of increased stack heights to justify greater emissions, the concept of Good Engineering Practice (GEP) stack height is being employed in the United States. A GEP stack height is defined as:

> ". . . the height necessary that emissions from the stack do not result in excessive concentrations of any air pollutant in the immediate vicinity of the source as a result of atmospheric downwash, eddies and wakes which may be created by the source itself, nearby structures or nearby terrain obstacles."[1]

Preceding page blank

The GEP stack height definition is based on the observed phenomena that in the immediate vicinity of a structure or terrain obstacle, atmospheric flow is adversely disrupted by aerodynamic forces. Some finite stack height is, therefore, necessary to insure that emissions do not result in excessive ground-level concentrations. The GEP definition identifies the minimum stack height at which significant adverse aerodynamic effects are avoided. It is also the maximum height for which a source can receive credit for the purpose of determining allowable emissions.

This paper summarizes the technical basis for determining GEP stack height. While the scientific consensus in general indicates that a case specific review is integral to assuring the prevention of adverse aerodynamic effects in the immediate vicinity of a given source, the literature also identifies generalized formulations that are designed to establish the minimum stack height to prevent this phenomena. Thus, this paper defines the basis for determining GEP from (1) general rules-of-thumb derived from the technical literature, and (2) fluid models that make it possible to simulate features of atmospheric flow that control the aerodynamic behavior of pollutants.

General Aerodynamic Effects

Atmospheric flow is disrupted by aerodynamic forces in the immediate vicinity of structures or terrain obstacles. Attached to the leeward side of a structure or terrain obstacle is a region where the flow is stagnant, yet highly turbulent, and conceptually perceived as an eddy. This region is often referred to as the cavity and can be simply defined as the region where emissions of some visible tracer can be seen circulating to the lee of and returning towards a structure or terrain obstacle. The entire region of disturbed flow, called the wake, extends considerably above as well as downwind beyond the cavity as shown in Figure 1. The disrupted flow in the immediate vicinity of either building structures or terrain obstacles can both enhance the vertical dispersion of emissions from the source and reduce the effective height of emissions. For elevated sources, these aerodynamic effects may cause an increase in the maximum ground-level concentrations.

A review of the literature[3] clearly indicates that the aerodynamic influences and the extent of the wake are highly dependent on the particular shape and design of the obstruction. The extent of the wake also depends on the characteristics of the approaching atmospheric flow. Additional discussions of the aerodynamically-induced disruption around obstacles can be found, for example, in Cermak,[4] Halitsky,[5] Scorer,[6] and Hunt et al.[7]

Building Effects

The literature identifies generalized formulations that are designed to establish minimum stack heights to prevent aerodynamic effects. One such formulation is the "2.5 times rule," which specifies that stacks designed to discharge their effluent at least 2.5 times the height of the highest nearby structure would escape building influences. This rule apparently arose during the early part of this century as a practical formula.

Hawkins and Nonhebel[8] report that the rule had been successfully used by the British electricity generating industry during the previous 20 years. A British Government report that summarizes the informed opinion in 1954 presents the 2.5 times rule as successfully used in practice.[9] According to Sutton,[10] the rule was probably originally deduced by Sir David Brunt from W. R. Morgan's study of the height of disturbances over a ridge in connection with an investigation into the disaster of an airship. No matter what the origins of the rule may be, it is considered a reasonable working rule that is extensively referenced and generally supported by scientific literature.

A more general formulation that prescribes the stack height sufficient to avoid significant building influences has been presented both by Lucas[11] and Briggs.[12] They state that a stack should equal the height of the building plus 1.5 times the height or width, whichever is less. This formulation is equal to the "2.5 times rule" when the building width is greater than its height. In a series of wind-tunnel tests, Snyder and Lawson[13] showed that this formulation is adequate for a stack close to a building whose height is three times its width, and for a building whose width is twice its height. The well-established 2.5 times rule is found to be the consensus opinion as the stack height necessary to avoid significant effects for buildings whose projected width is greater than its height, although individual studies show some deviation. For tall buildings, where the width is less than the height, the stack height need only be equal to the height of the building plus 1.5 times its width.

Few literature references on building effects contain specific data that can be used to quantitatively evaluate these rules-of-thumb on building influences. However, the available data tends to substantiate the general rules. Figure 2 presents data from studies defining the necessary stack height to avoid significant wake effects.[13-19] The wake height (h_w) estimate is formulated by

$$h_w = H + 1.5L, \qquad (1)$$

where H is the height of the structure or nearby structure and L is the lesser dimension (height or width) of the structure or nearby structure. The data from Meroney and Yang[16] and Lord et al.[19] came from observations of plume centerlines of a smoke plume. The wake height estimate was derived as the minimum plume centerline height found to be unaffected by the building. The other data in Figure 2 are derived from vertical concentration profiles. For these data, the wake heights were defined as the plume centerline height where profiles both with and without the building were judged to be essentially the same.

Only three sets of ground-level measurements which can be used to define the increased maximum concentration in the building wake were found.[13,14,20,21] They are presented in Figure 3. A theoretical estimate of increased maximum concentration is also presented. The theoretical estimate assumes the building is very much wider than it is high, and should be considered as providing an upper estimate. For all three sets of data, the plume rise was very small and thus plume centerline height was nearly equal to stack height. The two sets of data where the building width is twice the building height and the data for the square building placed at a 45° diagonal to the wind are very similar. One should expect some differences among building types. Ground-level maximum concentrations associated with a stack 2.5 times the building height, which is the estimated wake height for these cases, are found to be increased by roughly 20 to 40 percent by the building wake.

The downwind extent of the highly turbulent region where there are significant effects is not as well defined as the height of the turbulent region. Based on the rather limited current literature, the downwind extent of the wake where effects are most significant is generally found to be within five times the height or width of the structure, whichever is less. This choice is most applicable to a structure whose width is less than 10 times greater than its height. In situations where the structure is wider than 10 times its height, significant adverse effects may extend farther downwind.

GEP Calculation Technique

To minimize the adverse impact of structural obstacles, GEP stack height (H_G) should be based on the formulation

$$H_G = H + 1.5L \qquad (2)$$

Both the height and width of the structure should be determined from the frontal area of the structure, projected onto a plane perpendicular to the direction of the wind. If the structure is asymmetrical, the GEP stack height should be based on the plane projection lying upwind from the source (stack) which results in greatest justifiable height. The plane projection may have a multitude of heights or widths, particularly for a multi-layered structure. Each combination of the height, H, and lesser dimension (height or width), L, must be evaluated for each segment of the structure to determine which one results in the greatest GEP stack height as defined by Equation (2). The area in which a nearby structure can have a significant influence on a source should be limited to five times the height or width of the structure, whichever is less, downwind. The area of influence becomes diminishingly small as the height-to-width ratio of a structure increases.

The plume has to remain entirely outside of the building wake to result in no effect on ground-level concentrations. This requires that the stack be placed somewhat above the disturbed flow since part of a plume emitted above the wake can, in a short distance, spread downward and thus be affected. In some instances, plume rise may be sufficient to keep the plume emitted above the disturbed flow without the need of a stack higher than the disturbed flow. For most sources, even those with a relatively high exit velocity, a wind speed of 15-20 m/s will result in significantly reduced plume rise and thus increase the potential for adverse effects. For this reason, plume rise generally need not be considered in the determination of the maximum stack height necessary to avoid significant wake influences.

Figure 4 illustrates an application to three types of buildings. A GEP stack should have an emission point above the shaded regions of the vertical cross-section or else the stack should be placed outside the shaded regions, R, of the horizontal cross-section to avoid adverse aerodynamic effects. For both the tall, thin structure and the short, long structure, the expected sphere of adverse influence is less than that found for the moderately tall, cubical structure. To meet the intent of the Clean Air Act, the GEP stack height is also the maximum height for which a source can obtain credit in determining allowable emission limitations.

Use of Fluid Models to Determine GEP Stack Height

Where terrain features are of concern, no general rules-of-thumb are available. Thus, it is necessary to determine GEP stack height on a case-by-case basis through the use of appropriate field studies or fluid model studies. Field studies or fluid model studies may also be used to show that a stack height near structures is needed to prevent excessive pollutant concentrations. An excessive pollutant concentration is a maximum ground-level concentration that is a specified percent in excess of the maximum ground-level concentration experienced in the absence of downwash, wakes or eddy effects produced by nearby structures or terrain.

In most instances, fluid model studies are preferable to field studies since field studies are much more expensive and time consuming, notwithstanding the difficulties in relating a measure of excessive concentration to the adverse effects of structures or terrain. In addition, there must be an area near the site of the source where the atmospheric flow is similar except for differences caused by the structures or terrain nearby the source.

The determination of the good engineering practice stack height requires that the aerodynamically-induced effects from structures or nearby terrain be simulated. Fluid model studies are especially suited to examine such effects. However, certain similarity criteria must be considered if fluid model studies are to accurately reproduce atmospheric phenomena. The document entitled, "Guidelines for Fluid Modeling of Atmospheric Diffusion," reviews the fundamental principles and practical applications of fluid models.[22] Specific guidance for using fluid model studies in the determination of GEP stack height is provided in a separate document.[23]

Essential elements necessary for determining GEP stack height include accurate simulation of (1) boundary layer conditions to properly characterize dispersion; (2) plume rise to properly depict behavior of the effluent near the obstruction; and (3) structure and terrain features to create a representative turbulent field. The trajectory of the plume from the stack should be modeled in an appropriately simulated atmospheric boundary layer flow prior to examining the effects of the structure(s) and/or elevated terrain. Ground-level concentration measurements in the wake of and in absence of either the structure or terrain obstacle are needed to assess the increase in maximum concentrations. It is very important that the determination of the maximum ground-level concentrations be supported by several vertical and lateral concentration profiles throughout the study area. Where detailed field information describing the situation is available, the model study should be designed to best assimilate it.

The GEP stack height is determined by comparing the maximum ground-level concentration found with inclusion of the adverse effects of the nearby structures and/or terrain to the maximum ground-level concentration in the absence of the special features. GEP stack height is that height at which the concentration excess with the structure or terrain feature is not less than some specified percent of the concentration without the features. Modelers may evaluate the effects for several increasingly tall stacks. In other cases, it may be sufficient only to demonstrate that a particular stack is not in excess of GEP.

Conclusions

Atmospheric flow is disturbed by aerodynamic forces in the immediate vicinity of structures or terrain obstacles. The scientific literature generally indicates that case specific reviews are necessary to determine the appropriate steps that should be taken to avoid adverse effects in the immediate vicinity of sources. However, the literature also identifies several generalized formulations which are designed to establish a stack height to minimize the affects of particular phenomena near building structures.

An evaluation of the literature reveals that GEP stack height should be based on the wake height near the building, defined as the height of the structure plus 1.5 times the height or width, whichever dimension is less. Several sets of ground-level concentration measurements, both in the wake of and in the absence of a building, illustrate that maximum concentration increases of 20-40 percent are associated with GEP stack heights. In addition, fluid model studies are a very practical means of determining GEP stack height. The increase of ground-level maximum concentration can be simply related to the aerodynamic effects of structures and/or elevated terrain.

The definition of GEP stack height is essential to determining allowable pollutant emissions from a source. Stacks taller than GEP would allow excessive emissions to increase the atmospheric loading of pollutants. Thus, good engineering practice in construction of stacks is necessary to minimize both adverse aerodynamic effects and to foster the use of constant emission controls.

References

1. U. S. Congress, Government Printing Office, "The Clean Air Act as Amended, August 1977," Washington, Serial No. 95-11, Sec. 123, pp. 64-65, 1977.

2. Environmental Protection Agency, "1977 Clean Air Act Amendments for Stack Heights--Proposed Regulatory Revisions, Federal Register, 44, 9, Friday, January 12, 1979.

3. Environmental Protection Agency, "Technical Support Document for Determination of Good Engineering Practice Stack Height," Research Triangle Park, NC, 1978 (Draft).

4. Cermak, J.E., "Aerodynamics of Buildings," in Annual Review of Fluid Mechanics, Vol. 8, M. Van Dyke, and W. G. Vincenti (Co. Ed.), Annual Reviews, Inc., Palo Alto, CA, pp. 75-106, 1976.

5. Halitsky, J., "Gas Diffusion Near Buildings," Meteorology and Atomic Energy - 1968, D. H. Slade (Ed.), Chapter 5-5, 1968.

6. Scorer, R. S., Air Pollution, Pergamon Press, Oxford, England, pp. 107-123, 1968.

7. Hunt, J.C.R., C. J. Abell, J. A. Peterka, and H. Woo, "Kinematical studies of the flows around free or surface mounted obstacles; applying topology to flow visualization," J. Fluid Mech. Vol 86, Part 1, pp. 179-200, 1978.

8. Hawkins, J.E. and G. Nonhebel, "Chimneys and the dispersal of smoke," J. of the Institute of Fuel, Vol. 28, p. 530, 1955.

9. Beaver, S.H. (Chairman), "Report of government committee on air pollution," Her Majesty's Stationary Office, Cmd. 9322, November 1954.

10. Sutton, O.G., "Discussion before the institute in London, 23.d, May 1960" J. Institute of Fuel, Vol. 33, p. 495, 1960.

11. Lucas, D.H., "Choosing chimney heights in the presence of buildings," Proceedings of the International Clean Air Conference, Melbourne, Australia, May 15-18, p. 47, 1972.

12. Briggs, G.A., "Diffusion estimation for small emissions," Atmospheric Turbulence and Diffusion Laboratory, NOAA, Oak Ridge, TN, ATDL No. 75/15, 1973 (Draft).

13. Snyder, W.H., and R. E. Lawson, Jr., "Determination of a necessary height for a stack close to a building--a wind tunnel study," Atmospheric Environment, Vol. 10, p. 683, 1976.

14. Ukeguchi, N.H., H. Sakata, and Y. Ide, "Study on stack gas diffusion," Mitsubishi Technical Bulletin No. 52, 1967.

15. Huber, A.H., and W. H. Snyder, "Building wake effects on short stack effluents," Third Symposium on Atmospheric Turbulence Diffusion and Air Quality, Raleigh, NC, 1976.

16. Meroney, R.N., and B. T. Yang, "Wind-tunnel study on gaseous mixing due to various stack heights and injection rates above an isolated structure," USAEC Report No. COO-2053-6, 1971.

17. Jensen, M., and N. Frank, "Model-scale tests in turbulent wind," Danish Technical Press, Copenhagen, 1965.

18. Sherlock, R.H., and E. A. Stalker, "The control of gases in the wake of smokestacks," ASME Journal, p. 455, June 1940.

19. Lord, G.R., W. D. Baines, and H. J. Leutheusser, "On the minimum height of roof-mounted chimneys, results of an exploratory wind-tunnel study," Report TP-6409, Technical Publication Series, Dept. of Mechanical Engineering, University of Toronto, 1964.

20. Britter, R.E., J. C. R. Hunt, J. S. Puttock, "Predicting pollution concentrations near buildings and hills," presented at the Conference on Systems and Models in Air and Water Pollution, at the Institution of Measurement, London, Sept. 22-24, 1976.

21. Robins, A.G., and I. P. Castro, "A wind tunnel investigation of plume dispersion in the vicinity of a surface mounted cube." Atmospheric Environment, Vol. 17, p. 291, 1977.

22. Snyder, W.H., "Guidelines for Fluid Modeling of Atmospheric Diffusion," Environmental Protection Agency, Research Triangle Park, NC, 27711, 1979 (Draft).

23. Environmental Protection Agency, "Guidelines on the Use of Fluid Models in the Determination of Good Engineering Practice Stack Height," Research Triangle Park, NC, 1979 (Draft).

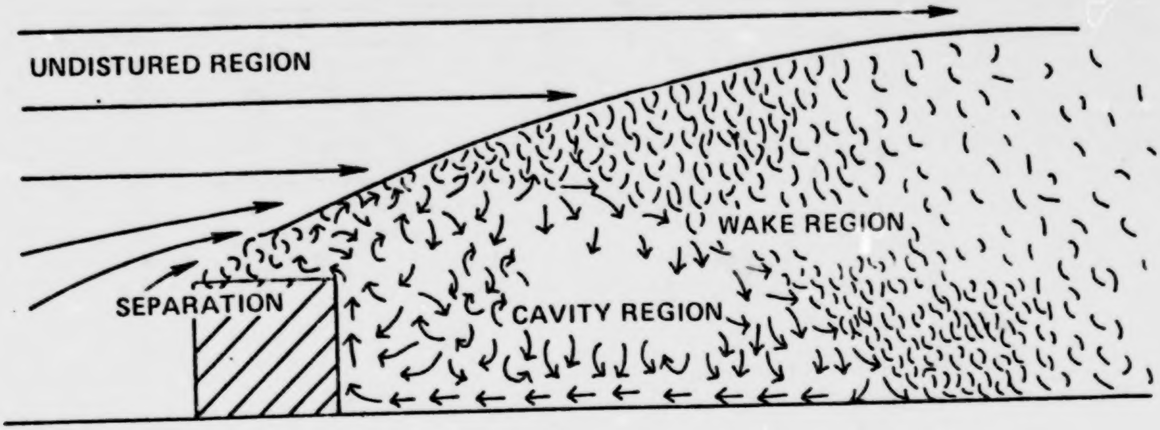
UNDISTURED REGION
WAKE REGION
SEPARATION
CAVITY REGION

Figure 1. Diagrammatic sketch of envelope and cavity regions behind a building (SIDE VIEW).

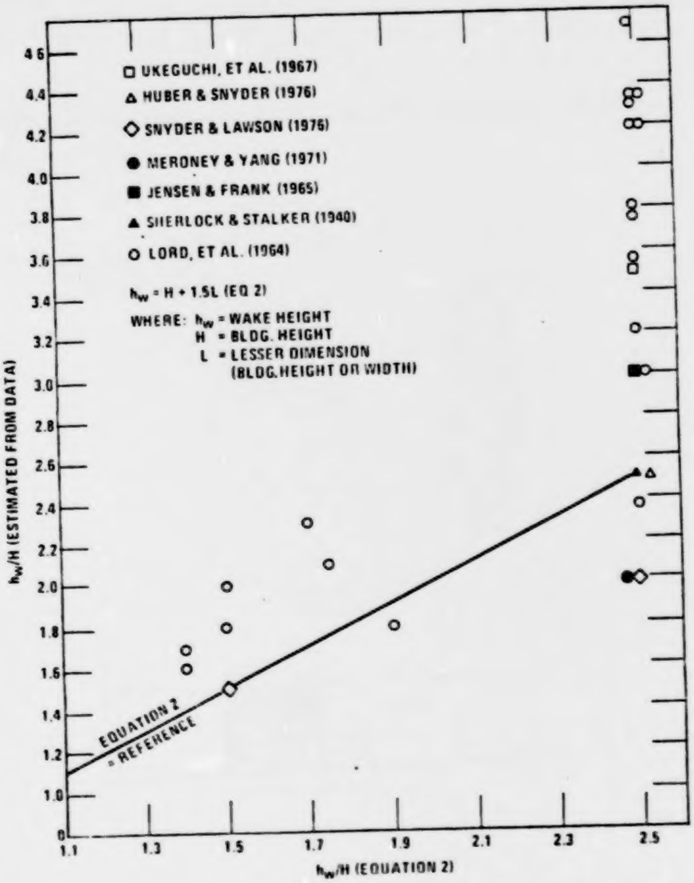

Figure 2. Wake height estimate.

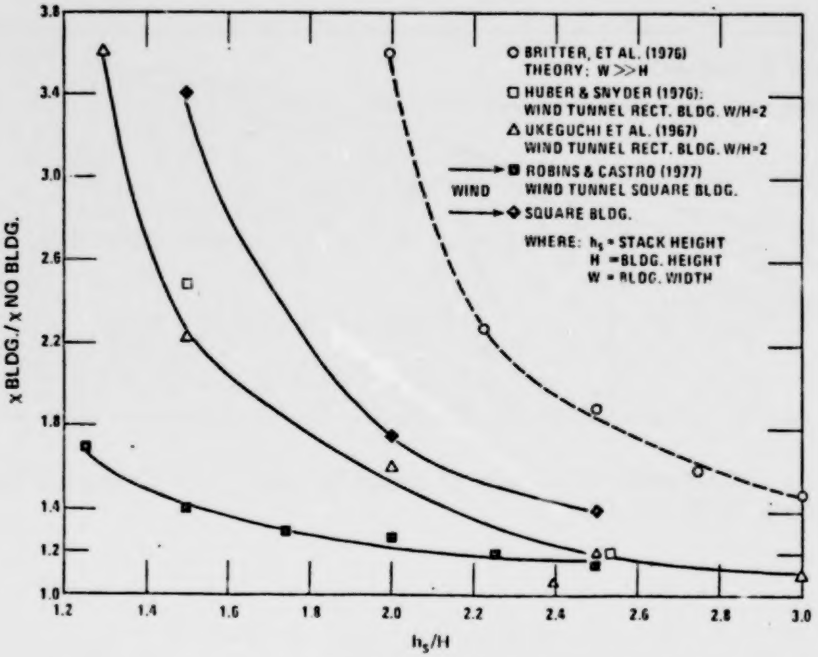

Figure 3. Increased maximum ground-level concentrations in building wake.

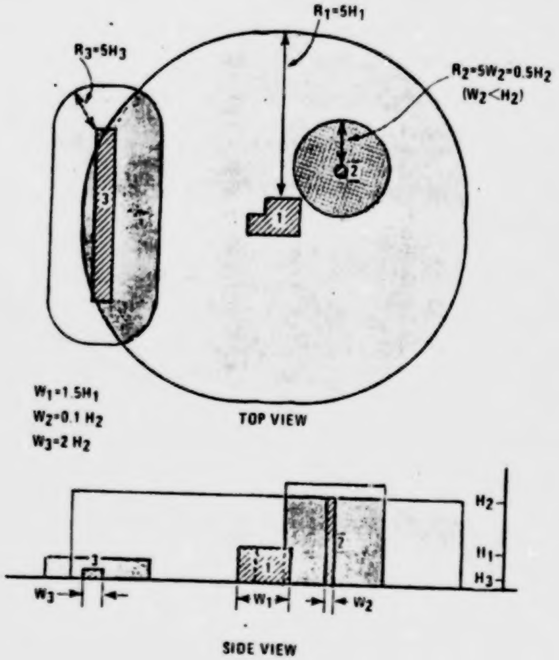
$R_1=5H_1$
$R_3=5H_3$
$R_2=5W_2=0.5H_2$
$(W_2<H_2)$
1
2
3
$W_1=1.5H_1$
$W_2=0.1\ H_2$
$W_3=2\ H_2$
TOP VIEW
H_2
H_1
H_3
W_3
W_1
W_2
SIDE VIEW

Figure 4. Determination of the immediate vicinity, R, for three types of structures.

Discussion:

Venkatram:

Does the GEP regulation define what a building is?

Tikvart (response):

The regulation refers to aerodynamic effects associated with the source, nearby structures, or terrain obstacles. Skeleton structures would have to be identified on an individual basis as an attempt to circumvent the intent of the regulation. However, a practical problem arises when a judgment must be made concerning the influence of a cooling tower associated with a power plant. This issue has not yet been resolved.

Question:

Who decides whether fluid modeling should be done?

Tikvart (response):

The proposed regulations require that when a stack height increase is requested, a fluid modeling study is required to demonstrate the need for a higher stack. For new sources, the source can request a fluid modeling study if it is believed that rules-of-thumb result in a stack height that is too short.

Barrett:

Is a zone of influence of five building heights adequate?

Tikvart (response):

Generally for most regularly shaped buildings, this zone of influence is an adequate rule-of-thumb. However, it is recognized that for buildings that have a width which is much greater than its height, e.g., a long, low building, the zone of influence can be 10 building heights or greater downwind. If this is judged to be an important factor in determining GEP stack height, then a fluid modeling study should be conducted.

10TH NATO /CCMS INTERNATIONAL TECHNICAL MEETING ON AIR POLLUTION MODELING AND ITS APPLICATION

TOPIC 6

Heavy Gases

Preceding page blank

FAILURE PROBLEMS AND DISPERSION PROCESSES OF HEAVY GASES

by

B. Gutsche

Freie Universität Berlin

Institut für Geophysikalische Wissenschaften

Thielallee 50

D - 1000 Berlin 33

F. Vahrenholt

Umweltbundesamt - Federal Environmental Agency

Bismarckplatz 1

D - 1000 Berlin 33

Summary:

Due to uncontrolled release various components, e. g. heavy and hazardous gases are being emitted into the atmosphere.

Within this paper the following aspects are being discussed

- which substances are occuring in specific plants,
- under which conditions in case of accidents are these substances emitted,
- what is the amount in which these substances are being expected to be released (exemplary) in such situations,
- how are the transmission conditions,
- what are the suitable methods for describing adequately the transmission processes (as well dispersion as transformation processes)

First analyses of the existing situation and preliminary results of some numerical calculations will be presented as well as ways and methods to define protection distances.

Preceding page blank

1. General problem substances and emission conditions

The environmental catastrophe of Seveso threw into the full glare of publicity the fact that there are production processes in the chemical and related industries in the course of which highly toxic substances may escape to the environment.

After the catastrophe of Seveso the risk of chemical facilities has been investigated in detail in the Federal Republic of Germany. Thereby the responsible authorities realized, however that there are in the Federal Republic, apart from the relatively safe production of trichlorophenol, a series of similar processes in the course of which substances of only slightly lower toxicity than tetrachlorodibenzodioxin (TCDD) occur - but in greater quantities. In this connection it is irrelevant, whether these substances occur as initial materials, intermediate products, by-products, end products, the products of accidents or as process materials in the plants concerned.

Prompted by the accident of Seveso, the Federal Environmental Agency compiled a schedule of highly toxic substances. As a result of the various modes of exposure of toxins (oral, inhalation, dermal) and due to the use of various experimental animals (mice, rats, rabbits), the criteria used to classify a substance as highly toxic resulted in a kind of toxicological criteria catalogue. This schedule of highly toxic substances covers 145 substances.

Certainly the risk depends not only on the toxicity (including the carcinogenic, teratogenic and mutagenic property) of a substance, but also on the quantity of the substance and the relation between possible accidents and installed measures of security. High requirements must to be satisfied at units, in which substances are handled with high temperature or high pressure like reaction vessels, agitator and pressure vessel plants, distillation plants, storage facilities and pipework.

Critical quantities, which lead to considerable injuries of the (vicinity) neighborhood in the case of an outbreak, are given in the following table:

Fluorine	2 tonnes
phosgene	2 tonnes
chlorine	10 tonnes
vinylchloride	10 tonnes
sulfur dioxide	25 tonnes
ammonia	50 tonnes

The experience of the past confirm this:

For one of substances listed in the schedule of toxins - namely phosgene - investigation have been carried out at a selected plant to establish the effects to be anticipated in the event of an accident and the probability of such an accident occuring.

As maximum credible accidents were investigated

1. The flanged connection at the phosgen tank breaks off, Fluid phosgen is streaming outside due to the pressure in the tank and the diameter of the piping.

2. A tank is busting by a raising of the pressure in the phosgene storage or by influence from outside (aeroplane crash) and fluid phosgen is suddenly set free, which vaporizes at atmospheric pressure.

   The probability of occurence has been calculated with 10^{-5} to 10^{-6}/year.

a) chlorine

year	country	quantity lost(tonnes)	persons affected casualties	fatalities
1926	France	25	?	19
1929	USA	25	30	1
1939	Roumania	21-25	400	68
1947	Finland	30	120	19
1952	Germany	15	200	7
1957	USA	?	210	8
1974	Spain	1	100	4
1975	USA	?	89	4

b) phosgene

1928	Germany	11	200	11

c) ammonia

1968	France	19	15	5
1969	USA	64	?	6
1973	South Africa	38	65	17

Table: Experiences of the past

In this model case and whereby 30 m^3 phosgen break out an average wind velocity of 1 m/sec. and a stable layer within the atmosphere a region of 1.7 km^2 would be contaminated with a dosis (concentration x time, which is higher than the lethal dosis LC_{50} (75 ppm for 30 minutes)

The demand for minimizing the risk of hazardous installations aims in the first instance at appropriate technical and organizing measures in order to prevent such accidents or to lower the likelihood of an event. For this is necessary an investigation of each process using an accident analysis which is usual already for atomic energy power stations. The risk, defined as product from the probability of an event accident frequency and its effects of injury, may also be lowered by minimizing the effects to be anticipated in the event. This can for example be done by adequate regulations, which rules on minimum distance between chemical facility and residential areas. Such regulations are giving appropriate protection if based on suitable dispersion calculations. These calculations are also necessary to manage active emergency schemes.Only on this way disaster plans and emergency schemes may be developed, which have in view a special substance and a distinct accident.

Beginning with the results of an accident analysis which describe in detail all the possible sources of technical failure and human error fault tree analysis and taking into account the particular physical and chemical properties the typical emission sources and the dispersion conditions the measures and procedures have to be fixed. Following measures can be thought of depending on the type of installation, the accident to be anticipated (e. g. emission of toxic substances, explosion, fire), the meteorologic conditions and the structure of the affected area.

Fixing immission limits in the event of an accident, which if they are exeded leads to catastrophe protection measures; denomination of the to included persons and organizations; to keep ready vehicles and other resources; arrangements which should be done by the population itself; sealing off of the affected area; medical provision of the population; reuse of injured people; evacuation of persons and decontamination plans which lay down the procedure for the disposal of substances which are long-lived in the environment. Some of these measures (immission limits, evacuation, decontamination plans) including regular safety drills presume other models of dispersion calculation than the Gaussian dispersion model, hitherto most commonly used.

2. Transmission conditions and their numerical treatment

A consequent theoretical treatment of the spread of heavy gases in failure situations would imply the use of a coupled system of partial differential equations for all relevant hydro- and thermodynamical variables including the mass conservation laws for all participating components.

Such a treatment of failure problems seems to represent a long-distance aim of the moment.

Concerning the numerical structure of mathematical procedures to be applied in such cases experiences exist from two scientific fields

- climate simulations under the consideration of anthropogenic influences; e. g. the work done by MANABE and WETHERALD,
- investigations of development and spread of photochemical smog.

At this place, we want to present - alternatively to the methods applied by VAN ULDEN or EIDSVIK and others - some first steps into the direction of a long-distance aim as mentioned above.

2.1 Application of integrated Gaussian puff-models

The TÜV Rheinland calculated immission concentrations to be expected in the case of a phosgene-tank explosion using the conventional equations noted in the following table. 42.300 kg Phosgene were emitted within 1 sec. in an emission height of about zero meters.

As an example for these calculations we present in Fig. 1 for stable atmospheric stratification and a wind speed of 1 m/s isolines of LC_{50} - and TDLo - values. The meanings of these values are the following:

LC_{50}: the lethal concentration with a mortability-probability of 50 %;

TDLo: the lowest published toxic dose.

In the Federal Republic of Germany the following values are in discussion for phosgene:

LC_{50} = 75 ppm = 308 mg/m^3 for 30 minutes;
TDLo = 25 ppm = 103 mg/m^3 for 30 minutes.

The estimation of a death-rate within a given region due to much an accident does not seem to be legitimate due to the weaknesses of the applied method.

2.2 Finite-Difference Methods

In spite of the fact that already integrated Gaussian puff models require as well a lot of computer time and core as additional input data they are not more than the very first step into the direction cited above.

The next step, a bit more complicated than integrated Gaussian puff model, consists of the application of finite-difference procedures requiring even the three-dimensional structure of the meteorological field for each time step as input data. Due to the sparingness of such data mathematical-meteorological models have to be developed, preceding these dispersion models and delivering these three-dimensional input data field to them.

GAUSSian dispersion formula

1. Normal situation (GAUSSian plume solution)

$$S = \frac{Q}{2\pi \bar{u} \sigma_y \sigma_z} \exp\left\{- \frac{y^2}{2\sigma_y^2}\right\} \left[\exp\left\{- \frac{(z-h)^2}{2\sigma_z^2}\right\} + \right.$$

$$\left. + \exp\left\{+ \frac{(z+h)^2}{2\sigma_z^2}\right\}\right]$$

2. Case of an explosion (integrated GAUSSian puff model)

$$S(t) = \int_0^t dt' \frac{Q(t')}{\sqrt{[4\pi(t-t')]^3 k_x k_y k_z}} \times$$

$$\exp\left\{- \frac{[x - \bar{u}(t-t')]^2}{4k_x(t-t')} - \frac{y^2}{4K_y(t-t')}\right\} +$$

$$\left[\exp\left\{- \frac{(z-h^2)}{4k_z(t-t')}\right\} + \exp\left\{- \frac{(z+h)^2}{4k_z(t-t')}\right\}\right]$$

Fig. 1: LC_{50}- and TDLo-values for stable atmospheric stratification wind speed 1 m/s (calculation by TÜV Rheinland)

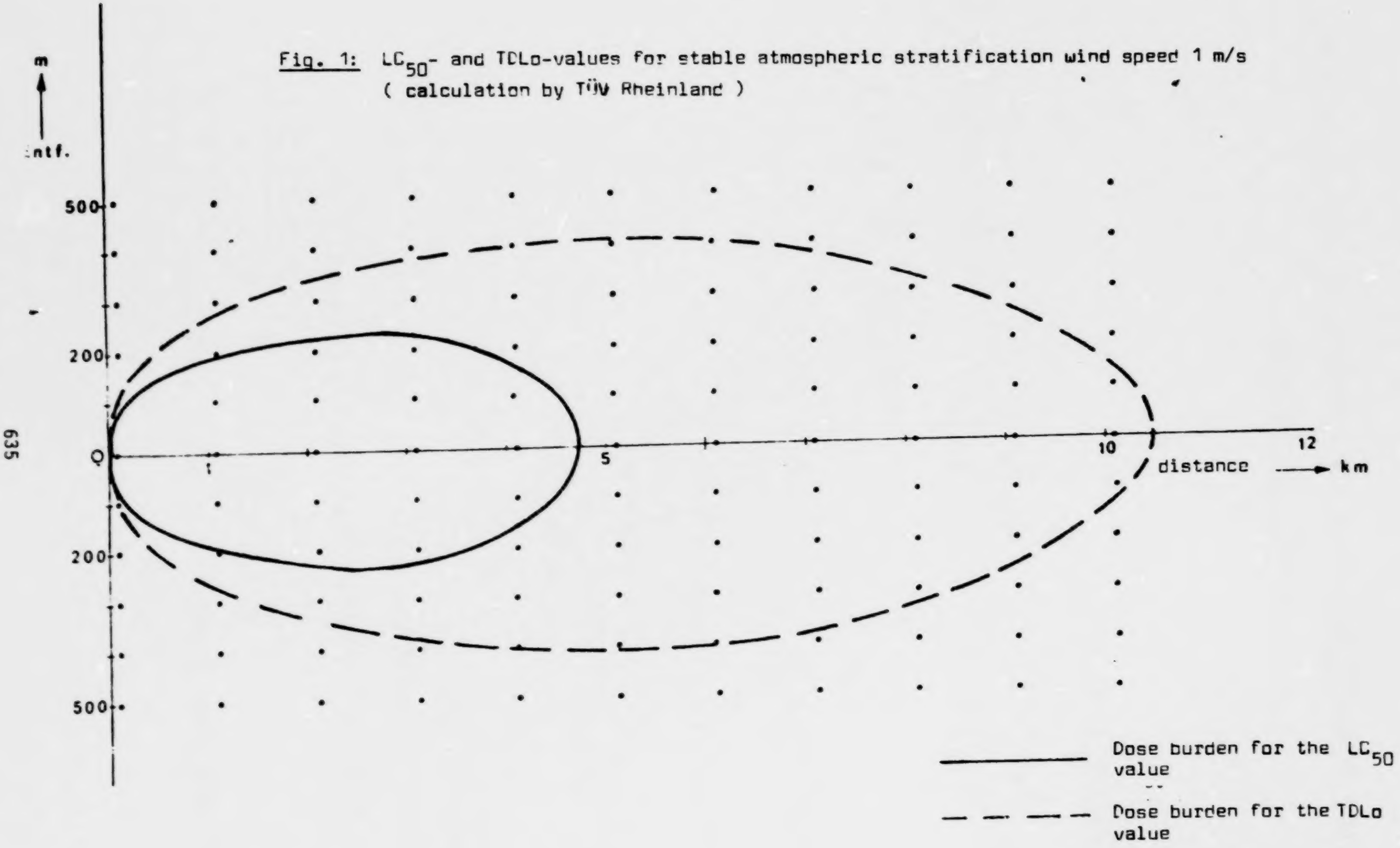

SIMPLE FINITE-DIFFERENCE SCHEME FOR DESCRIBING THE SPREAD OF POLLUTANTS AFTER A TANK EXPLOSION

Differential Equation

$$\frac{\partial s(\mathbf{r},t)}{\partial t} = \frac{ds(\mathbf{r},t)}{dt} = \mathbf{v}(\mathbf{r},t)\cdot\nabla s(\mathbf{r},t) + \mathbf{K}(\mathbf{r},t)\,\nabla^2 s(\mathbf{r},t)$$

Approximations:

1. constant mass - bilance

2. horizontal homogeneity

Method of solution

Two-step difference method

1. step Advection (treated using backward-differences)

$$\frac{\partial s_1}{\partial t} = -\,\overline{u}\,\frac{\partial s(x,y,z;t)}{\partial x}$$

2. step: Diffusion (Treated using central differences)

$$\frac{\partial s_2}{\partial t} = K_{ii}\,\frac{\partial^2 s(x,y,z;t)}{\partial x^2}$$

Fig. 2: LC_{50} - and TCLo-values for stable atmospheric stratification

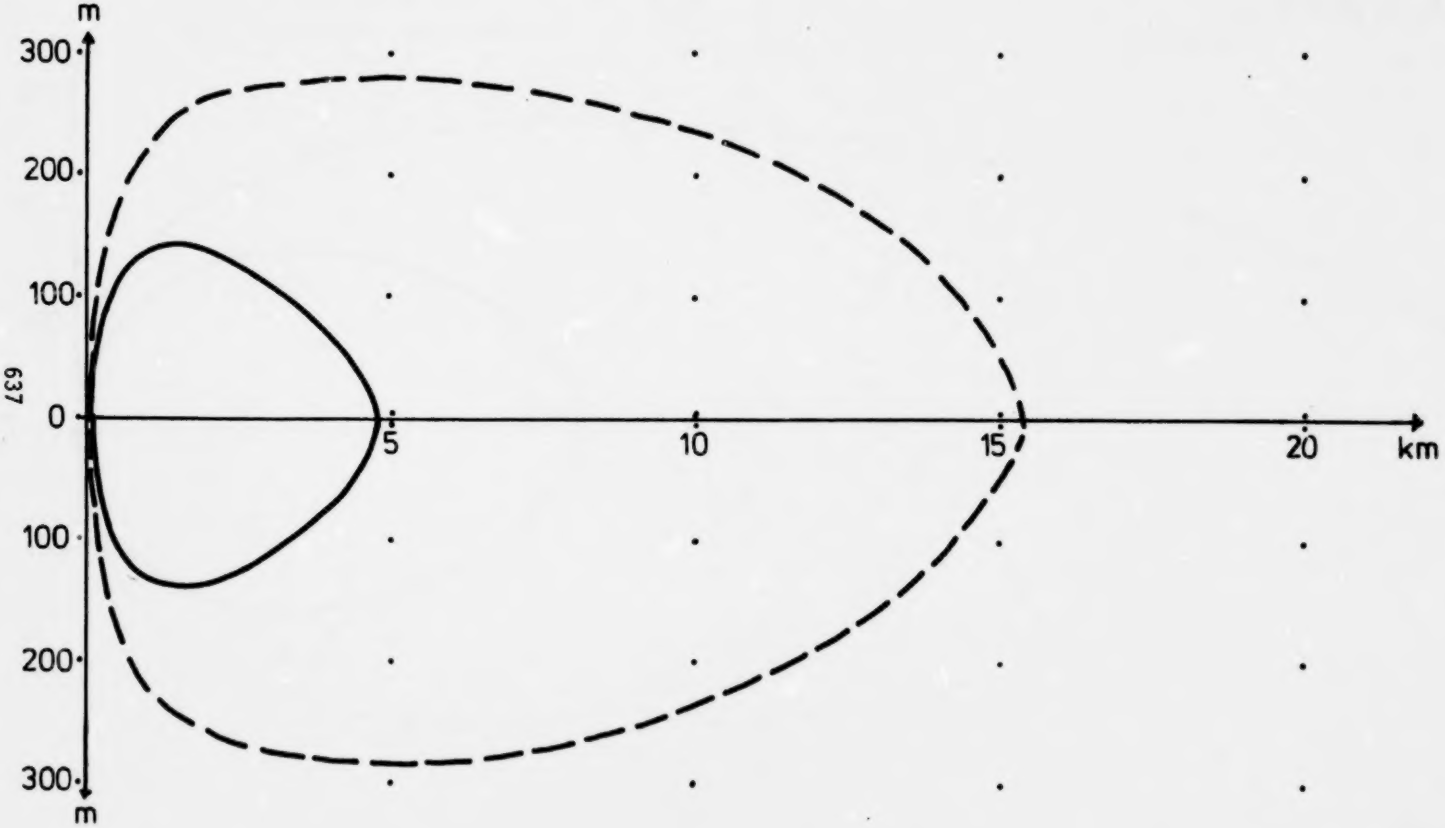

Dose burden atm. stratification slightly stable   1) LC50 = 308 mg/m^3 f. 30 Min. ———   2) TDLo = 103 mg/m^3 f. 30 Min. — — —

Fig. 3.: LC_{50}- and TCLo-values for neutral atmospheric stratification

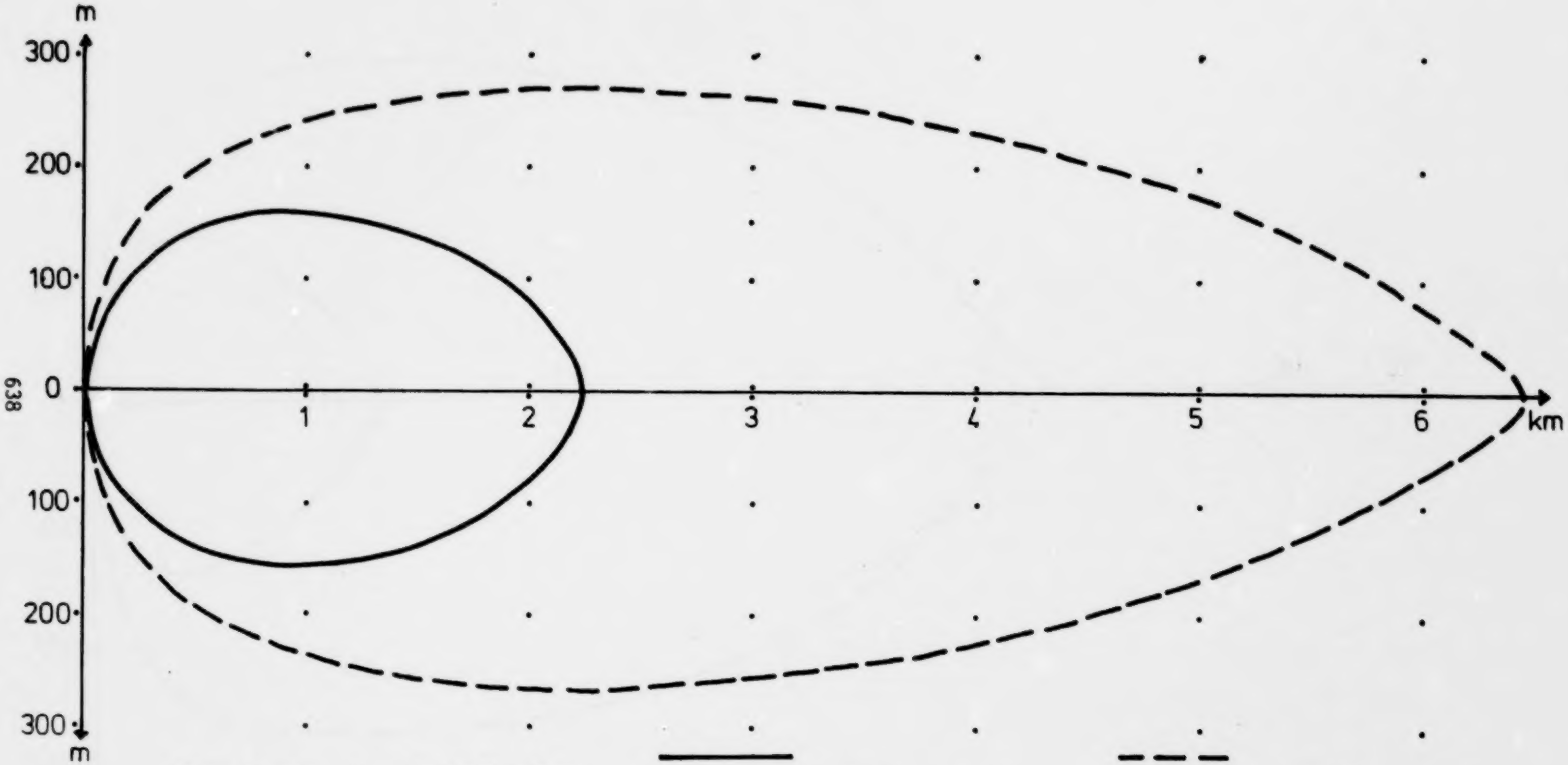

Dose burden atm. stratification
slightly stable

1) LC50 = 308 mg/m^3 f. 30 Min.

2) TCLo = 103 mg/m^3 f. 30 Min.

Fig. 4: LC_{50}- and TDLo-values for unstable atmospheric stratification

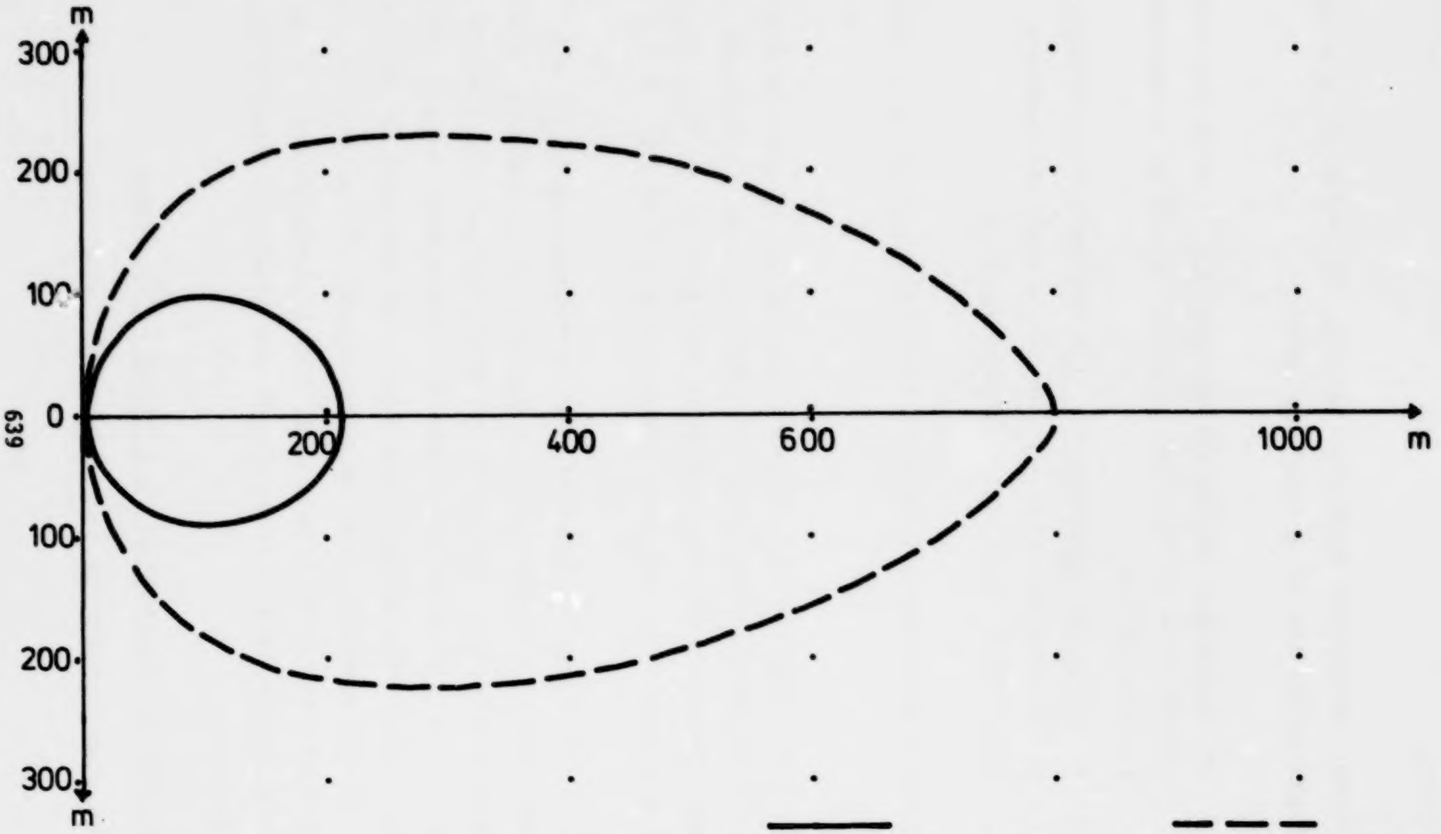

Dose burden atm. stratification
slightly stable

1) 308 mg/m^3 f. 30 Min.

2) TDLo = 103 mg/m^3 f. 30 Min.

In the following table the general way of applying finite-difference methods to coupled systems of partial differential equations has been demonstrated.

The original dispersion equation for the transmission process has been separated by use of a two-step-method:

1. step: an advection differential-equation, which has been transformed to a difference-equation by use of a backward-difference-method;
2. step: a diffusion equation, which has been transformed to a difference-equation by use of central differences (in the special procedure applied here).

The resulting difference-equations have been solved by a step-by-step-process.

To compare the results with those cited above by the TÜV Rheinland using an integrated Gaussian puff model the same conditions have been used, though this szenario does not seem to be very realistic for the authors. Only the wind speed was a bit higher (1.5 m/s).

Fig. 2 - 4 show the isolines of the corresponding LC_{50}- and TDLo-values for stable, indifferent, and unstable atmospheric stratifications. Field structure and order of magnitude of the results are comparable with the results of the TÜV Rheinland, though the methods which have been applied here are much more flexible as well with respect to the complexity of meteorological situations, to the consideration of weak-wind situations, local circulations, topography, and to the incorporation of physical and chemical transformation processes.

2.3 The particle-in-cell-method on a Monte Carlo Basis

A further step forward to the "demanded ideal model system" seems to be the very flexible particle-in-cell-method on a Monte-Carlo-Basis.

The mixed Eulerian-Lagrangian particle-in-cell-method is based on representing the continuous concentration field by means of a finite system of mass points whereby each point corresponds with a defined mass and its location is identical with the centre of gravity of the mass that it represents. Displacement of the particles, which stands for the transmission process of the material they represent, follows the trajectories resulting from local meteorological conditions. Use of the particle-in-cell method for the two-dimensional simulation of the random walk of vehicle exhaust gases in a street was carried out by Gutsche . Here, the transition probability V (Q, t/P,t..) of a particle moving from location P to location Q in the time t - t.. is characterised by the Einstein-Kolmogorow equation.

$$\begin{aligned} V\,(Q,\ t/P\ldots t..) - \int & V\,(Q,\ t/P',\ t') \\ & \times V\,(P',\ t'/P\ldots t..)\,dV_r \\ & \text{for } t.. < t' < t. \end{aligned}$$

When the process properties are given in the form of transition probabilities, the probability of a particle W (N/i, j) being at locations (i, j) after N steps is, using the two-dimensional Markow process.

$$W(N/i,j) = p^{\frac{i\ +i}{2}}\ q^{\frac{i\ -\ i}{2}}\ r^{\frac{j\ +\ j}{2}}\ s^{\frac{j\ -\ j}{2}}$$

$$\times \sum_{\delta = 0}^{\frac{N-\ i\ -\ j}{2}} \begin{pmatrix} N \\ N-\ j\ -\ \delta \end{pmatrix} \begin{pmatrix} N-\ j\ -\ \delta \\ \frac{N-\ i\ -\ j}{2} \end{pmatrix} \genfrac{}{}{0pt}{}{\frac{N-\ i\ -\ j}{2}}{\delta}$$

$$\times (pq)^{\frac{N-\ \ i\ -\ j}{}\ -\ \delta} (rs)^{\delta}$$

$$\text{for}\quad \frac{1}{2}\,(N-\ \ i\ \ j\ ) \in N \cup \{0\}$$

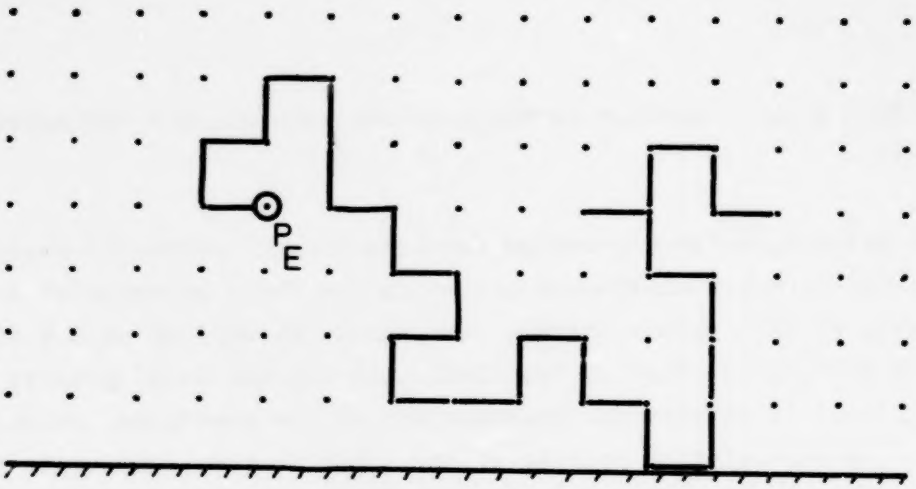

Fig. 5: Example for a two-dimensional random walk with slip boundary conditions
(Point of emission of particles P_E)

and $W(N/i, j) = 0$ elsewhere.

In the above, p and q represent the transition probabilities in the positive or negative x direction, and r and s, the transition probabilities in the positive or negative y direction.

The advantages of this method (retention of absolute positivity and mass and absolute numerical stability) must be weighed against the disadvantages of high storage capacity and computer time requirements and the need to use extremely large numbers of particles in order to achieve adequate accuracy.

Though the last-mentioned disadvantages still represent a hindrance to successfully transferring this simulation of the stochastic diffusion process with a particle-in-cell method to complex urban air pollution problems, it, nevertheless, seems to be one of the most promising methods for handling such problems in the near future, especially due to its extreme flexibility concerning all kinds of initial and boundary conditions. Till now this model type has only been applied with success to the spread of automotive emissions in street canyons and to the development of photochemical smog.

3. Conclusions

Theoretical and numerical methods for the treatment of the spread of heavy gases under failure situations exist, but all these methods - viewed upon as the state of the art in 1979 - seem to be only intermediate approximations on the way to the demanded "ideal solution" of the problem. Nevertheless, these knowledges have to be used for the formulation of ad hoc-measures in the sense, that we must be prepared already for failure problems in the times where this "ideal solution" does not yet exist and perhaps the corresponding computer does not yet exist, too.

THE UNSTEADY GRAVITY SPREAD OF A DENSE CLOUD IN A CALM ENVIRONMENT.

A.P. van Ulden,
Royal Netherlands Meteorological Institute,
De Bilt,
The Netherlands.

Abstract

The differences between stationary and non-stationary gravity currents are investigated. The one-dimensional and axisymmetric spread of a dense cloud with an almost constant volume are considered. It is shown that the commonly used Froude-number scaling is not always applicable. The reason is that a cloud never reaches a steady state. Analytic solutions are obtained for the case that surface friction can be neglected.

Introduction

In this paper we consider the spread of a dense cloud released instantaneously on a horizontal surface in a calm ambient fluid. Such a cloud will spread axisymmetrically over the ground by the action of gravity. This feature has been observed in field experiments (Van Ulden, 1974; Picknett, 1978) and in the laboratory (Hall, 1977). The spreading cloud has the appearance of an axisymmetric gravity current i.e. the cloud attains the shape of a cylinder with a sharp leading edge. The leading edge resembles the gravity current head that has been described for stationary one-dimensional spread by Benjamin (1968), Simpson (1972) and Simpson and Britter (1979). The latter type of spread can be described by a simple Froude-number relation:

$$U = \alpha\sqrt{g\frac{\Delta\rho}{\rho}\,h}\ , \tag{1}$$

where U is the velocity of the leading edge, α an empirical constant, $\Delta\rho$ the density difference between the two fluids, h a height scale and ρ a reference density. It is the purpose of this paper to investigate wether this type of scaling can also be applied to instationary gravity spreading. We do so both for one-dimensional and for axisymmetric spread.

Analysis

We consider an instantaneous release of a cloud with a mass m_0, that is greater than that of an equal volume of the lighter ambient fluid by an amount Δm. This mass surplus is a conserved quantity for the case considered in this paper, in which no heat transfer and no phase transitions take place. It is independent of the degree of mixing with the lighter fluid.

First we consider the one-dimensional spread in a deep channel with constant width B: the so called modified lock exchange process (Simpson and Britter, 1979). We denote the dimensions of the cloud by the distance X of the leading edge from the origin and by the densimetric mean height H of the upper density interface, that is defined by

Preceding page blank

$$H = 2\bar{z} \ , \tag{2}$$

where $\bar{z}$ is the height of the center of mass of the dense cloud.
We further have the cloud volume

$$V = BHX \ , \tag{3}$$

the mean density difference

$$\Delta\rho \equiv \Delta m/V \ , \tag{4}$$

the mean cloud density

$$\rho_c \equiv \rho_a + \Delta\rho \ , \tag{5}$$

where ρ_a is the density of the ambient fluid and the total mass of the cloud

$$m_c = \rho_c V \ , \tag{6}$$

or

$$m_c = \rho_a V + \Delta m \ . \tag{7}$$

In this representation the state of the cloud is described by the conserved quantities Δm and ρ_a and by the variables H and X. The latter variables may change by two processes. First we have the mean- not turbulent - velocities due to gravity spreading. These are characterized by the mean horizontal velocity U_X at the leading edge and by the mean downward velocity W_H at the upper interface. For continuity reasons these velocities are related to each other by

$$W_H = -(H/X)U_X \ . \tag{8}$$

Secondly we have the turbulent motions caused by the encounter of the leading edge of the dense fluid and the ambient fluid. Experiments (e.g. Simpson and Britter, 1979) show that the leading edge remains quite sharp. Therefore it seems reasonable to assume that the velocity of the leading edge is equal to the mean horizontal velocity just behing the leading edge:

$$dX/dt = U_X \ . \tag{9}$$

On the other hand the upper interface behind the leading edge is rather distorted. There entrainment of ambient fluid takes places that tends to increase the mean cloud height. This implies that entrainment corresponds with a relative upward motion of the dense fluid. We characterize this upward motion with an entrainment velocity W_e, that is defined by

$$W_e = \frac{dH}{dt} - W_H \ . \tag{10}$$

An alternative - but equivalent - definition of W_e is:

$$W_e = \frac{1}{\rho_a BX} \frac{dm_c}{dt} . \tag{11}$$

So W_e determines the rate at which the cloud mass increases. From (8) - (10) we see that dX/dt and dH/dt are determined by V_X and W_e. So in order to describe the spread of the cloud we need expressions for V_X and W_e. We will derive such expressions by considering the energy budget of the cloud.

The energy budget

Due to its mass surplus the cloud possesses an amount of potential energy (PE) equal to:

$$PE = g\Delta m\bar{z} ,$$

or

$$PE = \tfrac{1}{2}g\Delta mH , \tag{12}$$

This potential energy is the energy source for gravity spreading. As the cloud height decreases energy is transformed first into kinetic energy (KE) of the mean velocities, then into turbulence (TE) and from turbulence partly by entrainment back into potential energy, partly by viscous dissipation into internal heat (IH).

As there is no external energy source the total energy in a large control volume is conserved:

$$\frac{dPE}{dt} + \frac{dKE}{dt} + \frac{dTE}{dt} + \frac{dIH}{dt} = 0 . \tag{13}$$

Let us evaluate the various terms in this equation.
From (12) and (10) we have for the potential energy:

$$\frac{dPE}{dt} = \tfrac{1}{2}g\Delta mW_H + \tfrac{1}{2}g\Delta mW_e . \tag{14}$$

Since W_H is negative and W_e positive the potential energy decreases by gravity spreading and increases by entrainment of air.
The kinetic energy is mainly due to the mean outward horizontal spreading velocity. We neglect the contributions to the kinetic energy of secondary flows. This implies that we assume that in the bulk sense hydrostatic equilibrium is maintained. From the continuity equation it follows that the velocity U increases linearly with the distance x from the origin:

$$U(x) = (x/X)U_X . \tag{15}$$

The total kinetic energy is thus approximately given by

$$KE = B \int_0^X \tfrac{1}{2}\rho_c U^2 dx .$$

This yields

$$KE \approx \frac{1}{6} m_c U_X^2 \tag{16}$$

and

$$\frac{dKE}{dt} = \frac{1}{3} m_c U_X \frac{dU_X}{dt} + \frac{1}{6} U_X^2 \frac{dm_c}{dt} . \tag{17}$$

Using (7) and (11) we may write this equation as

$$\frac{dKE}{dt} = \frac{1}{3} m_c U_X \frac{dU_X}{dt} + \frac{1}{6} m_c U_X^2 \frac{\rho_a W_e}{\rho_c H} . \tag{17}$$

The third term in the energy equation (13) is determined by the turbulent energy equation integrated over the control volume (Monin and Yaglon, 1971):

$$\frac{dTE}{dt} = SP - BD - D . \tag{18}$$

Here SP stands for shear production, BD for buoyant destruction and D for the dissipation into internal heat. The transport terms that are present in the energy equation are assumed to vanish at the boundaries of the control volume.

The shear production of turbulence occurs mainly at the leading edge. We will assume that the contributions to the production due to friction with the surface and at the density interface behind the leading edge can be ignored (Simpson and Britter, 1979, Britter, 1979).

The leading edge of a gravity current that advances over a no-slip horizontal surface will have a distinct nose at some height above the surface. Below the nose lighter fluid is overrun by the dense fluid. This leads to the lobes and clefts structure with enhanced production of turbulence and mixing of the two fluids that has been described by Allan (1971) and Simpson (1972). Above the nose Kelvin - Helmholz instabilities develop that grow and turn over in a breaking zone behind the head. Here a strong production of turbulence and mixing of the two fluids occurs.

We may estimate the total production of turbulence at the leading edge as follows. The advancing head encounters undisturbed fluid at a rate proportional to BHV$_X$. The undisturbed fluid is accelerated and receives kinetic energy that scales with $\frac{1}{2}\rho_a U_X^2$. Therefore the total production rate of turbulence at the leading edge should scale as:

$$SP \approx \tfrac{1}{2}\beta B H \rho_a U_X^3 ,$$

or

$$SP \approx \tfrac{1}{2}\beta \frac{\rho_a}{\rho_c} m_c \frac{U_X^3}{X} . \tag{19}$$

The second term in the turbulent energy equation is the buoyant destruction. This term is just equal to the potential energy gain by entrainment of ambient fluid:

$$BD = \tfrac{1}{2} g \Delta m W_e \ . \qquad (20)$$

Finally the dissipation equals the gain in internal heat in the energy equation:

$$D = \frac{dIH}{dt} \ . \qquad (21)$$

Using (14) - (21) we may write the energy equation (13) as:

$$\frac{1}{3} m_c U_X \frac{dU_X}{dt} + \frac{1}{6} m_c U_X^{2} \frac{\rho_a W_e}{\rho_c H} + \tfrac{1}{2} g \Delta m W_H + \tfrac{1}{2} \ \frac{\rho_a}{\rho_c} m_c \frac{U_X^{3}}{X} = 0 \ . \qquad (22)$$

By dividing this equation by $\frac{1}{3} m_c V_X$ and by using (4), (6) and (18) we obtain a bulk momentum equation:

$$\frac{dU_X}{dt} + \frac{1}{2} \frac{\rho_a W_e U_X}{\rho_c H} - \frac{3}{2} \frac{g \Delta \rho H}{\rho_c X} + \frac{3}{2} \beta \frac{\rho_a}{\rho_c} \frac{U_X^{2}}{X} = 0 \ . \qquad (23)$$

We may interpret the various terms in this equation as follows. The first term represents the acceleration/deceleration of the gravity current, the second term the effect of the increase of the cloud mass, the third term the bulk static pressure gradient and the fourth term the bulk dynamic pressure gradient. We will use this equation to investigate the differences between steady-state gravity spreading and the non-steady spreading of a cloud.

The steady-state gravity current.

For a steady-state gravity current $dU_X/dt = 0$. In this case the momentum equation may be written as:

$$U_X^{2} + \frac{W_e U_X X}{3 \beta H} = \frac{1}{\beta} \frac{g \Delta \rho H}{\rho_a} \ . \qquad (24)$$

where we have multiplied (23) by $2X/3\beta$.
Since we want to solve (24) for U_X, we make an estimate for W_e in terms of U_X. We make the assumption (Tennekes, 1973) that the potential energy gain by entrainment is a fixed fraction γ of the turbulent energy production. Using (19), (20), (4) and (6) we then obtain:

$$W_e = \gamma \beta \frac{\rho_a U_X^{3}}{g \Delta \rho X} \ . \qquad (25)$$

The momentum equation now becomes

$$U_X^{2} \left(1 + \gamma \frac{\rho_a U_X^{2}}{3 g \Delta \rho H}\right) = \frac{1}{\beta} \frac{g \Delta \rho H}{\rho_a} \ . \qquad (26)$$

In order to estimate the constants γ and β we use the experimental results and the analysis by Simpson and Britter (1979). These authors used a height scale h_4, that is approximately one half of our densimetric mean height H. Using this relation and extropolating the SB results to the case of an infinetely deep channel we find that

$$U_X^2 \approx \alpha^2 \frac{g\Delta\rho H}{\rho_a} , \qquad (27)$$

with $\alpha^2 \approx 1.0$.
It further follows from the SB experiments that $\gamma \approx 0.1$. This implies that the entrainment term in (26) is quite small.

Upon neglecting the entrainment term in (26) we retrieve the Froude-number scaling (27) from our momentum equation with

$$\alpha^2 \approx \frac{1}{\beta} \approx 1.0 . \qquad (28)$$

The value of α^2 and thus of β is somewhat dependent of the height of the nose of the gravity current as shown in the SB paper. This need not concern us in this paper, since we are primarily interested in the differences between the steady and the unsteady gravity current.

The unsteady gravity current

Neglecting the entrainment in (23) we have as approximate equation for the unsteady gravity current:

$$\frac{dU_X}{dt} - \frac{3}{2} \frac{g\Delta\rho H}{\rho_c X} + \frac{3}{2} \beta \frac{\rho_a U_X^2}{\rho_c X} = 0 . \qquad (29)$$

The solution of this equation is:

$$U_X^2 = \alpha^2 \frac{g\Delta\rho H}{\rho_a} \{1 - (\frac{X_o}{X})^{\frac{3\rho_a}{\alpha^2\rho_c}}\} + U_o^2 (\frac{X_o}{X})^{\frac{3\rho_a}{\alpha^2\rho_c} + 1} , \qquad (30)$$

where

$$\alpha^2 = \frac{1}{\beta - \frac{\rho_c}{3\rho_a}} . \qquad (31)$$

and where U_o and X_o are the initial values of U_X and X. Let us envestigate the behaviour of this equation for the case that the initial velocity $U_o = 0$. It follows that the spreading rate first increases due to the static pressure gradient. Later it decreases due to the development of the dynamic pressure gradient and the decrease of the static pressure gradient. In this respect we may note that crudely H is inversely proportional to X. The asymptotic behaviour of (30) for large values of X/X_o is interesting. We may distinguish betwgen two different cases.
I. $\alpha^2 > 0$. These values of α^2 are obtained when $\rho_c < 3\beta\rho_a$.
The asymptotic solution is:

$$U_X^2 = \alpha^2 \frac{g\Delta\rho H}{\rho_a} . \qquad (32)$$

In this case the Froude-number scaling is retrieved. The value of α however is different from that for the steady-state gravity current. With $\beta \simeq 1.0$ and $\rho_a/\rho_c < 1$ we find

$$\alpha \geqslant 1.2 \; . \tag{33}$$

This value is at least 20% higher than the steady state value. The difference increases with increasing density difference. The explanation for this feature is that a cloud never reaches a steady-state. The gravity current continuously has to be decelerated and therefore its velocity is allways somewhat above its steady-state equilibrium. The relative importance of the deceleration of the cloud, that scales with ρ_c, in comparison with the dynamic pressure gradient, that scales with ρ_a, increases with increasing density difference. This result contradicts the results obtained by Simpson and Britter (1979). The present theory shows however that the omittance of the term between brackets in (30) may easily lead to an underestimate for α.

II. $\alpha^2 < 0$. This occurs when $\rho_c > 3\beta\rho_a$.

The asymptotic solution is:

$$U_X{}^2 = -\alpha^2 \frac{g\Delta\rho H}{\rho} \left(\frac{X}{X_0}\right)^{-\frac{3\rho_a}{\alpha^2\rho_c}} \; . \tag{34}$$

In this case the Froude-number scaling is not retrieved. The velocity U_X vanishes more slowly with increasing X/X_0 than in the former case. This is caused by the weakening of the dynamic pressure gradient for decreasing values of the density ratio ρ_a/ρ_c. Of course we realize that the above results are based on the assumption that β is a constant for all values of ρ_a/ρ_c and that the direct effect of surface friction is small in comparison with the dynamic pressure gradient. The latter requrement is not easily met in experimental practice for small ρ_a/ρ_c, when the dynamic pressure gradient is relatively small.

Axisymmetric spread

In the same way as for the one-dimensional spread we may derive a bulk momentum equation. It reads:

$$\frac{dV_R}{dt} - \frac{2g\Delta\rho H}{\rho_c R} + 2\,\beta\frac{\rho_a}{\rho_c}\frac{V_R{}^2}{R} = 0 \; . \tag{37}$$

Here R is the cloud radius and V_R the velocity of the leading edge. The solution of this equation is:

$$V_R{}^2 = 2\,\frac{g\Delta\rho H}{\rho_a}\left\{1 - \left(\frac{R_0}{R}\right)^{\frac{4\rho_a}{\alpha^2\rho_c}}\right\} + V_0{}^2\left(\frac{R_0}{R}\right)^{\left(\frac{4\rho_a}{\alpha^2\rho_c} + 2\right)} \; . \tag{38}$$

where R_0 is the initial radius and

$$\alpha^2 = \frac{1}{\beta - \frac{1}{2}\frac{\rho_c}{\rho_a}} \; . \tag{39}$$

Now for $\alpha^2 > 0$ the asymptotic solution is (with $V_o = 0$)

$$V_R^2 = \alpha^2 \frac{g\Delta\rho H}{\rho_a} . \qquad (40)$$

With $\beta = 1.0$ and $\rho_a/\rho_c < 1$ we obtain

$$\alpha > 1.4 . \qquad (41)$$

This is about 20% higher than the value for the one-dimensional current and at least 40% higher than that of the stationary current.

Conclusions

We have derived simple bulk momentum equations that describe the one-dimensional and axisymmetric gravity spread of a dense cloud. The analytic solutions of these equations show that this spread differs from steady state gravity spreading. The reason is that the spreading cloud never reaches a steady-state.

The present theory provides a tool to analyze this type of gravity spreading. It further is a step toward a more complete description of gravity spreading because in principle the effects of surface friction etc. can be incorporated in the momentum equations derived in this paper. These results imply that the analysis of the gravity spreading of a cloud as made e.g. by Van Ulden (1974) has to be revised. Research in this direction is being undertaken.

References

1. J.R.L. Allan, Mixing at turbidity heads and its geological implications, J. Sedimentary Petrology, 41, 97-113, 1971.

2. T.B. Benjamin, Gravity currents and related phenomena, J. Fluid Mech., 31, 209-248, 1968.

3. R.E. Britter, The spread of a negatively buoyant plume in a calm environment, Atm. Environment, 13, 1241-1247, 1979.

4. D.J. Hall, Further experiments on a model of an escape of heavy gas, Warren Spring Laboratory, Report LR 312 (AP), 1979.

5. A.S. Monin and A.M. Yaglon, Statistical Fluid Mechanics, 393-400, 1971.

6. R.G. Picknett, Field experiments on the behaviour of dense clouds, Chemical Defence Establishment Porton, Report No. Ptn IL 1154/78, 1978.

7. J.E. Simpson, Effects of lower boundary on the head of a gravity current, J. Fluid Mech., 53, 759-768, 1972.

8. J.E. Simpson and R.E. Britter, The dynamics of the head of a gravity current advancing over a horizontal surface, J. Fluid Mech., 94, 477-495, 1979.

9. H. Tennekes, A model for the dynamics of the inversion above a convenctive boundary layer, J. Atm. Sci., 30, 558-567, 1973.

10. A.P. van Ulden, On the spreading of a heavy gas released near the ground, Int. Loss Prevention Symp., The Netherlands (edited by C.H. Rushmann), Elsevier Amsterdam, 221-226, 1974.

Discussion:

(Rapporteur: P. Prahm):

Kaiser:

Can your approach be modified to include the case in which the puff of dense gas is very cold, so that there is a possibility that turbulence will be generated because the gas is heated by the ground?

Van Ulden (response):

Yes, but then this should be accounted for in the energy equation.

Venkatram:

I noticed V term in your equations. Could you eyplain how it is estimated?

Van Ulden (response):

It can be estimated by different conventional procedures.

Schulte:

Does your model include the effects of the heat of evaporisation such as one has with ammonia?

Van Ulden (response):

No, the model does not include any heat effects but can e. g. treat chlorine and freon. Ammonia is much more complicated!

THE INVESTIGATION INTO THE SPREADING AND DISPERSION OF A HEAVY GAS CLOUD BY MEANS OF PLANT DAMAGES IN THE AFFECTED AREA

by

C.G.Booij
Landbouwhogeschool
Wageningen
Netherlands

Abstract. The methods used in the investigation of the effects of a chlorine spill on the affected area,in which heavy plant damages were found,are reported.
The judging of the appearance of stricken in comparison with that of plants,exposed to a known concentration during a known exposure time,played a big role in this investigation. The results of exposure tests lead to the drafting of an exposure - effect - relationship that was used in estimating the conditions that must have existed in the affected area.

Introduction

On a dreary summer day,some years ago,at approx.5.20 a.m. some 5 tons of liquid chlorine escaped within 9 minutes from a large hole in a pipeline inside an unoccupied building.

There is no need to reveal,where this happened,as the cause of this accident was so trivial that it might have happened anywhere.

Part of the liquid flashed immediately,but most of it dropped on the floor and formed a pool that spread out to the ground outside the building via the slit underneath the closed doors.There it evaporated and the cloud was carried away by the light southern wind (1 to 1.5 m/s) to the nearby town at some 500 metres distance,thus crossing a 60 metres wide canal and a 400 metres stretch of rough grass land.

It passed through and over the fairly densily populated residential and industrial area of the town and reached the railway station (at 1800 m from the source) after approx.20 minutes, at the time of arrival of two trains by which some 200 labourers came to their work.

All of the train passengers suffered moderate to light eye - and throat irritation.Many people in the town complained about the strong smell,still present 3 hours after the leak occurred.Some people that were outside in this towns quarter when it was hit by the cloud complained about sickness and/or severe irritation of the throat,eyes and nose.

But only three men were treated in hospital for some hours, returning to work the same or the following day,and one operator of the factory involved was treated in an oxygen tent,recovering well and fast.

So there were no human casualties.

As for the fauna,some paroquets and a rabbit were killed, some hens were in such a bad condition that they had to be slaughtered and a goat was injured badly in its respiratory system.(The investigators forgot to look for dead wild birds,but it may be assumed that the harm done to this group of animals must have been extremely light,as nobody of the towns people reported any findings on this subject.)

No harm was done to commodities etc.outside the building.

But the flora in the affected area was in a terrible state. Many small plants (in a limited area) were killed,very many were severely damaged and had lost their leaves and nearly all plants, hedges and trees in the area were at least slightly damaged, showing discoloured leaves.

As a matter of fact the boundaries of the affected area were deduced from the appearance of the plants.Plant damage formed an important subject in the whole of the investigation of the accident.

A factory managment does not install measuring gear just for the purpose of determining the loss of material during an accident,nor for the indication of concentrations of spilled material somewhere around the premises that may never occur.

So in the case that is discussed now there were no (exact) data on the flow rate of chlorine through the leak,nor on the duration of that flow,nor on concentrations in the affected area.

That means,that the total amount of spilled chlorine and its effects on the environment had to be estimated on the basis of the results of calculations,interviews,simulations,site inspections,tests,plain reasoning and hypotheses,which should fit like the pieces of a giant jig saw puzzle.

Therefor each one of the results was cross checked against all others of the available data,which was some sort of running the gauntlet.

Some observations

Interviews,simulation of actions of operating personel, observations inside the building inwhich the leak occurred and some calculations led to the conclusion that the duration of the escape must have been 9 minutes or thereabout.

The flow rate was calculated and recalculated after cross checking over and over again and was estimated to be approximately 8 kg/s,so that the total amount was sized up to 5 tons.

From this quantity some 18% flashed off immediately,i.e.0.9 tons were emitted within the above mentioned 9 minutes.

The remaining liquid dropped on the floor and spread out outside the building.But doing so it hit relatively hot ground

on which it boiled off,thus limiting the spreading.
The surface temperature deminished due to the heat extraction form the ground and the boiling stopped.It was replaced by non-boiling evaporation.

It could be estimated from eye witness reports and calculations that the boiling stopped six minutes after the leak had been closed.In this time another 2.7 tons may have evaporated,so that the total amount of chlorine vapour that was emitted within 15 minutes was about 3.6 tons;1.4 tons of liquid remained on the ground and evaporated slowly.The last whiffs of cloud on the factory site were seen about 3 hours after the leak was closed.

The produced clouds slumped immediately,forming a pan cake with a 10% chlorine content,which was pushed forward to the canal by the slight wind.

"Like a flock of lambs" - that was the description that one of the eye witnesses gave of the clouds rolling over the southern bank of the canal.That observation fitted well with those on the plants on this bank.All lower plants were killed,but the stronger thistles showed heavy damage up to 40 cm height and green leaves above that mark.

The cloud spread out over the canal water and filled the space above it.The normal height of the northern bank over the water is 3 metres,but there is a slip-in harbour more or less opposite the storage area on the factory site,where the chlorine evaporated.The quay height is approx.1.5 m above the water.
The cloud filling the space above the water formed a buffer from which only moderate dispersion took place according to the eye witnesses.This buffer grew untill it reached the quay height and there it started flowing over the adjacent area before slumping completely.and eventually dispersing.This happened just before the boiling of the liquid pool stopped,so that only some 500 kilograms of chlorine (in an approx.10% cloud) spread over the lower part of the rough grass land.

There is one storey house alongside the slip-in harbour.
The family living in this house slept with their windows closed, because of the frequently occurring stench from an other factory nearby.And so they slept well although the chlorine clouds played around their house.They awoke at 6 o'clock,when all was over bar shouting,their garden a ruins,their chickens nearly dead but their canaries in the aviary in the shrubs behind the house, on top of the chicken run,sang lustily like one o'clock!(fig.1)

And 50 metres away people stood on the bridge over the canal, 5 to 10 metres above the clouds and they remained there all the time,without suffering more than a slight smell.

Most of the plants in the garden (potatoes,broad beans,etc.) were dead.So were most of the plants in the lower part of the rough grass land running up to the boundary of the inhabited towns quarter.And even in that quarter,in line with this lower grass land,several dead plants were found.Here too the killed rabbit and the injured goat were found!

On the higher part of the rough grass land no dead plants were found,though severely damaged plants were found in the area adjacent to the lower part.More to the east only moderately and slightly damaged plants were found.The total width of the stricken area was 300 m at the northern bank increasing to 400 m near the boundary of the towns quarter.

The total width of the affected area in the town remained more or less constant (400 to 600 metres),which must be due to the limited lateral spreading between the houses.

Severe plant damage was found up to approx.800 metres from the source and in some spots even further away.These remote effects must be attributable to lingering parts of the chlorine clouds,for in general a distinct decrease in damage in relation to the distance could be observed.This observation was used in an attempt to assess concentrations to which people in the affected area must have been exposed.

There were only a few people about though,because most of the inhabitants slept and most of them slept with closed windows.

Exposure - effect - relationship for plants

A large number of photographs have been made of all sorts of plant,hedges and trees all over the affected area of the town, within 72 hours after the accident occurred.
From the study of these photos it followed,that the investigation should be limited to the area up to 1800 m from the source (i.e. south of the railway station).The photos north of this station showed too large inconsistencies for which no valid explanation could be found,unless lingering cloud parts were assumed.
Furthermore the photos south of the station showed the worst damages.

This study also showed that the investigation should be concentrated on stinging nettles to start with as these photos covered the chosen area to a large extend.

So the complete series of pictures of stinging nettles was collected and it was given to a panel of 5 independent observers, who should judge them on the severity of plant damage and arrange them accordingly.

Then a series of tests was carried out with fresh stinging nettles in an unaffected area near the factory involved.

In each test a group of plants was exposed to a known concentration during a known exposure time.A photo was made of each group of plants a few hours after the exposure.
These photos were given to three panels of observers with the same assignment as mentioned above.

These panels agreed fairly well in their arrangements,which indicated that this method of judgment by photos could be justified.

Then the panels were asked to insert the photos of the plants in the affected area into the package of photos from the tests.

Here again the panels showed a remarkable unanimity, as only 3% of the individual observations deviated.

So a rough indication of the conditions in the affected area could be given.

The tests were then extended to other plants that had been damaged in the towns quarter. The Instituut voor Plantenziektekundig Onderzoek (Institute for Phytopathological Research) in Wageningen, closely related to the University of Agriculture, did a large number of tests in their test warehouses.

Stinging nettles, thistles, broad beans, persicaria, sweet-williams, mugwort, petunia and waybread were grown and groups of each one of these families were then exposed to a combination of exposure time and concentration of chlorine.
These combinations were chosen so as to give the best information about the relationship between the exposure load and the effect thereof in this type of short exposure.

It was found that this relationship could best be expressed as:

$$E :: c^2 . t_{ex} \qquad (1)$$

in which

E = observed effect (severity of damage)
c = chlorine concentration in mg/m^3
t_{ex} = exposure time in minutes.

From this equation it follows that a high concentration during a short exposure time may give a worse effect than a low concentration during a long exposure time.

This also means that the severest damage to a plant, exposed to a varying concentration, may be inflicted during the short time in which the highest concentration occurred.

This result was applied to the case under study, for which an exposure time for the highest concentration of approx. 10 to 15 minutes had been estimated.

And again a good agreement between test results and local observations was found, which more or less confirmed the justification of the applied method.

Chlorine absorption in plants

The same series of tests were also used to determine the amount of chlorine that was absorbed by the plants.

It was found, that the chlorine content in the plants depends largely on the concentration in the gas cloud to which the plants are exposed, as long as the plants are not killed.

Some types of plants absorb more chlorine than others under the same conditions,so for instance thistles.

The average absorption in the tested types of plants however varies with the dose to which they were exposed,i.e.:

$$C \;::\, c\;.t_{ex} \qquad (2)$$

in which

C = chlorine content in plants in weight% in dry material
c = chlorine concentration in air in mg/m^3
t_{ex} = exposure time in minutes.

The average absorption varied from 0.1% at a dose of 100 $mg.min/m^3$ to 5% at a dose of $5.\ 10^6$ $mg.min/m^3$.

The average dose on the rough grass land must have been something like 10^4 $mg.min/m^3$,which means that the mean chlorine content in the plants in this stretch of land must have been 0.5% in dry.In average 1 kg of dry material grows on 1 m^2 (incl. shrubs,hedges and small trees) of this land.
So the chlorine absorption in this area may have amounted to approx. 1 ton,of which some 600 kg may have been neutralized within the first 10 minutes.

Comparison of "measured" and calculated concentrations.

From the foregoing it follows,that

- the boundary of the towns quarter was exposed to far less than 5 tons of chlorine
- the exposure was delayed due to the neutralization of the first clouds passing over the grass land
- the remaining load was spread out over a width of 300 to 400 m.
- the remaining load was spread out over a considerably longer time than the duration of the leak.

In the towns quarter itself more chlorine will have been neutralized by the plants.

From the plant damages it was apparent that the lateral dispersion in the town was suppressed;the vertical dispersion will have been suppressed due to the gravity influences on the (still heavy) cloud.

All this beeing taken into account the concentrations in the towns quarter have been calculated,using the Gaussian formula, splitting the calculations into two parts,i.e.:
a.for the towns boundary,starting from a 300 m wide line source,
b.for various photographed plant locations in the towns quarter south of the railway station,starting from a 450 m wide line source at the towns boundary.The results of this procedure showed fair agreement with those from the plant judging.

And although no exactness can be claimed for each one of these approaches,the results gave some more confidence in the applicability of the applied methods.

Effects on man.

The main objective of the investigation was to make out,if this accident had produced dangerous situations for man.

An exposure - effect - relationship for the respiratory system of man was derived in analogy to the one for plants,and this was applied to the data that were found in the above mentioned procedures.(Afterwards it was found out,that Eisenberg et.al. had published a similar relationship in their report "Vulnerability Model".)[1]

From this it was concluded,that there may have existed a fatal situation during a very short time (1 minute) in a small area at the towns boundary,in line with the lowered grass land.

A dangerous,but not fatal,situation may have occurred at the towns boundary near the centre of the cloud path and this situation may have existed for some 10 minutes,from 5.30 to 5.40 a.m.

Severe irritations may have been inflicted on men,out in the streets up to 1000 m from the source;this situation again may have existed for maximum 10 minutes at this far distance, but at the towns boundary it may have lasted for nearly two hours.

Moderate and light irritations will have been possible all over the towns quarter during more than two hours.

These conclusions were checked against the experiences of several people,that had been in the stricken area,for instance police officers,post men,paper boy,railway men,people going to their work.The news boy for instance had been crossing the area for more than an hour,protecting himself only with a wetted handkerchief and a scarf,without severe complaints.The police officers on the other hand reported sick after driving their car through the heaviest parts of the cloud for no more than two minutes.

All reports from these people fitted fairly well in the overall picture that had been derived from the plant judgments, calculations and interviews with factory personnel.

Conclusion.

Judging of plant damages by means of photographs may play an important role in investigating the effects of a release of an agressive and toxic gas.

References.

1. N.A.Eisenberg,C.J.Lynch,R.J.Breeding,
"Vulnerability Model:A Symulation System for Assessing Damage Resulting from Marine Spills".Enviro Control,Rockville,USA, 1975.

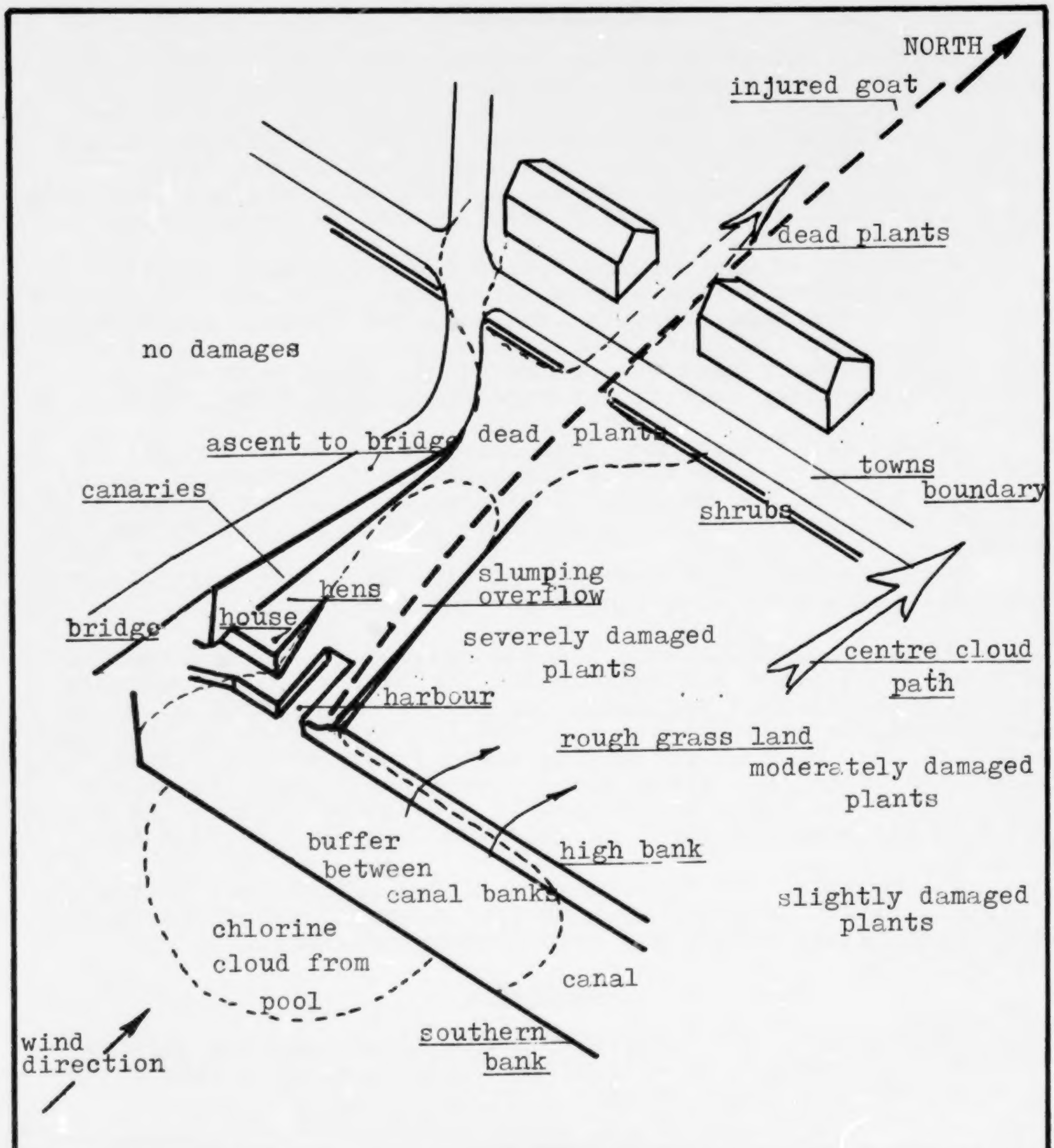
NORTH
injured goat
dead plants
no damages
ascent to bridge
dead plants
towns boundary
canaries
shrubs
slumping overflow
hens
house
bridge
severely damaged plants
centre cloud path
harbour
rough grass land
moderately damaged plants
buffer between canal banks
high bank
slightly damaged plants
chlorine cloud from pool
canal
southern bank
wind direction

FIG.1 SITUATION CLOUD IN CANAL AND OVER ROUGH GRASS LAND

FIELD TRIALS ON THE RELEASE OF HEAVY GASES

by

J. McQuaid
Research and Laboratory Services Division
Health and Safety Executive
Red Hill, Sheffield S3 7HQ, UK

Abstract. In 1976, the UK Health and Safety Executive (HSE) commissioned the Chemical Defence Establishment (CDE) to carry out a programme of field trials on the dispersion of heavier-than-air gases in the atmosphere. In each trial a quantity of up to 200 kg of gas at atmospheric pressure and temperature was rapidly released from an enclosure and the subsequent behaviour of the cloud was studied. A total of 42 trials was performed in a variety of atmospheric conditions and covering a range of initial densities. This paper presents the background to the programme, describes the trials and summarises the results obtained. HSE is currently considering a proposal to conduct further field trials, in which quantities of up to 10 tonnes of heavier-than-air gas would be released. The details of this proposal are discussed.

Introduction

The UK Advisory Committee on Major Hazards (ACMH) was appointed in 1974 to advise on measures of control over installations (excluding nuclear installations) which have the potential to present major hazards to employees or to the public or to the environment. The Committee issued its First Report in 1976.[1] In that report, the ACMH expressed themselves as unhappy about the state of knowledge on the behaviour of a massive release of gas from industrial operations in which large quantities of toxic or flammable gas are stored or handled. At an early stage in their work, the Committee asked HSE to consider instituting an experimental programme to clarify the areas of doubt which existed at the time. In response to this request, HSE identified the experiments that were most urgently needed and that were considered to be feasible, given the difficulty and expense that the Committee itself acknowledged were associated with this kind of research. A programme of work was drawn up in two parts: (i) a series of moderate-scale field experiments on the dispersion of heavier-than-air gas and (ii) a further series of field trials, consecutive to (i), involving larger quantities of gas more closely approaching the scale of possible releases from industrial operations and which would draw on the experience and knowledge gained from the first series. This paper describes the outcome of (i) and considers the proposal for (ii).

The Formulation of the Research Programme

The Practical Problems

The release of a hazardous fluid after an accidental loss of containment can take many forms. No single, feasible programme of research could hope to simulate all of the variables that influence the ultimate consequences of such a loss of containment. An obvious initial restriction on the programme was therefore to consider only the definition, in space and time, of the distribution of concentration following the release. The effects of ignition, in the case of a flammable gas, or the response of the population, in the case of a toxic gas, are issues that are being pursued separately and ultimately can only be resolved when the concentration field has been defined.

Once this restriction had been accepted, the following questions were considered:

(i) What modes of cloud formation should be examined?

(ii) At what scale should the experiment be carried out?

(iii) What are the significant parameters?

The answers to these questions will be influenced by some or all of the following:

(i) The circumstances under which the most hazardous releases occur.

(ii) The state of existing (or developing) knowledge both analytical and experimental.

(iii) The feasibility of a scale experiment that takes account of existing technology, the availability of facilities, the likely expense and the probability of a successful outcome.

The Form of Trials Chosen

An examination of catastrophic failures that have resulted in the release of hazardous material to the atmosphere showed that those failures in which a large amount of material was released in a short time were the most important from the point of view of the severity of the consequences. It was decided therefore that in the experimental programme short-term releases would be assigned a higher priority than continuous ones.

The material released could be in the form of a gas, a liquid or a two-phase mixture. It appears to be a characteristic of catastrophic failures, however, that, irrespective of the conditions that prevail immediately upon loss of containment, a cloud forms very quickly around the failed container. This cloud once formed then has to mix with the atmosphere before it is rendered safe. It therefore seemed plausible to consider a division of events into:

(i) the release history, from loss of containment up to the formation of a cloud, and

(ii) the dispersion history of the cloud so formed.

Divided in this way, part (i) could then be separately examined in order to relate the initial cloud size, shape, density and whatever else is found to be important, to conditions when containment is lost - including the storage conditions, the flow from the breach, the percentage flash evaporation of material, the energy available for projecting the contents into the surrounding atmosphere, and so on. The mechanism of cloud formation is specific to particular cases and improved understanding is more likely to accrue from several independent lines of investigation than from simulations of particular cases. Several such lines of investigation were identified and are being pursued as part of HSE's research programme. But part (ii) provided a promising possibility for work of general application since it is common to many different cases. On grounds of the probability of a generally useful outcome, a study of part (ii) was assigned a higher priority than a study of part (i).

A review of relevant previous work was carried out.[2] This showed that previous programmes generally had quite specific objectives related to the type of escape of prime concern to the sponsoring organisation and gave results of limited general application. HSE was able to benefit from the experiences of others, and thus identify difficulties and frame a programme that would provide broad conclusions applicable to a wide range of conditions. To do this, it was essential to limit the number of variables as much as possible and to have an experimental arrangement where close control could be exercised on the release conditions. These requirements suggested the use of a wind tunnel but problems of scaling and the lack of suitable tunnel facilities in the UK ruled out this solution and it was decided that field trials should be carried out. It was concluded that the quasi-instantaneous release of a cloud of dense gas would be potentially the most rewarding topic for investigations, taking account of the frequency of historical occurrences and the lack of previous work, even for neutrally-buoyant gases.

In an experimental programme on such releases, it was considered that the simulant source should satisfy the following criteria:

(i) the volume and configuration of the released gas cloud must be repeatable;

(ii) the physical conditions of the released gas and the duration of the release must be repeatable;

(iii) the energy input into the cloud from the release mechanism (eg sudden rupture releasing stored pressure energy, or vigorous flashing of a liquid stored above its normal boiling point, or rapid evaporation of a fully-refrigerated liquefied gas contacting hot surfaces) must be minimised or indeed eliminated altogether.

To satisfy these criteria, the source necessarily had to be a preformed cloud of gas at ambient pressure and temperature in a container which could be rapidly removed and whose removal would not unduly disturb the cloud but would leave it ready to respond to the dispersive forces acting on it.

Although the ACMH had envisaged experimental releases of tonnage quantities, the mechanism of the density-driven behaviour was not well enough understood to provide reasonable assurance that a large release would not be wasteful of effort. A large release would also pose difficulties of organisation, since range safety considerations, given the inadequate knowledge, severely limited the choice of facilities. It was therefore decided to commence with a series of trials that could safely be conducted on a range of 1 km extent and to consider, at a later date, in the light of the results obtained, the feasibility of the larger releases originally envisaged. It was estimated that releases of up to 200 kg of heavy gas could be accommodated within the constraint. The range facilities at the Chemical Defence Establishment, Porton Down were identified as suitable and indeed that establishment has considerable experience and a long tradition of conducting field trials on dispersion in the atmosphere. The range at Porton Down offers both flat and sloping sites that are unobstructed and have uniform ground roughness.

Further stimulus to this choice of experiment was provided by the work of van Ulden[3] which offered an analysis of dispersion from the chosen source configuration. An analytical framework therefore existed which fortunately coincided with the identified need and this combination was the final determinant in deciding the way to proceed.

In summary, the experimental configuration adopted consisted of the sudden release of up to 200 kg of gas as a preformed cloud of defined shape and its dispersal over uniform and unobstructed flat or sloping ground.

Objectives of the Trials

The broad objective of the trials was to determine the concentration distribution in space and time consequent upon the release of a cloud as defined above, and specific objectives were to study the effects of

(i) the initial density of the cloud;

(ii) the atmospheric stability and wind speed;

(iii) the ground roughness, and,

(iv) the ground slope.

The Programme of Trials

Experimental Conditions

The volume and configuration of the initial cloud were the same in all experiments and were obtained by use of a collapsible-sided plastic tent in the form of a cube of volume 40 m^3. The tent was filled with a mixture of Refrigerant-12 (dichlorodifluoromethane, CCl_2F_2) and air to produce clouds of the desired initial relative densities. It was decided that most of the trials would be carried out on as flat a site as was available on the Porton range.

A total of 42 trials was carried out, not all of which were classed as successful. In these trials the following ranges of independent variables were covered.

Initial density of mixture (relative to air)	1.0 - 4.2
Wind speed m/s	0.4 - 7.6
Pasquill atmospheric stability category	B - G
Roughness height mm	2 - 150
Slope	Level to 1 in 14

The full description is given in the report on the trials which is now available.[4] The list of trials is given in Table 1.

Experimental Procedure

In all the trials, orange coloured smoke was added to the dense vapour/air mixture which was then vigorously stirred. The smoke coloured mixture was left a few seconds to become quiescent and then released. On operation of the release mechanism the tent collapsed to the ground in less than 1 second. The trial site was marked out with surveying poles to give horizontal and vertical distance scales and the behaviour and progress of the cloud was monitored by cine cameras at ground level from directions perpendicular to the mean wind direction and from a motorised overhead camera. Up to ten continuous vapour concentration monitors and up to one hundred and twenty dosage samplers were located downwind of the source. Standard meteorological measurements were taken during each trial.

Thus, for each trial (given a successful functioning of all systems) data were obtained on cloud height, length and width and on the movement of the cloud across the trial site as a function of time. Supplementary information on vapour concentration and dosage was also obtained. Because of various instrumentation difficulties and such factors as late shifts in wind direction, a complete set of data was not obtained for each trial.

Broad Conclusions from the Report of the Trials

Only the more important and reasonably well-validated results of the trials will be summarised in this paper. The interested reader is referred to the detailed report of the results of the trials.[4] Part 1 of that report describes the measurement techniques, gives a summary of the results and presents a model of the dispersion process which is used in the analysis of the results. Parts 2 and 3 of the report contain the complete set of raw data obtained in the trials. An edited film in which material from the filmed records of the trials appears is being prepared.

The trial data illustrate the considerable influence of density on the dispersion process. In the absence of any appreciable wind, there is a clear demonstration of the expected rapid radial outflow. A cloud with a raised front in the shape of a doughnut is formed which continues to spread radially for a considerable time. In the presence of a ground slope, there is a pronounced flow downhill and a noticeable feature is the persistence of the doughnut shape on the downhill side.

When there is a wind present, the dense vapour in the outflow from the source advances for a time against the wind. On the downwind side, the cloud forms a transient horseshoe shape which may be attributable to its behaviour as a pseudo-solid body with the wind constrained to move around it. Initially at least the source container will produce the same effect, and the observed shape may be due to the persistence of the effect for the first few seconds after the container falls to the ground. As the cloud is carried downwind it assumes a wedge-shaped form with the base of the wedge at the leading front, with some suggestion of a nose above ground level due to the wind shear. The depth of the cloud falls initially in conformity with gravity-spreading models and reaches a minimum after which mixing produced by atmospheric turbulence induces vertical dispersion. The transition from dispersion dominated by gravitational effects to dispersion dominated by atmospheric effects is covered by the trial data. With a ground slope and the wind uphill, the initial flow against the wind was sustained for a longer time, as might be expected.

Regarding the specific objectives listed earlier, an analysis has been carried out[4] consisting of an examination of pairs of experiments for which, as nearly as possible, only one of the listed parameters was varied. The results of this analysis may be summarised as follows:

Initial Cloud Density. Increasing the initial cloud density increases the cloud width, decreases the cloud volume, the minimum cloud depth and the time to reach this depth and has little effect on the cloud length.

Wind Speed. The higher the wind speed, the larger the minimum cloud depth, the time to reach this depth, the cloud volume and the cloud length while the cloud width is not affected. The effect of stability category was not analysed but since stability is roughly correlated with wind speed (for a given solar radiation level) the above conclusions broadly apply also for increasing instability.

Roughness Length. The range of measurements available to determine the effect of roughness length was limited but nonetheless it was concluded that increasing roughness increased the cloud volume, width and length. In other words, the larger the roughness, the greater the rate of dilution of the cloud. The minimum depth and the time to reach it are unaffected.

Ground Slope. Cloud movement uphill has no effect on the minimum depth; its influence on the other parameters was not clear from the available measurements. Since the spatial average concentration in the cloud is inversely proportional to the cloud volume, the observations on cloud volume imply that the concentration increases with initial cloud density and decreases with wind speed and roughness.

These qualitative observations, while providing a useful picture of behaviour, are not of direct use for practical purposes, for which an analytical framework is required which will allow a quantitative description of the effects. Comparisons with predictions of models of dispersion of heavier-than-air gases are currently being undertaken and it is expected that the results of these comparisons will appear in the literature in the near future.

Proposal for Large-Scale Field Trials

The trials discussed so far were expected not only to be scientifically important in their own right but also to provide a sound base for deciding the need for large scale trials and how they should be performed, both from the point of view of economics and of feasibility within the constraint of available range facilities in the UK. In 1978, HSE commissioned a study of releases of up to 10 tonnes of heavy gas. This study was carried out under contract by the Chemical Defence Establishment. The study was concerned only with the feasibility and the design of the experiments, in particular the design of an improved release configuration. HSE is currently considering, in conjunction with informed interests in government, industry and universities, the need for larger-scale trials and the form they should take.

It is intended that the trials would again study the dispersion of rapidly-formed clouds. Because of the much larger scale, the mechanical type of release mechanism is not considered practicable. A number of possible alternatives were investigated and it was concluded that a double-walled, plastic enclosure would be the most suitable. The double wall, divided into cells and inflated to a low pressure, provides an acceptably rigid structure and can be readily disintegrated with explosive fuse. Some tests with an enclosure of 100 m^3 volume have shown that the method is practicable and high-speed film of the disintegration shows that there appears to be no significant disturbance of the contained gas.

Because of the much greater cost, the number of trials would be fewer than in the series described earlier. It is therefore important that the proposed trials should concentrate on the areas of greatest uncertainty. The principal objective would be to determine whether there was any effect of scale on conclusions drawn from the smaller-scale tests. Some of the questions that should be considered before any decision is taken will be framed below.

The discussion of the way in which the scale of the release can influence the dispersion processes can be conveniently divided into two parts. The first considers the possible additional factors that would cause differences to be expected between dispersion on the scale of the first series of experiments and of much more massive releases, and the second considers the same question vis-a-vis the scale of wind-tunnel experiments.

Considering the first part, it is assumed in currently available analytical models of density-influenced dispersion that the cloud has no effect on the surrounding atmosphere. This assumption is not supported by experimental evidence obtained in wind tunnel studies[5,6] where it was observed that both the mean velocity and the three components of turbulence are significantly affected in regions where the concentration of source fluid had fallen to zero. The implication is that the rate at which turbulence energy can be transferred from one point to another in the ambient flow is not sufficient to maintain the energy levels that prevail in the absence of the clouds. The work that needs to be done to transfer the dense fluid against the gravity forces (ie to produce vertical mixing) is larger than can be immediately supplied. Thus the heavy gas cloud affects the atmospheric structure outside itself. The range of the effect and its persistence downwind would be expected to depend on the size of the release.

The qualitative result would be a reduction in the rate of dispersion of large clouds compared to that predicted by models validated only for smaller-scale experiments. This tendency of the models to err on the optimistic side would support the case for larger-scale trials.

Most of the available models for gravity-influenced dispersion do not take account of the continuous variation of wind speed with height. Small-scale releases will disperse in a region of the atmospheric boundary layer with different properties from those that would be encountered by a large-scale release. In particular the smaller releases will be subjected to larger wind shear effects so that the longitudinal spreading of a rapidly-released cloud will be greater for small-scale releases.

Conversely, the larger the release, the greater will be the effect of thermal stratification of the atmospheric boundary layer, since the effect of stratification on the properties of the boundary layer increase with height. Close to the ground the velocity distribution is unaffected by the density stratification. The effect on the velocity at any particular height depends on the ratio of the height to the Monin-Obukhov stability length which decreases as the stability increases.[7] Thus the dispersion of a small-scale release may be relatively insensitive to stability effects and conclusions drawn from such experiments could be misleading.

For very large releases of toxic materials, the cloud behaviour for long downwind distances may have to be evaluated because of the very low concentrations at which some materials continue to demonstrate adverse effects. Additional factors influencing the dispersion then enter, but because the density difference will have been reduced to a very low value it would be expected that the methods available for long-range dispersion of passive materials would be applicable.

The possible difficulty of scaling dense gas releases in a wind tunnel has been discussed by Hall, Barrett and Ralph.[8] They were unable to conclude that Reynolds number effects could be ignored, that is to say, regions would exist in the wind tunnel model of a dense gas cloud in which the mixing was affected directly by viscosity. Hall[6] remarked that 'the problem cannot properly be resolved without comparison with full-scale measurements and at the time of writing such data do not exist'. In this context, the results of the trials described earlier may be taken as 'full-scale measurements'. As part of the study of scale effect, HSE is to commission a wind-tunnel simulation of the Porton releases in order to examine whether Reynolds number effects are significant. This would provide guidance on the applicability of wind tunnel studies of dispersion in plant areas and around buildings and other topographical features, for which even experiments on the scale already carried out would be infeasible.

References

1. Advisory Committee on Major Hazards, First Report, Her Majesty's Stationery Office, London, 1976.

2. J. McQuaid, "Dispersion of Heavier-than-Air Gases in the Atmosphere: Review of Research and Progress Report on HSE Activities", Health and Safety Laboratories Technical Paper No. 8, Research and Laboratory Services Division, Health and Safety Executive, Sheffield S1 2GQ, UK, 1979.

3. A.P. van Ulden, "On the Spreading of a Heavy Gas Released near the Ground", Proc. 1st Int. Symp. on Loss Prevention and Safety Promotion in the Process Industries, Delft, The Netherlands, 1974.

4. R.G. Picknett, "Field Experiments on the Behaviour of Dense Clouds", Report No. Ptn IL 1154/78, Chemical Defence Establishment, Porton, Contract Report to Health and Safety Executive, Sheffield S1 2GQ, UK, 1978.

5. J. McQuaid, "Some Experiments on the Structure of Stably-Stratified Shear Flows", Technical Paper P21, Safety in Mines Research Establishment, Sheffield S3 7HQ, UK, 1976.

6. D.J. Hall, "Further Experiments on a Model of an Escape of Heavy Gas", Report No. LR 312 (AP), Warren Spring Laboratory, Stevenage, Herts, UK, 1977.

7. J.L. Lumley and H.A. Panofsky, "The Structure of Atmospheric Turbulence", Interscience, New York, 1964.

8. D.J. Hall, C.F. Barrett and M. Ralph, "Experiments on a Model of an Escape of Heavy Gas", Report No LR 217 (AP), Warren Spring Laboratory, Stevenage, Herts, UK, 1974.

© Crown Copyright 1979

TABLE 1 List of trials

Experiment Number	Initial Relative Density	Wind Speed m/s	Roughness Length mm	Pasquill Stability Category
Prelim	1.6	3.9	2	B
1	1.9	6.1	2	C/D
2	2.2	7.6	2	D
3	2.3	5.5	2	D
4	1.2	2.8	2	C/D
5	2.5	4.0	20	D
6	1.7	2.8	20	C/D
7	1.1	1.2	2	B/C
8	2.0	<0.5	2	F/G
9	1.8	0.7	2	F
10	2.5	0.4	2	F
11	2.4	2.0	2	E
12	2.4	5.7	20	C
13	2.2	5.9	20	C/D
14	1.5	7.2	2	C/D
15	2.0	6.4	2	D
16	1.4	1.7	20	B
17	1.7	3.5	20	C
18	1.1	3.2	20	E
19	2.9	5.5	20	C/D
20	2.1	5.3	20	C
21	1.3	4.7	20	B/C
22	2.8	2.0	2	C
23	1.9	2.1	150	B
24	1.9	2.5	150	B
25	3.1	2.9	150	C
26	3.4	4.0	2	B/C
27	1.9	4.7	2	B/C
27A	1.0	4.7	2	B/C
28	2.1	5.1	2	C
29	4.2	4.3	2	C
29A	1.0	4.5	2	C
30	2.6	3.0	2	C
31	1.6	6.7	2	C
32	2.7	1.8	10	C
33	2.2	2.0	10	B/C
34	2.1	1.6	10	B
35	2.6	5.2	10	C/D
36	1.5	4.7	10	C/D
37	2.2	5.1	10	C/D
38	1.3	0.6	10	F/G
39	1.03	1.8	10	E/F

Discussion:

Venkatram:

From the point of view of modelling it might have been useful to measure the turbulence intensity. The ratio of the turbulent velocity (vertical) to the initial setting velocity would characterise the experiments.

McQuaid (response):

Some turbulence measurements were made during the experiments, including the intensity of the vertical component. It is interesting to note that these measurements showed no effect of the presence of the cloud, a result that is perhaps surprising.

Schnatz:

What do you think is the influence of the downward movement of the sidewalls on the initial turbulence of the cloud and secondly what do you think is the influence of the remaining roof on the cloud spread. In one of the pictures of the film it could be seen that a proportion of the cloud was captured below the top for a few seconds and then travelled separately from the rest of the cloud.

McQuaid (response):

I think it must be stated that any choice of release mechanism will have its disadvantages. There is no ideal solution. An important consideration is that the release conditions should be repeatable and this is achieved I think, with the configuration adopted. This would not be the case, for instance, with sudden rupture of a pressurised container as in the experiment described by Dr. van Ulden. In the study carried out in connection with the proposed large scale trials, some experiments were carried out on explosive disintegration of the plastic enclosure containing the gas. High-speed film of the release did not show any signifi-

McQuaid (response, cont.):

cant effect on the cloud and one might imagine that this mode of release would be more disturbing than the mechanical collapse of the sides as in the early trials. But specific measurements were not carried out which would help to answer the question of the effect of the initial disturbance. With regard to the observation on the effect of the roof of the enclosure, I do not recall noticing this. It is a fact that each person who views this film sees different things, and even after having seen it several times, new features emerge. I shall certainly look out with interest for the effect you have remarked upon when next I show it.

A MODEL FOR HEAVY GAS DISPERSION IN THE ATMOSPHERE

by

K.J. Eidsvik
Norwegian Institute for Air Research
P.O. Box 130, N-2001 Lillestrøm
Norway

Abstract. A simple model for the dispersion of heavy and cold gas clouds is developed. The horizontal dimension of the cloud is assumed to increase due to the gravity fall of the cloud. The cold cloud is heated from below and from air entrainment. The initial entrainment velocity is assumed to be linearly proportional to the front velocity and decay as its square.
The entrainment at the upper surface is estimated as for atmospheric inversions and density interfaces in laboratory flows. The model predictions are shown not to be critically dependent on coefficient variations. Experimental data on heavy gas dispersion are predicted reasonably accurate.

Introduction

The Problem

The production, transportation and storage of large quantities of heavy, explosive or poisonous gases may present serious hazards to the public. A cloud of methane, propane or butane may be flammable if the mean volume concentration is higher than approximately 1%. A cloud of chlorine may be poisonous at concentrations of approximately 10^{-5}%. If an accidental release occurs in unfavourable atmospheric flows, the resulting cloud could be hazardous far away from the source. Several investigations have been done towards estimating the spread of such clouds [1,2,3,4,5,6,7,8,9,10,11]. Recent experiments at Porton, have contributed substantially to relevant data, [11]. Most proposed models are very simple and all involve uncertain ad hoc assumptions. Although it may be claimed that models fit the data, the fit could easily be caused by the incomplete, sparse and stochastic data, and the number of coefficients used for curve fitting. Our model can predict important aspects of heavy gas spreading as revealed by the Porton data, with adjustment of only one coefficient for initial entrainment [12].

Outline of the process

Experimental evidence suggests that the spreading from an instantaneous heavy gas source may conveniently be referred to in terms of a rapid phase of initial slumping, an intermediate phase of less vigorous development, and finally a phase of passive scalar diffusion.

If the gas release is sufficiently rapid, the initial phase is characterized by a vortex ring at the peripherial cloud boundary. In the Porton experiments it is estimated that a significant fraction of the gas mass is contained in this vortex ring, [11]. The characteristic duration of this phase is t_I. Both the characteristic time for the slumping and heating of a cold cloud, are probably of the same order of magnitude, [9]. The release or initial air entrainment has been estimated as significant in various experiments, [5,10,11]. A physically realistic modelling of the initial phase would be extremely difficult. It depends on which of the many possible ways the gas is released. It involves nonequilibrium boiling and nonequilibrium thermal interaction between two complicated turbulent flows. A reasonably realistic model for the gas flow alone would probably require a very complicated turbulence model, [13,14,15]. As the initial mean gas flow is definitly three-dimensional and of small scale, a very small grid size would be necessary along all spatial direction over a large spatial domain. With todays computers such a model would not be feasible. In addition the model would be uncertain due to uncertain closure schemes. It is instead hoped that a simple ad hoc model can predict the approximate bulk properties of the cloud at the end of the initial phase.

For the intermediate stage, $t \geq O(t_I)$, the gas mixture is still denser than air and continues to spread radially due to gravity. Because of surface stress and heat transfer, it is probably a well developed turbulent flow. The turbulence is likely to give a reasonably homogeneous air-gas mixture inside the cloud. The horizontal dimension of the cloud, r, is much larger than the height, h, assumed to be reasonably well defined. The assumed large mean flow gradients near the upper cloud boundary, suggest that the flow may be subject to Kelvin Helmholz instability. This instability would imply an effective dilution of the gas cloud. For $t > t_I$ it is assumed that the flow adjusts its gradient Richardson number over the interface so that Kelvin Helmholz instability is almost always avoided. If the above concepts of the flow are realistic, the dispersion can not be realistically estimated by using K-theories of turbulence, [7,8]. In the bulk cloud there will be large vertical turbulent transports in spite of negligible mean gradients, and across the large mean gradients ("interface") the turbulent transport may be small. It is also difficult to use numerical models of the Reynolds equations for mean flow computations because the resolution of the grid must be very small in the neighbourhood of the cloud boundaries. Our model is mainly meant to be applicable for this intermediate stage of cloud development.

As the density difference between the cloud and atmosphere vanishes, the dispersion must approach that of a passive scalar. At this stage the gas concentration may have decreased to non-hazardous concentrations so that sufficient accuracy may be achieved by designing the heavy gas model to have an approximately correct limiting behaviour as the density difference vanishes.

A dispersion model for a heavy gas cloud

The model

Any dispersion model for heavy gas must, as mentioned, be far from "first principles". It must also be uncertain due to the few experimental data. The model should therefore be simple and well behaved with parsimonious use of experimental coefficients. The key equations of our model are as follows [12]

$$\pi\rho(t)r^2(t)h(t) = M_g + M_a(t) \tag{1}$$

$$\frac{dr}{dt} = U_g = \alpha_1 \left(gh\frac{\Delta\rho}{\rho}\right)^{\frac{1}{2}} \tag{2}$$

$$\frac{dM_a}{dt} = \rho_a \pi r^2 \left(\frac{dh}{dt}\right)_* \tag{3}$$

$$\left(\frac{dh}{dt}\right)_* = \frac{dh_d}{dt} + 2\,\frac{h}{r}\,\frac{dr_d}{dt} \tag{4}$$

$$\frac{dr_d}{dt} = \frac{\alpha_5}{U_g(0)}\,U_g{}^2(t) \tag{5}$$

$$\frac{dh_d}{dt} = \frac{\alpha_4}{\alpha_6{}^* + R_i}\,w \tag{6}$$

$$R_i = \frac{gh\frac{\Delta\rho}{\rho}}{w_2} \tag{7}$$

$$w^2 = (\alpha_2\, w_T)^2 + (\alpha_3\, w_m)^2 \tag{8}$$

$$w_T = \left((\overline{\theta w})_0\,\frac{gh}{T}\right)^{1/3} \tag{9}$$

$$w_m = u_* = \left(\frac{1}{2}\,c_f\right)^{\frac{1}{2}} U \tag{10}$$

$$U^2 = (\frac{2}{3} U_g)^2 + U_a{}^2 \qquad 11$$

$$\frac{dT}{dt} = \frac{1}{h} ((\overline{\theta w})_o - (\overline{\theta w})_h) H(M_a(t) - M_{ad}) \qquad 12$$

$$(\overline{\theta w})_0 = \frac{1}{2} c_f U(T_a(0) - T) \qquad 13$$

$$(\overline{\theta w})_h = ((T_a - T) + \frac{L_w}{c_{pa}} \chi_w H(T_{da} - T)) \frac{\rho_a c_{pa}}{\rho\ c_p} (\frac{dh}{dt})_* \qquad 14$$

It is assumed that the static pressure is constant and the laws of an ideal gas and gas mixtures are valid. Equation 1 defines the characteristic density, ρ, radius, r, and height, h, of the cloud. M_g is released mass of gas and M_a is entrained air. Experimental coefficients are, α_i. Equation 2 describes the gravity speed of the cloud front as a function of the acceleration of gravity, g, and the density difference between the gas mixture and air, $\Delta\rho = \rho - \rho_a$. The equations 3 to 11 describe the entrainment of air. Sideways entrainment velocity is $\frac{dr_d}{dt}$. Vertical entrainment velocity is $\frac{dh_d}{dt}$. w is the characteristic turbulent velocity in the gas cloud. $(\overline{\theta w})$ is the temperature flux, c_f is the surface drag coefficient and U is the free-stream velocity set equal to the quadratic sum of the cloud area average of the gravity velocity and the wind velocity, U_a. Equation 12 to 14 describes the enthalpy equation. H is the generalized Heavyside function. M_{ad} is the air mass necessary to evaporate the droplets of liquid gas thrown into the air-gas cloud during the release process. L_w, χ_w and T_{da} are the latent heat, mixing ratio and dew point of water vapour. c_p and c_{pa} are spesific heat at constant pressure for gas mixture and air respectively.

The model has the approximate correct behaviour as the density difference vanish and the gas cloud becomes passive [12].

Sensitivity analysis

It is essential that model predictions do not vary too much when the coefficients are varied over their normal range of uncertainty. The coefficient variations may be contained in the independent α_1, α_2, α_4, α_5 and α_6. The horizontal size of the cloud is predicted to depend little upon the entrainment process so that the variation with α_1 is simple. In the limit as $\Delta\rho \rightarrow 0$ the cloud height increases linearly with α_6; $\alpha_6{}^* = \alpha_4\ \alpha_6{}^{-1}$. The most interesting variability may therefore be discussed in terms of the three coefficients $\alpha_2 \in (0.2, 1.0)$, $\alpha_4 \in (0.2, 5.0)$ and $\alpha_5 \in (0.0, 1.0)$ [12].

It is noted that the sideways entrainment velocity equation 5 is a quadratic function of the front velocity instead of the traditional linear. Figure 1 illustrates one aspect of the difference between a linear and quadratic sideways entrainment equation. The sideways entrainment rate of air dominate at all interesting times unless the exponent in the sideways entrainment equation is higher than one. A linear sideways entrainment equation also turns out to give a large variation of cloud spreading with small variations of α_5. To obtain a simple, well behaved model, the quadratic sideways entrainment equation is used.

Figure 2 illustrates a representative variation of cloud state for two different values of the sideways entrainment coefficient, α_5. It is indicated that the entrainment equation 5, affects the dispersion significantly only in the initial stages. The prediction of the cloud state at the end of the slumping stage is not critically dependent on the entrainment coefficient α_5.

Figure 3 illustrates a representative variation of cloud state for two different values of the entrainment coefficient, α_4. It is indicated that the entrainment equation 6, affects the dispersion significantly only after the initial stages. The predicted state of the cloud is not critically dependent on the coefficient α_4.

Figure 4 illustrates the variation of cloud state for two different values of the coefficient α_2 to characterize the importance of the convective turbulence in relation to mechanical turbulence. The gas chosen is methane to maximize the effect of heat transfer. The predicted state of the cloud is dependent, but not critically, on α_2.

It is therefore concluded that the model is reasonably well behaved. If reasonably chosen coefficients enable the model to explain interesting aspects of experimental data on heavy gas dispersion, there is reason to believe that the model may be physically realistic. The traditionally accepted coefficients are: $\alpha_1 = 1.3$, $\alpha_2 = 0.7$, $\alpha_3 = 1.3$, $\alpha_4 = 3.5$, and $\alpha_6 = 0.3$. The ad hoc coefficient $\alpha_5 = 0.5$ is chosen so as not to give too large initial entrainment.

Data comparison

The Porton experiments contain the bulk of the quantitative experimental data on the spreading of heavy gases in the atmosphere [11]. The field experiments were carried out with an instantaneous source of 40 m^3, with densities in the range of 1.03 to 4.2 relative to air. The gas temperature was equal to the atmospheric temperature. Orange smoke was used to make the cloud visible. The cloud dispersion was monitored by side-view photographs, by gas dosage measurements and by continuous measurements of gas concentration.

We use the data from the flat sites only. Using the friction velocity and mean wind speed for each experiment, the estimated friction coefficient at the different flat sites are as follows: $z_o = 2$ mm → $c_f \simeq 7 \cdot 10^{-3}$; $z_o = 10$ mm and $z_o = 20$ mm → $c_f \simeq 1.4 \cdot 10^{-2}$ and $z_o = 150$ mm → $c_f = 5 \cdot 10^{-2}$. These groups contain 10, 18 and 3 experiments respectively. Judged relative to the large stochastic variability of atmospheric flows, this is so small a sample size that only subjective "statistical methods" are used. Neither Picknet nor we have discovered, from the data, any "significant" dependence between dispersion variables and surface roughness [11,12]. The reason is probably that the experiments are few and most of them are accociated with a narrow range of c_f-values. In the following, we will use $c_f = 1.4 \cdot 10^{-2}$ for model predictions.

The variables used to characterize the cloud were its height, downwind and crosswind cloud dimensions, and the average volume concentration, [11]. The difference between the downwind and crosswind cloud dimensions, caused by the combined effect of turbulence and mean wind shear, is not too large and cannot be discribed by our model. The observed crosswind cloud size is associated with the predicted 2r. As most of the gas mass may be contained in a intense vortex ring it must be difficult to estimate a representative cloud height, [17]. The visually observed height h_*, could be more representative for the ring than for the whole cloud. Redistribution of the mass from a circumferential ring of radius $(h_*/2)$ evenly over the cylindrical cloud of radius r gives a cloud height of $(2\pi/4 \cdot h_*^2/r)$. In the neighbourhood of its minimum, h_* is observed to be of the order 1/10 r, so that a representative height could sometimes have been overestimated by a large factor. This difference is illustrated in Figure 5. The ambiguity will affect the concentration curves linearly so that a representative concentration could have been underestimated by a large factor.

The predicted cloud development resembles very much the observed one, are illustrated in Figures 2,3 and 5. The largest discrepancy is apparently between the observed and predicted cloud height, illustrated in Figure 5. This apparent discrepancy could easily been made much smaller, without large increase of other types of errors, by using a larger initial entrainment coefficient, α_5. However, because the discrepancy may not be real, or also because the initial entrainment in the Porton experiments could be large due to the particular gas release mechanism, α_5 is not chosen to minimize this (apparent?) error.

With a general agreement between the actual and predicted cloud development, the data may be represented in terms of a few variables instead of functions. We choose: time to minimum cloud height $t(h_{min})$, transverse cloud dimension, $2r(t=10\text{ sec})$, and volume concentration $c(t=10\text{ sec})$. Most of the Porton experiments were associated with reasonably high winds. As illustrated in Figure 2, the spreading will then occur at reasonably small Richardson numbers, and therefore approach passive scalar dispersion when $t > O(10\text{ sec})$. The most dominant variations of the three dispersion variables are shown in the Figures 6,7 and 8. Predicted isolines are also shown. Considering the simplicity of the model, the complexity of the heavy gas process, the uncertainty of the coefficients and the inevitable randomness and possible bias associated with the data, the similarity between the predicted and actual values is judged to be remarkable.

Predicted spread

The simple model has been found to be well conditioned and to explain important aspects of the existing experimental data on heavy gas dispersion. The experimental data cover only "points" in the phase space spanned by "reasonable" release and environmental conditions. It is of interest to discuss the model prediction over a portion of this space of more relevance to hazard.

Figure 9 illustrates the variation of the "hazard" variables, t(c=1%) and r(c=1%) with released mass of propane. The approximate relations, obtained from Figure 9, show that the variations with the released mass are slow.

$$t(c=1\%) \propto M_g^{1/3} \qquad 15$$

$$r(c=1\%) \propto M_g^{2/5} \qquad 16$$

Equation 15 expresses the same type of law that are approximately valid for a small passive scalar cloud, which have a linear increase of its three dimensions with the time.

Figure 10 illustrates the variation of the variables t(c=1%) and r(c=1%) with the ratio, δ, of liquid evaporated initially in the air-gas mixture. There is practically no dependence for propane. The spread of a heavy methane cloud is somewhat more dependent upon δ. However, for the small, most realistic values of δ, the dependence is not decisive. The variation with initial cloud shape, h(o)/r(o), was also found to be small.

Environmental variations are illustrated in Figure 11. There is a significant variation of the variables t(c=1%) and r(c=1%) with both wind speed and the roughness of the underlying surface. The maximum "hazard" distance, x(c=1%), of the order

$$x(c=1\%) \simeq U_a t(c=1\%) + r(c=1\%) \qquad 17$$

shows a small variation with the wind speed. With other conditions kept constant, the hazard from a heavy gas release is predicted to be more serious in calm wind conditions, mainly because t(c=1%) is high.

For temparatures in the neighbourhood of 10°C, there are only small predicted variations of the dispersion with the water vapour content. The predicted variations with the stratification of the atmosphere, $\partial T_a/\partial z$, are also found to be negligible. However, it should be noted that the variation of atmospheric stratification has only been included in the $\Delta\rho = (\rho-\rho_a(z))$ and $(T-T_a(z))$ terms. The associated change of atmospheric turbulence has not been taken into account.

Concluding remarks

We have tried to describe the dynamics of the most essential state variables of a heavy gas cloud as simply as possible. Possible refinements of some approximations are obvious, but the design of a consistent and significantly more realistic model seems to introduce complications. The complications are accociated with for instance: the coupling between the release and entrainment processes, the coupling between the atmospheric flow and the gravity induced flow, and the spatial variations of the gas cloud characteristics.

The present model is attractive in that the results do not depend critically upon uncertainties about numerical coefficients. The model does asymptotically predict the spreading of a passive scalar cloud as the density difference vanish. With an ad hoc initial entrainment equation, the model gives a remarkably accurate prediction of the Porton experimental data, which constitute the bulk of the existing data on heavy gas dispersion.

The potential hazard of a large (accidental) gas release is predicted to vary significantly with the state of the underlying surface and of the atmosphere, especially so in the neighbourhood of the potentially most hazardous conditions; low wind speed.

References

1. D. Burges, J. Biordi and J. Murphy, 1972. Hazards of spillage of LNG into water. Bureau of Mines, Pittsburg, Pa. PMSRC Rep.no. 4177.
2. G.F. Feldbauer, J.J. Heigl, W. Mc Queen and W.G. Mag, 1972. Spills of LNG on water - "Vaporization & downwind drift of combustible mixtures". Esso Reseach & Engineering Company. Florham Park. Rep.no. EEGIE-72.
3. V.A. Fay, 1973. Unusual fire hazard of LNG tanker spills. Combust.Sci.Technol., 7, 47-49.
4. American Gas Association Project, 1974. LNG safety program interim report on phase II work. Battelle, Columbus, Ohio. American gas Project IS-3-1.
5. A.P. van Ulden, 1974. On the spreading of a heavy gas released near the ground. 1st international loss prevention symposium. The Hague/Delft, Netherland. Elsevier, Amsterdam, pp. 221-226, 431-439.
6. A.E. Germeles and E.M. Drake, 1975. Gravity spreading and atmospheric dispersion of LNG varpour clouds. The 4th int. symposium on transport of hazardous cargoes by sea and inland waterways. Jacksonville, Florida, pp. 519-539.

7. Science Application, 1976. LNG terminal risk assessment study for Point Conception, California. La Jolla, California.

8. P.H.M. te Riele, 1977. Atmospheric dispersion of heavy gases emitted at or near ground level. 2nd. international loss prevention symposium. Heidelberg, pp. 347-357.

9. K.J. Eidsvik, 1978. Dispersion of heavy gas clouds in the atmosphere. Lillestrøm. NILU OR 32/78.

10. G.D. Kaiser and B.C. Walker, 1978. Releases of anhydrous ammonia from pressurized containers. Atmos.Environ. 12, 2289-2300.

11. R.G. Picknett, 1978. Field experiments on the behaviour of dense clouds. Chemical Defence Establishment Porton Down. Salisbury, Wilts., England. Report Ptn. IL 1154/78/1.

12. K.J. Eidsvik, 1979. A model for heavy gas dispersion in the atmosphere. Lillestrøm. NILU OR 18/79.

13. R.E. Britter and J.E. Simpson, 1978. Experiments on the dynamics of a gravity current head. J. Fluid Mech. 88, pp. 223-240.

14. J.W. Deardorff, 1974. Three-dimensional numerical study of the height and mean structure of a heated planetary boundary layer. Boundary-layer Meteorol. 7, 81-106.

15. C. Donaldson and A.J. Bilanin, 1975. Vortex wakes of conventional Aircraft. Neuilly Sur Seine. AGARD-AG-204.

16. O. Zeman and H. Tennekes, 1977. Parameterization of the turbulent energy budget at the top of the daytime atmospheric boundary layer. J. Atmos.Sci. 34, 111-123.

17. R.G. Picknett and C.D. Jones, 1978. Private communication, Sheffield.

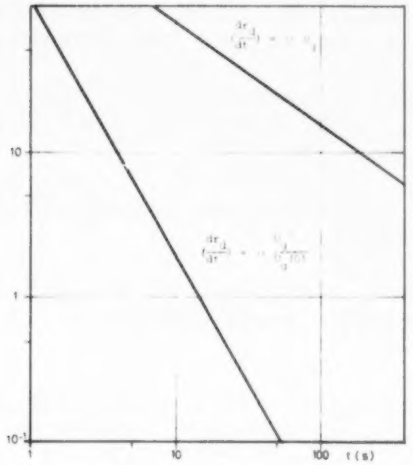

Figure 1: Ratio of entrainment rate of air at the cloud side and top. Release: V(o)= 40 m^3 freon-air mixture, $\rho(o)/\rho_a$=2 $h(o)/r(o)$ = 1.84, $T_g = T_a$, U_a = 0, c_f=$1.4 \cdot 10^{-2}$, α_1 = 1.4, α_2=0.7, α_3 = 1.3, α_4 = 2.5, α_5 = 0.8, α_6 = 0.3.

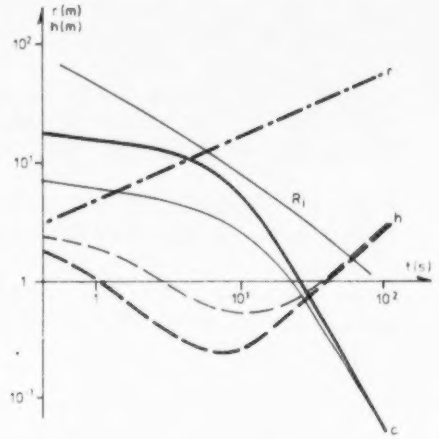

Figure 2: Variation of initial entrainment. Heavy curves: α_5 = 0.5. Thin curves: α_5=1.0 Release of V(o) = 40 m^3 freon-air mixture. $\rho(o)/\rho_a$ = 2, $h(o)/r(o)$ = 1.84, $T_g = T_a$, U_a = 2 ms^{-1}, c_f= $1.4 \cdot 10^{-2}$, α_1 = 1.4, α_2 = 0.7, α_3 = 1.3, α_4 = 2.5, α_6 = 0.3.

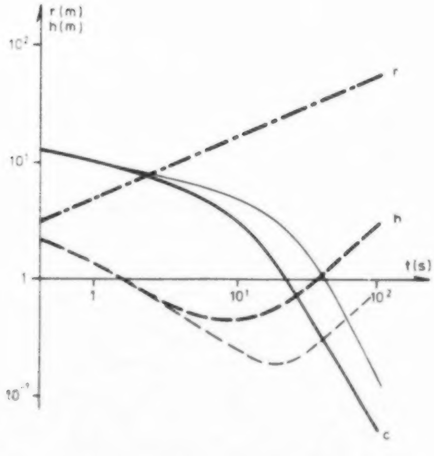

Figure 3: Variation of vertical entrainment. Heavy curves: α_4 = 5.0. Thin curves: α_4 = 0.2. Release of V(o) = 40 m^3 freon-air mixture, $\rho(o)/\rho_a$ = 2, $h(o)/r(o)$ = 1.84, $T_g = T_a$, U_a = 2 ms^{-1}, c_f = $1.4 \cdot 10^{-2}$, α_1 = 1.4, α_2 = 0.7, α_3 = 1.3, α_5 = 0.8, α_6 = 0.3.

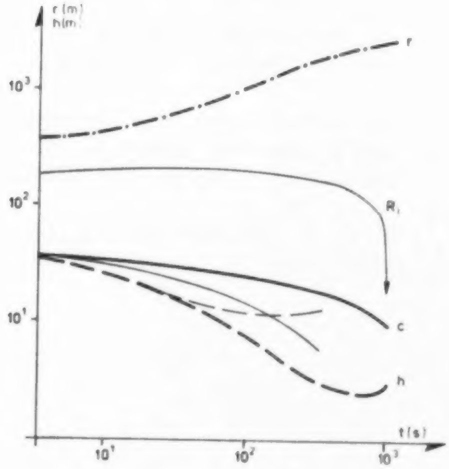

Figure 4: Variation of convective entrainment. Heavy curves: α_2 = 0.5. Thin curves: α_2 = 2.5. Release of 10^7 kg metane at boiling temperature. δ = 0.5, $h(o)/r(o)$ = 0.25. U_a = 0.5 ms^{-1}, c_f = $2 \cdot 10^{-3}$, $T_a - T_{da}$ = 5, α_1 = 1.3, α_3 = 1.3, α_4 = 3.5, α_5 = 0.5, α_6 = 0.3.

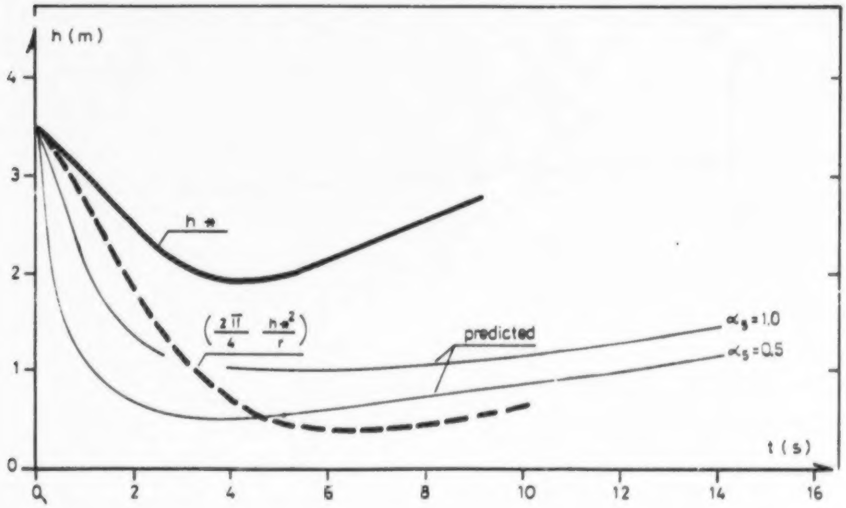

Figure 5: Mean observed and "corrected" height variation for the Porton experiments no: (13,20,28,37), and predicted variation for $\alpha_5 = 0.5$ and $\alpha_5 = 1.0$, $\rho(o)/\rho_a = 2.15$, $U_a = 5.4\ ms^{-1}$, $c_f = 1.4 \cdot 10^{-2}$.

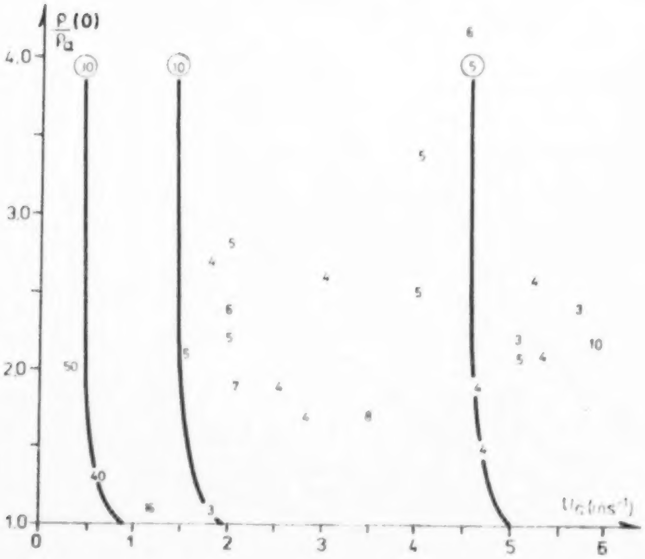

Figure 6: Porton data for time in second to minimum cloud height. Isocurves for predicted values. $c_f = 1.4 \cdot 10^{-2}$, $\alpha_1 = 1.3$, $\alpha_2 = 0.7$, $\alpha_3 = 1.3$, $\alpha_4 = 3.5$, $\alpha_5 = 0.5$, $\alpha_6 = 0.3$.

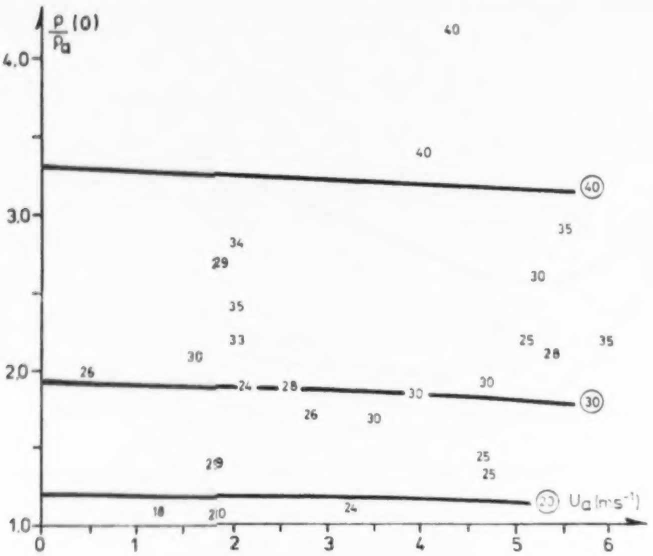

Figure 7: Porton data for transvers cloud dimension in metres 10 sec from release. Isocurves for predicted values. $c_f = 1.4 \cdot 10^{-2}$, $\alpha_1 = 1.3$, $\alpha_2 = 0.7$, $\alpha_3 = 1.3$, $\alpha_4 = 3.5$, $\alpha_5 = 0.5$, $\alpha_6 = 0.3$.

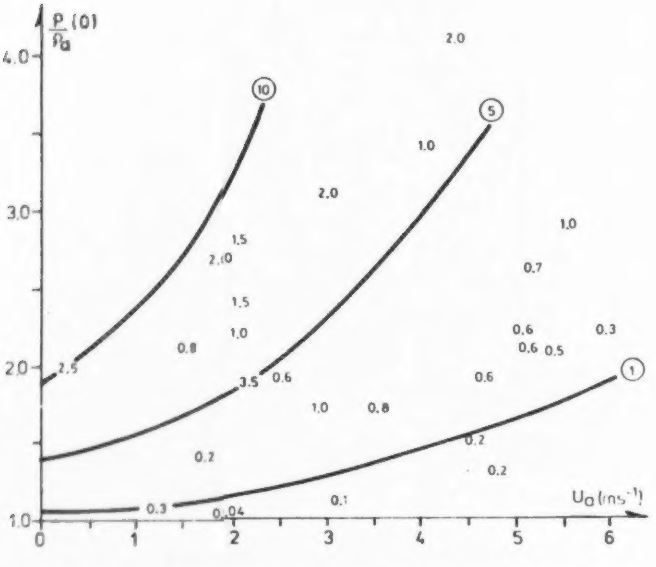

Figure 8: Porton data for volume concentration in percent 10 sec from release. Isocurves for predicted values. $c_f = 1.4 \cdot 10^{-2}$, $\alpha_1 = 1.3$, $\alpha_2 = 0.7$, $\alpha_3 = 1.3$, $\alpha_4 = 3.5$, $\alpha_5 = 0.5$, $\alpha_6 = 0.3$.

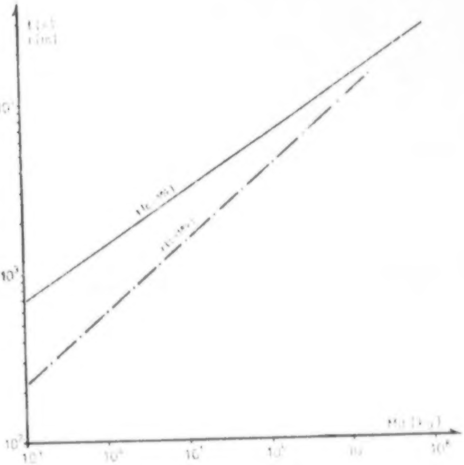

Figure 9: Mass variation. Time to and radius at 1% mass concentration as functions of released mass of propane. $\delta = 0.1$, $h(o)/r(o) = 0.25$, $c_f = 2 \cdot 10^{-3}$, $U_a = 0.5\ ms^{-1}$, $T_a - T_{da} = 5$, $\alpha_1 = 1.3$, $\alpha_2 = 0.7$, $\alpha_3 = 1.3$, $\alpha_4 = 3.5$, $\alpha_5 = 0.5$, $\alpha_6 = 0.3$.

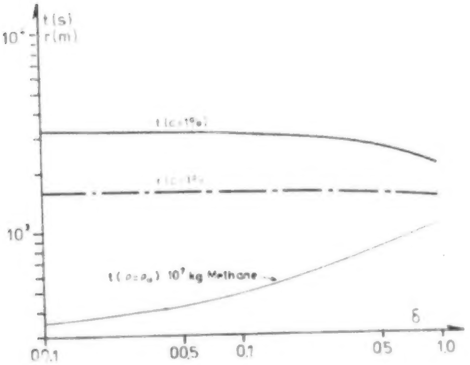

Figure 10: Evaporation of aerosol. Time to and radius at 1% mass concentration as function of the mass ratio evaporated in an air-propane cloud. $M_g = 10^5$ kg, $h(o)/r(o) = 0.25$, $c_f = 2 \cdot 10^{-3}$, $U_a = 0.5\ ms^{-1}$, $T_a - T_{da} = 5$, $\alpha_1 = 1.3$, $\alpha_2 = 0.7$, $\alpha_3 = 1.3$, $\alpha_4 = 3.5$, $\alpha_5 = 0.5$, $\alpha_6 = 0.3$.

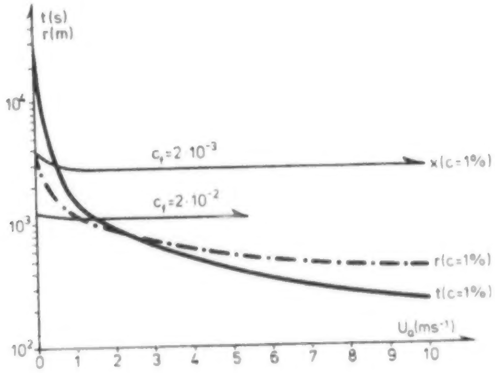

Figure 11: Environmental variations. "Hazard" variables as function of wind speed and surface roughness. Propane, $M_g = 10^5$ kg, $\delta = 0.1$, $h(o)/r(o) = 0.25$, $\alpha_1 = 1.3$, $\alpha_2 = 0.7$, $\alpha_3 = 1.3$, $\alpha_4 = 3.5$, $\alpha_5 = 0.5$, $\alpha_6 = 0.3$.

Discussion:

(Rapporteur: E. Runca)

A. P. Van Ulden:

Did you compare your model with low wind speed cases of the Porton trials?

K. J. Eidsvik (response):

I did, but not to large dispersion times.

G. Schnatz:

In the last diagram is atmospheric dispersion included?

K. J. Eidsvik (response):

Atmospheric dispersion is not included.

PHYSICAL MODELING OF ATMOSPHERIC DISPERSION OF HEAVY GASES RELEASED AT THE GROUND OR FROM SHORT STACKS

by

Robert N. Meroney
Professor, Colorado State University
Fort Collins, Colorado USA

Abstract. The past decade has seen a significant increase in the quantity of toxic or hazardous gases transported or stored under conditions which may result in a denser-than-air gas upon escape. Motion in the atmospheric boundary layer can be simulated in boundary-layer wind tunnels with sufficient accuracy to permit realistic scaling of escape hazards, pretest planning for field experiments, and a post-test opportunity to extend the value of limited field measurements.

Concentration measurements have been evaluated for bent-over plumes during releases in quiescent and crosswind conditions. Expressions were developed for plume rise height, "touchdown" distance and concentration variations. Heavy gases released at the ground surface exhibit a "pancaking" behavior.

Introduction

Laboratory simulation of negatively buoyant emissions into the earth's boundary layer is a valuable predictive tool to describe the motions of potentially hazardous chemicals such as propane, butane, chlorine, liquified natural gas, freon, etc. In this paper are discussed some of the simulation criteria, special instrumentation, and results of wind tunnel investigations of dense plume behavior. Such wind tunnel data can be correlated in a manner that yields an emperical prediction of vapor dispersion from full scale releases; nonetheless, certain facility and gas specific limitations must be recognized when interpreting an experimental program.

Prior Experience: Laboratory Simulation of Dense Gas As Cryogenic Spills

Dense gas plumes may result whenever the fractional density ratio, Δ, is greater than zero, i.e.

$$\Delta = -\left(\frac{C_{p_o}}{C_p}\right)\left(\frac{T-T_o}{T_o}\right)+ 1 - \left(\frac{28.9}{m_o}\right)+ \left(8 \frac{\dot{M}w}{\dot{M}_o}\right) \qquad (1)$$

where C_p is a specific heat capacity at constant pressure, M_o is the mean molecular weight of the effluent, and $\dot{M}_w$ and $\dot{M}_o$ are the mass flux of liquid water and total mass flux of the effluent respectively. If $\Delta > 0$ the plume is heavier than air and may fall to the ground rather close to the source if

$$Fr = \frac{U}{\sqrt{g\Delta d_o}} < C \qquad (2)$$

where C lies between 0.7 to 7.7 depending on surface roughness, wind speed and stratification condition. Prediction of the behavior of dense plumes is also often aggravated by the influence of surface interaction, heat transfer, latent heat release, and a transient character.

A number of controlled laboratory experiments have been prepared previously to evaluate the significance of density on gaseous plume dispersion. Sakagami and Kato measured diffusion and vapor rise from a small 5 x 10 cm LNG well in the floor of a 50 x 50 cm cross-section x 200 cm length wind tunnel.[1] They confirmed a tendency for the gas to remain concentrated at ground level. Boyle and Kneebone released LNG on water, precooled methane, and propane in a specially built 1.5 x 1.2 m cross-section by 5 m long asbestos-wall wind tunnel.[2] No attempt was made to scale the atmospheric surface layer velocity profile or turbulence. They concluded room-temperature propane simulated a LNG spill quite well, but the pre-cooled methane runs lofted suggesting to the authors incorrect release temperature or exaggerated heat transfer from the ground surface. Hoot and Meroney considered point source releases of heavy gases from short stacks in wind tunnels.[3] Hoot and Meroney found that releasing ground level gases with specific gravities as great as 3.0 only slightly shifted the decay of maximum concentrations with distance despite significantly different plume cross-sections. Hall considered transient and continuous releases on a rough surface (plume height - roughness height) and on up- and down-hill slopes.[4,5] Hall reported shallow, wide plumes whose shapes were considerably altered by 1 in 12 ground slopes.

Tests were conducted by Neff et al. in wind tunnel facilities to evaluate the rate of dispersion and the extent of downwind hazards associated with the rupture of typical large LNG storage tanks.[6] Concentrations and temperature measurements, and photographic records were obtained for different wind speeds, wind direction and constant boiloff rates under both neutral and stable atmospheric stratifications. Subsequent measurements by Meroney et al. examined transient releases in similar configurations as well as dense plumes on uphill slopes, and buoyant plume lift off situations.[7,8] Different model release gases were used to simulate the behavior of the cold methane plume--heavy isothermal gas mixtures (CO_2, Freon-12 and air, or Argon) or light-cold mixtures (He and N_2).

Currently research on LNG spill behavior over irregular terrain is being performed at Colorado State University for the U.S. Coast Guard and Gas Research Institute, USA.[9] Small scale models of the LNG Release Pond and surrounding topography at China Lake Naval Weapons Testing Center, California, are being examined in a meteorological wind tunnel. Mean and transient concentration contours have been mapped. Overall plume geometry and behavior have been recorded photographically. Results will be used to plan a field experiment and validate tunnel methodologies.

Laboratory Simulation of Dense Plumes

The reliability of the use of wind tunnel shear layers for modeling atmospheric flows has been demonstrated by several investigators.[10] Specific problems associated with the dispersion of cold natural gas plumes have been previously discussed by Meroney et al.[11,12]

Wind tunnel flow characteristics and physical size are such that most of the requirements for similarity with the atmosphere can only be approximated with varying degrees of accuracy. This does not eliminate the possibility of making useful studies of diffusion by means of small-scale models but limits the range of length scales and thermal conditions for which the studies are feasible. Each similarity requirement will be examined in an effort to determine the necessary approximation imposed by the physical model and the resulting limitations imposed upon a dispersion study.

Grouping independent variables which govern dense vapor dispersion into dimensionless parameters with air density, ρ_a, wind velocity at reference height, U_H, and reference height, H, as reference variables and where Q is volume source rate of the dense gas and ρ_g is dense gas density yields

$\frac{U_H H}{\nu}$ - Reynolds number

$\frac{\rho_a U_H^2}{g(\rho_a - \rho_g)H}$ - Modified Froude number

$\frac{\rho_g Q^2}{\rho_a U_H^2 H^4}$ - Momentum ratio

$\frac{\rho_g - \rho_a}{\rho_a}$ - Gas density ratio

$\frac{Q}{U_H H^2}$ - Non-dimensional spill rate

$\frac{g(T_H - T_o)H}{T\, U_H^2}$ - Bulk Richardson number of inverse atmospheric Froude number

$\frac{\delta}{H}, \frac{D}{H}, \frac{h}{H}, \frac{k}{H}$ - Various length scale ratios associated with shear layer thickness, δ, dike or building diameters, D; structure height, h; and roughness length, k.

For a model test to be completely representative of the full-scale event, values of at least these ten dimensionless numbers plus similarity in approach flow velocity and turbulence profiles should be the same in the model test as at full-scale. Since it is not possible to retain exactly the same values of all these numbers at full- and model scale some latitude must be tolerated. (Indeed in many cases the full-scale values are not even well defined.) One may accept variation in these parameters to the extent that such lassitude does not jeopardize the representativeness of the model.

The Reynolds number cannot be made equal for model and prototype for scales ranging from 1:100 to 1:600. Fortunately equality is not required if the magnitude and quality of the shear layer turbulence is similar to the full-scale--hence the use of specially designed meteorological wind tunnels.[10] It is possible to obtain full-scale values of the remaining non-dimensional parameters by reducing the reference velocity, U_H, to very low values (of the order of 0.2 m/s to simulate a 3 m/sec full-scale wind) and increasing the atmospheric temperature difference (T_H-T_o) as necessary. In some cases investigators modify the density ratio $(\rho_a-\rho)/{}_g\rho_a$ to permit the use of larger and more convenient values of U_H.[4,13] Unfortunately this also modifies inertial effects, time scale ratios, and volume dilution rates so this is not proposed herein.

Previous experiments by Hoot and Meroney, Bodurtha, Van Ulden, and Boyle and Kneebone have confirmed that the Froude number is the parameter which governs plume spread rate, trajectory, plume size and entrainment when gases remain negatively buoyant during their entire trajectory.[3,14,15,2] In the case of spills of LNG buoyancy of the plume will be a function of both mole fraction of methane and temperature. Thus, depending upon the relative rate of entrainment of ambient gases versus rate of thermal transport from surrounding surfaces the state of buoyancy may vary from negative to positive.

Earlier measurements for cold methane releases now suggest that heat transfer effects may be small over the significant time scales associated with non-calm situations (i.e., $U_p > 1$ m/sec); hence gas density should be adequately simulated by isothermal high molecular weight gas mixtures.[6,7] This agrees with the result independently reported by Boyle and Kneebone that room temperature propane simulated an actual LNG spill quite well.[2]

Facilities and Equipment

Simulation of the atmospheric surface layer in Bounday Layer Wind Tunnels has been considered in some detail by previous authors. Special procedures required to inject cold gas plumes are considered by Meroney et al.[12] Representation of transient sources require additional tools recommended below.

Variable Source Rate Simulation

To obtain an accurate prediction of the extent of hazard associated with the spill of a low vapor pressure liquid such as LNG, ammonia, or Freon, the model should simulate the variable boiloff rate of the gas characteristic to that of the spill configuration.

Variable gas flow rate curves may be obtained by use of a programmed cam to close a micrometer needle value controlling the flow of simulation set at a predetermined rate.

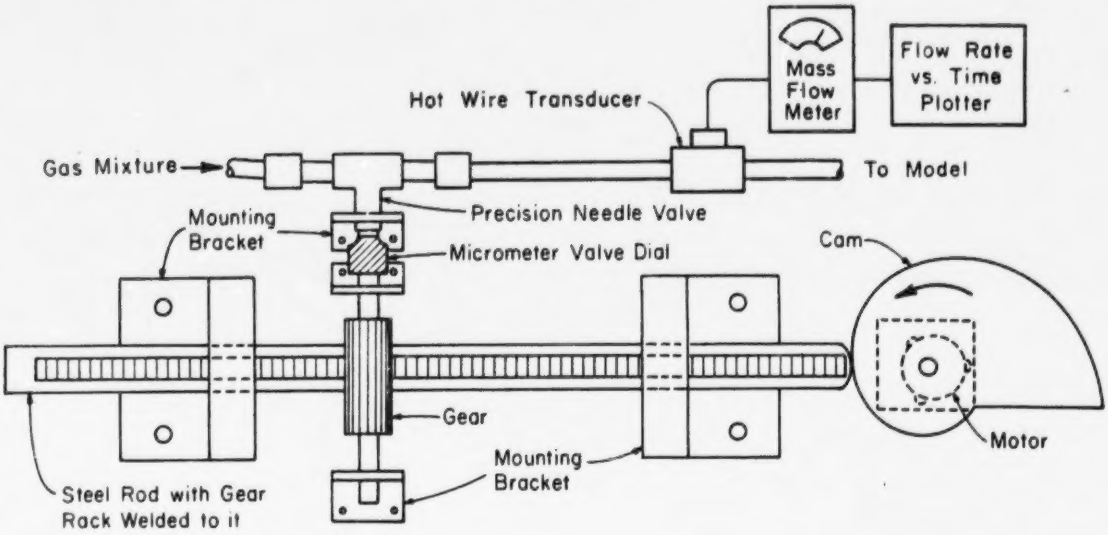
Mass Flow Meter
Flow Rate vs. Time Plotter
Hot Wire Transducer
Gas Mixture
To Model
Mounting Bracket
Precision Needle Valve
Micrometer Valve Dial
Cam
Gear
Motor
Mounting Bracket
Steel Rod with Gear Rack Welded to it

Figure 1. Variable Flow Rate Control Valve

Transient-Concentration Instrumentation

The transient nature of most chemical spills to be simulated necessitate the use of a fast response, temperature compensated concentration transducer. An aspirated dual-film probe was designed recently at Colorado State University. As noted in Figure 2 dual films operated at different current levels permitted compensation for temperature drift, while a flared inlet reduced the noise of pressure fluctuations. Calibration suggests a noise level of 0.1% by volume CO_2 or Argon and an upper frequency response of 1000 Hz.

Variable-Area-Source Release

When low vapor pressure liquids spill on an uncontained surface, density causes the liquid to grow radially outward until all the liquid is vaporized. Generally this growth is thought to be linear with time. Since no cryogenic fluid is generally used in model tests, the resultant variable area nature of the release must be simulated by means of auxiliary equipment installed beneath the wind tunnel floor.

A variable area source devise has been constructed for the current China Lake spill series. As shown in Figure 3 it consists of a contoured honeycomb surface together with a mercury filled bladder. The device has been constructed at a diameter of 0.25 meters; however a larger version may be possible. A simple alternative for the larger size releases is a set of concentric anuluses metered by flowraters and monitored by cam operated solenoid valves.

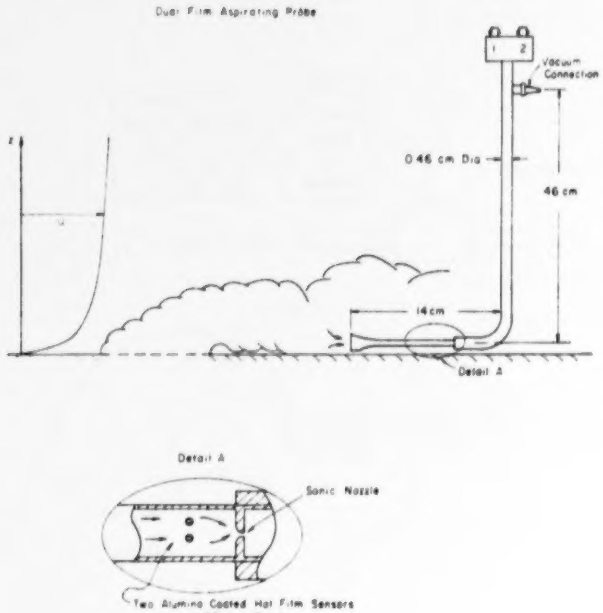
Dual Film Aspirating Probe
z
U
1
2
Vacuum Connection
0.46 cm Dia
46 cm
14 cm
Detail A
Detail A
Sonic Nozzle
Two Alumina Coated Hot Film Sensors
(50 μm Dia)

Figure 2. Dual Film Aspirating Concentration Probe

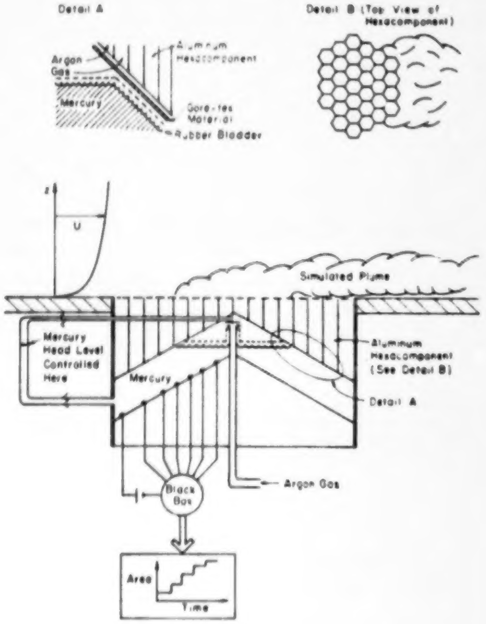
Detail A
Argon Gas
Aluminum Hexacomponent
Mercury
Gore-tex Material
Rubber Bladder
Detail B (Top View of Hexacomponent)
z
U
Simulated Plume
Mercury Head Level Controlled Here
Mercury
Aluminum Hexacomponent (See Detail B)
Detail A
Argon Gas
Black Box
Area
Time

Figure 3. Variable Area Source Model

Test Program Results

The purpose of this paper is to report the character of results of utilizing wind tunnels as a tool to study dense gas released rather than present comprehensive results. Extended discussions of the dense gas release cases examined at Colorado State University are available in report format.[6,7,8,9,16,17]

Dense Plume Dynamics Associated With Structures, Ground Level Release

Density differences were observed by Hoot and Meroney to have significant effect on the downstream diffusion patterns of a ground source.[17] Lateral spread rate increased and vertical spread rate decreased in the vicinity of a release over that displayed by a neutrally buoyant plume as shown in Figure 4. The effect of variation of maximum centerline concentration with distance was primarily multiplicative. Echols prepared corrections to Gaussian plume calculations from this data to provide corrections to conventional Gaussian plume predictions when estimating hazards due to hydrogen sulphide release.[18]

When dense gas clouds result from a breach in a storage tank, the heavy gas may rapidly spread laterally outside the aerodynamic wake region downwind of the tank. In such cases the portion of the plume outside the wake will not be mixed by the turbulent intensity excess present in the wake region, and bifurcated plume profiles will exist at ground level as suggested by the sketch in Figure 5. The tank and bund structure may mix gases vertically immediately downwind as shown in the figure; however, surface concentrations generally vary with distance in a manner noted by Figure 4.

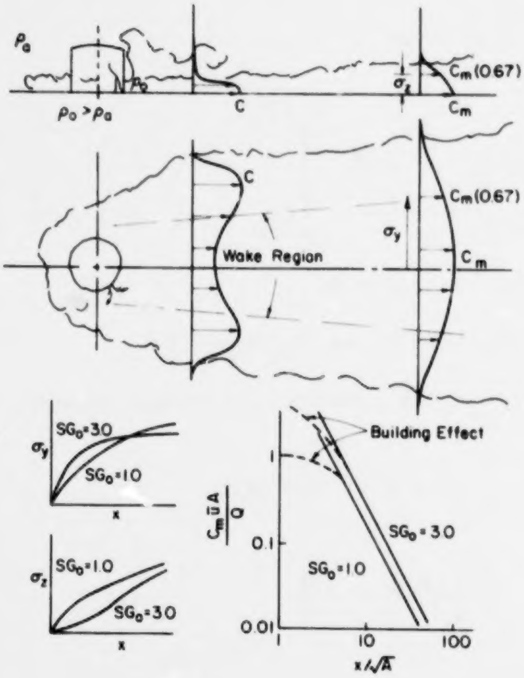
ρ_a
ρ_o
$\rho_o > \rho_a$
C
σ_z
$C_m(0.67)$
C_m
C
$C_m(0.67)$
σ_y
Wake Region
C_m
$SG_o=3.0$
σ_y
$SG_o=1.0$
x
$SG_o=1.0$
σ_z
$SG_o=3.0$
x
Building Effect
$\frac{C_m \bar{u} A}{Q}$
1
0.1
0.01
$SG_o=3.0$
$SG_o=1.0$
1
10
100
$x/\sqrt{A}$

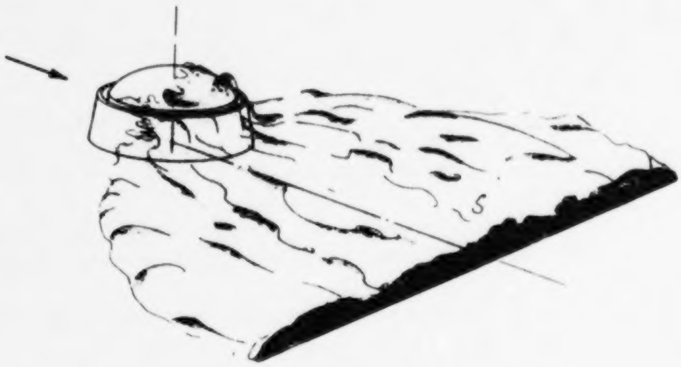

Figure 4. Dense Plume Dispersion Ground Source Release

Figure 5. Dense Gas Spreading Downwind of a Tall Dike About a Storage Tank

Dense Plume Dynamics Associated With Structures - Elevated Releases

Hoot and Meroney proposed a method to estimate surface concentrations based on emperical tuning of an analytical plume theory.[3,17] The components of the analysis requires one to first estimate plume rise, Δh, as

$$\frac{\Delta h}{d_o} = 1.32\ (S.G.)^{2/3}\ (F_{RH})^{2/3}\ (R), \qquad (3)$$

where $S.G. = \rho_o/\rho_a$

$R \quad = w_o/u$

$$F_{RH} = U/\sqrt{g\Delta d_o}\ , \text{ and}$$

downwind distance to maximum plume rise, $\bar{x}$, as

$$\frac{\bar{x}}{d_o} = (\mathrm{S.G.})\ (F_{RH})^2\ (R)\ . \qquad (4)$$

Touchdown distance, x_{TD}, may be evaluated from

$$\frac{x_{TD}-\bar{x}}{d_o} = 0.56\left[\frac{\left(\frac{h_s}{d_o} + 2\,\frac{\Delta h}{d_o}\right)^3 - \left(\frac{\Delta h}{d_o}\right)^3}{R}\ .\right]^{1/2} F_{RH} \qquad (5)$$

(Symbols are defined in Figure 6)

Note that as $u \to 0$, $F_{RH} \to 0$, $\bar{x} \to 0$, $\Delta h \to 0$ and $x_{TD}/h_s \to 3\ F_{RH}$. The constant, 3, compares well to the value 4.5 proposed by Briggs based on Bodurtha's visualization experiments.[19]

At touchdown the surface concentrations are of the order

$$\frac{C_{TD}\ u h_B^2}{Q} = 3.1\left(\frac{2\Delta h + h_s}{h_B}\right)^{-2} \qquad (6)$$

Concentrations decrease from their touchdown values at a negative 0.65 power of distance, x, until the curve intercepts the -1.7 slope behavior of a ground source as shown in Figure 6.

ACKNOWLEDGMENTS

Authors gratefully acknowledge support via R & D Associates, Marina del Rey, California, USA, from American Gas Association Project IS-128-1 and Department of Energy Contract EE77C031364 as well as direct support through Department of Transportation Contract No. DOT-CG-75279-A.

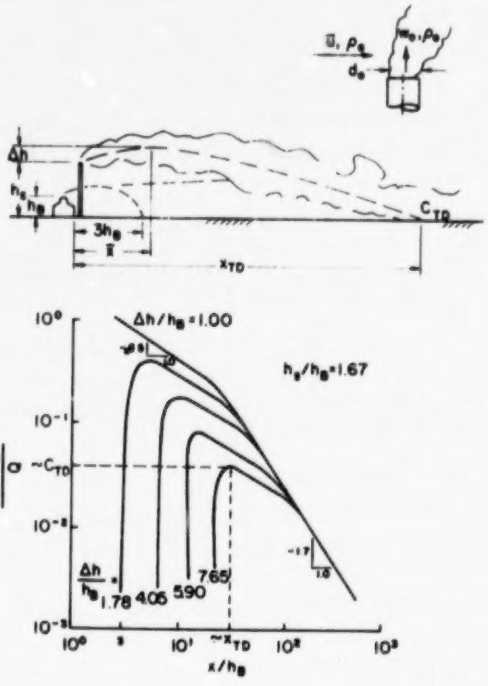

Figure 6. Dispersion of Dense Plumes From Short Stacks

References

1. J. Sakagami and M. Kato, "Diffusion and Vapour Rise of Methane Vapour From a Real Source in Air Stream," Natural Science Report of Ochanomizu University, Japan, 19: 59-66, 1968.

2. G. J. Boyle and A. Kneebone, "Laboratory Investigation Into the Characteristics of LNG Spills on Water, Evaporation, Spreading and Vapor Dispersion," Shell Research, Ltd., Report to API, 1973.

3. T. G. Hoot and R. N. Meroney, "The Behavior of Negatively Buoyant Stack Gases," 67th Annual Meeting APCA, Denver, CO, 74-210, June 9-13, 1973.

4. D. J. Hall, C. F. Barrett, and M. O. Ralph, "Experiments on a Model of an Escape of Heavy Gas," Warren Spring Laboratory Report CR 882 (AP), Department of Trade and Industry, U.K., 1975.

5. D. J. Hall, "Further Experiments on a Model of an Escape of Heavy Gas," Warren Spring Laboratory Report CR 1341 (AP) Department of Trade and Industry, U.K., 1977.

6. D. E. Neff, R. N. Meroney, and J. E. Cermak, "Wind Tunnel Study of the Negatively Buoyant Plume Due to an LNG Spill," Colorado State University, Ft. Collins, CER76-77DEN-RNM-JEC22, 1976.

7. R. N. Meroney, D. E. Neff, J. E. Cermak, and M. Megahed, "Dispersion of Vapor From LNG Spills - Simulation in a Meteorological Wind Tunnel," Colorado State University, Ft. Collins, CER76-77RNM-JEC-DEN-MM57, 1977.

8. R & D Associates and Fluid Mechanics and Wind Engineering Program Staff, Colorado State University, "LNG Wind Tunnel Simulation and Instrumentation Assessments," RDA-TR-105700-003 or DOE Report SAN/W1376-01, 1978.

9. D. E. Neff and R. N. Meroney, "Dispersion of Vapor From LNG Spills-Simulation in a Meteorological Wind Tunnel of Spills at China Lake Naval Weapons Center, California," Colorado State University, Ft. Collins, CER78-79DEN-RNM41, 1979.

10. J. E. Cermak, "Applications of Fluid Mechanics to Wind Engineering--A Freeman Scholar Lecture," J. of Fluid Engineering, 97: 9-38, 1975.

11. R. N. Meroney, J. E. Cermak and D. E. Neff, "Dispersion of Vapour From LNG Spills--Simulation in a Meteorological Wind Tunnel," Proc. of 3rd AMS Symposium on Atmospheric Turbulence, Diffusion and Air Quality, Raleigh, N.C. 243-246, October 19-22, 1976.

12. R. N. Meroney, D. E. Neff and J. E. Cermak, "Wind Tunnel Simulation of LNG Spills," Proc. of American Gas Association Transmission Conference, Montreal, Canada, T217-T223, May 8-10, 1978.

13. N. Isyumov and H. Tamaka, "Wind Tunnel Modeling of Stack Gas Dispersion--Difficulties and Approximations," Proceedings Fifth International Conference on Wind Engineering, Fort Collins, Colorado, USA, Pergamon Press, 2 vols, 1979.

14. F. T. Bodurtha, Jr., "The Behavior of Dense Stack Gases," J. of APCA, Vol. 11, No. 9, pp. 431-437, 1961.

15. A. P. Van Ulden, "On the Spreading of a Heavy Gas Released Near the Ground," Loss Prevention and Safety Promotion Seminar, Delft, Netherlands, 1974.

16. P. T. Harsha, "LNG Safety Program Topical Report, Wind Tunnel Tests of Vapor Dispersion From Land Facilities," RDA-TR-1100-002, AGA Project IS-128-1, 1976.

17. T. G. Hoot, R. N. Meroney, and J. A. Peterka, "Wind Tunnel Tests of Negatively Buoyand Plumes," Colorado State University, Fort Collins, CER73-74TGH-RNM-JAP13, 1973.

18. W. T. Echols, "Estimating the Hazardous Radius of Exposure From Accidental Releases at Hydrogen Sulfide Gas," Proceedings of 1976 Conference on Control of Hazardous Material Spills, New Orleans, Louisiana, April 25-28, 1976.

19. G. A. Briggs, "Diffusion Estimation for Small Emissions," Atmospheric Turbulence and Diffusion Laboratory Report No. 79, NOAA, Oak Ridge, Tennessee, 61 p. 1973.

Discussion:

Van Ulden:

Did you study the influence of a high dike situated at greater distance from the source? The volumen endosed by the dike, then should be sufficiently large to contain all the dense gas that is released. In that case the dike may prevent the dense gas to spread further than the dike!

Meroney (response):

No, we did not study this.

Young:

Have you come to any conclusions about the effects of various types of enclosures on either the delay times for heavy gas spread or containment?

Meroney (response):

He has not studied these particular problems in enough detail to answer these questions.

COMPARISON OF A WIND TUNNEL MODEL OF A DENSER-THAN-AIR GAS SPILL WITH FIELD EXPERIMENTS

by

D.J.Hall *
Warren Spring Laboratory, Stevenage,
Herts, UK.

Abstract The behaviour of denser-than-air gas spills has become a matter of considerable interest over the last few years because many such materials are potentially hazardous. Wind tunnel modelling is a very convenient way of investigating such spills, but because of specific difficulties in scaling them the accuracy of these models remains uncertain until they can be compared with suitable full scale data. Some well documented field trials of denser-than-air gas spills are now available and it has been possible to compare these with similar wind tunnel experiments carried out prior to the trials. The comparison shows good agreement.

*Presented by C.F.Barrett

Preceding page blank

Introduction

Many potentially hazardous gases are either naturally denser-than-air (for example, propane, butane, chlorine) or are stored in refrigerated or compressed form so that they will be denser-than-air if released to the atmosphere (for example, Liquefied Natural Gas, Ammonia). There is thus some interest in the characteristics of accidental spills of these materials and they may be expected to behave differently to releases of neutrally or positively buoyant materials whose behaviour is generally better known.

In the last few years a number of wind tunnel model simulations of denser-than-air gas spills have been reported 1,2,3. The usefulness of wind tunnel modelling of atmospheric dispersion problems is well established, as is its general accuracy for many types of pollutant releases. However, the special characteristics of a denser-than-air spill near the ground, a significant density driven flow component and high plume stability levels, cause particular problems of model scaling which may well affect the accuracy of a small scale model of such a spill. The problems of dense gas spill model scaling are fully discussed in the reports noted above, but the validity of such models will remain uncertain until suitable comparisons can be made with large scale field trials.

Until recently suitable field data have not existed, but in the last year the results of thoroughly documented field trials carried out at Porton Down, England, have become available,[4]. These involved an instantaneous release of, typically, 40 m^3 of gas of varying densities under a range of atmospheric conditions. Measurements of the plume size were made from photographs of the smoke-filled plume and concentrations were recorded in the plume using both dosage meters and continuously recording monitors at specific points. The wind tunnel experiments [2], which were carried out some time before the Porton field trials, were of a general nature designed to model a range of, mostly large scale, spill conditions, including short duration spills. Provided that Richardson Number modelling is applied a comparison between these wind tunnel experiments and the Porton trials is possible, and the results are shown in this short paper.

Determination of Model Scale

The range of values of density ratio, $\frac{\Delta\rho}{\rho}$, for the released gas and windspeed, U, for the Porton trials are shown in fig 1. Though these cover a considerable range of conditions the size of the spill is quite modest compared with many spills of practical interest and the wind tunnel model was primarily designed to cover these larger spills. As a result there is only a limited overlap between the experimental range of the Porton trials and that of the wind tunnel model, and this overlap requires that Richardson Number modelling be applied (that is, matching values of Richardson Number, R_i(= $g\frac{\Delta\rho}{\rho}\frac{L}{U^2}$) at model and full scale). The shortest puff release time (2_s) at the highest windspeed used in the wind tunnel experiments seemed most likely to match the field trials. The solid line in fig 1 is the line of constant Richardson Number corresponding to this particular model test and shows the range of conditions in the Porton trials that it will match on this basis. Trial No 33 sits on the line and was used for the comparison since it produced a full set of data. Trial No. 25, near the line, was also considered but suffered from an uncertain windspeed and incomplete data output.

Two of the continuous monitor results from the trial were at distances from the source that matched fairly closely sample points in the wind tunnel model and these have been compared. Also, times for 'arrival' and 'departure' of the plume at different downwind distances were available for both model and field trial and these too have been compared. The length scale of the model test, L, was fixed at $^1/34.2$ by matching the volume of gas released. Windspeed on the model was determined at 5.85 cms height, the scale equivalent of the 2m reference height used in the trials. The time scale of the wind tunnel experiment, t, then came out at 10.8 times full scale by matching values of $\frac{Ut}{L}$, the appropriate dimensionless scaling parameter.

The respective operating conditions for the field trial and the model test are thus:

	Field Trial No 33	Model Test
Scale, L.	1/1	1/34.2
Volume of Release	40 m^3	1 l.
Time of Release	Instantaneous	2 s.
Density of Release/Density of Air,	2.2	5.74
$\frac{\Delta\rho}{\rho}$	1.2	4.74
Windspeed	2.0 ms^{-1} at 2 m height	.63 ms^{-1} at 58.5mm height
Time scaling	x1	x10.8
Atmospheric Stability	B-C (near Neutral)	C-D (Neutral)

Results

Figs 2 and 3 show comparisons between 'continuous monitor' measurements from the field trial at distances of 15 m and 25 m downwind of the source respectively. In fig 2 the continuous monitor was at 15 m from the source, while the nearest sample point in the wind tunnel was at an equivalent distance of 17.4 m from the source. The wind tunnel measurements indicated that between the equivalent of 15 m and 17.4 m downwind the peak concentration fell by 31%, so the model values were scaled by this amount for the comparison. In fig 3 the field trial measurements were at 25m and the wind tunnel monitor at an equivalent distance of 26.1 m, differences in peak concentration between these distances was small, so model and trial were compared directly.

Fig 4 shows comparisons of 'arrival' and 'departure' times, of the plume at different downwind distances. The original figure of the Porton report, from which fig 4 has been taken, showed only times derived from photographic records of smoke releases. In fact some further data is available from the continuous monitor results (including those of figs 2 and 3) and these have been added to the figure. 'Departure' times from smoke and continuous monitor results are a similar, but 'arrival' times differ a little.

Discussion

The level of agreement between wind tunnel model and field trial seems generally very good. The peak concentrations, the form of concentration distribution with time, and the 'arrival' and 'departure' times all match quite well. 'Arrival' times from the continuous monitor results agree more closely with the wind tunnel results than do those from the smoke measurements.

There are some characteristics of the wind tunnel model which do not precisely match the field trials. These are:

1) The model surface roughness was proportionately greater than that of the field trial by a factor of about seven in Z_o. This might reduce velocities near the ground, thus affecting 'arrival' and 'departure' times, though probably not by very much. Otherwise this difference should not be important.

2) The model gas release took a significant time to enter the tunnel, the equivalent of 22 seconds at field trial time scales. The wind tunnel experiments showed significant effects of release time on plume front velocity and peak concentration. This difference would probably cause lower peak concentrations and longer plume arrival times to occur on the model. One might also argue that it would be better to treat the midpoint of the model release time as the zero time point for the comparison. If this were done the continuous monitor results of figs 2 and 3 would show closer agreement than before, so would the 'arrival' times in fig 4. The 'departure' times in fig 4 would agree a little less well, but not significantly so.

3) The effective height of the release was lower on the model, equivalent to about one metre, than in the field trial, where the tent was about 3m high. This difference would mostly affect plume front velocities in the density driven part of the plume, and thus 'arrival' times, and, possibly, maximum plume size.

The expected effects of these differences, mainly reduced plume front velocities and reduced peak concentrations on the model, are the main differences that appear in the comparison.

Conclusions

Despite some differences in the test arrangements, the wind tunnel model shows remarkably close agreement to the Porton field trial to which it can be matched using Richardson Number scaling. It is thus an encouraging step on the way to validating wind tunnel models of denser-than-air gas spills. A more thorough comparison would be desirable and it is intended to do this in the near future. Because of the relatively modest scale of the Porton field trials compared with the size of many spills of practical interest their value for validation purposes, though important, must remain limited. The need for a well documented large-scale spill remains.

References

1. D.J.Hall, C.F.Barrett, M.O.Ralph. Experiments on a Model of an Escape of Heavy Gas. Warren Spring Laboratory Rept No LR217 (AP) Nov 1975, Stevenage, U.K.

2. D.J.Hall. Further Experiments on a model of an Escape of Heavy Gas Warren Spring Laboratory Rept No LR312 (AP) May 1979, Stevenage, U.K.

3. R.N.Meroney, J.E.Cermak, D.E.Neff. Dispersion of Vapour from LNG Spills - Simulation in a Meteorological Wind Tunnel. Presented at AMS Third Symposium on Atmospheric Turbulence, Diffusion and Air Quality, Oct 19-22, 1976, Raleigh N.C.,U.S.A.

4. R.G.Picknett. Field experiments on the Behaviour of Dense Clouds. Chemical Defence Establishment, Porton Down Rept No Ptn 1L 1154/78/1 Sept 1978. U.K.

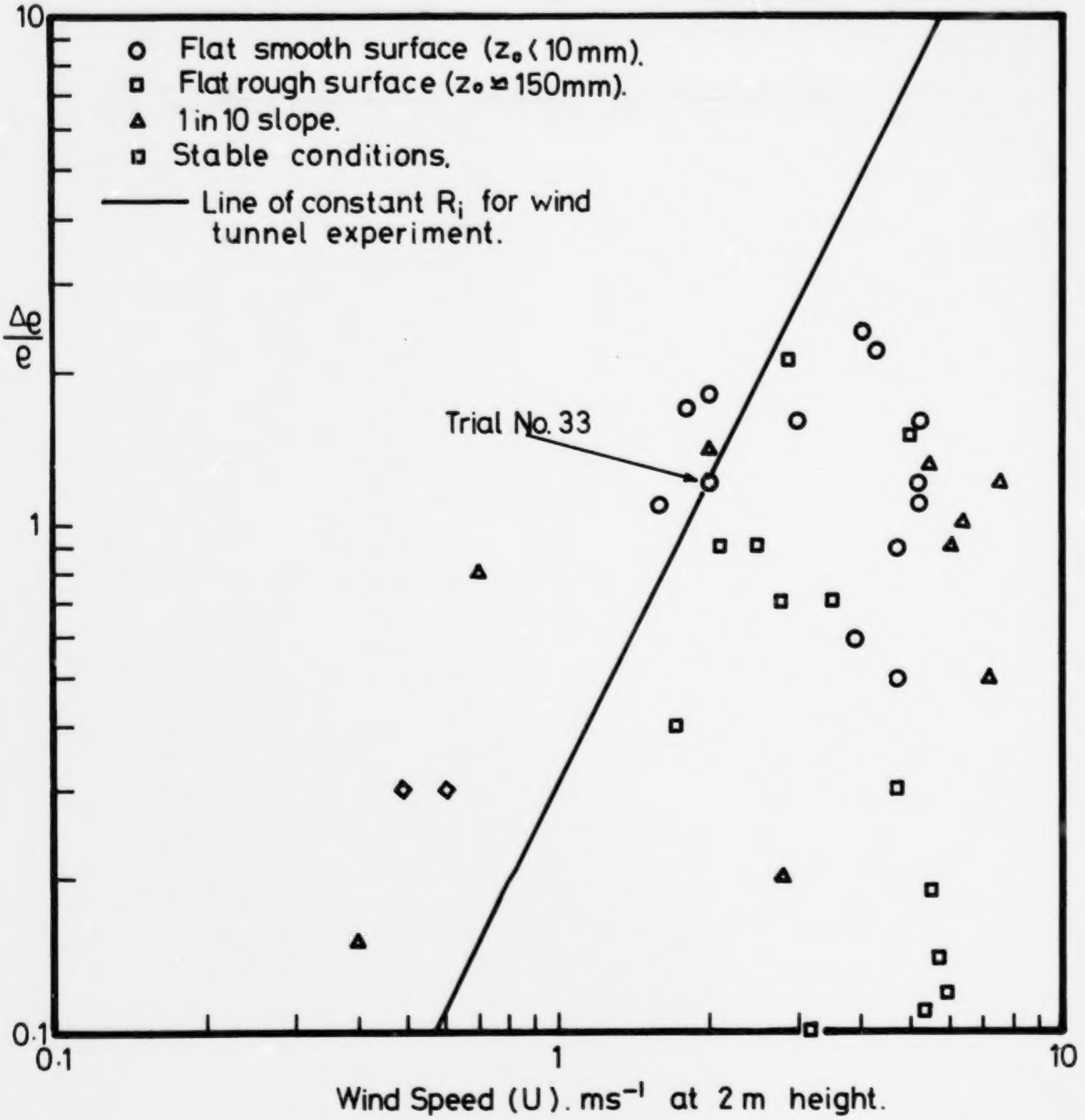

Fig. 1 Porton Field Trials - Range of Experimental Variables.

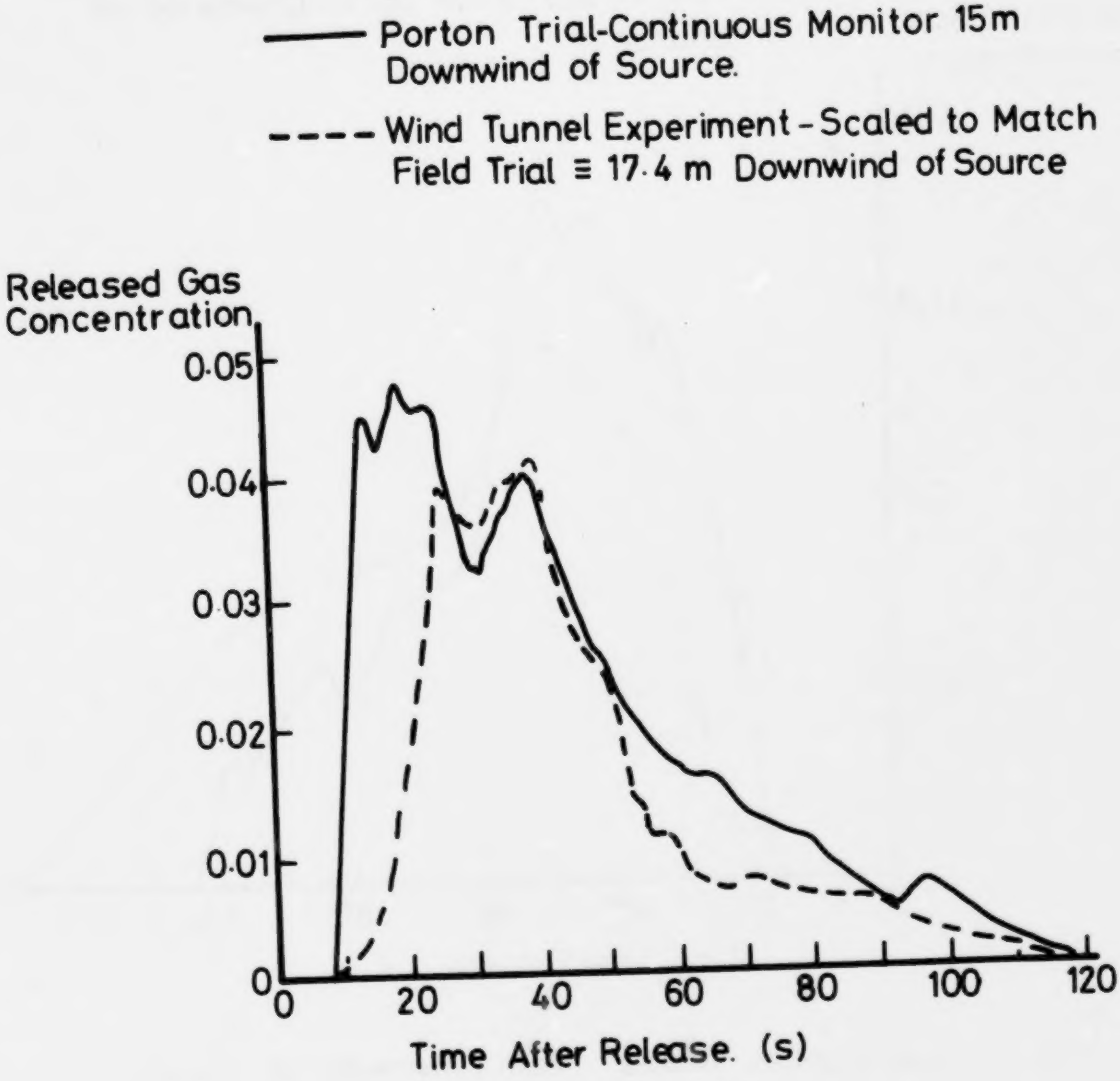

Fig. 2 Gas Monitor Traces 15m Downwind of Source.
Trial No.33

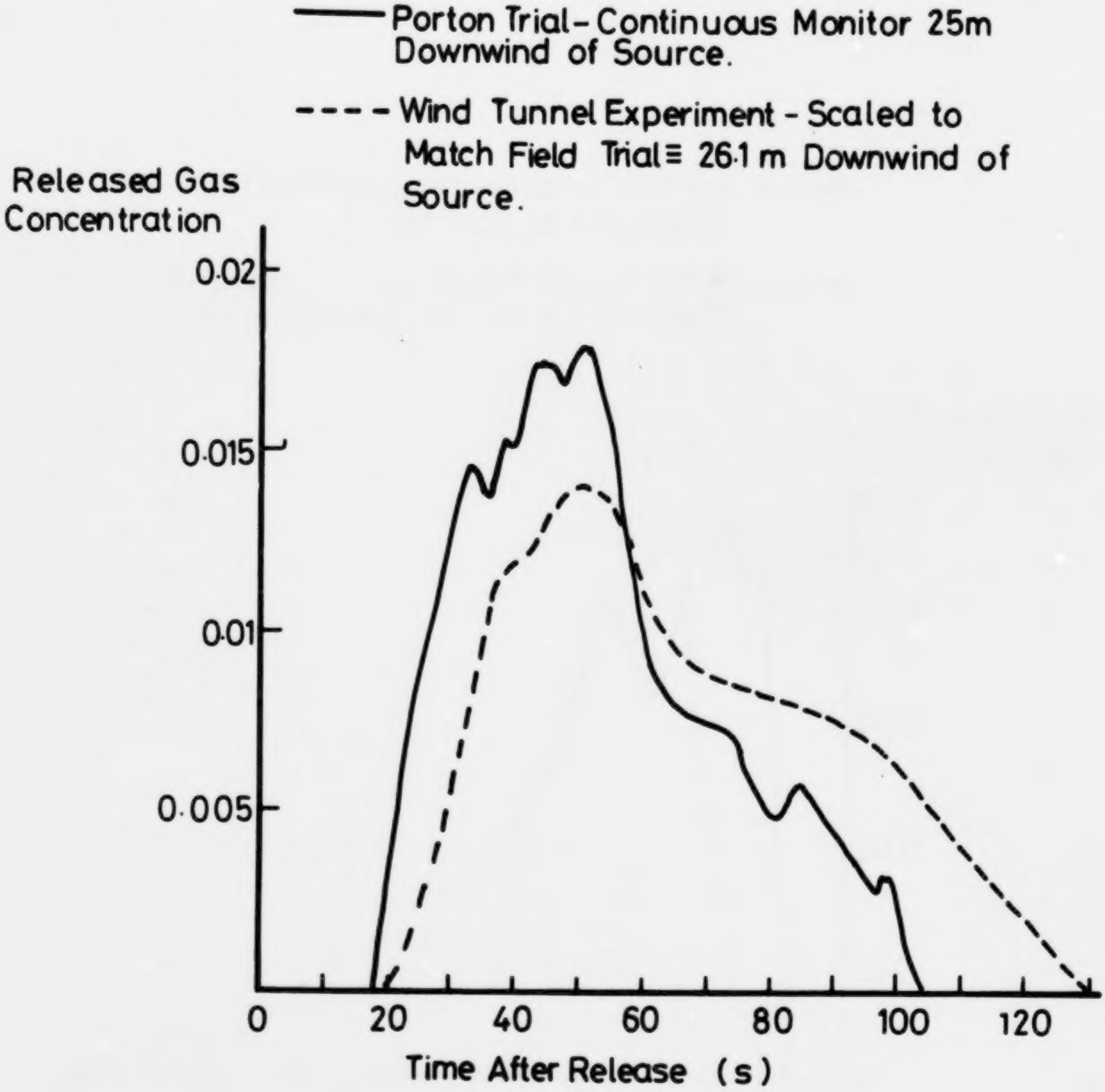

Fig. 3 Gas Monitor Traces 25m Downwind of Source. Trial No. 33.

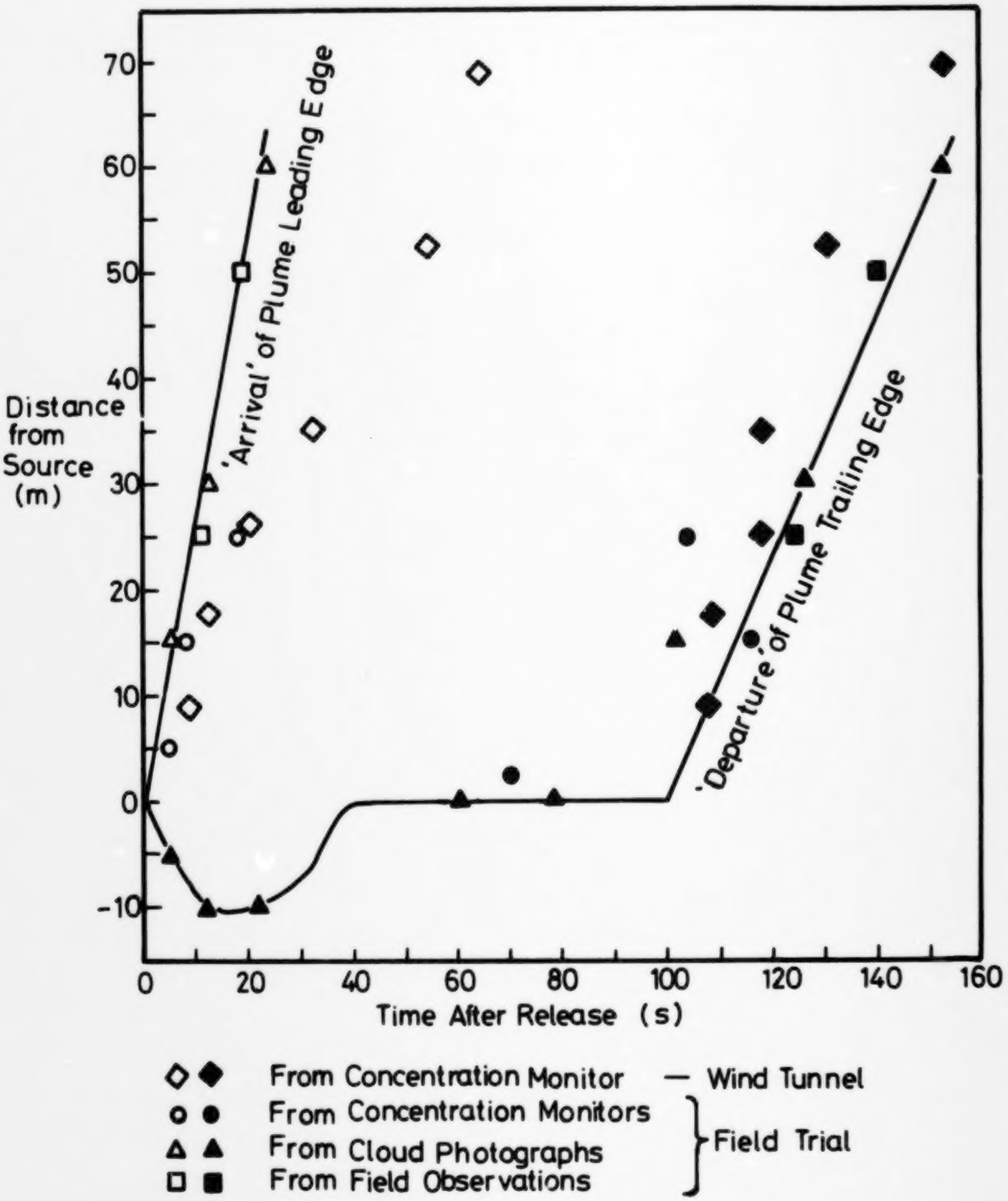

Fig. 4 Movement of Gas Plume
Trial No. 33.

AGENDA

Tuesday, October 23, 1979

Chairman: Dieter Jost

INTRODUCTORY PRESENTATIONS

Chairman: H. Fortak

Rapporteur: R. V. Portelli

1. Luigi Santomauro

TALL STACKS; MANAGEMENT

2. Werner Klug

TALL STACKS; IMPACTS ON THE ATMOSPHERE

PRESENTATIONS AND DISCUSSIONS ABOUT TOPIC I

TALL STACKS

Chairman: T. Schneider

Rapporteur: C. D. Whiteman

1. G. Fronza et al.

FORECAST OF FUMIGATION EPISODES AROUND A TALL STACK

(P. Bolzern, G. Fronza, Istituto di Elettronica; Centro Teoria dei Sistemi; Politecnico di Milano, Milano, Italy)

2. M. Benarie

HOW DO TALL STACKS INFLUENCE ON LONG RANGE TRANSPORT?

(M. Benarie, Institut national de recherche chimique appliquée - IRCHA Boite postale No. 1; 91710 Vert Le Petit, France)

3. A. Venkatram et al.

MODELING OF DISPERSION FROM TALL STACKS

(A. Venkatram, Ontario Ministry of the Environment, Air Quality and Met.

Preceding page blank

Section, 135 St. Clair Avenue West, Toronto, Ont. MAV 1P5;
R. Vet, Vet Consultants Ltd., Toronto, Ont. Canada)

4. H. Fortak

ON THE EFFECTIVENESS OF EXTREMELY TALL STACKS

(H. Fortak, Freie Universität Berlin, Theoretische Meteorologie, Thielallee 49, 1000 Berlin 33)

Chairman: L. Santomauro
Rapporteur: A. Venkatram

5. P. Guillot

DISPERSION OF POLLUTANTS FROM TALL STACKS STUDIED BY REMOTE SENSING TECHNIQUES DURING EEC JOINT CAMPAIGNS

(P. Guillot, Commission of the European Communities; Environment and Raw Materials Research Programmes; 200 Rue de la Loi, 1049 Brussels, Belgium)

6. R. V. Portelli

THE NANTICOKE STUDY: EXPERIMENTAL INVESTIGATION OF DIFFUSION FROM TALL STACKS IN A SHORELINE ENVIRONMENT

(R. V. Portelli, Atmospheric Environment Service; Fisheries and Environment Canada; 4905 Dufferin Street, Downsview, Ont. M3H 5T4, Canada)

7. N. Gillani

EXPERIMENTAL INVESTIGATION OF ATMOSPHERIC SULFUR TRANSPORT AND TRANSFORMATION IN THE STATE PROGRAM

(Wm. E. Wilson, F. Schiermeier, US Environmental Protection Agency, Environmental Sciences Research Laboratory, MD-84, Research Triangle Park, North Carolina 27711, USA)
N. V. Gillani, Dept. of Mechanical Engineering, Washington University, St. Louis, Missouri 63130, USA)

8. A. E. Saab et al.

DEVELOPMENT OF PRACTICAL CALCULATIONS FOR ESTIMATING DISPERSION FROM ELEVATED SOURCES

(A. E. Saab, J. P. Granier, Electricité de France, Direction des études et recherches, 6, Quai Watier, 78400 Chatou, France)

Chairman: M. Bénarie
Rapporteur: N. Gillani

9. M. M. Millàn

EXPERIMENTAL OBSERVATIONS OF THE PLUME FROM A TALL STACK OUT TO 400 km

(M. M. Millàn, Atmospheric Environment Service; Fisheries and Environment Canada; 4905 Dufferin Street, Downsview, Ont. M3H 5T4, Canada)

10. E. L. Petersen et al.

ELEVATED SOURCE SF_6-TRACER DISPERSION EXPERIMENTS IN THE COPENHAGEN AREA

(S. E. Gryning, E. L. Petersen, Risø National Laboratory, Met. Section, 4000 Roskilde; E. Lyck, Danish National Agency of Environmental Protection Air Pollution Lab., 1401 Copenhagen K., Denmark)

11. D. A. Trout

A REVIEW OF HORIZONTAL AND VERTICAL DISPERSION COEFFICIENTS APPLIED IN THE CALCULATION OF GROUND LEVEL POLLUTANT CONCENTRATIONS RESULTING FROM EMISSIONS FROM TALL STACKS UNDER VERY UNSTABLE ATMOSPHERIC CONDITIONS

(D. A. Trout, US Environmental Protection Agency, Region V, Chicago, Illinois, USA)

ROUND TABLE DISCUSSION

M. E. Smith, P. R. Maul, T. Schneider, H. Fortak, A. L. Berger

Chairman: W. Klug
Rapporteur: R. V. Portelli

Wednesday, October 24, 1979

PRESENTATIONS AND DISCUSSIONS ABOUT TOPIC II

COMPLEX TERRAIN AND WEAK WIND CONDITIONS

Chairman: E. Weber
Rapporteur: G. Fronza

1. B. Henderson-Sellers

A GROSS PARAMETER PLUME MODEL; THEORY AND APPLICATION FOR NON-PLANAR TOPOGRAPHY AND FOR NEGATIVELY BUOYANT EFFLUENTS

(B. Henderson-Sellers, University of Salford, Dept. Civil Eng. Salford M5 4WT, England)

2. J. C. Weil

BUOYANT PLUME RISE OVER A TWO-DIMENSIONAL HILL

(J. C. Weil, Martin Marietta Corp., Environmental Center, 1450 South Rolling Road, Baltimore, Maryland 21227, USA)

3. G. Tebaldi

ANALYSIS BY MEANS OF METEOROLOGICAL AND PHYSICAL CONSIDERATIONS ABOUT THE TRANSPORT AND GROUND DEPOSITION OF THE TCDD, EMITTED THE 10TH JULY, 1976 FROM THE ICMESA FACTORY

(A. Cavallaro, G. Tebaldi, R. Gualdi, Laboratorio provinciale Igiene e profilassi - Reparto Chimico, Via Juvara 22, Milano, Italy)

Rapporteur: J. Tikvart

4. C. D. Jones

STATIONARITY OF THE CONCENTRATION INTERMITTENCY IN SHORT-RANGE ATMOSPHERIC DISPERSION

(C. D. Jones, Porton Down, Salisbury, Wilts SP4 oJQ, England)

5. H. Reuter et al

THE INFLUENCE OF LOW LEVEL INVERSIONS ON THE DISPERSION OF ATMOSPHERIC POLLUTANTS

(H. Kolb, H. Reuter, Universität Wien, Institut für Meteorologie und Geophysik, Hohe Warte 38, 1190 Wien, Austria)

6. Gisela Tangermann

NUMERICAL SIMULATIONS OF AIR FLOW AND POLLUTANT DISPERSION OVER COMPLEX TERRAIN

(Gisela Tangermann, Meteorologisches Institut der Universität Karlsruhe, 7500 Karlsruhe, Federal Republic of Germany)

Chairman: G. C. Holzworth
Rapporteur: A. Braig

7. T. B. McKee et al.

TEMPERATURE INVERSION DESTRUCTION IN MOUNTAIN VALLEYS - IMPLICATIONS FOR AIR POLLUTION DISPERSION

(C. D. Whiteman, T. B. McKee, Colorado State University, Dept. of Atmospheric Science, Fort Collins, Colorado 80523, USA)

8. F. Wippermann

TRAJECTORIES UNDER A STRONG TEMPERATURE INVERSION IN A MOUNTAINOUS AREA

(F. Wippermann, H. J. Koppert, Technische Hochschule Darmstadt, Institut für Meteorologie, Hochschulstr. 1, 6100 Darmstadt, Federal Republic of Germany)

Rapporteur: Helga Kolb

9. M. W. Chan et al.

DEVELOPMENT AND VALIDATION ON AN AIR POLLUTION MODEL FOR COMPLEX TERRAIN APPLICATIONS

(M. W. Chan, Sara J. Head, S. Machiraju, Aero Vironment, Inc., 145 Vista Avenue, Pasadena, California 91107, USA)

10. H.-T. Liu et al.

PHYSICAL MODELING OF PLUME DISPERSION IN COMPLEX TERRAIN WITH AN ELEVATED INVERSION

(H.-T. Liu, Flow Research Com., 21414, 68th Avenue South, Kent, Washington 98031;
J.-T. Lin, United Industries Corp., Bellevue, Washington, USA)

Chairman: B. Gutsche
Rapporteur: D. A. Trout

11. G. C. Holzworth

A STUDY OF DISPERSION OVER COMPLEX TERRAIN IN THE SOUTHEASTERN UNITED STATES

(George C. Holzworth, Meteorology and Assessment Division, Env. Sciences Research Lab., EPA, Research Triangle Park, North Carolina 27711, USA;
K. E. Pickering & R. C. Koch, Geomet. Inc.; 15 Firstfield Road, Gaithersburg, Maryland 20760, USA)

12. L. Santomauro et al.

EXPERIMENTAL DETERMINATION OF DIFFUSION COEFFICIENTS ABOVE AN URBAN AREA

(L. Santomauro, V. Maestro, C. Barberis, Osservatorio Meteorologico di Brera, 20121 Milano, Italy)

13. G. A. Davidson et al.

A COMPARISON OF SOME INTEGRAL PLUME RISE MODELS WITH FIELD OBSERVATIONS

(G. A. Davidson, P. R. Slawson, University of Waterloo, Dept. of Mechanical Engineering, Waterloo, Ont. N2L 3G1, Canada;
S. G. Djurfors, Syncrude Canada Ltd. 10030 - 107 Street, Edmonton, Alberta T5J 3E5, Canada)

14. R. J. Yamartino et al.

ANALYSIS OF SEVERAL LOW WIND SPEED TRACER EXPERIMENTS

(R. J. Yamartino, Argonne National Laboratory, 9700 South Cass Avenue, Illinois 60439 USA;
P. G. Lühring, R. Stern, Freie Universität Berlin, Institut für Geophysikalische Wissenschaften, Thielallee 50, 1000 Berlin 33)

Chairman: H. Reuter
Rapporteur: B. Henderson-Sellers

15. W. G. Hübschmann

DIFFUSION OF ATMOSPHERIC POLLUTANTS BEING EMITTED FROM TALL STACKS

(W. G. Hübschmann, K. Nester, P. Thomas, Kernforschungszentrum Karlsruhe GmbH, Postfach 3540, 7500 Karlsruhe, Federal Republic of Germany)

16. D. Camuffo et al.

TESTS ON ATMOSPHERIC DIFFUSION WITH TRACERS IN AN URBAN AREA

(D. Camuffo, CNR Laboratorio Chimica e Tecnologia Radioelementi, Corso Stati Uniti, I - 35100 Padowa;
M. De Bortoli, P. Gaglione, IRC Euratom, Chemical Division, ISPRA, Varese, Italy)

17. K. J. Vogt et al.

AN EXTENSION OF THE GAUSSIAN PLUME MODEL FOR THE CASE OF CHANGING WHEATHER CONDITIONS

(K. J. Vogt, J. Straka, H. Geiß, Kernforschungsanlage Jülich GmbH, Postfach 365, 5170 Jülich 1, Federal Republic of Germany)

Thursday, October 25, 1979

PRESENTATIONS AND DISCUSSIONS ABOUT TOPIC III

MULTIPLE SOURCES

Chairman: A. Berger
Rapporteur: R. J. Yamartino

1. L. Prahm et al.

REGIONAL SOURCE QUANTIFICATION MODEL FOR SULPHUR OXIDES IN EUROPE

(L. P. Prahm, National Agency for Environmental Protection, Danish Air Pollution Laboratory, Risø National Lab., 4000 Roskilde;
K. Conradsen, L. B. Nielsen, Institute of Mathematical Statistics and Operations Research, Denmark's Technical University, 2800 Lyngby, Denmark)
A. Eliassen, Norwegian Meteorological Institute, Postbox 320, Blindern, Oslo 3, Norway)

2. J. H. Weaving et al.

AN EXPERIMENTAL AND THEORETICAL INVESTIGATION OF PHOTO-CHEMICAL POLLUTION IN TURIN

(J. H. Weaving, S. F. Benjamin, Browns Lane Allesley, Coventry CV5 9LR, England)
P. P. Gaddo, F. Repetto, Committee of Common Market Automobile Constructors (CCMC), 1040 Brussels, Belgium)

3. Giovanna Finzi et al.

MULTIVARIATE REAL-TIME PREDICTORS OF SULPHUR DIOXIDE CONCENTRATIONS IN MILAN CITY

(D. Barbieri, M. Baroni, G. Finzi, Centro Teoria dei Sistemi CNR, c/o Istituto di Elettrotecnical ed Elettronica; Politecneco di Milano, Piazza Leonardo da Vinci 32, 20133 Milano, Italy)

4. J. G. Kretzschmar

SOME COMMENTS ON THE VALIDATION OR VERIFICATION OF MULTIPLE SOURCE MODELS FOR IMPACT ASSESSMENT

(J. G. Kretzschmar, Studiecentrum voor Kernenergie, S. C. K. /C. E. N., Boeretang 200, 2400 Mol, Belgium)

5. E. Runca et al

COMPARISON OF FINITE DIFFERENCE AND GALERKIN TECHNIQUES APPLIED TO THE NUMERICAL TREATMENT OF ADVECTION AND DIFFUSION OF AIR POLLUTANTS

(E. Runca, P. Melli, Centro Scientifico IBM, Roma, Italy)

PRESENTATIONS AND DISCUSSIONS ABOUT TOPIC IV

MESOSCALE DIFFUSION

Chairman: F. Nieuwstadt
Rapporteur: K. Herrmann

1. D. Henderson et al.

THE DEVELOPMENT AND APPLICATION OF MATHEMATICAL MODEL OF MESOSCALE DIFFUSION OF ATMOSPHERIC POLLUTANTS

(D. Henderson, United States Dept. of the Interior, National Park Service WASO Air Quality Office, P. O. Box 25287, Denver, Colorado 80225; Mei-Kao Liu and Michael Wojcik, System Applications, Inc. 950 Northgate Drive, San Rafael, California 94903, USA)

2. Helen ApSimon et al.

APPLICATION OF THE MESO-SCALE DIFFUSION MODELS MESOS AND TALD TO ACCIDENTAL RELEASES OF RADIO ACTIVITY

(H. ApSimon, J. Wrigley, Imperial College, London, England)
J. Le Grand, A. Desprès, Commissariat à l'Energie Atomique, Fontenay-aux Roses, France)

3. J. E. Lewis et al.

VARIATION OF ACID RAIN CONCENTRATIONS WITH SUMMER PRECIPITATION EVENTS IN THE SCHEFFERVILLE QUEBEC AREA

(J. E. Lewis, B. Hrebenyk, McGill University, Department of Geography, Burnside Hall, 805 Sherbrooke Street West, Montreal, PQ H3A, Quebec, Canada)

4. W. E. Davis et al.

THE USE OF TIME AVERAGED PRECIPITATION FOR WET REMOVAL IN A REGIONAL AIR POLLUTION ASSESSMENT MODEL

(W. E. Davis, W. J. Eadie, Battelle Pacific Northwest Lab., Battelle Boulevard, Richland, Washington, 99352, USA)

Chairman: Prof. Fiocco
Rapporteur: Ch. M. Bhumralkar

5. R. Berkowicz et al.

SPECTRAL TURBULENT DIFFUSIVITY THEORY APPLIED FOR POINT SOURCE DISPERSION

(R. Berkowicz, Danish Meteorological Institute, 100 Lyngbyvey,
2100 Copenhagen, Denmark)
L. P. Prahm, National Agency for Environmental Protection, Air Pollution
Lab., Risø National Laboratory, 4000 Roskilde, Denmark)

6. J. D. Reid

MODELLING DRIFT OF FOREST PESTICIDE SPRAY USING THE MONTE CARLO METHOD

(J. D. Reid, Atmospheric Environment Service, Boundary Layer Research
Division, 4905 Dufferin Street, Downsview, Ont., M3H 5T4, Canada)

7. A. Berger et al.

A STATISTICAL STUDY OF AIR TRAJECTORIES IN CONNEXION WITH THE OBSERVED LEVEL OF MESO-SCALE POLLUTION

(A. Berger, G. Deman, Cl. Demuth, P. Hecq, Université Catholique de
Louvain, Institut d'Astronomie et de Géophysique Georges Lemaitre,
Chemin du Cyclotron 2, 1348 Louvain-La-Neuve, Belgium)

8. P. R. Maul

THE MATHEMATICAL MODELING OF THE MESO-SCALE AND LONG-RANGE TRANSPORT OF SULPHUR COMPOUNDS

(P. R. Maul, Central Electricity Generating Board, Scientific Sciences
Department, Ratcliffe-on-Soar, Nottingham, NG II OEE, England)

Chairman: J. Tikvart
Rapporteur: D. Jost

9. K. Herrmann

MODELLING INTERREGIONAL TRANSPORT OF SO_2

(K. Herrmann, BASF Aktiengesellschaft, Abt. TUU/L1 - K 210,
6700 Ludwigshafen, Federal Republic of Germany)

10. N. D. van Egmond et al.

EVALUATION OF A MESO-SCALE MODEL OF THE DISPERSION OF SULPHUR DIOXIDE

(N. D. van Egmond, Rijksinstituut voor de Volksgezondheid, Bilthoven;
C. Huygen, IMG /TNO Div. of Technology for Society, P.O. Box 342,
7300 AH Apeldoorn,The Netherlands)

11. C. M. Bhumralkar et al.

AIR POLLUTION MODEL FOR CALCULATING SHORT-TERM DAILY REGIONAL PATTERNS AND TRANSFRONTIER EXCHANGES OF AIRBORNE SULFUR IN EUROPE

(C. M. Bhumralkar, W. B Johnson, R. L. Mancuso, D. E. Wolf, Stanford
Research International, 333 Ravenswood Ave., Menlo Park, California
94025, USA;
J. Pankrath, Umweltbundesamt, Bismarckplatz 1, 1000 Berlin 33)

Friday, Oct. 26, 1979

PRESENTATIONS AND DISCUSSIONS ABOUT TOPIC V

REGULATORY APPLICATIONS

Chairman: Prof. Dreyhaupt
Rapporteur: J. McQuaid

1. S. R. Hayes et al.

THE CHANGING REGULATORY ENVIRONMENT: AN APPRAISAL OF MODEL NEEDS IN THE ANALYSIS AND EXAMINATION OF POTENTIAL AIR QUALITY IMPACTS OF NO_x EMISSIONS FROM LARGE POINT SOURCES

(S. R. Hayes, P. M. Roth, D. R. Souten, R. W. Bergstrom, Systems Applications, Inc. 950 Northgate Drive, San Rafael, California 94903, USA)

2. M. E. Smith

THE CURRENT ROLE OF TALL STACKS IN THE UNITED STATES — TECHNOLOGY VERSUS POLITICS

(M. E. Smith, Meteorological Evaluation Services Inc., 134 Broadway, Amityville, N. Y. 11701, USA)

3. L. Kropp et al.

SENSITIVITY OF MODEL CALCULATIONS ON THE METEOROLOGICAL DATA AND ITS RELEVANCE TO REGULATORY ASPECTS

(L. Kropp, W. Bahmann, Technischer Überwachungsverein Rheinland e. V., Postfach 10 17 50, 5000 Köln 1, Federal Republic of Germany)

4. J. W. S. Young

TOTAL ENVIRONMENTAL PREDICTION - AIR QUALITY COMPONENT

(J. W. S. Young, Atmospheric Environment Service Canada, Dispersion Div., 4905 Dufferin Street, Downsview, Ont. M3H 5T4, Canada)

5. J. Tikvart

THE USE OF GOOD ENGINEERING PRACTICE STACK HEIGHTS IN AIR POLLUTION CONTROL

(J. A. Tikvart, Alan H. Huber, United States Environmental Protection Agency, Office of Air Quality Planning and Standards, MD - 14, Research Triangle Park, North Carolina, 27711, USA)

PRESENTATIONS AND DISCUSSIONS ABOUT TOPIC VI

HEAVY GASES

Chairman: J. W. S. Young

Rapporteur: L. Prahm

1. B. Gutsche et al.

FAILURE PROBLEMS AND DISPERSION PROCESSES OF HEAVY GASES

(B. Gutsche, Freie Universität Berlin, FB 24 /WE 4 - Fachrichtung Meteorologie, Thielallee 49, 1000 Berlin 33,
Christa Ludwig, Fritz Vahrenholt, Umweltbundesamt, Bismarckplatz 1, 1000 Berlin 33)

2. A. P. van Ulden

THE UNSTEADY GRAVITY SPREAD OF A DENSE CLOUD IN A CALM ENVIRONMENT

(A. P. van Ulden, Koninklijk Nederlands Meteorologisch Instituut, Postbus 201, 3730 AE De Bilt, The Netherlands)

3. C. G. Booij

THE INVESTIGATION INTO THE SPREADING AND DISPERSION OF A HEAVY GAS CLOUD BY MEANS OF PLANT DAMAGES IN THE AFFECTED AREA

(C. G. Booij, van Huevenstraat 46, 6824 MR Arnhem, The Netherlands)

4. J. McQuaid

FIELD TRIALS ON THE RELEASE OF HEAVY GASES

(J. McQuaid, Research and Laboratory Services Division, Health and Safety Executive, Sheffield S3 7HQ, England)

Chairman: J. G. Kretzschmar

Rapporteur: E. Runca

5. K. J. Eidsvik

A MODEL FOR HEAVY GAS DISPERSION IN THE ATMOSPHERE

(K. J. Eidsvik, Norwegian Institute for Air Research, P. B. 130,
2001 Lillestrom, Norway)

6. R. N. Meroney

PHYSICAL MODELING OF ATMOSPHERIC DISPERSION OF HEAVY GASES RELEASED AT THE GROUND OR FROM SHORT STACKS

(R. N. Meroney, Colorado State University, Department of Civil Engineering, Fort Collins, Colorado 80523, USA)

10TH NATO /CCMS INTERNATIONAL TECHNICAL MEETING ON AIR POLLUTION MODELING AND ITS APPLICATION

October 23 - 26, 1979

Rome, Italy

List of Participants

Preceding page blank

LIST OF PARTICIPANTS

AUSTRIA

KOLB Helga
University of Vienna
Hohe Warte 38

A - 1190 Vienna

PILLMANN Werner
Technical University of Vienna, and
Österreichisches Bundesinstitut
für Gesundheitswesen
Kegelgasse 19/4

A - 1030 Vienna

REUTER Heinz
University of Vienna
Hohe Warte 38

A - 1190 Vienna

BELGIUM

BERGER André
Université Catholique de Louvain
2, Chemin du Cyclotron,

B - 1348 Louvain-La-Neuve

BULTYNCK Henri
Studiecentrum voor Kernenergie
S.C.K. / C.E.N.
Boeretang 200

B - 2400 Mol

DEMUTH Claude
Université Catholique de Louvain
2, Chemin du Cyclotron

B - 1348 Louvain-La-Neuve

GUILLOT Pierre
Commission of the European Communities
200, rue de la Loi

B - 1049 Brussels

HECQ Pierre
Université Catholique de Louvain
2, Chemin du Cyclotron

B - 1348 Louvain-La-Neuve

KRETZSCHMAR Jean G. V.
Studiecentrum voor Kernenergie
S.C.K. /C.E.N.
Boeretang 200

B - 2400 Mol

WEAVING J. H.
Committee of Common Market
Automobile Constructors (CCMS)
18 Square de Meeûs

B - 1040 Brussels

DE WISPELAERE Christiaan
Programmatie van het Wetenschapsbeleid
Wetenschapsstraat 8

B - 1040 Brussels

CANADA

DAVIDSON A.
University of Waterloo
Dept. of Mechanical Engineering,

Waterloo, Ontario N2L 3G1

DJURFORS Sven G.
Syncrude Canada Ltd
10030 - 107 St.

Edmonton, Alberta

LEWIS John
Mc Gill University - Dept. of Geography
805 Sherbrook St. W.

Montreal, P. Q. H3A 2K6

MILLAN Millan
Atmospheric Environment Service
Fisheries and Environment Canada
4905 Dufferin Street

Downsview, Ontario M3H 5T4

PORTELLI Ron
Atmospheric Environment Service
Fisheries and Environment Canada
4905 Dufferin Street

Downsview, Ontario M3H 5T4

VENKATRAM Akula
Ontario Ministry of Environment
880 Bay Str. 4 Flr.

Toronto, Ontario M5S 1Z8

YOUNG James W. S.
Atmospheric Environment Service
Fisheries and Environment Canada
4905 Dufferin Street

Downsview, Ontario M3H 5T4

DENMARK

BERKOWICZ Ruwim
Danish Meteorological Institute
100 Lyngbyvey

DK - 2100 Copenhagen

JENSEN Niels Otto
Risø National Laboratory

DK - 4000 Roskilde

LYCK Erik
National Agency of Environmental
Protection, Air Pollution Laboratory
29 Strandgade 29

DK - 1041 Copenhagen K

MARKVORSEN Jørgen S.
Cowiconsult
45, Teknikerbyen

DK - 2830 Virum

PETERSEN Erik L.
Risø National Laboratory
Air Pollution Laboratory

DK - 4000 Roskilde

PRAHM Lars P.
National Agency for Environmental Protection
Air Pollution Laboratory
Risø National Laboratory

DK - 4000 Roskilde

FRANCE

BENARIE Michel
Institut National
de Recherche Chimique Appliquée
I R C A
B. P. 1

F - 91710 Vert Le Petit

GOBERT Thierry
Electricité de France
Septen, Tour EDF - Cedec 8

F - 92080 La Defense

SAAB Assaad E.
Electricité de France
6 Quai Watier

F - Chatou

GERMANY, FEDERAL REPUBLIC OF

AHRENS Dieter
Landesanstalt für Umweltschutz
Hertzstr. 173
D - 7500 Karlsruhe 1

BRAIG Anton
Battelle Institut e. V.
Am Römerhof 35
D - 6000 Frankfurt/Main

DREYHAUPT Franz J.
Ministerium fuer Arbeit, Gesundheit
und Soziales
Horionplatz 1
D - 4000 Düsseldorf

FISCHER Klaus
Deutsche Gesellschaft
für Wiederaufarbeitung
von Kernbrennstoffen
Buenteweg 2
D - 3000 Hannover

FORTAK Heinz
Freie Universität Berlin
Institut für Theoretische Meteorologie
Thielallee 49
D - 1000 Berlin 33

GUTSCHE Bernd
Freie Universität Berlin
FB 24/WE 4
Fachrichtung Meteorologie
Thielallee 49
D - 1000 Berlin 33

HERRMANN Klaus
BASF Aktiengesellschaft
Abt. TUU/LI-K 210
D - 6700 Ludwigshafen

HÜBSCHMANN Wolfgang
Kernforschungszentrum Karlsruhe GmbH
Postfach 3540
D - 7500 Karlsruhe

JOST Dieter
Umweltbundesamt
Bismarckplatz 1
D - 1000 Berlin 33

JÜRGEN Frank
Rheinisch-Westfälischer
Technischer Überwachungsverein
Steubenstr. 53

D - 4300 Essen

KLUG Werner
Institut für Meteorologie
Technische Hochschule Darmstadt

D - 6100 Darmstadt

KROPP Lothar
TÜV Rheinland Köln
Postfach 10 17 50

D - 5000 Köln 1

KUHR Klaus D.
Universität Hannover
Immelmannstr. 9

D - 3200 Hildesheim

LOEBEL Jürgen
VDI-Kommission
Reinhaltung der Luft
Postfach 1139

D - 4000 Düsseldorf

LÜHRING Paul G.
Freie Universität Berlin
Institut für Geophysikalische
Wissenschaften
Thielallee 50

D - 1000 Berlin 33

MEINL Herbert
Dornier System GmbH

D - 7990 Friedrichshafen

MORAWA Christa
Umweltbundesamt
Bismarckplatz 1

D - 1000 Berlin 33

MÜLLER Hans G.
Dornier System GmbH

D - 7990 Friedrichshafen

NEUMANN Gesa
Kernforschungszentrum Karlsruhe
Abt. für Angewandte Systemanalyse

D - 7500 Karlsruhe

SCHMITT Alfred
Ministerium für Arbeit, Gesundheit
und Soziales
Horionplatz 1

D - 4000 Düsseldorf

SCHNATZ Gottfried
Battelle Institut
Am Römerhof 35

D - 6000 Frankfurt /M. 90

SCHULTZ Heinrich
Universität Hannover
Theodor Storm Str. 5

D - 3007 Gelwelen

STRAKA Jan
Kernforschungsanlage Jülich GmbH
Postfach 365

D - 5170 Jülich 1

VOGT Kurt J.
Kernforschungsanlage Jülich GmbH
Postfach 365

D - 5170 Jülich 1

WEBER Erich
Bundesministerium des Innern
Ref. U II 8
Graurheindorfer Str. 198

D - 5300 Bonn

WIPPERMANN Friedrich
Technische Hochschule Darmstadt
Institut für Meteorologie

D - 6100 Darmstadt

ISRAEL

DAYAN Nissim
Israel Institute for Biological Research
P. O. Box 19

IL - Ness-Ziona

EYAL Ehud
Israel Institute for Biological Research
P. O. Box 19

IL - Ness-Ziona

ITZCHACK Ariel
Israel Institute for Biological Research
P. O. Box 19

IL - Ness-Ziona

KAPLAN Hadassah
Israel Institute for Biological Research
P. O. Box 19

IL - Ness-Ziona

ITALY

ANFOSSI Domenico
Laboratorio di Cosmo-Geofisica
C. N. R. - Università degli Studi di Torino
Corso Fiume 4

I - Torino

BELLOMO Bruno
ENEL
Via G. B. Martini 3

I - Roma

BONINO Giuseppe
Laboratorio di Cosmo-Geofisica
C. N. R. - Università degli Studi di Torino
Corso Fiume 4
I - Torino

CAGNETTI Pietro
CNEN - Casaccia
Via Anguillarese

I - 0060 Roma

CAMUFFO Dario
C. N. R.
Corso Stati Uniti - Camin

I - 35100 Padova

CARTA Gian Paolo
AGIP S. p. A.

I - San Donato Milanese

COLACINO Michele
Istituto di Fisica dell'Atmosfera
C. N. R.
Piazza Sturzo 31

I - Roma

DE CECCO Gianfranco
CNEN
Viale Regina Margherita 125

I - Roma

FERRARA Vincenzo
CNEN - Casaccia
Via Anguillarese

I - 0060 Roma

FINZI Giovanna
Centro Teoria dei Sistemi CNR
c/o Istituto di Elettrotecnica
ed Elettronica
Politecneco di Milano
Piazza Leonardo da Vinci 32

I - 20133 Milano

FIOCCO Giorgio
Istituto di Fisica dell'Atmosfera
C. N. R. e Università di Roma
Piazza Sturzo 31

I - Roma

FRONZA Giorgio
Istituto di Elettronica - Centro Teoria
dei Sistemi - Politecnico di Milano
Via Ponzio 34/5

I - Milano

GAGLIONE Pietro
Centro Comune di Varese - Divisione Chimica

I - Ispra, Varese

GIOVANELLI Giorgio
FISBAT - C. N. R.
Via dei Castagnoli 1

I - Bologna

GIOVANNINI Ivano
TECNECO

I - S. Ippolito (Pistoia)

LEVY Antonio
TECNECO

I - S. Ippolito (Pistoia)

LONGHETTO Arnaldo
ENEL
Bastioni Porta Volta 10

I - Milano

LUPINI Renzo
Facoltà di Ingegneria
Dip. Matematica
Via della Montagnola

I - Ancona

MELLI Pietro
Centro Scientifico IBM
Via del Giorgione 129

I - Roma

PAGLIARI Marcello
ENEL CRTN
Bastioni Porta Volta 10

I - Milano

RICHIARDONE Renzo
Laboratorio di Cosmo-Geofisica del CNR
Corso Fiume 4

I - Torino

RUNCA Elidoro
IBM Italia
Via del Giorgione 129

I - Roma

SANDRONI Santiono
Centro Comune di Ricerca CEE
Euratom Ispra

I - Ispra

SANTOMAURO Luigi
Osservatorio Meteorologico di Brera
Via Brera 28

I - Milano

SILVI Cesare
C N E N
Viale Regina Margherita 125

I - Roma

SOLARI Augusto
E. N. I.
Via Borgatti 25

I - Roma

TAMBURRANO Aldo
CNEN
Viale Regina Margherita 125

I - Roma

TEBALDI Giancarlo
Laboratorio Provinciale di Igiene
e Profilassi
Via Iuvara 22

I - Milano

TIRABASSI Tiziano
FISBAT - C. N. R.
Via dei Castagnioli 1

I - Bologna

ZAMPARO Gino
AGIP - S. p. A.

I - San Donato Milanese

JAPAN

INOUYE Rikita
Hokkaido University
13-8 Kita

J - Sapporo

THE NETHERLANDS

BOOIJ C. G.
Landbouwhogeschool
Van Huevenstraat 46

NL - Wageningen

HUYGEN C.
IMG - TNO - Division of Technology
for Society
P. O. Box 214

NL - Delft

NIEUWSTADT, F.
Royal Netherlands Meteorological Institute
Utrechtseweg 297

NL - AE 3730 De Bilt

SCHNEIDER Toni
National Institute of Public Health
P. O. Box 1

NL - Bilthoven

STEENKIST Ruud
KEMA
Utrechtseweg 310

NL - Arnhem

VAN DEN HOUT K. Dick
TNO - Inst. Env. Hygiene
Postbus 214

NL - Delft

VAN EGMOND Klaas
Dutch National Institute
of Public Health
P. O. Box 1

NL - Bilthoven

VAN ULDEN Aad
K N M I - Royal Netherlands
Meteorological Inst.
P. O. Box 201

NL - 3730 AE De Bilt

ZWERVER Saidjah
Ministerie van Volksgezondheid
en Milieu-Hygiene

NL - Leidschendam

NORWAY

EIDSVIK Karl
Norvegian Institute for Air Research
P. O. Box 130

N - 201 Lillestrom

SWEDEN

BRINGFELT Bjorn
SMHAI - Swenska Meteorological
and Hydrological Institute
SMHAI, Fack

S - 60101 Norrkoping

SWITZERLAND

TERCIER Philippe
Institut Météorologique Suisse
Section de la Protection de l'Air
Vignette 18

CH - 1530 Payerne

UNITED KINGDOM

BARRET C. F.
Warren Spring Laboratory
Gunnels Wood Road

GB - Stevenage

BENJAMIN Stephen F.
B. L. Technology Ltd.
Brown Lane

GB - Coventry

HARRIS N. C.
ICI Ltd. Mondial Division

GB - Northwich Cheshire

HENDERSON-SELLERS B.
University of Salford
Dept. Civil Eng.

GB - Salford M 5 4WT

JONES C. C.
CDE Porton Down Salisbury

GB - Wilts SP4 0JQ

KAISER Geoffrey
United Kingdom
Atomic Energy Authority
17 Bowden Close

GB - Culchet, Warrington

MAUL Philip R.
Central Electricity Generating Board
Midlands Region, Scientific Sciences Dept.
Scientific Services Centre
Ratcliffe-On-Soar

GB - Nottingham, NG 11 0EE

McQUAID James
Health and Safety Executive
Research and Laboratory Services Div.

GB - Red Hill Sheffield S3 7HQ

UNITED STATES OF AMERICA

BERRY Michael
US Environmental Protection Agency
Environmental Criteria and Assessment Office
Research Triangle Park

North Carolina, 27711 /USA

BHUMRALKAR Chandrakant
SRI - Stanford Research International
333 Ravenswood Avenue

Menlo Park, California 94025 /USA

CHAN Michael W.
Aero Vironment Inc.
145 Vista Avenue

Pasadena, Ca. 91107 /USA

DAVIS William E.
Battelle Pacific Northwest Laboratory
Battelle Boulevard, Richland

Washington 99352 /USA

GILLANI Noor
Washington University
Dept. of Mechanical Engineering
Box 1185

St. Louis, MO. 63130 /USA

HAYES Stanley R.
Systems Applications, Inc.
950 Northgate Drive

San Rafael, California, 94960 /USA

HENDERSON Donald
US Dept. of the Interior
National Park
Service WASO Air Quality Office
P. O. Box 25287

Denver, Colorado 80225 /USA

HOLZWORTH George
US Environmental Protection Agency
EPA - Meteorology (MD - 80)

Research Triangle Park N.C. 27711 /USA

LIU Hsien-Ta
Flow Research Company
21414 68th Avenue South Kent

Washington 98055 /USA

McKEE T. B.
Colorado State University
Dept. of Atmospheric Science

Fort Collins, Colorado 80523 /USA

MERONEY Robert
Colorado State University
Department of Civil Engineering

Fort Collins Colorado 80523 /USA

SCHULZE Richard
Trinity Consultants
P. O. Box 31481

Dallas, Texas 75231 /USA

SMITH Maynard
Meteorological Evaluation Services
134 Broadway

Amityville, N. Y. 11701 /USA

TIKVART Joseph A.
U.S. Environmental Protection Agency

Research Triangle Park, N. C. 27711 /USA

TROUT Dennis
US Environmental Protection Agency
Air Programs Branch 5AHAP
230 South Dearborn

Chicago, Ill. 60604 /USA

WEIL Jeffrey
Martin Marietta Corp.
1450 S. Rolling Road

Baltimore, M. D. 21227 /USA

WHITEMAN C. David
Colorado State University
1912 Springfield Dr.

Fort Collins Colorado /USA

YAMARTINO Robert
Argonne National Laboratory
9700 South Cass Avenue

Argonne, Ill. 60439 /USA